



P H D
T H E
S I S

STUDY OF

RESPONSE
SURFACE
MODELS

FOR THE CHARACTERIZATION OF
THE PERFORMANCE IN
REFRIGERATION EQUIPMENTS
and
HEAT PUMPS

January 2023

Javier Marchante Avellaneda

Supervisors

José Miguel Corberán Salvador

Emilio Navarro Peris



UNIVERSITAT
POLITÈCNICA
DE VALÈNCIA



PHD THESIS

Study of Response Surface Models for the characterization of the performance in Refrigeration Equipments and Heat Pumps

Author:

Javier Marchante Avellaneda

Supervisors:

Prof. José Miguel Corberán
Prof. Emilio Navarro Peris

*A thesis submitted in fulfillment of the requirements for the degree of
Doctor of Philosophy in Industrial Engineering and Production*


in the

Instituto Universitario de Investigación en Ingeniería Energética
Departamento de Termodinámica aplicada

UNIVERSITAT POLITÈCNICA DE VALÈNCIA

January 8, 2023

Note

This PDF document has been created by the typesetting system L^AT_EX (T_EXLive Team, 2022) and the  package for dynamic documents *knitr*¹. The purpose of *knitr* is to provide researchers with a powerful tool able to convert their work into a quality publishable document. It is based on *Reproducible Research* through the means of *Literate programming*.


Originally defined by Donald Knuth (Knuth, 1984), Literate programming is a programming paradigm that allows a program or source code to be defined as literature understandable to human beings. It is the basic idea behind dynamic documents and allows your research to be reported using a mix of program code and narrative. The 3 steps used by Literate Programming to generate the final document are:

- Parse the source document and separate code from narratives.
- Execute the source code and return the results.
- Mix the results from the source code with the original narratives, creating the final report or dissertation.

Therefore, this workflow allows our research results to be compiled (often implemented as program code) into numeric or graphical output, and the output to be inserted into our literal writings (like documentation). This has the main advantage of obtaining a dynamic document: If we modify or update our research results, the final document will be updated too. The other advantage is allowing our work to be reproducible.

The term reproducible research was first proposed by Jon Claerbout (Fomel and Claerbout, 2009). The idea is that the final product of our work is not just the published document. All datasets, the steps used to obtain our results, as well as the programming environment² are important too.

This means that, with *knitr* and a proper construction in our computer to define the programming environment, it is possible to reproduce our work (there is usually no human intervention when we generate a dynamic document).

¹This free tool integrates , or other programming languages, with the most common typesetting systems like L^AT_EX, Markdown, HTML, etc.

²Packages used, environment variables defined, etc.

Note

knitr is an open source package, and is therefore free to use in your research. It is thoroughly documented on the website <https://yihui.org/knitr/>. Another useful reference is the published book “*Dynamic Documents with R and knitr*” (Xie, 2015).

Finally, you can find the most recent stable version of this package hosted on CRAN (<https://cran.r-project.org/web/packages/knitr/index.html>) and the development version hosted on Github (<https://github.com/yihui/knitr>).

To my parents
Pedro *and* Isabel

Acknowledgments

First and foremost, I am extremely grateful to my supervisors, Prof. José Miguel Corberán Salvador and Prof. Emilio Navarro Peris, for their unwavering support, assistance at every stage of this research project, and patience during my doctoral studies training. Despite all the day-to-day work, they have always been willing to dedicate their time and knowledge to me, awakening my research interest. Thanks also to Prof. José González Maciá, who opened the doors of the IUIIE, allowing me to grow both professionally and personally.

Thanks a lot to my family at IUIIE. I will not mention names so as not to be too longwinded, but I would like to say that each of them is a great person. We are an excellent research team, and the result of our efforts is high-quality work. On the other hand, I cannot think of a better place to work. They are also wonderful people on a human level and make it possible to come with the best smile on my face.

Thanks to Hatef, Davide, and Yang for their warm welcome during my stay in Stockholm at KTH. They are also a great research team, and I have fond memories of them. I hope to see you soon.

I would like to acknowledge the financial support that has made this PhD thesis possible. The doctoral fellowship FPU15/03476 was founded by “*El Ministerio de Educación, Cultura y deporte*” inside the program “*Formación de Profesorado Universitario*”, and the GEOTECH project (Nº 656889) founded by the European Union under the “*Horizon 2020 Framework Programme for European Research and Technological Development*”.

Many thanks to everyone involved in the AHRI “*Low-GWP Alternative Refrigerants Evaluation Program*”. Their tremendous effort and excellent reports have made it possible to carry out a large part of the analysis on compressors. Thank you very much for publishing all this information openly and thus allowing researchers to improve science.

My appreciation also goes out to my family and friends. To my mother for her advice and help. To my father for never being afraid to get his hands dirty and helping me to disassemble and repair anything. To my sister for sharing good moments since we were kids. To my grandparents for their love and affection. And to my girlfriend for being by my side and creating unforgettable memories and experiences. Without their love and support, finishing this work would have

Acknowledgments

been impossible. Also, to my friends for making me grow as a person and sharing so many special moments since childhood.

Finally, I wish to give my wholehearted support to José Miguel's family and conclude by dedicating a few words in my mother tongue in memory of José Miguel Corberán. Sadly he died in July of this year, leaving a huge void to the IUIIE's team.

“Porque podemos cerrar los ojos y pensar en que se ha ido. Sin embargo, es mejor mantenerlos bien abiertos y contemplar lo que José Miguel ha construido con los años. Porque su legado es precioso. Elaborado durante años con esmero y perseverancia. Todos aquellos que lo han conocido saben de lo que hablo. Hablo de una persona de sonrisa eterna, afable, amable y con un entusiasmo que contagia a los que rodea. Una persona con afán por el saber y por la enseñanza. Quizás una de las cosas más importantes en la ciencia es la complicada tarea de divulgar y transmitir adecuadamente conocimiento. Sin lugar a dudas, en esto último José Miguel destacaba. Experto en transmisión de calor, era capaz de hacernos llegar la magia de la termodinámica a los aspectos más comunes de nuestras vidas, como por ejemplo a la cocina de nuestras casas. Nos proveía de herramientas tan valiosas como el pensamiento crítico y analítico, ayudando a perfilar y mejorar nuestro “yo” investigador a base de alimentar nuestra curiosidad. Escribo estas palabras con el máximo afecto y cariño y sintiéndome afortunado de todo lo que he podido aprender de él. Con tu prematura marcha dejas un gran vacío, pero si de algo estoy seguro es de que las personas jamás nos dejan. Su esencia queda, su voz se escucha, incluso sentimos su sonrisa, eternamente alimentada de los recuerdos de todos aquellos que te hemos conocido.”

We will keep your memory alive by continuing your valuable work.

Javier Marchante

Valencia, Spain (2022)

Abstract

In a context of global warming concerns and global energy policies, in which heating and cooling systems in buildings account for a significant amount of the global energy consumption, heat pump systems are widely considered as a really interesting option for enabling high efficiency and also for being renewable energy sources. In this sense, an accurate characterization of these units is of vital importance to improve their design and implement efficient control strategies, when the unit is integrated in more complex systems.

Against this background, this PhD thesis focuses on heat pump modelling in order to create map-based models able to accurately characterize the global performance of these units for the entire working range.

In the first part of this work, many experimental tests have been obtained for a new Dual Source Heat Pump prototype tested in the framework of the European project GEOTeCH. Due to the dual typology, the experimental results include performance data for the two main heat pump technologies: Air Source Heat Pumps and Ground Source Heat Pumps. By using all this experimental information, this first part focuses on obtaining empirical polynomial models capable of accurately predicting energy consumption and heating and cooling capacities as a function of external variables. Such variables are easy to measure and are usually recorded in real installations. Therefore, these models characterize the heat pump as a single component, simplifying its implementation in global models of more complex systems where these units are installed. Furthermore, selecting the empirical model approach, this part also includes some critical aspects, such as how to obtain the best polynomial expression, or how to perform the required experimental test matrices, i.e., how many tests should be conducted and where in the operating range.

Finally, the second part of this PhD thesis is dedicated to modelling one of the main components of these units, the compressor. In this case, the development of an extensive database including numerous calorimetric tests on the two main compressor technologies, reciprocating and scroll compressors, has allowed the detailed analysis of the response surfaces of their performance parameters, i.e., the energy consumption and mass flow rate as a function of the evaporation and condensation temperatures. Using this information, and following an approach similar to that used in the first part, this second part reviews the models included

Abstract

in the current compressor characterization standard, the AHRI 540 (2020), in order to check whether they are appropriate or, on the contrary, whether we should use of other types of polynomial expression. Critical issues such as the number of points needed to characterize each compressor technology, where to place them in the experimental domain, how to prevent possible overfitting in the model adjustment to minimize extrapolation or interpolation problems, or how to extrapolate results for predicting other refrigerant or suction conditions, are discussed in depth.

Resumen

En un contexto de creciente preocupación por el calentamiento global y de políticas energéticas internacionales, en el cual los sistemas de climatización de los edificios suponen una parte importante del consumo energético global, los sistemas de bombas de calor son considerados como opciones muy interesantes debido a su alta eficiencia y por ser fuentes de energía renovables. En este sentido, una caracterización precisa de estos equipos es de vital importancia con el objetivo de mejorar su diseño y, en aquellos casos dónde este tipo de unidades se integren como parte de sistemas más complejos, implementar estrategias de control eficientes.

En este contexto, esta tesis doctoral se centra en el modelado de bombas de calor con el fin de obtener modelos que permitan conocer con precisión el desempeño global de estas unidades en todo el rango de trabajo.

En la primera parte del trabajo, se han realizado numerosos ensayos experimentales utilizando un nuevo prototipo de bomba de calor dual, obtenidos dentro del marco de trabajo del proyecto europeo GEOTeCH. Debido a la tipología híbrida de esta unidad, los resultados experimentales obtenidos incluyen datos de desempeño para las principales tecnologías de bombas de calor: las bombas de calor aerotérmicas y geotérmicas. Haciendo uso de toda esta información experimental, esta primera parte del trabajo se centra en obtener modelos polinómicos para la predicción del consumo eléctrico y las capacidades de calefacción y refrigeración en función de las variables externas a la unidad. Dichas variables son fáciles de obtener y suelen medirse en instalaciones reales. Por tanto, estos modelos caracterizan a la bomba de calor como un único componente, simplificando su implementación en modelos globales de sistemas más complejos donde se instalan estas unidades. Además, seleccionado un enfoque empírico para el modelado, en esta parte también se analizan algunos aspectos relevantes, como los términos a incluir en el polinomio, o cómo conformar las matrices experimentales de ensayo necesarias, es decir, cuántos puntos experimentales realizar y dónde situarlos en el rango de operación.

Por último, la segunda parte de la tesis doctoral está dedicada a modelar uno de los componentes principales en estas unidades, el compresor. En este caso, el desarrollo de una extensa base de datos que incluye numerosos ensayos calorimétricos de las dos principales tecnologías de compresores, pistón y scroll,

ha permitido el análisis detallado de las superficies de respuesta del consumo eléctrico y el caudal másico de refrigerante en función de las temperaturas de evaporación y condensación. A partir de esta información y siguiendo un enfoque similar al utilizado previamente, en esta segunda parte se revisan los modelos incluidos en la norma actual de caracterización de compresores, el estándar AHRI 540 (2020), para comprobar si son adecuados o si, por el contrario, debemos utilizar otro tipo de expresiones polinómicas. También se analizan en profundidad cuestiones críticas como el número de puntos necesarios para caracterizar cada tecnología de compresor, dónde situarlos en el dominio experimental, cómo evitar un posible sobreajuste del modelo minimizando problemas de extrapolación o interpolación, o cómo extrapolar los resultados para predecir con otros refrigerantes u otras condiciones de aspiración.

Resum

En un context de creixent preocupació per l'escalfament global i de polítiques energètiques internacionals, en el qual els sistemes de climatització dels edificis suposen una part important del consum energètic global, els sistemes de bombes de calor són considerats com a opcions molt interessants a causa de la seva alta eficiència i perquè són fonts d'energia renovables. En aquest sentit, una caracterització precisa d'aquests equips és de vital importància amb l'objectiu de millorar el seu disseny i, en aquells casos on aquest tipus d'unitats s'integren com a part de sistemes més complexos, implementar estratègies de control eficients.

En aquest context, aquesta tesi doctoral se centra en el modelat de bombes de calor per obtenir models que permetisquen conèixer amb precisió el funcionament d'aquestes unitats a tot el rang de treball.

A la primera part del treball, s'han realitzat nombrosos assajos experimentals utilitzant un nou prototip de bomba de calor dual, obtinguts dins del marc de treball del projecte europeu GEOTECH. A causa de la tipologia híbrida d'aquesta unitat, els resultats experimentals obtinguts inclouen dades de funcionament per a les principals tecnologies de bombes de calor: les bombes de calor aerotèrmiques i geotèrmiques. Fent ús de tota aquesta informació experimental, aquesta primera part del treball se centra a obtenir models polinòmics per a la predicció del consum elèctric i les capacitats de calefacció i refrigeració en funció de les variables externes a la unitat. Aquestes variables són fàcils d'obtenir i se solen mesurar en instal·lacions reals. Per tant, aquests models caracteritzen la bomba de calor com un únic component, simplificant-ne la implementació en models globals de sistemes més complexos on s'instal·len aquestes unitats. A més, seleccionat un enfocament empíric per al modelatge, en aquesta part també s'analitzen alguns aspectes rellevants, com els termes a incloure al polinomi, o com conformar les matrius experimentals d'assaig necessàries, és a dir, quants punts experimentals realitzar i on situar-los al rang d'operació.

Per acabar, la segona part de la tesi doctoral està dedicada al modelat d'un dels components principals d'aquestes unitats, el compressor. En aquest cas, el desenvolupament d'una extensa base de dades que inclou nombrosos assajos calorimètrics de les dues principals tecnologies de compressors, pistó i scroll, ha permès l'anàlisi detallat de les superfícies de resposta del consum elèctric i el cabal màssic de refrigerant segons les temperatures d'evaporació i de conden-

sació. A partir d'aquesta informació i seguint un enfocament similar a l'utilitzat prèviament, en aquesta segona part es revisen els models inclosos a la norma actual de caracterització de compressors, l'estàndard AHRI 540 (2020), per comprovar si són adequats o si, per contra, cal utilitzar un altre tipus d'expressions polinòmiques. També s'analitzen en profunditat qüestions crítiques com el nombre de punts necessaris per caracteritzar cada tecnologia de compressor, on situar-los al domini experimental, com evitar un possible sobreajust del model minimitzant problemes d'extrapolació o interpolació, o com extrapolat els resultats per predir amb altres refrigerants o altres condicions d'aspiració.

Contents

Note

Acknowledgments

Abstract

Foreword v

List of Figures xiii

List of Tables xix

Nomenclature xxiii

I Main document

1 Introduction	1
1.1 Motivation	1
1.2 Background and state of the art	4
1.3 Aims of the study	17
1.4 Methodology	20
1.5 Structure of the thesis	23
2 Database	25
2.1 Introduction	25
2.2 Dual Source Heat Pump	26
2.3 Compressor performance data	45
2.4 Summary of datasets	47
3 Characterization of HPs: Empirical model approach	53
3.1 Introduction	53
3.2 Response variables and independent variables in the DSHP	59
3.3 IMST-ART and the virtual test database	65

3.4	Exploring functionals with the virtual database	67
3.5	DoE: Generating the experimental test matrices	85
3.6	Adjusting the polynomial models with the experimental data	93
3.7	Final results	102
4	Characterization of compressors: Empirical model approach	107
4.1	Introduction	108
4.2	Scroll compressors	112
4.3	Reciprocating compressors	142
4.4	Comparison of technologies	166
4.5	Summary of results for the polynomial models analyzed	171
5	Conclusions	175
5.1	Main conclusion for DSHP characterization	175
5.2	Main conclusions for scroll compressors	177
5.3	Main conclusions for reciprocating compressors	179
5.4	Future research	180
	Bibliography	I
	R-Packages and software	XIII
	Python-Packages and software	XVII
	Publications	XIX
 II Appendixes		
A	R workflow	a-1
A.1	Introduction	a-1
A.2	How to calculate thermophysical properties and the error propagation in R	a-1
A.3	R extensions	a-3
A.4	Python extensions	a-12
B	DSHP: Components description	b-1
B.1	Refrigerant	b-1
B.2	Heat exchangers	b-2
B.3	Expansion valve	b-4
B.4	Compressor	b-5
B.5	Pipes and refrigerant charge	b-5

C	Auxiliaries characterization	c-1
C.1	DSHP parasitic consumption	c-1
C.2	Fan characterization	c-2
C.3	Fluid properties for the brine and water loops	c-3
C.4	BPHE pressure drop	c-4
C.5	Circulation pumps (secondary side)	c-7
D	Uncertainty analysis	d-1
D.1	Estimation of measurement uncertainty	d-1
D.2	Instrumentation uncertainty specifications	d-6
E	Experimental test matrices	e-1
E.1	Winter Ground	e-2
E.2	Summer Ground	e-3
E.3	DHW Ground	e-4
E.4	DHW User	e-5
E.5	Winter Air	e-6
E.6	Summer Air	e-7
E.7	DHW Air	e-8
F	Experimental results DSHP	f-1
F.1	Winter Ground	f-2
F.2	Summer Ground	f-5
F.3	DHW Ground	f-7
F.4	DHW User	f-9
F.5	Winter Air	f-11
F.6	Summer Air	f-14
F.7	DHW Air	f-17
G	Empirical models DSHP	g-1
G.1	Introduction	g-1
G.2	Winter Ground	g-2
G.3	Summer Ground	g-5
G.4	DHW Ground	g-8
G.5	DHW User	g-11
G.6	Winter Air	g-14
G.7	Summer Air	g-17
G.8	DHW Air	g-20
H	Contour plots scroll compressors	h-1
H.1	Contour plots of scroll performance variables	h-1

I	Contour plots reciprocating compressors	i-1
I.1	Contour plots of reciprocating performance variables	i-1
J	Model summary tables for scroll compressors	j-1
J.1	Model summary tables for the characterization of \dot{W}_c , \dot{W}_{esp} and \dot{m}_{ref}	j-1
K	Model summary tables for reciprocating compressors	k-1
K.1	Model summary tables for the characterization of \dot{W}_c , \dot{W}_{esp} and \dot{m}_{ref}	k-1
L	Design of experiments in compressor characterization	l-1
L.1	Introduction	l-1
L.2	Classical experimental designs	l-3
L.3	Computer-aided experimental designs	l-5
L.4	Generating the experimental samples	l-7
L.5	Analysis of results	l-8
L.6	Summary of results	l-14
L.7	Summary tables DoE samples	l-16
L.8	Source code to obtain computer-aided designs	l-19

Foreword

The construction and adjustment of a model is a common process that researchers face today. Usually, we import a dataset into a statistical software program with all the experimental results for the physical system analyzed. Then, the main objective will be to adjust a model so that it is able to characterize the behavior of this physical system.

In general, this behavior is represented by the response variable of interest y and there is a set of predictors, or independent variables, x_1, x_2, \dots, x_n that fix the value of y .

In some systems this relationship between y and x 's might be known "exactly", based on physical principles or chemical laws. Therefore, we could obtain a model with the form $y = g(x_1, x_2, \dots, x_n) + \epsilon$, where ϵ represents the residual "error" for the model adjusted.

This type of relationship is often called a **mechanistic model**. Unfortunately, this is not the common situation, where the underlying mechanism is not fully understood, and therefore the function g is unknown.

In this situation, researchers must approximate this unknown function g with the **empirical model** approach: $y = f(x_1, x_2, \dots, x_n) + \epsilon$. The most common functionals selected to adjust this function f are first-order or second-order polynomials and these types of empirical model are called **response surface models**.

Of course, we require some knowledge of statistical experimental design, regression modelling techniques and graphical representation methodologies to make a proper adjustment for the final response surface models. All these tools have been popularly called **Response Surface Methodology (RSM)**.

The present work will show how to make a good adjustment of this type of model in the field of refrigeration and Heat Pumps (HPs). It includes the **Design of Experiments (DoE)** methodologies to perform the experimental test matrices, the development of the response surface models and the final adjustment with the experimental data.

Software Information and Conventions

This section shows how to set the programming environment necessary to reproduce the present work. The source code was compiled in [Ubuntu 20.04 LTS \(KDE neon distribution\)](#)³ in order to construct the programming environment in an open source operating system.

The main tool used was the [R](#) language (R Core Team, 2022) and the IDE RStudio (RStudio Team, 2022). Additionally, the [Python](#)⁴ language is also required in order to calculate the thermophysical properties of the refrigerants with *Coolprop* and *Refprop 10* software (Bell et al., 2014; Lemmon et al., 2018).

The environment variables below are included in `/etc/environment` in order to fix the [Python](#) distribution and *Refprop 10* paths:

- `RETICULATE_PYTHON="/home/username/anaconda3/bin/python3"`
- `RPprefix="/opt/Refprop_10/"`

Finally, an installed distribution of [L^AT_EX](#) is also required (T_EXLive Team, 2022) and the session information of [R](#) and [Python](#) are attached below with the complete list of additional packages required:

R-Session information

```
print(sessionInfo(), FALSE)

## R version 4.1.3 (2022-03-10)
## Platform: x86_64-pc-linux-gnu (64-bit)
## Running under: KDE neon User - 5.25
##
## Matrix products: default
## BLAS:   /usr/lib/x86_64-linux-gnu/blas/libblas.so.3.9.0
## LAPACK: /home/jamarav/anaconda3/lib/libmkl_rt.so.1
##
## attached base packages:
## [1] grid      stats    graphics
## [4] grDevices utils   datasets
## [7] methods  base
```

³Linux distribution based on [Debian](#) and developed by Canonical Ltd.

⁴The selected distribution of [Python](#) installed was [Anaconda Inc.](#) (2022).

```
##
## other attached packages:
## [1] scales_1.1.1
## [2] AlgDesign_1.2.0
## [3] RcmdrMisc_2.7-2
## [4] sandwich_3.0-1
## [5] car_3.0-12
## [6] carData_3.0-5
## [7] tikzDevice_0.12.3.1
## [8] pacman_0.5.1
## [9] fields_13.3
## [10] viridis_0.6.2
## [11] viridisLite_0.4.0
## [12] spam_2.8-0
## [13] metR_0.12.0
## [14] isoband_0.2.5
## [15] modelsummary_0.9.5
## [16] gt_0.3.1
## [17] ggfortify_0.4.14
## [18] GGally_2.1.2
## [19] ppcor_1.1
## [20] MASS_7.3-55
## [21] lemon_0.4.5
## [22] cowplot_1.1.1
## [23] ggpubr_0.4.0
## [24] kableExtra_1.3.4
## [25] gridExtra_2.3
## [26] reticulate_1.24
## [27] nls.multstart_1.2.0
## [28] Metrics_0.1.4
## [29] quantities_0.1.6
## [30] errors_0.3.6
## [31] udunits2_0.13.2
## [32] units_0.8-0
## [33] ggthemes_4.2.4
## [34] forcats_0.5.1
## [35] stringr_1.4.0
## [36] dplyr_1.0.8
## [37] purrr_0.3.4
## [38] readr_2.1.2
## [39] tidyr_1.2.0
```

```
## [40] tibble_3.1.6
## [41] ggplot2_3.3.5
## [42] tidyverse_1.3.1
## [43] knitr_1.37
##
## loaded via a namespace (and not attached):
## [1] colorspace_2.0-2
## [2] ggsignif_0.6.3
## [3] class_7.3-20
## [4] ellipsis_0.3.2
## [5] htmlTable_2.4.0
## [6] base64enc_0.1-3
## [7] fs_1.5.2
## [8] proxy_0.4-26
## [9] rstudioapi_0.13
## [10] fansi_1.0.2
## [11] lubridate_1.8.0
## [12] xml2_1.3.3
## [13] splines_4.1.3
## [14] Formula_1.2-4
## [15] jsonlite_1.7.3
## [16] broom_0.7.12
## [17] cluster_2.1.2
## [18] dbplyr_2.1.1
## [19] png_0.1-7
## [20] compiler_4.1.3
## [21] httr_1.4.2
## [22] backports_1.4.1
## [23] assertthat_0.2.1
## [24] Matrix_1.4-0
## [25] fastmap_1.1.0
## [26] cli_3.1.1
## [27] formatR_1.11
## [28] htmltools_0.5.2
## [29] tools_4.1.3
## [30] dotCall64_1.0-1
## [31] gtable_0.3.0
## [32] glue_1.6.1
## [33] maps_3.4.0
## [34] tables_0.9.6
## [35] Rcpp_1.0.8
```



```
## [36] cellranger_1.1.0
## [37] vctr_0.3.8
## [38] filehash_2.4-2
## [39] svglite_2.1.0
## [40] xfun_0.29
## [41] rvest_1.0.2
## [42] lifecycle_1.0.1
## [43] rstatix_0.7.0
## [44] zoo_1.8-9
## [45] hms_1.1.1
## [46] RColorBrewer_1.1-2
## [47] rpart_4.1.16
## [48] latticeExtra_0.6-29
## [49] reshape_0.8.8
## [50] stringi_1.7.6
## [51] highr_0.9
## [52] nortest_1.0-4
## [53] e1071_1.7-9
## [54] checkmate_2.0.0
## [55] rlang_1.0.1
## [56] pkgconfig_2.0.3
## [57] systemfonts_1.0.3
## [58] evaluate_0.14
## [59] lattice_0.20-45
## [60] htmlwidgets_1.5.4
## [61] tidyselect_1.1.1
## [62] plyr_1.8.6
## [63] magrittr_2.0.2
## [64] R6_2.5.1
## [65] generics_0.1.2
## [66] Hmisc_4.6-0
## [67] DBI_1.1.2
## [68] foreign_0.8-82
## [69] pillar_1.7.0
## [70] haven_2.4.3
## [71] withr_2.4.3
## [72] nnet_7.3-17
## [73] survival_3.2-13
## [74] abind_1.4-5
## [75] modelr_0.1.8
## [76] crayon_1.4.2
```

```
## [77] utf8_1.2.2
## [78] tzdb_0.2.0
## [79] rmarkdown_2.11
## [80] jpeg_0.1-9
## [81] readxl_1.3.1
## [82] data.table_1.14.2
## [83] reprex_2.0.1
## [84] digest_0.6.29
## [85] webshot_0.5.2
## [86] munsell_0.5.0
```

Python-Session information

```
session_info.show()
## -----
## CoolProp          6.4.1
## matplotlib        3.5.1
## numpy             1.21.5
## pandas            1.4.2
## session_info      1.0.0
## -----
## Python 3.9.12 (main, Apr  5 2022, 07:05:27) [GCC 7.5.0]
## Linux-5.15.0-41-generic-x86_64-with-glibc2.31
## -----
## Session information updated at 2023-01-08 22:11
```


List of Figures

1.1	Phases of Modelling and Simulation	6
1.2	Modelling paradigms	7
1.3	Conceptual model classification	9
1.4	P-h diagram (R32 - reference state IIR)	12
1.5	Vapour compression cycle	12
1.6	GEOTeCH consortium	17
2.1	DSHP basic diagram	29
2.2	DSHP 3D	32
2.3	DSHP experimental test rig (diagram)	33
2.4	Experimental test rig	34
2.5	IMST-ART GUI	38
2.6	IMST-ART compressor submodel: Adjustment results \dot{m}_{ref}	43
2.7	IMST-ART compressor submodel: Adjustment results \dot{W}_c	43
2.8	IMST-ART compressor submodel: Heat losses	44
2.9	IMST-ART model vs experimental data in WG mode	45
3.1	Response Curve vs Response Surface	55
3.2	Steps to obtain polynomial models	58
3.3	Winter Ground: Response (blue) and control (red) variables	60
3.4	Winter Air: Response (blue) and control (red) variables	62
3.5	Summer Air: Response (blue) and control (red) variables	64
3.6	WG: Correlation matrix \dot{W}_c	68
3.7	WG: Correlation matrix \dot{Q}_c	71
3.8	WG: Correlation matrix \dot{Q}_e	72
3.9	WG: Linear model and stepwise model	76
3.10	WG: Linear model diagnostic plots	76
3.11	WG: Stepwise model diagnostic plots	77
3.12	WG: \dot{W}_c and \dot{W}_c/f_c vs pressure ratio	79
3.13	WG: Correlation matrix \dot{W}_c/f_c	79
3.14	WG: Correlation matrix \dot{Q}_c/f_c	80
3.15	WG: Correlation matrix \dot{Q}_e/f_c	80
3.16	WG: \dot{W}_c/f_c model	82

3.17	WG: \dot{W}_c / f_c model diagnostic plot	82
3.18	Factorial design: 2^3	86
3.19	Central Composite Design: Face centered (left-hand) vs Circumscribed (right-hand)	89
3.20	Box & Behnken design	90
3.21	DoE comparison (WG mode)	91
3.22	WG mode: IMST-ART compressor consumption vs calculated values (CCD vs Taguchi designs)	92
3.23	Response surface y (blue) and tangent plane (orange) at the point y_0	96
3.24	Example 3.1: Experimental readjustment for different values of k_j . Original model (blue surface) and readjusted model (orange surface)	99
4.1	η_c as a function of P_r (AHRI 11 R410A and AHRI 21 R404A)	114
4.2	η_c contour plot, temp. domain (AHRI 11 R410A and AHRI 21 R404A. SH=11K)	115
4.3	η_c as a function of P_r at given levels of T_e (AHRI 11 R410A and AHRI 21 R404A)	116
4.4	\dot{W}_c as a function of T_c at given levels of T_e (AHRI 11 R410A and AHRI 21 R404A)	117
4.5	\dot{W}_c contour plot, temp. domain (AHRI 11 R410A and AHRI 21 R404A. SH=11K)	118
4.6	3D plot of \dot{W}_c , temp. domain (AHRI 11 R410A and AHRI 21 R404A. SH=11K)	118
4.7	\dot{W}_c contour plot, press. domain (AHRI 11 R410A and AHRI 21 R404A. SH=11K)	119
4.8	η_v as a function of P_r (AHRI 11 R410A and AHRI 21 R404A)	121
4.9	η_v contour plot, temp. domain (AHRI 11 R410A and AHRI 21 R404A. SH=11K)	121
4.10	\dot{m}_{ref} contour plot, temp. domain (AHRI 11 R410A and AHRI 21 R404A. SH=11K)	123
4.11	3D plot of \dot{m}_{ref} , temp. domain (AHRI 11 R410A and AHRI 21 R404A. SH=11K)	123
4.12	3D plot of \dot{W}_c , temp. domain (left-hand) and pressure domain (right-hand) (AHRI 11 and 4 different refrigerants)	125
4.13	3D plot of \dot{W}_c , temp. domain (left-hand) and pressure domain (right-hand) (AHRI 21 and 5 different refrigerants)	125
4.14	3D plot of \dot{m}_{ref} , temp. domain (left-hand) and pressure domain (right-hand) (AHRI 11 and 4 different refrigerants)	127
4.15	3D plot of \dot{m}_{ref} , temp. domain (left-hand) and pressure domain (right-hand) (AHRI 21 and 5 different refrigerants)	127
4.16	\dot{W}_c model errors (AHRI 11, 21 and Cuevas (2009))	130

4.17	\dot{W}_c prediction extrapolating for other refrigerants (AHRI 11 and 21). <i>Correlation 2a</i> (left-plot) and <i>Correlation 3a</i> (right-plot)	132
4.18	Dabiri correction to other suction conditions (AHRI 11 R410A and DR5)	133
4.19	\dot{m}_{ref} model errors (AHRI 11, 21 and Cuevas (2009))	136
4.20	Optimal Design. Fedorov (7, 9, 11 test points). AHRI 21 R404A	137
4.21	Optimal Design. Fedorov (5, 6, 7 test points). AHRI 21 R404A	139
4.22	Random samples error models (AHRI 21 R404A. SH=11K)	141
4.23	η_c contour plot, temp. domain (AHRI 30 R134a and AHRI 21 R404A. SH=11K)	143
4.24	η_c and \dot{W}_c as a function of P_r, T_e at given levels of T_c (AHRI 30 R134a)	144
4.25	\dot{W}_c contour plot, press. domain, reciprocating compressor (left-hand AHRI 17, 18, 28, 30, 59) and scroll compressor (right-hand AHRI 11, 21) for its reference refrigerant	145
4.26	\dot{W}_{esp} contour plot, press. domain, reciprocating compressor (left-hand AHRI 17, 18, 28, 30, 59) and scroll compressor (right-hand AHRI 11, 21) for its reference refrigerant	147
4.27	\dot{W}_{esp} contour plot, press. domain, with P_r and P'_r isolines of AHRI 59 for its reference refrigerant	148
4.28	P_r vs P'_r (AHRI 17, 18, 28, 30, 59, 11, 21 and its reference refrigerant)	149
4.29	η_v as a function of P_r (AHRI 30 R134a and AHRI 21 R404A)	149
4.30	\dot{m}_{ref} contour plot, press. domain, reciprocating compressor (left-hand AHRI 17, 18, 28, 30, 59) and scroll compressor (right-hand AHRI 11, 21) for its reference refrigerant	150
4.31	3D plot of \dot{W}_c , temp. domain (left-hand) and pressure domain (right-hand) (AHRI 59 and 6 different refrigerants)	152
4.32	Energy consumption model errors (AHRI 30, 59)	157
4.33	Mass flow rate model errors (AHRI 30, 59)	160
4.34	Polygonal Design (7, 9, 11 test points). AHRI 21 R404A	163
4.35	Random samples error models including \dot{W}_{esp} results (AHRI 21 R404A)	165
4.36	3D plot of \dot{W}_c , temp. domain (AHRI 30 R134a and AHRI 59 R410A. SH=11K)	166
4.37	\dot{W}_{is} dependence as a function of working conditions	168
4.38	η_v and η_c vs P_r in scroll and reciprocating compressors	169
4.39	η_v/η_c vs P_r in scroll (AHRI 11 and 21) and reciprocating (AHRI 30 and 59) compressors	170
4.40	Summary model errors: scroll compressor	172
4.41	Summary model errors: reciprocating compressor	173
A.1	R session workflow	a-3

B.1	RTPFHx circuits	b-2
C.1	Fan characterization	c-2
C.2	Operating map of a variable speed circulation pump	c-7
C.3	Condenser capacity correction with the heat injected by the circulation pump	c-9
D.1	Steps to obtain the expanded uncertainty to report	d-5
G.1	Winter Ground mode: Empirical model	g-4
G.2	Summer Ground mode: Empirical model	g-7
G.3	DHW Ground mode: Empirical model	g-10
G.4	DHW User mode: Empirical model	g-13
G.5	Winter Air mode: Empirical model	g-16
G.6	Summer Air mode: Empirical model	g-19
G.7	DHW Air mode: Empirical model	g-22
H.1	Contour plots AHRI 11 ; R410A ; SH=11K	h-2
H.2	Contour plots AHRI 33 ; R32+R134a ; SH=11K	h-3
H.3	Contour plots AHRI 21 ; R404A ; SH=11K	h-4
H.4	Contour plots AHRI 24 ; DR5 ; SH=11K	h-5
H.5	Contour plots AHRI 38 ; L41b ; SH=11K	h-6
H.6	Contour plots AHRI 39 ; R32 ; SH=11K	h-7
H.7	Contour plots AHRI 58 ; R454B ; SH=11K	h-8
H.8	Contour plots AHRI 34 ; DR7 ; SH=11K	h-9
H.9	Contour plots AHRI 36 ; L40 ; SH=11K	h-10
H.10	Contour plots AHRI 65 ; R447A ; SH=11K	h-11
H.11	Contour plots AHRI 66 ; HPR2A ; SH=11K	h-12
H.12	Contour plots Cuevas(2009) 50Hz ; R134a ; SH=6.8K	h-13
I.1	Contour plots AHRI 17 ; R22 ; SH=11K	i-2
I.2	Contour plots AHRI 18 ; R134a ; SH=22K	i-3
I.3	Contour plots AHRI 28 ; R404A ; SH=11K	i-4
I.4	Contour plots AHRI 29 ; DR7 ; SH=11K	i-5
I.5	Contour plots AHRI 49 ; R455A ; SH=11K	i-6
I.6	Contour plots AHRI 50 ; DR3 ; SH=11K	i-7
I.7	Contour plots AHRI 30 ; R134a ; SH=11K	i-8
I.8	Contour plots AHRI 35 ; DR7 ; SH=11K	i-9
I.9	Contour plots AHRI 37 ; L40 ; SH=11K	i-10
I.10	Contour plots AHRI 51 ; R404A ; $T_s=20^\circ\text{C}$	i-11
I.11	Contour plots AHRI 59 ; R410A ; SH=11K	i-12
I.12	Contour plots AHRI 64a ; R404A ; SH=10K	i-13

I.13 Contour plots AHRI 67a ; ARM25 ; SH=10K i-14

I.14 Contour plots AHRI 69a ; ARM20b ; SH=10K i-15

I.15 Contour plots AHRI 64b ; R404A ; SH=10K i-16

I.16 Contour plots AHRI 67b ; ARM25 ; SH=10K i-17

I.17 Contour plots AHRI 69b ; ARM20b ; SH=10K i-18

L.1 Non-orthogonal experimental domains. Internal combustion engine (left-hand) and scroll compressor (right-hand) 1-2

L.2 Classical designs: 3^2 , CCD, SCD and HD (AHRI 21 R404A and SH=11K) 1-4

L.3 AHRI 11 R410A-CCD vs R32-HD (SH=11K) 1-9

L.4 Clustering 6, 9, and 12 points (AHRI 11 R410A and SH=11K) 1-9

L.5 Optimal design using Fedorov's algorithm for 6, 9, and 12 points (AHRI 11 R410A and SH=11K) 1-10

L.6 Polygon Design 6, 9, and 12 points (AHRI 11 R410A and SH=11K) . 1-11

List of Tables

1.1	Conceptual models: advantages/disadvantages	11
2.1	Operating conditions (secondary fluid values) ^a	27
2.2	Operating modes	28
2.3	DSHP components	31
2.4	Instrumentation	36
2.5	Compressor submodel coefficients	42
2.6	DSHP experimental campaign	48
2.7	DSHP virtual tests	49
2.8	Calorimeter data (AHRI Reports)	50
2.9	New refrigerants composition (Low GWP HFC mixtures)	51
3.1	Number of coefficients in polynomials of degree d with k inputs	56
3.2	WG: Linear model and stepwise model coefficients	75
3.3	WG: \dot{W}_c/f_c model	81
3.4	Two blocks for a 2^3 design	87
3.5	DoE methodology results: Performance prediction in WG mode	92
3.6	WG: \dot{Q}_c/f_c model adjusted with the virtual and experimental database	94
3.7	WG: \dot{Q}_c model readjusted with the experimental database	100
3.8	Prediction errors for the final polynomial models	104
4.1	\dot{W}_c models (AHRI 11, 21 and Cuevas (2009))	129
4.2	\dot{m}_{ref} models (AHRI 11, 21 and Cuevas (2009))	134
4.3	Regression model adjusted with OD sample, 9 tests (AHRI 21 R404A)	138
4.4	Regression model adjusted with OD sample, 6 tests (AHRI 21 R404A)	140
4.5	\dot{W}_c models (AHRI 30, 59)	155
4.6	\dot{m}_{ref} models (AHRI 30, 59)	159
4.7	Regression model adjusted with PD sample, 9 tests (AHRI 21 R404A)	163
B.1	Data of the designed RTPFHx	b-3

B.2	BPHEs specifications	b-4
B.3	Compressor specifications	b-5
C.1	Water Properties	c-4
C.2	Propylenglycol Properties (30% mass fraction)	c-4
C.3	ΔP (User - Plate model: F85 SWEP)	c-6
C.4	ΔP (DHW - Plate model: B26 SWEP)	c-6
C.5	ΔP (Ground - Plate model: F80AS SWEP)	c-6
C.6	Regression coefficients DHW and User pumps	c-8
C.7	Regression coefficients Ground pump	c-8
E.1	WG mode: CCD (30 test points)	e-2
E.2	SG mode: CCD (30 test points)	e-3
E.3	DHWG mode: CCD (20 test points)	e-4
E.4	DHWU mode: CCD (20 test points)	e-5
E.5	WA mode: CCD (30 test points)	e-6
E.6	SA mode: CCD (30 test points)	e-7
E.7	DHWA mode: CCD (20 test points)	e-8
F.1	WG: Experimental results	f-2
F.2	SG: Experimental results	f-5
F.3	DHWG: Experimental results	f-7
F.4	DHWU: Experimental results	f-9
F.5	WA: Experimental results	f-11
F.6	SA: Experimental results	f-14
F.7	DHWA: Experimental results	f-17
G.1	Winter Ground: Polynomial models adjusted with the virtual database	g-2
G.2	Winter Ground: Experimental readjustment	g-3
G.3	Summer Ground: Polynomial models adjusted with the virtual database	g-5
G.4	Summer Ground: Experimental readjustment	g-6
G.5	DHW Ground: Polynomial models adjusted with the virtual database	g-8
G.6	DHW Ground: Experimental readjustment	g-9
G.7	DHW User: Polynomial models adjusted with the virtual database	g-11
G.8	DHW User: Experimental readjustment	g-12
G.9	Winter Air: Polynomial models adjusted with the virtual database	g-14
G.10	Winter Air: Experimental readjustment	g-15
G.11	Summer Air: Polynomial models adjusted with the virtual database	g-17

G.12 Summer Air: Experimental readjustment	g-18
G.13 DHW Air: Polynomial models adjusted with the virtual database	g-20
G.14 DHW Air: Experimental readjustment	g-21
J.1 Energy consumption models (AHRI 11, 33)	j-2
J.2 Mass flow rate models (AHRI 11, 33)	j-3
J.3 Energy consumption models (AHRI 21)	j-4
J.4 Mass flow rate models (AHRI 21)	j-5
J.5 Energy consumption models (AHRI 24, 38, 39, 58)	j-6
J.6 Mass flow rate models (AHRI 24, 38, 39, 58)	j-7
J.7 Energy consumption models (AHRI 34, 36)	j-8
J.8 Mass flow rate models (AHRI 34, 36)	j-8
J.9 Energy consumption models (AHRI 65)	j-9
J.10 Mass flow rate models (AHRI 65)	j-9
J.11 Energy consumption models (AHRI 66)	j-10
J.12 Mass flow rate models (AHRI 66)	j-10
J.13 Energy consumption models (Cuevas(2009))	j-11
J.14 Mass flow rate models (Cuevas(2009))	j-11
K.1 Energy consumption models (AHRI 17)	k-2
K.2 Mass flow rate models (AHRI 17)	k-2
K.3 Energy consumption models (AHRI 18)	k-3
K.4 Mass flow rate models (AHRI 18)	k-4
K.5 Energy consumption models (AHRI 28, 29, 49, 50)	k-5
K.6 Mass flow rate models (AHRI 28, 29, 49, 50)	k-6
K.7 Energy consumption models (AHRI 30)	k-7
K.8 Mass flow rate models (AHRI 30)	k-7
K.9 Energy consumption models (AHRI 35, 37)	k-8
K.10 Mass flow rate models (AHRI 35, 37)	k-8
K.11 Energy consumption models (AHRI 51)	k-9
K.12 Mass flow rate models (AHRI 51)	k-9
K.13 Energy consumption models (AHRI 59)	k-10
K.14 Mass flow rate models (AHRI 59)	k-11
K.15 Energy consumption models (AHRI 64a, 67a, 69a)	k-12
K.16 Mass flow rate models (AHRI 64a, 67a, 69a)	k-13
K.17 Energy consumption models (AHRI 64b, 67b, 69b)	k-14
K.18 Mass flow rate models (AHRI 64b, 67b, 69b)	k-15
L.1 AHRI 11 (R410A). Energy consumption	l-12
L.2 AHRI 11 (R410A). Mass flow rate	l-12
L.3 AHRI 11. Summary table DoE samples results	l-16
L.4 AHRI 21. Summary table DoE samples results	l-17

L.5 AHRI 33. Summary table DoE samples results 1-18

Nomenclature

Symbol Description

A	Area (m ²).	P_{atm}	Atmospheric pressure. 1.013 (bar).
D_h	Hydraulic diameter (m).	P_c	Condensation pressure (bar).
dT_c	Temperature difference of the secondary fluid across the condenser (K).	P_e	Evaporation pressure (bar).
dT_e	Temperature difference of the secondary fluid across the evaporator (K).	$P_{h,user}$	Circulation pump hydraulic power, user loop (W).
f_c	Compressor frequency (Hz).	$P_{h,ground}$	Circulation pump hydraulic power, ground loop (W).
f_f	Fanning friction factor (-).	$P_{h,DHW}$	Circulation pump hydraulic power, DHW loop (W).
f_{fan}	Fan speed (%).	P_r	Pressure ratio between compressor inlet and outlet (-).
h_1	Enthalpy at compressor suction (kJ/kg).	\dot{Q}_c	Condenser capacity (W).
h_{2s}	Enthalpy at compressor discharge (isentropic compression) (kJ/kg).	$\dot{Q}_{cooling}$	Cooling capacity (W).
L	Length (m ²).	\dot{Q}_e	Evaporator capacity (W).
\dot{m}	Mass flow rate (kg/s).	$\dot{Q}_{heating}$	Heating capacity.
\dot{m}_{dhw}	Water mass flow rate, DHW loop in the DSHP (kg/h).	Re	Reynolds number (-).
\dot{m}_{ground}	Brine mass flow rate, ground loop in the DSHP (kg/h).	RH	Relative humidity (%).
\dot{m}_{map}	Compressor mass flow rate adjusted to map suction conditions (kg/s).	T_a or T_{ai}	Air inlet temperature to the RTPFHx (°C or K).
\dot{m}_{ref}	Refrigerant mass flow rate (kg/h).	T_c	Dew point condensation temperature (°C).
\dot{m}_{user}	Water mass flow rate, user loop in the DSHP (kg/h).	T_{ci}	Inlet temperature of the secondary fluid to the condenser (°C or K).
n	Compressor speed (rps).	T_{co}	Outlet temperature of the secondary fluid to the condenser (°C or K).
		$T_{coil,in}$	Inlet temperature of the refrigerant.

	erant to the RTPFHx in the DSHP (°C).	\dot{V}_{user}	Secondary volume flow rate, user loop (m ³ /s).
$T_{coil,out}$	Outlet temperature of the refrigerant to the RTPFHx in the DSHP (°C).	w_{ai}	Humidity ratio at RTPFHx inlet conditions (kg _{water} /kg _{dry air}).
T_d	Compressor discharge temperature (°C).	\dot{W}_c	Compressor energy consumption (W or kW).
$T_{d,in}$	Inlet temperature of the refrigerant to the DHW HX in the DSHP (°C).	$\dot{W}_{DHW,pump}$	Circulation pump energy consumption, DHW loop (W).
$T_{d,out}$	Outlet temperature of the refrigerant to the DHW HX in the DSHP (°C).	\dot{W}_{DSHP}	DSHP energy consumption (W).
T_e	Dew point evaporation temperature (°C).	\dot{W}_{fan}	Fan energy consumption (W).
T_{ei}	Inlet temperature of the secondary fluid to the evaporator (°C or K).	$\dot{W}_{ground,pump}$	Circulation pump energy consumption, ground loop (W).
T_{eo}	Outlet temperature of the secondary fluid to the evaporator (°C or K).	\dot{W}_{HP}	HP energy consumption (W).
$T_{g,in}$	Inlet temperature of the refrigerant to the Ground HX in the DSHP (°C).	\dot{W}_{is}	Compressor isentropic power (W).
$T_{g,out}$	Outlet temperature of the refrigerant to the Ground HX in the DSHP (°C).	\dot{W}_{par}	Parasitic consumption (W).
$T_{u,in}$	(Inlet temperature of the refrigerant to the User HX in the DSHP (°C).	w_{sat}	Humidity ratio at saturated conditions (kg _{water} /kg _{dry air}).
$T_{u,out}$	Outlet temperature of the refrigerant to the User HX in the DSHP (°C).	$\dot{W}_{user,pump}$	Circulation pump energy consumption, user loop (W).
\dot{V}	Volume flow rate (m ³ /s).	Δh_{is}	Enthalpy difference of an isentropic compression (kJ/kg).
\dot{V}_{DHW}	Secondary volume flow rate, DHW loop (m ³ /s).	Δh_{23}	Enthalpy difference across the condenser (kJ/kg).
\dot{V}_{ground}	Secondary volume flow rate, ground loop (m ³ /s).	Δh_{13}	Enthalpy difference across the evaporator (kJ/kg).
v	Velocity (m/s).	ΔP	Pressure drop (Pa).
V_s	Compressor swept volume (m ³).	ΔP_{DHW}	Secondary fluid pressure drop, DHW loop (Pa).
		ΔP_{ground}	Secondary fluid pressure drop, ground loop (Pa).
		ΔP_{user}	Secondary fluid pressure drop, user loop (Pa).
		Δw	$w_{ai} - w_{sat}$ (kg _{water} /kg _{dry air}).
		$\Delta w'$	$\max[w_{ai} - w_{sat}, 0]$ (kg _{water} /kg _{dry air}).
		δT_e	Difference temperature between primary and secondary

	loop in the evaporator (temperature approach) (K).	μ	Dynamic viscosity (Pa·s).
		ξ	Compressor heat losses (%).
η_c	Compressor efficiency (%).	ρ_s	Density (kg/m ³).
η_p	Circulation pump electric motor efficiency (%).	ρ_s	Refrigerant density at compressor suction conditions (kg/m ³).
η_v	Volumetric efficiency (%).		

Acronym Description

AHRI	Air-Conditioning, Heating and Refrigeration Institute.	GHGs	Greenhouse gases.
AIC	Akaike Information Criterion.	GSHP	Ground Source Heat Pump.
ASHP	Air Source Heat Pump.	GUI	Graphical User Interface.
BIC	Bayesian Information Criterion.	GWP	Global Warming Potential.
BPHE	Brazed Plate Heat Exchanger.	HBP	High Back Pressure.
ccp	Correlation coefficient of Pearson.	HD	Hexagonal Design.
CCD	Central Composite Design.	HFC	Hydrofluorocarbons.
CD	Clustering Design.	HFO	Hydrofluoro-olefin.
COP	Coefficient of Performance. \dot{Q}_c / \dot{W}_c	HGLS	Hyper-Graeco-Latin-Square design.
CO ₂	Carbon dioxide.	HP	Heat Pump.
CV _{RMSE}	Coefficient of Variation of the RMSE. $RMSE / mean(y)$ (%).	HVAC	Heating, Ventilating and Air-Conditioning.
DHW	Domestic Hot Water.	HX	Heat exchanger.
DHWA	Domestic Hot Water Air operating mode (DSHP).	IVW	Inverse-Variance Weighting.
DHWG	Domestic Hot Water Ground operating mode (DSHP).	LBP	Low Back Pressure.
DHWU	Domestic Hot Water User operating mode (DSHP).	LRL	Lower Range Limit.
DoE	Design of Experiments.	MBP	Medium Back Pressure.
DSHP	Dual Source Heat Pump.	MRE	Maximum Relative Error (%).
EEV	Electronic Expansion Valve.	OD	Optimal Design.
EIR	Energy Input to cooling output Ratio. Inverse of COP.	OLS	Ordinary Least Squares.
EU	European Union.	$pccp$	Partial correlation coefficient of Pearson.
GEOTeCH	Geothermal Technology for economic Cooling and Heating.	PD	Polygonal Design.
		PHE	Plate Heat Exchanger.
		R&D	Research and Development.
		RH	Relative Humidity (%).
		PID	Proportional Integral Derivative controller.
		RMSE	Root Mean Square Error (W, kg/h).

RSM	Response Surface Methodology.	SG	Summer Ground operating mode (DSHP).
RTD	Resistance Temperature Detector.	TSM	Taylor Series Method.
RTPFHx	Round Tube Plate Fin Heat exchanger.	URL	Upper Range Limit.
SA	Summer Air operating mode (DSHP).	WA	Winter Air operating mode (DSHP).
SCD	Small Composite Design.	WG	Winter Ground operating mode (DSHP).
		WSHP	Water Source Heat Pump.

Part I

Main document

1

Introduction

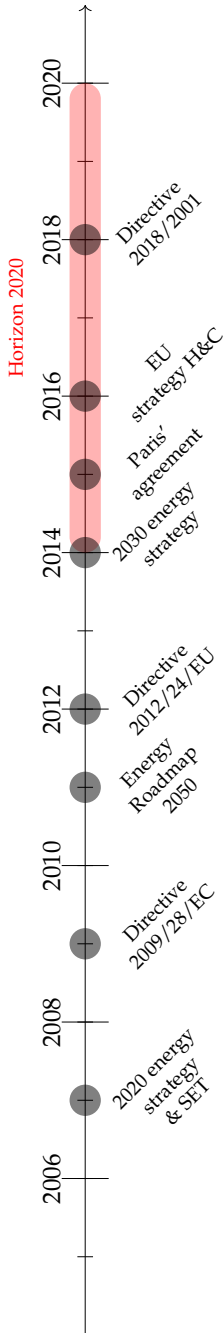
CONTENTS

1.1	Motivation	1
1.1.1	Institute for Energy Engineering (IUIIE). Thermal area projects	3
1.2	Background and state of the art	4
1.2.1	Modelling and simulation	4
1.2.2	Computerized models	6
1.2.3	Conceptual models	8
1.2.4	Heat pumps. Fundamentals and classification	11
1.2.5	Heat pump modelling	13
1.3	Aims of the study	17
1.4	Methodology	20
1.5	Structure of the thesis	23

1.1 Motivation

Industrialization has always seemed to be the key to wealth and better living. The rise of the telecommunications and transport sector, the evolution towards a globalized society or improvements to production in many fields are just some of the advantages and consequences of technological innovations. However, the rapid evolution of society over the last century has also been accompanied by other disadvantages. Mainly, the current extreme climate changes.

At present, the adverse effects of CO₂ have motivated a reduction in dependence on fossil fuels. The emission of greenhouse gases (GHGs) and other pollutants, together with the fossil fuel shortages (Sürmeli et al., 2007), are promoting the use of other alternative power sources.



Industrialization not only involves technological innovations, it also implies economic and social transformations. Nowadays, many countries, especially those in Europe, direct their policies with the objective of mitigating the current global warming. Therefore, in the last decade, the European Commission has published a set of regulations with the current environmental roadmap.

For example, in March 2007 it introduced *Europe's 2020 energy strategy* with the following guidelines:

- A reduction of at least 20% in GHGs by 2020, from a 1990 baseline - rising to 30% if the conditions become favourable.
- A 20% share of renewable energies in the European Union (EU) energy consumption by 2020.

In the same year, it also published the *Strategic Energy Technology Plan*, which aimed to coordinate funding efforts in technology research in order to accelerate the transition to low-carbon energy systems. In line with this, in April 2009, it also adopted the *Renewable Energy Directive 2009/28/EC*, publishing its revision in December 2018 (*Directive 2018/2001*), with the main objective of promoting renewable energies.

Subsequently, these measures have been backed up in order to limit the rising global temperatures to "well below 2°C, aiming for 1.5°C" by 2100 (United Nations, 2015), with the following more ambitious efficiency targets:

1. *Europe's 2030 energy strategy*:

- 40% reduction in GHGs from a 1990 baseline.
- 27% share of renewable energies in EU energy consumption by 2030.
- 27% improvement in energy efficiency.

2. *Energy Roadmap 2050*:

- 80-95% reduction in GHGs from a 1990 baseline.

In parallel to this politic framework, the European Commission has supported research, innovation and market uptake projects that help to promote clean energies. The current *Horizon 2020 programme*, available for over 7 years (2014-2020) with nearly €80 billion of funding support, is helping to couple research and innovation with an emphasis on “*excellent science*”, “*industrial leadership*” and tackling “*societal challenges*”. Such “*societal challenges*” include, amongst others, decarbonization of the global energy supply.

In this regard, the *EU Strategy on Heating and Cooling* sets an estimation that the heating and cooling sector uses 50% of the total energy consumed in Europe. Moreover, this document reported that around half of the buildings installed before 1992 in Europe are provided with heat by fossil fuel boilers with an efficiency of 60% or lower. Regarding this concern, this *EU Strategy on Heating and Cooling*, as well as the previous *Directive 2012/24/EU* on energy efficiency, enacted to promote residential energy consumption from renewable energy sources, aroused considerable interest in Heat Pumps (HPs) as an alternative option for space heating in buildings.

Concerning Heat Pump units, Ground Source Heat Pump systems (GSHPs) are one of the least carbon-intensive Heating, Ventilating and Air-Conditioning (HVAC) technologies (Bayer et al., 2012; Rees, 2016). In addition, compared to Air Source Heat Pumps (ASHPs), GSHPs present more stable source temperatures. This results in increased efficiency, with the only negative aspect being their installation cost. Over the past few years, manufacturers have been improving the design of these systems and developing new concept units such as Dual Source Heat Pumps (DSHPs) with the corresponding increase in system complexity.

In this framework, with the current increase in the complexity of HPs in order to improve their efficiency and cost savings, the design stage has taken on more importance for the industry. This has given rise to a need for additional simulation tools that offer direct feedback to manufacturers during the design process.

Therefore, due to the growing importance and the current role of HP systems in the heating and cooling sector, it seems a beneficial area of research to study different modelling methodologies in order to characterize their performance and behavior. The main objective will be to offer highly accurate models which are able to support researchers and manufacturers.

1.1.1 Institute for Energy Engineering (IUIIE). Thermal area projects

The IUIIE is a multidisciplinary research centre with more than 20 years of research activity, located at the Polytechnic University of Valencia (UPV). Its main objectives are to improve current R&D solutions related to the energy sector.

The present PhD thesis has been conducted within the thermal area projects group. This research group has extensive experience in the design and modelling of thermal systems. Some of its main activities are:

- Development of computer simulation tools for the characterization of refrigeration equipment and their components based on the vapour compression cycle.
- Studies for the use of new refrigerants in commercial and prototype units.
- The analysis and study of the heat and mass transfer processes involved in this type of system.

As a result of its activities over the last few years, the thermal area projects group has produced several PhD theses and contributions in international conferences and journals. For further information, see https://iie.webs.upv.es/publicacion_category/revistas/.

1.2 Background and state of the art

This section will try to offer a general overview of modelling and simulation in the field of engineering. The specific focus of this PhD thesis is heat pump modelling. Therefore, the general review of the state of the art will take into account the simulation strategies for the characterization of HPs and their components.

1.2.1 Modelling and simulation

Nowadays, simulation tools are increasingly being used by manufacturers in the industry with the aim of improving the quality of their products. In addition, the need to stand out from the competition has led the companies to invest more financial resources in the development of their own simulation software.

Better design tools will lead to a decrease in development costs and simplify the design phase of “*new products*” or the improvement of “*catalogue products*”. In the field of engineering, the increasing complexity of designs for the machines that surround us in our daily life has made the use of these tools indispensable.

The main purpose of these simulation tools is clear: Obtaining an accurate representation of the systems or components modelled, and characterizing their behavior. The list below enumerates the basic requirements that must always be met in order to obtain a good model.

1. Low computational time.
2. Straightforward, easy implementation.
3. Possibility to obtain simulation results for all the working maps for the system or component modelled.

There are some general terms linked to the simulation process. The terms “*model*”, “*modelling*” and “*simulation*” are used in a wide range of disciplines. Consequently, these terms have a range of meanings that are both context-specific and discipline-specific, (Knepell and Arangno, 1993) and (Neelamkavil, 1987). According to AIAA (1998), we can define these terms as:

Model: “A representation of a physical system or process intended to enhance our ability to understand, predict, or control its behavior”.

Modelling: “The process of construction or modification of a model”.

Simulation: “The exercise or use of a model. (That is, a model is used in a simulation)”.

AIAA G-077-1998(2002)
American Institute of Aeronautics and Astronautics

Figure 1.1 on next page shows the basic phases and processes within simulation and modelling adopted by the Society for Computer Simulation.

In this figure, it is possible to identify two types of models: *conceptual models* and *computerized models*.

The first of these two typologies is composed of all the information, mathematical modelling data and mathematical equations that characterize the physical system or its components. It is produced by analysis and observations from reality.

The second one is the *computerized model*. Basically, this typology represents the *conceptual model* developed as a computer program, in other words, its virtualization.

This virtual representation allows designers to check whether design specifications are met by using “**virtual tests**” rather than “**physical experiments**”.

Thanks to virtualization, researchers can obtain direct feedback on design processes which, likewise, allows for a more comprehensive exploration of design alternatives and a better performing final design.

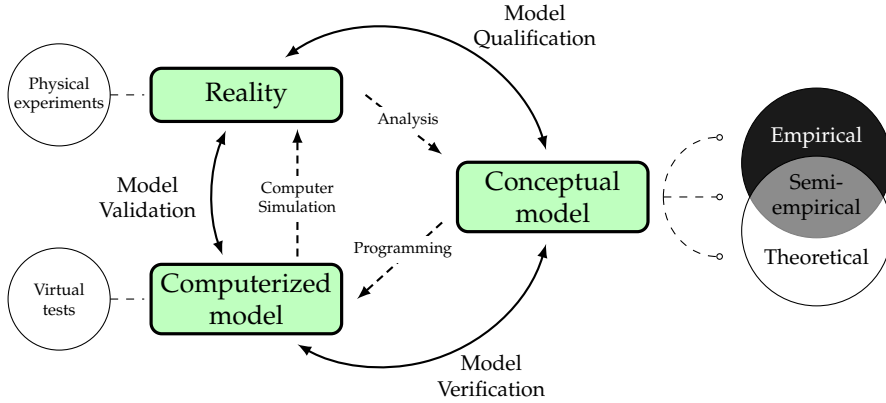


Figure 1.1: Phases of Modelling and Simulation

Therefore, a *virtual test* has the following advantages over a *physical experiment*:

1. It reduces the development costs for the systems or components modelled. The use of a computer is cheaper than investing in a test rig with all the necessary measurement equipment, especially now, considering how powerful the modern personal computer is, and how cheap it is to acquire.
2. It allows prototypes be adapted to the current regulations using virtualization at the design stage. The process of upgrading a model with new components is easy and does not increase the development costs.
3. It makes it possible for a large amount of simulation data to be obtained. *Physical experiments* are limited to compact test matrices due to the time required to reach steady conditions, as well as the test duration. By contrast, models are able to run large working maps with low simulation times.

Next, we will address in greater detail both model typologies noted above: “*Computerized*” and “*conceptual*” models.

1.2.2 Computerized models

Sinha et al. (2001) present an interesting review of the *computerized model* paradigms available that researchers may adopt to develop highly accurate models (Figure 1.2).

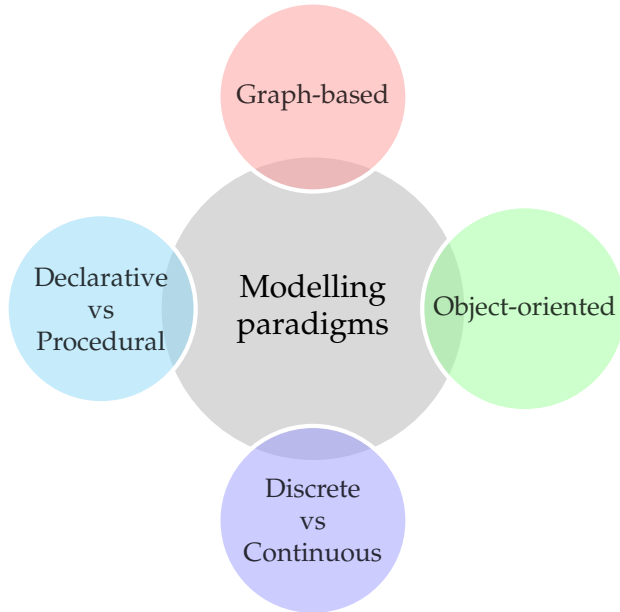


Figure 1.2: Modelling paradigms

A first possibility is the use of “*graph-based*” models. This modelling paradigm represents interconnected systems in many different modelling domains. Tools like MATLAB/Simulink, Modelica or TRNSYS are examples of this type of simulation environment.

Another possibility is to opt for “*language-based*” modelling. Currently, there are many simulation languages that researchers can use, but the two main approaches to consider are the: “*Declarative*” or “*Procedural*” programming languages.

On the one hand, “*Procedural*” languages define models through assignments describing their control flow. These assignments express a dependent variable as a function of independent variables, and must be evaluated in the order defined by the user. This is the classical programming approach which places the emphasis on “*how*” the model obtains the results (the set of procedures and functions defined in the model). Examples of this programming language are Fortran, C, and Pascal.

On the other hand, “*Declarative*” or “*equation-based*” languages do not impose a fixed causality on the model. In these languages, the model is defined by a set of equations that establishes relationships between states, their derivatives, and time.

It has the advantage that it does not define the mathematical causality of equations, so that the same model can be used for any causality imposed by other system components. This allows the researcher to focus on the logic of the problem rather than on a detailed algorithmic implementation of the simulation model. Languages like Modelica or EES use this modelling paradigm.

The third classification is related to the changes to the state variables over time with two possible approaches: “*Discrete*” and “*Continuous*” modelling. Many physical phenomena, such as rigid body motion, flow of electric currents, fluid flow, or heat flow, evolve as continuous functions of time and are therefore best modelled by a set of differential algebraic equations (Ascher and Petzold, 1998; Cellier and Greifeneder, 1991). Physical events and digital components, on the other hand, generate outputs at discrete points in time and space; they are best modelled using discrete variables or impulse functions (Zeigler et al., 2000; Glynn, 1989; Koenig et al., 1967). A good overview of the principles and industrial applications of discrete-event simulation can be found in Zeigler et al. (2000) and Banks (1998).

Finally, the last possibility is “*Object-oriented*” modelling with the important benefits of encapsulation. The code is structured using public objects with accessible properties and methods. This approach lets researchers reuse code, optimizing the model construction process and obtaining more compact simulation codes. The advantage of encapsulation is that a system can be modelled by composing and connecting the interfaces of its sub-systems, independently of future implementations and changes (Diaz-Calderon et al., 2000; Zeigler et al., 1991). A clear example of this type of language is Python, whose philosophy emphasizes the readability of the code. Currently, this high-level programming language is becoming more popular amongst researchers for exploratory data analysis.

All the modelling paradigms noted above are useful and allow researchers to develop really complex models. The choice of one over another will depend on the researchers preferences and the characteristics of the system being modelled.

1.2.3 Conceptual models

Now, setting aside the typology of *computerized models* and focusing on *conceptual models*, the first thing to remember is the general definition of model introduced in Subsection 1.2.1 on page 5. Usually, this definition remains too general. There are different levels of detail that we can consider in a model construction, and these levels of detail will depend on the available information about the system and the model purpose.

For example, if we take the refrigeration compressor as a case study, we will need more or less input information depending on the level of detail considered, according to Rasmussen and Jakobsen (2000).

Considering that this previous level of knowledge may be used to develop a classification, the Figure 1.3 presents different conceptual model typologies.

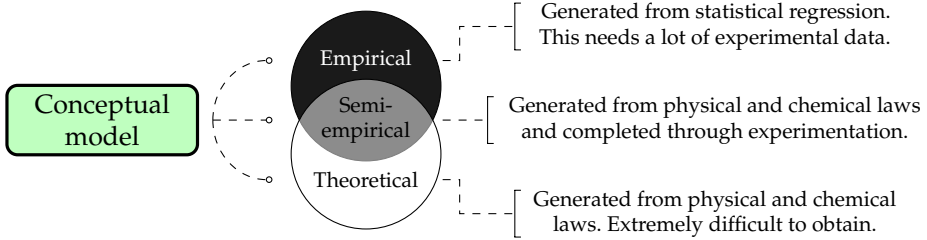


Figure 1.3: Conceptual model classification

The first possibility is to construct a simple model for the characterization of compressor performance. This type of model represents numerical relationships between “*independent variables*” (the control variables in the system) and “*response variables*” (the objective variables that we want to characterize). Typically, this category is referred to as a “*black-box*” or “*empirical*” model and it is constructed by regression analysis of the common data provided by manufacturers. In the field of compressors these data are:

- Condensation temperature (T_c) and evaporation temperature (T_e), as *independent variables*.
- Mass flow rate (\dot{m}_{ref}) and compressor energy consumption (\dot{W}_c), as *response variables*.

Therefore, *black-box* models do not directly describe any physical phenomena that take place inside the compressor. However, they will provide simple correlations able to describe the compressor performance over the experimental domain delimited by the test results used for the regression adjustment.

At the other extreme, there is the “*white-box*” or “*theoretical*” model. This typology requires the highest level of knowledge of the compressor’s boundary conditions and geometric measurements (compressor displacement, geometric parameters of its internal components, ambient temperature, etc.).

Once the above information is known, the compressor is divided into its individual parts, as control volumes, that are coupled together in terms of flows of energy and mass. Therefore in a *theoretical* model, all processes are only described using fundamental equations (conservation of mass, energy and momentum, Navier-Stokes equations, etc.). Then these differential equations are applied through the different fixed control volumes. However, as shown by Rasmussen and Jakobsen (2000):

“A true “White-box” model of a compressor may probably never be developed – the knowledge needed for developing such a model being too extensive to gather and organize.”

Purdue University conference, paper 1429
Rasmussen and Jakobsen (2000)

According to this, when the physical system modelled involves a high degree of complexity, like the compression process in refrigeration compressors, it is necessary to simplify and abstract the problem.

This leads us to the third and final conceptual model typology: The “grey-box” or “Semi-empirical” model. As a combination of the previous two typologies noted above, the “grey-box” model may also contain fundamental equations together with numerical relations. This simplifies the most complex processes and excludes input parameters which are difficult to collect. Of course, this third typology can be divided into different groups according to:

- The number of simplifying hypotheses.

- The discretization employed in the compressor:
 - phenomena-oriented models.
 - construction-oriented models.

Thus, the phenomena-oriented models are focused on general phenomena fixing the control volumes in the compression chamber. Typically, the compression chamber is divided into three control volumes (pre-compression, compression and post-compression). Then, as the number of control volumes is increased, the model characterizes the specific components of the compressor. Under these conditions the model becomes a construction-oriented model.

Finally, to sum up the discussion above, Table 1.1 summarizes the main advantages and disadvantages of these different typologies of conceptual model.

Table 1.1: Conceptual models: advantages/disadvantages

Items	Advantages	Disadvantages
Empirical	-Low computational time -Useful for programming control systems -Simplicity	- Possible error prediction in non-tested domains
Semi-empirical	-It is able to model the most complex processes -It provides a general idea about how the system works	-It is not able to extrapolate when some internal inputs are changed
Theoretical	-Useful in the design of systems -It does not need empirical data -It is able to obtain magnitudes which are difficult to measure	-Complicated to obtain -High computational time -It requires a lot of input parameters (Maybe difficult to obtain)

1.2.4 Heat pumps. Fundamentals and classification

Nowadays, the use of heat pumps (or refrigeration equipment) is widespread in heating and air-conditioning applications for buildings.

The purpose of a heat pump is to extract heat from a lower temperature source and transfer it to a higher temperature sink at a “*useful*” level. According to this working principle, heat pumps and refrigeration equipment are basically the same equipment with the same components. The only difference is the desired production of heating or cooling that the equipment provides to the user.

Although various forms of thermodynamic cycle can be used to transfer heat between source and sink, the predominant form is based on the vapour compression cycle. Of course, the heat transfer from a lower temperature source to a higher temperature sink must be done under the constraints of the second law of thermodynamics. Therefore, the addition of work (or, more generally, exergy) to the system is required. To accomplish this, the unit is provided with the components shown in Figure 1.5, and Figure 1.4 on next page presents the state of the refrigerant throughout the cycle.

These main components are:

1. Compressor.
2. Heat exchangers.
 - (a) Condenser.
 - (b) Evaporator.
3. Expansion valve.

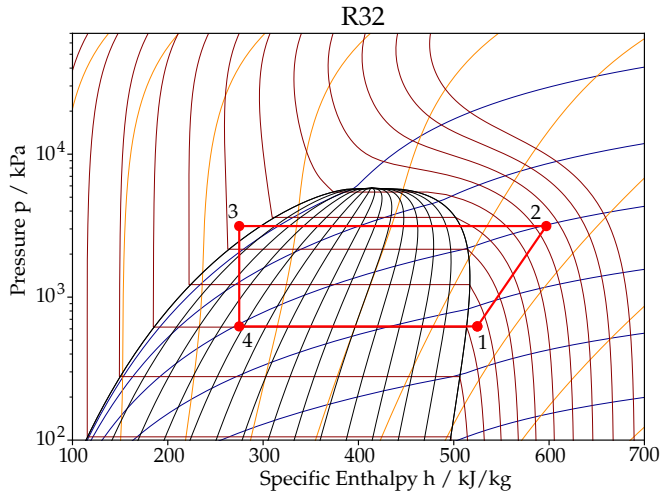


Figure 1.4: P-h diagram (R32 - reference state IIR)

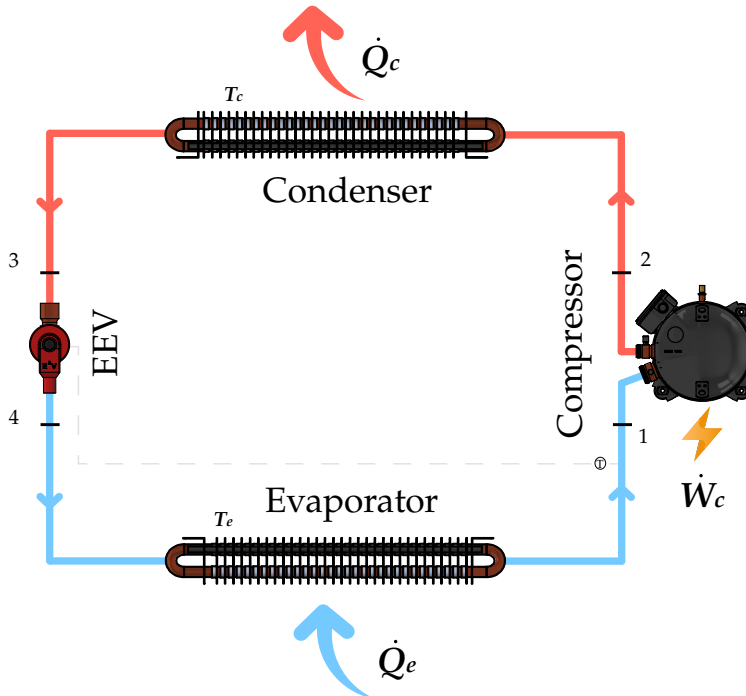


Figure 1.5: Vapour compression cycle

In this type of cycle, the compressor pumps the refrigerant and maintains two appropriate levels of pressure, P_e and P_c . At the lower pressure side, the liquid refrigerant is vaporized, absorbing heat, and at the higher pressure side, the vapour refrigerant is condensed, discharging heat. These two heat transfer processes are quantified by the condenser and evaporator capacities (\dot{Q}_c and \dot{Q}_e). Of course, the main reason for the interest in using heat pumps is that they take less work compared to the heating and cooling effect. This work is provided to the compressor (\dot{W}_c), usually as an electrical power supply.

The three variables named above (\dot{Q}_c , \dot{Q}_e and \dot{W}_c) are known as “*performance*” in heat pump applications. The study of how to obtain simple and accurate empirical models for their characterization will be the main objective of the present PhD thesis.

As concerns heat pump technology, it is possible to develop a classification according to the type of source used.

HP technologies:

1. **Air Source Heat Pump** (ASHP) \Rightarrow Secondary fluid: Air.
2. **Ground/Water Source Heat Pump** (GSHP/WSHP) \Rightarrow Secondary fluid: Brine or water.

The heat pump prototype tested in the current work is a Dual Source Heat Pump allowing the equipment to work as an ASHP or GSHP. It also includes the ability to reverse the cycle (air source and ground source refrigeration equipment) including an additional operating mode to provide domestic hot water production when it supplies chilled water (water source heat pump¹). Therefore, this PhD dissertation will study how to characterize the main technologies available in heat pumps and refrigeration equipment field (air/ground/water source units).

1.2.5 Heat pump modelling

The modelling of heat pumps and refrigeration equipment can be beneficial when analyzing more complex systems where such units are integrated. In this sense, characteristics of a desirable model are simplicity and dependence on parameters that can easily define an average user and be monitored in real installations. Hamilton and Miller (1990) presented a classification for air conditioning equipment models, similar to that already shown in a previous section for compressors (Rasmussen and Jakobsen, 2000), again differentiating between “*equation-fit*” models (empirical models) and “*deterministic*” models (theoretical models).

¹These units are also included in solar assisted installations.

Therefore, heat pump models also can be generally classified in terms of the degree of complexity and empiricism. Some of them can provide simple correlations as black-box models to directly predict heat pump performance (\dot{Q}_c , \dot{Q}_e , \dot{W}_c) in steady-state conditions. Other models can develop a more detailed definition, modelling its components. In past years, some detailed simulation tools have assisted heat pump manufacturers. Some examples of these simulation tools are the ORNL Heat Pump Design Model (Fischer, S.K. Rice, 1983), the CYCLE_D-HX software (Brown et al., 2021), the VapCyc and Coil Designer software (Richardson et al., 2002; Richardson, 2006; Jiang et al., 2006), or the simulation tool IMST-ART (Corberán et al., 2002; Thermal Area IUIIE, 2019) developed by the IUIIE, where the heat pump unit is implemented by defining its individual components (commonly with the data extracted from the manufacturer's catalog). Then, some authors developed other types of heat pump model with a greater or lesser degree of complexity, e.g., (Stoecker and Jones, 1982; Dabiri, 1982; Domanski and Didion, 1985; Bourdouxhe et al., 1998; Jin and Spitler, 2002, 2003; Lemort and Bertagnolio, 2010; Dos Santos et al., 2022). Jin (2002) and also Madani (2012) present a good review of this kind of thermodynamics-based model, which also includes some equation-fit models. Another good review of modelling methods in HVAC applications is provided by Afram and Janabi-Sharifi (2014).

We will now focus on this second type of model, the equation-fit model. These are commonly developed as black-box models by regression analysis and experimental data. The main advantages of these typologies are a higher prediction accuracy for the adjusted experimental domain and a very low computational time. Fortunately, the unit performance is continuous with only smooth trends, so polynomial models are usually efficient functionals to describe them. In this sense, compressors, which are the basis for the heat pump performance, are very well studied in such types of empirical models, and it is well known that AHRI polynomials (AHRI 540, 2020) can characterize their performance with high accuracy. Compressor performance is characterized by selecting condensation and evaporation temperatures as independent variables, which can be suitable parameters if the main objective is to develop a compressor model that can be implemented as a model component. But, to develop a polynomial model for heat pump performance, the main problem is that these temperatures are internal parameters and therefore unknown (commonly, such temperatures are only monitored in research). However, evaporation and condensation temperatures are dependent on boundary conditions at the evaporator and condenser side. Therefore, polynomials based on the external parameters, i.e., source/sink temperatures, should be able to characterize the unit performance.

Allen and Hamilton (1983) already presented the idea of employing second-order polynomials with the evaporator and condenser outlet temperatures (secondary fluid) to predict the full load performance (evaporator capacity and en-

ergy consumption of chillers). For example, the evaporator capacity was defined by adjusting the following polynomial equation:

$$\dot{Q}_e = a_0 + a_1 T_{eo} + a_2 T_{co} + a_3 T_{eo} T_{co} + a_4 T_{eo}^2 + a_5 T_{co}^2 \quad (1.1)$$

And in a similar way, the energy consumption:

$$\dot{W}_c = b_0 + b_1 T_{eo} + b_2 T_{co} + b_3 T_{eo} T_{co} + b_4 T_{eo}^2 + b_5 T_{co}^2 \quad (1.2)$$

Thus, this simple kind of model can provide the ability to include the heat pump unit as a simple component when a more complex system layout must be implemented. As reported by Afjei and Dott (2011), such “map-based” models are most widespread in dynamic simulation programs like TRNSYS, ESP-r, Energy-Plus, IDA ICE and MATLAB/Simulink.

Similarly to Allen’s model, other authors have published other types of polynomial models. For example, Tabatabaei et al. (2016) characterize the performance in air source heat pumps as a function of air temperature. Afjei et al. (1997) provided similar functions to Hamilton implemented as TRNSYS type, but for heat pump applications (prediction of condenser capacity and energy consumption). This same methodology is employed inside EnergyPlus², for the evaporator capacity, while for the consumption, a polynomial for the Energy Input to cooling output Ratio (EIR), i.e., the inverse of the COP, was employed instead of the energy consumption. The output of these correlations is multiplied by the reference performance to give the full-load cooling capacity or energy consumption at specific temperature operating conditions (i.e., at temperatures different from the reference temperatures):

$$\frac{\dot{Q}_e}{\dot{Q}_{e,reference}} = a_0 + a_1 T_{eo} + a_2 T_{ci} + a_3 T_{eo} T_{ci} + a_4 T_{eo}^2 + a_5 T_{ci}^2 \quad (1.3)$$

$$\frac{EIR}{EIR_{reference}} = b_0 + b_1 T_{eo} + b_2 T_{co} + b_3 T_{eo} T_{co} + b_4 T_{eo}^2 + b_5 T_{co}^2 \quad (1.4)$$

However, the main problem with these kind of models is that they only take into account the variation of the inlet (or outlet) temperatures of the secondary fluid to the evaporator and the condenser. So, the space of the independent variables domain is only 2D. As is described above, the usual procedure used by these authors was to characterize the performance at full load and then apply a correction for part load operation.

Unfortunately, new refrigeration and heat pump units are currently incorporating variable speed compressors and also variable speed circulation pumps and fans. Therefore, the characterization of new and future equipment with so many

²EnergyPlus (See Electric Chiller Model Based on Condenser Entering Temperature).

independent variables must include more than two independent variables. In this sense, only a few authors have included improvements to the previous models. Ruschenburg et al. (2014), according to results in Pärish et al. (2014), updated Afjei's model considering the mass flow change in sink³. So, Ruschenburg also defined second-order polynomials selecting the evaporator inlet temperature and substituting the condenser outlet by the condenser mean temperature to predict the condenser capacity and COP in heat pump applications:

$$\dot{Q}_c = a_0 + a_1 T_{eo} + a_2 T_{c,mean} + a_3 T_{eo} T_{c,mean} + a_4 T_{eo}^2 + a_5 T_{c,mean}^2 \quad (1.5)$$

$$COP = b_0 + b_1 T_{eo} + b_2 T_{c,mean} + b_3 T_{eo} T_{c,mean} + b_4 T_{eo}^2 + b_5 T_{c,mean}^2 \quad (1.6)$$

On the other hand, the studies from Yuan and Grabon (2011) and Verhelst et al. (2012) provide correlations including compressor speed as an additional variable. In Verhelst's case, the functionals obtained for air source heat pumps were second-order polynomials as a function of condenser outlet temperature, air temperature and compressor speed:

$$\dot{Q}_c = a_0 + a_1 T_a + a_2 T_{co} + a_3 f_c + a_4 T_a T_{co} + a_5 f_c T_a + a_6 f_c T_{co} + a_7 T_a^2 + a_8 T_{co}^2 + a_9 f_c^2 \quad (1.7)$$

$$\dot{W}_c = b_0 + b_1 T_a + b_2 T_{co} + b_3 f_c + b_4 T_a T_{co} + b_5 f_c T_a + b_6 f_c T_{co} + b_7 T_a^2 + b_8 T_{co}^2 + b_9 f_c^2 \quad (1.8)$$

As we can see, the current models in the literature include from 1 to 3 independent variables. Unfortunately, this number of parameters is still insufficient because current units with variable speed components have a 5D domain (compressor speed, sink/source temperatures, and sink/source mass flow rate). Furthermore, another essential aspect not generally taken into consideration is related to efficient experimental test acquisition. Domains with a large number of variables represents a significant challenge⁴ when defining the experimental samples to be tested. Thus, the minimum number of test points necessary and their location in the experimental domain are issues not addressed by previous studies. Such issues are particularly relevant if we want proper model adjustment and accuracy, including non-excessive experimental costs.

³The mass flow on the sink side is much more volatile than on the source side in typical residential applications.

⁴For example, a full factorial test in a 5D domain and 5 levels, requires a total of 3125 tests.

Finally, to conclude this section, it is important to remark on the importance of using simple and compact models in heat pump applications. These can be implemented in a simple way in more complex systems allowing, for example, the optimization of these or implementing improvements in their control (Madani et al., 2011a,b; Cazorla-Marín et al., 2018a,b; Cazorla Marín, 2019). Another interesting challenge can also be the use of these models for fault detection (Cho et al., 2014; Kim et al., 2006, 2009, 2010), detecting possible deviations in the machine's behavior compared to that which is expected.

1.3 Aims of the study

The present work is part of the 4-year *Geothermal Technology for Economic Cooling and Heating* (GEOTeCH) project. It is funded by the European Commission, within the *Horizon 2020 programme*, for the implementation of cost-effective geothermal systems. The project consortium is formed of several industrial and research partners from different European countries, presented in Figure 1.6.



Figure 1.6: GEOTeCH consortium

Its Work Packages include the design and testing of an innovative prototype of DSHP. This type of unit is able to work as a GSHP and ASHP, whilst also providing Domestic Hot Water (DHW) and working as a reversible unit. Therefore, due to the great complexity of this unit, several challenges were addressed in this project.

One of them was to determine the best control strategy, and for that, we noticed the importance of using simple and compact models to characterize the DSHP performance. Due to the dual typology of this unit, it was necessary to perform a dynamic model in TRNSYS (Cazorla Marín, 2019), implementing a global model of the system to determine an efficient control strategy, i.e., determine when the unit should work as a geothermal or aerothermal heat pump.

For this purpose, precise correlations are required characterizing the heat pump as individual equipment depending on the external variables of the unit. Such external variables are those commonly available when developing a global model of the system and allow the adjustment of heat pump correlations from the manufacturer's catalog data or experimental laboratory results. One of the main objectives of this PhD will be to characterize the DSHP as a single component.

Heat pump models as a single component are useful and necessary when modelling any system that includes these units as an integral part. Moreover, using polynomial models results in an easy integration in any dynamic simulation tool, for example, as a TRNSYS type. This PhD will select this approach, characterizing the DSHP as a single component with the simplicity of polynomial models. This brings us the opportunity to extend the applicability of this work. This type of model is easy to use by any potential user that requires to describe the behavior of a heat pump unit. Some examples of application could be studies focused on control management, techno-economic studies, or fault detection, which can benefit from an easy implementation of heat pump's behavior.

However, as already shown in Subsection 1.2.5, this topic—the development of heat pump polynomial models—is at present poorly developed. It comprises a limited number of publications by some authors considering very simple units with a limited number of boundary variables. As previously mentioned, current units include a large number of variable speed components and the number of independent variables that determine the unit performance has increased. Another challenge is the limited experimental information available in the literature. The development of accurate polynomial models requires a huge dataset of experimental results. They allow the unit performance to be characterized over the entire working map. In this sense, another objective of this PhD will be to analyze statistical methodologies capable of reducing the required experimental information, i.e., select the most appropriate location of the experimental runs and obtain as much experimental information as possible. Once this analysis selects the most appropriate methodology, the following step will be to generate

a large amount of experimental information. Due to the hybrid typology of the DSHP and the ability to reverse the cycle, we can generate experimental results for different HP and refrigeration equipment technologies. All of this by testing the same unit. Therefore, valuable experimental information in this research field will be generated.

Finally, another objective to include in this work will be to focus on the modelling of compressors. In these units, the compressor is the most complicated component to characterize, and researchers commonly require it when developing detailed heat pump models by modelling the individual components. This field is much more developed, and the literature has a large volume of experimental information to perform the analysis. In this sense, the objectives will be the same as those previously described for the modelling of heat pumps, i.e., determine the most suitable polynomial model to characterize compressors and establish a methodology to fix the minimum size and location of the experimental points for the adjustment. This part will apply all the previous knowledge acquired at the DSHP characterization stage. In this sense, it will allow us to provide missing information not available in the current standard for compressor characterization. Unfortunately, no indications are given on how to define the experimental matrices covering the entire working map and required to adjust the polynomial models. Moreover, other relevant issues will also be analyzed, such as if the models included in the standard are adequate or how to extrapolate to other suction conditions.

To conclude this section, this item list shows a brief summary enumerating the abovementioned objectives:

1. Characterize the performance in GSHPs and ASHPs taking the external variables only into account as available information. This will allow response models to be obtained for the performance with an experimental adjustment that depends on the information provided by manufacturers from their catalogue products.
2. Obtain the individual characterization of HP components, specifically that of the most important element, the compressor. Similar to the previous point, simple compressor modelling can help to develop detailed HP models where it is necessary to include several submodels for its components.
3. The several response models developed will be compact and easy to program. This will ensure the HP equipment is easy to implement in global models of the system, regardless of the programming environment or model paradigm selected. The approach selected will use polynomial models.

4. Explore and fix the most adequate methodologies in order to perform the experimental test matrices. The main objective will be to define the exactly location of the experimental points and the minimum number required for the polynomial adjustment. After that, generate a huge dataset of experimental results for the available heat pump and refrigeration equipment technologies.
5. Adjustment of the final response models must consider the selection of the minimum experimental points with the maximum statistical inference. Therefore, the present work has to take into account methodologies in order to perform the experimental test matrices.

1.4 Methodology

In order to carry out the objectives above, it was necessary to have access to a reliable database⁵ on the performance of different HP technologies, as well as compressor calorimeter data.

The experimental data used in this PhD thesis was generated from the experimental campaign of the GEOTeCH project in the laboratories of the IUIIE. This dataset includes the performance data for the DSHP tested. In order to generate the experimental data, several methodologies for properly selecting the experimental matrices were also evaluated to select an adequate one in terms of experimental sample size and model accuracy.

In addition to the experimental data from the DSHP, this study was complemented with a comprehensive database of simulation results using the IMST-ART simulation software. The main objective was to make an in-depth analysis of the best polynomials to describe the unit performance in order to adjust, in a second step, to the GEOTeCH's experimental database. So, possible deviations between the IMST-ART model and the real performance of the unit were eliminated, resulting in accurate and easy-to-implement polynomial models.



On the other hand, this work also includes other datasets in order to conduct an in-depth analysis of the most important component of this equipment, the compressor. The main objective was to select also suitable polynomial models for compressor characterization as a single component. Compressor models are widely used in research and industry because this component significantly influences the unit performance. Therefore, map-based compressor models are

⁵For further information about the database, see Chapter 2.

helpful in a large number of applications. This part also includes methodologies for properly selecting the experimental matrices, with the main objective of setting the minimum number of tests and their location in the compressor envelope. These types of issues, although relevant, are not included in the current standard for compressor characterization (AHRI 540, 2020).

In view of the above, the methodology used for the development of the target models includes the following steps:

1. Collection of data from the bibliography.
2. Construction of a high precision experimental test rig for monitoring the DSHP.
3. Collection of experimental data for the DSHP.
4. Development and validation of a detailed model for the DSHP in the simulation software IMST-ART (Corberán et al., 2002; Thermal Area UIIE, 2019).
5. Construction of an extensive database of virtual tests generated with the IMST-ART model.
6. Study of the response surfaces using the virtual test database.
7. Construction of empirical models for the characterization of the DSHP performance using the virtual database.
8. Adjustment of the empirical models to the experimental data by using compact experimental samples.
9. Study of the response surfaces for the compressor performance using the calorimeter data collected from the bibliography.
10. Construction of empirical models for the characterization of the compressor performance.
11. Adjustment of the empirical compressor models to the experimental data by using compact experimental samples.




As concerns the means and software tools required to develop the present study, it was necessary to select a proper tool able to analyze a large amount of data. The main tool selected was the  software (R Core Team, 2022) and the IDE RStudio (RStudio Team, 2022).  is a procedural language-based programming software with a large number of extension packages with different statistical utilities. It allows a wide variety of statistical and graphical techniques to be employed such as linear and non-linear modelling, in addition to being an open source software.


The other software tools used in this PhD thesis were:

- IMST-ART (Corberán et al., 2002; Thermal Area IUIIE, 2019).
- Engineering Equation Solver (EES), (Klein, S.A., 2020).
- Microsoft Excel.
- Catalogue data from manufacturers.
- Python (Python Core Team, 2022).



In order to calculate the thermophysical properties for the refrigerants, two approaches were selected.

On the one hand, in the DSHP database (working with R32), the thermophysical properties were calculated with the software EES. This declarative programming language is able to obtain the thermophysical properties for the most common refrigerants and mixtures used in the industry. It also allows the corresponding propagation of error to be obtained for the variables calculated in the vapour compression cycle.

On the other hand, this option was dismissed for the calorimeter database due to the huge amount of experimental data obtained with *new mixtures*⁶. In this case, the approach selected was to provide  with the ability to calculate the thermophysical properties. The solution adopted was to use *Coolprop* and *Refprop 10* software working with  *Python*⁷. The  package *quantities*, an integration of the *units* and *errors* packages, was also used to obtain the propagation of error. For more details about these implementations see Appendix A.

Finally, this document has been created by the typesetting system \LaTeX (T_EXLive Team, 2022) and the  package for dynamic documents *knitr*⁸ (Xie, 2021).

⁶Not available in EES software.

⁷The section “*Software Information and Conventions*” includes the extension packages used in the  and  *Python* programming environments. Complete reference in “*R-Packages and software*” and “*Python-Packages and software*”.

⁸For further information about dynamic documents and reproducible research see the “*Note*” page.

1.5 Structure of the thesis

The main part of this document is structured in 5 chapters. In the current chapter (**Chapter 1**) has been introduced the motivation behind this research and a general review of modelling and simulation in heat pumps, including the aims of this study and the methodology used. To achieve these objectives the document has been structured in the following chapters:

- **Chapter 2:** This chapter presents a description of the DSHP tested and an overview of the database generated and collected in this work. This database includes performance data for the main HP technologies (ASHP and GSHP) and calorimeter data for scroll and reciprocating compressors, and it will be used to develop the models described in chapters 3 and 4.
- **Chapter 3:** This chapter explores the empirical model approach to characterize the performance of HPs. It describes a new methodology on how to develop the models and how to adjust them to the experimental data. This chapter also introduces Design Of Experiments (DoE), a statistical methodology to assist the experimental campaign. It is used to answer the questions: *“How many test points do we need?”* and *“Where should we locate the test points in the experimental domain?”*
- **Chapter 4:** This chapter focuses on the most important component of HPs, the compressor. The response surface for the main compressor technologies, reciprocating and scroll compressors, are analyzed. Then, this chapter presents the development of several simple empirical models to characterize the compressor performance and how to perform the experimental matrices necessary for their adjustment.
- **Chapter 5:** This final chapter sums up the main conclusions extracted from the results of this work and presents the future research.

2

Database

CONTENTS

2.1	Introduction	25
2.2	Dual Source Heat Pump	26
2.2.1	Operating conditions	27
2.2.2	Operating modes	28
2.2.3	System and components	31
2.2.4	Test rig	33
2.2.5	DSHP experimental results	37
2.2.6	DSHP simulation results	37
2.2.6.1	IMST-ART software	38
2.2.6.2	Detailed model in IMST-ART	39
2.2.6.3	Compressor sub-model and experimental validation for the IMST-ART model	40
2.3	Compressor performance data	45
2.4	Summary of datasets	47

2.1 Introduction

In order to perform an in-depth analysis of suitable model strategies able to characterize the performance in HPs, it is necessary to have access to a large volume of data. For this reason, the present chapter shows the database developed as part of the current PhD thesis. This database will allow the development of the final empirical models (Chapter 3) for the characterization of the DSHP and an additional analysis concerning modelling in refrigeration scroll and reciprocating compressors (Chapter 4).

Specifically, this work provides experimental data obtained from the test campaign performed on a DSHP. This has enabled us to extend the analysis to both main HP technologies, GSHPs and ASHPs. Furthermore, these experimental results have been complemented by a large amount of simulation results generated by a detailed model of the DSHP in the IMST-ART software (Corberán et al., 2002; Thermal Area IUIIE, 2019).

Additionally, the database developed includes calorimeter test data for scroll and reciprocating compressors, available in the current scientific literature.

The following sections show the working principles of the DSHP tested, the test bench used for the experimental campaign, the IMST-ART model developed and a summary of all the data included in the database.

2.2 Dual Source Heat Pump

The concept behind the innovative heat pump being tested is its ability to operate with a dual source: air and ground. This allows the use of the ground source to be minimized, in order to reduce the required size of the borehole heat exchangers with the corresponding cost savings. Furthermore, this concept is able to use the air source instead of the ground source whenever it is more convenient from an efficiency point of view, leading to a superior seasonal performance compared with current technology.

The DSHP tested in this PhD thesis is one of the three prototypes designed and tested inside the framework of the GEOTeCH project. The main characteristics of this first prototype are the following:

- Reversible unit¹.
- Domestic Hot Water (DHW) production.
- Nominal heating capacity: 8 kW.
- Plug&Play construction.
- Refrigerant: R32.

¹It satisfies the entire heating and cooling demand.

In particular, this prototype was designed by the Italian company *HiRef* in collaboration with the *IUIIE*. The next three sections provide a summary of the operating conditions, the operating modes available in this unit and its main components.

For additional information about the design of this unit, my Master thesis could be consulted (Marchante-Avellaneda, 2017), or the Deliverable 4.1 and 4.3 (Corberán et al., 2016b,a) from the WP4 in the GEOTECH project. Other good references are Marchante-Avellaneda et al. (2018a); Cazorla-Marín et al. (2018a).

2.2.1 Operating conditions

The operating conditions of the DSHP have been set in terms of user side and source/sink side, as they were defined in Corberán et al. (2016b), Table 2.1.

These temperature values are used to define the range conditions that need be evaluated to characterize the performance of this unit and they represent the maximum temperature range in which the system will work.

Table 2.1: Operating conditions (secondary fluid values)^a

Primary operation (Secondary operation is DHW with user side 50-55 °C)	User Temp. (°C)	Source/sink Temp. (°C)		Source/sink Temp. (°C)	
		(COLD CLIMATE)		(WARM CLIMATE)	
		Ground	Air	Ground	Air
Heating-low temperature (radiant floor)	35/40	-5/10	5/15	5/20	5/20
Heating-medium temperature (convector/radiator)	40/45	-5/10	5/15	5/20	5/20
Heating-high temperature (radiator)	45/55	-5/10	5/15	5/20	5/20
Winter-DHW	50/55	-5/10	18/30	5/20	5/25
Cooling-high temperature (radiant surface)	18/26	10 ^b /30	18/30	10/35	18/40
Cooling-medium temperature (air handling)	12/16	10 ^b /30	18/30	10/35	18/40
Cooling-low temperature (air handling & dehumidification)	6/10	10 ^b /30	18/30	10/35	18/40
Summer-DHW	50/55	10 ^b /30	18/30	10/35	18/40

^a User temp. defined as supply temp. and ground and air temp. as return (borehole) and air inlet (coil) temp;

^b Free-cooling for brine temperatures below 10 °C;

As an example, for low temperature heating (radiant floor), the water temperature to the user side (production of the heat pump) is expected to be somewhere between 35 and 40°C. In this situation, when the ground source is selected, the brine temperature to the heat pump is expected to vary between -5 and 10°C (cold climate), and between 5 and 15°C in the air, when the heat pump works with the air source.

2.2.2 Operating modes

In order to cover all demands, the DSHP is able to operate in nine² different working modes, which are summarized in Table 2.2. They are primarily classified depending on the season: when the system operates in summer mode, it will work as a chiller; when it operates in winter mode, it will work as a heat pump.

The unit is also able to operate in free-cooling conditions when the return temperature from the borehole loop is lower than 10°C. However, this extra mode is not included in Table 2.2 because in this condition, the unit is switched off and the present work only analyzes the working maps of the unit.

Table 2.2: Operating modes

Mode	Summer		Mode	Winter	
	Condenser	Evaporator		Condenser	Evaporator
Heating & Cooling					
1-SA ¹	Air	User	4-WA ⁶	User	Air
2-SG ²	Ground	User	5-WG ⁷	User	Ground
DHW & Cooling					
3-DHWU ³	DHW	User			
Domestic Hot Water					
6S-DHWA ⁴	DHW	Air	6W-DHWA ⁴	DHW	Air
7S-DHWG ⁵	DHW	Ground	7W-DHWG ⁵	DHW	Ground

¹ SA: Summer Air;

² SG: Summer Ground;

³ DHWU: Domestic Hot Water User;

⁴ DHWA: Domestic Hot Water Air;

⁵ DHWG: Domestic Hot Water Ground;

⁶ WA: Winter Air;

⁷ WG: Winter Ground;

²There are 7 working modes + Winter and Summer conditions for the DHW production = 9 operating modes.

According to Table 2.2, the unit is provided with three Brazen Plate Heat Exchanger (BPHEs) to cover the User and DHW demands and for the heat transfer in the Ground side. Then, a Round Tube Plate Fin Heat exchanger (RTPFHx) is also installed for the heat transfer in the air side. Figure 2.1 shows a simple diagram of the DSHP including the appointed heat exchangers.

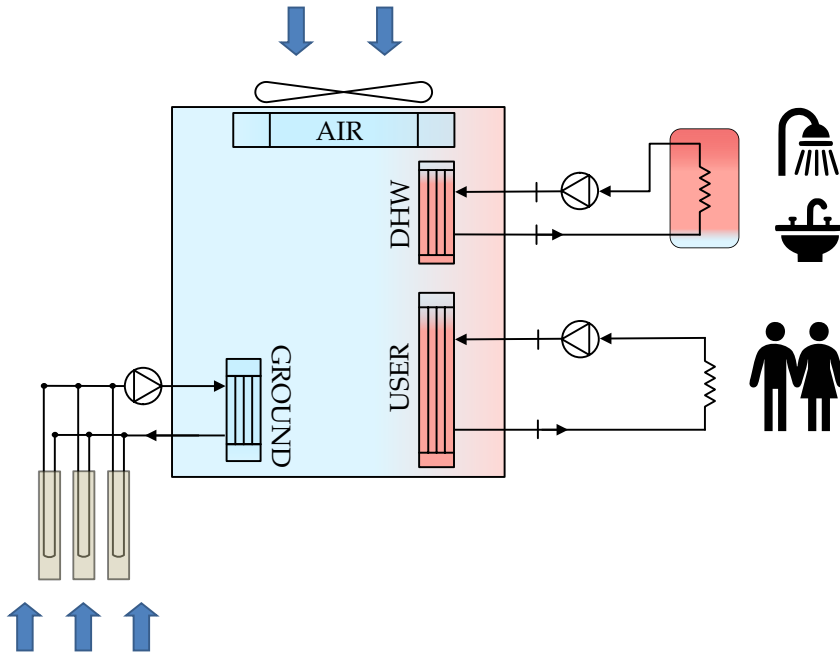


Figure 2.1: DSHP basic diagram

Finally, a brief description is given below for the 9 operating modes:

- Mode 1: SUMMER (AIR). The unit is working as a chiller, so producing chilled water at the internal heat exchanger (USER in Figure 2.1). Condensation occurs at the air-to-refrigerant HX³ (AIR in Figure 2.1).
- Mode 2: SUMMER (GROUND). The unit is working as a chiller, so producing chilled water at the internal heat exchanger (USER in Figure 2.1). Condensation occurs at the brine-to-refrigerant HX (GROUND in Figure 2.1).

³HX: Heat exchanger.

- Mode 3: SUMMER (DHW - USER). The unit is working as a chiller, so producing chilled water at the internal heat exchanger (USER in Figure 2.1). Condensation occurs at the dedicated BPHE (DHW in Figure 2.1). The nomenclature DHW - USER refers to the fact that the DHW is produced employing the USER (internal circuit) as the heat source. This gives the name to the system layout: “*full recovery*”. In this mode, the system is producing chilled water and DHW at the same time. The DHW production is therefore conditional on the existence of the cooling load⁴.
- Mode 4: WINTER (AIR). The unit is working as a heat pump, so producing hot water at the internal heat exchanger (USER in Figure 2.1). Evaporation occurs at the air-to-refrigerant HX (AIR in Figure 2.1).
- Mode 5: WINTER (GROUND)⁵. The unit is working as a heat pump, so producing hot water at the internal heat exchanger (USER in Figure 2.1). Evaporation occurs at the brine-to-refrigerant HX (GROUND in Figure 2.1).
- Mode 6S: SUMMER (DHW - AIR). The unit is working in summer conditions as a heat pump, so producing DHW at the dedicated BPHE (DHW in Figure 2.1). Evaporation occurs at the air-to-refrigerant HX (AIR in Figure 2.1). The nomenclature DHW - AIR refers to the fact that the DHW is produced employing AIR as the heat source. DHW production is therefore independent of the building’s thermal load with no chilled water production.
- Mode 7S: SUMMER (DHW - GROUND). The unit is working in summer conditions as a heat pump, so producing DHW at the dedicated BPHE (DHW in Figure 2.1). Evaporation occurs at the brine-to-refrigerant HX (GROUND in Figure 2.1). The nomenclature DHW - GROUND refers to the fact that the DHW is produced employing the brine coming from the ground as the heat source. DHW production is therefore independent of the building’s thermal load with no chilled water production.
- Mode 6W: WINTER (DHW - AIR). The unit is working in winter conditions as a heat pump, so producing DHW at the dedicated BPHE (DHW in Figure 2.1). Evaporation occurs at the air-to-refrigerant HX (AIR in Figure 2.1). This mode is identical to Mode 6S but the operating temperatures will be remarkably different.

⁴The most efficient operating mode.

⁵The unit has been designed considering WG as the main operating mode.

- Mode 7W: WINTER (DHW - GROUND). The unit is working in winter conditions as a heat pump, so producing DHW at the dedicated BPHE (DHW in Figure 2.1). Evaporation occurs at the brine-to-refrigerant HX (GROUND in Figure 2.1). This mode is identical to Mode 7S but the operating temperatures will be remarkably different.

2.2.3 System and components

The system layout of this unit was designed to satisfy all the operating modes, i.e. heating, cooling and DHW production both during winter and during summer. In Corberán et al. (2016b), there is an extensive analysis of how to design the system layout. The final solution⁶ was to connect the air and ground HXs in parallel with a suitable interconnection of 10 solenoid valves (combining them with 7 check valves) in the refrigeration circuit. This configuration allows selection of the desired source/sink interconnecting the HXs with an inverter scroll compressor and the Electronic Expansion Valve (EEV). Additionally, a liquid receiver is installed at the condenser outlet—in the liquid line before the EEV—to store any liquid refrigerant that will be excess to requirements in some modes and operating conditions. Therefore, the HP operates with a subcooling of $\approx 0\text{K}$ and the EEV sets a constant superheat of 5K at the suction pipe. Table 2.3 shows a summary of the main components installed in this unit. A more detailed description of these components is given in Appendix B.

Table 2.3: DSHP components

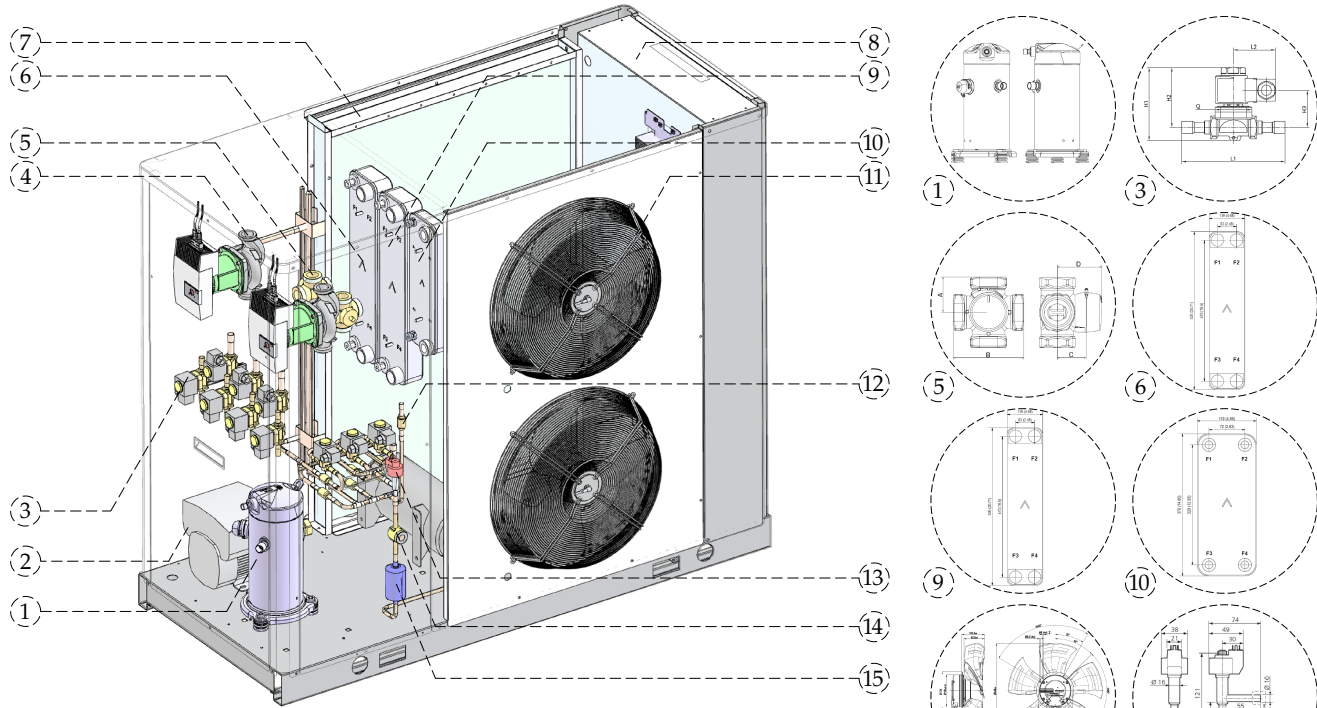
Component	Manufacturer	Hydraulic loop	Size
Compressor XHV-025	Copeland	-	25 cm ³
BPHE F85	SWEP	User	1.08 m ²
BPHE F80AS	SWEP	Ground	1.08 m ²
BPHE B26	SWEP	DHW	0.656 m ²
RTPFHx	-	Air	38.56 m ²
Liquid receiver	-	-	6.6 l
EEV E2V14	Carel	-	8.3 kW (R410a)

On the next page, the Figure 2.2 shows the final design for the DSHP with all the components described above. This figure does not show the connection pipes⁷.

⁶This system layout design is referenced as the “Full recovery system” in Corberán et al. (2016b).

⁷Hiref confidential agreement.

Figure 2.2: DSHP 3D



- | | | |
|--|------------------------------------|------------------------|
| 1. Scroll compressor. XHV0251P (Copeland) | 7. RTPFHx (Prototype) | 13. EEV. E2V24 (Carel) |
| 2. Circulation pump (Ground). CME3-2 (Grundfoss) | 8. Electronics | 14. Sight glass |
| 3. Solenoid valve. 1078/M12 and 1078/5 (Castel) | 9. BPHE (User). F85 (Sweep) | 15. Filter drier |
| 4. Circulation pump (User/DHW). Stratos Para 25/1 (Wilo) | 10. BPHE (DHW). B26 (Sweep) | |
| 5. 4-way valve. VRG142+ARA632 (ESVE) | 11. Fans. A3G450-AC28-51 (EBM) | |
| 6. BPHE (Ground). F80AS (Sweep) | 12. Check valves. 3132/M10 (Carel) | |

2.2.4 Test rig

This section introduces the experimental test rig used to carry out the entire experimental campaign on the DSHP. As mentioned in the sections above, the DSHP includes three internal BPHEs and one RTPFHx, in order to work in all the operating modes described in Subsection 2.2.2. Therefore, the experimental test rig includes three different hydraulic loops⁸ and the unit is located inside a climatic chamber, which is able to set the temperature and humidity conditions required.

Figure 2.3 shows a simple diagram and Figure 2.4 some photographs of the experimental test rig with the DSHP installed.

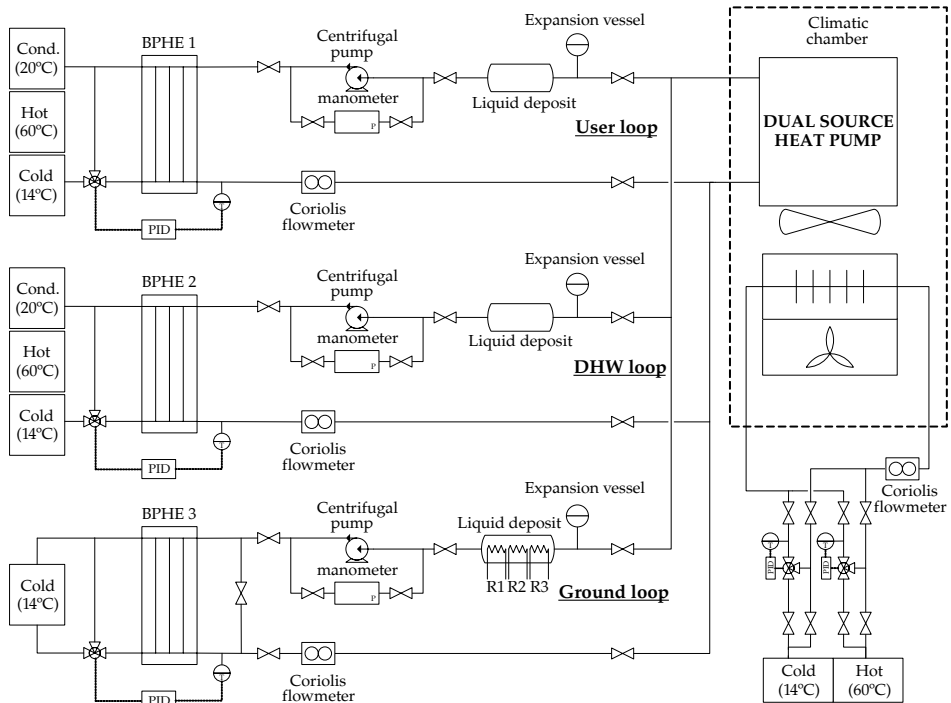


Figure 2.3: DSHP experimental test rig (diagram)

⁸User, DHW and Ground loops.

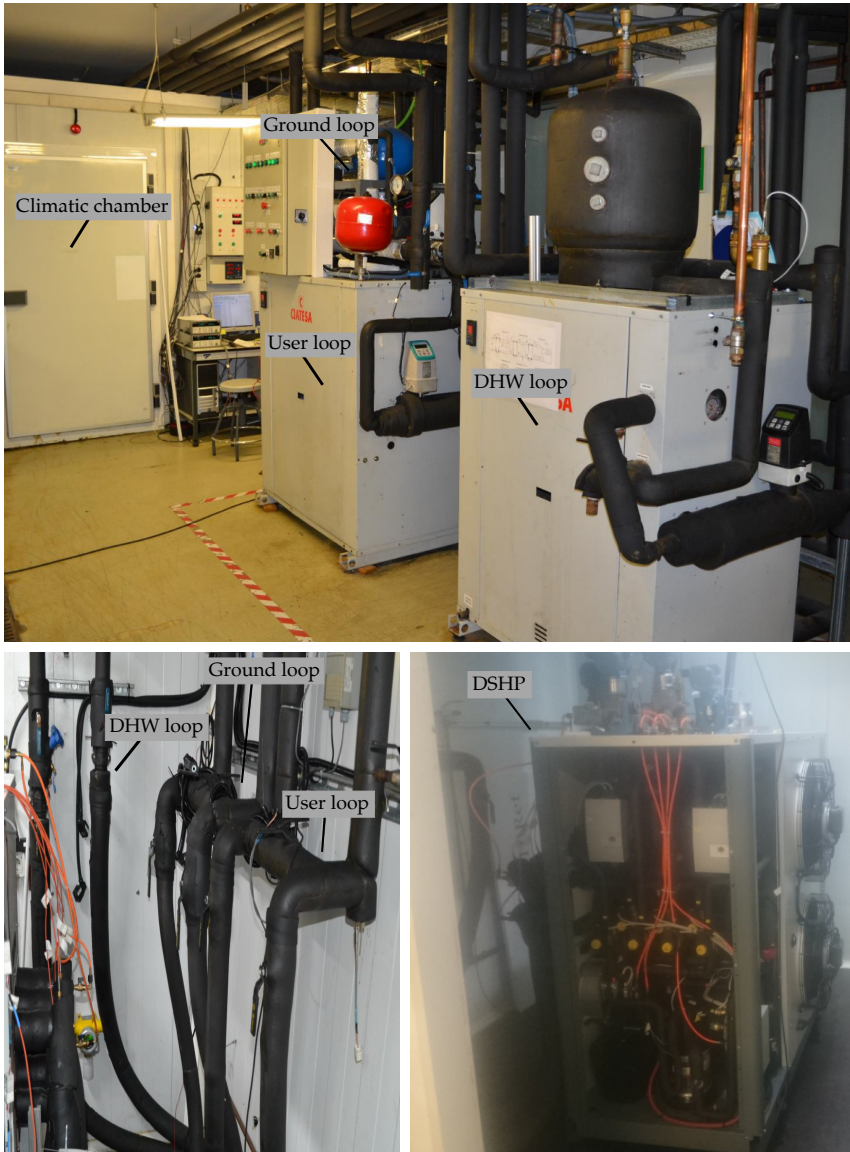


Figure 2.4: Experimental test rig

The three hydraulic loops are able to set the desired return temperatures to the DSHP, working with three external PHEs and a set of 3-way valves actuated by PID controllers. These PHEs dissipate or absorb the thermal loads with three external water circuits: hot water (60°C – Summer modes), cold water (14°C – Winter modes) and condensation water (20°C – specific situations).

The first hydraulic loop (User) simulates the building demand when the DSHP selects an operating mode with the User BPHE active.

Then, the second loop (Ground) reproduces the conditions of the ground simulating the return temperature from the borehole heat exchanger when the unit works as a geothermal HP. This hydraulic loop is not connected to the external hot water circuit. Instead, a set of three electric heating resistors compensate for the drop in temperature when the unit works in Winter mode.

Finally, the third loop (DHW) sets the conditions when the unit produces DHW simulating the DHW demand. The configuration for this loop is similar to the previous one.

The selected working fluids were water for the User and DHW loops and propylene glycol⁹ in the Ground loop, working at 1.6 – 2 bar. The rest of the elements located in the hydraulic loops are listed below:

- Hand valves ⇒ Allows the desired hydraulic loops to be connected according to the operating mode tested.
- Expansion vessels ⇒ Compensate the change in volume of the secondary fluid due to the temperature change.
- Buffer tanks ⇒ Prevent sudden changes in conditions.
- External circulation pumps ⇒ Circulate the secondary fluid.

The capacities of the heat pump were determined at the water/brine side, including the use of Coriolis flow meters to ensure high accuracy when measuring the secondary mass flow. Additionally, Resistance Temperature Detectors (RTDs) were also used to measure the supply and return temperatures of the secondary fluid in each loop.

Finally, in order to monitor and to measure the temperature in other locations¹⁰, a total of 24 T-type thermocouples were installed. Two absolute pressure transmitters were also provided in the suction and discharge pipes and a power meter was fitted to measure the total power input and the compressor consumption.

Table 2.4 shows the model, units and location for all the sensors/actuators installed.

⁹30% (mass fraction) to prevent the secondary fluid from freezing when the DSHP operates in the Winter Ground mode.

¹⁰Refrigerant circuit measurements.

Table 2.4: Instrumentation

Sensor/actuator	Model	Units	Measurement	Location
Thermocouple	T-type (class 1)	2	$T_s ; T_d$	Compressor inlet/outlet
		2	$T_{rec,in} ; T_{rec,out}$	Inlet/outlet liquid receiver
		2	$T_{EEV,in} ; T_{EEV,out}$	Inlet/outlet EEV
		2	$T_{coil,in} ; T_{coil,out}$	Inlet/outlet RTPFHx (refrigerant)
		10	$T_{C1,in}$ and $T_{C1,out}$ to $T_{C5,in}$ and $T_{C5,out}$	Inlet/outlet RTPFHx circuits
		6	$T_{g,in} ; T_{g,out} ; T_{u,in} ; T_{u,out} ; T_{d,in} ; T_{d,out}$	Inlet/outlet BPHE (refrigerant)
RTDs	PT100	6	$T_{co} ; T_{ci} ; T_{eo} ; T_{ei}$	Inlet/outlet BPHE (secondary)
		2	T_a^*	Inlet RTPFHx (air side)
Pressure transducer	Rosemount 2088 (absolute)	1	P_e	Suction pressure
	Rosemount 3051 (absolute)	1	P_c	Discharge pressure
	Rosemount 3051 (relative)	1	$(P_d - P_{EEV})$	ΔP from discharge to inlet EEV
	Yokogawa (relative)	1	$\Delta P_{water} ; \Delta P_{brine}$	ΔP secondary
Humidity sensor	HUMICAP 180	1	RH	Climatic chamber humidity
Humidifier	Hygromatik HL 80	1	-	Climatic chamber
Flowmeter	Siemens Mass 2100 DL15 (Coriolis)	1	\dot{m}_{user}	User hydraulic loop
		1	\dot{m}_{dhw}	DHW hydraulic loop
		1	\dot{m}_{ground}	Ground hydraulic loop
Powermeter	A2000 Multifunctional Power meter	2	$\dot{W}_{DSHP} ; \dot{W}_c^\dagger$	Connected to HP power
Pitot	Vaisala HMP141A	1	$p_{total} - p_{static} \Rightarrow v_a$ (Air side)	Air velocity (RTPFHx outlet)
		1	-	User hydraulic loop
3-way valve	SKD62 Landis & Steafa	1	-	DHW hydraulic loop
		1	-	Ground hydraulic loop
		1	-	User hydraulic loop
PID	KS 90-1 (PMA)	1	-	DHW hydraulic loop
		1	-	Ground hydraulic loop
		1	-	Ground hydraulic loop
Datalogger	Agilent 34972	2	-	Climatic chamber
		2	-	Room

* Average value;

† This measurement includes the inverter consumption;

2.2.5 DSHP experimental results

The DSHP has been tested in the test bench described above including two experimental test campaigns.

The first one was carried out with the objective of evaluating the operation of this prototype and identifying possible design improvements. This set of tests mainly includes the nominal conditions for all the operating modes, the evaluation of the frost formation in the RTPFHx¹¹, parametric studies for the variable speed compressor and fan, the evaluation of the compressor oil return, and additional tests in order to check the change in between operating modes. The main conclusions of all these results are reported in Corberán et al. (2017b).

Then, the second experimental campaign included more extensive test conditions for all the operating modes. Basically, these experimental results were obtained in order to adjust the final empirical models developed in Chapter 3. The test conditions were defined according to the operating conditions described in Subsection 2.2.1 and the use of Design of Experiments methodologies, as will be described in Chapter 3. Table 2.6 on page 48 shows a summary of all the experimental test data obtained in the first and second experimental campaigns.

Finally, the data for the characterization of the unit performance at each test point had been recorded at steady-state conditions over 45 minutes with an interval of 5 seconds between measurements. Then, the experimental values for the monitored variables in each individual test were reported as the mean of all measurements recorded throughout the test duration without outliers, in order to minimize random error. The corresponding error analysis for the measurements is included in Appendix D.

2.2.6 DSHP simulation results

This section introduces an additional model of the DSHP developed for each operating mode in the commercial simulation tool IMST-ART. The main objective of this detailed model was to generate the complete working maps of the unit as a virtual test and then, to find better empirical equations for the characterization of the unit performance.

These **simulated results** are composed of **21875 points** including all the operating modes. Table 2.7 on page 49 shows the level values for the control variables considered. We can obtain the total number of virtual tests generated in IMST-ART as the full factorial for the total number of control variables and their levels.

¹¹The analysis of frost formation in this unit only included some additional tests to check the performance penalty due to frost formation. Due to its dual typology, it was not necessary to characterize the unit's performance under frost formation conditions. In this sense, once the capacity decreases due to the frost formation (the RTPFHx inlet area decrease), the unit must select the ground as the source and change the operating mode.

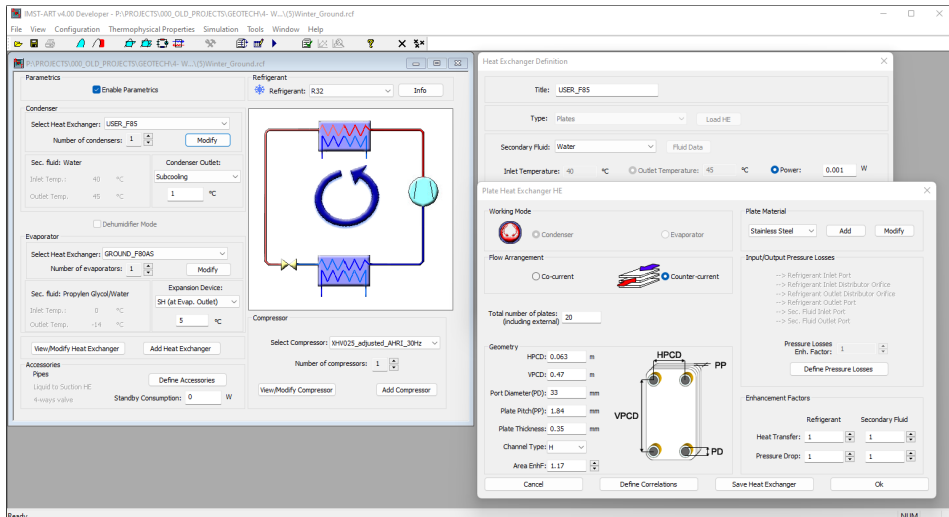
Additionally, the IMST-ART model was also used to compare and select the best experimental design from the DoE methodologies studied, in order to perform the experimental test matrix for the second experimental campaign. This comparison is described in the next chapter.

The following subsections includes a brief summary describing the IMST-ART simulation tool and how the DSHP model was implemented.

2.2.6.1 IMST-ART software

IMST-ART is a software package developed at the Polytechnic University of Valencia for the analysis and optimization of heat pumps and refrigeration equipment based on the vapour compression cycle. IMST-ART is based on a long experience on the detailed modelling of these units and is fully targeted to assist the design of components and systems, especially envisaged from the beginning of its development as a design tool for industrial use. The main feature of the program is the accurate evaluation of the unit performance including a high accurate modelling of every single component at the same time. In that way, any modification in one or several components can be always assessed from the perspective of the global performance of the unit. Figure 2.5 shows a screenshot of the IMST-ART Graphical User Interface (GUI).

Figure 2.5: IMST-ART GUI



This software is able to take into account in the simulation most of the components of vapour compression based units: compressor, heat exchangers, piping and accessories. The global model of the system is divided in submodels: compressor, heat exchangers (HX), expansion valve, accessories, and piping.

Each submodel involves a series of non-linear equations and in the case of the heat exchangers, maybe also the solution of a system of ODEs, which is discretized with a finite volume technique. The global set of equations forms a complex system of non-linear equations AEs or DAEs which is solved through a Newton like solver. The independent variables chosen for the global set of equations are pressure and enthalpy in each inlet and outlet point. This choice assures a smooth variation of the variables, not given by other choices like temperature or quality. The main characteristics of the employed models appeared in Corberán et al. (2002) and Corberán et al. (2005).

The HX model is based on the discretization of the HX in cells along the refrigerant and secondary fluid paths, assuming one-dimensional flow. The model is able to take into account both heat transfer and pressure drop, with local evaluation of the heat transfer coefficient and friction factor, by built-in correlations, as well as of the fluid properties. This model is able to take into consideration most of the geometrical and operation parameters of current evaporators and condensers.

The compressor submodel includes four different ways to define it: constant efficiencies, polynomial correlations for the efficiencies as a function of the pressure ratio, data tables from the manufacturer's catalog data, and AHRI polynomials.

2.2.6.2 Detailed model in IMST-ART

As concerns the DSHP detailed model, it was implemented by being provided with all the geometric and performance data for the individual components installed in the DSHP to IMST-ART (compressor, HX, etc.). These data were extracted from the manufacturers' catalogs. The option selected for the compressor submodel was to introduce the compressor performance as AHRI polynomials.

Unfortunately, the AHRI polynomials for the variable speed compressor were not available for the R32 refrigerant. When this unit was designed, there were no variable speed compressors with the required capacity, so a compressor designed to use R410A was installed, changing the lubricant oil to the one recommended by the manufacturer.

Consequently, this model in ART has been updated at the end of the experimental campaign. At first, the model was constructed to characterize the compressor efficiency with the available data for R410A. However, once the experimental campaign concluded, the experimental results were used to update the compressor sub-model in ART. All the virtual tests generated in ART have been

repeated with the updated model, including the results for the comparison between the experimental designs set out above.

The next subsection shows the construction for the final compressor sub-model introduced in ART and the validation with the experimental results.

2.2.6.3 Compressor sub-model and experimental validation for the IMST-ART model

Once the experimental campaign was concluded, the experimental results afforded us an opportunity to adjust a model for the variable speed compressor, working with R32 as the refrigerant.

The process to adjust a model for refrigerant compressors is not an easy task. The complicated heat and mass transfer processes inside the compressor makes it difficult to obtain a simple model with a high degree of precision. Furthermore, in variable speed compressors, the velocity is an extra factor to be taken into consideration.

In the current scientific literature, a lot of studies have been conducted on the characterization of constant speed compressors. One of the most common types is the efficiency method, widely used when the required precision is not particularly high.

In order to increase the accuracy of the model, another extended methodology used is map-based models (AHRI 540, 2020), which characterize the compressor performance (\dot{W}_c and \dot{m}_{ref}) with empirical polynomials at specific working conditions of constant superheat or suction temperature. These polynomials are adjusted as a function of condensation temperature (T_c) and evaporation temperature (T_e) at dew point. However, as mentioned above, the performance of inverter compressors are also a function of velocity (f_c). In other words, there are three independent variables in the model: T_c , T_e and f_c .

In order to include the frequency (velocity) dependence in the map-based models, Shao et al. (2004) analyzed the performance curves of three inverter rotary compressors. As described in this work, when operating at a certain frequency, the performance of variable speed compressors is similar to that of a constant speed compressor. Additionally, the authors concluded that the dependence of the compressor performance on the evaporation and condensation temperature is almost independent of the frequency. With these two assumptions, the authors provide the following model for the characterization of variable speed rotary compressors.

First of all, a nominal frequency is selected adjusting the Equation 2.1 and Equation 2.2 for the prediction of the compressor power input and the mass flow rate at this frequency:

$$\dot{m}_{ref}^* = a_0 + a_1 T_e + a_2 T_c + a_3 T_e T_c + a_4 T_e^2 + a_5 T_c^2 \quad (2.1)$$

$$\dot{W}_c^* = b_0 + b_1 T_e + b_2 T_c + b_3 T_e T_c + b_4 T_e^2 + b_5 T_c^2 \quad (2.2)$$

The equations above includes the main terms of the map-based models defined in the standard AHRI 540 (2020). These terms are the linear predictors (T_e , T_c), quadratic terms (T_e^2 , T_c^2) and the two-factor interaction term ($T_e \times T_c$) of the condensation temperature and the evaporation temperature.

Then, Equation 2.3 and Equation 2.4 correct the other compressor frequencies to the performance at the nominal frequency:

$$k_M = \frac{\dot{m}_{ref}}{\dot{m}_{ref}^*} = c_0 + c_1(f_c - f_c^*) + c_2(f_c - f_c^*)^2 \quad (2.3)$$

$$k_P = \frac{\dot{W}_c}{\dot{W}_c^*} = d_0 + d_1(f_c - f_c^*) + d_2(f_c - f_c^*)^2 \quad (2.4)$$

The two equations above include two interceptions, c_0 and d_0 . If we consider that at a compressor frequency of 0 Hz the mass flow rate and power input values are zero, both coefficients become 1. However, the authors also reported that these two coefficients must be included in the regression adjustment.

As they conclude, this implies that the frequency values are not zero when the mass flow rate and power input values are at zero and, this difference is due to the slip ratio of the asynchronous electric motor and the internal friction force of the compressor.

Therefore, we must also consider these terms in the regression adjustment in order to increase the accuracy of the model by including the effect of the slip.

Table 2.5 shows the regression coefficients adjusted to the experimental results of the DSHP. Then, in order to introduce the model in ART, the abovementioned model was recomposed as a set of second-order AHRI polynomials by considering different discretized levels for the value of the compressor speed.

As map-based models are obtained at constant superheat values, the experimental test included in the compressor submodel adjustment have been previously filtered. This unit is designed to work at a constant superheat value of 5K but, when the discharge temperature is higher than 120°C, the EEV injects some liquid at the compressor suction in order to limit it. Additionally, the EEV was not able to set the 5K of superheat in some tests in Summer Air, and particularly, Summer Ground modes, with the presence of bubbles upstream of the EEV¹².

Excluding these tests, the final adjustment takes a total of 196 experimental points into consideration.

Table 2.5: Compressor submodel coefficients

	\dot{m}_{ref}^* (kg/h)		\dot{W}_c^* (W)		k_M (-)		k_P (-)
a_0	1.040e+02	b_0	8.936e+02	c_0	9.941e-01	d_0	9.975e-01
a_1	1.605e+00	b_1	-2.170e+01	c_1	2.105e-02	d_1	2.021e-02
a_2	-3.973e-01	b_2	2.414e+00	c_2	4.249e-06	d_2	7.471e-05
a_3	3.192e-02	b_3	5.531e-01				
a_4	3.864e-02	b_4	-2.770e-01				
a_5	1.134e-03	b_5	4.403e-01		f_c^*		50 Hz

¹ Temperatures (°C);

² Compressor frequency (Hz);

As we can see in the table above, the adjusted values for the coefficients c_0 and d_0 are close to 1. This means that the effect of the slip on the compressor performance is a second-order effect, so it contributes to a slight correction.

Then, Figure 2.6 and Figure 2.7 show the deviation of the adjusted model with the experimental data. These plots also include the Maximum Relative Error (MRE), the Root Mean Square Error (RMSE), and the Coefficient of Variation of the RMSE (CV_{RMSE} ¹³). Furthermore, the error bars as expanded uncertainty with a confidence interval of 95% are also included for the experimental results¹⁴.

¹²These two operating modes have lower values of pressure ratio with high values of mass flow rate. We included an extra refrigerant charge in order to eliminate the flash gas effect without success. This problem was reported in Corberán et al. (2017b).

¹³This coefficient is calculated by dividing RMSE by the average of the analyzed variable.

¹⁴HP capacities have been obtained at the secondary side. Therefore, the error bars for the refrigerant mass flow rate have been obtained with the corresponding analysis of error propagation.

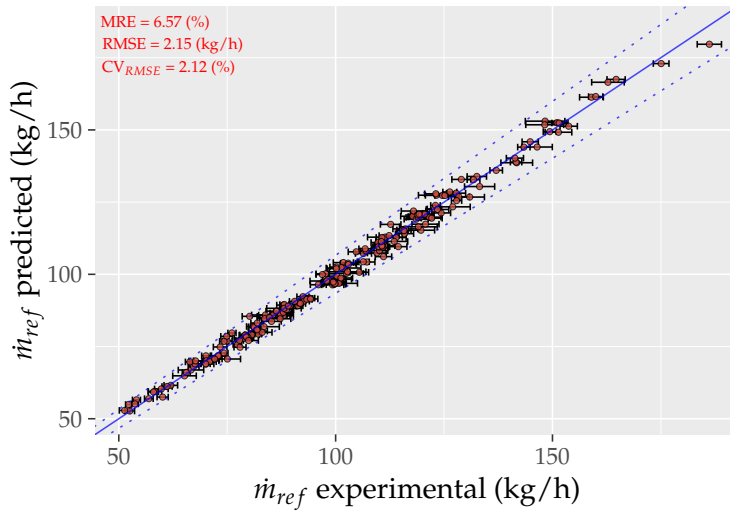


Figure 2.6: IMST-ART compressor submodel: Adjustment results \dot{m}_{ref}

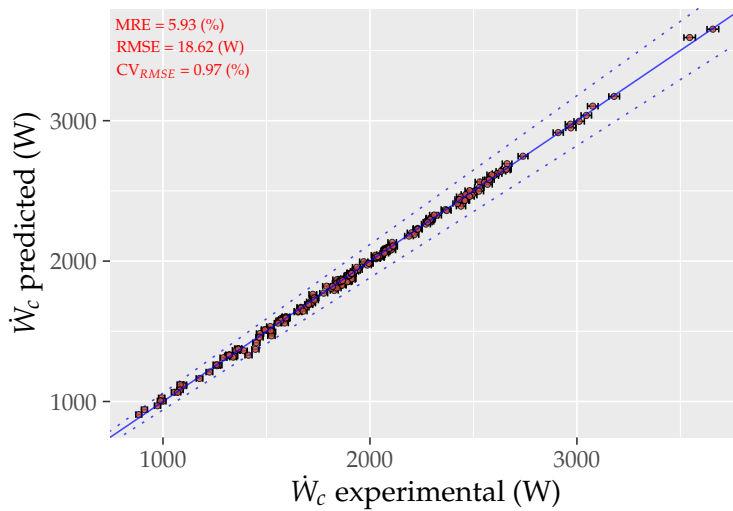


Figure 2.7: IMST-ART compressor submodel: Adjustment results \dot{W}_c

As a result of the comparison with the experimental data, we can confirm that the methodology presented by Shao et al. (2004) is also valid for the scroll compressor installed in the unit. The adjusted model presents a maximum relative error of around 7% in the mass flow rate prediction and 6% in the compressor power input, both with low values for the RMSE and CV_{RMSE} errors.

Once the compressor model was adjusted, the last step to finalize the compressor submodel in ART was to include the compressor heat losses extracted from the analysis of the experimental data (Equation 2.5). Figure 2.8 represents the calculated heat losses for the experimental test points. These values have been introduced in ART as mean heat loss values in each operating mode.

$$\xi = \frac{\dot{m}_{ref} \cdot [h_2(P_c, T_2) - h_1(P_e, T_1)]}{\dot{W}_c} \times 100 \quad (2.5)$$

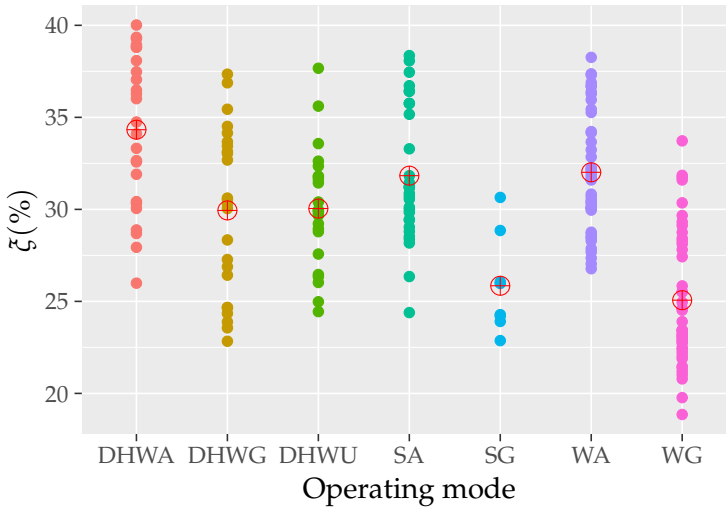


Figure 2.8: IMST-ART compressor submodel: Heat losses

Finally, to conclude with the IMST-ART model, Figure 2.9 below shows the prediction of \dot{W}_c and \dot{Q}_c in ART compared with the experimental results in Winter Ground mode. The final IMST-ART adjusted model, including the submodel of the compressor described above, demonstrates a maximum relative error in the prediction of the DSHP performance of less than 10% in all operating modes.

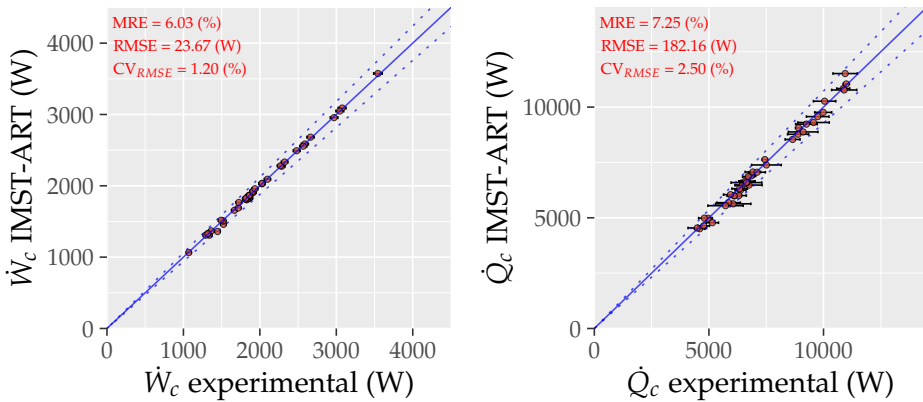


Figure 2.9: IMST-ART model vs experimental data in WG mode (\dot{W}_c and \dot{Q}_c)

2.3 Compressor performance data

A few years ago, the Air-Conditioning, Heating, and Refrigeration Institute (AHRI) launched an industry-wide cooperative research program to identify and evaluate promising alternative refrigerants in heat pump applications. This program was referred to as the “*Low GWP Alternative Refrigerants Evaluation Program*”, and it generated a large amount of compressor calorimeter data, among other results. The following summary on the project’s website includes the results obtained and the project’s framework:

“In response to environmental concerns raised by the use of high-global warming potential (GWP) refrigerants, AHRI has established this industry-wide cooperative research program to identify and evaluate promising alternative refrigerants for major product categories. The AHRI Low-GWP Alternative Refrigerants Evaluation Program (AREP) includes compressor calorimeter testing, system drop-in testing, soft-optimized system testing, and heat transfer testing. All tests other than heat transfer coefficient measurements are expected to be performed at participating companies’ laboratories, using their own resources, at their own expense. The Low-GWP AREP program is managed by a technical committee reporting to the AHRI Executive Committee. The AHRI Research Department administers the Low-GWP AREP program, and coordinates and disseminates information and reports among the participating companies and the observers.”



AHRI Low-GWP AREP
Air-Conditioning, Heating, and Refrigeration Institute

The compressor calorimeter data are included in 25 test reports evaluating the compressor performance for scroll and reciprocating compressor technologies. They include the results for the base refrigerant of the compressor analyzed together with the evaluation of new mixtures at different suction temperature or suction superheat working conditions. Their references are included below:

Scroll: AHRI 11 (Shrestha et al., 2013a), AHRI 21 (Shrestha et al., 2013b), AHRI 24 (Rajendran and Nicholson, 2013), AHRI 33 (Shrestha et al., 2014), AHRI 34 (Rajendran and Nicholson, 2014a), AHRI 36 (Rajendran and Nicholson, 2014c), AHRI 38 (Rajendran and Nicholson, 2014e), AHRI 39 (Rajendran and Nicholson, 2014f), AHRI 58 (Rajendran et al., 2016a), AHRI 65 (Rajendran et al., 2016b), and AHRI 66 (Suindykov et al., 2016).

Reciprocating: AHRI 17 (Borges Ribeiro and Marchi Di Gennaro, 2013a), AHRI 18 (Borges Ribeiro and Marchi Di Gennaro, 2013b), AHRI 28 (Sedliak, 2013a), AHRI 29 (Sedliak, 2013b), AHRI 30 (Sedliak, 2013c), AHRI 35 (Rajendran and Nicholson, 2014b), AHRI 37 (Rajendran and Nicholson, 2014d), AHRI 49 (Sedliak, 2015a), AHRI 50 (Sedliak, 2015b), AHRI 51 (Boscan and Sanchez, 2015), AHRI 59 (Lenz and Shrestha, 2016), AHRI 64 (P erouffe and Renevier, 2016a), AHRI 67 (P erouffe and Renevier, 2016b), and AHRI 69 (P erouffe and Renevier, 2016c).

In addition to this extensive database and excellent experimental data, this work includes additional data for an inverter scroll type compressor published in Cuevas and Lebrun (2009). Chapter 4 analyzes only the operation of fixed-speed compressors. Therefore, the data analyzed from Cuevas' work includes only the experimental data for the nominal speed (50 Hz).

A summary of the main information provided in these reports is included in the Table 2.8 on page 50. Table 2.9 on page 51 shows the composition of the new mixtures evaluated in this project.

Due to the large amount of data collected from this excellent work we have been able to analyze the compressor performance in scroll and reciprocating compressors. This study is included in Chapter 4.

2.4 Summary of datasets

Finally, to conclude this second chapter, this section shows the summary of the experimental data and virtual tests included in the developed database (Table 2.6, Table 2.7 and Table 2.8).

Table 2.6: DSHP experimental campaign

Test	Summer Air	Summer Ground	DHW User	Winter Air	Winter Ground	DHW Air	DHW Ground	Total test points
Nominal conditions	1	1	1	2	2	2	2	227
Variation f_c (User 40/45)	-	-	-	4	4	-	-	
Variation f_c (User 30/35)	-	-	-	4	4	-	-	
Variation f_{fan}	-	-	-	3	-	-	-	
Frost formation	-	-	-	4	-	-	-	
Test matrices (DoE)	30	20	20	30	30	20	20	
Winter Ground as DHW	-	-	-	-	3	-	-	
Double evaporator (WA/WG)	-	-	-	4	-	-	-	
Extra test	1	1	2	-	6	3	3	

Table 2.7: DSHP virtual tests

f_c Hz	T_{co} or T_{ci} °C	dT_c or f_{fan} K or %	T_{eo} or T_{ei} °C	dT_e or f_{fan} K or %	Virtual tests *
SA: ($f_c, T_{ci}, f_{fan}, T_{eo}, dT_e$)					
[30, 40, 50, 60, 70]	[15, 21, 27, 33, 39]	[20, 35, 50, 65, 80]	[6, 9, 12, 15, 18]	[2, 3, 5, 7, 9]	3125
SG: ($f_c, T_{ci}, dT_c, T_{eo}, dT_e$)					
[30, 40, 50, 60, 70]	[6, 11, 16, 21, 26]	[2, 3, 5, 7, 9]	[6, 9, 12, 15, 18]	[2, 3, 5, 7, 9]	3125
DHWU: ($f_c, T_{co}, dT_c, T_{eo}, dT_e$)					
[30, 40, 50, 60, 70]	[50, 52, 55, 58, 60]	[5, 10, 20, 30, 40]	[6, 9, 12, 15, 18]	[2, 3, 5, 7, 9]	3125
WA: ($f_c, T_{co}, dT_c, T_{ei}, f_{fan}$)					
[30, 40, 50, 60, 70]	[35, 40, 45, 50, 55]	[2, 3, 5, 7, 9]	[4, 7, 11, 15, 19]	[20, 35, 50, 65, 80]	3125
WG: ($f_c, T_{co}, dT_c, T_{ei}, dT_e$)					
[30, 40, 50, 60, 70]	[35, 40, 45, 50, 55]	[2, 3, 5, 7, 9]	[-5, 0, 5, 10, 15]	[2, 3, 5, 7, 9]	3125
DHWA: ($f_c, T_{co}, dT_c, T_{ei}, f_{fan}$)					
[30, 40, 50, 60, 70]	[50, 52, 55, 58, 60]	[5, 10, 20, 30, 40]	[5, 11, 17, 23, 29]	[20, 35, 50, 65, 80]	3125
DHWG: ($f_c, T_{co}, dT_c, T_{ei}, dT_e$)					
[30, 40, 50, 60, 70]	[50, 52, 55, 58, 60]	[5, 10, 20, 30, 40]	[-5, 2, 10, 18, 25]	[2, 3, 5, 7, 9]	3125

* 5 levels for each of the 5 control variables $\Rightarrow 5^5 = 3125$ virtual tests by operating mode \Rightarrow Total virtual tests: **21875**;

Table 2.8: Calorimeter data (AHRI Reports)

Report	Compressor model	Manufacturer	Displacement <i>cm³/rev</i>	Refrigerants tested	Test cond.* °C	Test points [†]	Total tests
Scroll compressors							
AHRI 11	ZP21K5E-PFV	Copeland	20.32	R410A/R32/DR5/L41a	a/b/c	196/166/189/186	737
AHRI 21	ZS21KAE-PFV	Copeland	50.96	R404A/ARM31a/D2Y65/L40/R32+R134a	c/a/b	191/186/183/173/133	866
AHRI 24	ZP31K5E-PFV	Copeland	29.50	DR5	a	22	22
AHRI 33	ZP21K5E-PFV	Copeland	20.32	R410A/R32+R134a	a/b/c	196/168	364
AHRI 34	ZF18K4E-TFD	Copeland	98.04	DR7	a	19	19
AHRI 36	ZF18K4E-TFD	Copeland	98.04	L40	a	19	19
AHRI 38	ZP31K5E-PFV	Copeland	29.50	L41b	a	30	30
AHRI 39	ZP31K5E-PFV	Copeland	29.50	R32	a	23	23
AHRI 58	ZP31K5E-PFV	Copeland	29.50	R454B	a	29	29
AHRI 65	ZP122KCE-TFD	Copeland	112.30	R447A	a	23	23
AHRI 66	SH161A4	Danfoss	151.70	HPR2A	a	28	28
Cuevas(2009)	-	-	54.40	R134a	f	18	18
Reciprocating compressors							
AHRI 17	NJ7240F	Embraco	34.38	R22/R1270	a	12/12	24
AHRI 18	EG80HLR	Embraco	7.15	R134a/N13a/ARM42a	b	12/8/12	32
AHRI 28	NEK2134GK	Embraco	8.77	R404A/L40	c/a/b	36/36	72
AHRI 29	NEK2134GK	Embraco	8.77	DR7	c/a/b	36	36
AHRI 30	NEK6214Z	Embraco	16.80	R134a/R1234yf	c/a/b	45/45	90
AHRI 35	CS14K6E-TF5	Copeland	47.15	DR7	a/b	52	52
AHRI 37	CS14K6E-TF5	Copeland	47.15	L40	a/b	51	51
AHRI 49	NEK2134GK	Embraco	8.77	R455A	c/a/b	36	36
AHRI 50	NEK2134GK	Embraco	8.77	DR3	c/a/b	36	36
AHRI 51	4GE-23-40P	Bitzer	971.26	R449A/R404A	e	12/12	24
AHRI 59	H84B223ABC	Bristol	30.51	R410A/L41-1/DR5A/ARM71a/D2Y60/R32	a	15/15/15/15/17/15	92
AHRI 64a	FH2511Z	Tecumseh	74.23	R404A/DR7	d/e	28/23	51
AHRI 64b	FH4540Z	Tecumseh	74.23	R404A/DR7	d/e	34/27	61
AHRI 67a	FH2511Z	Tecumseh	74.23	ARM25	d	37	37
AHRI 67b	FH4540Z	Tecumseh	74.23	ARM25	d	16	16
AHRI 69a	FH2511Z	Tecumseh	74.23	ARM20b	d/e	30	30
AHRI 69b	FH4540Z	Tecumseh	74.23	ARM20b	d	16	16

* Test conditions: **a.** $SH = 11 K$; **b.** $SH = 22 K$; **c.** $T_s = 18 ^\circ C$; **d.** $SH = 10 K$; **e.** $T_s = 20 ^\circ C$; **f.** $SH = 6.8 K$;

† Total test points: **2934**;

Table 2.9: New refrigerants composition (Low GWP HFC mixtures)

Refrigerant name	ASHRAE name ^{abc}	Company	Refrigerant composition	% molar mass (% mass)
DR5	≈ R454B	Dupont	R32/R1234yf	0.852/0.148 (0.725/0.275)
L41a	≈ R459A	Honeywell	R32/R1234yf/R1234ze(E)	0.856/0.08/0.064 (0.730/0.150/0.120)
ARM31a	-	Arkema	R32/R134a/R1234yf	0.452/0.173/0.375 (0.280/0.210/0.510)
D2Y65	R454A	Deikin	R32/R1234yf	0.541/0.459 (0.350/0.650)
L40	-	Honeywell	R32/R152a/R1234yf/R1234ze(E)	0.566/0.111/0.129/0.194 (0.400/0.100/0.200/0.300)
R32+R134a	-	-	R32/R134a	0.662/0.338 (0.500/0.500)
R32+R134a	-	-	R32/R134a	0.969/0.031 (0.941/0.059)
DR7	R454A	Dupont	R32/R1234yf	0.552/0.448 (0.360/0.640)
L41b	-	Honeywell	R32/R1234ze(E)	0.856/0.144 (0.730/0.270)
HPR2A	-	Mexichem	R32/R1234ze(E)/R134a	0.871/0.094/0.035 (0.760/0.180/0.060)
N13a	-	Honeywell	R134a/R1234yf/R1234ze(E)	0.447/0.172/0.381 (0.420/0.180/0.400)
ARM42a	≈ R516A	Arkema	R134a/R152a/R1234yf	0.072/0.175/0.754 (0.070/0.110/0.820)
DR3	R454C	Dupont	R1234yf/R32	0.625/0.375 (0.785/0.215)
L41-1	R446A	Honeywell	R32/R1234ze(E)/Butane	0.81/0.158/0.032 (0.680/0.290/0.030)
DR5A	R454B	Dupont	R32/R1234yf	0.829/0.171 (0.689/0.311)
ARM71a	R459A	Arkema	R32/R1234yf/R1234ze(E)	0.823/0.144/0.033 (0.680/0.260/0.060)
D2Y60	≈ R454A	Deikin	R32/R1234yf	0.594/0.406 (0.400/0.600)
ARM25	R465A	Arkema	R32/R1234yf/Propane	0.335/0.517/0.149 (0.210/0.711/0.079)
ARM20b	R457B	Arkema	R32/R1234yf/R152a	0.515/0.369/0.116 (0.350/0.550/0.100)

^a Refrigerant designation according to ANSI/ASHRAE Standard 34 (2019);

^b - : Development mixture;

^c ≈ : Development mixture with a similar composition to an ASHRAE-designated mixture;

3

Characterization of HPs: Empirical model approach

CONTENTS

3.1	Introduction	53
3.2	Response variables and independent variables in the DSHP ...	59
	3.2.1 Winter Ground and Winter Air modes	60
	3.2.2 Summer and DHW modes	64
3.3	IMST-ART and the virtual test database	65
3.4	Exploring functionals with the virtual database	67
	3.4.1 Winter Ground polynomial models	68
	3.4.2 Winter Air polynomial models	83
3.5	DoE: Generating the experimental test matrices	85
	3.5.1 DoE comparison	90
3.6	Adjusting the polynomial models with the experimental data .	93
3.7	Final results	102

3.1 Introduction

The term Response Surface Methodology (RSM) was first introduced by Box and Wilson (1951). In this work, they described the application of RSM to chemical processes, and it had a profound impact on industrial applications and experimentation, including for RSM as a new branch of knowledge in statistics able to characterize processes when the reality becomes complex.

The term RSM can be defined as a set of mathematical and statistical techniques that allow us to analyze a physical process and construct suitable empirical models for its characterization. Often, researchers carry out experiments in order to understand a physical process, where one or several control variables

potentially influence some performance measure of interest. This performance measure is the response variable y and the several inputs controlled are referred to as predictors or independent variables (x_1, x_2, \dots, x_n) .

Thanks to RSM, researchers have adequate tools to explore the relationships between y and x 's in order to develop accurate models for the prediction of y .

Regarding these models, they can be obtained in two situations. When researchers have a great deal of knowledge about the physical phenomena studied, they can deduce the form of the functional relationship between the response and the independent variables. In this case, we use the mechanistic model approach.

Unfortunately, this is not the common situation in experimentation. Usually, the phenomena analyzed are complex and not sufficiently understood to permit the mechanistic approach. In this situation, RSM are able to approximate empirical models to the true relationship between y and x 's. In many applications, the underlying relationship between y and x 's implies smooth changes in the response variable and we can characterize it by adjusting some polynomial equations. Box and Wilson (1951) propose the second-order polynomial as the appropriate functional. Thus, if we consider a response variable y and two independent variables x_1 and x_2 , we can define the true relationship between y and x 's as:

$$y = g(x_1, x_2) + \epsilon \quad (3.1)$$

where the unknown function g^1 is probably non-linear and ϵ^2 is referred to other sources of variability such as the measurement error on the response. Then, if we approximate this function near the point (x_{10}, x_{20}) using the two-term Taylor series, we will obtain:

$$\begin{aligned} g(x_1, x_2) \approx & g(x_{10}, x_{20}) + (x_1 - x_{10}) \left. \frac{\partial g(x_1, x_2)}{\partial x_1} \right|_{x_1=x_{10}, x_2=x_{20}} \\ & + (x_2 - x_{20}) \left. \frac{\partial g(x_1, x_2)}{\partial x_2} \right|_{x_1=x_{10}, x_2=x_{20}} \\ & + \frac{(x_1 - x_{10})^2}{2} \left. \frac{\partial^2 g(x_1, x_2)}{\partial x_1^2} \right|_{x_1=x_{10}, x_2=x_{20}} \\ & + \frac{(x_2 - x_{20})^2}{2} \left. \frac{\partial^2 g(x_1, x_2)}{\partial x_2^2} \right|_{x_1=x_{10}, x_2=x_{20}} \\ & + \frac{(x_1 - x_{10})(x_2 - x_{20})}{2} \left. \frac{\partial^2 g(x_1, x_2)}{\partial x_1 \partial x_2} \right|_{x_1=x_{10}, x_2=x_{20}} \end{aligned} \quad (3.2)$$

¹The function g is a continuous and differentiable function.

²We assume in a regression model that ϵ has a normal distribution with a mean of zero.

which leads to a general second-order polynomial equation as Box and Wilson (1951) suggest:

$$y = \beta_0 + \beta_1 x_1 + \beta_2 x_2 + \beta_{11} x_1^2 + \beta_{22} x_2^2 + \beta_{12} x_1 x_2 \quad (3.3)$$

where $\beta_1 = \left. \frac{\partial g(x_1, x_2)}{\partial x_1} \right|_{x_1=x_{10}, x_2=x_{20}}$, etc.

And now, if we consider a number of k predictors, we will obtain the following equation:

$$y = \beta_0 + \sum_{i=1}^k \beta_i x_i + \sum_{i=1}^k \beta_{ii} x_i^2 + \sum_{i < j}^k \sum_{j=1}^k \beta_{ij} x_i x_j \quad (3.4)$$

That is, the general quadratic equations including k independent variables that fix the value of y .

Of course, the number of predictors will be fixed by the type of physical process characterized. In this regard, if we characterize a response variable with only one independent variable, we will obtain a response curve such as that shown in Figure 3.1 on the left. Then, if there are two predictors, and we represent the dependence of y with them in a three-dimensional space, we will obtain a response surface such as Figure 3.1 on the right.

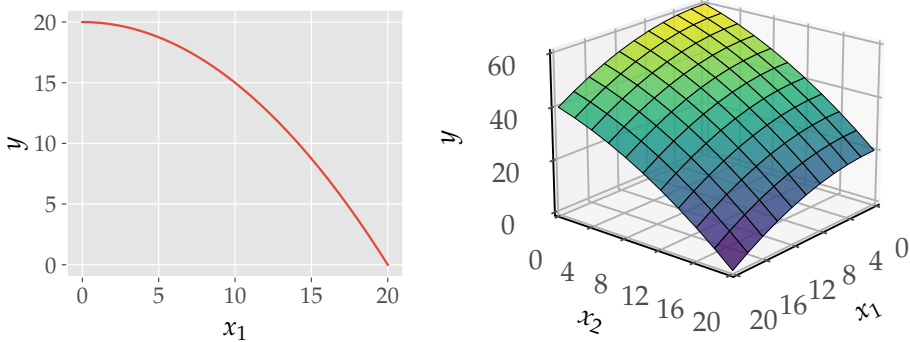


Figure 3.1: Response Curve vs Response Surface

Both examples above include a maximum of two predictors but, in general, when the number k of predictors is greater than two, we still talk of a response surface in the $(k + 1)$ -dimensional space. Therefore, we obtain a hypersurface, where only sectional representation of the surface is possible in the three-dimensional space.

Against this background, the empirical equation to adjust will include a specific number of coefficients (β 's), according to the number (k) of independent variables involved in the process and the polynomial degree (d) selected to model the response.

In general, a polynomial is said to be of order d if it contains the linear terms for the independent variables (x 's) and the product of d of the x 's. For example, when $d = 2$ and $k = 2$ we consider a second-order polynomial including x_1 , x_2 , x_1^2 , x_2^2 , the interaction term x_1x_2 and an interception. On the other hand, when $d = 3$ and $k = 3$, the model includes the terms x_1 , x_2 , \dots , x_1^3 , $x_1x_2^2$, $x_1x_2x_3$, etc.

Table 3.1, extracted from the book by Box and Draper (2007), shows the total number of coefficients for specific values of k and d .

Table 3.1: Number of coefficients in polynomials of degree d with k inputs

Number of variable inputs k	Degree of Polynomial, d			
	1	2	3	4
	Planar	Quadratic	Cubic	Quartic
2	3	6	10	15
3	4	10	20	35
4	5	15	35	70
5	6	21	56	126

As shown in the table above, when we have high values of k and d , the complete polynomial model includes a high number of regression coefficients (β 's). Commonly, the selection of a second-order polynomial is enough to model most of the physical processes and predict the values of the response with good precision. The quadratic terms help to reproduce curvature effects, and two-factor interaction terms³ ($x_i x_j$) are common in many processes.

³The interaction terms are included when an independent variable has a different effect on the response depending on the values of another independent variable.

However, in most practical contexts, high-order interaction terms are not usual and suggest that the predictors are not independent. Furthermore, the selection of high-order polynomials is not recommended to prevent an overfitting in the response.

For example, the models proposed in the current compressor characterization standards (AHRI 540, 2020) include third-degree polynomials and two predictors (10 coefficients according to Table 3.1), and it is well known that they may have significant extrapolation errors.

Therefore the second-order polynomial is selected as a basis to model the performance of the DSHP in this chapter. Then, other concepts related to transformations in the response and significant terms are also included in order to simplify the adjusted models.

Finally, the following sections describe the complete process employed to adjust the models developed in this chapter.

As a brief introduction, Figure 3.2 on next page shows the steps performed when shaping and adjusting the polynomial models. This process has been followed for each of the seven operating modes, including mainly the following steps:

- Generation of the unit working maps in each operating mode. For this purpose, the detailed model of the DSHP in IMST-ART has been used to obtain simulation data.

- Study of the simulation data to compose suitable polynomial expressions in each operating mode.

- Determination of the most appropriate experimental design to perform the experimental test matrices. The IMST-ART model is also used for this purpose.

- Generate the experimental results on the test bench.

- Adjustment of the polynomials to the experimental data. At this point, a novel methodology has been defined to combine the information extracted from the simulation and experimental data.

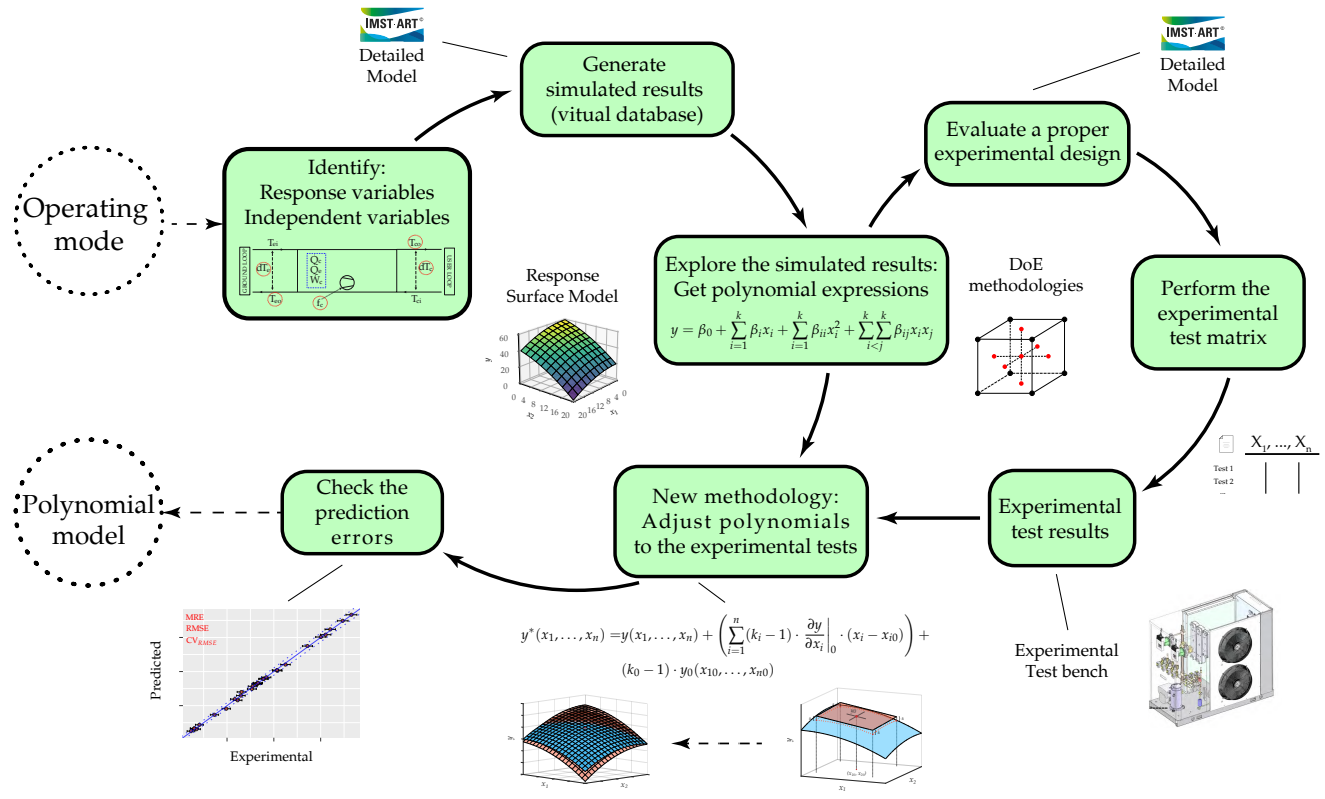


Figure 3.2: Steps to obtain polynomial models

3.2 Response variables and independent variables in the DSHP

The performance of a vapour compression heat pump or refrigeration equipment is characterized by three response variables: condenser capacity (\dot{Q}_c), evaporator capacity (\dot{Q}_e) and compressor or unit energy consumption (\dot{W}_c or \dot{W}_{HP}).

At the same time, in variable speed units, the value of the performance will be a function of the compressor frequency (f_c) and the operating conditions at the evaporator and condenser heat exchangers (HXs). Therefore, the independent variables to model the performance are the compressor frequency and a set of variables that fix the boundary conditions for the condenser and the evaporator.

Regarding the boundary conditions in the HX, there are two possible approaches in order to select the independent variables this includes:

On the one hand, we can select the independent variables in the primary loop as evaporation and condensation temperatures. This is the common approach used, for example, in the characterization of the main component in HPs, the compressor. Nevertheless, the use of condensation and evaporation temperatures has the disadvantage of needing measurements in the refrigerant loop. These measurements are monitored by researchers in the laboratory but they are not usually available in real installations.

Then, on the other hand, another approach is to select the independent variables in the secondary loop. In this situation, the boundary conditions for the condenser or evaporator are characterized by only two independent variables, and these variables can be any combination of the three variables controlled in the secondary loops: inlet and outlet temperatures, and mass flow rate. This corresponds to the normal operation of these units. The source/sink conditions and user demand, together with the compressor frequency, set the condensation and evaporation temperatures in the refrigerant loop.

Therefore, due to the fact that secondary loop variables are usually monitored in real installations and are easy to measure, they will be selected as independent variables in order to construct the final correlations for the characterization of the performance in this unit. In this sense, the final models will depend only on the external variables, which will make it easier to use in many possible scenarios.

Now, we are going to identify the set of independent variables for the DSHP. The following subsection describes the independent variables involved in the process for the main operating modes, Winter Ground or Winter Air modes, when the DSHP works as a brine-to-water HP or air-to-water HP.

3.2.1 Winter Ground and Winter Air modes

Figure 3.3 shows a schematic diagram for Winter Ground mode including the independent variables in the hydraulic loops (User and Ground loops), the response variables of interest (\dot{Q}_c , \dot{Q}_e and \dot{W}_c) and the compressor frequency (f_c).

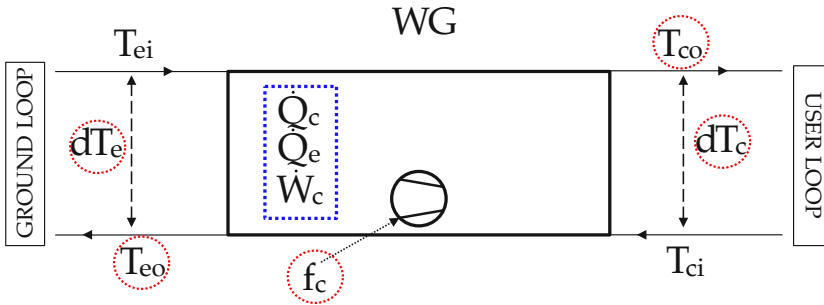


Figure 3.3: Winter Ground: Response (blue) and control (red) variables

In this operating mode, the HP works as a geothermal HP. For that reason, the variables controlled on the test bench are the compressor frequency, the mass flow rate in the hydraulic loops (controlled by the frequency of the circulation pumps), the return temperature in the Ground BPHE (T_{ei} , this is the brine return temperature from the borehole HX) and the supply temperature in the User BPHE (T_{co} , this is the hot water supply temperature to the building).

This set of 5 independent variables can be selected in order to model the performance of the unit. However, the independent variables highlighted in red in the figure above were the independent variables selected to model the performance in this operating mode.

The temperature difference across the BPHE (dT_c and dT_e) in the secondary loops was selected rather than the mass flow rate because, in real installations, the inlet and outlet temperatures are usually always measured and monitored while mass flow rate is seldom measured. This is an equivalent representation of the mass flow rate in the secondary loops. When we increase or decrease the velocity of the circulation pumps, the values of dT_c and dT_e also decrease or increase for a given capacity. Both dT_c and dT_e are defined as positive, i.e. $dT_c = T_{co} - T_{ci}$ and $dT_e = T_{ei} - T_{eo}$.

Additionally, the outlet temperature in the secondary side of the BPHE (T_{eo}) was also selected rather than T_{ei} in the evaporator and keeping T_{co} in the condenser. Due to the fact that the BPHEs in this unit always work in counter-current, the secondary outlet temperatures are a better representation of the evaporation or condensation temperatures, which set the refrigerant conditions in the HXs and therefore the performance of the unit.

Selecting the 5 independent variables described above (f_c , T_{eo} , dT_e , T_{co} and dT_c), Equation 3.5, Equation 3.6 and Equation 3.7 allow to the performance of the DSHP to be calculated to include the effect of the auxiliary components:

Winter Ground - Performance including the auxiliary components

$$\dot{Q}_{heating} = \dot{Q}_c(f_c, T_{eo}, dT_e, T_{co}, dT_c) + [\eta_p \cdot \dot{W}_{user,pump} - P_{h,user}] \quad (3.5)$$

$$\dot{Q}_{cooling} = \dot{Q}_e(f_c, T_{eo}, dT_e, T_{co}, dT_c) - [\eta_p \cdot \dot{W}_{ground,pump} - P_{h,ground}] \quad (3.6)$$

$$\dot{W}_{DSHP} = \dot{W}_c(f_c, T_{eo}, dT_e, T_{co}, dT_c) + \dot{W}_{par} + \dot{W}_{user,pump} + \dot{W}_{ground,pump} \quad (3.7)$$

On the one hand, the variables $\dot{Q}_{heating}$ and $\dot{Q}_{cooling}$ are the capacities including the heat injected by the circulation pumps⁴, where $\dot{Q}_{heating}$ rejects the heat from the condenser to the User and $\dot{Q}_{cooling}$ absorbs the heat from the Ground in the evaporator. Then, \dot{W}_{DSHP} is the total electrical consumption of the unit and it is calculated by adding the parasitic and circulation pumps consumption to the compressor energy consumption.

On the other hand, the highlighted parts in the equations above are the variables \dot{W}_c , \dot{Q}_c and \dot{Q}_e and they exclude the effect of the auxiliary components. As mentioned above, they have been selected as response variables to obtain the empirical models in this chapter (if we exclude the effects of the auxiliary components over the response variables, we will simplify the construction of the response models).

Due to the fact that the inlet and outlet temperatures in the secondary side are measured in the connection pipes of the unit with the hydraulic loops and the unit is equipped with internal circulation pumps, the calculated capacities in the secondary loops are $\dot{Q}_{heating}$ and $\dot{Q}_{cooling}$. Therefore, these capacities have been corrected with Equation 3.5 and Equation 3.6 to obtain the values of \dot{Q}_c and \dot{Q}_e . Regarding \dot{W}_c , it is directly measured on the test bench and it includes the inverter losses. In the following sections, we will refer to the performance of the unit as \dot{W}_c , \dot{Q}_e and \dot{Q}_c . However, the characterization of the auxiliary components is also included in Appendix C, and the equations above together with the expressions defined in Appendix C allows the effect of the auxiliary components to be included in the empirical models developed in this chapter.

Now, setting aside the Winter Ground mode and focusing on the Winter Air mode, Figure 3.4 shows the variables involved in the process when the unit works as an air-to-water HP.

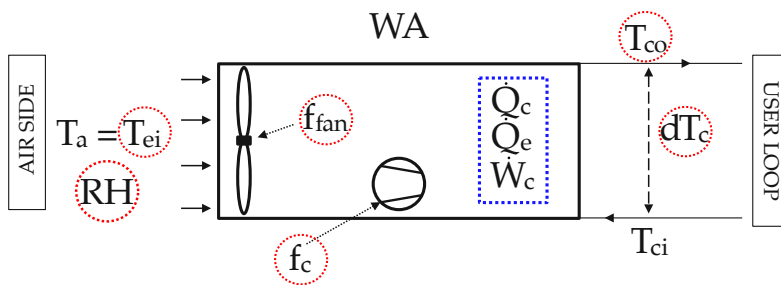


Figure 3.4: Winter Air: Response (blue) and control (red) variables

⁴The heat injected by the circulation pump is calculated as the product of electrical consumption with the electric motor efficiency and removing the hydraulic power. It increases the heating capacity and decreases the cooling capacity.

This figure includes the same independent variables selected in Winter Ground with the exception of the variables which are related to the evaporator. In Winter Air, the unit works with the Round Tube Plate Fin Heat Exchanger (RTPFHx) as the evaporator and therefore the variables T_{co} and dT_c are replaced by the air temperature at the inlet of the RTPFHx (T_{ei} , this is the temperature set in the climatic chamber) and the frequency of the fan (f_{fan} , fixed with the unit control of the DSHP on the test bench). Furthermore, the relative humidity (RH) is an extra variable to take into account.

Due to the fact that the RTPFHx works as an evaporator, it may involve condensation of humid air—sensible and latent capacity—on the heat transfer surfaces when the external wall surfaces of the round tubes are below the corresponding dew point temperatures. As will be seen in Subsection 3.4.2, the inclusion of RH as an extra independent variable will be necessary in the calculation of the capacities and it is excluded from the compressor energy consumption.

Taking into account the selected independent variables (f_c , T_{ei} , f_{fan} , RH , T_{co} and dT_c), Equation 3.8, Equation 3.9⁵ and Equation 3.10 are the expressions to calculate the performance including the effect of the auxiliary components:

Winter Air - Performance including the auxiliary components

$$\dot{Q}_{heating} = \dot{Q}_c(f_c, T_{ei}, f_{fan}, RH, T_{co}, dT_c) + [\eta_p \cdot \dot{W}_{user,pump} - P_{h,user}] \quad (3.8)$$

$$\dot{Q}_{cooling} = \dot{Q}_e(f_c, T_{ei}, f_{fan}, RH, T_{co}, dT_c) \quad (3.9)$$

$$\dot{W}_{DSHP} = \dot{W}_c(f_c, T_{ei}, f_{fan}, T_{co}, dT_c) + \dot{W}_{par} + \dot{W}_{user,pump} + \dot{W}_{fan} \quad (3.10)$$

In this case, the electrical consumption of the circulation pump in the evaporator side is replaced by the electrical consumption of the fan. Regarding the calculated capacity in the RTPFHx, it is not directly estimated from the air side⁶. It has been obtained by first estimating the refrigerant mass flow rate from the balance in the condenser.

⁵The test bench does not include the required sensors to quantify the fan's static pressure difference and air flow rate. Moreover, this unit is not designed for duct connection, and following the guidelines of the BS EN Standard 14511-3:2018, a correction of the capacity with the heat injected by fans is not required (It is expected to be low).

⁶This method was rejected because it implies a higher degree of complexity and it is necessary to attach an airflow measuring device, such as a nozzle airflow measuring apparatus, in the air discharge.

Then, like Winter Ground mode, the highlighted parts in the equations above (\dot{W}_c , \dot{Q}_c and \dot{Q}_e) will be the response variables correlated in this chapter and they exclude the effect of the auxiliary components. The Appendix C also includes the characterization of the fan.

3.2.2 Summer and DHW modes

The subsection above analyzes the independent variables selected in the main operating modes, Winter Ground and Winter Air. As concerns the remaining operating modes, Summer Ground, DHW Ground and DHW User modes operate with two BPHEs as evaporator and condenser (brine-to-water or water-to-water HP).

They will have the same schematic diagram as Winter Ground (Figure 3.3 on page 60) but work with the corresponding hydraulic loops selected in each operating mode (see Subsection 2.2.2 on page 28). Therefore, they will include the same independent variables as Winter Ground mode. Equation 3.5, Equation 3.6 and Equation 3.7 must be modified to include the correction with the corresponding circulation pumps (this depends on the hydraulic loops selected).

Then, on the other hand, DHW Air mode operates with the RTPFHx as the evaporator including the same independent variables as Winter Air mode and replacing the User loop with the DHW loop in the condenser. Equation 3.8 and Equation 3.10 must be modified including the correction with the circulation pump in the DHW loop.

Finally, Figure 3.5 is the schematic diagram for Summer Air mode, and the only difference from Winter Air mode is that now the condenser is the RTPFHx and the evaporator is the User BPHE. Therefore, it will include the independent variables f_c , T_{eo} , dT_e , T_{ci} and f_{fan} . The relative humidity is not included as an independent variable because there are no dehumidification conditions when the RTPFHx works as a condenser.

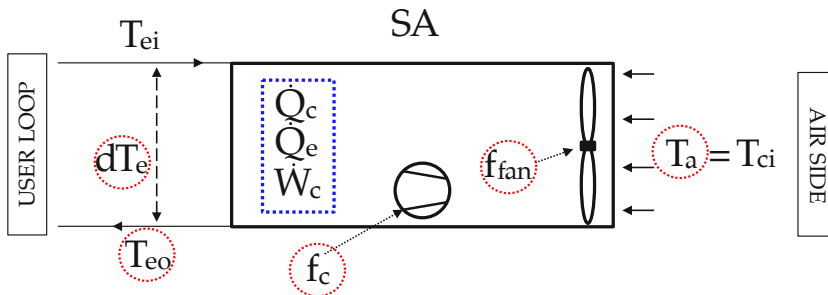


Figure 3.5: Summer Air: Response (blue) and control (red) variables

Equation 3.11, Equation 3.12 and Equation 3.13 are the expressions to calculate the performance including the effect of the auxiliary components in Summer Air mode:

Summer Air - Performance including the auxiliary components

$$\dot{Q}_{heating} = \dot{Q}_c(f_c, T_{eo}, dT_e, T_{ci}, f_{fan}) \quad (3.11)$$

$$\dot{Q}_{cooling} = \dot{Q}_e(f_c, T_{eo}, dT_e, T_{ci}, f_{fan}) - [\eta_p \cdot \dot{W}_{user,pump} - P_{h,user}] \quad (3.12)$$

$$\dot{W}_{DSHP} = \dot{W}_c(f_c, T_{eo}, dT_e, T_{ci}, f_{fan}) + \dot{W}_{par} + \dot{W}_{user,pump} + \dot{W}_{fan} \quad (3.13)$$

3.3 IMST-ART and the virtual test database

Once we have identified all the independent variables for the 7 operating modes, the second step is to look for the functionals that are able to predict the response variables (\dot{Q}_c , \dot{Q}_e and \dot{W}_c) with the highest accuracy in the experimental domain.

For this purpose, researchers usually carry out experimental campaigns in order to characterize the performance of units, such as the characterization of refrigerating compressors in the 2-dimensional space defined by the condensation and evaporation temperatures (AHRI 540, 2020).

However, as we have identified in the subsections above the experimental domain for new heat pumps and refrigeration equipment is increased because many of them incorporate variable speed compressors and also variable speed circulation pumps and fans. In the DSHP, this experimental domain is a 6-dimensional space in Winter Air and DHW Air modes —RH is an extra parameter— and a 5-dimensional space for the rest of operating modes (Winter Ground, Summer Ground, DHW Ground, DHW User and Summer Air).

Unfortunately, the characterization of equipment with so many independent variables can not be completed exhaustively by experimentation because of the huge amount of data required. The definition of the experimental points to test will be a function of the number of independent variables and the number of levels⁷ selected for each one.

⁷In experimentation, the number of levels of independent variables is the number of specific values measured on a continuous scale.

For example, if we consider the Winter Ground mode with 5 independent variables, we will obtain the following full factorial test plans:

- 3 levels for each variable $\Rightarrow 3^5 = 243$ test points.
- 4 levels for each variable $\Rightarrow 4^5 = 1024$ test points.
- 5 levels for each variable $\Rightarrow 5^5 = 3125$ test points.

Considering therefore that the performance dependence with each independent variable is not linear and it includes at least some curvature, the number of levels to be considered should be around 4 or 5. This results in really large experimental matrices with around 1000 or 3000 test points, and in this unit these amount of points must be tested in each of the 7 operating modes (around 7000 or 21000 test points). Of course, it would be completely unfeasible to conduct a full factorial plan, due to the significant amount of time and effort needed and an alternative approach is required.

Against this background, we had to deal with the following challenges:

1. *“How can the full factorial plans be reduced?”*
2. *“Which is the functional that better fits the heat pump performance?”*

The solution adopted in this work to answer the questions above was to combine the use of some Design of Experiments (DoE) methodologies and the generation of virtual tests with the simulation tool IMST-ART.

On the one hand, the DoE methodology allow us to obtain compact test matrices with the objective of simplifying the experimental stage. These methodologies substitute the full factorial plan with a minimum amount of test points with the maximum statistical inference.

On the other hand, current simulation tools in the field of engineering bring us the opportunity to substitute experimentation with simulation results. This allow us to generate a huge amount of simulation data that would otherwise be impossible to obtain by experimentation.

In this regard, the IMST-ART model of the DSHP introduced and validated in Chapter 2 was used to perform a virtual database with simulation data for the entire working maps of the DSHP. The generated database includes the full factorial for the 5 control variables, selecting 5 levels for each one.

Therefore, a high-resolution mesh grid of virtual tests for the response surfaces was generated, allowing us to explore the better polynomials to predict the HP performance and, once the polynomial models were obtained, they were adjusted with the experimental results of the sample defined by the DoE.

Table 2.7 on page 49 shows the levels selected for the variables controlled on the test bench in order to simulate the full factorial plans and generate a virtual database with a total of **21875 points**.

In Winter Air and DHW Air modes, the relative humidity was also included as an independent variable in the polynomial models to take into account the dehumidification process in the evaporator. However, in order to decrease the number of simulation points, it is not included in the full factorial, and the humidity conditions in the air are fixed as a dry and wet bulb temperature difference of 1°C in air inlet temperatures of less than 11°C . Then, the humidity ratio corresponding to the moist air conditions of $11(10)^\circ\text{C}$ is fixed in air inlet temperatures greater than 11°C .

According to the methodology described above, Section 3.4 explores the best functionals for the polynomial models, Section 3.5 shows the comparison between different DoE methodologies and the construction of the final experimental test matrices and Section 3.6 describes the final adjustment of the polynomial models obtained in Section 3.4 with the experimental results.

3.4 Exploring functionals with the virtual database

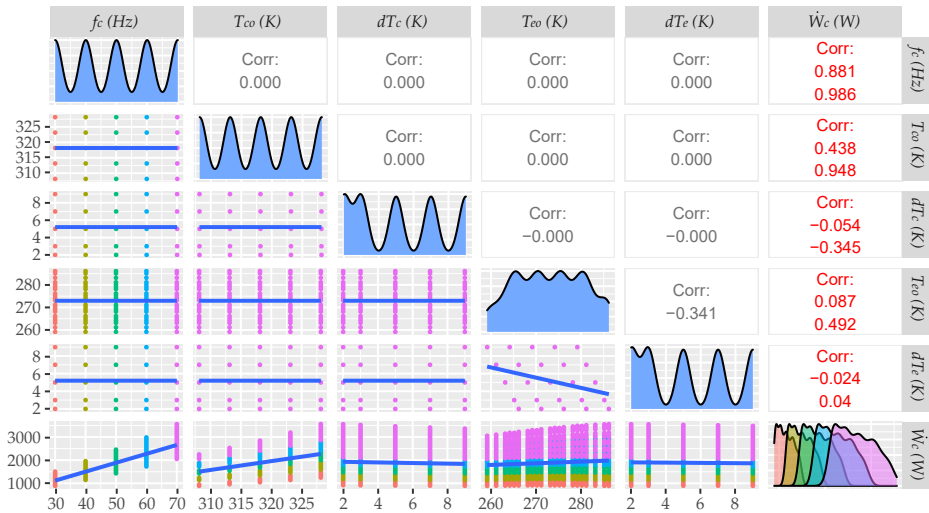
The development of an empirical polynomial model is not an easy task and it involves the use of statistical and graphical techniques in order to find a suitable functional to characterize the response variables of interest. As mentioned above, the response variables selected are \dot{W}_c , \dot{Q}_c and \dot{Q}_e and they will be characterized for the 7 operating modes. Therefore, we need to find 21 polynomial equations to characterize the performance of the DSHP. In order to describe the process appropriately and obtain the best polynomial equations, this section includes the construction of the polynomial models for the main operating mode, Winter Ground. Furthermore, Subsection 3.4.2 describes how to include the dehumidification effect in Winter Air for the characterization of the capacities. Then, Section 3.7 and Appendix G shows a summary for the final polynomial models developed in the 7 operating modes, including the adjustment to the experimental data (this adjustment will be described in Section 3.6).

3.4.1 Winter Ground polynomial models

Starting with the characterization of the performance in Winter Ground mode, the first thing to do is to explore the relationship between the independent variables and the response variables.

Typically, matrix correlation plots are the most common graphs to show this. For example, selecting \dot{W}_c to start the analysis, Figure 3.6 provides the correlation matrix⁸ for this response variable.

Figure 3.6: WG: Correlation matrix \dot{W}_c



It includes the following information:

- The density plots with the representation of the data distribution for the independent and response variables (the diagonal of the matrix). In these density plots, the y-axis is rescaled between 0 and 1, where the x-axis shows the data distribution for each variable. In this sense, the independent variables show a single density curve—we can observe the different levels considered—to simplify the visualization. On the other hand, several density curves have been included for each compressor frequencies in the response variable (\dot{W}_c , right lower corner plot). This will be useful later when analyzing transformations on the response variable to simplify the final models.

⁸This type of plot can be generated easily in  with the graphical package ggplot2 (Wickham et al., 2021a) and the extension package GGally (Schloerke et al., 2021).

- Scatter plots with all the bivariate representations (at the lower part of the diagonal). It also includes a linear adjustment for all the data represented in each plot. These graphs are very useful for analyzing the various dependencies between the response and independent variables.
- Color series in the scatter plots. The selected variable to define the series is the compressor frequency (f_c). That is the main independent variable, as we will soon see.
- The correlation coefficient of Pearson (ccp) and the partial correlation coefficient of Pearson ($pccp$) (at the upper part of the diagonal). These coefficients measure the level of correlation between variables. They will be discussed in more detail later.
- Variable labels at the top (x-axis) and right side (y-axis). By combining them, we can identify: the variables considered on the scatter plot axes, the pair of variables to which the correlation coefficients refer, and the variable considered in the density plots.

As we can see, only the last row and column provides us with information about the relationship between \dot{W}_c and the independent variables. The other plots are the combination between independent variables, and therefore it does not demonstrate any dependence. The only dependence is presented in the plot T_{e0} vs dT_e . This is because the real control variable on the test bench, and also the one selected to generate the full factorial in the virtual test, is T_{ei} ($T_{e0} = T_{ei} - dT_e$).

However, we obtained better results in the performance characterization when we took T_{e0} as the independent variable rather than T_{ei} . As previously discussed, the secondary outlet temperatures are a better representation of the evaporation and condensation temperature when the BPHE work in counter-current, so we took T_{e0} as the independent variable rather than T_{ei} , and therefore it is included in the correlation matrix.

First, we are going to analyze the results of the statistical coefficients of Pearson. These two coefficients measure the relationship between two continuous variables and show how strong this is. The value varies between -1 and 1, with the following results:

- 1 indicates a strong positive relationship.
- -1 indicates a strong negative relationship.
- A result of zero indicates no relationship at all.

This helps us to identify which are the most important independent variables. As given in Figure 3.6, the main independent variable that fixes the value of \dot{W}_c is the compressor frequency with a strong positive relationship. This is consistent with the normal operation of compressors. When the compressor speed is increased, the mass flow rate and the electrical consumption also increase.

In this case, the values for the correlation coefficient and the partial correlation coefficient among \dot{W}_c and f_c are 0.881 and 0.986. The difference between them is that the partial correlation coefficient measures the dependence between the response and one independent variable, when the effect of the other independent variables is removed. Therefore, it is a better statistical indicator when we have so many independent variables, removing the interaction effect between them. As we can see in the correlation matrix above, the value of the partial correlation coefficient always indicates a stronger dependence compared to the correlation coefficient in all the relationships between the response and independent variables. As we will soon see, this value of 0.986 between \dot{W}_c and f_c will allow us to transform the response and simplify the model construction.

The second main independent variable is T_{co} which also has a strong positive relationship with the compressor consumption ($pccp = 0.948$). Once again, this result is to be expected, due to the fact that the compressor installed in the DSHP is a scroll compressor. As has been reported in Marchante-Avellaneda et al. (2023a), and as we will see in Chapter 4, when the frequency remains constant, the electrical consumption in scroll compressors is mainly fixed by the condensation temperature (or condensation pressure). Now, if we set the boundary conditions in the condenser, selecting the independent variables in the secondary loop, this dependence will be reproduced mainly by T_{co} and, to a lesser extent, dT_c . In this case, the $pccp$ of dT_c is -0.345 with a slight negative dependence. When the value of dT_c is increased, the mass flow rate in the secondary loop of the condenser decreases. So, for a given supply temperature to the building, we have a slight reduction in the condensation temperature and pressure ratio, a slight rise in the compressor efficiency, and therefore a small reduction in \dot{W}_c .

Then, regarding the independent variables relating to the evaporator, we have a positive relationship between \dot{W}_c and T_{eo} ($pccp = 0.492$, a secondary dependence compared to f_c and T_{co}), and a null or really small effect with dT_e ($pccp = 0.04$). The effect of the evaporation temperature/pressure on \dot{W}_c was also analysed in Chapter 4 for a large number of scroll compressors, and it presented a positive (low range of evaporation pressure) or negative relationship (middle range of evaporation pressure). In this case, we obtained similar results for the relationship between \dot{W}_c and T_{eo} : a positive relationship in the WG mode (low range of P_e) and a negative relationship in SG mode with a $pccp = -0.596$ (middle range of P_e).

From the discussion above we can say that, in WG mode, the compressor consumption is mainly fixed by f_c and T_{co} with a strong positive relationship. Then, we have a secondary positive dependence with T_{eo} and small dependencies with dT_c (negative) and dT_e (really small and slight positive).

These results can also be observed in the scatter plots of the correlation matrix. Of course, having so many independent variables makes identifying the relationships a complicated process. The clearest dependencies can be seen for the main variables f_c and then T_{co} . As mentioned above, the first one shows a clear positive dependence and, by selecting a specific level of frequency, we can observe a vertical deviation due to the effect of the other independent variables. This deviation is even greater as f_c increases, and it is confirmed by the density plot of \dot{W}_c (The range on the x-axis of the density plot, the right lower corner plot, increases at higher compressor frequencies). Therefore, if we construct a polynomial model to correlate \dot{W}_c , we will need to consider some interaction terms with f_c . Then, the scatter plot of T_{co} shows the same positive dependence with a high degree of vertical deviation. In this case, thanks to the color series, we can identify that this vertical deviation is mostly caused by f_c .

Now, making the same analysis on \dot{Q}_c and \dot{Q}_e , Figure 3.7 and Figure 3.8 shows the correlation matrices for the capacities.

Figure 3.7: WG: Correlation matrix \dot{Q}_c

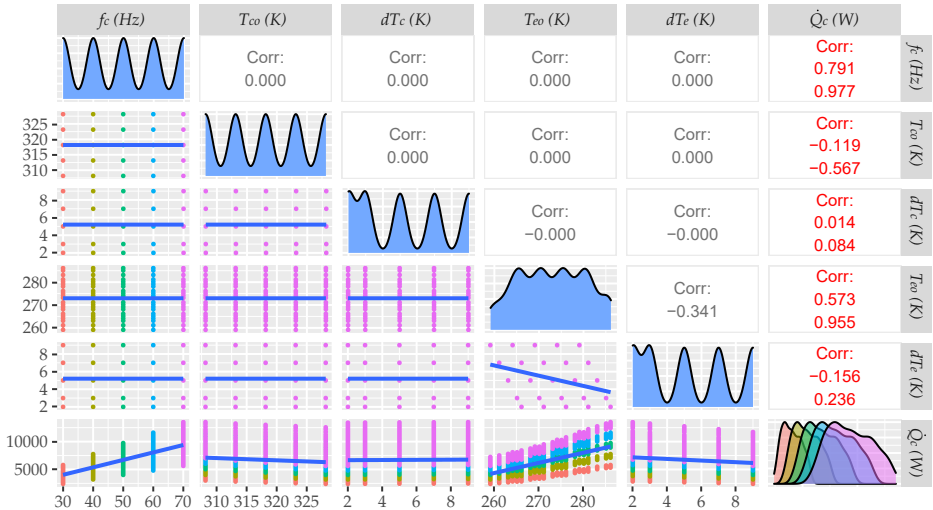
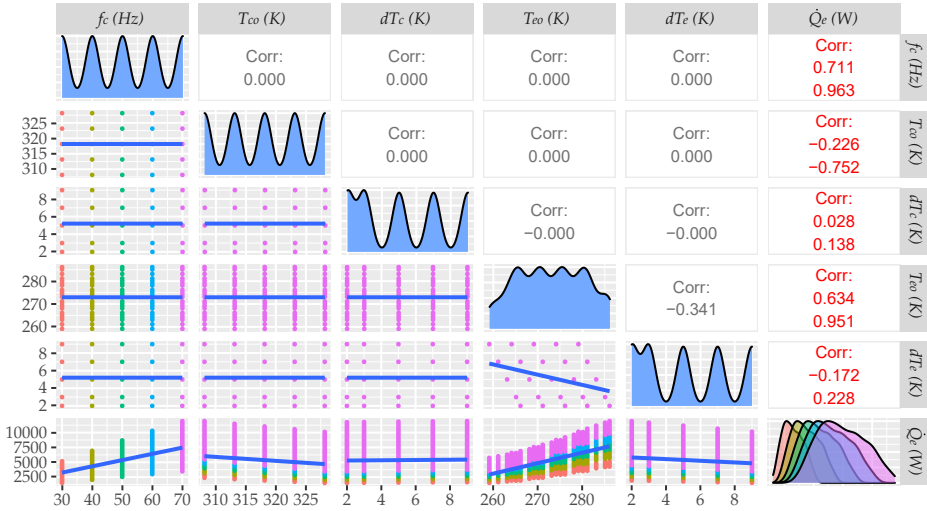


Figure 3.8: WG: Correlation matrix \dot{Q}_e 

According to the calculated values of the $pccp$, the order from the most important variables (strong dependence) to secondary variables (slight dependence) is:

- $\dot{Q}_c \Rightarrow f_c$ (0.977), T_{eo} (0.955), T_{co} (-0.567), dT_e (0.236) and dT_c (0.084).
- $\dot{Q}_e \Rightarrow f_c$ (0.963), T_{eo} (0.951), T_{co} (-0.752), dT_e (0.228) and dT_c (0.138).

Therefore, the main independent variable is still f_c with the same strong positive relationship. We have always obtained the same results for all the response variables (\dot{W}_c , \dot{Q}_c and \dot{Q}_e) in the 7 operating modes. However, for the capacities, the other main independent variable is T_{eo} rather than T_{co} . In this case, as has been reported in Marchante-Avellaneda et al. (2023a), the mass flow rate in scroll compressors is mainly fixed by the evaporation temperature for a given compressor speed, and therefore T_{eo} is now the second main relationship concerning the capacities and, to a lesser extent dT_e .

Then, as concerns the condenser, T_{co} presents a negative dependence and dT_c a slight positive dependence.

On the one hand, when we have high values of hot water production, the condensation temperature is also higher; therefore for a fixed value of evaporation temperature, the pressure ratio increases and the volumetric efficiency on the compressor is decreased, with a negative effect on the capacities. On the other hand, as mentioned above, when dT_c is increased, the mass flow rate in the secondary loop of the condenser decreases. So, we have a slight reduction in the condensation temperature, a slight rise in the volumetric efficiency, and therefore a small rise in the capacities.

Once a preliminary analysis of the relationships between the response and the independent variables has been concluded, the second step is to find a suitable polynomial model to reproduce them.

In this sense, the first model to test would be a simple linear model including all the independent variables. This is the simplest model that we can build, and it should always be the first step when we construct a response surface model. Firstly selecting \dot{W}_c to construct a response surface model, Figure 3.9 and Table 3.2 on the left side show the results for the linear model. These figures and tables can be found on pages 75 and 76. Moreover, they include the results of a second model (stepwise model) that uses automatic term selection tools to simplify the comparison between these two models. This second model will be introduced later, when we finish analyzing the simple linear model.

Analyzing the results, we can establish that this first model, the linear model, with so few terms is not able to predict \dot{W}_c with good accuracy. The graph predicted vs experimental (Figure 3.9-left on page 76) shows high values for MRE, RMSE and CV_{RMSE} . In addition, we can see how the represented points describe a parabola, which is indicative that there are some non-linear relationships not explained by the model. The latter can also be checked in the model's diagnostic plots⁹ (Figure 3.10 on page 76).

The residuals vs fitted plot also shows a parabolic dependence, indicating that the residuals are not uncorrelated due to the unexplained relationships. Furthermore, the normal q-q plot indicates that the residuals do not have a normal distribution. Hence, we need to add more terms to the polynomial model in order to explain these relationships.

Regarding the steps to add terms in a polynomial model, there are different approaches which can be used.

⁹These plots allow us to check whether the regression model works well for the adjusted data. The residual vs fitted plot can reveal relationships not explained by the model. Then the normal q-q plot shows if residuals are normally distributed.


For example, it is possible to construct the model adding terms until the added term is not statistically significant (forward regression). This statistical significance is measured by the p -value¹⁰ considering that a predictor should be included in the model when it has a p -value < 0.05 . Table 3.2 on page 75 also includes the p -value of the predictors adding significance stars to the calculated regression coefficients.

Then, the other option is to use the reverse method (backward regression). In this case, we select a specific polynomial degree including all the predictors in the model (linear terms, interaction terms, etc.). Then, the predictors with highest p -value are removed iteratively until only significant predictors remain.

In both cases, we get compact polynomial models able to predict the response variable with a low deviation. It is important to note that lower order terms should not be removed from the model before higher order terms in the same independent variable, even if it shows a non significant p -value (see Faraway, 2005, pg. 130-131).

It is likely that the methods described above are useful in many applications and provide us with a simple way to construct accurate polynomial models. However, when we have a significant number of independent variables, these methodologies become unwieldy.

In order to simplify the model construction when a significant number of independent variables are involved in the modeled process, a third option is to use the stepwise regression. In this case, the model construction is carried out by an automatic procedure. This method combines backward elimination and forward selection in a criterion-based procedure.¹¹

Selecting this third option applied to a second-order polynomial model and considering the AIC criterion, the stepwise regression procedure obtains the model provided in Figure 3.9 and Table 3.2 on the right side. The `stepAIC()`  function (see Venables and Ripley, 2022, pg. 143) has been used to facilitate the application of the stepwise regression procedure.

¹⁰The p -value is a statistical coefficient to test the null hypothesis over a predictor in a linear regression model. A p -value < 0.05 is statistically significant and it indicates strong evidence against the null hypothesis.

¹¹Commonly, the most used criteria are the Akaike Information Criterion (AIC) and the Bayesian Information Criterion (BIC). Both are statistical coefficients that inform the relationship between the model's prediction error and the number of predictors selected. For model comparison, the model with the lowest AIC or BIC score is preferred.

Table 3.2: WG: Linear model and stepwise model coefficients

	\dot{W}_c (W) (linear model)	\dot{W}_c (W) (stepwise regression model)
(Int.)	-1.413e+04 ($\pm 1.92e+02$)***	7.096e+04 ($\pm 1.35e+03$)***
f_c	3.850e+01 ($\pm 2.26e-01$)***	-2.704e+02 ($\pm 1.63e+00$)***
T_{co}	3.825e+01 ($\pm 4.53e-01$)***	-3.918e+02 ($\pm 6.18e+00$)***
dT_c	-1.310e+01 ($\pm 1.25e+00$)***	1.834e+02 ($\pm 8.66e+00$)***
T_{eo}	7.286e+00 ($\pm 4.53e-01$)***	-6.209e+01 ($\pm 5.62e+00$)***
dT_e	1.500e+00 ($\pm 1.33e+00$)*	-1.498e+01 ($\pm 1.06e+01$)**
(f_c^2)		1.461e-01 ($\pm 2.28e-03$)***
(T_{co}^2)		3.798e-01 ($\pm 9.11e-03$)***
(dT_c^2)		4.150e-01 ($\pm 7.68e-02$)***
(T_{eo}^2)		-2.150e-01 ($\pm 9.11e-03$)***
(dT_e^2)		-1.318e-01 ($\pm 8.02e-02$)**
$f_c \times T_{co}$		7.586e-01 ($\pm 3.81e-03$)***
$f_c \times dT_c$		-2.919e-01 ($\pm 1.05e-02$)***
$f_c \times T_{eo}$		1.989e-01 ($\pm 3.81e-03$)***
$f_c \times dT_e$		3.437e-02 ($\pm 1.12e-02$)***
$T_{co} \times dT_c$		-5.157e-01 ($\pm 2.10e-02$)***
$T_{co} \times T_{eo}$		5.586e-01 ($\pm 7.62e-03$)***
$T_{co} \times dT_e$		1.297e-01 ($\pm 2.24e-02$)***
$dT_c \times T_{eo}$		-8.192e-02 ($\pm 1.98e-02$)***
$T_{eo} \times dT_e$		-9.163e-02 ($\pm 2.78e-02$)***
Num.Obs.	3125	3125
R2 Adj.	0.978	1.000
AIC	37089.8	23799.3
MRE (%)	33.735	5.354
RMSE (W)	91.212	10.829
CV _{RMSE} (%)	4.835	0.574
Range (W)	[890, 3558]	[890, 3558]

^a + p < 0.1, * p < 0.05, ** p < 0.01, *** p < 0.001;

^b Temperatures (K);

^c Compressor frequency (Hz);

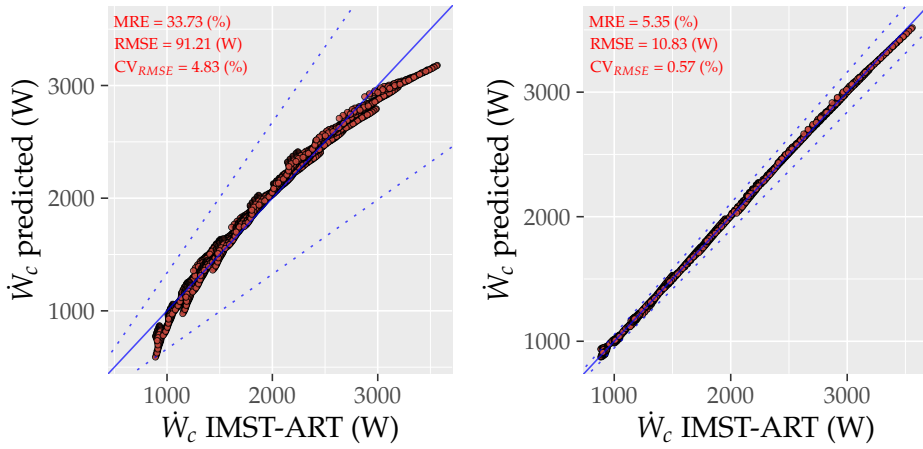


Figure 3.9: WG: Linear model and stepwise model

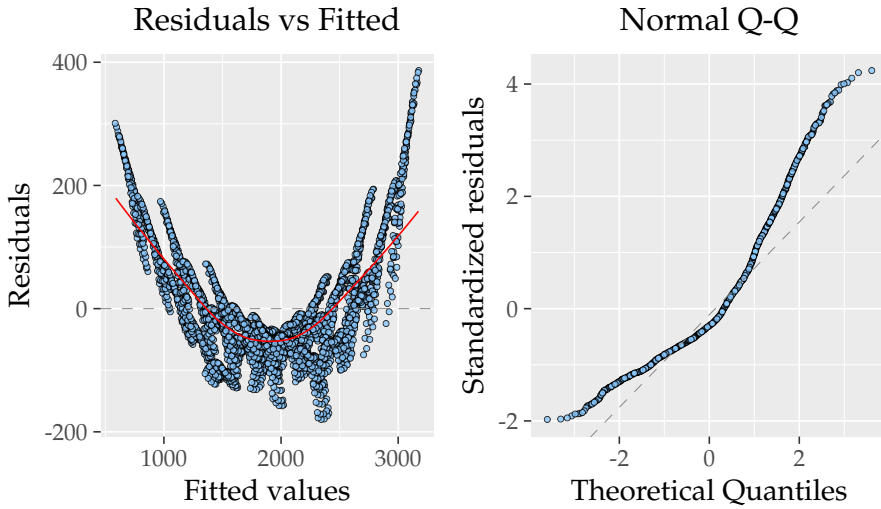


Figure 3.10: WG: Linear model dignostic plots

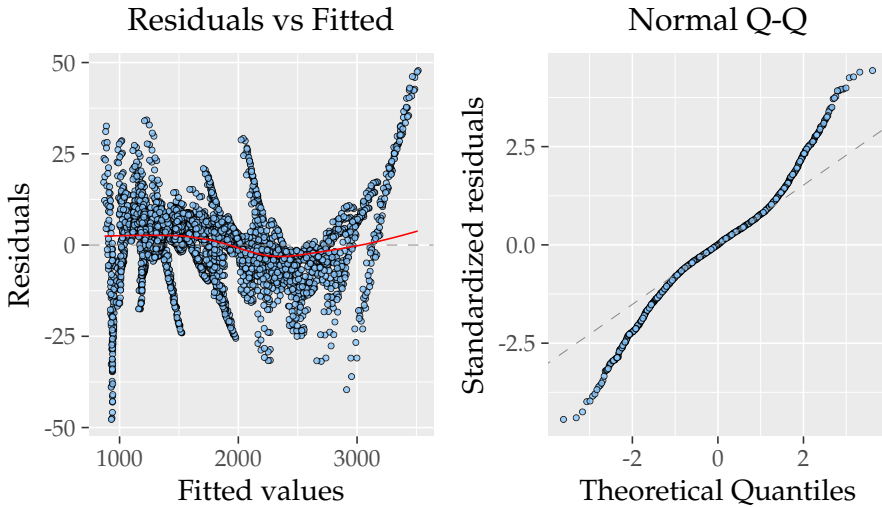


Figure 3.11: WG: Stepwise model diagnostic plots

Let us now consider the results for this second model. We can see that the values of MRE and RMSE have decreased significantly. Moreover, the Figure 3.11 shows a lower scale in the residuals with low grouping patterns and all the regression coefficients included in Table 3.2 on page 75 are statistically significant.

Regarding these regression coefficients, we can compare them with the coefficients obtained at the beginning in the adjustment of the first model. If we look at the sign of each of the coefficients in the simple linear model, we can see that they correspond to the sign obtained in the calculation of the partial correlation coefficients of Pearson (Figure 3.6 on page 68). On the other hand, the second model proposed does not keep this equality. This is completely normal due to a greater number of predictors having been introduced, which may include interaction terms and quadratic terms for the same independent variable. This means that the effect of an independent variable on the response variable is divided into several terms of the model.

However, if we take a look at the total number of terms included in the second model, we will notice that the stepwise methodology has only eliminated one term ($dT_c \times dT_e$), with a total of 20 regression coefficients. It is possible that some terms provide little information despite being statistically significant and the model can be further compacted, but with a total of 20 coefficients the model obtains approximately 5% of MRE. Removing terms will increase this error.

In this sense, applying a transformation in the response variable can simplify the model construction and improve the prediction results. This is a common technique used in regression models. For example, the Box-Cox power transformation is commonly applied when models violate the normality assumption (see Kabacoff, 2011, pg. 199-200). Another possibility is to carry out a transformation using the independent variables. For this purpose, we need to know and understand the physical process modeled.

From the results obtained in the correlation matrices, we could see that the most relevant independent variable is f_c when we characterize the compressor consumption and also the capacities, with a strong positive dependence. Mainly, the compressor speed will fix the refrigerant mass flow rate in the primary loop and hence the electrical consumption in the compressor and the capacities. From the equations to calculate the compressor efficiency and the volumetric efficiency, Equation 3.14, Equation 3.15 and Equation 3.16 show how to remove the main dependence of the compressor speed in the unit performance:

$$\dot{W}_c = \frac{\dot{m}_{ref} \Delta h_{is}}{\eta_c} \Rightarrow \dot{W}_c = \rho_s n V_s \frac{\eta_v}{\eta_c} \Delta h_{is} \Rightarrow \boxed{\frac{\dot{W}_c}{n} = \rho_s V_s \Delta h_{is} \frac{\eta_v}{\eta_c}} \quad (3.14)$$

$$\dot{Q}_c = \dot{m}_{ref} \Delta h_{23} \Rightarrow \dot{Q}_c = \rho_s n V_s \eta_v \Delta h_{23} \Rightarrow \boxed{\frac{\dot{Q}_c}{n} = \rho_s V_s \eta_v \Delta h_{23}} \quad (3.15)$$

$$\dot{Q}_e = \dot{m}_{ref} \Delta h_{13} \Rightarrow \dot{Q}_e = \rho_s n V_s \eta_v \Delta h_{13} \Rightarrow \boxed{\frac{\dot{Q}_e}{n} = \rho_s V_s \eta_v \Delta h_{13}} \quad (3.16)$$

Therefore, a possible transformation to apply could be to divide the response variables by f_c , so we obtain \dot{W}_c/f_c , \dot{Q}_c/f_c , and \dot{Q}_e/f_c as new response variables. Figure 3.12 shows the effect when we apply this transformation, plotting \dot{W}_c and \dot{W}_c/f_c as a function of the pressure ratio. Clearly, the major effects of f_c are removed from the response variable \dot{W}_c/f_c . The figure on the left side shows different groups or levels for the electrical consumption depending on the compressor speed but, once the transformation is applied, the figure on the right side shows how these levels converge in a single group with only a slight dependence of the compressor speed¹².

¹²The efficiencies show a slight dependence on speed in scroll compressors.

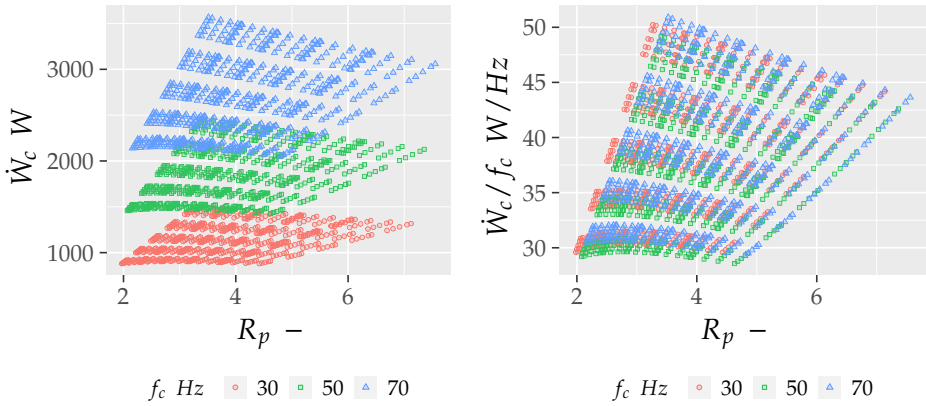


Figure 3.12: WG: \dot{W}_c and \dot{W}_c/f_c vs pressure ratio

At this time, it is important to keep in mind that, when a transformation is applied, the interpretations must be based on the transformed variables, not on the original variables. Thus, it is recommended to regenerate the correlation matrices and recheck the dependencies of the new response variables with the independent variables. Figure 3.13, Figure 3.14 and Figure 3.15 are the correlation matrices generated for the new response variables.

Figure 3.13: WG: Correlation matrix \dot{W}_c/f_c

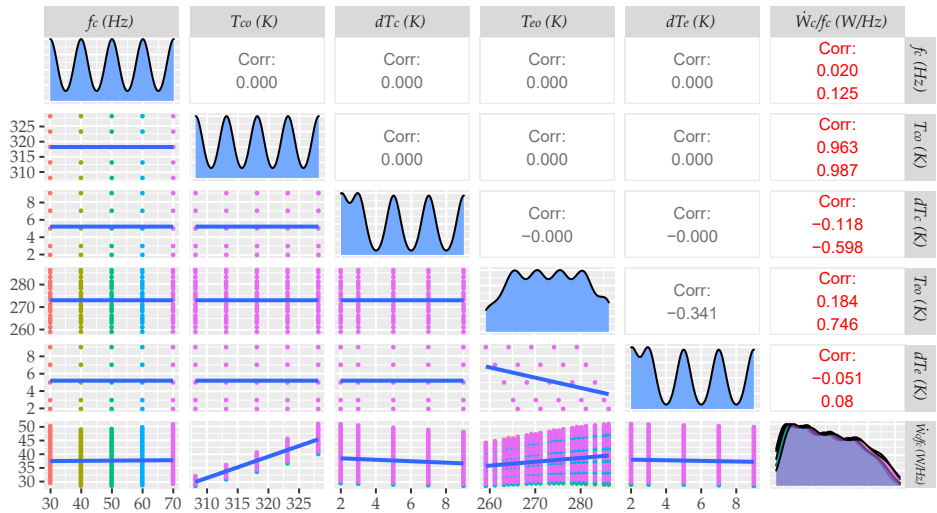


Figure 3.14: WG: Correlation matrix \dot{Q}_c / f_c

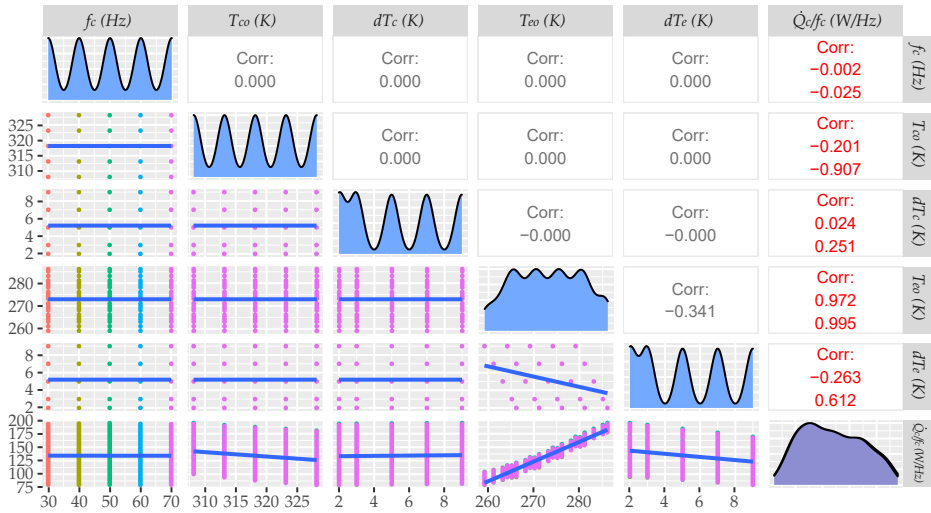
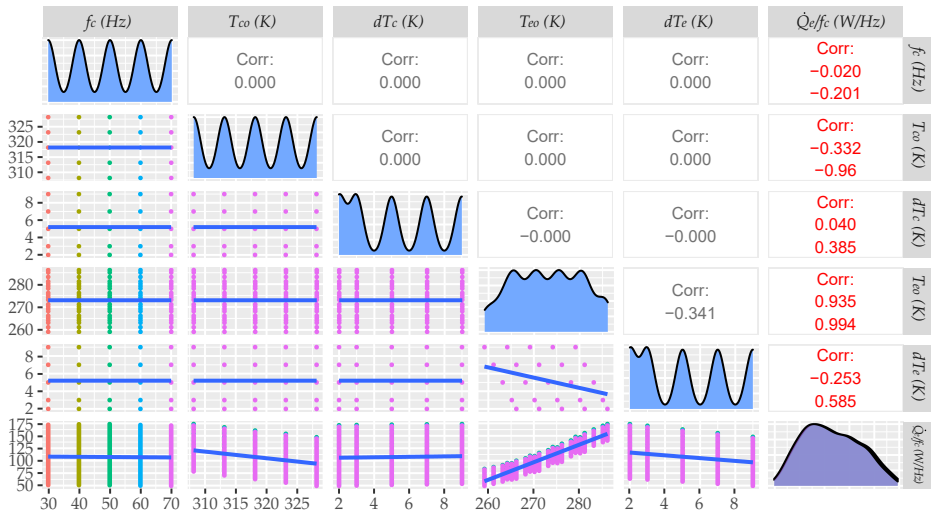


Figure 3.15: WG: Correlation matrix \dot{Q}_e / f_c



If we look at the correlation matrices included above, we will also see that the dependence on the compressor frequency has been practically removed. Then, regarding the values of the $pccp$, we can see that they increase for the rest of the independent variables, maintaining the same sign. Therefore, the rest of the dependencies continue to maintain the same trend with a greater significance.

Let us now include a final response surface model for the characterization of \dot{W}_c/f_c rather than \dot{W}_c . In order to build it, the stepwise regression method was applied considering a second-order polynomial with a greater penalty in the terms of inclusion. The objective was to include only the most relevant terms to obtain a compact polynomial model without distribution patterns in the residuals plot. The independent variable f_c is also included in order to reproduce the second-order dependencies that the transformation has not eliminated. Moreover, an extra term ($1/f_c$) was also included to decrease the error prediction. This coefficient corresponds to an interception term when we recalculate \dot{W}_c from \dot{W}_c/f_c . Table 3.3, Figure 3.16 and Figure 3.17 include the results for this last model.

Table 3.3: WG: \dot{W}_c/f_c model

	\dot{W}_c/f_c (W/Hz)
(Int.)	1.162e+03 ($\pm 1.35e+01$)***
(T_{co}^2)	7.612e-03 ($\pm 1.00e-04$)***
T_{co}	-6.997e+00 ($\pm 6.74e-02$)***
(T_{eo}^2)	-3.968e-03 ($\pm 7.56e-05$)***
T_{eo}	-1.214e+00 ($\pm 4.83e-02$)***
dT_c	3.013e+00 ($\pm 7.38e-02$)***
dT_e	3.174e-02 ($\pm 1.74e-03$)***
f_c	-1.602e-01 ($\pm 1.08e-02$)***
($1/f_c$)	2.991e+02 ($\pm 2.53e+00$)***
$T_{co} \times T_{eo}$	1.089e-02 ($\pm 7.90e-05$)***
$T_{co} \times dT_c$	-1.029e-02 ($\pm 2.32e-04$)***
$T_{eo} \times f_c$	1.125e-03 ($\pm 3.95e-05$)***
Num.Obs.	3125
R2 Adj.	1.000
AIC	-4384.6
MRE (%)	1.385
RMSE (W)	5.524
CV_{RMSE} (%)	0.293
Range (W)	[890, 3558]

^a + $p < 0.1$, * $p < 0.05$, ** $p < 0.01$, *** $p < 0.001$;

^b Temperatures (K);

^c Compressor frequency (Hz);

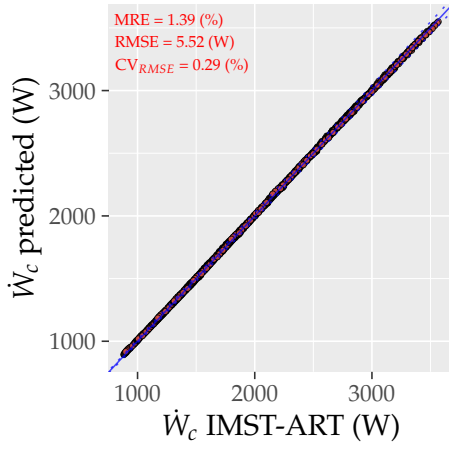


Figure 3.16: WG: \dot{W}_c/f_c model

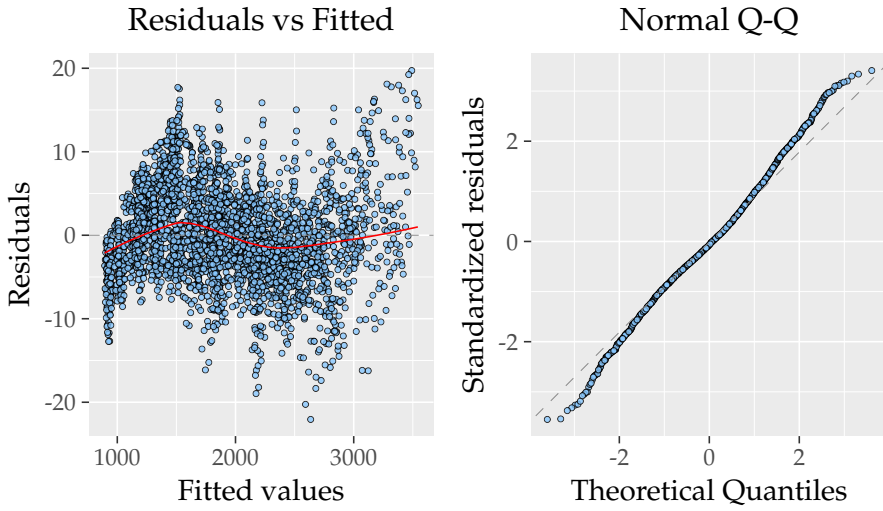


Figure 3.17: WG: \dot{W}_c/f_c model diagnostic plot

As can be seen in the results included above, this last model improves the results of the second model adjusted with a significant reduction in the number of regression coefficients, with an MRE of less than 2%. The values of MRE, RMSE and CV_{RMSE} have been recalculated for the compressor consumption rather than \dot{W}_c/f_c in order to compare the results with the previous models adjusted. Moreover, the Figure 3.17 on the left side shows a lower scale in the residuals without grouping patterns and the residuals have a normal distribution (Figure 3.17-right). These residuals have also been recalculated as values for the compressor consumption.

Therefore, due to the fact that this last model has a lower prediction error with only 12 coefficients, it has been selected as the final model for the characterization of the compressor energy consumption in Winter Ground. Regarding the capacities, if we apply the same steps described above, we will obtain the same polynomial model but with the interaction term $T_{co} \times dT_c$ removed as a non significant term. These results are summarized in Section 3.7 on page 102 and Appendix G, together with the models obtained for the rest of the operating modes.

3.4.2 Winter Air polynomial models

In order to not extend the explanation, this subsection only includes some special aspects to consider when we characterize an aerothermal unit. This mainly relates to how to include the dehumidification effect in the unit performance when the RTPFHx works as an evaporator.

This effect does not influence the characterization of the compressor consumption, but it must be included in the characterization of the capacities. It directly affects the evaporator capacity, increasing its value due to the extra latent capacity when dehumidification conditions are present. Then, this rise in the evaporator capacity will also modify the value of the condenser capacity ($\dot{Q}_c = \dot{Q}_e + \xi \dot{W}_c$).

As in Winter Ground mode, the response variables characterized have been \dot{W}_c/f_c , \dot{Q}_c/f_c and \dot{Q}_e/f_c and the polynomial models have been obtained considering a second-order polynomial and the stepwise methodology. The independent variables to include are f_c , T_{ei} , f_{fan} , T_{co} , dT_c and the humidity conditions fixed by RH . Additionally, during the model construction, it was found that applying a transformation over the predictor f_{fan} and considering $1/f_{fan}$ as an independent variable improved the results. Then, the extra term $1/f_c$, considered in Winter Ground, is also included.

Regarding the humidity conditions in the evaporator, the independent variable fixed on the test bench is the relative humidity (RH) of the climatic chamber.

At the beginning, this variable was considered in the model's construction in order to introduce the dehumidification effect. However, directly considering RH

as a predictor only slightly improved the results, and the analysis of the residuals continued to show effects not explained by the model.

This was an expected value due to the fact that the dehumidification process in the RTPFHx occurs only when the external wall surfaces of the round tubes are below the corresponding dew point temperatures, but:

1. "How can we reproduce the dehumidification effect in a polynomial model?"
2. "Which is the independent variable to include when the external variables are the only input information?"

Clearly, the independent variable selected must be able to increase the capacity value taking into account the latent heat under dehumidification conditions. On the other hand, this term should not modify the value of the capacity when there is no condensation in the RTPFHx.

The solution adopted was to estimate the difference between the air inlet humidity ratio (w_{ai}) and the air humidity ratio considering an air temperature equal to the evaporation temperature¹³ (w_{sat}). Of course, we will need to include the air inlet temperature, the relative humidity and some estimation for the evaporation temperature as input information. This estimation of the evaporation temperature will be necessary to build the polynomial models taking just the external variables into account as available information.

Therefore, in order to estimate the evaporation temperature, a constant temperature approach has been considered. For Winter Air mode, this temperature approach is calculated as the mean of the values obtained in the virtual database, i.e. $\delta T_e = 6$ K. Then, the evaporation temperature and the difference in the humidity ratio are estimated as:

$$T_e \approx T_{ai} - \delta T_e \quad (3.17)$$

$$\Delta w = w_{ai}(T_{ai}, RH, P_{atm}) - w_{sat}(T_{ai} - \delta T_e, P_{atm}) \quad (3.18)$$

The values calculated with the equation above can be positive or negative. If the calculated value is positive, we will have condensation in the RTPFHx. Therefore, in order to reproduce the dehumidification process adequately, we must to recalculate Δw as:

$$\Delta w' = \max [w_{ai}(T_{ai}, RH, P_{atm}) - w_{sat}(T_{ai} - \delta T_e, P_{atm}), 0] \quad (3.19)$$

¹³We consider that the temperature in the external wall surfaces of the round tubes is equal to the evaporation temperature.

Therefore, the $\Delta w'$ calculated with Equation 3.19 provides us with an independent variable able to modify the capacity value only when we have dehumidification conditions in the RTPFHx. The only requirement will be to estimate $\Delta w'$ as is described above using a psychrometric chart or any software able to obtain the psychrometric properties of the humid air. In order to calculate these properties, the *HAPropsSI()* function available in the *Coolprop* software has been used.

Finally, the polynomial models adjusted for Winter Air mode include f_c , T_{ei} , f_{fan} , T_{co} , dT_c and $\Delta w'(T_{ai}, RH, \delta T_e, P_{atm})$ as independent variables. These models are summarized in Section 3.7 and Appendix G.

3.5 DoE: Generating the experimental test matrices

Once the polynomial models have been obtained, the next step is to define the experimental test matrices. The objective will be to obtain experimental results in order to adjust the polynomial models generated in the section above. For that purpose, the Design of Experiments (DoE) methodologies are a powerful tool that can be used to define a suitable sample of experimental points with the maximum statistical inference.

DoE is defined as a branch of statistics that deals with planning and conducting the experimental stage and it is used together with the RSM in order to construct empirical polynomial models. DoE methodologies can in turn be divided into two main typologies. The first one is known as classical DoE and it comprises a set of experimental matrices with an arrangement that is well documented in the literature. The other typology is computer-aided design, where the experimental test matrices are built with complex calculations assisted by computer.

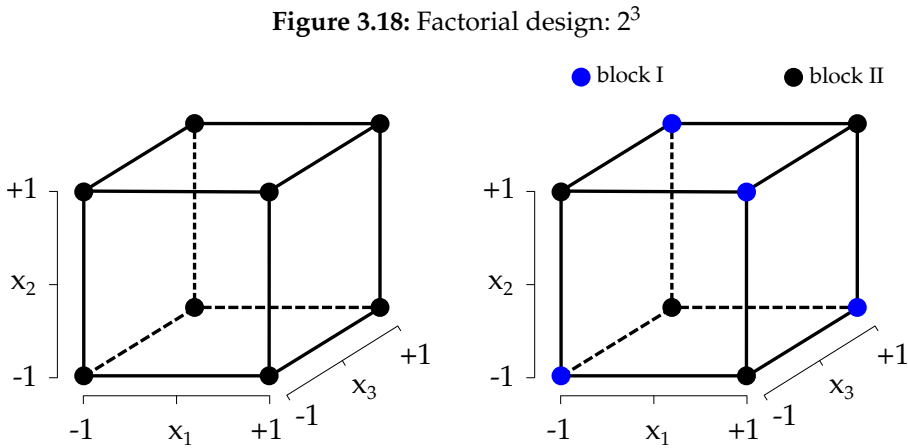
In this chapter we are going to see the use of the first typology, the classical DoE. This typology is easy to implement and, selecting the proper experimental design, we are able to adjust the second-order polynomial models constructed in the previous section using the experimental results. Regarding the second typology, it will be selected in Chapter 4 to explore other alternatives in order to construct experimental designs.

Regarding the classical DoE methodologies, probably the simplest and most extended methodology is factorial design. A complete factorial design with k independent variables is obtained by choosing n_{x_1} levels of independent variable x_1 , n_{x_2} levels of independent variable x_2 , \dots , and n_{x_k} levels of independent variable x_k . Therefore, the total number of points will be $n = n_{x_1} \times n_{x_2} \times \dots \times n_{x_k}$.

In general, this methodology is really useful and the experimental matrices constructed as a factorial design have the property of orthogonality. This is an important property because orthogonality guarantees that we can always estimate the effect of one independent variable or interaction free from any influence due to any other independent variable or interaction.

However, the main problem with this methodology is that the number of tests increases rapidly when we include a greater number of variables or levels. For example, with the 5 independent variables selected in this unit and considering only 3 levels for each one, we would have a total of $3^5 = 243$ experimental points. In this regard, the concepts of blocking and fractionating the experimental designs are really interesting as ways to decrease the total number of experimental points (Box and Draper, 2007, chap. 5). These concepts can be clarified with a simple example.

Figure 3.18 on the left side shows a complete two-level factorial including three independent variables, and the same factorial design is divided in two blocks and represented on the right side.



In the 2^3 design represented above we have a total of 8 runs in which each independent variable occurs at just two levels (-1 and $+1$). The first possibility is to run the complete factorial design in a random order, testing all the points included in Table 3.4.

Table 3.4: Two blocks for a 2^3 design

x_1	x_2	x_3	$x_1x_2x_3$	Block
-1	-1	-1	-1	I
+1	-1	-1	+1	II
-1	+1	-1	+1	II
+1	+1	-1	-1	I
-1	-1	+1	+1	II
+1	-1	+1	-1	I
-1	+1	+1	-1	I
+1	+1	+1	+1	II

However, a better approach may have been to run the experimental design in a series of randomized blocks. Suppose, for example, that we are characterizing the velocity at the inlet section of an RTPFHx¹⁴ and the independent variables in Table 3.4 are the fan speed, the temperature set in the climatic chamber and the humidity. Each experimental run in the Table 3.4 includes the velocity measured with an anemometer at different measuring points (grid arrangement) on the inlet section, and then the inlet velocity is estimated as the mean of these measurements. Therefore, we need considerable time to complete each run and we anticipate that we will need a couple of days to complete the entire test matrix, with two operators taking the experimental measurements. With this type of experimental arrangement, there is a new independent variable to consider: the operator that takes the measurements.

In order to remove the effect of the operator, the experimental runs can be taken in the two blocks represented in Table 3.4. The first block will be run by operator A and the second one by operator B. These blocks have been built considering the negative terms of the three-factor interaction term ($x_1x_2x_3$) column in block I, and its positive terms in block II. So, the blocking factor is the variable operator and their effect is confounded with the three-factor interaction term (blocking generator). Thus, we lose the ability to obtain an accurate estimation of this three-factor interaction term¹⁵, but with the important benefit of having eliminated the effect of the operator variable (Blocks I and II remain orthogonal and altering the apparent effect of the three-factor interaction term with the operator effect does not change the estimate of any of the other effects).

Suppose now that it is not possible to obtain the experimental measurement for the two blocks mentioned above. Our testing capacity is limited and we are interested in obtaining a more compact experimental design.

¹⁴Round Tube Plate Fin Heat exchanger.

¹⁵As mentioned above, high order interaction terms are usually negligible.

In this situation, we can build a fractional design taking only the experimental measurements corresponding to block I (2^{3-1} fractional design; blue points in Figure 3.18 on page 86). This experimental arrangement allow us to run only 4 of the 8 experimental points included in the full factorial design.

Of course, this loss of information will result in not being able to estimate the three-factor interaction term by having selected only one of the blocks. This is not important because, as mentioned above, the effect of this interaction is confounded with the operator, as well as being negligible. Additionally, selecting only one of the blocks will result in the estimation of the main variables being confounded with the two-factor interaction terms¹⁶ (aliasing). This is not a desirable effect because the two-factor interaction terms may not be negligible, so in the example above a fractional design is not recommended.

However, when the process characterized involves a high number of independent variables, the main terms are aliased by high order interaction terms. For example, considering 5 independent variables and two blocks (the blocking generator is the five-factor interaction term), the effect of x_1 is aliased with the four-factor interaction term $x_2x_3x_4x_5$, expected to be negligible. So, fractional design allows us to construct more compact experimental designs with negligible loss of information when the process includes a large number of independent variables.

Against this background, a total of 4 different experimental designs¹⁷ have been selected from the technical literature in order to determine the best experimental design to characterize the DSHP¹⁸:

- Central Composite Design (Box and Wilson, 1951).
- Box & Behnken (Box and Behnken, 1960).
- Hyper-Graeco-Latin-Square (Fisher, 1971).
- Taguchi's matrix L16b (Taguchi, 1987).

¹⁶Aliasing occurs when the design does not include all of the combinations of factor levels.

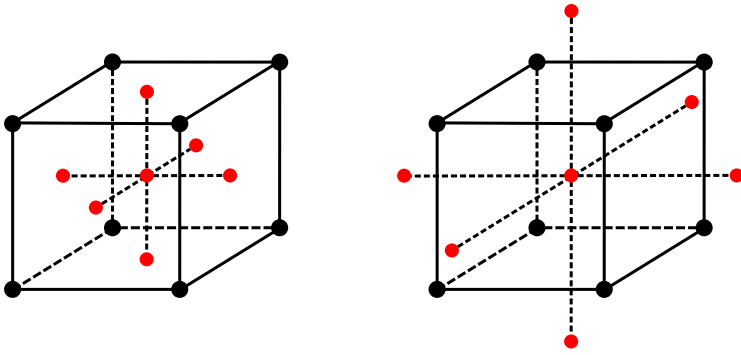
¹⁷They are able to adjust second-order polynomial models with a reduced number of runs.

¹⁸The required levels for the independent variable is fixed by each design. These levels have been selected considering the same variable range used in the virtual test full factorial.

The first design, the Central Composite Design (CCD) is the design most commonly used to adjust second-order models. It is obtained adding axial runs and replicated center points to a 2^k design, so it fixes a total of 3 or 5 levels for the independent variables. These extra points allow us to estimate the curvature effects and the addition of replicated center points provides some increase in the robustness of the design to outlying observations.

Figure 3.19 shows a CCD design including three independent variables in the three dimensional space:

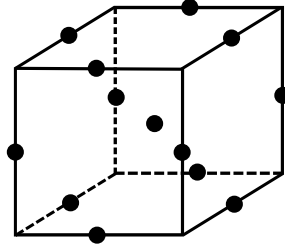
Figure 3.19: Central Composite Design: Face centered (left-hand) vs Circumscribed (right-hand)



As shown in the figure above, we can select different distances for the extra axial points. The CCD can be built as a face centered design, which defines a cuboidal region with only 3 levels for the independent variables, or as a circumscribed design, which defines a spherical region including 5 levels for the independent variables. This last typology has been selected to increase the total number of levels and extend the experimental region being characterized. Box and Draper (2007, chap. 15, Table 15.5) includes the CCD selected for a total of 5 independent variables with 49 experimental runs divided into three blocks.

The second design (Box & Behnken) is an alternative to the CCD. It requires only 3 levels for each independent variable, so it needs a lower number of experimental runs compared to the CCD. This design is built by combining two-level factorial designs with incomplete blocks in a particular manner. For example, selecting three independent variables, the Box & Behnken design includes the midpoints of edges and three replications at the center, Figure 3.20. The Box & Behnken design selected for 5 independent variables is provided in Box and Draper (2007, chap. 15, Table 15.9). It includes 46 experimental runs.

Figure 3.20: Box & Behnken design



The third design selected is the Hyper-Graeco-Latin-Square (HGLS). This type of design was used by Ronald Fisher to design field experiments in agriculture. It is an orthogonal design including the same levels for all the independent variables. The selected HGLS including 5 independent variables is reported in Heckert et al. (2002, section 5.3.3.2.3). It considers a total of 25 experimental runs.

Finally, the last design selected is a Taguchi design. This Japanese engineer has provided a lot of experimental design arrangements constructed for a different number of experimental variables and levels. They are easy to use, as it is only necessary to identify a design with the corresponding number of independent variables. The selected design was the Taguchi's matrix L16b for 5 independent variables and 4 levels (<https://www.york.ac.uk/depts/maths/tables/l16b.htm>).

3.5.1 DoE comparison

Once we have selected a proper set of experimental designs, the next step is to identify the best experimental design to characterize the DSHP. The approach used to identify it was to conduct a comparative study between these designs for the prediction of the performance in the main operating mode, Winter Ground. This comparative study was carried out with the IMST-ART model. Figure 3.21 shows a simple diagram including the necessary steps to compare the different experimental designs with the simulated results obtained with the IMST-ART model. The main objective will be to identify the most advantageous design in terms of prediction accuracy and sample size to perform the experimental matrices to be tested.

First, we obtained the simulated results with the IMST-ART model for the experimental runs defined by each experimental design, and then we adjusted the polynomial models developed in the previous section with these simulation results (i.e. with the sample defined by the experimental design).

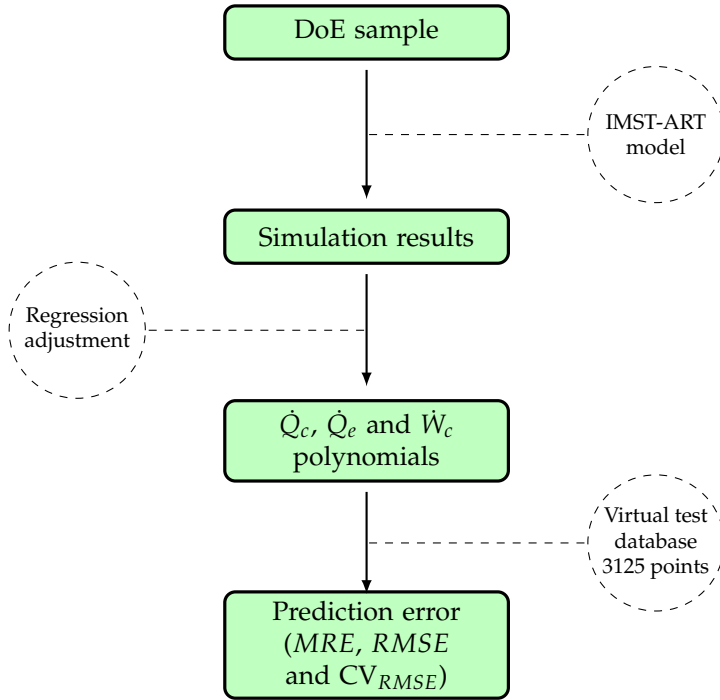


Figure 3.21: DoE comparison (WG mode)

Finally, the predictions from those fitted polynomials were compared with the virtual database¹⁹ covering the entire domain. This gave us a criterion to quantitatively compare the different methodologies and additionally investigate further reduction of the corresponding test matrices by taking only part of their orthogonal blocks.

The results for the comparison between the different DoE arrangements selected is summarized in Table 3.5 on next page. This table shows the Maximum Relative Error (MRE), the Root Mean Square Error (RMSE) and the Coefficient of Variation of the RMSE (CV_{RMSE} ²⁰) obtained for each performance parameter. As can be observed, the maximum deviation is very low for most of the methodologies, taking into account the small number of points in the test matrix employed to adjust the polynomials and the broadness of the 5D solution domain considered.

¹⁹3125 performance values in WG mode

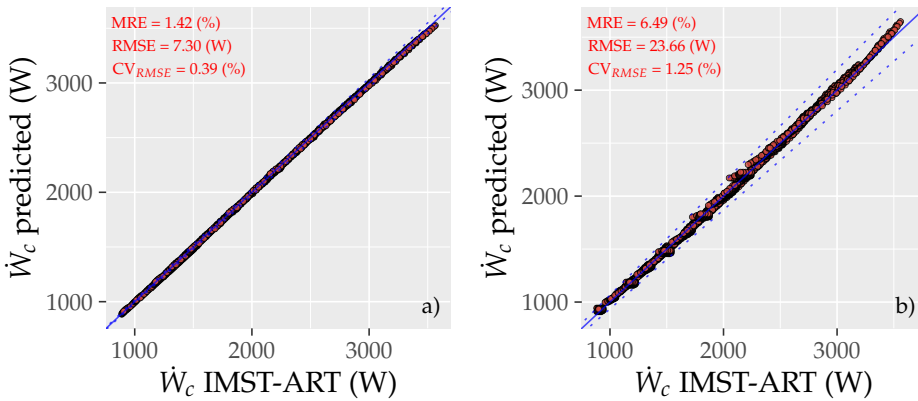
²⁰This coefficient is calculated by dividing RMSE by the average of the analyzed variable.

Table 3.5: DoE methodology results: Performance prediction in WG mode

	\hat{Q}_c			\hat{Q}_e			\hat{W}_c			Test Points
	MRE	RMSE	CV_{RMSE}	MRE	RMSE	CV_{RMSE}	MRE	RMSE	CV_{RMSE}	
	%	W	%	%	W	%	%	W	%	
CCD (Blocks I + III)	1.98	34.29	0.51	3.05	34.47	0.64	1.42	7.30	0.39	30
Box & Behnken	2.63	42.24	0.63	4.84	42.74	0.80	1.55	6.19	0.33	46
Hyper-Graeco-Latin-Square	1.98	35.15	0.52	3.08	34.64	0.65	1.51	7.15	0.38	25
Taguchi	2.44	43.04	0.64	4.81	42.83	0.80	6.49	23.66	1.25	16

As can be seen, the solution provided by the CCD taking into consideration only blocks I and III²¹, which means utilizing only 30 test points, was highly accurate when it comes to determining the response surface. Also, the HGLS provides outstanding results with only 25 points. Still, **we selected the CCD methodology as the final design** with orthogonal blocks I and III, given that it is a very well established and perfectly defined methodology providing very clear and ordered test matrices. Just as an example, Figure 3.22 shows the results of the compressor consumption for the CCD and Taguchi methodologies, clearly demonstrating how the polynomial fitted to the points defined by the CCD methodology is able to perfectly describe the whole response surface of 3125 points (virtual database).

Figure 3.22: WG mode: IMST-ART compressor consumption vs calculated values with the polynomial model fitted to a) blocks I and III of CCD, and b) Taguchi



²¹ As mentioned above, a fractional design offers a compact design with negligible loss of information when we have a high number of independent variables. Removing the block II in the CCD allows us to reduce the number of test points from 49 to 30.

To conclude this section, the experimental test matrices built with the CCD methodology are included in Appendix E. They were used in order to select the experimental points tested on the experimental test bench.

Each of these matrices include a total of 30 experimental points excluding DHW operating modes. The matrices of these modes remove the independent variable T_{co} , reducing the total number of test points to 20. Due to DHW modes are aimed at producing domestic hot water, the value of T_{co} is expected to be constant. However, in order to improve the power prediction of the models, the variable T_{co} is included in the DHW polynomial models built with the virtual database. As we do not have different experimental levels for the T_{co} variable, we will exclude T_{co} from the adjustment applied in the next section (Section 3.6). Therefore, the effect of T_{co} included in the polynomial models is only based on the simulated results generated with the IMST-ART model.

3.6 Adjusting the polynomial models with the experimental data

This section explains how to make the final adjustments to the polynomial models using the experimental results. It is important to remember that the adjusted polynomial models above were obtained using the virtual database generated with the IMST-ART model. Consequently, these polynomial models include the following prediction errors:

- Deviation between the adjusted regression model and the IMST-ART model.
- Deviation between the IMST-ART model and the experimental results.

Therefore, this final readjustment using the experimental results is necessary in order to reduce the prediction errors in the polynomial models.

The readjustment uses the following information:

- The polynomial models adjusted with the IMST-ART-generated virtual database (Section 3.4).
- The experimental results of the samples defined in the chosen experimental design, the Central Composite Design (Section 3.5).

However, “how do we go about readjusting the polynomial models correctly?”

One option is to take the same functional produced with the virtual database and readjust it directly with the experimental data. This involves simply recalculating the model’s regression coefficients while using the same polynomial expression.

Taking the WG operating mode as an example to explore this possibility, Table 3.6 shows the regression model obtained for the \dot{Q}_c prediction adjusted with the virtual database (left column) and the 30 experimental points from the CCD (right column).

Table 3.6: WG: \dot{Q}_c/f_c model adjusted with the virtual and experimental database

	\dot{Q}_c/f_c (W/Hz) (virtual database)	\dot{Q}_c/f_c (W/Hz) (experimental database)
(Int.)	4.617e+03 ($\pm 7.31e+01$)***	2.149e+02 ($\pm 3.44e+03$)
(T_{co}^2)	9.011e-03 ($\pm 5.43e-04$)**	6.477e-03 ($\pm 2.12e-02$)
T_{co}	-1.003e+01 ($\pm 3.65e-01$)***	4.673e+00 ($\pm 1.50e+01$)
(T_{eo}^2)	4.359e-02 ($\pm 4.09e-04$)**	4.623e-02 ($\pm 1.81e-02$)***
T_{eo}	-2.405e+01 ($\pm 2.62e-01$)***	-9.982e+00 ($\pm 1.29e+01$)
dT_c	2.669e-01 ($\pm 8.87e-03$)**	-2.879e-01 ($\pm 3.14e-01$)+
dT_e	8.238e-01 ($\pm 9.44e-03$)***	6.423e-01 ($\pm 3.16e-01$)***
f_c	2.826e-01 ($\pm 5.87e-02$)**	1.897e+00 ($\pm 3.55e+00$)
($1/f_c$)	-1.275e+02 ($\pm 1.37e+01$)***	1.159e+03 ($\pm 8.04e+02$)**
$T_{co} \times T_{eo}$	1.278e-02 ($\pm 4.27e-04$)***	-3.444e-02 ($\pm 2.64e-02$)*
$T_{eo} \times f_c$	-1.270e-03 ($\pm 2.14e-04$)***	-5.405e-03 ($\pm 1.29e-02$)
Num.Obs.	3125	30
R2 Adj.	0.999	0.995
AIC	6170.0	112.5
MRE (%)	5.603 ^d	2.071
RMSE (W)	145.119 ^d	59.187
CV _{RMSE} (%)	2.147 ^d	0.876
Range (W)	[2415, 13500]	[4293, 9988]

^a + p < 0.1, * p < 0.05, ** p < 0.01, *** p < 0.001;

^b Temperatures (K);

^c Compressor frequency (Hz);

^d MRE, RMSE and CV_{RMSE} are calculated with respect to the experimental data and \dot{Q}_c values;

As mentioned in Section 3.4, for the selected functional, a transformation is applied to the response variable, returning a regression model for \dot{Q}_c/f_c . This is why the prediction errors, MRE and RMSE included in Table 3.6 relate to \dot{Q}_c , after obtaining the prediction model and multiplying by f_c . Furthermore, these errors have been calculated while considering the deviation between the prediction

of the regression model and experimental data, including the virtual database-adjusted model.

As we can see from the results, the virtual database-adjusted model has an MRE = 5.6%, an RMSE = 145W and a $CV_{RMSE} = 2.1\%$ for the prediction of the 30 experimental points from the CCD. This is a relatively low prediction error, meaning the IMST-ART model in itself produces good prediction results.

The model adjusted directly with the experimental data, on the other hand, gives a lower prediction error, with an MRE = 2.1%, an RMSE = 59.2W and a $CV_{RMSE} = 0.88\%$. Though it should be noted that many of the regression coefficients are non-significant and do not always maintain the same sign when compared to the virtual database-adjusted regression coefficients.

The T_{co} coefficient, for example, changes from $-1.003e+01$ to $4.673e+00$. Generally speaking, a change in the sign of the coefficient, and therefore its tendency as a predictor, does not make sense if we assume the points generated in the virtual database have a lower deviation than the experimental results. This arbitrary tendency to modify the sign of the regression coefficients coupled with the fact that many of them are non-significant was also observed for the \dot{W}_c and \dot{Q}_e models, regardless of which operating mode is selected.

One possible explanation could be the large difference in the number of points used in the adjustment. It is important to highlight that the virtual database-adjusted polynomials include a full factorial design at five levels for the five independent variables. This equates to a total of 3125 points compared to the 30 points selected in the CCD.

Even though these 30 points were carefully selected in order to obtain as much experimental information as possible, this selection is unable to produce a model homologous to the one generated with the virtual database. In an ideal situation, the tendencies would be the same for all the regression coefficients. If, furthermore, we consider that many of the coefficients have a $p\text{-value} > 0.05$ when adjusting with the experimental data, then this seems to indicate that we should contemplate a more compact model when using the experimental sample from the CCD to get a model homologous to the virtual database-adjusted model.

As such, we can conclude that it would be ill-advised to adjust the model's regression coefficients directly with the experimental data. However:

1. *"Can the information from the virtual database be combined with the experimental results?"*
2. *"Can we improve the prediction error in the models without substantially changing the models obtained with the virtual database?"*

A second option, and the one finally chosen, is to keep the virtual database-adjusted model, including the values for the regression coefficients, and then

readjust using the experimental data. This readjustment employs the partial derivatives of the main terms (linear terms) and the value of the response variable at the CCD center point.

To simplify the explanation and so we can represent it in a 3D graph, let us consider using this new method to readjust a model for a response variable, y , that is only dependent on two independent variables, x_1 and x_2 .

This gives us an initial linear model (Equation 3.20):

$$y = (x_1, x_2) = f(x_1, x_2) \quad (3.20)$$

This model would be adjusted with the virtual database. In this case, as it only depends on two independent variables, we can create a 3D graph of this model, commonly called a response surface (Figure 3.23).

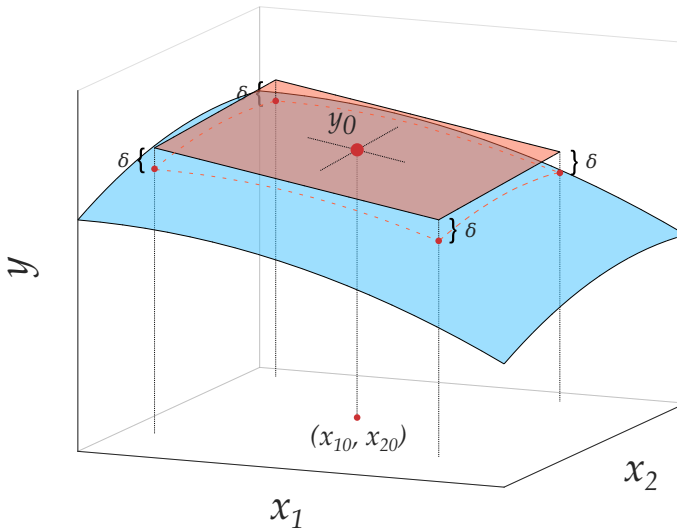


Figure 3.23: Response surface y (blue) and tangent plane (orange) at the point y_0

Figure 3.23 shows the response surface for the model $y(x_1, x_2)$ and the tangent plane at the point $y_0(x_{10}, x_{20})$. This point should be taken as the center point defined in the CCD.

The tangent plane at $y_0(x_{10}, x_{20})$ derives from the equation:

$$z(x_1, x_2) = y_0(x_{10}, x_{20}) + \sum_{i=1}^2 \left. \frac{\partial y}{\partial x_i} \right|_0 \cdot (x_i - x_{i0}) \quad (3.21)$$

To avoid having to modify the response surface, and while also readjusting with the experimental data, we can apply the following correction:

Subtracting the tangent plane equation from the original model for response variable y , then reintroducing it but while including the correction terms (k_0 , k_1 , k_2), gives us Equation 3.22:

$$y^*(x_1, x_2) = k_0 \cdot y_0(x_{10}, x_{20}) + \left(\sum_{i=1}^2 k_i \cdot \frac{\partial y}{\partial x_i} \Big|_0 \cdot (x_i - x_{i0}) \right) + \underbrace{\left[y(x_1, x_2) - y_0(x_{10}, x_{20}) - \left(\sum_{i=1}^2 \frac{\partial y}{\partial x_i} \Big|_0 \cdot (x_i - x_{i0}) \right) \right]}_{\delta(x_1, x_2)} \quad (3.22)$$

By simplifying and rearranging terms, we get Equation 3.23:

$$y^*(x_1, x_2) = y(x_1, x_2) + \left(\sum_{i=1}^2 (k_i - 1) \cdot \frac{\partial y}{\partial x_i} \Big|_0 \cdot (x_i - x_{i0}) \right) + (k_0 - 1) \cdot y_0(x_{10}, x_{20}) \quad (3.23)$$

Considering that $y(x_1, x_2)$ is a linear function, the new response variable $y^*(x_1, x_2)$ will also be a linear function. Therefore, coefficients k_0 , k_1 and k_2 could be adjusted to the experimental data from the CCD by linear regression, where $y^*(x_1, x_2)$ is the new model adjusted to the experimental data. We know the function $y(x_1, x_2)$, and calculating the partial derivatives is straightforward, and we know the coordinates and value of the CCD center point, x_{10} , x_{20} and y_0 .

The method described above applies a readjustment without deforming or modifying the response surface, it merely changes its position. Coefficients k_1 and k_2 mean the response surface can be rotated around the x_1 and x_2 axes, taking the CCD center point y_0 as an anchor point. The term k_0 also adds a further degree of freedom for making corrections by raising or lowering the response surface in the y axis.

With respect to the expected value for coefficients k_1 and k_2 , performing the regression adjustment will return positive values close to 1 if only small corrections are required. This will only occur if the model used to generate the virtual database has a low prediction error. If the coefficients are negative, it is indicative of a poor fit of the model used for the simulated results or possibly a measurement error in the experimental points due to the instruments' uncertainty.

In the next step, we take an arbitrary function, $y = 60 - 0.03x_1^2 - 0.06x_2^2 + 2x_2$, and a center point at the coordinates $x_{10} = x_{20} = 10$ to illustrate the adjustment:

Example 3.1: Experimental readjustment

Polynomial model:

CCD center point:

$$y = 60 - 0.03x_1^2 - 0.06x_2^2 + 2x_2$$

$$x_{10} = 10$$

$$\left. \begin{array}{l} \rightarrow \frac{\partial y}{\partial x_1} \Big|_0 = -0.06x_{10} = -0.6 \\ \rightarrow \frac{\partial y}{\partial x_2} \Big|_0 = 2 - 0.12x_{20} = 0.8 \end{array} \right\}$$

$$x_{20} = 10$$

$$y_0 = 71$$

Polynomial model adjusted:

$$y^* = y + (k_1 - 1) \cdot \frac{\partial y}{\partial x_1} \Big|_0 \cdot (x_1 - x_{10}) + (k_2 - 1) \cdot \frac{\partial y}{\partial x_2} \Big|_0 \cdot (x_2 - x_{20}) + (k_0 - 1) \cdot y_0$$

$$y^* = y + (k_1 - 1) \cdot (-0.6) \cdot (x_1 - 10) + (k_2 - 1) \cdot 0.8 \cdot (x_2 - 10) + (k_0 - 1) \cdot 71$$

Figure 3.24 shows how incorporating some arbitrary values for the set of coefficients k_i , presumably obtained from the linear regression adjustment to a set of experimental data, repositions the response surface in the above example depending on the values used for k_i . The blue surface represents the original model $y(x_1, x_2)$ and the orange surface is the model readjusted with the experimental data $y^*(x_1, x_2)$.

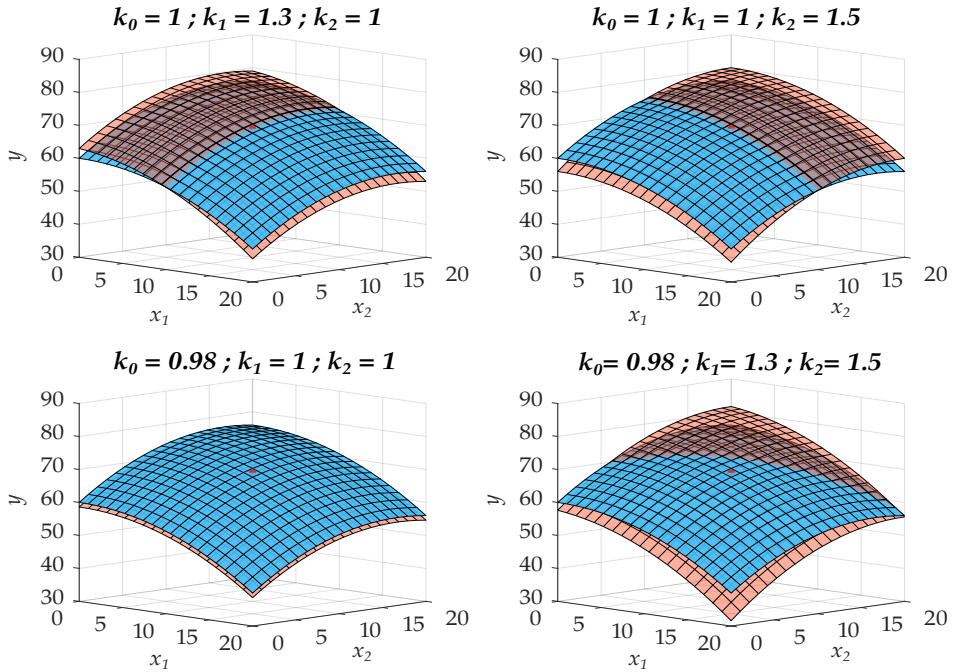


Figure 3.24: Example 3.1: Experimental readjustment for different values of k_i . Original model (blue surface) and readjusted model (orange surface)

The top left and right graphs show the effect of readjusting the k_1 or k_2 terms only, allowing the response surface to be rotated about the x_1 and x_2 axes and center point y_0 . The bottom left graph reveals a slight, constant vertical difference between the two surfaces upon adjusting with k_0 and, lastly, the bottom right graph shows the readjustment using the three coefficients k_i .

This method can be applied regardless of the number of independent variables included in the model. Rearranging Equation 3.23 and taking the general case of n independent variables in the model leads to the general equation:

$$y^*(x_1, \dots, x_n) = y(x_1, \dots, x_n) + \left(\sum_{i=1}^n (k_i - 1) \cdot \frac{\partial y}{\partial x_i} \Big|_0 \cdot (x_i - x_{i0}) \right) + (k_0 - 1) \cdot y_0(x_{10}, \dots, x_{n0}) \quad (3.24)$$

We can now appreciate how the use of such readjustment means we can take advantage of both the simulated results from the IMST-ART model and the experimental results.

By conserving the response surface obtained with a full factorial of 3125 simulated points, we have produced a robust model adjusted throughout the experimental domain, thus ruling out the possibility of extrapolation errors. What is more, the possible deviation in the simulated data used for the adjustment with respect to the experimental results is subsequently corrected using the new readjustment methodology described above. This means we can even improve the results from the polynomial models compared to the original model in IMST-ART.

Returning to the \hat{Q}_c model presented in Table 3.6 and readjusting according to the aforementioned method, we obtain the following values for the adjustment coefficients k_i :

Table 3.7: WG: \hat{Q}_c model readjusted with the experimental database

	\hat{Q}_c^* (W)
\hat{Q}_{c0}	1.012e+00 ($\pm 5.66e-03$)***
$k_1(x_1 = f_c)$	9.997e-01 ($\pm 3.33e-02$)***
$k_2(x_2 = T_{e0})$	1.070e+00 ($\pm 4.47e-02$)***
$k_3(x_3 = dT_e)$	7.679e-01 ($\pm 5.68e-01$)*
$k_4(x_4 = T_{c0})$	7.735e-01 ($\pm 2.14e-01$)***
Num.Obs.	30
R2 Adj.	1.000
AIC	368.1
MRE (%)	3.543
RMSE (W)	91.488
CV_{RMSE} (%)	1.354
Range (W)	[4293, 9988]

^a + p < 0.1, * p < 0.05, ** p < 0.01, *** p < 0.001;

^b Temperatures (K);

^c Compressor frequency (Hz);

The above coefficients were obtained by first taking the \dot{Q}_c/f_c model shown in Table 3.6 on page 94 adjusted with the virtual database (left column). Then we multiplied the \dot{Q}_c/f_c model by f_c to get a new polynomial expression, eliminating the transformation carried out on the response variable. Next, we calculated the partial derivatives with respect to each of the independent variables in this new polynomial for \dot{Q}_c and applied Equation 3.24 on page 100. Lastly, considering k_0, k_1, \dots, k_5 to be adjustment coefficients, we applied a regression adjustment using the 30 experimental points from the CCD²².

As we can see, the readjustment leads to an improvement in the model's prediction error. The MRE is just 3.5% instead of 5.6%, the RMSE is 91.5 W compared to 145 W and the CV_{RMSE} is 1.35% instead of 2.15%, thus improving on the prediction error for the original regression model and the IMST-ART model.

With regard to the values of the resulting coefficients, it is notable that they are all positive and close to 1, so the readjustment causes a slight repositioning of the response hypersurface and does not change the sign and therefore the tendency of the coefficients. A negative value was only returned in the case of the predictor dT_c , which indicates that the trend of the condenser capacity with dT_c in the experimental results is not the same as the one obtained in the simulated results.

This negative value was confirmed as being due to experimental uncertainty. The condenser capacity is calculated by means of the secondary balance, obtaining lower water flow rates compared to the evaporator and therefore increasing the experimental uncertainty. This, coupled with the fact that the capacity has very little dependence on the variable dT_c , is responsible for this change in tendency in the experimental readjustment. Therefore, since the model in IMST-ART is insensitive to the measurement uncertainties and given this coefficient exercises an insignificant correction on the model, dT_c was disregarded in the experimental readjustment by eliminating the factor k_5 .

Having finished the description of how to readjust the models to the experimental data, the final results are summarised in Appendix G.

²²The 30-point CCD in WG includes four replicas for the center point. The experimental readjustment is made while taking into account the values of $\dot{Q}_{c0}, f_{c0}, \dots$, that is, the mean of the experimental results for the four center point replicas.

3.7 Final results

Appendix G includes the \dot{W}_c , \dot{Q}_c and \dot{Q}_e models for all operating modes summarized in:

- A first table for each operating mode contains the \dot{W}_c/f_c , \dot{Q}_c/f_c and \dot{Q}_e/f_c polynomial models adjusted with the virtual database. In this table, the polynomial model prediction errors (MRE, RMSE and CV_{RMSE}) are calculated with respect to the simulation results, thus reconverting the values for the estimation of \dot{W}_c , \dot{Q}_c and \dot{Q}_e .
- A second table is also attached with values for the k_i adjustment coefficients obtained from the readjustments with the experimental data. In this case, the prediction errors are expressed with respect to the experimental results. Thus we can obtain the final regression models based on these two tables and Equation 3.24 on page 100.
- Lastly, a series of figures is included as a visual comparison of the adjustment of these models, the model adjusted with the virtual database and the final regression model readjusted with the experimental data.

Regarding the values obtained for the k_i coefficients, the water-to-water and brine-to-water modes obtained positive values close to 1. The DHW User, DHW Ground and Summer Ground modes also obtained a negative value in the k coefficient for the predictor dT_c , therefore, as in Winter Ground mode, it has been removed from the experimental readjustment. Additionally, the Summer Ground mode only includes the k_i coefficients for the main predictors f_c , T_{eo} and T_{co} , due to the rest of coefficients became negative. This is because, as mentioned in the previous chapter (see page 42), the EEV was not able to set the 5K of superheat in some test, with the presence of bubbles upstream of the EEV, and therefore, only 8 experimental points from the total of the 30 test are available for the experimental readjustment.

Then, regarding to the air modes, they obtained similar results that the previous ones. Only, the k coefficient for the predictor f_{fan} in Winter Air and DHW Air modes gets a higher value for the readjustment of \dot{W}_c , and probably indicates that the fan characterization included in the IMST-ART model could be improved. However this coefficient has the same trend with a positive value and therefore, it has not been removed. Finally, some values of the k_i coefficients for the predictors dT_c and dT_e obtained negatives values in the air modes, due to the experimental uncertainty. They have also been removed from the experimental readjustment.

Once the final models have been included in Appendix G, we can see that all the fitted models have a low prediction errors. As a summary, Table 3.8 on next page includes the MRE, RMSE and CV_{RMSE} of the empirical models built for the prediction of \dot{W}_c , \dot{Q}_c and \dot{Q}_e in the 7 operating modes. In order to be in a position to assess whether the experimental readjustment improves the prediction errors, this table includes the prediction error of the original models built with the virtual database and the models readjusted with the methodology described in Section 3.6. Both errors refer to the prediction of the experimental data.

We can see that the prediction errors decrease in the 7 operating modes. Therefore, the empirical models improve the prediction errors of the IMST-ART model, with a value of 1-3% of MRE in most models. Moreover, this polynomial equations are easy to implement, regardless of the programming or simulation tool selected.

Finally, at the end of this section, an example of how to recompose the model with the summarized data provided in Appendix G is included for the \dot{W}_c prediction in Winter Ground mode (Example 3.2).

Table 3.8: Prediction errors for the final polynomial models

	\dot{W}_c		\dot{Q}_c		\dot{Q}_e	
	PM ^a	PMA ^b	PM ^a	PMA ^b	PM ^a	PMA ^b
Winter Ground						
MRE (%)	2.850	2.131	5.603	3.543	4.589	3.351
RMSE (W)	18.181	13.488	145.119	91.488	124.549	77.069
CV _{RMSE} (%)	0.970	0.720	2.147	1.354	2.317	1.434
Summer Ground						
MRE (%)	10.794	1.087	6.979	2.235	5.735	2.122
RMSE (W)	32.104	6.612	261.855	83.672	186.385	80.695
CV _{RMSE} (%)	2.989	0.616	2.943	0.940	2.378	1.029
DHW Ground						
MRE (%)	5.228	1.756	6.862	4.721	4.559	2.100
RMSE (W)	71.717	18.918	257.677	129.369	149.604	64.792
CV _{RMSE} (%)	3.512	0.927	3.449	1.732	2.415	1.046
DHW User						
MRE (%)	5.051	1.505	3.791	2.776	5.775	1.672
RMSE (W)	71.294	15.290	125.186	111.968	273.251	56.137
CV _{RMSE} (%)	3.406	0.730	1.351	1.208	3.625	0.745
Winter Air						
MRE (%)	1.673	1.966	12.379	2.783	13.305	3.325
RMSE (W)	13.864	12.000	621.020	84.117	523.350	83.303
CV _{RMSE} (%)	0.726	0.629	8.085	1.095	8.177	1.302
Summer Air						
MRE (%)	6.523	1.225	6.854	2.791	6.820	2.399
RMSE (W)	71.757	10.685	398.599	88.533	327.614	66.111
CV _{RMSE} (%)	4.377	0.652	4.335	0.963	4.053	0.818
DHW Air						
MRE (%)	4.597	1.681	15.202	4.378	16.962	5.854
RMSE (W)	62.919	17.653	899.789	138.660	813.285	166.491
CV _{RMSE} (%)	3.026	0.849	10.646	1.641	11.474	2.349

^a Polynomial model adjusted with the virtual database and predicting the experimental data;

^b Polynomial model readjusted with the experimental data;

Example 3.2: WG: Final polynomial model for the \dot{W}_c prediction*Polynomial model:*

$$\dot{W}_c = f_c \cdot (a_0 + a_1 \cdot T_{c0}^2 + a_2 \cdot T_{c0} + a_3 \cdot T_{e0}^2 + a_4 \cdot T_{e0} + a_5 \cdot dT_c + a_6 \cdot dT_e + a_7 \cdot f_c + a_8 \cdot 1/f_c + a_9 \cdot T_{c0} \cdot T_{e0} + a_{10} \cdot T_{c0} \cdot dT_c + a_{11} \cdot T_{e0} \cdot f_c)$$

$$\rightarrow \left. \frac{\partial \dot{W}_c}{\partial f_c} \right|_0 = (a_0 + a_1 T_{c0}^2 + a_2 T_{c0} + a_3 T_{e0}^2 + a_4 T_{e0} + a_5 dT_c + a_6 dT_e + a_7 f_{c0} + a_8 1/f_{c0} + a_9 T_{c0} T_{e0} + a_{10} T_{c0} dT_c + a_{11} T_{e0} f_{c0}) + f_{c0} (a_7 - a_8 1/f_{c0}^2 + a_{11} T_{e0}) = 5.186e+01$$

$$\rightarrow \left. \frac{\partial \dot{W}_c}{\partial T_{e0}} \right|_0 = f_{c0} (a_3 (2T_{e0}) + a_4 + a_9 T_{c0} + a_{11} f_{c0}) = 7.033e+00$$

$$\rightarrow \left. \frac{\partial \dot{W}_c}{\partial dT_e} \right|_0 = a_6 f_{c0} = 1.587e+00$$

$$\rightarrow \left. \frac{\partial \dot{W}_c}{\partial T_{c0}} \right|_0 = f_{c0} (a_1 (2T_{c0}) + a_2 + a_9 T_{e0} + a_{10} dT_c) = 3.859e+01$$

$$\rightarrow \left. \frac{\partial \dot{W}_c}{\partial dT_c} \right|_0 = f_{c0} (a_5 + a_{10} T_{c0}) = -1.304e+01$$

where:

$$a_0 = 1.162e+03 \quad a_3 = -3.968e-03 \quad a_6 = 3.174e-02 \quad a_9 = 1.089e-02$$

$$a_1 = 7.612e-03 \quad a_4 = -1.214e+00 \quad a_7 = -1.602e-01 \quad a_{10} = -1.029e-02$$

$$a_2 = -6.997e+00 \quad a_5 = 3.013e+00 \quad a_8 = 2.991e+02 \quad a_{11} = 1.125e-03$$

CCD center point:

$$\dot{W}_{c0} = 1856.612 \text{ (W)}$$

$$dT_{e0} = 4.972 \text{ (K)}$$

$$f_{c0} = 50 \text{ (Hz)}$$

$$T_{c0} = 318.272 \text{ (K)}$$

$$T_{e0} = 273.184 \text{ (K)}$$

$$dT_{c0} = 5.078 \text{ (K)}$$

Polynomial model adjusted:

$$\begin{aligned} \dot{W}_c^* = & \dot{W}_c + (k_1 - 1) \cdot \left. \frac{\partial \dot{W}_c}{\partial f_c} \right|_0 \cdot (f_c - f_{c0}) + (k_2 - 1) \cdot \left. \frac{\partial \dot{W}_c}{\partial T_{e0}} \right|_0 \cdot (T_{e0} - T_{e0}) + \\ & (k_3 - 1) \cdot \left. \frac{\partial \dot{W}_c}{\partial dT_e} \right|_0 \cdot (dT_e - dT_{e0}) + (k_4 - 1) \cdot \left. \frac{\partial \dot{W}_c}{\partial T_{c0}} \right|_0 \cdot (T_{c0} - T_{c0}) + \\ & (k_5 - 1) \cdot \left. \frac{\partial \dot{W}_c}{\partial dT_c} \right|_0 \cdot (dT_c - dT_{c0}) + (k_0 - 1) \cdot \dot{W}_{c0} \end{aligned}$$

where:

$$k_0 = 1.000e+00 \quad k_2 = 1.070e+00 \quad k_4 = 1.046e+00$$

$$k_1 = 9.815e-01 \quad k_3 = 1.274e+00 \quad k_5 = 1.163e+00$$

4

Characterization of compressors: Empirical model approach

CONTENTS

4.1	Introduction	107
4.2	Scroll compressors	112
4.2.1	Response surface analysis	113
4.2.1.1	Energy consumption analysis	114
4.2.1.2	Mass flow rate analysis	120
4.2.2	Evaluation of compressor correlations	124
4.2.2.1	Correlation for energy consumption	124
4.2.2.2	Correlation for mass flow rate	126
4.2.3	Comparison of correlations	128
4.2.3.1	Energy consumption comparison	128
4.2.3.2	Mass flow rate comparison	132
4.2.4	Experimental points required	137
4.3	Reciprocating compressors	142
4.3.1	Response surface analysis	142
4.3.1.1	Energy consumption analysis	143
4.3.1.2	Mass flow rate analysis	149
4.3.2	Evaluation of compressor correlations	151
4.3.2.1	Correlation for energy consumption	151
4.3.2.2	Correlation for mass flow rate	154
4.3.3	Comparison of correlations	154
4.3.3.1	Energy consumption comparison	154
4.3.3.2	Mass flow rate comparison	159
4.3.4	Experimental points required	161
4.4	Comparison of technologies	166
4.5	Summary of results for the polynomial models analyzed	171

4.1 Introduction

Nowadays, mathematical models allow estimation of the refrigeration or heat pump (HP) system's performance, and, therefore, are very useful in assisting the system's design, analysis, and control. The heart of any refrigeration or HP system is the compressor. As reported Chua et al. (2010), the development and improvement of compressor technologies can lead to a reduction in HP electricity consumption of more than 80%. Therefore, its precise description is essential in evaluating the global system performance.

Regarding the compression process, scroll and reciprocating **compressors** are two of the technologies most frequently used for **applications** from **100 W** up to **100 kW**. Over the years, numerous models have been proposed in the literature to estimate the compressor behavior.

The term "compressor model" could be defined as the mathematical transcription of the thermodynamic processes inside the compressor shell. These models mainly aim to predict the compressor performance, i.e., the compressor energy consumption and refrigerant mass flow rate, and they can be classified depending on the detailed level of knowledge (Rasmussen and Jakobsen, 2000). Thus, we can consider theoretical models, based on modelling the thermodynamics of the involved processes across the compressor, or entirely empirical, i.e., based on functionals (for instance, polynomials).

Theoretical models can be purely theoretical (based only on physical principles), or theoretical but adjusted with some empirical coefficients, which help fit the results to performance data, adjusting for effects that have not been adequately represented in their formulation. We will call this last type of model semi-empirical. A thorough review of compressor models has been included in several recent papers, for instance in Byrne et al. (2014) and Hermes et al. (2019).

Although many semi-empirical models have been proposed over the years, fully empirical models are the approach most frequently used by the community to accurately represent compressor behavior. It is the way that most compressor manufacturers report their compressor performance according to the compressor characterization standard (AHRI 540, 2020).

As reported in Cheung and Wang (2018), when semi-empirical models have been compared with empirical models, in the cases where many experimental data points are available all across the compressor envelope, fully empirical models show better agreement in the representation of the compressor performance. This is because semi-empirical models employ pre-defined functionals, with some coefficients that need to be adjusted to experimental data, but with dependences on the input variables that are implicit to the functional and, therefore, cannot be changed in the model's adjustment.

However fully empirical models involve no physics and require experimental data to be fitted. If enough experimental data is available, they will be more flexible allowing their shape to be adapted to the actual compressor performance surface.

Semi-empirical models are, in contrast, able to capture the influence of the main variables in the performance, for instance, pressure ratio, and hence, can give a reasonably good estimation of the compressor performance with a reduced amount of experimental data. However, they cannot reproduce the actual compressor performance with high accuracy. See, for example, Jähnig et al. (2000), Navarro et al. (2007), Cuevas and Lebrun (2009), Tello-Oquendo et al. (2019), and the recent paper by Hermes et al. (2019).

The classical fully empirical model used to characterize the compressor performance is the 10-coefficient third-degree AHRI polynomial (AHRI 540, 2020). These polynomials can accurately predict the compressor performance, i.e., refrigerant mass flow rate, and compressor energy consumption, across its entire working envelope by fitting the 10 coefficients to the experimental data. This approach is mathematically consistent according to the Taylor theorem approach of functions. It considers that a polynomial with a higher degree will produce similar results requiring more experimental points to find the polynomial parameters. However, there is no clear explanation for using a third-degree polynomial to reproduce the compressor performance in the literature. That point is especially critical, considering that the cubic exponent introduces a very sensible term to the location of the experimental information. Furthermore, it could introduce significant deviations when the amount of data is not high or is not appropriately placed over the entire operating range as it is in Jähnig et al. (2000). Therefore, the main disadvantages of AHRI polynomials may be summarized as follow:

- It could introduce important deviations in the prediction of compressor behavior if experimental compressor data are not sufficient or they are not properly distributed.
- The number of experimental data required to have a confident curve is significantly high. The third-degree polynomials give great flexibility to reproduce complex response surfaces. However, the significant number of terms may overfit¹ the simplest response surfaces, and cubic terms could introduce interpolation or extrapolation problems. Therefore, the adjustment of linear regression models should always aim at finding the most compact and simple model that offers the required accuracy.

¹We say a model is overfitted when it fits too closely to the training data but obtains high prediction errors with non-training points (interpolation and extrapolation errors). It occurs because the model is too complicated or has too many features. Generally, by increasing the degree of the polynomial in simple response surfaces, we increase the number of turning points and degrees of freedom of the polynomial, which can lead to capturing noise and not just the underlying trends.

With these two considerations in mind, a few authors have proposed other empirical models, intending to reduce the number of experimental test points required for their fitting and improve the interpolation and extrapolation capabilities of the functionals in comparison with the AHRI polynomial. Among these, the first to be mentioned should be the more compact second-degree polynomial proposed by Shao et al. (2004) for rotary compressors, the functional proposed by Aute et al. (2014), and the proposed by Navarro-Peris et al. (2013).

Considering everything set out above, one should think about three critical questions related to selecting AHRI polynomials when map-based models are required for accurate predictions:

1. *“Is it mandatory to use all of the coefficients of the third-degree polynomials?”*
2. *“What is the minimum number of points required to accurately predict the compressor performance?”*
3. *“Where should these points be placed?”*

Thus, even though the industry widely adopts AHRI polynomials, there is no clear explanation in the literature about these issues, or at least a mathematical analysis that justifies the use of third-degree polynomials to characterize compressors.

On the other hand, related to the second question, it is surprising that the AHRI 540 (2020) does not specify guidelines for the size and location of the experimental samples. Even more so with the sensitivity of the proposed third-degree polynomial models if poor or bad experimental samples are used for its adjustment. One reason is the lack of a wide database of compressor performance over the whole compressor envelope for any compressor design and refrigerants based on experimental results. This experimental database is especially important. Although manufacturers supply the compressor performance map in a wide range of operating conditions, it is usually unclear whether that information comes from internal experimental tests or corresponds to values estimated from some model or interpolation procedure. In this sense, currently, only a few authors have analyzed the topic of how to perform the experimental matrices, see, Aute et al. (2015), Aute and Martin (2016) and Cheung and Wang (2018).

From that point of view, a project founded by AHRI through “*Low-GWP Alternative Refrigerants Evaluation Program*” which supports a massive test campaign of compressors working with different refrigerants has been especially relevant.

Based on all the experimental tests performed under this program and other experimental compressor data available in the literature like the one supplied by Cuevas and Lebrun (2009), this chapter analyzes the energy consumption and mass flow rate of scroll and reciprocating compressors. The main objective will be to better understand its response surfaces’ shape and dependence on the operating parameters in order to provide proper map-based models, selecting in particular the polynomial approach.

From the literature review, it has been found that some authors are currently using other more sophisticated approaches, such as non-parametric models (Afram and Janabi-Sharifi, 2014; Nishiguchi et al., 2010; Nebot-Andrés et al., 2020) or neural networks (Ma et al., 2020). However, these tools lack the simplicity of the AHRI polynomials, significantly reducing the number of potential users. Furthermore, most of these works available have only been tested with a reduced number of compressors and refrigerants; thus, the global applicability of them must be still tested with a wider amount of data.

Therefore, from the response surfaces analysis conducted in this chapter, we will clarify if the third-degree polynomial proposed by the standard is adequate or, in the case that it is not required, determine the optimum degree of the polynomial. Then, using these results, the minimum number of experimental data and where they should place will be addressed. This will reduce the time dedicated to characterizing a compressor properly, considering accurate map-based models, and avoiding undesired deviations in the results obtained from using this kind of model to extrapolate data.

This chapter is structured in two parts. First, the results for scroll compressors and then for reciprocating compressors are included. Both parts include the analysis of the response surface shape, proper polynomial models for its characterization, how to set up the experimental test matrices, and how many points they contain. The polynomials reported include two approaches to select the independent variables. They are defined in terms of temperature (T_e and T_c) or pressure (P_e and P_c). As will be seen below, models defined in terms of pressures have several advantages over those defined in terms of temperature. However, the latter has also been considered due to their widespread use in this type of application.

4.2 Scroll compressors

As is included in Chapter 2, a few years ago, AHRI disclosed a series of performance data for different compressors (scroll and reciprocating), with conventional and new refrigerants and mixtures. These experimental results are included in several reports within the AHRI “*Low-GWP Alternative Refrigerants Evaluation Program*”, including all of their experimental results in the database developed in this PhD thesis.

The following sections will show the analysis conducted in scroll compressors, including the analysis of the experimental data reported by Cuevas and Lebrun (2009) and the following AHRI reports: AHRI 11 (Shrestha et al., 2013a), AHRI 21 (Shrestha et al., 2013b), AHRI 24 (Rajendran and Nicholson, 2013), AHRI 33 (Shrestha et al., 2014), AHRI 34 (Rajendran and Nicholson, 2014a), AHRI 36 (Rajendran and Nicholson, 2014c), AHRI 38 (Rajendran and Nicholson, 2014e), AHRI 39 (Rajendran and Nicholson, 2014f), AHRI 58 (Rajendran et al., 2016a), AHRI 65 (Rajendran et al., 2016b), and AHRI 66 (Suindykov et al., 2016).

This provides us with experimental information for a total of 7 different scroll compressors, and 16 different refrigerants: R410A, R32, DR5, L41a, R404A, ARM31a, D2Y65, L40, R32+R134a, DR7, L41b, R454B, R447A, HPR2A, R32+R34a, R134a.

In these tests, the evaporation and condensation temperatures were changed and conducted at constant superheat and, in some cases, at constant temperature at the compressor inlet, which allowed the influence of this variable on compressor performance to be analyzed. For additional information regarding the main characteristics, composition of new mixtures tested, and test conditions of the analyzed compressors, please refer to Table 2.8 and Table 2.9 on page 50 and 51.

The analysis of the scroll **energy consumption** data have shown two different trends depending on the application range: for **MBP** (Medium Back Pressure) and **HBP** (High Back Pressure) conditions, the compressor energy consumption is almost **independent of the evaporation temperature**. While, for **LBP** (Low Back Pressure) conditions, the compressor energy consumption **decreases** significantly **with** the reduction of the **evaporation temperature** with some kind of hyperbolic behavior. **AHRI 11** and **AHRI 21** compressors were selected as representative of the M/HBP and LBP conditions respectively.

These compressors were selected as they have the **densest test matrix** in its corresponding category and were tested with different refrigerants. The results presented in this chapter will be shown in terms of these two compressors, but the same analysis was verified with the rest of the compressors included in the database. Therefore, the conclusions presented are applicable to all the scroll compressors analyzed in this work. This information is included in Appendix H and Appendix J. The compressor reported in Cuevas and Lebrun (2009) belongs to the M/HBP category.

4.2.1 Response surface analysis

The characterization of compressor performance from the point of view of vapour compression systems depends on a volumetric variable that could be the mass flow or the volumetric efficiency and on an energy consumption variable that could be the energy consumption itself or another variables like the compressor efficiency.

The compressor and volumetric efficiency are given by Equation 4.1 and Equation 4.2. Traditionally, they have been very attractive variables for compressor modelling as they are adimensional and do not show a strong dependence on compressor size or refrigerant.

$$\eta_c = \frac{\dot{m}_{ref}(h_{2s} - h_1)}{\dot{W}_c} = \frac{\dot{m}_{ref}\Delta h_{is}}{\dot{W}_c} \quad (4.1)$$

$$\eta_v = \frac{\dot{m}_{ref}}{\rho_s V_s n} \quad (4.2)$$

These facts have made some authors focus on these variables to model the compressor behavior. Moreover, other authors have proposed non-dimensional parameters, similar to the efficiencies, which are even more general and provide a slightly better estimation of the compressor performance. See, for example, Pierre (1982), Da Riva and Del Col (2011) or Navarro-Peris et al. (2013).

4.2.1.1 Energy consumption analysis

Even considering the previously commented advantages, characterizing the compressor energy consumption in terms of the compressor efficiency is more complex than just fitting a polynomial directly to the energy consumption, as shown in the following.

Figure 4.1 represents the compressor efficiency versus pressure ratio for the compressors ZP21K5E-PFV (report AHRI 11) and ZS21KAE-PFV (report AHRI 21), taking into account all the experimental points tested with the reference refrigerants, R410A and R404A. Three sets of data were measured, corresponding to three different conditions at the suction: constant superheat of 11K, constant superheat of 22K, and constant return temperature of 18°C.

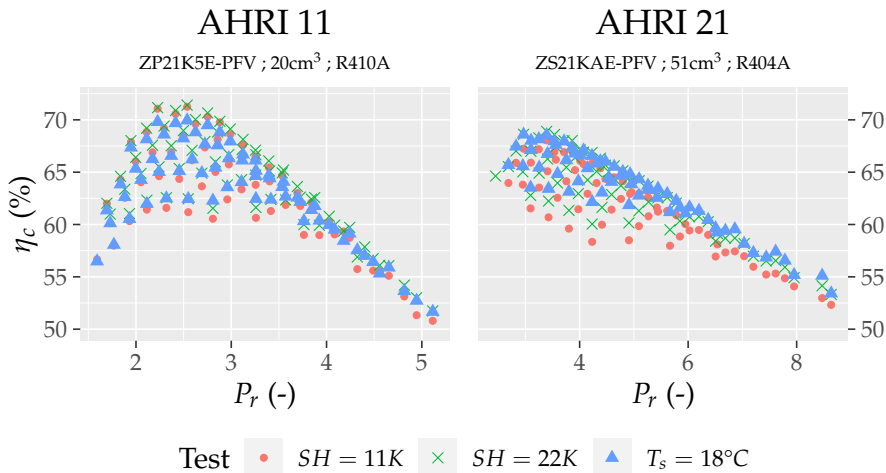


Figure 4.1: η_c as a function of P_r (AHRI 11 R410A and AHRI 21 R404A)

Figure 4.1 shows the typical shape as a function of the pressure ratio. It shows that a critical variable in the description of compressor efficiency is the pressure ratio, which in some way justifies why this consideration is extended in the literature.

However, the figure also shows that, in this case, where the experimental data includes the entire compressor envelope, there are other complex cross-influences between the evaporator and condensation temperatures, leading to a wide scattering across the average trend versus pressure ratio. The usual statement that the compressor efficiency has its optimum at a certain pressure ratio is a great simplification. It is only valid for compressors with an approximately constant evaporation range, like compressors for air conditioning or chillers. Furthermore, looking at the results in global terms, it is observed that this local maximum is shifted to higher pressure ratios as evaporation pressure increases.

Figure 4.2 plots compressor efficiency as a function of evaporation and condensation temperatures for a constant superheat of 11K and the reference refrigerant for each compressor. It also includes, in red points, the location in the experimental domain for the experimental test available for the refrigerant and conditions mentioned. One can see the high resolution available in both compressors with a total of approximately 65 test points for each of them.

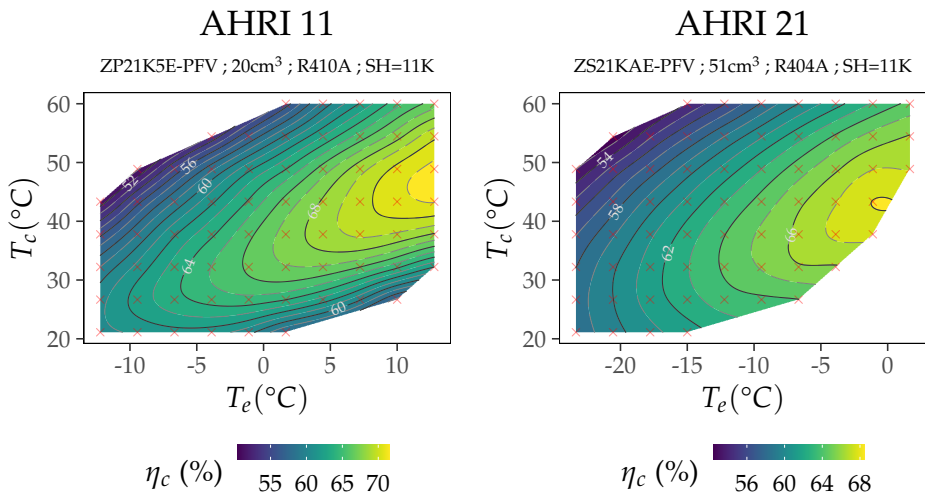


Figure 4.2: η_c contour plot, temp. domain (AHRI 11 R410A and AHRI 21 R404A. SH=11K)

This figure shows that compressor efficiency depends on both variables—evaporation and condensation temperatures—and its maximum values are placed at the highest evaporation temperature values.

Additionally, from the experimental data in the reports, it can be stated that the compressor inlet temperature has a noticeable influence on compressor efficiency, as it tends to rise as superheat rises.

In general, the highest efficiencies are found for superheats of 22K, except at low evaporation temperatures where a return temperature of 18°C is imposed, and the superheat is higher than 22K. It is possible to notice this with a simple plot of the compressor efficiency depending on the evaporation temperature for each level of condensation temperature (Figure 4.3).

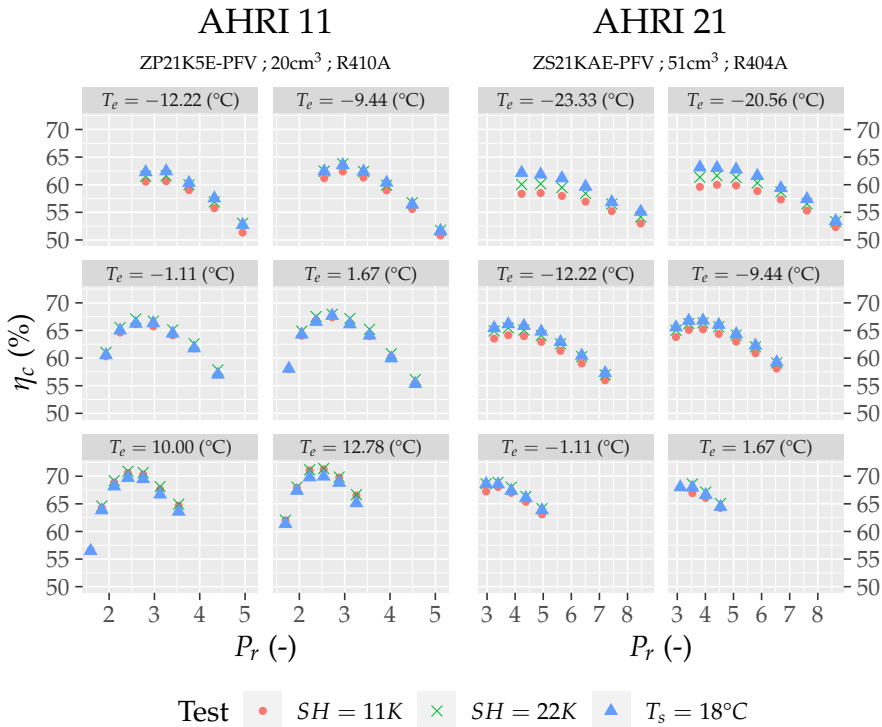


Figure 4.3: η_c as a function of P_r at given levels of T_e (AHRI 11 R410A and AHRI 21 R404A)

In other words, compressor efficiency is a complex function of evaporation and condensation conditions plus the superheat. Moreover, selecting the compressor efficiency as a response variable and considering the shape observed in Figure 4.2, one can see that the location of the experimental sample is critical, where the location of the optimum efficiency is a priori unknown. Therefore, these features make developing a function representing this variable to characterize the energy consumption and perform the corresponding test matrices a challenging tasks.

In contrast, if one represents the compressor consumption versus the evaporation and condensation temperatures (Figure 4.4), the influence of superheat is reduced significantly. So, if the suction conditions considered in the adjustment of the polynomials are modified, it is unnecessary to make any correction to the energy consumption. It can be considered independent of the suction temperature or SH.

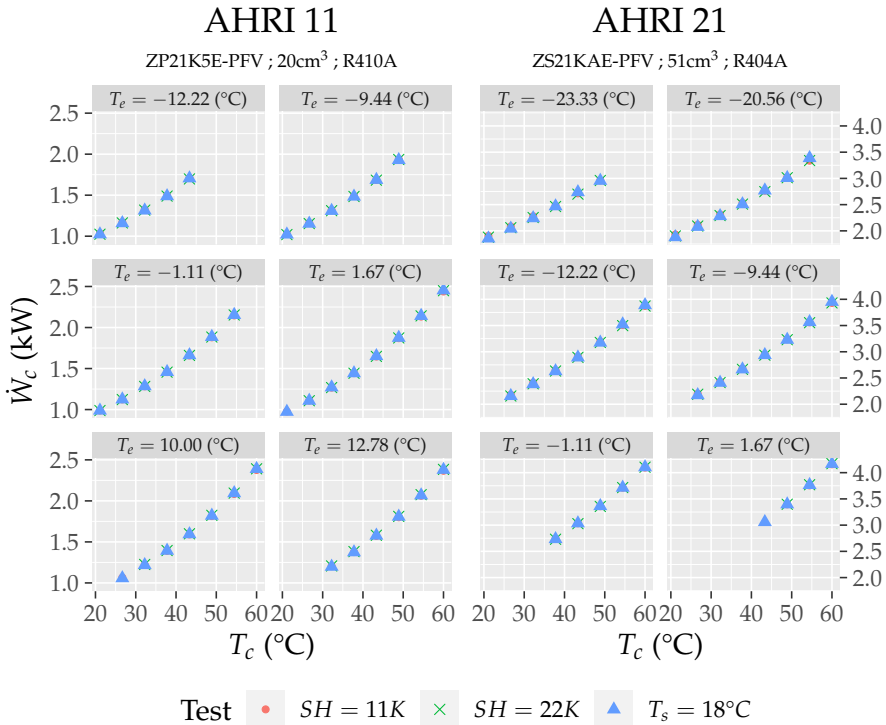


Figure 4.4: \dot{W}_c as a function of T_c at given levels of T_e (AHRI 11 R410A and AHRI 21 R404A)

Turning to the response surface shape analysis, Figure 4.5 represents a contour plot for the AHRI 11 and AHRI 21 compressor consumption vs. condensation and evaporation temperatures, and Figure 4.6 the same representation in a 3D plot. These figures show that the **condensation temperature** is the variable with the **strongest influence** on scroll energy consumption; the **evaporation temperature** also **influences** but **at a lower level**.

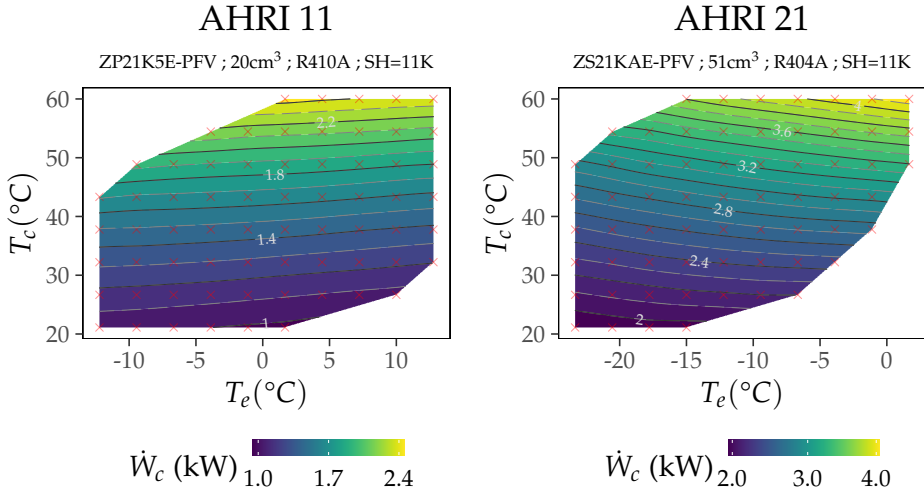


Figure 4.5: \dot{W}_c contour plot, temp. domain (AHRI 11 R410A and AHRI 21 R404A. SH=11K)

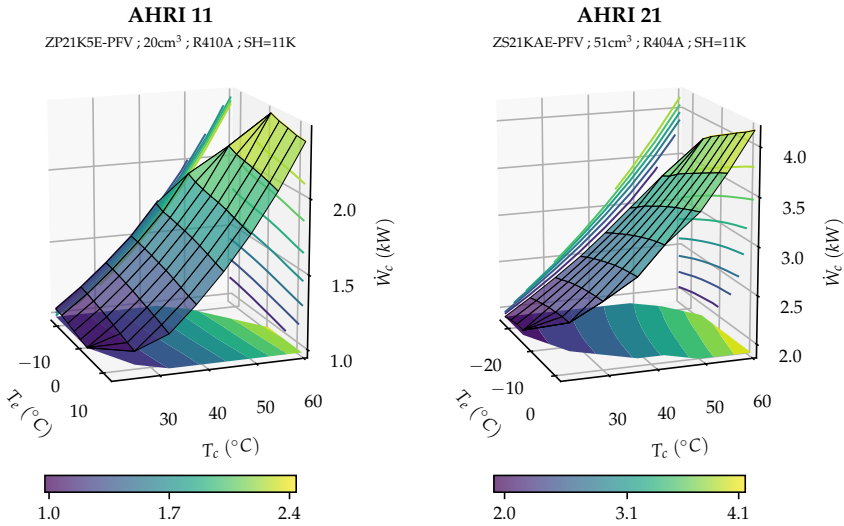


Figure 4.6: 3D plot of \dot{W}_c , temp. domain (AHRI 11 R410A and AHRI 21 R404A. SH=11K)

As can be seen in Figure 4.5 and Figure 4.6, the energy consumption of scroll compressors mainly depends on the condensation temperature, increasing with it. Then, there is a slight dependence on the evaporation temperature, but in this case, the energy consumption dependency with that variable will depend on the application range. In this case, for energy consumption, the global trend is significantly more straightforward than the representation of compressor efficiency.

From the construction of pure empirical models, Figure 4.5 clearly shows that energy consumption is a more suitable variable for building this kind of empirical model (polynomial models). It presents a monotonic behavior with smooth trends for the entire working map. Hence, if an adjusted polynomial model is used to predict the compressor energy consumption, it will contain fewer terms than a polynomial used to predict the compressor efficiency. This will have the consequence that this polynomial will be more robust, have fewer extrapolation problems, and require fewer experimental points to predict the compressor behavior accurately.

Regarding the trends of the response surface, one can observe different trends depending on the application range for the evaporation conditions. The same graph as in Figure 4.5 can be plotted as a function of pressures, where we can also plot the various pressure ratio isolines, including more information (Figure 4.7).

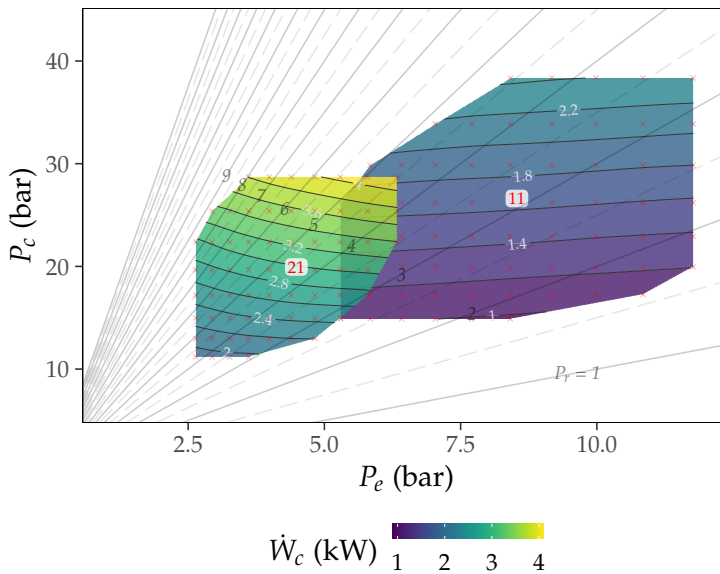


Figure 4.7: \dot{W}_c contour plot, press. domain (AHRI 11 R410A and AHRI 21 R404A. SH=11K)

This representation in terms of pressure is more appropriate when analyzing the dependence of consumption on the range of pressures.

In this graph, we can see how, at lower evaporation pressure values, we obtain a higher density and smaller distance in the pressure ratio isolines and, therefore, a greater range of P_r variation. Thus, the AHRI 21 compressor, which has been tested at low evaporation pressures (LBP, higher P_r values), shows a decreasing trend in the consumption with decreasing evaporation pressure. In contrast, AHRI 11 compressor shows a “slight” increasing trend with decreasing evaporation pressure (M/HBP, lower P_r values).

All M/HBP analyzed scroll compressors in the referenced AHRI reports, and the one tested by Cuevas and Lebrun (2009), show this slight increase in the compressor consumption, almost linear, with the decrease in the evaporation pressure. While the compressors in reports AHRI 21, AHRI 34, and AHRI 36 show the consumption decreasing trend with the decrease in the evaporation pressure. It should be pointed out that the compressors in reports AHRI 34 and AHRI 36 are for Low Temperature (LT) applications, including the highest values of pressure ratio, and, in fact, they are liquid injection types.

Therefore, it can be concluded that the dependence of the scroll compressor consumption with the evaporation conditions is weak, and it depends on the application range, with a slight hyperbolic decline for LBP applications while there is a slight linear increase for M/HBP applications.

Figure 4.5 and Figure 4.7 are replicated for the rest of the compressors available in the database. All the working maps generated are included in Appendix H. This appendix includes both representations of consumption as a function of condensation and evaporation temperature, as well as a function of condensation and evaporation pressure. In the pressure plot, the isolines of the pressure ratio have also been included to easily identify the variation range for the pressure ratio in the compressor envelope.

4.2.1.2 Mass flow rate analysis

Figure 4.8 shows the volumetric efficiency of compressors ZS21KAE-PFV (AHRI 21) and ZP21K5E-PFV (AHRI 11) for their corresponding reference refrigerants R404A, and R410A, respectively, and the three different inlet conditions. Moreover, Figure 4.9 also represents the volumetric efficiency as a contour plot, function of the evaporation and condensation temperatures, for a constant superheat of 11K and the same reference refrigerants.

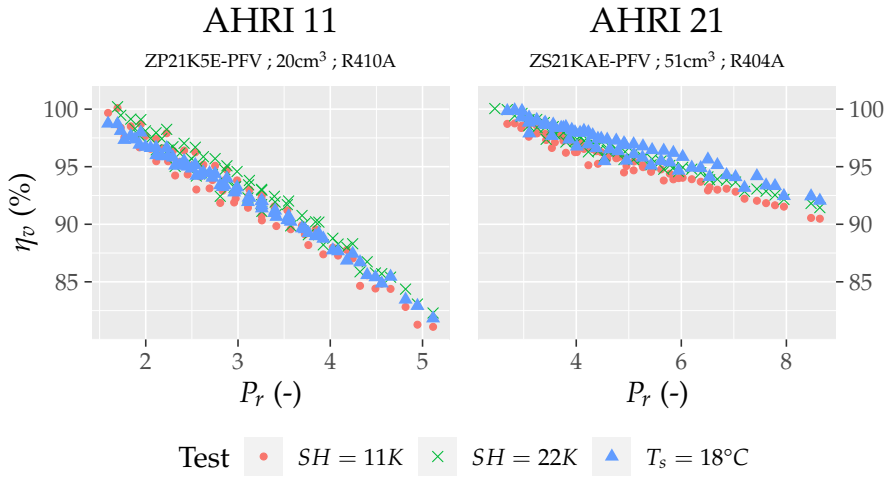


Figure 4.8: η_v as a function of P_r (AHRI 11 R410A and AHRI 21 R404A)

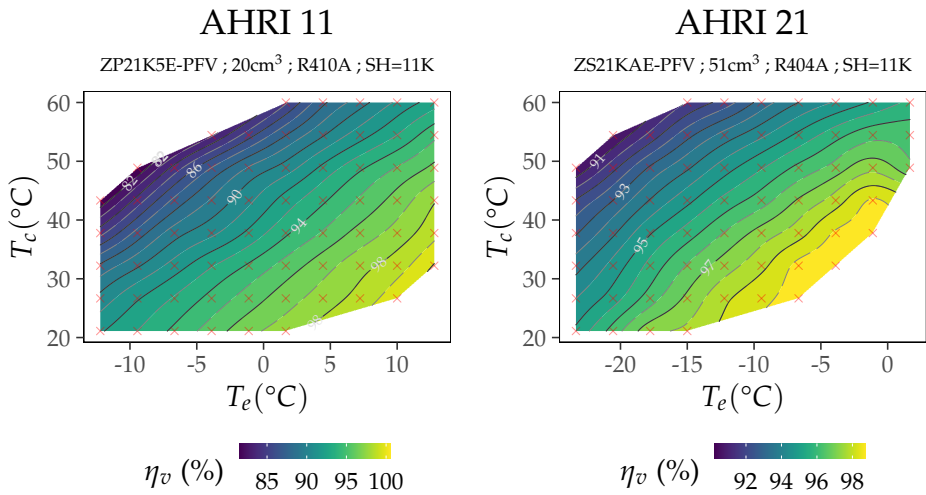


Figure 4.9: η_v contour plot, temp. domain (AHRI 11 R410A and AHRI 21 R404A. SH=11K)

As can be observed, Figure 4.8 shows a clear primary dependence of η_v with pressure ratio, as many references in the literature describe, with a decreasing trend when the pressure ratio increases.

However, it also becomes clear that the relationship is not strictly linear but more complex, and there are also other influences. The significant impact of the inlet conditions on the volumetric efficiency is evident, with higher volumetric efficiencies at higher superheats.

This behavior is well known, and there are ways to detect this effect and correct it in estimating the mass flow rate. The most frequently employed correction is the one proposed by Dabiri (Dabiri and Rice, 1981).

There is also an influence of the evaporation and condensation temperatures, not explained by the pressure ratio. One can see that there are groups of points distinguishable in Figure 4.8, corresponding to the same evaporation (T_e) or condensation temperatures (T_c).

On the other hand, the contour plot shows a surface that, despite being simpler than the one shown above for the compressor efficiency, still presents greater irregularities compared to the mass flow rate, as we will see below.

Therefore, volumetric efficiency is a good parameter to characterize the compressor mass flow rate when a simple correlation is required. However, it is not the right way to perform accurate map-based models. In fact, the AHRI standard (AHRI 540, 2020) is based on the direct correlation of the compressor mass flow rate.

Figure 4.10 and Figure 4.11 show the mass flow rate of AHRI 11 and AHRI 21 compressors in a contour plot and a 3D plot as a function of evaporation and condensation temperatures for the case with a constant superheat of 11K.

As can be observed, at constant superheat, the mass flow rate surface is quite smooth, mainly dependent on the evaporation temperature, with a very slight curvature and a much weaker dependence on the condensation temperature, again almost linear.

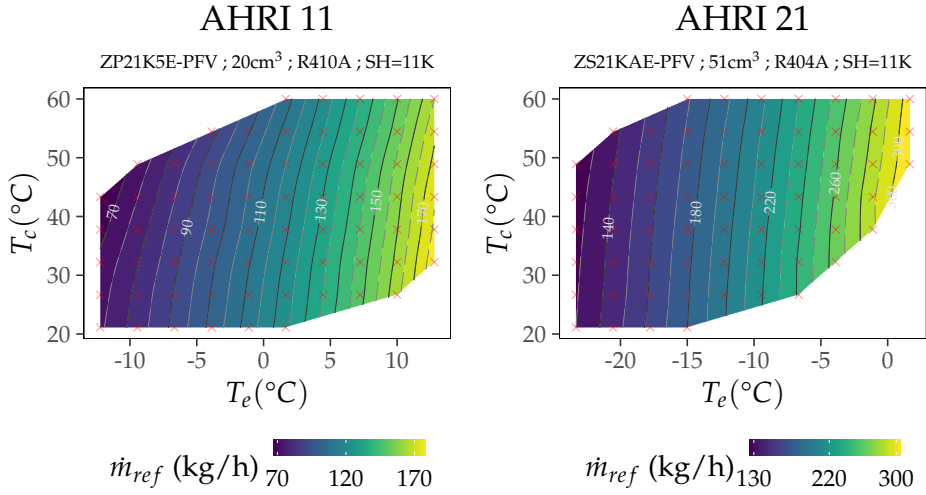


Figure 4.10: \dot{m}_{ref} contour plot, temp. domain (AHRI 11 R410A and AHRI 21 R404A. SH=11K)

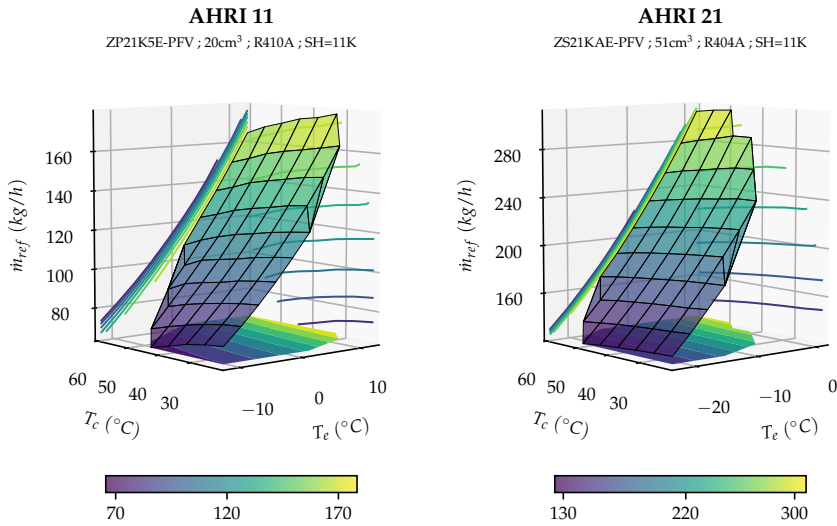


Figure 4.11: 3D plot of \dot{m}_{ref} , temp. domain (AHRI 11 R410A and AHRI 21 R404A. SH=11K)

Finally, this same representation for the mass flow rate has been conducted in all AHRI reports referred to above and the test data included in Cuevas and Lebrun (2009). They have found that the trends observed in Figure 4.10 and Figure 4.11 are the same for all compressors and refrigerants. The contour plots of the mass flow rate for the rest of compressors are included in Appendix H.

4.2.2 Evaluation of compressor correlations

From all the information about the shape of the response surface for the compressor energy consumption and mass flow rate, in this section, the suitability of AHRI polynomials to reproduce the compressor behavior will be studied, and the significance of the different terms of that correlation analyzed. From it, the best correlation for scroll compressors based on these polynomials is proposed.

4.2.2.1 Correlation for energy consumption

Looking at the surface representing the compressor consumption versus the condensation and evaporation temperatures (Figure 4.5 on page 118), it is evident that the 10-coefficient AHRI polynomial (AHRI 540, 2020) is able to fit these results. Of course, the only requirement will be to have a minimum amount of data available, all of which is well distributed across the entire working map.

However, the question is whether all the coefficients are necessary to reproduce the behavior, or if the same goodness of fit can be obtained using polynomials with a lower number of coefficients. Regarding that question, a second-order polynomial with only 6 coefficients, like the one used by Shao et al. (2004) for rotary compressors, can be used without significantly reducing the prediction capabilities of the AHRI polynomials. The use of this model was previously analyzed in Chapter 2, also showing good prediction capabilities to characterize scroll compressors. Thus, the polynomial supplied by Equation 4.3 could properly represent the energy consumption of scroll and rotary compressors.

$$\dot{W}_c = c_0 + c_1 T_e + c_2 T_c + c_3 T_e T_c + c_4 T_e^2 + c_5 T_c^2 \quad (4.3)$$

Though, when one plots the compressor consumption for different refrigerants, although the surfaces show similar trends, they are at different levels. This displacement almost disappears when the representation is made as a function of refrigerant saturation pressures instead of temperatures.

Figure 4.12 and Figure 4.13 show the compressor energy consumption for AHRI 11 and AHRI 21 compressors as a function of working conditions for different refrigerants tested.

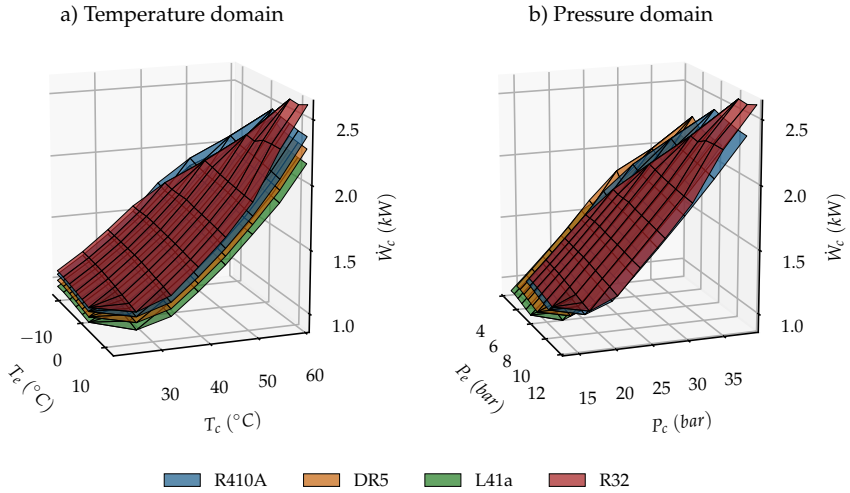


Figure 4.12: 3D plot of \dot{W}_c , temp. domain (left-hand) and pressure domain (right-hand) (AHRI 11 and 4 different refrigerants)

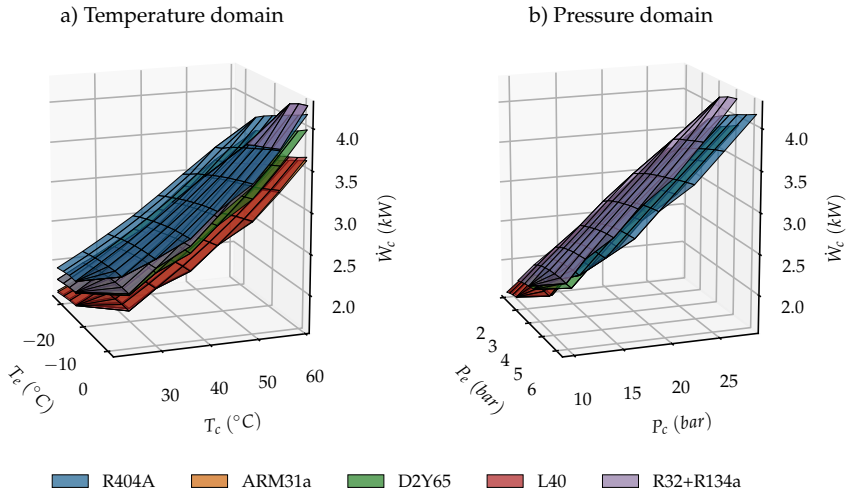


Figure 4.13: 3D plot of \dot{W}_c , temp. domain (left-hand) and pressure domain (right-hand) (AHRI 21 and 5 different refrigerants)

From these figures, one can see that the representation based on the pressure domain is much more universal than the temperatures. This results from the fact that the compressor does not see temperatures but compresses a reheated gas from the pressure at the inlet (suction) up to the pressure at the outlet (discharge). Of course, the temperature influences the density of the raked refrigerant and, therefore, the mass flow rate and heat transfer, but with minor changes in the compressor consumption if the pressure domain is selected.

The same representation of Figure 4.12 and Figure 4.13 as a function of evaporation and condensation pressures has been obtained for all the refrigerants and compressors included in the referenced reports, obtaining similar conclusions. Thus, it can be determined that the compressor energy consumption as a function of inlet and outlet saturation pressures is much more independent of the refrigerant and more representative of the compressor. Furthermore, a correlation of polynomials based on the condensation and evaporation pressures can be as effective as the one based on the dew temperatures.

The right-hand side of Figure 4.12 and Figure 4.13 shows that the compressor consumption surface is quite flat for the pressure domain representation. Therefore, the pressure domain representation can simplify the objective response surface. A simple linear polynomial containing linear terms on both evaporation and condensation pressures and one cross-term with their product leads to a robust correlation with good precision for all the analyzed compressors and refrigerants. It also has the advantage of fitting the model with a small experimental sample due to the reduced number of terms in the correlation. This polynomial will be referred to as *Correlation 1a* in the following comparison of results.

$$\text{Correlation 1a: } \dot{W}_c = c_0 + c_1P_e + c_2P_c + c_3P_eP_c \quad (4.4)$$

Suppose that now we want to increase the accuracy of the correlation. In that case, and based on the dependences shown in Figure 4.5 on page 118, a second-order dependence on the condensation pressure should be incorporated. This incorporation will improve the fitting at high condensation pressures where the linear behavior is slightly broken. A second-order term on the evaporation temperature will also improve the goodness of fit for LBP compressors. Adding those two terms to *Correlation 1a*, one gets the following second correlation:

$$\text{Correlation 2a: } \dot{W}_c = c_0 + c_1P_e + c_2P_c + c_3P_eP_c + c_4P_c^2 + c_5P_e^2 \quad (4.5)$$

Finally, *Correlation 2a* but in the temperatures domain, which is the one proposed by Shao for variable speed rotary compressors, will be analyzed.

$$\text{Correlation 3a: } \dot{W}_c = c_0 + c_1T_e + c_2T_c + c_3T_eT_c + c_4T_e^2 + c_5T_c^2 \quad (4.6)$$

In *Correlation 3a*, the evaporation and condensation temperatures correspond to dew temperatures.

4.2.2.2 Correlation for mass flow rate

The same behavior observed in energy consumption can be extrapolated to refrigerant mass flow rate (Figure 4.14 and Figure 4.15).

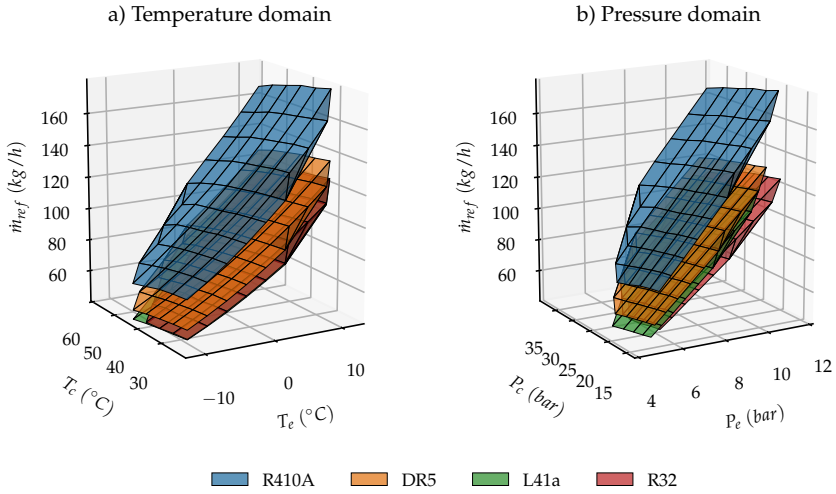


Figure 4.14: 3D plot of \dot{m}_{ref} , temp. domain (left-hand) and pressure domain (right-hand) (AHRI 11 and 4 different refrigerants)

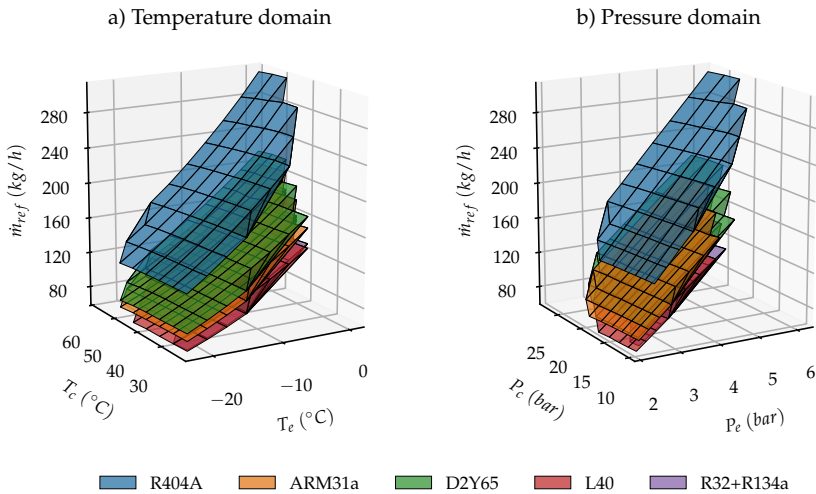


Figure 4.15: 3D plot of \dot{m}_{ref} , temp. domain (left-hand) and pressure domain (right-hand) (AHRI 21 and 5 different refrigerants)

In this case, when the representation is made in terms of pressures, the mass flow rate dependence is more linear, and the surfaces are in some way regularized. However, the surfaces corresponding to different refrigerants do not converge when they are represented as a function of pressures. This is because the refrigerant density at the compressor inlet strongly influences the mass flow rate.

The correlations analyzed in terms of pressures have been simplified as *Correlation 1b* and *Correlation 2b*:

$$\text{Correlation 1b: } \dot{m}_{ref} = c_0 + c_1 P_e + c_2 P_c \quad (4.7)$$

$$\text{Correlation 2b: } \dot{m}_{ref} = c_0 + c_1 P_e + c_2 P_c + c_3 P_e P_c \quad (4.8)$$

In the same way, the previous correlation is also performed for the temperature domain. This correlation is precisely the same as that proposed by Shao et al. (2004) for variable speed rotary compressors, referred to as *Correlation 3b*.

$$\text{Correlation 3b: } \dot{m}_{ref} = c_0 + c_1 T_e + c_2 T_c + c_3 T_e T_c + c_4 T_e^2 + c_5 T_c^2 \quad (4.9)$$

From these three equations, *Correlation 1b* has a smaller number of coefficients than the models contemplated for the energy consumption. In this sense, the reduction of terms does not reduce the number of experimental tests required, but improves the stability and sensitivity of the obtained results when extrapolating from the experimental data.

4.2.3 Comparison of correlations

4.2.3.1 Energy consumption comparison

Table 4.1 shows the fitting results obtained for the compressors AHRI 21 and AHRI 11, and the one tested by Cuevas and Lebrun (2009). The fitting has included the 3 correlations proposed plus the AHRI polynomials. However, the last ones were not included in the table as they did not improve the fitting quality and some of the coefficients were not statistically significant. The table includes the values of the coefficients obtained for the different correlations, the **Maximum Relative Error** (MRE) in %, the **Root Mean Square Error** (RMSE) in **W** and the **Coefficient of Variation**² of the RMSE (CV_{RMSE}) in %. These errors are plotted in Figure 4.16 to simplify the comparison. The correlations are fitted to all available test points for each compressor and refrigerant, including all different suction conditions. The coefficients are meant to provide the **compressor consumption** in **kW** with temperatures expressed in **°C** and **pressures** in **bar**. Summary tables like Table 4.1 are also included in Appendix J for the rest of the scroll compressors.

²This indicates how much variation or randomness there is between the data and the model, calculated by dividing RMSE by the average of the characterized variable (ASHRAE Guideline 14, 2014).

Table 4.1: \dot{W}_c models (AHRI 11, 21 and Cuevas (2009))

	\dot{W}_c (kW) Correlation 1a	MRE (%) RMSE ^d (W)	\dot{W}_c (kW) Correlation 2a	MRE (%) RMSE ^d (W)	\dot{W}_c (kW) Correlation 3a	MRE (%) RMSE ^d (W)	Fluid \dot{W}_c Range [W] (N° tests)
AHRI 11							
c_0	2.758e-01 (±3.21e-02)***	2.57 12.86 (0.82)	3.242e-01 (±1.71e-02)***	0.72 4.95 (0.32)	7.719e-01 (±1.52e-02)***	1.21 7.26 (0.46)	R410A [973, 2454] (66/64/66)
c_1	-2.954e-02 (±3.78e-03)***		-1.080e-02 (±3.35e-03)***		-3.930e-03 (±7.03e-04)***		
c_2	5.846e-02 (±1.32e-03)***		4.813e-02 (±8.03e-04)***		1.002e-03 (±8.13e-04)*		
c_3	4.317e-04 (±1.49e-04)***		-1.346e-04 (±7.70e-05)***		-2.073e-05 (±1.79e-05)*		
c_4			-2.900e-04 (±2.19e-04)**		-7.612e-05 (±2.16e-05)***		
c_5			2.913e-04 (±1.87e-05)***		4.470e-04 (±1.02e-05)***		
c_0	4.033e-01 (±4.90e-02)***	2.71 16.88 (1.09)	3.962e-01 (±4.44e-02)***	3.19 12.53 (0.81)	7.952e-01 (±3.69e-02)***	3.12 14.43 (0.93)	R32 [1005, 2607] (59/52/55)
c_1	-4.484e-02 (±5.35e-03)***		-1.635e-02 (±9.11e-03)***		-6.163e-03 (±1.90e-03)***		
c_2	5.235e-02 (±2.17e-03)***		4.307e-02 (±2.28e-03)***		6.100e-04 (±2.09e-03)		
c_3	1.305e-03 (±2.24e-04)***		5.302e-04 (±2.86e-04)***		6.753e-05 (±5.38e-05)*		
c_4			-6.050e-04 (±6.31e-04)+		-7.108e-05 (±5.18e-05)**		
c_5			3.195e-04 (±6.40e-05)***		4.836e-04 (±2.82e-05)***		
c_0	2.880e-01 (±4.59e-02)***	4.95 17.94 (1.21)	3.566e-01 (±3.65e-02)***	4.19 10.61 (0.71)	7.815e-01 (±2.79e-02)***	4.62 13.00 (0.87)	DR5 [929, 2401] (66/61/62)
c_1	-3.288e-02 (±5.73e-03)***		-1.259e-02 (±7.84e-03)**		-2.703e-03 (±1.34e-03)***		
c_2	5.778e-02 (±2.07e-03)***		4.479e-02 (±1.86e-03)***		-1.732e-03 (±1.51e-03)*		
c_3	6.835e-04 (±2.46e-04)***		-2.444e-04 (±2.03e-04)*		-3.607e-05 (±3.49e-05)*		
c_4			3.952e-05 (±5.62e-04)		-4.084e-05 (±4.05e-05)*		
c_5			4.213e-04 (±4.72e-05)***		4.626e-04 (±1.91e-05)***		
c_0	2.959e-01 (±2.68e-02)***	2.29 10.48 (0.75)	3.021e-01 (±1.56e-02)***	1.02 4.64 (0.33)	6.949e-01 (±1.39e-02)***	1.25 6.33 (0.45)	L41a [888, 2211] (65/60/61)
c_1	-3.105e-02 (±3.48e-03)***		-7.373e-03 (±3.52e-03)***		-4.315e-03 (±6.73e-04)***		
c_2	5.503e-02 (±1.26e-03)***		4.661e-02 (±8.34e-04)***		1.556e-03 (±7.57e-04)***		
c_3	7.344e-04 (±1.56e-04)***		2.042e-04 (±9.94e-05)***		2.430e-05 (±1.78e-05)**		
c_4			-8.129e-04 (±2.66e-04)***		-8.312e-05 (±1.99e-05)***		
c_5			2.678e-04 (±2.27e-05)***		3.922e-04 (±9.70e-06)***		
AHRI 21							
c_0	7.650e-01 (±5.09e-02)***	2.34 21.50 (0.74)	5.876e-01 (±4.24e-02)***	1.54 13.44 (0.46)	1.364e+00 (±4.87e-02)***	2.19 14.04 (0.48)	R404A [1856, 4172] (64/63/64)
c_1	-2.086e-03 (±1.26e-02)		1.100e-01 (±1.53e-02)***		-1.109e-02 (±2.35e-03)***		
c_2	8.803e-02 (±2.51e-03)***		8.301e-02 (±2.97e-03)***		2.082e-02 (±1.91e-03)***		
c_3	4.986e-03 (±5.92e-04)***		7.071e-03 (±5.14e-04)***		4.832e-04 (±3.59e-05)***		
c_4			-1.782e-02 (±2.11e-03)***		-2.083e-04 (±4.68e-05)***		
c_5			-8.686e-05 (±8.80e-05)+		4.177e-04 (±1.93e-05)***		
c_0	6.718e-01 (±3.77e-02)***	1.89 17.42 (0.70)	5.179e-01 (±2.66e-02)***	1.29 9.40 (0.38)	1.165e+00 (±3.50e-02)***	1.65 9.73 (0.39)	ARM31a [1582, 3615] (58/64/64)
c_1	1.598e-02 (±1.16e-02)**		1.197e-01 (±1.21e-02)***		-8.665e-03 (±1.68e-03)***		
c_2	8.459e-02 (±2.19e-03)***		8.342e-02 (±2.20e-03)***		1.830e-02 (±1.38e-03)***		
c_3	5.617e-03 (±6.37e-04)***		8.578e-03 (±4.93e-04)***		4.503e-04 (±2.64e-05)***		
c_4			-2.242e-02 (±2.11e-03)***		-1.556e-04 (±3.31e-05)***		
c_5			-2.473e-04 (±7.69e-05)***		3.626e-04 (±1.40e-05)***		
c_0	7.080e-01 (±4.13e-02)***	2.61 18.41 (0.68)	5.574e-01 (±3.23e-02)***	1.61 11.01 (0.41)	1.260e+00 (±4.30e-02)***	1.85 11.98 (0.44)	D2Y65 [1724, 3988] (56/64/63)
c_1	1.104e-03 (±1.11e-02)		1.028e-01 (±1.33e-02)***		-1.027e-02 (±2.11e-03)***		
c_2	8.712e-02 (±2.20e-03)***		8.351e-02 (±2.41e-03)***		1.873e-02 (±1.71e-03)***		
c_3	5.247e-03 (±5.58e-04)***		7.683e-03 (±4.92e-04)***		4.824e-04 (±3.30e-05)***		
c_4			-1.886e-02 (±2.10e-03)***		-1.699e-04 (±4.21e-05)***		
c_5			-1.473e-04 (±7.70e-05)***		4.285e-04 (±1.75e-05)***		

(Continued on Next Page...)

Table 4.1: \dot{W}_c models (AHRI 11, 21 and Cuevas (2009)) (continued)

	\dot{W}_c (kW) Correlation 1a	MRE (%) RMSE ^d (W)	\dot{W}_c (kW) Correlation 2a	MRE (%) RMSE ^d (W)	\dot{W}_c (kW) Correlation 3a	MRE (%) RMSE ^d (W)	Fluid \dot{W}_c Range [W] (N° tests)
AHRI 21							
c_0	6.068e-01 (±3.96e-02)***		5.295e-01 (±2.68e-02)***		1.306e+00 (±8.29e-02)***		
c_1	-5.817e-03 (±1.03e-02)		1.081e-01 (±1.53e-02)***		-1.140e-02 (±4.77e-03)***		
c_2	1.029e-01 (±2.53e-03)***	1.46	8.812e-02 (±2.52e-03)***	0.91	1.395e-02 (±3.43e-03)***	1.28	R32+R134a
c_3	5.034e-03 (±5.82e-04)***	15.50 (0.38)	7.895e-03 (±9.05e-04)***	8.89 (0.33)	4.759e-04 (±8.47e-05)***	13.62 (0.51)	[1740, 4268]
c_4			-2.128e-02 (±3.22e-03)***		-2.337e-04 (±9.03e-05)***		(40/48/45)
c_5			9.119e-05 (±1.11e-04)		5.739e-04 (±3.56e-05)***		
Cuevas (2009)							
c_0	9.187e-02 (±2.82e-01)		1.779e-01 (±3.01e-01)		1.384e+00 (±6.61e-01)***		
c_1	-3.761e-02 (±3.32e-02)*		-2.548e-03 (±4.63e-02)		1.959e-02 (±2.08e-02)+		
c_2	1.549e-01 (±1.11e-02)***	3.16	1.321e-01 (±2.82e-02)***	2.58	-3.100e-02 (±2.45e-02)*	3.05	R134a
c_3	-6.756e-04 (±1.08e-03)	60.775 (1.75)	-1.101e-03 (±2.41e-03)	51.17 (1.47)	-1.686e-04 (±3.38e-04)	54.48 (1.57)	[1449, 5424]
c_4			-9.498e-04 (±2.62e-03)		-2.660e-04 (±2.11e-04)*		(18)
c_5			5.152e-04 (±8.52e-04)		7.654e-04 (±2.24e-04)***		

^a + p < 0.1, * p < 0.05, ** p < 0.01, *** p < 0.001; Confidence interval of 95% for regression coefficients;

^b Temperatures (°C);

^c Pressures (bar);

^d The values in brackets are the CV_{RMSE} (%);

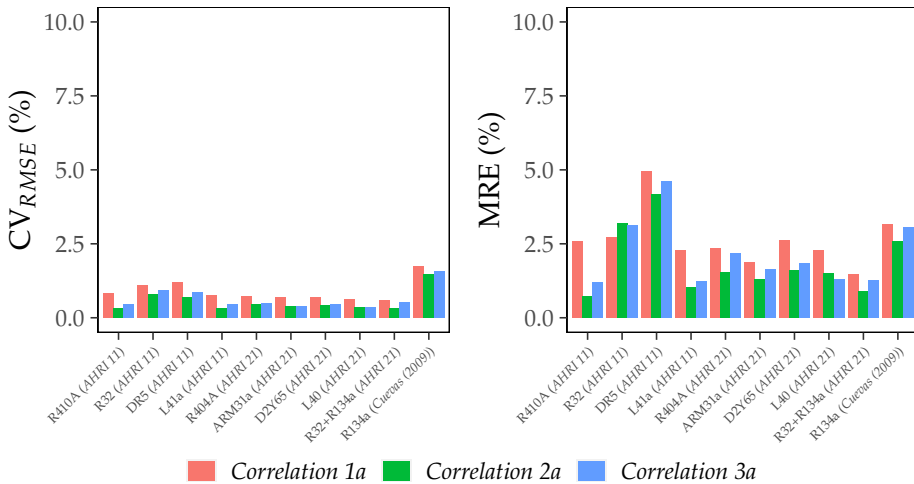


Figure 4.16: \dot{W}_c model errors (AHRI 11, 21 and Cuevas (2009))

As shown in Table 4.1, both MRE and RMSE are very low for all the analyzed correlations, providing a very good representation of the compressor consumption across the entire envelope. Typically, the analysis of the significance of the coefficients in the model uses statistical terms such as the *p-value* (p), where a term with a *p-value* < 0.05 is considered significant. Therefore, this table also includes the confidence intervals and *p-value* for each coefficient. The three correlations were fitted with the same amount of data for each compressor and refrigerant.

We can observe a low prediction error when analyzing firstly *Correlation 1a* and *Correlation 2a* (pressure domain). *Correlation 1a* allows the energy consumption to be characterized by including only two linear terms (P_e and P_c) and the interaction term ($P_e \times P_c$). As shown in the analysis performed in Subsubsection 4.2.2.1 on the dependence and shape of the response surfaces for energy consumption, the use of the pressure domain results in the linearization of the dependencies with P_e and P_c . Therefore, taking the pressure domain into consideration allows us to characterize the energy consumption without quadratic terms and with a low prediction error. Thus, we obtain a simple and compact correlation that will need fewer experimental tests for the adjustment. On the other hand, if we want to increase the model's accuracy and a larger experimental sample is available, adding the quadratic terms in *Correlation 2a* allows us to decrease the prediction error slightly. Moreover, we can see that the *p-values* (p) and the confidence intervals obtained for the coefficients of *Correlation 2a* are still low, so the addition of these terms is statistically significant. Thus, adding coefficients allows for a better fitting of the experimental results but probably implies the necessity of a higher number of experimental points. Finally, *Correlation 3a* (temperature domain) obtains slightly lower prediction errors than *Correlation 1a* but these are slightly higher than *Correlation 2a*. In this case, we can see that all terms included in the correlation are statistically significant due to the greater complexity of the surface when using the temperature domain, where the quadratic terms have greater relevance. Therefore, the highest accuracy is reached with *Correlation 2a*, proving that the correlation with pressures is better than with temperatures and, as discussed above, less dependent on the refrigerant employed. Furthermore, another advantage of using the pressure domain is to extend the applicability of these models to transcritical cycles, where the condensation pressure remains constant as opposed to the condensation temperature.

As mentioned in Subsubsection 4.2.2.1, using pressures instead of temperatures allows a correlation which is even more independent of the refrigerant. For example, Figure 4.17 on next page shows the results of extrapolating with other refrigerants. This figure shows *Correlation 2a* (left-plot) and *Correlation 3a* (right-plot), adjusting its coefficients with the base refrigerants (AHRI 11 \Rightarrow R410A and AHRI 21 \Rightarrow R404a) and extrapolating the predicted energy consumption values for the other refrigerants available in these datasets.

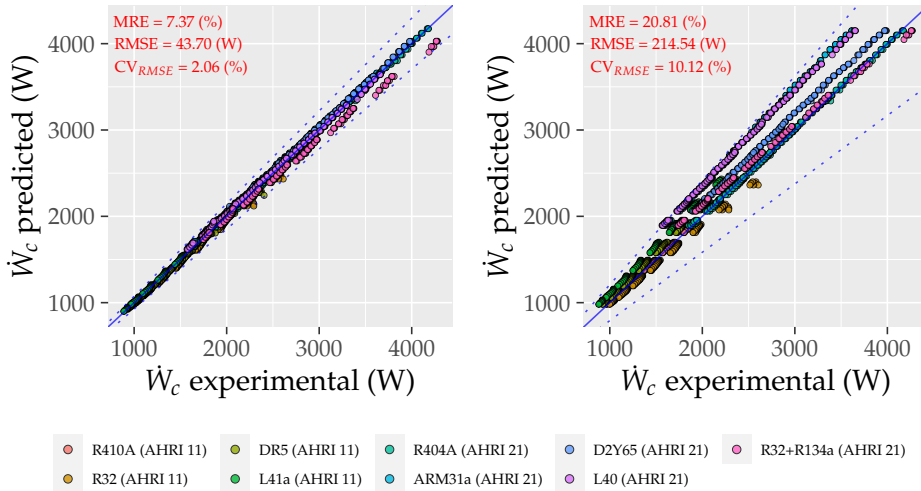


Figure 4.17: \dot{W}_c prediction extrapolating for other refrigerants (AHRI 11 and 21). *Correlation 2a* (left-plot) and *Correlation 3a* (right-plot)

In this case, one can see how the prediction errors are significantly lower when using pressures instead of temperatures (Pressure domain: $CV_{RMSE} = 2.06\%$ vs Temperature domain: $CV_{RMSE} = 10.12\%$). Finally, the compressor of Cuevas and Lebrun (2009) was selected because their results were obtained in a totally different framework to the AHRI reports. Hence it could be a good indicator of the general application of the results obtained. In this case, their polynomials show slightly higher RMSE when fitted to those results, but the surface is very similar to the other M/HBP compressors in the AHRI report. In this sense, a higher experimental uncertainty could explain the slightly higher deviation.

4.2.3.2 Mass flow rate comparison

A similar summary table to the previous one obtained for the energy consumption has been generated for the mass flow rate (Table 4.2 on page 134). The Table includes the values of the coefficients (estimates) for *Correlation 1b*, *Correlation 2b*, and *Correlation 3b*, as well as the **Maximum Relative Error** (MRE) in %, the **Root Mean Square Error** (RMSE) in **kg/h** and the **Coefficient of Variation** of the RMSE (CV_{RMSE}) in %. These errors are plotted in Figure 4.19 in order to simplify the comparison. The coefficients are meant to provide the compressor **mass flow rate** in **kg/h** with **temperatures** expressed in **°C** and **pressures** in **bar**. Summary tables, like Table 4.2, are also included in Appendix J for the rest of the scroll compressors.

Regarding the suction conditions used, for each compressor and refrigerant, the correlations were fitted to the data tested at constant SH (SH=11K in the AHRI reports and SH=6.8K in Cuevas and Lebrun (2009)). Similar results were obtained with these correlations adjusted for the rest of the available suction conditions.

On the other hand, the use of the Dabiri correlation (Dabiri and Rice, 1981) for correcting suction conditions has also been tested on the data analyzed. The application of this correction makes use of a linear correlation (Equation 4.10)³.

$$\frac{\dot{m}_{ref}}{\dot{m}_{ref,map}} = 1 + F \left(\frac{\rho_s}{\rho_{s,map}} - 1 \right) \quad (4.10)$$

Taking as an example the experimental results for the AHRI 11 report, Figure 4.18 shows an example of the error obtained with the Dabiri correction. These results are generated by fitting the *Correlation 2b* to the R410A and DR5 mixtures at a superheat of 11K, extrapolating for a superheat of 22K and a suction temperature of 18°C, and considering the reported value of the coefficient F in Dabiri and Rice (1981) (F=0.75).

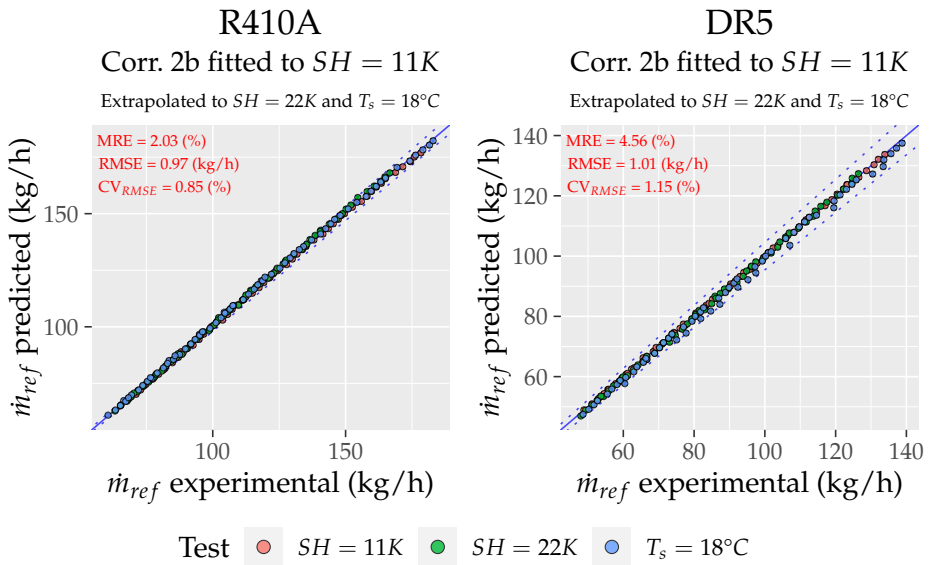


Figure 4.18: Dabiri correction to other suction conditions (AHRI 11 R410A and DR5)

³The term map refers to the reference suction conditions in which the linear terms of the polynomial are adjusted. By applying the Dabiri correction, we can extrapolate to other suction conditions.

As can be shown in Figure 4.18, the prediction errors are low in both refrigerants; lower for the R410A and slightly higher for the DR5.

Considering also that this correction uses a liner correction with the density ratio, no major extrapolation problems are expected with its application. So, we can conclude that using this correction provides a good accuracy for extrapolation to other suction conditions.

Table 4.2: \dot{m}_{ref} models (AHRI 11, 21 and Cuevas (2009))

	\dot{m}_{ref} (kg/h) Correlation 1b	MRE (%) RMSE ^d (kg/h)	\dot{m}_{ref} (kg/h) Correlation 2b	MRE (%) RMSE ^d (kg/h)	\dot{m}_{ref} (kg/h) Correlation 3b	MRE (%) RMSE ^d (kg/h)	Fluid \dot{m} Range [kg/h] (N° tests)
AHRI 11 (SH = 11K)							
c_0	-4.472e+00 ($\pm 7.47e-01$)***	1.61 0.61 (0.52)	-1.032e+00 ($\pm 2.55e+00$)	1.37 0.57 (0.49)	1.170e+02 ($\pm 1.45e+00$)***	1.42 0.40 (0.34)	R410A [66, 178] (66)
c_1	1.658e+01 ($\pm 8.24e-02$)***		1.617e+01 ($\pm 2.98e-01$)***		4.082e+00 ($\pm 6.73e-02$)***		
c_2	-6.726e-01 ($\pm 2.38e-02$)***		-8.171e-01 ($\pm 1.05e-01$)***		1.242e-01 ($\pm 7.82e-02$)**		
c_3			1.661e-02 ($\pm 1.18e-02$)**		4.019e-03 ($\pm 1.73e-03$)***		
c_4					5.603e-02 ($\pm 2.12e-03$)***		
c_5					-6.558e-03 ($\pm 9.85e-04$)***		
R32							
c_0	-3.185e-01 ($\pm 1.10e+00$)	2.24 0.86 (1.05)	-9.252e+00 ($\pm 3.49e+00$)***	1.67 0.70 (0.86)	7.745e+01 ($\pm 2.33e+00$)***	2.16 0.54 (0.66)	R32 [46, 123] (59)
c_1	1.129e+01 ($\pm 1.28e-01$)***		1.227e+01 ($\pm 3.84e-01$)***		2.960e+00 ($\pm 1.17e-01$)***		
c_2	-6.301e-01 ($\pm 3.93e-02$)***		-2.390e-01 ($\pm 1.51e-01$)**		3.423e-01 ($\pm 1.31e-01$)***		
c_3			-4.173e-02 ($\pm 1.58e-02$)***		9.063e-05 ($\pm 3.25e-03$)		
c_4					3.534e-02 ($\pm 3.34e-03$)***		
c_5					-9.097e-03 ($\pm 1.74e-03$)***		
DR5							
c_0	-2.305e+00 ($\pm 3.87e-01$)***	1.33 0.32 (0.36)	-2.829e-01 ($\pm 1.29e+00$)	1.02 0.29 (0.33)	8.896e+01 ($\pm 6.93e-01$)***	0.65 0.19 (0.21)	DR5 [49, 134] (66)
c_1	1.346e+01 ($\pm 4.59e-02$)***		1.320e+01 ($\pm 1.62e-01$)***		3.075e+00 ($\pm 3.21e-02$)***		
c_2	-6.068e-01 ($\pm 1.31e-02$)***		-6.976e-01 ($\pm 5.68e-02$)***		9.685e-02 ($\pm 3.73e-02$)**		
c_3			1.121e-02 ($\pm 6.85e-03$)**		3.664e-03 ($\pm 8.23e-04$)**		
c_4					3.874e-02 ($\pm 1.01e-03$)***		
c_5					-5.486e-03 ($\pm 4.70e-04$)***		
L41a							
c_0	-3.876e+00 ($\pm 5.04e-01$)***	1.87 0.41 (0.52)	1.350e+00 ($\pm 1.17e+00$)*	1.22 0.27 (0.33)	8.315e+01 ($\pm 9.38e-01$)***	0.99 0.25 (0.32)	L41a [43, 122] (65)
c_1	1.291e+01 ($\pm 6.38e-02$)***		1.222e+01 ($\pm 1.53e-01$)***		2.803e+00 ($\pm 4.49e-02$)***		
c_2	-5.266e-01 ($\pm 1.79e-02$)***		-7.731e-01 ($\pm 5.42e-02$)***		-7.364e-02 ($\pm 5.07e-02$)**		
c_3			3.171e-02 ($\pm 6.81e-03$)***		4.679e-03 ($\pm 1.17e-03$)***		
c_4					3.476e-02 ($\pm 1.40e-03$)***		
c_5					-2.793e-03 ($\pm 6.41e-04$)***		
AHRI 21 (SH = 11K)							
c_0	4.801e+00 ($\pm 9.67e-01$)***	1.09 0.80 (0.40)	-4.720e+00 ($\pm 2.29e+00$)***	0.85 0.53 (0.26)	3.056e+02 ($\pm 3.24e+00$)***	0.75 0.49 (0.24)	R404A [124, 308] (63)
c_1	5.093e+01 ($\pm 2.12e-01$)***		5.332e+01 ($\pm 5.70e-01$)***		9.744e+00 ($\pm 1.57e-01$)***		
c_2	-7.107e-01 ($\pm 4.24e-02$)***		-2.385e-01 ($\pm 1.13e-01$)***		-1.708e-02 ($\pm 1.25e-01$)		
c_3			-1.156e-01 ($\pm 2.67e-02$)***		-5.005e-03 ($\pm 2.38e-03$)***		
c_4					9.452e-02 ($\pm 3.07e-03$)***		
c_5					-4.410e-03 ($\pm 1.25e-03$)***		

(Continued on Next Page...)

Table 4.2: \dot{m}_{ref} models (AHRI 11, 21 and Cuevas (2009)) (continued)

	\dot{m}_{ref} (kg/h) Correlation 1b	MRE (%) RMSE ^d (kg/h)	\dot{m}_{ref} (kg/h) Correlation 2b	MRE (%) RMSE ^d (kg/h)	\dot{m}_{ref} (kg/h) Correlation 3b	MRE (%) RMSE ^d (kg/h)	Fluid \dot{m} Range [kg/h] (N° tests)
AHRI 21 (SH = 11K)							
c ₀	1.362e+00 (±3.74e-01)***	0.73 0.33 (0.26)	-7.923e-01 (±1.09e+00)	0.92 0.29 (0.23)	1.966e+02 (±1.67e+00)***	0.92 0.28 (0.22)	ARM31a [73, 200] (64)
c ₁	4.077e+01 (±1.01e-01)***		4.145e+01 (±3.35e-01)***		6.563e+00 (±8.21e-02)***		
c ₂	-5.273e-01 (±1.85e-02)***		-4.026e-01 (±6.20e-02)***		-7.248e-02 (±6.65e-02)*		
c ₃			-3.794e-02 (±1.82e-02)***		-1.204e-03 (±1.24e-03)+		
c ₄					6.842e-02 (±1.71e-03)***		
c ₅					-1.931e-03 (±6.86e-04)***		
c ₀	2.573e+00 (±6.38e-01)***	1.24 0.55 (0.40)	-6.429e-01 (±1.95e+00)	1.62 0.50 (0.37)	2.089e+02 (±2.58e+00)***	1.33 0.44 (0.32)	D2Y65 [81, 214] (64)
c ₁	3.888e+01 (±1.52e-01)***		3.977e+01 (±5.30e-01)***		6.772e+00 (±1.27e-01)***		
c ₂	-5.252e-01 (±2.84e-02)***		-3.566e-01 (±1.01e-01)***		5.783e-02 (±1.03e-01)		
c ₃			-4.516e-02 (±2.61e-02)***		2.105e-04 (±1.92e-03)		
c ₄					6.698e-02 (±2.66e-03)***		
c ₅					-3.509e-03 (±1.06e-03)***		
c ₀	1.311e+00 (±4.82e-01)***	1.04 0.42 (0.38)	-4.331e-01 (±1.55e+00)	1.29 0.41 (0.36)	1.661e+02 (±2.13e+00)***	1.04 0.32 (0.29)	L40 [64, 175] (61)
c ₁	3.668e+01 (±1.41e-01)***		3.723e+01 (±4.83e-01)***		5.692e+00 (±1.09e-01)***		
c ₂	-5.020e-01 (±2.56e-02)***		-3.967e-01 (±9.25e-02)***		2.149e-01 (±8.51e-02)***		
c ₃			-3.196e-02 (±2.71e-02)*		2.328e-03 (±1.70e-03)**		
c ₄					6.098e-02 (±2.20e-03)***		
c ₅					-4.778e-03 (±8.68e-04)***		
c ₀	2.304e+00 (±7.79e-01)***	1.76 0.61 (0.51)	1.800e+00 (±2.71e+00)	1.75 0.61 (0.51)	1.697e+02 (±5.23e+00)***	1.33 0.53 (0.44)	R32+R134a [68, 179] (48)
c ₁	3.519e+01 (±2.50e-01)***		3.532e+01 (±7.17e-01)***		5.883e+00 (±3.05e-01)***		
c ₂	-8.091e-01 (±4.61e-02)***		-7.783e-01 (±1.65e-01)***		4.069e-01 (±2.15e-01)***		
c ₃			-7.643e-03 (±3.93e-02)		7.470e-03 (±5.21e-03)**		
c ₄					6.584e-02 (±6.07e-03)***		
c ₅					-8.758e-03 (±2.22e-03)***		
Cuevas (2009) (SH = 6.8K)							
c ₀	-1.155e+01 (±1.04e+01)*	3.93 6.03 (1.37)	4.247e+00 (±2.63e+01)	4.70 5.65 (1.29)	1.332e+02 (±5.43e+01)***	2.76 4.48 (1.02)	R134a [198, 904] (18)
c ₁	4.766e+01 (±1.01e+00)***		4.575e+01 (±3.08e+00)***		6.381e-01 (±1.71e+00)		
c ₂	-1.706e+00 (±4.99e-01)***		-2.297e+00 (±1.03e+00)***		1.318e+00 (±2.01e+00)		
c ₃			6.580e-02 (±1.01e-01)		7.263e-03 (±2.78e-02)		
c ₄					1.500e-01 (±1.73e-02)***		
c ₅					-1.610e-02 (±1.84e-02)+		

^a + p < 0.1, * p < 0.05, ** p < 0.01, *** p < 0.001; Confidence interval of 95% for regression coefficients;

^b Temperatures (°C);

^c Pressures (bar);

^d The values in brackets are the CV_{RMSE} (%);

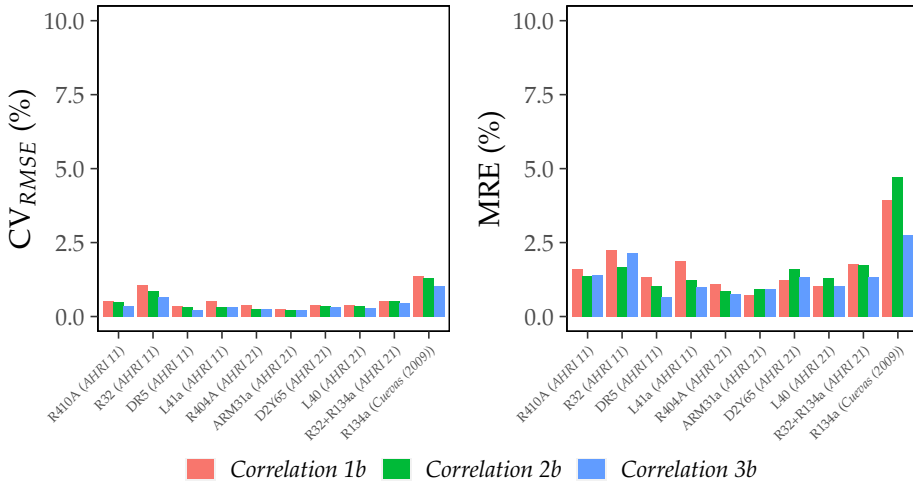


Figure 4.19: \dot{m}_{ref} model errors (AHRI 11, 21 and Cuevas (2009))

Analyzing the results from Table 4.2 and Figure 4.19, one can observe that the accuracy level reached is similar to the one comparing the correlations proposed for the energy consumption. In this case, the AHRI polynomial was also tested, resulting in a large number of non-significant terms and collinearity between them, more than in the case of the consumption characterization due to the more straightforward response surface for the mass flow rate (almost a plane dependent on evaporation conditions). Therefore it has been removed from the summary tables due to it overfits the simpler response surface of the mass flow rate. The fact that we have many non-significant terms clearly signals an overfit in the model. We have already mentioned the problems that this entails when setting up a model, where, despite reducing the error in training points, we greatly increase the prediction error in new points (interpolation/extrapolation errors).

In general, the three proposed correlations show similar prediction errors with the additional advantage of including fewer terms in the models fitted in pressures. We can observe that the pressure domain eliminates the use of quadratic terms due to the linearization of the response surfaces. Thus, we obtain simple and compact correlations that will need fewer experimental tests for the adjustment. Then, adding the interaction term ($P_e \times P_c$) slightly decreases the prediction errors between *Correlation 1b* and *Correlation 2b*. Table 4.2 shows the results obtained from this analysis, which also includes the corresponding *p-value* and confidence interval for each coefficient. In general, all the coefficients included in the correlations are statistically significant (low *p-values*).

4.2.4 Experimental points required

One essential question about properly characterizing the compressor performance is how many points are required and where should these be placed in the working domain. This question has been widely addressed in the field of Design of Experiments (DoE), including classical methodologies and more sophisticated methods like computer-aided calculations in Optimal Designs (OD). This last typology, OD, has the advantage of selecting points in non-regular domains (Atkinson and Donev, 1992), like the temperatures or pressure domains in scroll compressors (Appendix L includes a detailed discussion on several methodologies suitable to the experimental domain of compressors).

Regarding OD designs, these theories assume that the model describing the data is known and the application domain is defined. Based on that, the D-Optimal criteria described in Fedorov (1972) has been selected as it is especially well indicated for linearized problems with a non-regular operation domain.

Furthermore, this methodology is well documented, and many open source tools include preprogrammed algorithms, providing an easy and automatic way to perform experimental test matrices to characterize compressor performance (R Core Team, 2022; Wheeler, 2019). The challenge relating to selecting a proper sample which gives statistically significant results is not included in the current standard (AHRI 540, 2020).

Taking as a first example the *Correlation 3a* and *Correlation 3b* (temperature domain) for the characterization of mass flow rate and power consumption, Figure 4.20 shows the ubication domain of the experimental points for 7, 9, and 11 experimental measurements. These points have been selected with the D-Optimal criteria as mentioned above. The samples show that most of the tests must be placed at the operating limits of the compressor. Then, a few tests must be placed in the center. This result is similar to the one obtained by Aute et al. (2015).

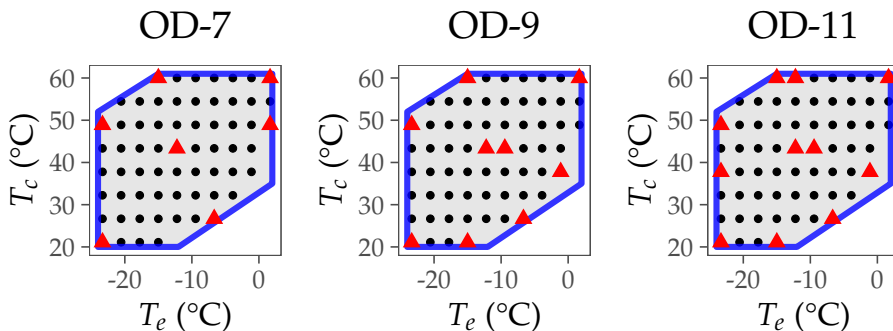


Figure 4.20: Optimal Design. Fedorov (7, 9, 11 test points). AHRI 21 R404A

Once the location of tests points was determined, a fit of the models was done using the samples proposed by the Fedorov technique and the whole matrix of experimental points (SH=11K, SH=22K, and $T_s = 18^\circ\text{C}$ for \dot{W}_c model and SH=11K for \dot{m}_{ref} model) in order to check the prediction error for all the experimental data available. From these results the 9 experimental measurements sample obtained the best results between sample size and prediction accuracy for the models adjusted. Table 4.3 shows these results obtained considering the second-order polynomial (*Correlation 3a* and *Correlation 3b*) and 9 experimental measurements. This table also includes in brackets the MRE, RMSE and CV_{RMSE} obtained when fitting the original AHRI polynomial and selecting a sample of 11 test points.

Table 4.3: Regression model adjusted with OD sample, 9 tests (AHRI 21 R404A)

	All points ^c		Sample OD (9 test points) ^c	
	\dot{W}_c (kW)	\dot{m}_{ref} (kg/h)	\dot{W}_c (kW)	\dot{m}_{ref} (kg/h)
$Int.$	1.364e+00 ($\pm 4.87\text{e-}02$)***	3.056e+02 ($\pm 3.24\text{e+}00$)***	1.329e+00 ($\pm 1.27\text{e-}01$)**	3.057e+02 ($\pm 6.93\text{e+}00$)***
T_e	-1.109e-02 ($\pm 2.35\text{e-}03$)***	9.744e+00 ($\pm 1.57\text{e-}01$)***	-1.386e-02 ($\pm 6.32\text{e-}03$)**	9.659e+00 ($\pm 3.40\text{e-}01$)***
T_c	2.082e-02 ($\pm 1.91\text{e-}03$)***	-1.708e-02 ($\pm 1.25\text{e-}01$)	2.217e-02 ($\pm 5.46\text{e-}03$)***	-7.665e-02 ($\pm 2.73\text{e-}01$)
$T_e:T_c$	4.832e-04 ($\pm 3.59\text{e-}05$)***	-5.005e-03 ($\pm 2.38\text{e-}03$)***	5.365e-04 ($\pm 9.11\text{e-}05$)***	-3.487e-03 ($\pm 4.70\text{e-}03$)+
T_e^2	-2.083e-04 ($\pm 4.68\text{e-}05$)***	9.452e-02 ($\pm 3.07\text{e-}03$)***	-2.499e-04 ($\pm 1.38\text{e-}04$)*	9.376e-02 ($\pm 6.86\text{e-}03$)***
T_c^2	4.177e-04 ($\pm 1.93\text{e-}05$)***	-4.410e-03 ($\pm 1.25\text{e-}03$)***	4.088e-04 ($\pm 5.97\text{e-}05$)***	-3.258e-03 ($\pm 2.77\text{e-}03$)*
Num.Obs.	191	63	9	9
RMSE (W, kg/h)	14.043	0.491	15.691 (16.193 ^d)	0.584 (0.833 ^d)
CV_{RMSE} (%)	0.484	0.244	0.540 (0.558 ^d)	0.290 (0.414 ^d)
MRE (%)	2.194	0.751	2.504 (2.630 ^d)	0.872 (1.308 ^d)
Range (W, kg/h)	[1856, 4172]	[124, 308]	[1856, 4172]	[124, 308]

^a $p < 0.1$, * $p < 0.05$, ** $p < 0.01$, *** $p < 0.001$;

^b Temperatures ($^\circ\text{C}$);

^c Models: Correlation 3a (\dot{W}_c) and Correlation 3b (\dot{m}_{ref});

^d MRE, RMSE and CV_{RMSE} for the original AHRI polynomial fitted with OD and 11 experimental points;

As can be seen, the Maximum Relative Error (MRE), Root Mean Square Error (RMSE), CV_{RMSE} and the differences in the polynomial parameters when 9 experimental points were selected began to be very small (the errors refers to the prediction of all the available test points), this number being a rational number of points required to characterize scroll compressors. Moreover, looking at the MRE, RMSE and CV_{RMSE} values in brackets, one can see that the AHRI polynomial fit does not improve the accuracy and slightly increases the prediction error. Therefore, the AHRI polynomial includes many terms, overfitting these types of simpler response surfaces.

On the other hand, it must be noted that test points in the compressor limit usually have a higher experimental error than points in the center. The fitting process weighted the relative influence on the final solution of the different points with their error.

Therefore, the Inverse-Variance Weighting (IVW) was selected rather than the classical Ordinary Least Squares (OLS) adjustment. The regression adjustment includes a vector of weights with the same length as the experimental sample. This vector is constructed as the inverse experimental variance, i.e., the inverse of the square of the combined standard uncertainty (Taylor and Kuyatt, 1994).

Similar results can be reproduced considering the pressure domain. In this case, the experimental design is constructed in the same way as described above. We must consider that the optimal design methodologies must know the functional to be applied. This means that in the case of having different functionals for the characterization of the energy consumption and mass flow rate, we should consider the functional with more terms when planning the experimental design. Therefore, if *Correlation 2a* is selected for the energy consumption, we will obtain an experimental design equivalent to the previous one (we have the same polynomial terms between *Correlation 2a* and *Correlation 3a*); to ensure proper correlation for the mass flow rate, *Correlation 2b* is to be selected due to its higher precision.

However, if the intention is to decrease the experimental cost with only a slight increase in the prediction error, another pertinent option is to select *Correlation 1a* for the energy consumption. In this case, the proper correlation for the mass flow rate is still *Correlation 2b* due to the fact that the experimental sample must be able to adjust the functional for the energy consumption. Therefore, selecting *Correlation 1a* for the energy consumption and *Correlation 2b* for the mass flow rate, Figure 4.21 shows the ubication domain of the experimental points for 5, 6, and 7 experimental measurements using Fedorov technique.

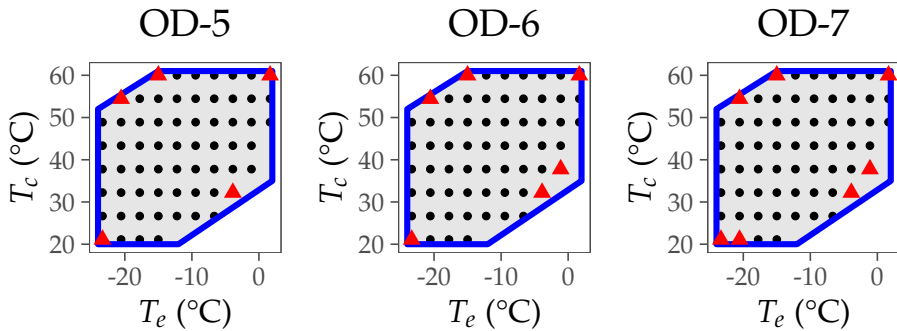


Figure 4.21: Optimal Design. Fedorov (5, 6, 7 test points). AHRI 21 R404A

The results obtained are similar to the previous ones. The samples show that most of the tests must be placed at the operating limits of the compressor.

However, if the polynomial model does not include quadratic terms, the experimental sample will not include center points. This does not result in a significant increase in the prediction error. As shown in Table 4.4, selecting a sample of 6 points results in a prediction error similar to the previous case, with only a slight increase in the RMSE. In this case, 6 experimental measurements obtained the best results between sample size and prediction accuracy for the models adjusted.

Table 4.4: Regression model adjusted with OD sample, 6 tests (AHRI 21 R404A)

	All points ^c		Sample OD (6 test points) ^c	
	\dot{W}_c (kW)	\dot{m}_{ref} (kg/h)	\dot{W}_c (kW)	\dot{m}_{ref} (kg/h)
$Int.$	7.650e-01 ($\pm 5.09e-02$)***	-4.720e+00 ($\pm 2.29e+00$)***	8.364e-01 ($\pm 2.14e-01$)**	-3.359e+00 ($\pm 1.57e+00$)*
P_e	-2.086e-03 ($\pm 1.26e-02$)	5.332e+01 ($\pm 5.70e-01$)***	-1.666e-02 ($\pm 5.61e-02$)	5.286e+01 ($\pm 4.67e-01$)***
P_c	8.803e-02 ($\pm 2.51e-03$)***	-2.385e-01 ($\pm 1.13e-01$)***	8.510e-02 ($\pm 1.20e-02$)**	-3.209e-01 ($\pm 7.64e-02$)**
$P_e:P_c$	4.986e-03 ($\pm 5.92e-04$)***	-1.156e-01 ($\pm 2.67e-02$)***	5.439e-03 ($\pm 2.96e-03$)*	-9.212e-02 ($\pm 2.18e-02$)**
Num.Obs.	191	63	6	6
RMSE (W, kg/h)	21.495	0.532	25.120 (16.193 ^d)	0.594 (0.833 ^d)
CV_{RMSE} (%)	0.740	0.264	0.865 (0.558 ^d)	0.295 (0.414 ^d)
MRE (%)	2.345	0.850	2.608 (2.630 ^d)	0.818 (1.308 ^d)
Range (W, kg/h)	[1856, 4172]	[124, 308]	[1856, 4172]	[124, 308]

^a + p < 0.1, * p < 0.05, ** p < 0.01, *** p < 0.001;

^b Temperatures (°C);

^c Models: Correlation 1a (\dot{W}_c) and Correlation 2b (\dot{m}_{ref});

^d MRE, RMSE and CV_{RMSE} for the original AHRI polynomial fitted with OD and 11 experimental points;

Finally, we must illustrate the importance of obtaining a good experimental design, ensuring the robustness of the proposed correlations and the AHRI polynomial against which random samples will be analyzed. Sometimes the compressor data supplied have not been obtained using an appropriate experimental design. Depending on the model used, this can lead to significant prediction errors when interpolating or extrapolating data. This can be especially critical in the case of fitting the original AHRI polynomial, where cubic terms add further instability to the model.

Considering the original AHRI polynomial and the models proposed for the performance characterization in scroll compressors, Figure 4.22 includes a box plot showing the prediction errors (MRE and CV_{RMSE}) for the entire dataset of the AHRI 21 report and its reference refrigerant (R404A), and selecting a total of 50 random samples. The sample size selected in all models has been 11 points in order to be able to fit the largest model (original AHRI polynomial).

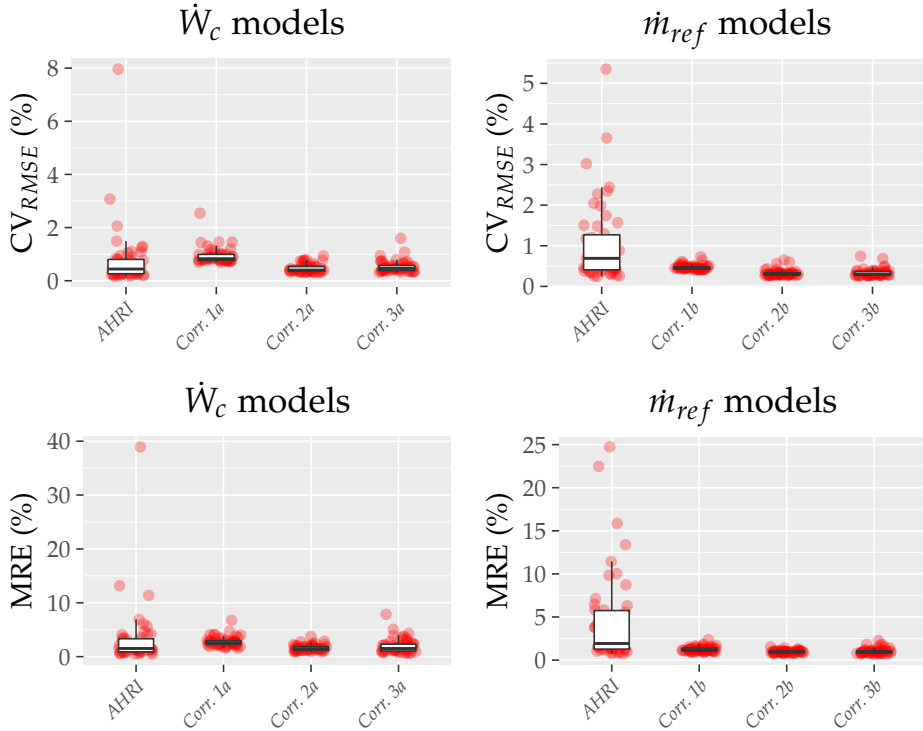


Figure 4.22: Random samples error models (AHRI 21 R404A. SH=11K)

The results have shown that the models proposed in this work obtain greater stability and robustness than the original AHRI polynomial, thanks to the elimination of the cubic terms, which are not required for scroll compressors and prevent overfitting the model.

The AHRI polynomial for predicting the mass flow rate shows a higher number of random samples with high error values, where the intention is to characterize the almost linear dependence of the mass flow rate on evaporation conditions by using many terms and, therefore, greatly overfitting the model. In this sense, the other models present a great robustness thanks to the elimination of unnecessary terms, reaching an acceptable degree of accuracy, and even using random experimental samples for the adjustment.

Specifically, Correlations 2a and 2b have obtained the best results, very similar to the rest of the proposed correlations. As concerns the simplest models proposed (Correlations 1a and 1b), one can see that they only present a slight increase in error and could be interesting options if limited resources are available for experimentation.

4.3 Reciprocating compressors

Once the analysis of the characterization of scroll compressors has been concluded, the following sections will show an equivalent analysis applied to reciprocating compressor characterization. It includes all the data extracted from the AHRI reports and contains the reciprocating compressor tests: AHRI 17 (Borges Ribeiro and Marchi Di Gennaro, 2013a), AHRI 18 (Borges Ribeiro and Marchi Di Gennaro, 2013b), AHRI 28 (Sedliak, 2013a), AHRI 29 (Sedliak, 2013b), AHRI 30 (Sedliak, 2013c), AHRI 35 (Rajendran and Nicholson, 2014b), AHRI 37 (Rajendran and Nicholson, 2014d), AHRI 49 (Sedliak, 2015a), AHRI 50 (Sedliak, 2015b), AHRI 51 (Boscan and Sanchez, 2015), AHRI 59 (Lenz and Shrestha, 2016), AHRI 64 (Pérouffe and Renevier, 2016a), AHRI 67 (Pérouffe and Renevier, 2016b), AHRI 69 (Pérouffe and Renevier, 2016c).

This provide us experimental information for a total of 9 different reciprocating compressors, and 20 different refrigerants: R22, R1270, R134a, N13a, ARM42a, R404A, L40, DR7, R1234yf, R455A, DR3, R449A, R410A, L41-1, DR5A, ARM71a, D2Y60, R32, ARM25, ARM20b. Those reports also include many refrigerants tested and different suction conditions. Therefore, this part checked the effect of the suction conditions and refrigerant on the compressor performance again. Table 2.8 on page 50 summarizes the main characteristics of the reciprocating compressors included in the AHRI reports, and Table 2.9 on page 51 includes the composition for the new mixtures tested.

From the analysis of all these compressor consumption data, again, two different behaviors, depending on the application range, have been identified:

- Low/Medium evaporation pressure conditions (L/MBP).
- High values of evaporation pressure (HBP).

Based on the number of points, AHRI 30 (L/MBP) and AHRI 59 (HBP) compressors were selected as the basis to perform all the current analyses. The results obtained with these compressors were verified with the rest to confirm the general application of the obtained conclusions. The results for the rest of the compressors are supplied in Appendix I and Appendix K.

4.3.1 Response surface analysis

Similar to the analysis of scroll compressor response surfaces, the following sections will represent the response surfaces of mass flow and energy consumption, including other variables of interest, such as compressor efficiency and volumetric efficiency. They will be analyzed and also compared with the previous response surfaces obtained in scroll compressors.

Regarding the contour plots shown in this part, the advantages of using pressures rather than temperatures as the basis for representation has previously been explored. Therefore this part will directly include contour plots represented in the pressure domain for the energy consumption and the mass flow rate. It will allow the addition of the pressure ratio isolines, enriching the graphs due to the relevance of this variable on the performance. Moreover, it will simplify the explanation of the proposed functional for a new response variable introduced in this part, the specific consumption (\dot{W}_{esp}), which, as seen below, will give us some advantages when characterizing reciprocating compressors.

4.3.1.1 Energy consumption analysis

Figure 4.23 shows an example of the compressor efficiency map for a reciprocating compressor (AHRI 30, left-hand plot) and for a scroll compressor (AHRI 21, right-hand plot) at constant suction conditions (SH=11K).

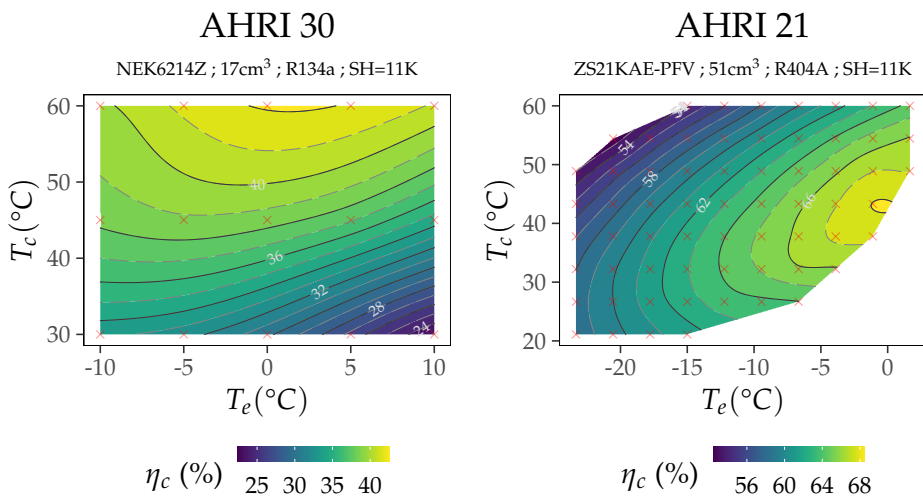


Figure 4.23: η_c contour plot, temp. domain (AHRI 30 R134a and AHRI 21 R404A. SH=11K)

In Figure 4.23, the compressor efficiency depends on both variables, evaporation and condensation temperature. The scroll compressor (AHRI 21) shows the zone of maximum efficiency at the highest evaporation temperature values. On the other hand, for the reciprocating compressor (AHRI 30), the highest efficiency values are obtained at the highest condensation temperature values without an absolute maximum and including the lower values at high evaporation temper-

atures (low pressure ratio). Other reciprocating compressors have also been analyzed resulting in similar contour diagrams to that obtained in the AHRI 21, such as the AHRI 59 compressor (HBP). In general, it has been noticed that the response surfaces for the compressor efficiency do not show smooth trends, requiring an empirical model with many parameters. Then, another interesting feature to analyze is the dependence on suction conditions. Figure 4.24 shows the compressor efficiency and energy consumption vs the pressure ratio and evaporation temperature for the AHRI 30 compressor, including three different suction conditions (SH=11K, SH=22K and $T_s = 18^\circ\text{C}$), and the reference refrigerant (R134a). This figure also includes different subplots for each level of condensation temperature to simplify the visualization.

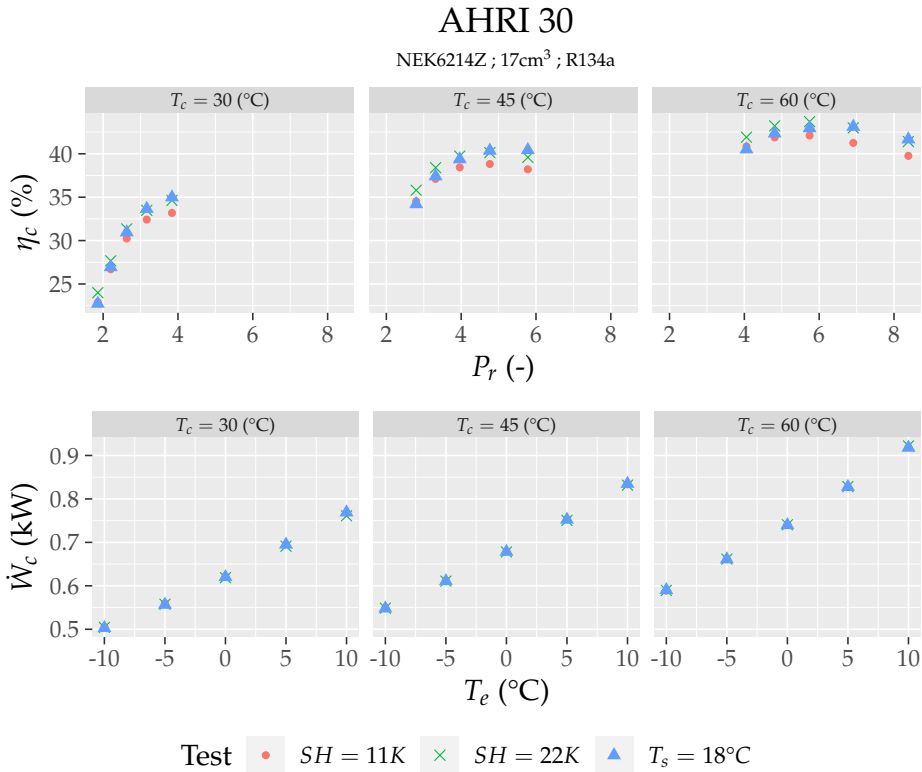


Figure 4.24: η_c and \dot{W}_c as a function of P_r , T_e at given levels of T_c (AHRI 30 R134a)

As shown in Figure 4.24, the suction temperature or SH level only affects the

compressor efficiency, with no apparent effect on the energy consumption. For instance, it is possible to observe how the compressor efficiency increases with the superheat level. These results agree with those already obtained in scroll compressors. On the other hand, the energy consumption shows an almost main linear dependence on the evaporation temperature (it increases for higher values of T_c) and a slight dependence on the condensation temperature. The condensation temperature only includes a slight dependence on most of the compressors analyzed. Only the reports AHRI 51 and AHRI 59 include a major dependence on the condensation temperature which corresponds to the HBP compressors. In order to show these trends, Figure 4.25 includes the energy consumption maps of several reciprocating reports (left-hand plot), and the energy consumption maps already analyzed for the scroll compressors (right-hand plot). This figure is plotted in terms of condensation and evaporation pressure in order to include the pressure ratio isolines. The plot also includes a label to identify the AHRI report.

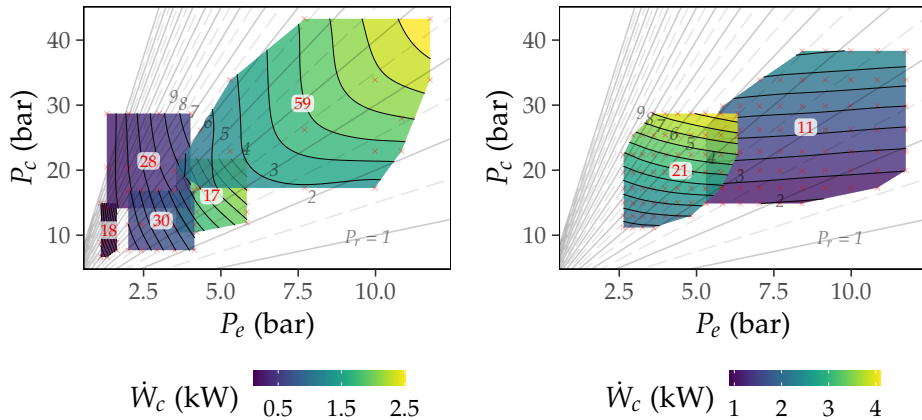


Figure 4.25: \dot{W}_c contour plot, press. domain, reciprocating compressor (left-hand AHRI 17, 18, 28, 30, 59) and scroll compressor (right-hand AHRI 11, 21) for its reference refrigerant

As can be observed in Figure 4.25, the energy consumption in reciprocating compressors has two behaviors, depending on the application range of the compressor. For L/MBP compressors, the energy consumption depends mainly on evaporation pressure. In this case, the response surfaces are simpler and, as it will be seen later, this will probably require less terms for polynomial fitting. For example, AHRI 18 and AHRI 28 compressors (LBP) show this main dependency with these trends. Then, if the application range of the evaporation pressure increases (MBP compressors), the dependence of the energy consumption with the

condensation temperature also increases, like in the AHRI 30 and AHRI 17 compressors (MBP). Finally, for the higher evaporation pressure values (HBP), the response surface conforms to the second type of behavior observed, like in the AHRI 59 compressor, depending on the energy consumption in evaporation and condensation conditions. Therefore, in order to obtain a good characterization, it will be necessary to use a higher number of terms, including terms dependent on the condensation temperature.

Summing up the trends observed, and contrary to what is observed in scroll compressors where the consumption depends mainly on the condensation pressure (Figure 4.25-right), the most significant variable in reciprocating compressors is the evaporation pressure with a secondary dependence on the condensation pressure in L/MBP applications or only significant in HBP applications. These differences between reciprocating and scroll compressors may be caused by their different behavior in terms of mass flow rate. Considering that the energy consumption is related to the level of mass flow rate through the compressor, an important difference between these two technologies is the dependence of the volumetric efficiency on the pressure ratio.

On the one hand, in reciprocating compressors (and piston machines) there is a high dependence caused by the influence of the “*dead space*”. If we check the pressure ratio isolines in the figure above, we will notice a lower distance between them at lower evaporation pressure values. Therefore, we will have a high variation in the pressure ratio/mass flow rate for the energy maps that shows only a main dependence with the evaporation pressure.

To conclude the analysis on the energy consumption characterization, an alternative approach to unify the energy consumption behavior, regardless of the operating range and compressor technology, has been developed. Assuming that the differences in the energy consumption behavior are based on the different mass flow trend, a specific energy consumption has been defined as:

$$\dot{W}_{esp} = \frac{\dot{W}_c}{\dot{m}_{ref}} \quad (4.11)$$

It is fair to point out that this kind of approach (dividing energy parameter by the mass flow parameter) has been already undertaken by other authors. A clear example is shown in Pierre (1982), where the author specifies a correlation for the ratio between volumetric efficiency and compressor efficiency (η_v/η_c), instead of directly characterizing the compressor efficiency. This ratio of efficiencies has also been contemplated in this work, but finally the specific consumption was selected because it obtained a more homogeneous behavior, and the response surfaces were easier to characterize. Figure 4.26 shows the specific consumption maps for the previous compressors analyzed.

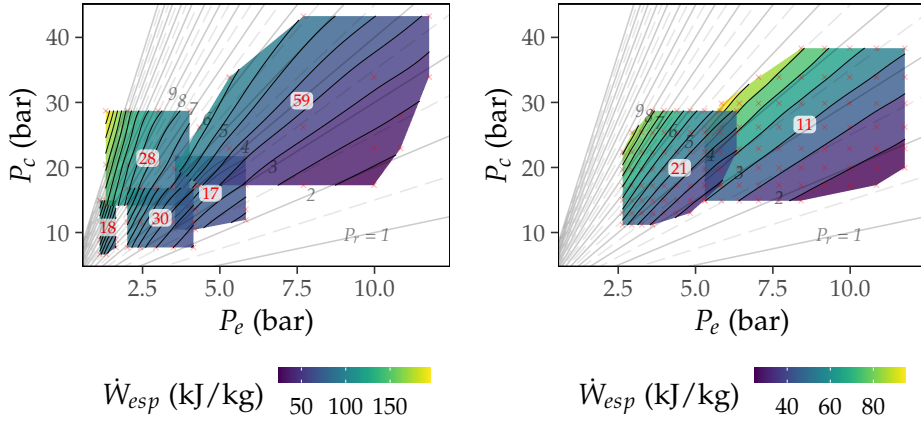


Figure 4.26: \dot{W}_{esp} contour plot, press. domain, reciprocating compressor (left-hand AHRI 17, 18, 28, 30, 59) and scroll compressor (right-hand AHRI 11, 21) for its reference refrigerant

We can see in Figure 4.26 how the response surfaces have a certain similarity for both compressor designs. Comparing the specific consumption with the pressure ratio isolines, it is seen that they intersect, forming a small angle. Thus, different values for the specific consumption at a constant pressure ratio are obtained. This is a consequence of the fact that the specific consumption is equivalent to the ratio of Δh_{is} to η_c (Equation 4.1 on page 113). Therefore, the specific consumption is not directly a function of the pressure ratio. However, as the pressure ratio isolines converge to a common vertex at the origin of pressures (0,0), the specific consumption isolines also seem to converge at a common vertex. If we consider this last assumption, the following change of variable can be done:

$$P'_r = \frac{P_c - z_c}{P_e - z_e} \quad (4.12)$$

Where z_c and z_e are the coordinates of the vertex of the specific consumption isolines in the pressure domain. Generally, these coordinates of z_c and z_e will depend on the compressor. Considering appropriate values of z_c and z_e , Figure 4.27 represents how the isolines of this new variable (P'_r) are distributed for the AHRI 59 compressor.

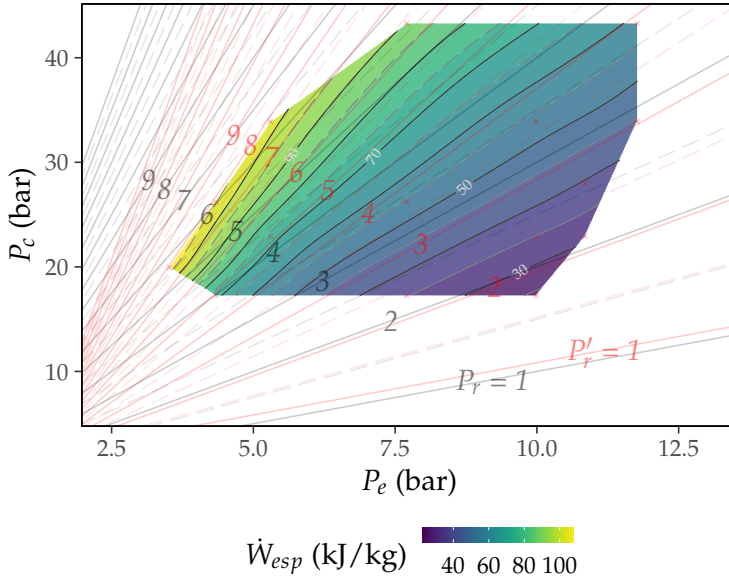


Figure 4.27: \dot{W}_{esp} contour plot, press. domain, with P_r and P'_r isolines of AHRI 59 for its reference refrigerant

Figure 4.27 shows how the P'_r isolines corresponds to the specific consumption isolines. Therefore, we can consider that the specific consumption is a function of this new variable:

$$\dot{W}_{esp} = f \left(\frac{P_c - z_c}{P_e - z_e} \right) \tag{4.13}$$

Finally, Figure 4.28 plots how this corrected pressure ratio could characterize the specific consumption with a simple polynomial correlation. We can see that the dependence is almost linear or with a slight curvature in some cases. Therefore, the values of z_c and z_e can be obtained simply by proposing a polynomial correlation as a function of P'_r and adjusting by nonlinear regression.

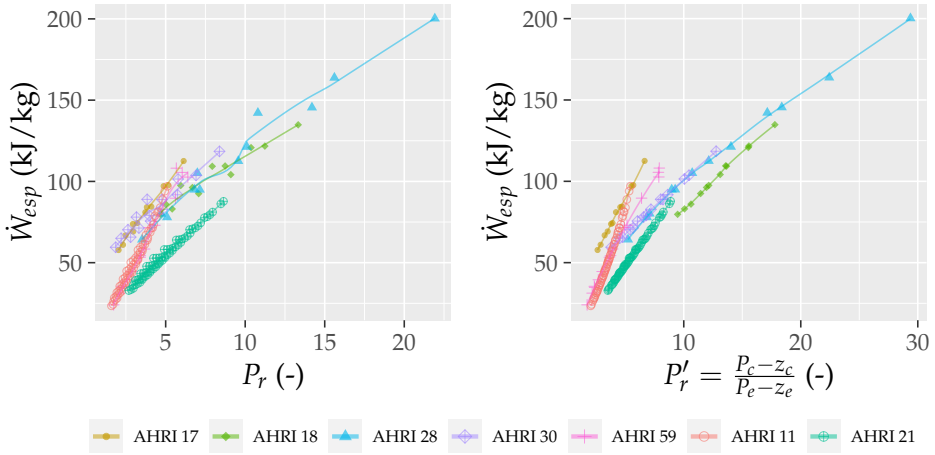


Figure 4.28: P_r vs P'_r (AHRI 17, 18, 28, 30, 59, 11, 21 and its reference refrigerant)

4.3.1.2 Mass flow rate analysis

Figure 4.29 shows the volumetric efficiency for a reciprocating compressor (AHRI 30, left-hand plot) and a scroll compressor (AHRI 21, right-hand plot) working with the reference refrigerant and three suction conditions.

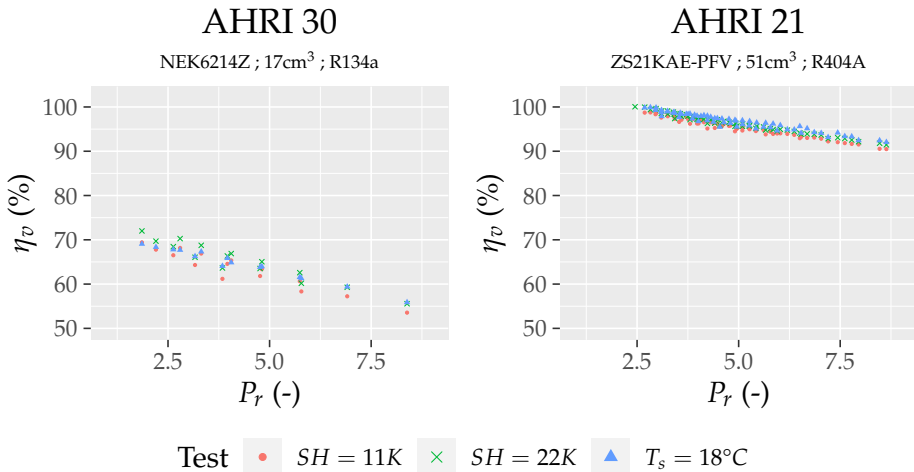


Figure 4.29: η_v as a function of P_r (AHRI 30 R134a and AHRI 21 R404A)

As shown in Figure 4.29, the only distinction between both compressors is a clear difference in volumetric efficiency values, which are much lower for reciprocating compressors. This is very well known due to the strong influence of the “dead space” in piston machines.

Except for the lower volumetric efficiency values in reciprocating compressor, both technologies obtain similar trends. Volumetric efficiency has a primary linear and negative tendency with pressure ratio—it decreases at higher values of P_r —and a secondary dependence on suction conditions. As mentioned previously in the scroll compressors analysis, this dependence on suction conditions is commonly rectified by the correction suggested by Dabiri and Rice (1981).

However, although volumetric efficiency is a good parameter for characterizing the compressor mass flow rate in general terms, we can see that the relationship with P_r is not strictly linear and it is not adequate to perform accurate map-based models. There are other second-order dependencies with condensation and evaporation temperature. Therefore, we can understand why using a polynomial depending on these two variables, as proposed by the AHRI standard (AHRI 540, 2020), can obtain lower prediction errors to characterize the mass flow rate directly.

In this sense, Figure 4.30 represents the mass flow rate maps as a function of evaporation and condensation pressures for the compressors already analyzed in the previous section.

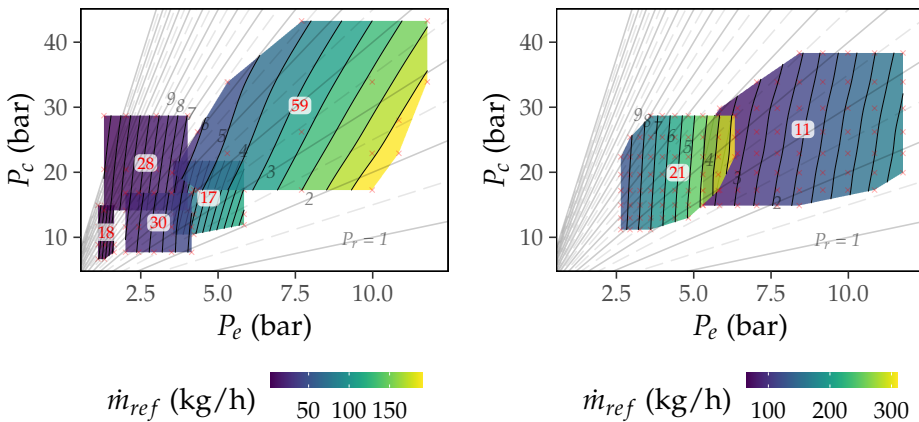


Figure 4.30: \dot{m}_{ref} contour plot, press. domain, reciprocating compressor (left-hand AHRI 17, 18, 28, 30, 59) and scroll compressor (right-hand AHRI 11, 21) for its reference refrigerant

The figure shows how the response surfaces for the mass flow rate are practically a plane which depends mainly on the evaporation conditions for most scroll and reciprocating compressors.

The condensation pressure increases its influence as evaporation pressure increases; this trend can be observed for the AHRI 59 (HBP) compressor. However, the response surfaces remain simple, with smooth changes, compared to those obtained in the previous section for the energy consumption, pointing to the fact that using the third-degree and 10-term polynomial provided in the AHRI standard, may not be necessary for characterizing the mass flow rate.

4.3.2 Evaluation of compressor correlations

Based on the results obtained in the previous sections, this section includes the analysis of several functionals to characterize reciprocating compressor performance. The proposed functionals consider the complexity of the response surface, ensuring this is characterized to minimize possible overfitting. Finally, the best correlation for reciprocating compressors based on these polynomials is proposed.

4.3.2.1 Correlation for energy consumption

Once the initial analysis of the dependence and shape of the response surface for the energy consumption and mass flow rate in reciprocating compressors has been completed, the next step is to define the polynomial model to be used.

As has been previously analyzed, in scroll compressors, the use of the 10-term AHRI polynomial (AHRI 540, 2020) was unnecessary due to the smoothness of the response surfaces.

However, in reciprocating compressors, Figure 4.25 has plotted more complex behavior of the energy consumption as a function of evaporation and condensation conditions that may imply the use of a larger number of terms in the polynomial overall, considering the different compressor behavior observed depending on the evaporation pressure range.

Regarding the mass flow rate in reciprocating compressors, the response surfaces obtained are still quite similar to those already analyzed in scroll compressors. They only include a slight increase in the dependence of the mass flow rate on the condensation pressure for HBP conditions.

Another essential aspect to consider, which has already been verified in scroll compressors, is the selection of the independent variables:

1. "Should we obtain a polynomial in terms of condensation and evaporation temperature?"
2. "Is there any advantage of building the model in terms of condensation and evaporation pressure?"

In scroll compressors, it has been found that if the consumption is plotted as a function of the refrigerant pressure, instead of temperatures, it turns out that the surfaces are much more similar to each other. Making the same assumption for reciprocating compressors, Figure 4.31 shows a 3D representation of the consumption response surfaces for the AHRI 59 compressor working with different refrigerants at the same SH level (11K).

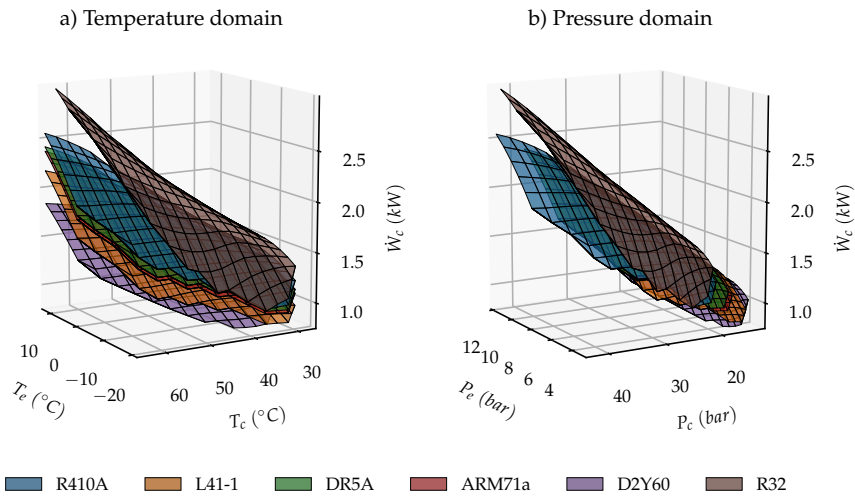



Figure 4.31: 3D plot of \dot{W}_c , temp. domain (left-hand) and pressure domain (right-hand) (AHRI 59 and 6 different refrigerants)

This figure shows the same effect when using a pressure domain in reciprocating compressors. Only the refrigerant R32 shows a slight difference, converging all the other refrigerants in the same plane. Therefore, selecting the pressure domain rather than the temperature domain for the energy consumption model will obtain more general results in both technologies when extrapolating to other refrigerants.

Due to the higher complexity observed in the energy consumption response surface of reciprocating compressors, the experimental results have been fitted to the basic correlation proposed by the AHRI standard in terms of temperatures and pressures, expressions (4.14) and (4.15). Then, additional term reduction methodologies have been applied to evaluate the possibility of reducing the number of significant terms in the correlations. Specifically, this reduction was made by the backward elimination procedure selecting the *BIC* (Bayesian Information Criterion). The tool selected has been the open-source programming language  (R Core Team, 2022) and the *stepwise()* function provided in the *R-RcmdrMisc* package (Fox, 2021).

$$\text{Temperature domain (T)} \quad \dot{W}_c = c_0 + c_1 T_e + c_2 T_c + c_3 T_e T_c + c_4 T_e^2 + c_5 T_c^2 + c_6 T_e T_c^2 + c_7 T_e^2 T_c + c_8 T_e^3 + c_9 T_c^3 \quad (4.14)$$

$$\text{Pressure domain (P)} \quad \dot{W}_c = c_0 + c_1 P_e + c_2 P_c + c_3 P_e P_c + c_4 P_e^2 + c_5 P_c^2 + c_6 P_e P_c^2 + c_7 P_e^2 P_c + c_8 P_e^3 + c_9 P_c^3 \quad (4.15)$$

Additionally, the energy compressor characterization as a function of the specific consumption has been evaluated (Equation 4.16), where P'_r is calculated by Equation 4.12, reported on page 147.

$$\dot{W}_{esp} = \frac{\dot{W}_c}{\dot{m}_{map}} = k_0 + k_1 P'_r + \dots + k_n P_r'^n \quad (4.16)$$

As shown in Figure 4.28 on page 149, the correction of P_r with the z_c and z_e terms resulted in a practically linear dependence with P'_r and sometimes with a slight curvature. The determination of the degree of the polynomial in Equation 4.16 with P'_r has been done iteratively. This means starting with the fit using a linear correlation and increasing the degree of the polynomial if necessary. The fit can be performed by nonlinear regression to obtain the k_0, \dots, k_n coefficients and the z_c and z_e coordinates. Then, representing the obtained results in a similar way to Figure 4.28 with the values of z_c and z_e obtained, provides a simple way to see whether it is necessary to increase the degree of the polynomial. We must remember that the suction conditions do not affect the energy consumption value, but they fix the mass flow rate through the compressor. Therefore, the specific consumption will also depend on the suction conditions. This means that to convert the specific consumption to energy consumption values, we must multiply by the mass flow rate considered in the adjustment of the coefficients k_0, \dots, k_n and z_c, z_e .

Selecting this approach allows the prediction of compressor energy consumption with a quite simple functional which depends on only 4 parameters (or 5/6 if we want to increase the prediction accuracy by increasing the degree of the polynomial), and is valid for reciprocating and scroll compressors. The use of this variable could help to represent the compressor energy consumption based on a significantly lower number of experimental tests.

4.3.2.2 Correlation for mass flow rate

Summing up the results for the mass flow rate analysis, Figure 4.30 shows that mass flow rate presents a more regular surface than the energy consumption. The response surface for the mass flow rate in reciprocating compressors is practically a plane depending on the evaporation conditions, and with a dependence on the condensation conditions that can also be significant. This dependence on the condensation conditions has already been identified for scroll compressors, but in a second-order dependence. However, the response surfaces for the mass flow rate in reciprocating compressors continue to show reasonably smooth trends. In this sense, it has been found that a second-order polynomial is enough to obtain low prediction errors. Furthermore, as in the analysis of the mass flow rate for scroll compressors, using pressures as independent variables allows the response surfaces to be smoothed. Therefore, the correlations evaluated for the characterization of the mass flow rate in reciprocating compressors include a second-order polynomial evaluated in terms of temperature and pressure (Equation 4.17 and Equation 4.18). The use of these functionals, including term elimination methodologies, is also evaluated for the mass flow rate.

$$\text{Temperature domain (T)} \quad \dot{m}_{ref} = c_0 + c_1 T_e + c_2 T_c + c_3 T_e T_c + c_4 T_e^2 + c_5 T_c^2 \quad (4.17)$$

$$\text{Pressure domain (P)} \quad \dot{m}_{ref} = c_0 + c_1 P_e + c_2 P_c + c_3 P_e P_c + c_4 P_e^2 + c_5 P_c^2 \quad (4.18)$$

4.3.3 Comparison of correlations

This section analyzes the results obtained on reciprocating compressors for the proposed correlations, similar to the analysis performed on scroll compressors. The predictive ability of the proposed correlations will be checked, together with the significance of the different polynomial terms.

4.3.3.1 Energy consumption comparison

Table 4.5 shows the fitting results for the AHRI 30 and AHRI 59 compressors. The results for the rest of the compressors analyzed are included in Appendix K. The

AHRI (T) and AHRI (P) models are obtained by fitting the full polynomial with 10 terms (Equation 4.14 and Equation 4.15). Then, the AHRI (T-SW) and AHRI (P-SW) models are the polynomials obtained after applying the automatic term elimination methodology. These tables include the values of the regression coefficients, as well as the **Maximum Relative Error** in % (MRE), **Root Mean Square Error** (RMSE) in W and the **Coefficient of Variation** of the RMSE (CV_{RMSE}) in %. For each compressor and refrigerant, the correlations are fitted to all available test points, including all different suction conditions (as already seen in Figure 4.24, \dot{W}_c is independent of suction conditions). For the specific consumption adjustment, the suction conditions considered as \dot{m}_{map} are those used in adjusting the correlation for the mass flow rate included in the following section. The adjustment coefficients k_0, \dots, k_n and z_c and z_e have been adjusted by previously calculating the ratio \dot{W}_c/\dot{m}_{map} , where \dot{m}_{map} is the predicted mass flow rate, using Equation 4.18. Therefore, the prediction errors for the specific consumption include the possible increase in error due to the prediction errors for the mass flow rate. Concerning this error, we observed that it decreases if we divide the consumption by the prediction of the adjusted model for the mass flow rate, eliminating possible experimental noise. Finally, the coefficients are meant to provide the **energy consumption** in kW with **temperatures** in °C and **pressures** in bar and the **specific consumption** in kJ/kg with **pressures** in bar.

Table 4.5: \dot{W}_c models (AHRI 30, 59)

\dot{W}_c (kW)		MRE (%)	\dot{W}_c (kW)	MRE (%)	\dot{W}_c (kW)	MRE (%)	\dot{W}_c (kW)	MRE (%)	W_{esp} (kJ/kg)	MRE (%)	Fluid
AHRI (T-SW)	RMSE ² (W)		AHRI (P-SW)	RMSE ² (W)	AHRI (T)	RMSE ² (W)	AHRI (P)	RMSE ² (W)		RMSE ² (W)	W , Range [W] (N° tests)
AHRI 30											
c_0, z_c	5.292e-01 (±1.03e-02)**	0.78	9.481e-02 (±1.42e-02)**	1.73 (0.25)	5.292e-01 (±1.05e-02)**	1.67 (0.30)	1.481e-01 (±2.60e-02)**	1.67 (0.30)	-7.732e+00 (±8.98e-01)**	1.65	R134a
c_1, z_e	1.517e-02 (±1.45e-03)**		1.407e-01 (±1.14e-02)**		1.535e-02 (±1.46e-03)**		9.525e-02 (±6.64e-02)**		8.332e-02 (±1.15e-01)		[503, 922]
c_2, k_0	2.639e-03 (±4.84e-04)**		2.254e-02 (±2.59e-03)**		2.640e-03 (±4.85e-04)**		2.002e-02 (±2.61e-03)**		3.434e+01 (±2.18e+00)**		(15/15/15)
c_3, k_1	-1.543e-04 (±6.84e-05)**		-2.438e-03 (±2.93e-03)	0.78	-1.543e-04 (±6.82e-05)**	0.75	1.138e-03 (±2.74e-03)	0.75	6.649e+00 (±3.39e-01)**	4.75 (0.69)	
c_4, k_2	1.327e-04 (±1.36e-05)**		-9.158e-04 (±1.77e-04)**		1.338e-04 (±5.15e-05)**		1.059e-02 (±2.08e-02)				
c_5, k_3	1.489e-05 (±5.35e-06)**		2.182e-04 (±5.54e-05)**		1.489e-05 (±5.33e-06)**		-8.479e-04 (±2.41e-04)**				
c_6	2.948e-06 (±7.56e-07)**		-3.189e-04 (±2.23e-04)**		2.948e-06 (±7.53e-07)**		1.956e-04 (±2.76e-05)**				
c_7					-2.540e-08 (±1.10e-06)		-4.119e-04 (±3.16e-04)*				
c_8					-2.022e-06 (±2.67e-06)		-1.290e-03 (±2.21e-03)				
c_9					(NA)		(NA)				
c_0, z_c	5.727e-01 (±1.43e-02)**	0.81	2.098e-01 (±5.93e-02)**	2.33 (0.33)	5.727e-01 (±1.46e-02)**	2.31 (0.33)	1.301e-01 (±1.26e-01)**	2.33 (0.33)	-9.501e+00 (±1.08e+00)**	1.58	R1234YF
c_1, z_e	1.004e-02 (±1.12e-04)**		1.245e-01 (±2.02e-02)**		9.293e-03 (±2.02e-03)**		1.886e-01 (±1.04e-01)**		4.370e-02 (±1.42e-01)		[531, 919]
c_2, k_0	2.420e-03 (±6.57e-04)**		-2.399e-03 (±9.96e-03)	0.85	2.420e-03 (±6.70e-04)**	0.77	9.614e-04 (±1.10e-02)	0.78	3.132e+01 (±1.83e+00)**	3.94 (0.56)	(15/15/15)
c_3, k_1	8.642e-05 (±8.84e-06)**		6.421e-03 (±3.03e-03)**		1.226e-04 (±9.42e-05)*		4.268e-03 (±2.26e-03)*		5.147e+00 (±2.88e-01)**		
c_4, k_2	-1.710e-05 (±6.97e-05)		-7.460e-03 (±1.63e-03)**		-1.710e-05 (±7.11e-05)		-2.338e-02 (±3.03e-02)				
c_5, k_3	9.289e-06 (±7.22e-06)**		2.101e-04 (±4.05e-04)		9.289e-06 (±7.37e-06)*		2.101e-04 (±4.02e-04)				
c_6	2.422e-06 (±1.49e-06)**		-1.484e-04 (±1.22e-04)*		4.015e-07 (±1.04e-06)		-1.484e-04 (±1.21e-04)*				
c_7					2.422e-06 (±1.52e-06)**		3.262e-04 (±4.61e-04)				
c_8					-1.185e-07 (±3.68e-06)		1.216e-03 (±3.01e-03)				
c_9					(NA)		(NA)				
AHRI 59											
c_0, z_c	8.272e-01 (±5.28e-01)**	1.87	2.277e-01 (±5.74e-01)	10.80 (0.60)	8.259e-01 (±7.13e-01)*	1.92	7.319e-02 (±1.01e+00)	2.01	2.092e+00 (±4.05e+00)	4.06	R410A
c_1, z_e	-4.112e-02 (±5.52e-03)**		3.157e-01 (±1.81e-01)**	12.91 (0.79)	-4.476e-02 (±3.13e-02)*	1.92	3.260e-01 (±2.26e-01)**	2.01	1.259e+00 (±6.84e-01)**	34.69 (2.13)	[918, 2552]
c_2, k_0	1.176e-02 (±3.83e-02)		-3.486e-02 (±3.77e-02)*	1.97	1.279e-02 (±5.39e-02)	1.92	-1.998e-02 (±9.05e-02)	2.01	-2.115e+00 (±7.02e-00)	4.06	(15)
c_3, k_1	1.475e-03 (±1.12e-04)**		1.594e-02 (±4.23e-03)**		1.664e-03 (±1.50e-03)*		1.685e-02 (±7.54e-03)*		1.625e+01 (±2.78e+00)**		
c_4, k_2	-1.168e-03 (±3.04e-04)**		-5.184e-02 (±2.50e-02)**		-1.477e-03 (±1.15e-03)*		-5.502e-02 (±3.48e-02)**		-3.059e-01 (±3.52e-01)*		
c_5, k_3	5.033e-04 (±8.80e-04)		-2.261e-04 (±6.72e-04)		4.708e-04 (±1.28e-03)		-8.609e-04 (±2.97e-03)				
c_6			-1.221e-04 (±7.30e-05)*		-1.914e-06 (±1.67e-05)		-1.096e-04 (±2.29e-04)				
c_7	1.033e-05 (±8.36e-06)*				1.574e-05 (±2.46e-05)		-9.845e-05 (±1.03e-03)				
c_8			1.399e-03 (±1.09e-03)*		-6.609e-06 (±1.75e-05)		1.646e-03 (±2.23e-03)				
c_9	-6.563e-06 (±6.42e-06)*				-6.304e-06 (±9.57e-06)		5.814e-06 (±4.35e-05)				

(Continued on Next Page...)

Table 4.5: \dot{W}_c models (AHRI 30, 59) (continued)

\dot{W}_c (kW)		MRE (%)	RMS E^d (W)	\dot{W}_c (kW)	MRE (%)	RMS E^d (W)	\dot{W}_c (kW)	MRE (%)	RMS E^d (W)	\dot{W}_c (kW)	MRE (%)	RMS E^d (W)	\dot{W}_{exp} (kJ/kg)	MRE (%)	RMS E^d (W)	Fluid W. Range [W] (N° tests)	
AHRI (T-SW)				AHRI (P-SW)	AHRI (T)	AHRI (P)											
AHRI 59																	
c_0, z_c	3.903e-01 (+1.21e-01)***			-1.029e-01 (+6.01e-01)	4.616e-01 (+5.02e-01)+	-1.029e-01 (+6.01e-01)				1.134e+00 (+3.55e+00)							
c_1, z_r	-4.238e-02 (+1.56e-02)**			1.208e-01 (+1.71e-01)	-4.044e-02 (+2.20e-02)**	1.208e-01 (+1.71e-01)				1.193e+00 (+4.36e-01)***							
c_2, k_0	3.906e-02 (+5.42e-03)**			5.558e-02 (+6.59e-02)+	3.353e-02 (+3.80e-02)+	5.558e-02 (+6.59e-02)+				-1.935e+01 (+1.327e+01)							
c_3, k_1	1.940e-03 (+7.44e-04)**			1.082e-02 (+6.88e-03)**	1.846e-03 (+1.06e-03)**	1.082e-02 (+6.88e-03)**				3.298e+01 (+1.178e+01)							
c_4, k_2	-2.378e-02 (+6.23e-04)**			-1.248e-02 (+3.34e-02)*	-2.320e-03 (+8.08e-04)**	-1.248e-02 (+3.34e-02)*				-3.247e+00 (+3.41e+00)+							
c_5, k_3	-3.194e-03 (+3.69e-05)**			-3.082e-03 (+2.61e-03)*	-1.866e-04 (+9.02e-04)	-3.082e-03 (+2.61e-03)*				1.827e-01 (+2.07e-01)*							
c_6	-7.662e-05 (+6.23e-03)**			-3.569e-04 (+2.53e-03)*	-6.603e-06 (+1.18e-05)	-3.569e-04 (+2.53e-03)*											
c_7	3.675e-05 (+1.28e-05)**			1.275e-03 (+1.20e-03)*	3.357e-05 (+1.73e-05)**	1.275e-03 (+1.20e-03)*											
c_8	-3.144e-05 (+1.06e-05)**			-2.038e-03 (+2.72e-03)	-3.106e-05 (+1.23e-05)*	-2.038e-03 (+2.72e-03)											
c_9	-3.968e-06 (+2.57e-06)**			5.484e-05 (+4.61e-05)*	-9.946e-07 (+6.74e-06)	5.484e-05 (+4.61e-05)*											
		1.64	7.04 (0.53)		1.78	8.23 (0.60)			1.65	6.94 (0.50)			1.78	8.23 (0.60)	4.72	L41-1 [779, 2173] (15)	
c_0, z_c	6.378e-01 (+2.13e-01)***			-2.728e-01 (+4.45e-01)	6.057e-01 (+2.66e-01)**	-2.728e-01 (+4.45e-01)				5.346e-01 (+2.77e-00)							
c_1, z_r	-3.622e-02 (+2.19e-03)**			2.738e-01 (+1.10e-01)**	-3.914e-02 (+1.17e-02)**	2.738e-01 (+1.10e-01)**				1.138e+00 (+4.02e-01)***							
c_2, k_0	2.351e-02 (+1.54e-02)**			3.476e-02 (+1.34e-02)+	2.627e-02 (+2.01e-02)*	3.476e-02 (+1.34e-02)+				-2.314e+01 (+1.211e+01)**							
c_3, k_1	1.366e-03 (+4.75e-05)**			1.288e-02 (+3.99e-03)**	1.508e-03 (+5.59e-04)**	1.288e-02 (+3.99e-03)**				1.359e+01 (+1.424e-01)***							
c_4, k_2	-1.779e-03 (+1.53e-04)**			-4.188e-02 (+1.86e-02)**	-1.857e-03 (+4.28e-04)**	-4.188e-02 (+1.86e-02)**				-3.487e+00 (+2.56e+00)*							
c_5, k_3	1.730e-04 (+3.52e-04)**			-2.207e-03 (+1.51e-03)*	1.031e-04 (+4.78e-04)	-2.207e-03 (+1.51e-03)*				2.054e-01 (+1.71e-01)*							
c_6		0.73	3.83 (0.25)	-1.607e-04 (+1.31e-04)*	-1.594e-06 (+6.24e-06)	-1.607e-04 (+1.31e-04)*			0.63	5.56 (0.38)			5.56 (0.38)	2.72	25.63 (1.53)	DR5A [884, 2416] (15)	
c_7	2.290e-05 (+4.30e-06)**			3.376e-04 (+5.96e-04)	2.491e-05 (+9.18e-06)**	3.376e-04 (+5.96e-04)			0.96	5.56 (0.38)							
c_8	-1.481e-05 (+5.09e-06)**			6.263e-04 (+1.30e-03)	-1.566e-05 (+6.52e-06)*	6.263e-04 (+1.30e-03)			0.96	5.56 (0.38)							
c_9	-3.968e-06 (+2.57e-06)**			2.512e-05 (+2.48e-05)*	-3.416e-06 (+3.57e-06)*	2.512e-05 (+2.48e-05)*			0.96	5.56 (0.38)							
c_0, z_c	6.062e-01 (+2.21e-01)***			-1.965e-01 (+2.87e-01)	6.062e-01 (+2.21e-01)***	-1.946e-01 (+3.34e-01)				1.126e+00 (+2.48e+00)							
c_1, z_r	-3.960e-02 (+9.70e-03)**			2.343e-01 (+5.51e-02)**	-3.960e-02 (+9.70e-03)**	2.322e-01 (+8.53e-02)**				1.180e+00 (+3.51e-01)***							
c_2, k_0	2.614e-02 (+1.67e-02)**			3.609e-02 (+2.83e-02)**	2.614e-02 (+1.67e-02)**	3.636e-02 (+3.34e-02)**				-2.169e+01 (+1.193e+01)**							
c_3, k_1	1.617e-03 (+4.44e-04)**			1.166e-02 (+2.06e-03)**	1.617e-03 (+4.44e-04)**	1.159e-02 (+3.55e-03)**				3.380e+01 (+1.15e-01)***							
c_4, k_2	-2.016e-03 (+3.55e-04)**			-3.376e-02 (+5.96e-03)**	-2.016e-03 (+3.55e-04)**	-3.329e-02 (+4.48e-02)**				-3.635e+00 (+2.37e-00)*							
c_5, k_3	6.141e-05 (+3.97e-04)			-2.154e-03 (+1.05e-03)*	6.141e-05 (+3.97e-04)	-2.157e-03 (+1.21e-03)*				2.160e-01 (+1.58e-01)*							
c_6	-3.325e-06 (+3.18e-06)			-3.325e-06 (+3.18e-06)	-3.325e-06 (+3.18e-06)	-2.031e-04 (+1.06e-04)**											
c_7	2.839e-05 (+7.62e-06)**			5.608e-04 (+2.60e-04)**	2.839e-05 (+7.62e-06)**	5.747e-04 (+4.86e-04)**											
c_8	-2.067e-05 (+5.41e-06)**			-2.067e-05 (+5.41e-06)**	-2.067e-05 (+5.41e-06)**	-3.868e-05 (+1.07e-05)											
c_9	-2.881e-06 (+2.96e-06)+			2.887e-05 (+1.59e-05)**	-2.881e-06 (+2.96e-06)+	2.914e-05 (+1.98e-05)*											
		0.53	3.05 (0.20)		0.76	4.25 (0.28)			0.53	3.05 (0.20)			0.73	4.25 (0.28)	3.23	25.63 (1.68)	ARM71a [866, 2371] (15)
c_0, z_c	5.652e-01 (+1.11e-01)***			1.719e-01 (+4.66e-01)*	6.993e-01 (+4.56e-01)**	1.885e-01 (+9.19e-01)				-2.173e+00 (+2.70e+00)							
c_1, z_r	-6.267e-02 (+1.43e-02)**			3.368e-01 (+1.84e-01)**	-5.921e-02 (+1.89e-02)**	3.264e-01 (+3.10e-01)**				9.097e-01 (+3.55e-01)***							
c_2, k_0	2.706e-02 (+5.13e-03)**			-3.258e-02 (+2.74e-02)*	1.666e-02 (+3.46e-02)	-3.222e-02 (+8.52e-02)				-3.296e+01 (+1.93e+01)**							
c_3, k_1	2.985e-03 (+6.94e-04)**			1.644e-02 (+7.58e-03)**	2.813e-03 (+9.26e-04)**	1.624e-02 (+9.42e-03)**				3.338e+01 (+9.42e+00)**							
c_4, k_2	-2.241e-03 (+5.75e-04)**			-5.908e-02 (+2.10e-02)**	-2.113e-03 (+7.39e-04)**	-5.677e-02 (+5.70e-02)+				-4.097e+00 (+1.66e+00)**							
c_5, k_3	-2.238e-04 (+3.53e-05)**			-2.635e-04 (+3.23e-05)	2.561e-05 (+8.21e-04)	-2.671e-04 (+3.54e-05)				2.327e-01 (+9.83e-02)**							
c_6	-2.244e-05 (+7.65e-03)**			-6.326e-04 (+2.86e-03)*	-2.049e-05 (+1.03e-05)*	-6.945e-04 (+3.81e-04)**											
c_7	3.761e-05 (+1.16e-05)**			1.728e-03 (+1.65e-03)*	3.476e-05 (+1.56e-05)**	1.788e-03 (+1.78e-03)*											
c_8	-2.007e-05 (+1.35e-05)**			4.260e-05 (+5.75e-05)	-1.879e-05 (+1.48e-05)*	-2.030e-04 (+4.58e-03)											
c_9		1.93	7.79 (0.65)		2.41	11.03 (0.92)			2.00	7.51 (0.62)			2.35	11.03 (0.91)	2.08	14.61 (1.21)	D2Y60 [787, 1838] (17)
c_0, z_c	1.682e+00 (+1.81e-00)+			3.755e-01 (+1.28e-00)	1.682e+00 (+1.81e-00)+	3.750e-01 (+1.48e-00)				6.101e+00 (+2.70e-00)**							
c_1, z_r	6.653e-02 (+1.03e-01)			2.646e-01 (+2.35e-01)*	6.653e-02 (+1.03e-01)	2.663e-01 (+3.17e-01)+				2.041e+00 (+3.26e-01)**							
c_2, k_0	-5.384e-02 (+1.34e-01)+			-2.654e-02 (+1.07e-01)	-5.384e-02 (+1.34e-01)+	-2.699e-02 (+1.31e-01)				-1.118e+01 (+3.88e-01)							
c_3, k_1	-4.311e-03 (+4.90e-03)+			3.930e-02 (+1.14e-02)**	-4.311e-03 (+4.90e-03)+	3.908e-02 (+2.52e-02)**				3.532e+01 (+2.05e+01)**							
c_4, k_2	2.181e-03 (+2.43e-03)+			-8.266e-02 (+2.96e-02)**	2.181e-03 (+2.43e-03)+	-8.255e-02 (+3.56e-02)**				-2.589e+00 (+4.39e-00)							
c_5, k_3	2.350e-03 (+3.19e-03)+			-3.992e-03 (+2.71e-03)*	2.350e-03 (+3.19e-03)+	-3.940e-03 (+6.00e-03)				1.207e-01 (+2.96e-01)							
c_6	7.572e-05 (+5.66e-05)**			2.858e-04 (+2.51e-04)*	7.572e-05 (+5.66e-05)**	2.957e-04 (+1.02e-03)											
c_7	-8.098e-05 (+5.18e-05)**			-2.451e-03 (+9.79e-04)**	-8.098e-05 (+5.18e-05)**	-2.469e-03 (+2.19e-03)*											
c_8	2.706e-05 (+2.59e-05)**			4.892e-03 (+1.84e-03)**	2.706e-05 (+2.59e-05)**	4.908e-03 (+2.66e-03)**											
c_9	-2.169e-05 (+2.47e-05)+				-2.169e-05 (+2.47e-05)+	-1.643e-06 (+1.63e-04)											
		1.11	9.94 (0.85)		2.13	15.22 (0.94)			1.11	9.94 (0.85)			2.11	15.22 (0.94)	5.57	54.65 (3.02)	R32 [896, 3083] (15)

^a + p < 0.1, * p < 0.05, ** p < 0.01, *** p < 0.001; Confidence interval of 95% for regression coefficients;

^b Temperatures (°C);

^c Pressures (bar);

^d The values in brackets are the CV_{RMS E} (%).

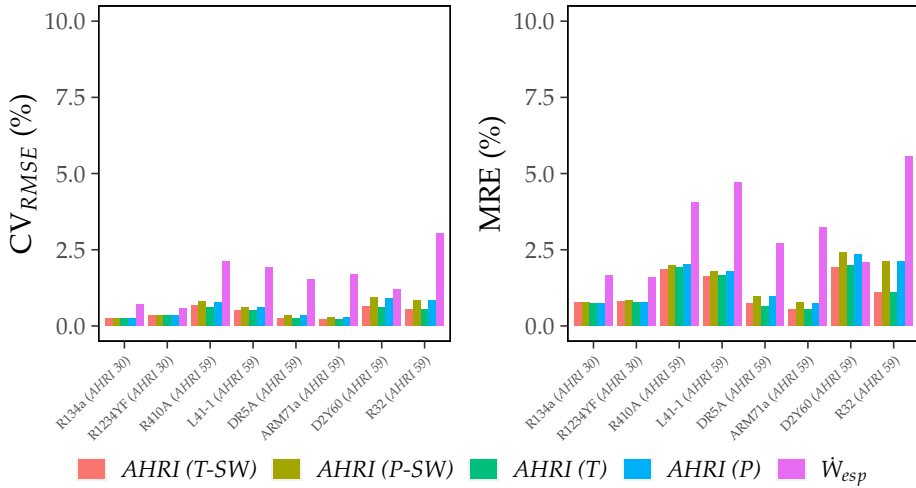


Figure 4.32: Energy consumption model errors (AHRI 30, 59)

As we can see from the results for the energy consumption (AHRI (T), AHRI (P), AHRI (T-SW) and AHRI (P-SW) correlations), the prediction errors are low for both temperature and pressure-fitted models. In the case of the AHRI 30 (L/MBP) compressor, we can observe that the term elimination methodologies obtain more compact models than in the AHRI 59 (HBP) compressor. Furthermore, it has been noticed that, in general, the compressors with LBP and MBP application ranges present large collinearity when trying to fit the 10-term AHRI polynomial. In the case of the AHRI 30 compressor, we can observe that the regression fit has not been able to estimate the cubic term (NA) referring to condensation conditions (T_c^3 or P_c^3) in the AHRI (T) and AHRI (P) models. Then, some regression coefficients show non-significance in the correlation with high p -values. This reinforces the hypothesis that this type of compressor, with more straightforward response surfaces, does not need such a large polynomial model, but the best polynomials required for each case are different. Therefore, it is advisable to eliminate terms to avoid overfitting in the model adjustment, but it is not possible to supply a general expression that is suitable for all the compressors and refrigerants.

Additionally, another possible approach could be to generate the compressor performance maps with other more sophisticated tools such as non-parametric regression models like a Thin-Plate-Spline regression model (Afram and Janabi-Sharifi, 2014; Green and Silverman, 1993). This allows a smooth interpolation, and accurate results can be obtained regardless of the complexity of the response surface.

On the other hand, we can also observe low prediction errors for the correlation of specific consumption, but these are slightly higher than the previous models. However, we must consider that the previous models have been fitted with a large number of terms and with samples that generally do not exceed 15 experimental points⁴. Therefore, we are not considering the possible extrapolation or interpolation errors that we can obtain when utilizing models with a large number of terms, as demonstrated previously in scroll compressors (see, Figure 4.22). Furthermore, as already shown in the previous sections, selecting \dot{W}_{esp} as the response variable brings some advantages, such as greater simplicity of the response surface (models with fewer terms) and higher similarity between compressor technologies (the same functional can be used to characterize reciprocating compressors or scroll compressors). Thus, for the \dot{W}_{esp} model, it has been verified that a major part of the analyzed reciprocating compressors achieves good results with a third-degree polynomial (Equation 4.16 on page 153). In some cases a lower degree for the polynomial also achieves good results but cannot be generalized. Regarding the significance of the coefficients, it is observed that sometimes one of the two terms z_c or z_e is non-significant. This means that the vertex coordinates of the specific consumption isolines can be considered on the coordinate or ordinate axis. However, considering the fact that neither terms (z_c, z_e) increases the prediction error, and many of the analyzed compressors obtain significance in both terms, it is recommended that both coefficients are considered in the fit in order to obtain a more general correlation. This correlation has also been tested for the scroll compressors analyzed in the first part of this chapter, obtaining similar results. In this case, for scroll compressors, second degree in Equation 4.16 is enough to obtain a low prediction error, and a linear correlation can be considered in many of the scroll compressors analyzed from the database. Therefore, the specific consumption can be characterized using a simple functional with a reduced number of terms. This type of correlation has the advantage of not using any statistical methodology of term elimination in order to obtain an expression for all the compressors. The response surfaces analyzed are quite similar regardless of the operating range or compressor technology used.

Summing up these results, this section includes several models in terms of temperature or pressure capable of accurately characterizing the energy consumption in reciprocating compressors. Similar prediction errors are obtained by fitting the model in terms of pressures or temperatures. However, as mentioned above, defining the model in terms of pressures results in less dependence on the refrigerant used, obtaining a more general approach to characterizing compressors, and with the additional advantage of being able to characterize compressors

⁴In some cases, the energy consumption data available for each compressor and refrigerant include different suction conditions. Therefore, for the energy consumption, the useful experimental information refers to a single suction conditions (\dot{W}_c is independent of suction conditions).

sors in transcritical cycles. Finally, an additional model for the characterization of the specific energy consumption is also analyzed. It has the main advantage of defining a simple polynomial equation able to accurately predict the energy consumption in both technologies, scroll and reciprocating compressors.

4.3.3.2 Mass flow rate comparison

Table 4.6 shows the fitting results for the AHRI 30 and AHRI 59 compressors. The results for the rest of the compressors analyzed are included in Appendix K. These tables contain the same information as those already analyzed for the energy consumption in the previous section, including the second-order polynomial models in terms of temperature and pressure (second-order polynomial (T) and (P)), and the same correlations after applying the automatic term elimination methodology (second-order polynomial (T-SW) and (P-SW)). Figure 4.33 also represents the error values of the CV_{RMSE} and MRE. These correlations have been obtained by selecting one of the available suction conditions for each compressor analyzed. The results have also been checked by adjusting the proposed functionals to the rest of the suction conditions with similar results. The coefficients are meant to provide the mass flow rate in kg/h with temperatures in °C and pressure in bar.

Table 4.6: \dot{m}_{ref} models (AHRI 30, 59)

\dot{m}_{ref} (kg/h) 2 nd order polynomial (T-SW)		MRE (%) RMSE (kg/h)	\dot{m}_{ref} (kg/h) 2 nd order polynomial (P-SW)		MRE (%) RMSE (kg/h)	\dot{m}_{ref} (kg/h) 2 nd order polynomial (T)		MRE (%) RMSE (kg/h)	\dot{m}_{ref} (kg/h) 2 nd order polynomial (P)		MRE (%) RMSE (kg/h)	Fluid = Range [kg/h] (N° tests)
AHRI 30 (SH = 11K)												
c ₀	3.048e+01 (+1.13e+00)***	0.66 0.09 (0.28)	-4.131e+00 (+1.17e+00)***	0.66 0.09 (0.28)	3.048e+01 (+1.21e+00)***	0.65 0.09 (0.28)	-4.598e+00 (+1.80e+00)***	0.69 0.09 (0.28)	R134a [18, 46] (15)			
c ₁	1.301e+00 (+8.84e-03)***		1.284e+01 (+7.91e-01)***		1.302e+00 (+3.60e-02)***		1.286e+01 (+9.00e-01)***					
c ₂	1.104e-01 (+5.33e-02)***		1.04e-01 (+5.70e-02)**		1.104e-01 (+5.70e-02)**		7.743e-02 (+1.85e-01)					
c ₃					-2.000e-05 (+7.72e-04)		-1.455e-03 (+2.33e-02)					
c ₄	1.678e-02 (+1.49e-03)***		-1.097e-01 (+1.28e-01)+		1.678e-02 (+1.60e-03)***		-1.097e-01 (+1.38e-01)					
c ₅	-2.222e-03 (+5.89e-04)***	-1.208e-02 (+6.57e-04)***	-2.222e-03 (+6.31e-04)***	-1.501e-02 (+6.90e-03)***								
AHRI 30 (SH = 11K)												
c ₀	3.757e+01 (+4.76e+00)***	2.18 0.35 (0.90)	1.871e+00 (+4.14e+00)	2.19 0.41 (1.05)	3.757e+01 (+4.76e+00)***	2.18 0.35 (0.90)	-3.628e+00 (+8.08e+00)	2.20 0.35 (0.90)	R1234YF [24, 55] (15)			
c ₁	1.334e+00 (+1.42e-01)***		1.245e+01 (+1.25e+00)***		1.334e+00 (+1.42e-01)***		1.445e+01 (+3.77e+00)***					
c ₂	1.118e-01 (+2.24e-01)		-5.278e-01 (+3.33e-01)**		1.118e-01 (+2.24e-01)		-1.034e-01 (+8.23e-01)					
c ₃	2.440e-03 (+3.04e-03)		7.869e-02 (+1.00e-01)		2.440e-03 (+3.04e-03)		7.869e-02 (+9.78e-02)					
c ₄	1.479e-02 (+6.28e-03)***				1.479e-02 (+6.28e-03)***		-3.030e-01 (+5.41e-01)					
c ₅	-2.102e-03 (+2.48e-03)+		-2.102e-03 (+2.48e-03)+	-1.736e-02 (+3.09e-02)								
AHRI 59 (SH = 11K)												
c ₀	1.777e+02 (+1.15e+01)***	5.41 1.10 (0.91)	-2.200e+01 (+1.20e+01)**	6.04 1.18 (0.88)	1.777e+02 (+1.15e+01)***	5.41 1.10 (0.91)	-2.041e+01 (+1.39e+01)**	5.66 1.15 (0.96)	R410A [31, 196] (15)			
c ₁	7.194e+00 (+4.54e-01)***		2.770e+01 (+1.15e+00)***		7.194e+00 (+4.54e-01)***		2.710e+01 (+2.51e+00)***					
c ₂	-9.504e-01 (+5.47e-01)**		-1.885e+00 (+7.50e-01)**		-9.504e-01 (+5.47e-01)**		-1.867e+00 (+7.90e-01)**					
c ₃	-3.083e-02 (+9.40e-03)***		-1.798e-01 (+4.20e-02)**		-3.083e-02 (+9.40e-03)***		-1.924e-01 (+6.39e-02)***					
c ₄	6.819e-02 (+1.09e-02)***				6.819e-02 (+1.09e-02)***		6.013e-02 (+2.21e-01)					
c ₅	-8.085e-03 (+6.04e-03)*	1.380e-02 (+1.29e-02)*	-8.085e-03 (+6.04e-03)*	1.528e-02 (+1.46e-02)*								
AHRI 59 (SH = 11K)												
c ₀	1.112e+02 (+9.50e+00)***	4.32 0.91 (1.22)	-1.340e+01 (+1.45e+01)+	9.08 1.29 (1.79)	1.112e+02 (+9.50e+00)***	4.32 0.91 (1.22)	-1.340e+01 (+1.45e+01)+	9.08 1.29 (1.79)	L41-1 [17, 126] (15)			
c ₁	5.180e+00 (+3.77e-01)***		1.992e+01 (+3.30e+00)***		5.180e+00 (+3.77e-01)***		1.992e+01 (+3.30e+00)***					
c ₂	-7.081e-01 (+4.54e-01)**		-1.265e+00 (+1.00e+00)*		-7.081e-01 (+4.54e-01)**		-1.265e+00 (+1.00e+00)*					
c ₃	-2.792e-02 (+7.80e-03)***		-2.369e-01 (+1.02e-01)**		-2.792e-02 (+7.80e-03)***		-2.369e-01 (+1.02e-01)**					
c ₄	5.887e-02 (+9.04e-03)***		3.145e-01 (+3.70e-01)+		5.887e-02 (+9.04e-03)***		3.145e-01 (+3.70e-01)+					
c ₅	-3.810e-03 (+5.01e-03)	1.897e-02 (+2.22e-02)+	-3.810e-03 (+5.01e-03)	1.897e-02 (+2.22e-02)+								

(Continued on Next Page...)

Table 4.6: \dot{m}_{ref} models (AHRI 30, 59) (continued)

\dot{m}_{ref} (kg/h) 2 nd order polynomial (T-SW)		MRE (%) RMSE (kg/h)	\dot{m}_{ref} (kg/h) 2 nd order polynomial (P-SW)		MRE (%) RMSE (kg/h)	\dot{m}_{ref} (kg/h) 2 nd order polynomial (T)		MRE (%) RMSE (kg/h)	\dot{m}_{ref} (kg/h) 2 nd order polynomial (P)		MRE (%) RMSE (kg/h)	Fluid # Range [kg/h] (N° tests)
AHRI 59 (SH = 11K)												
c_0	1.329e+02 (+4.99e+00)***	2.04 0.48 (0.52)	-1.817e+01 (+1.01e+01)**	4.72 0.85 (0.92)	1.329e+02 (+4.99e+00)***	2.04 0.48 (0.52)	-1.817e+01 (+1.01e+01)**	4.72 0.85 (0.92)	1.329e+02 (+4.99e+00)***	2.04 0.48 (0.52)	-1.817e+01 (+1.01e+01)**	DR5A [23, 151] (15)
c_1	5.708e+00 (+1.98e-01)***		2.189e+01 (+2.01e+00)***		5.708e+00 (+1.98e-01)***		2.189e+01 (+2.01e+00)***					
c_2	-6.890e-01 (+2.38e-01)***		-1.290e+00 (+6.22e-01)**		-6.890e-01 (+2.38e-01)***		-1.290e+00 (+6.22e-01)**					
c_3	-2.747e-02 (+4.10e-03)***		-1.962e-01 (+5.51e-02)***		-2.747e-02 (+4.10e-03)***		-1.962e-01 (+5.51e-02)***					
c_4	5.757e-02 (+4.75e-03)***		1.443e-01 (+1.93e-01)		5.757e-02 (+4.75e-03)***		1.443e-01 (+1.93e-01)					
c_5	-5.910e-03 (+2.63e-03)**		1.406e-02 (+1.24e-02)*		-5.910e-03 (+2.63e-03)**		1.406e-02 (+1.24e-02)*					
c_0	1.316e+02 (+5.93e+00)***	2.52 0.57 (0.64)	-1.580e+01 (+1.16e+01)*	4.93 0.98 (1.10)	1.316e+02 (+5.93e+00)***	2.52 0.57 (0.64)	-1.580e+01 (+1.16e+01)*	4.93 0.98 (1.10)	1.316e+02 (+5.93e+00)***	2.52 0.57 (0.64)	-1.580e+01 (+1.16e+01)*	ARM71a [23, 147] (15)
c_1	5.652e+00 (+2.35e-01)***		2.190e+01 (+2.36e+00)***		5.652e+00 (+2.35e-01)***		2.190e+01 (+2.36e+00)***					
c_2	-7.848e-01 (+2.83e-01)***		-1.428e+00 (+7.30e-01)**		-7.848e-01 (+2.83e-01)***		-1.428e+00 (+7.30e-01)**					
c_3	-2.836e-02 (+4.87e-03)***		-2.097e-01 (+6.65e-02)***		-2.836e-02 (+4.87e-03)***		-2.097e-01 (+6.65e-02)***					
c_4	5.795e-02 (+5.64e-03)***		1.636e-01 (+2.35e-01)		5.795e-02 (+5.64e-03)***		1.636e-01 (+2.35e-01)					
c_5	-4.531e-03 (+3.13e-03)**		1.825e-02 (+1.49e-02)*		-4.531e-03 (+3.13e-03)**		1.825e-02 (+1.49e-02)*					
c_0	1.415e+02 (+3.85e+00)***	6.55 1.51 (1.80)	-2.416e+01 (+1.41e+01)**	8.78 1.52 (1.81)	1.375e+02 (+1.47e+01)***	7.19 1.48 (1.77)	-1.933e+01 (+1.81e+01)*	7.37 1.46 (1.74)	1.415e+02 (+3.85e+00)***	7.19 1.48 (1.77)	-1.933e+01 (+1.81e+01)*	D2Y60 [25, 147] (17)
c_1	5.983e+00 (+4.51e-01)***		2.993e+01 (+1.88e+00)***		5.917e+00 (+5.21e-01)***		2.817e+01 (+4.44e+00)***					
c_2	-1.258e+00 (+8.43e-02)***		-1.920e+00 (+1.14e+00)**		-1.056e+00 (+7.11e-01)**		-1.974e+00 (+1.16e+00)**					
c_3	-3.242e-02 (+9.56e-03)***		-3.040e-01 (+9.00e-02)***		-3.103e-02 (+1.10e-02)**		-3.391e-02 (+1.21e-01)***					
c_4	5.958e-02 (+1.32e-02)***		2.951e-02 (+2.53e-02)*		5.771e-02 (+1.52e-02)**		2.148e-01 (+4.91e-01)					
c_5					-2.234e-03 (+7.79e-03)		3.524e-02 (+2.88e-02)*					
c_0	1.179e+02 (+2.13e+00)***	15.45 1.16 (1.41)	-1.346e+01 (+9.14e+00)**	13.19 1.19 (1.45)	1.123e+02 (+2.02e+01)***	10.26 1.08 (1.32)	-1.582e+01 (+1.32e+01)**	13.09 1.16 (1.42)	1.179e+02 (+2.13e+00)***	10.26 1.08 (1.32)	-1.582e+01 (+1.32e+01)**	R32 [18, 144] (15)
c_1	4.419e+00 (+1.11e-01)***		2.177e+01 (+2.26e+00)***		4.090e+00 (+7.20e-01)***		2.144e+01 (+2.72e+00)***					
c_2			-2.101e+00 (+1.51e-01)**		2.779e-01 (+9.74e-01)		-1.825e+00 (+9.03e-01)**					
c_3					7.716e-03 (+1.67e-02)		2.191e-02 (+1.25e-01)					
c_4	3.515e-02 (+7.61e-03)***		-2.891e-01 (+1.45e-01)**		3.165e-02 (+1.08e-02)**		-3.034e-02 (+2.25e-01)*					
c_5	-1.574e-02 (+1.07e-03)***				-1.904e-02 (+1.13e-02)**		-8.210e-03 (+2.92e-02)					

^a + p < 0.1, * p < 0.05, ** p < 0.01, *** p < 0.001; Confidence interval of 95% for regression coefficients;

^b Temperatures (°C);

^c Pressures (bar);

^d The values in brackets are the CV_{RMSE} (%);

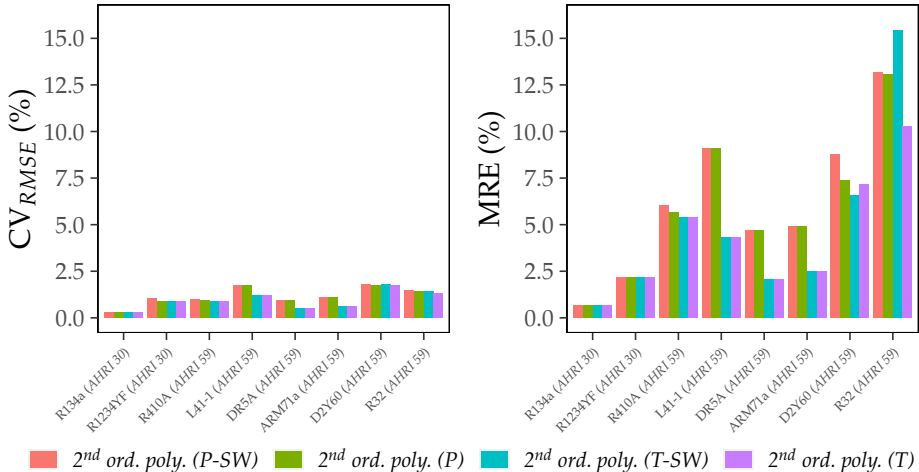


Figure 4.33: Mass flow rate model errors (AHRI 30, 59)

As we can see in the results, some compressors obtain a MRE of more than 5%. However, after checking these cases, it was noticed that these errors are due to one or two individual points at the lower values of the mass flow rate in each dataset, where the error measurement is higher. Furthermore, the values for the CV_{RMSE} are low in all cases, being a better indicator of the predictive power of the models because these individual points do not influence them. Therefore we can conclude that a second-order polynomial is enough to characterize the mass flow rate instead of using the full functional defined in the AHRI standard. The elimination of cubic terms makes it possible to obtain more compact polynomials with better predictive behavior, avoiding overfitting problems with the AHRI polynomials.

Nevertheless, most compressors obtain even more compact models by applying the automatic term elimination methodology. So, it is not possible to provide a general functional like in scroll compressors, where low prediction errors could be obtained by fitting a simple linear correlation and improving the results by adding an interaction term ($P_c \times P_e$). In reciprocating compressors, these functionals were only suitable for some compressors.

Therefore, using Equation 4.17 and Equation 4.18 to characterize the mass flow rate in reciprocating compressors will be recommended, considering the application of automatic term elimination methodologies as optional. Furthermore, due to the predictive power is similar in both correlations, it will be more suitable to use the correlation in terms of pressure (Equation 4.18). It provides a more general functional that can also characterize compressors in transcritical cycles.

4.3.4 Experimental points required

Once the models proposed in this work for the characterization of reciprocating compressors have been analyzed, we will focus again on selecting proper experimental samples for their adjustment. As commented before, this topic is addressed in the field of regression modelling by the so-called Design of Experiments methodologies, where computer-aided designs have the advantage of adapting to irregular domains, and therefore, they are suitable methodologies to apply over the compressor envelope⁵.


⁵Compressors have two areas of no operation, one limited by the high discharge temperatures, where the integrity of the compressor would be compromised, and another area limited by a low-pressure ratio with a considerable loss of efficiency.

These tools have already been analyzed in the scroll compressor analysis. In that case, the most adequate design was the optimal designs (OD). However, the reciprocating compressor tests analyzed in this second part do not include any fine-meshed dataset with which to perform a detailed analysis.

Therefore, one of the scroll compressors already analyzed has been selected to perform an analysis on the selection of optimal samples for the characterization of the specific consumption. This compressor is the ZS21KAE-PFV (Shrestha et al., 2013b) with a dataset of about 60 points for the same suction conditions and refrigerant (R404A and SH=11K). As previously shown, the response surfaces for the specific consumption are very similar for both compressor typologies (scroll and reciprocating), with similar results also obtained for the mass flow rate. Therefore, the conclusions obtained from the analysis of this massive dataset are easily extrapolated to reciprocating compressors.

Regarding the type of experimental design to be used, the model proposed for the specific consumption is adjusted using nonlinear regression tools. In previous analysis of scroll compressors, the use of linear models allowed the use of optimal designs (OD) employing the Fedorov algorithm. In this case, due to the fact that this methodology only contemplates the use of purely linear models, for the specific energy consumption, another type of design known as Cluster Designs (CD) and another typology, Polygonal Designs (PD) (Aute et al., 2015), have been selected.

Both typologies are based on the automatic grouping of points in clusters, considering their location in the experimental domain, and performing the experimental sample by selecting the centroid of each cluster. The main objective will be to obtain an experimental sample homogeneously distributed over the compressor envelope. Thus, the Polygonal Design differs from the pure Cluster Design in a first manual selection of the polygon vertexes defining the compressor envelope and completing the remaining points by grouping them by clusters.

Based on the results of both methodologies, the Polygonal Design can be considered a proper methodology for compressor characterization. It has the advantage of completely covering the experimental domain, regardless of the number of points to be included in the design in which, in the case of cluster design, compact samples tend to move away from the envelope edges. Selecting three samples of 7, 9 and 11 tests as an example, Figure 4.34 includes the samples generated by the Polygonal Design. The automatic selection has been performed by the open-source programming language  and the *k-means* algorithm from the *stats* base package.

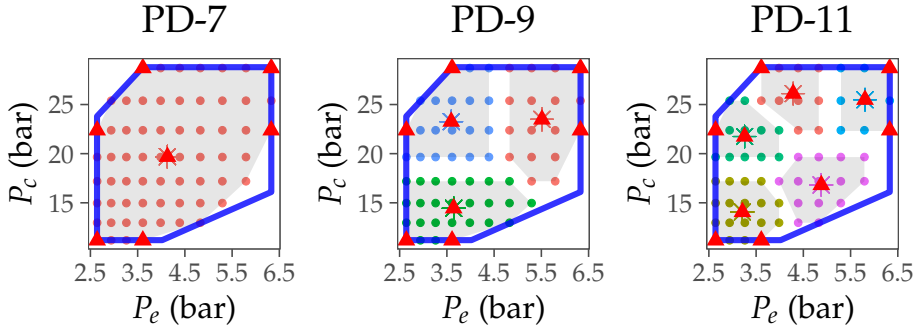


Figure 4.34: Polygonal Design (7, 9, 11 test points). AHRI 21 R404A

As can be observed in Figure 4.34, the Polygonal design obtains homogeneously distributed samples over the entire compressor envelope. The points in red are the corresponding sample performed by the PD. Then, once we know the location of the experimental points, we are able to fit the models proposed for the specific energy consumption and the mass flow rate. The mass flow rate model selected was the one proposed in scroll compressors, Equation 4.8, on page 128 due to the greater simplicity. It was also tested the one proposed in reciprocating compressor (Equation 4.18), and similar results were obtained. From the adjustment of these models with the different experimental designs, the sample of 9 points obtained the best results between sample size and prediction accuracy for the models adjusted, so it is included in Table 4.7 summarizing the main results of the predictive capabilities of the model.

Table 4.7: Regression model adjusted with PD sample, 9 tests (AHRI 21 R404A)

	All points ^c		Sample OD (9 test points) ^c	
	\dot{W}_{esp} (kJ/kg)	\dot{m}_{ref} (kg/h)	\dot{W}_{esp} (kJ/kg)	\dot{m}_{ref} (kg/h)
c_0, z_c	-6.117e+00 ($\pm 6.01e-01$)***	-4.720e+00 ($\pm 2.29e+00$)***	-6.417e+00 ($\pm 4.68e+00$)*	-2.285e+00 ($\pm 9.04e+00$)
c_1, z_e	-6.089e-01 ($\pm 1.05e-01$)***	5.332e+01 ($\pm 5.70e-01$)***	-6.221e-01 ($\pm 9.27e-01$)	5.245e+01 ($\pm 2.78e+00$)***
c_2, k_0	-2.652e+00 ($\pm 1.38e+00$)***	-2.385e-01 ($\pm 1.13e-01$)***	-2.135e+00 ($\pm 1.16e+01$)	-3.305e-01 ($\pm 3.97e-01$)+
c_3, k_1	1.013e+01 ($\pm 2.59e-01$)***	-1.156e-01 ($\pm 2.67e-02$)***	1.002e+01 ($\pm 2.39e+00$)***	-8.423e-02 ($\pm 1.17e-01$)
Num.Obs.	191	63	9	9
RMSE (W, kg/h)	24.070	0.532	30.236 (17.686 ^d)	0.698 (0.917 ^d)
CV _{RMSE} (%)	0.829	0.264	1.041 (0.609 ^d)	0.347 (0.456 ^d)
MRE (%)	2.845	0.850	3.048 (2.640 ^d)	0.968 (1.119 ^d)
Range (W, kg/h)	[1856, 4172]	[124, 308]	[1856, 4172]	[124, 308]

^a + p < 0.1, * p < 0.05, ** p < 0.01, *** p < 0.001;

^b Pressure (bar);

^c Models: Equation 4.16 (\dot{W}_{esp}) and Equation 4.8 (\dot{m}_{ref});

^d MRE, RMSE and CV_{RMSE} for the original AHRI polynomial fitted with PD and 11 experimental points;

In this case, the fitting process is performed as in Subsection 4.2.4 for scroll compressors, using the Inverse-Variance Weighting (IVW) rather than the conventional Ordinary Least Squares (OLS) adjustment.

Table 4.7 also includes the MRE, RMSE and CV_{RMSE} obtained when fitting the original AHRI polynomial and selecting a sample of 11 test points (in brackets). As can be seen, Maximum Relative Error (MRE), Root Mean Square Error (RMSE) and the differences on the polynomial parameters with the 9 experimental points sample began to be very small, being a rational number of required points. Moreover, looking at the MRE and RMSE values in brackets, one can see that the AHRI polynomial fit does not improve the accuracy and slightly increases the prediction error in the mass flow rate, with similar results seen for the energy consumption.

Finally, the prediction capabilities using random samples are also tested for the specific energy consumption polynomial. The same 50 random samples selected previously in the scroll analysis are used to adjust the functional for the specific energy consumption. The corresponding prediction errors obtained for the specific energy consumption are combined with the previous one obtained in the scroll analysis and these results are plotted in Figure 4.35. In this case, we can see that the stability of the model for specific consumption is also good. We do not obtain random samples that generate a bad fit of the model coefficients. This is partly due to the smoothness and simplicity of the response surface of the specific consumption, together with the fact that the proposed model contemplates a smaller number of possible terms including also a good accuracy. In this sense, the model's accuracy is slightly lower than the polynomial models proposed in scroll compressors. However, it has the following advantages:

- It has a good accuracy.
- The model shows a great robustness against extrapolation and interpolation problems.
- It is valid for both technologies.
- It requires a small sample size for the adjustment.

Therefore, we can conclude that it is a very interesting option when trying to characterize the consumption of compressors. It is also especially interesting in the case of reciprocating compressors, where the complexity of characterizing the energy consumption can be higher, and this approach provides us with a general polynomial expression requiring small sample sizes.

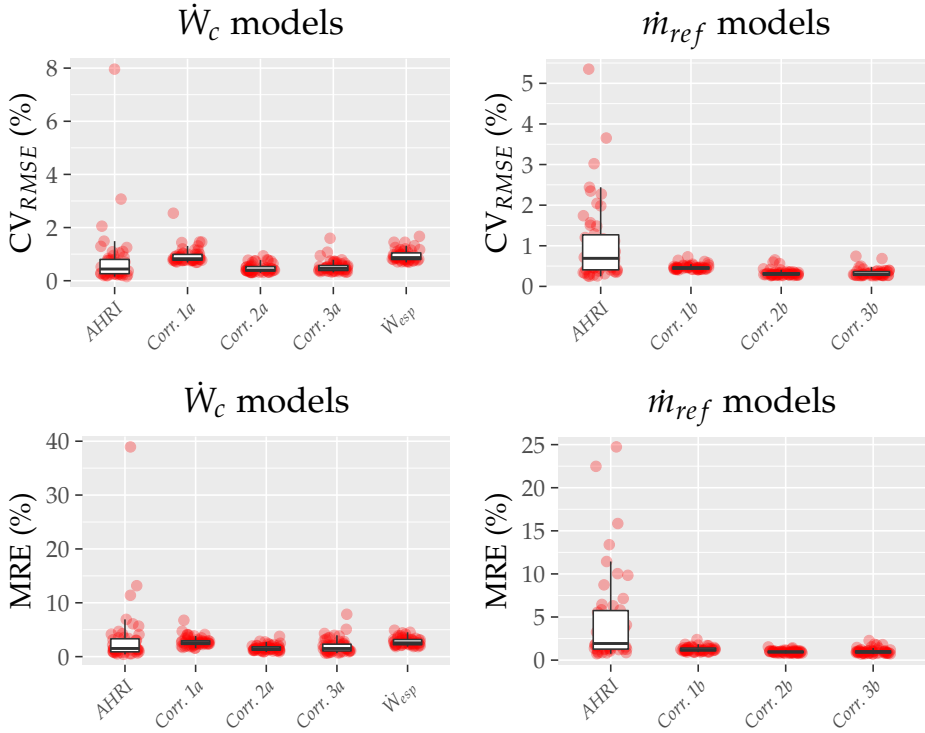


Figure 4.35: Random samples error models including \dot{W}_{esp} results (AHRI 21 R404A)

4.4 Comparison of technologies

Once we have finished the in-depth analysis of the performance response surfaces in scroll and reciprocating compressors, this section aims to compare the observed differences in a little more detail.

On the one hand, the mass flow rate shows a similar trend between technologies. In this sense, the reciprocating compressors, despite the higher dependence of the volumetric efficiency on the pressure ratio, still obtain surfaces mainly dependent on the suction temperature. This is because the suction conditions will set the density of the refrigerant at the suction port, so the compressor will pump at a higher or lower flow rate.

On the other hand, the energy consumption response surfaces shows the greatest difference in their behavior between technologies. These are more straightforward in scroll compressors (mainly dependent on condensation conditions), and can be more complex in reciprocating compressors (dependent on both condensation and evaporation conditions or mainly only dependent on evaporating conditions). Perhaps the latter case—the energy consumption in reciprocating compressors—is the most complicated case with different behaviors, as shown in Figure 4.36.

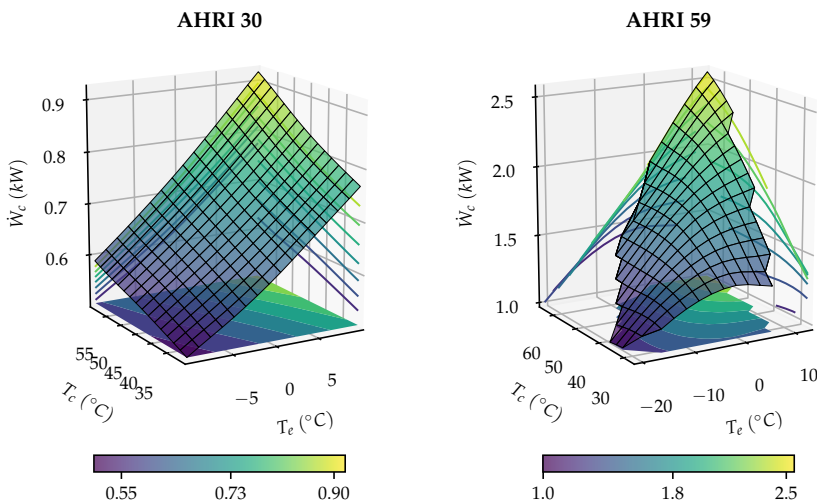


Figure 4.36: 3D plot of \dot{W}_c , temp. domain (AHRI 30 R134a and AHRI 59 R410A. SH=11K)

To understand these differences better, we will start from the definition of the theoretical power in compressors, considering the compression process as isentropic (adiabatic and reversible). This isentropic compression power (\dot{W}_{is}) is related to the compressor energy consumption according to Equation 4.19:

$$\dot{W}_c = \rho_s V_s n \Delta h_{is} \frac{\eta_v}{\eta_c} \quad (4.19)$$

Therefore, let us take a closer look at the highlighted terms of the above equation. We will refer to the blue one as the isentropic compression power and the red one as the ratio of efficiencies. Considering the same isentropic compression power for a specific refrigerant in the same range of working pressures, we can already intuit that the efficiency ratio will correct it and will have a different trend for each of the technologies due to the differences in the energy consumption already observed above.

Selecting first the isentropic compression power, Equation 4.25 shows how to obtain it as a function of the evaporation and condensation pressures. This equation can be obtained simply by considering the ideal gas assumption and substituting Equations 4.21, 4.22, 4.23, and 4.24 into Equation 4.20. We consider also that discharge and suction pressure in compressors are approximately the same as the evaporation and condensation pressures.

$$\dot{W}_{is} = \rho_s V_s n c_p (T_{2s} - T_s) \quad (4.20)$$

$$\frac{T_{2s}}{T_s} = \frac{P_c^{\frac{k-1}{k}}}{P_e} \quad (4.21)$$

$$\rho_s = \frac{P_e}{RT_s} \quad (4.22)$$

$$R = c_p - c_v \quad (4.23)$$

$$k = \frac{c_p}{c_v} \quad (4.24)$$

$$\dot{W}_{is} = V_s n \frac{k}{k-1} P_e \left[\frac{P_c^{\frac{k-1}{k}}}{P_e} - 1 \right] \quad (4.25)$$

Considering suitable values for the above variables, e.g., $V_s = 20 \text{ cm}^3$, $n_s = 3000 \text{ rpm}$, $k \approx 1.13$, and a wide working range, we can obtain the evolution of \dot{W}_{is} as a function of the operating conditions (Figure 4.37).

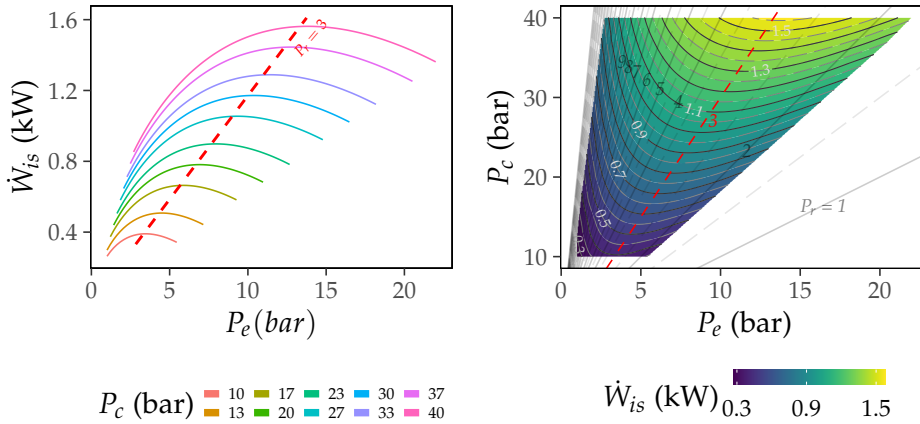


Figure 4.37: \dot{W}_{is} dependence as a function of working conditions

We can see from the figure above that the isentropic compression power is a complex surface depending on the operating conditions. Thus, this evolution of \dot{W}_{is} may be classified in two cases:

1. At constant inlet pressure: \dot{W}_{is} increases monotonically with the increasing discharge pressure. This is done in applications where the evaporator temperature remains constant and the condensation temperature changes.
2. At constant discharge pressure but with varying suction pressure: In this case, there is a maximum for \dot{W}_{is} at a specific pressure ratio (P_r).

The P_r at this maximum will depend on the characteristic isentropic expansion coefficient (k) of each refrigerant, but can be considered in the order of 3 (see Granryd et al., 2011, page 7:13). Commonly, this maximum is of special interest for the dimensioning of the compressor electric motor in order to provide the required power demand.

Analyzing Figure 4.37-right, we can see that it maintains some similarity with the consumption surfaces obtained in scroll compressors, where consumption depends mainly on the condensing conditions. However, in that case, no maximum was appreciated, which leads us to consider that the efficiency ratio corrects mainly in two zones, maximum and minimum of P_r . In the case of reciprocating compressors, this correction with the efficiency ratio should be more significant, due to the fact that in many of them, the consumption depended mainly on the evaporation conditions. We will now analyze the trend of the efficiency ratio (highlighted in blue in Equation 4.19) to better understand these differences. Thus, starting by identifying the different trends in volumetric and compressor

efficiency with the pressure ratio in both technologies is a pertinent approach. Figure 4.38 shows typical efficiency vs pressure ratio curves for scroll and reciprocating compressors.

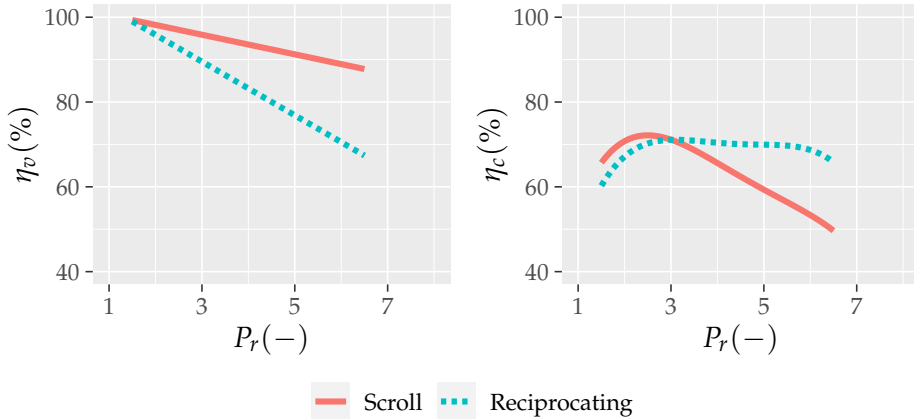


Figure 4.38: η_v and η_c vs P_r in scroll and reciprocating compressors

The following differences can be observed:

- **Volumetric efficiency** \Rightarrow It shows a practically linear negative trend with P_r in both technologies. However, it maintains a moderate decrease in scroll compressors while reciprocating compressors show a much higher degradation (This high dependence is caused by the influence of the “*dead space*”).
- **Compressor efficiency** \Rightarrow It presents a maximum in both technologies decreasing at low P_r , generally obtaining higher values in scroll compressors. However, scroll compressors show a significant decrease with increasing P_r whereas reciprocating compressors keep this efficiency almost constant. Scroll compressors are designed to operate in an optimum P_r , where lower or higher values of pressure ratio will decrease the compressor efficiency according to over and under compression phenomena (Winandy et al., 2002).

Now that the different trends in efficiencies according to technologies have been considered, we will move on to analyze the efficiency ratios. Considering what we have discussed above, the following behavior would be expected:

- η_v/η_c in Scroll compressors \Rightarrow This ratio includes volumetric efficiency

values that, although not constant, show a moderate drop. In the case of compressor efficiency, we obtain a large variation with a maximum efficiency and a pronounced drop at high P_r . Therefore the efficiency ratio should present a minimum value at optimum P_r , increasing at low P_r and high P_r .

- η_v/η_c in reciprocating compressors \Rightarrow In this case, we should get different behavior than with scroll compressors. The volumetric efficiency presents quite a pronounced drop with the pressure ratio. Regarding the compressor efficiency, we obtain a constant value in the medium and high-pressure ratio range with only a drop at low-pressure ratio values. Therefore the evolution of the efficiency ratio should demonstrate monotonic behavior with an increase in consumption at a low-pressure ratio and a decrease as the pressure ratio increases due to a greater drop in volumetric efficiency.

We can check this by plotting the ratio of efficiencies as a function of the pressure ratio for the compressors analyzed in this chapter, the AHRI 11 and 21 in scroll and the AHRI 30 and 59 in reciprocating (Figure 4.39). In this graph, we have also grouped each of the efficiency ratios relating to the same condensing pressure (joined by a trend line) in each compressor. The only purpose of this is to facilitate the visualization. As discussed throughout the chapter, the efficiencies are not a perfect function of P_r .

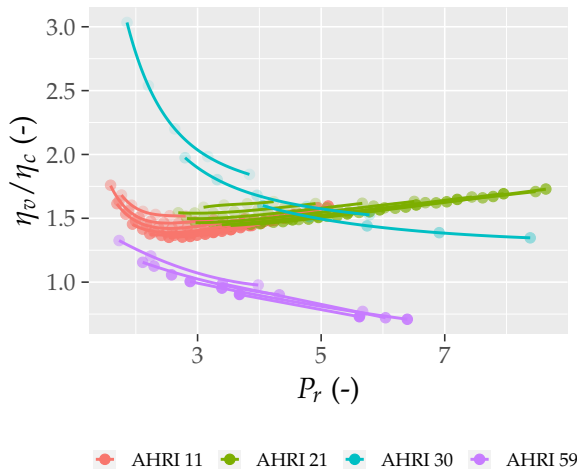


Figure 4.39: η_v/η_c vs P_r in scroll (AHRI 11 and 21) and reciprocating (AHRI 30 and 59) compressors

From these results, we can see that we obtain the expected trends.

The scroll compressors obtain an evolution of the efficiency ratio with a minimum P_r , with this value increasing at low and high P_r . Considering the evolution of the isentropic power, this translates into a greater increase in consumption at low and high P_r , where the isentropic power decreases. Therefore we obtain a flattening of the surface, making it more dependent on P_c .

Finally, concerning reciprocating compressors, we can observe the opposite effect at high P_r . In this case, the value of the efficiency ratio tends to decrease monotonically with increasing P_r . Therefore we will obtain a smaller increase in consumption at high P_r , accentuating the hyperbolic behavior of the consumption isolines and increasing the dependence on P_e . On the other hand, at low P_r we can see that, in the case of the AHRI 30 compressor, we obtain a considerable increase in the efficiency ratio. It has been found that, for those compressors with greater dependence on P_e (LBP), we obtain a very pronounced drop in compressor efficiency at low P_r , accentuating the dependence on P_e . In the case of AHRI 59, we can see that the efficiency ratio values do not present this significant increase. In this case, the compressors (M/HBP), where the most complex response surfaces for consumption were obtained, have not shown such a pronounced drop in compressor efficiency at low P_r .

4.5 Summary of results for the polynomial models analyzed

To conclude this chapter, some summary figures synthesize the prediction errors obtained with the various models presented in both scroll and reciprocating compressors. Figure 4.40 includes the CV_{RMSE} and MRE errors for the models obtained in scroll compressors and Figure 4.41 includes the same information for reciprocating compressors. An additional response variable to characterize the energy consumption, and not mentioned in the body of this chapter, was also included in these figures. This variable is the non-dimensional consumption calculated as $\dot{W}_c / (P_e V_s n)$. The reason for removing that was that the use of specific consumption allowed good predictions to be obtained for both technologies. However, the non-dimensional consumption is only a proper response variable to characterize the energy consumption when the compressor presents a moderate drop in volumetric efficiency with the pressure ratio. Even so, I consider it necessary to comment that all the results analyzed for the specific consumption also apply to the non-dimensional consumption in scroll compressors. Therefore, we can use the same functional with the advantage of modelling a response variable to characterize energy consumption independent of the accuracy of mass

flow rate measurement. As additional information, in appendices K and J, the non-dimensional consumption contour plots are also included to compare them with those obtained for specific consumption.

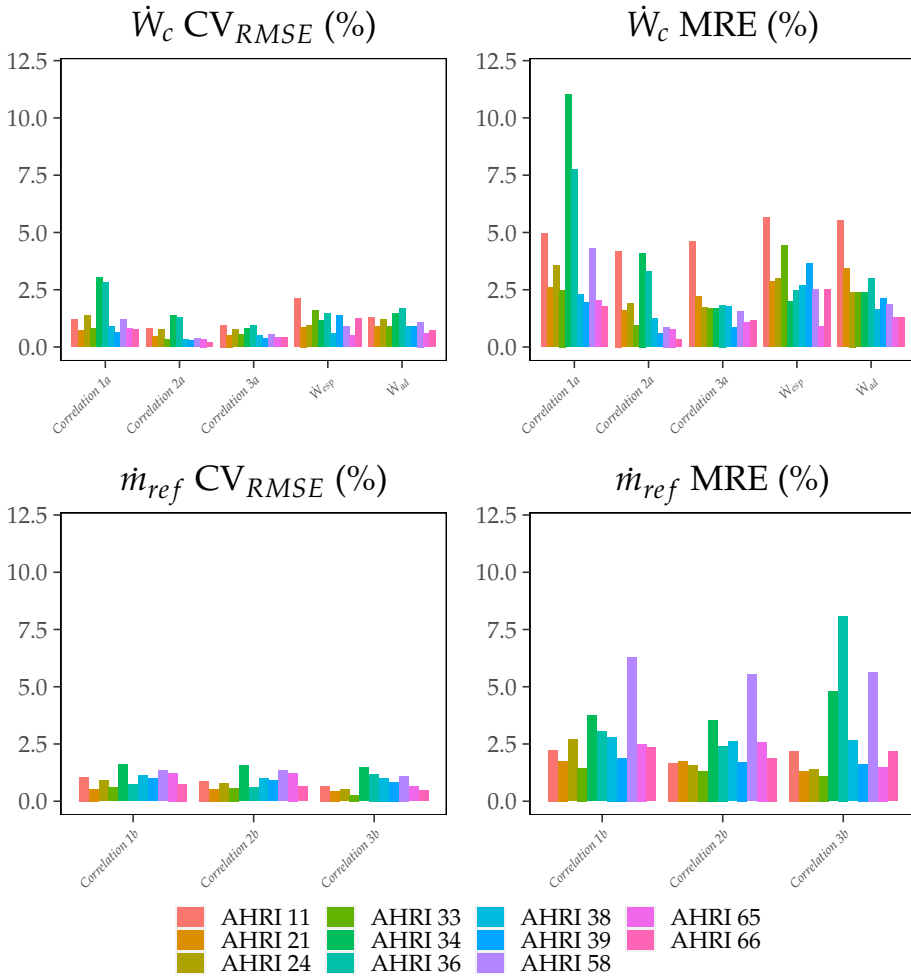


Figure 4.40: Summary model errors: scroll compressor

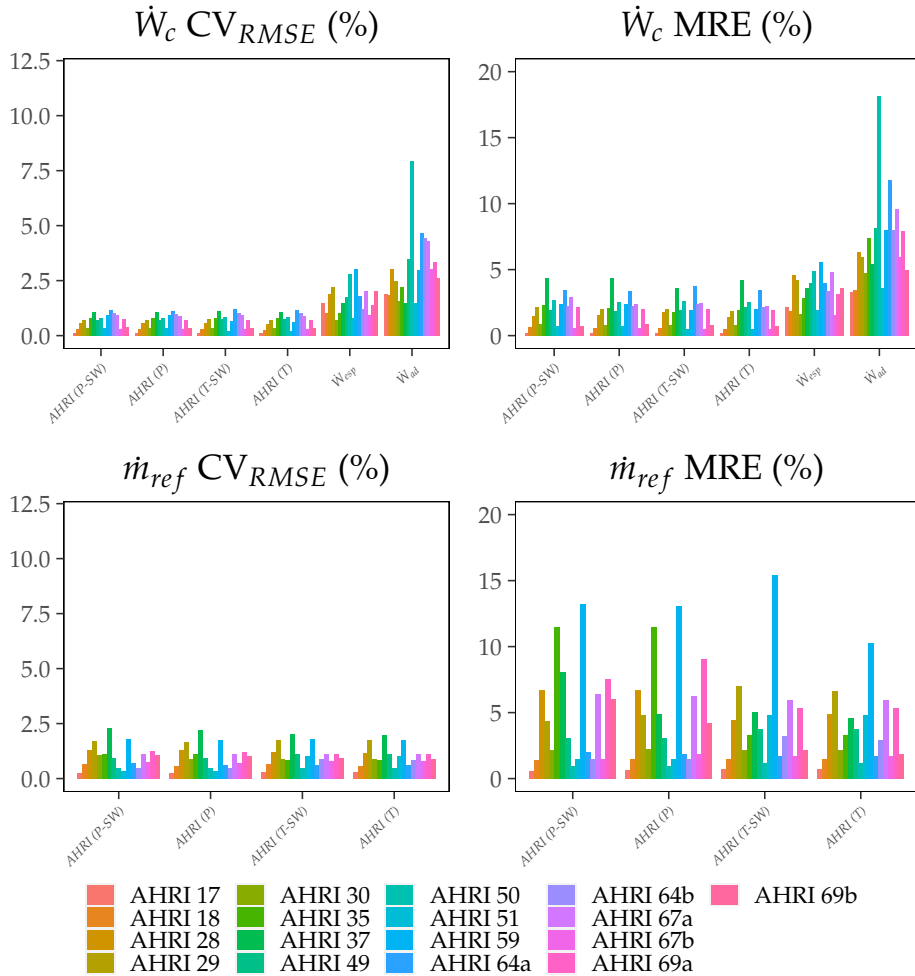


Figure 4.41: Summary model errors: reciprocating compressor

5

Conclusions

CONTENTS

5.1	Main conclusion for DSHP characterization	175
5.2	Main conclusions for scroll compressors	177
5.3	Main conclusions for reciprocating compressors	178
5.4	Future research	180

A thorough analysis of the characterization performance in the field of heat pumps and refrigeration equipment has been performed in this PhD thesis. In the first part of this PhD, this type of unit has been analyzed in depth using the empirical approach to propose simple polynomial models capable of accurately characterizing their performance. In this case, the HP unit is characterized as a single component. Then, this same approach has been used in the second part to accurately characterize one of the most important components of these units, the compressor.

Page XIX includes a list of publications derived from this work. These include deliverable reports from the European project GEOTeCH, publications in national and international conferences, and indexed journal articles.

The following main conclusions and results can be drawn from the performed study.

5.1 Main conclusion for DSHP characterization

- The new prototype of DSHP analyzed in this work operates with R32 refrigerant and includes a variable speed compressor which gives full capabilities for efficient modulating operation. The unit has turned out to be fully reliable with a smooth, simple, and fully automatic operation. It has been designed and thoroughly tested at the laboratory of the IUIIE with very accurate instrumentation by using a proper experimental test bench.

- This unit allowed the generation of a large amount of experimental data with a total of 227 test points. Thanks to the unit ability to select different heat sources, all the experimental data generated include the performance of the main heat pumps technologies —Air Source Heat Pumps, and Ground Source Heat Pumps— including data for an extended range of boundary conditions and also different operating modes (DHW application, heating mode, and cooling mode).
- The performance of current vapour compression heat pump and refrigeration units with variable speed components has, in general, 5 independent variables, for instance: inlet and outlet temperature of the secondary flow at the evaporator and the condenser, plus the compressor frequency. Therefore, the response surface for the evaporator capacity, condenser capacity, and energy consumption lies on a 5D domain.
- A testing campaign following a full factorial plan would require a huge number of test points, e.g., 3125 points with 5 levels for each independent variable. Therefore, some Design of Experiments methodology (DoE) must be applied to reduce the test matrix to a reasonable size.
- For the detailed analysis of the performance response surfaces, a dataset of virtual experiments was generated using a model developed in the commercial software IMST-ART. The ART model can predict the unit performance with an error of less than 10%. The performance maps generated with IMST-ART for the 7 operating modes include a total of 21875 simulation points.
- The performance of the unit can be characterized very efficiently by adequate polynomials. These polynomials have been obtained by the analysis of the virtual database. This analysis found that the polynomials include a smaller number of terms if we select the energy consumption and capacities divided by compressor speed as response variables. The independent variables selected to perform the polynomial models are the external variables.
- The IMST-ART model also allowed the evaluation of different DoE methodologies, defining which DoE methodology leads to a good compromise between the number of points for the fitting of the surface and the accuracy of the prediction. Thus, the Central Composite Design (CCD) is very good, requiring 30 test points respectively and allowing a very good characterization of the unit performance across the whole domain. This design was used to perform the experimental test matrices. They include the major part of the 227 experimental points tested.

- The polynomials generated from the virtual database were finally fitted using the experimental points defined by the CCD and a new methodology developed in this work. The fitting methodology used has proved adequate in the sense of being able to combine the extensive information obtained from the simulated data together with the experimental data.
- The developed polynomials were compared with the experimental performance data and provided a good prediction. The prediction error is very small, across the entire 5D domain: $< 2\%$ for the energy consumption and $\approx 3\%$ for the condenser and evaporator capacities.

5.2 Main conclusions for scroll compressors

- When the compressor is measured in a wide range of operating conditions, compressor and volumetric efficiencies show a complex shape inside its envelope. It is clearly sensitive to suction conditions (superheat). In contrast, the compressor consumption and mass flow rate are represented by smooth surfaces when plotted versus the evaporation and condensation temperatures (or pressures). For the energy consumption, it shows very little dependence on the superheat. Therefore, compressor consumption and mass flow rate are easier to characterize by fitting a polynomial than compressor efficiencies.
- For scroll compressors, it is not necessary to employ a 10 coefficients polynomial, as proposed in AHRI 540 (2020), to characterize the compressor. A second-order polynomial is accurate enough and requires fitting to many fewer test points.
- Shao et al. (2004) also uses a second-order polynomial to characterize rotary compressors. The correspondence with the Shao et al. (2004) results could indicate that all the conclusions drawn from the scroll compressor analysis can be extrapolated to rotary compressors. Unfortunately, the experimental database for these compressors was not so large and it was not possible to confirm this statement.
- It has found that the correlation will be smoother and more linear if the compressor consumption and mass flow rate are correlated with the condensation and evaporation pressures. Furthermore, it will also depend less on the refrigerant used for energy consumption and extends its applicability to transcritical cycles.

- The energy consumption of scroll compressors is quite plane and smooth trends are observed. A simple correlation with linear terms on the condensation and evaporation pressures together with a cross-term with their product requires only 4 coefficients. It provides a very simple and robust representation. Regarding the mass flow rate, correlation with linear terms on the condensation and evaporation pressures requires only 3 coefficients and provides a very simple and robust representation.
- This representation of these variables has an advantage in requiring fewer experimental point measurements to characterize the compressor energy consumption and mass flow rate appropriately than ARHI polynomials. But the most important thing is that the polynomials used for scroll compressors are quite linear and do not require cubic terms. Therefore, obtaining a good compressor performance prediction in this approach is less sensitive to where the points are measured and the error when extrapolation from experimental data is performed.
- The analyzed experimental design methodologies are suitable for the characterization of compressors. In this sense, computer-aided designs obtain the best results, being able to adapt the experimental design to irregular experimental domains. The methodologies analyzed in this PhD includes the Optimal Designs (OD), Cluster Designs (CD), and Polygonal Designs (PD).
- Although the standard does not specify anything about sampling selection, OD methodologies have been shown to obtain the best results for the proposed polynomial models for scroll compressors. Using the D-Optimal criterion and a proper size for the experimental sample will supply good results. In this sense, to increase the model's accuracy, 9 points is an adequate size for Correlations *3a*, *3b* (temperature domain) and for Correlations *2a*, *2b* (pressure domain). On the other hand, this sample size can be reduced to 6 points using *Correlation 1a* for the prediction of the energy consumption, decreasing the experimentation costs without a significant loss in accuracy. In this case, it is advisable to use *Correlation 2b* for the mass flow rate because the sample size is enough to obtain a good adjustment.

5.3 Main conclusions for reciprocating compressors

- The analysis of the compressor efficiencies response surface shows similar results to the ones obtained in scroll compressors. The response surface shows a complex shape, and it is sensitive to the suction conditions.
- The energy consumption response surfaces in reciprocating compressors are more complex than in scroll compressors. This complexity depends mainly on the working range of the compressor and may require the use of more complex polynomial models, with the inclusion of cubic terms as proposed by AHRI standard being justifiable.
- The energy consumption depends mainly on the evaporating temperature and two types of behavior have been identified. The L/MBP compressors analyzed have simpler response surfaces and depend mainly on the evaporation temperature with a slight dependence on condensation temperature. On the other hand, the HBP compressors obtain more complex response surfaces and evaporation and condensation temperatures have similar influence.
- Contrary to scroll compressors, the use of the original 10-term AHRI polynomial for reciprocating compressor characterization is justified. Furthermore, it has been found that the use of automatic term reduction methodologies are adequate in order to simplify the final polynomial model. This allows the elimination of possible collinearity effects in the models in the case of more straightforward response surfaces. Alternatively, other sophisticated strategies can be used to generate the compressor maps by a smooth interpolation. In this sense, non-parametric regression models such as a Thin-Plate-Spline regression model are demonstrated as good approaches. Nevertheless, it has been found that the expressions obtained with these techniques depend on the compressor and refrigerant.
- The compressor characterization in terms of the specific energy consumption significantly reduces the number of the parameters required by the functional in order to estimate the energy consumption and supply a general function depending only on 4 parameters (or 5/6 if we want to increase the prediction accuracy by increasing the degree of the polynomial) and unify the behavior for the two compressor technologies analyzed.
- The mass flow rate can be reproduced using second-order polynomials, so the use of third-order ARHI polynomials are not justified for this variable in reciprocating compressors.

- The prediction errors for approaches based on temperature or pressure are in the same range. However, the compressor consumption model parameters are more refrigerant-independent for a specific compressor if pressure variables are selected. Moreover, this approach allows also for characterizing compressors in transcritical cycles.
- Although the standard does not specify anything about sampling selection, PD methodologies can be used to select samples and perform the experimental test matrices in the compressor's field when non linear models must be adjusted. In this sense, to increase the model's accuracy, 9 points is an adequate size for the characterization of the specific energy consumption and mass flow rate.

5.4 Future research

Given the good results obtained and having developed an extensive experimental database, which includes performance data for various heat pump technologies and calorimetric tests of the main compressor technologies used in this sector, some beneficial areas of research are shown below:

- Test the applicability of the polynomial models developed for predicting the heat pump performance in other units. The methodology described here to perform the final fit to the experimental data allows adapting the models to other units if a minimum of experimental data is available.
- Extend the analysis of compressor characterization to other types of technology, e.g., rotary compressors. From the analysis carried out on the results published in Shao et al. (2004), it can be intuited that the characterization of this type of compressor can be similar to that of scroll compressors. However, this should be verified by performing an extensive experimental characterization, including a large number of test points.
- Another interesting aspect includes the characterization of variable speed compressors. The effect of speed on the response surfaces analyzed in this work is of particular interest in this regard. Moreover, the analysis of the appropriate experimental designs, the minimum number of points to be tested, and their location can be of special relevance in minimizing experimental costs when compressor speed is included as an additional variable.

- Analyze the characterization of other types of response variables in the field of compressors. In this sense, many of the calorimetric data in the database include temperature measurements, thus being able to analyze the characterization of heat losses in this type of component.
- Obtain adequate corrections to extrapolate the prediction of the mass flow rate to other types of refrigerants than the one used to fit the model. The corrections introduced in the standard only include the correction with the change of the suction temperature.
- Analyze the applicability of polynomial modelling for fault detection in these units. This field is known as Fault Detection and Diagnostic (FDD), where some authors propose the characterization of these units by measuring the deviation against forced failures, for example, the performance against an excess or lack of refrigerant charge. This would minimize costs by eliminating, for example, refrigerant detection sensors and provide the machine with a self-diagnostic capability.

Bibliography

- Afjei, T. and Dott, R. (2011). Heat pump modelling for annual performance, design and new technologies. In *12th Conference of International Building Performance Simulation Association*, pages 2431–2438.
- Afjei, T., Wetter, M., and Glass, A. (1997). *TRNSYS Type 204: Dual-stage compressor heat pump including frost and cycle losses*. TRNSYS Type version 2.0.
- Afram, A. and Janabi-Sharifi, F. (2014). Review of modeling methods for HVAC systems. *Applied Thermal Engineering*, 67(1-2):507–519.
- AHRI 540 (2020). AHRI 540 - Standard for performance rating of positive displacement refrigerant compressors and compressor units.
- AIAA (1998). *Guide for the Verification and Validation of Computational Fluid Dynamics Simulations (AIAA G-077-1998(2002))*. American Institute of Aeronautics and Astronautics, Inc.
- Allen, J. J. and Hamilton, J. F. (1983). Steady-state reciprocating water chiller models. In *Annual Meeting - Washington DC*. ASHRAE Transactions. Volume 89(2), pages 398–407.
- ANSI/ASHRAE Standard 34 (2019). Designation and Safety Classification of Refrigerants. Technical report, American Society of Heating and Air-Conditioning Engineers.
- Ascher, U. M. and Petzold, L. R. (1998). *Computer Methods for Ordinary Differential Equations and Differential-Algebraic Equations*. Society for industrial and applied Mathematics, Philadelphia, Pennsylvania.
- ASHRAE Guideline 14 (2014). Measurement of Energy, Demand, and Water Savings. Technical report, American Society of Heating and Air-Conditioning Engineers.
- Atkinson, A. C. and Donev, A. N. (1992). *Optimum Experimental Designs*. Oxford Statistical Science Series.

- Atkinson, A. C., Donev, A. N., and Tobias, R. D. (2007). *Optimum Experimental Designs, with SAS*. Oxford University Press Inc., 1 edition.
- Aute, V. and Martin, C. (2016). A comprehensive evaluation of regression uncertainty and the effect of sample size on the ahri-540 method of compressor performance representation. In *International Refrigeration and Air Conditioning Conference. Paper 2457*, West Lafayette, Indiana. Purdue University.
- Aute, V., Martin, C., and Radermacher, R. (2015). AHRI Project 8013 : A Study of Methods to Represent Compressor Performance Data over an Operating Envelope Based on a Finite Set of Test Data. *Air-Conditioning, Heating, and Refrigeration Institute*.
- Aute, V., Qiao, H., Kwon, L., Radermacher, R., Hall, G. M., and Park, C. (2014). Transient modeling of a multi-evaporator air conditioning system and control method investigation. In *11th IEA Heat Pump Conference 2014, May 12-16 2014, Montréal (Québec) Canada*.
- Banks, J. (1998). *Handbook of Simulation: Principles, Methodology, Advances, Applications, and Practice*. John Wiley & Sons.
- Bayer, P., Saner, D., Bolay, S., Rybach, L., and Blum, P. (2012). Greenhouse gas emission savings of ground source heat pump systems in Europe: A review. *Renewable and Sustainable Energy Reviews*, 16(2):1256–1267.
- Bell, I. H., Wronski, J., Quoilin, S., and Lemort, V. (2014). Pure and pseudo-pure fluid thermophysical property evaluation and the open-source thermophysical property library coolprop. *Industrial & Engineering Chemistry Research*, 53(6):2498–2508.
- Borges Ribeiro, G. and Marchi Di Gennaro, G. (2013a). TEST REPORT #17. Compressor Calorimeter Test of Refrigerants R-22 and R-1270. Technical report, Embraco.
- Borges Ribeiro, G. and Marchi Di Gennaro, G. (2013b). TEST REPORT #18. Compressor Calorimeter Test of Refrigerants R-134a, N-13a and ARM-42a. Technical report, Embraco.
- Boscan, M. and Sanchez, J. (2015). TEST REPORT #51. Compressor Calorimeter Test of Refrigerant Blend DR-33 (R449A) in a R-404A Reciprocating Compressor. Technical report, Bitzer US.
- Bourdouxhe, J.-P., Grodent, M., and Lebrun, J. (1998). *Reference guide for dynamic models of HVAC equipment*. ASHRAE.

- Box, G. E. and Draper, N. R. (2007). *Response Surfaces, Mixtures and Ridge Analyses*. John Wiley & Sons, Inc., 2nd edition.
- Box, G. E. P. and Behnken, D. W. (1960). Some New Three Level Design for Study of quantitative variables. *Technometrics*, 2(4):455–475.
- Box, G. E. P. and Wilson, K. B. (1951). On the Experimental Attainment of Optimum Conditions. *Journal of the Royal Statistical Society: Series B (Methodological)*, 13(1):1–38.
- Brown, J., Brignoli, R., Domanski, P., and Yoon, Y. (2021). CYCLE_D-HX: NIST Vapor Compression Cycle Model Accounting for Refrigerant Thermodynamic and Transport Properties; Version 2, User’s Guide.
- Byrne, P., Ghoubali, R., and Miriel, J. (2014). Scroll compressor modelling for heat pumps using hydrocarbons as refrigerants. *International Journal of Refrigeration*, 41:1–13.
- Cazorla Marín, A. (2019). *Modelling and Experimental Validation of an Innovative Coaxial Helical Borehole Heat Exchanger for a Dual Source Heat Pump System*. PhD thesis, Universitat Politècnica de València.
- Cellier, F. E. and Greifeneder, J. (1991). *Continuous System Modeling*. Springer-Verlag, New York.
- Cheung, H. and Wang, S. (2018). A comparison of the effect of empirical and physical modeling approaches to extrapolation capability of compressor models by uncertainty analysis: A case study with common semi-empirical compressor mass flow rate models. *International Journal of Refrigeration*, 86:331–343.
- Cho, J. M., Heo, J., Payne, W. V., and Domanski, P. A. (2014). Normalized performance parameters for a residential heat pump in the cooling mode with single faults imposed. *Applied Thermal Engineering*, 67(1-2):1–15.
- Chua, K. J., Chou, S. K., and Yang, W. M. (2010). Advances in heat pump systems: A review. *Applied Energy*, 87(12):3611–3624.
- Coleman, H. W. and Steele, W. G. (2018). *Experimentation, validation, and uncertainty analysis for engineers: Fourth edition*. John Wiley & Sons, Inc., 4th edition.
- Corberán, J. M., González, J., and Fuentes, D. (2005). Calculation of refrigerant properties by linear interpolation of bidimensional meshes. In *Proceedings of the IIR International Conference*, Vicenza, Italy. International Institute of Refrigeration (IIR).

- Corberán, J. M., González, J., Montes, P., and Blasco, R. (2002). 'ART' A Computer Code To Assist The Design Of Refrigeration and A/C Equipment. In *International Refrigeration and Air Conditioning Conference. Paper 570*, West Lafayette, Indiana. Purdue University.
- Cuevas, C. and Lebrun, J. (2009). Testing and modelling of a variable speed scroll compressor. *Applied Thermal Engineering*, 29(2-3):469–478.
- Da Riva, E. and Del Col, D. (2011). Performance of a semi-hermetic reciprocating compressor with propane and mineral oil. *International Journal of Refrigeration*, 34(3):752–763.
- Dabiri, A. E. (1982). A steady state computer simulation model for air-to-air heat pumps. In *Annual Meeting - Toronto, ON*. ASHRAE Transactions. Volume 88(2), pages 973–987.
- Dabiri, A. E. and Rice, C. K. (1981). A compressor simulation model with corrections for the level of suction gas superheat. In *Annual Meeting - Cincinnati, OH*. ASHRAE Transactions. Volume 87(2), pages 771–708.
- Diaz-Calderon, A., Paredis, C. J. J., and Khosla, P. K. (2000). Reconfigurable models: A modeling paradigm to support simulation-based design. 2000 Summer Computer Simulation Conference, Vancouver, Canada, 2000.
- Domanski, P. A. and Didion, D. A. (1985). Simulation of a heat pump operating with a nonazeotropic mixture. In *Annual Meeting, Honolulu, HI*. ASHRAE Transactions. Volume 91(2), pages 1368–1382.
- Dos Santos, C. G., Ruivo, J. P., Gasparini, L. B., Rosa, M. T. D. M., Odloak, D., and Tvrzská De Gouvêa, M. (2022). Steady-state simulation and optimization of an air cooled chiller. *Case Studies in Thermal Engineering*, 36.
- EnergyPlus Core Team (2022). *EnergyPlus: An open source building energy simulation program*. Version 22.1.0.
- European Commission (2007a). COM(2007) 723: The SET Plan a European Strategic Energy Technology Plan: Towards a Low Carbon Future.
- European Commission (2007b). COM(2008) 30 Final: 20 20 by 2020—Europe's Climate Change Opportunity. *alias: Europe's 2020 energy strategy*.
- European Commission (2009). Renewable Energy Directive 2009/28/EC.
- European Commission (2011a). COM(2011) 808: Horizon 2020 - The Framework Programme for Research and Innovation. *alias: Horizon 2020 programme*.

- European Commission (2011b). COM(2011) 885: Energy Roadmap 2050. *alias: Energy roadmap 2050*.
- European Commission (2012). Directive 2012/27/EU on energy efficiency, amending Directives 2009/125/EC and 2010/30/EU and repealing Directives 2004/8/EC and 2006/32/EC.
- European Commission (2014a). EUCO 169/14. *alias: Europe's 2030 energy strategy*.
- European Commission (2014b). Regulation (EU) N° 517/2014 of the european parliament and of the council of 16 April 2014 on fluorinated greenhouse gases and repealing Regulation (EC) No 842/2006. *European F-gas regulation*.
- European Commission (2015). Geothermal Technology for Economic Cooling. (H2020-LCE-2014-2, GEOTeCH-656889).
- European Commission (2016). COM(2016) 51: An EU Strategy on Heating and Cooling.
- European Commission (2018). Renewable Energy Directive 2018/2001 on the promotion of the use of energy from renewable sources.
- Faraway, J. J. (2005). *Linear Models With R*. CRC Press, Inc, New York.
- Fedorov, V. V. (1972). *Theory of Optimal Experiments Designs*. Academic Press.
- Fischer, S.K. Rice, C. (1983). *ORNL Heat Pump Model: A Steady-State Computer Design Model of Air-to-Air Heat Pumps*. Oak Ridge, TN (United States). Fortran-IV computer program.
- Fisher, S. (1971). *The Design of Experiments*. Hafner Press, New York, 9th edition.
- Fomel, S. and Claerbout, J. F. (2009). Guest editors' introduction: Reproducible research. *Computing in Science & Engineering*, 11(01):5–7.
- Glynn, P. W. (1989). A GSMP Formalism for Discrete Event Systems. In *Proceedings of the IEEE*, Vol. 77, No. 1, January 1989, pages 14–23. IIE Press.
- Granryd, E., Ekroth, I., Lundqvist, P., Melinder, Å., Palm, B., and Rohlin, P. (2011). *Refrigerating engineering*. KTH Royal Institute of Technology, Stockholm, 6th edition.
- Green, P. J. and Silverman, B. W. (1993). *Nonparametric Regression and Generalized Linear Models*. Chapman & Hall, 1st edition.
- Hamilton, J. F. and Miller, J. (1990). A simulation program for modeling an air conditioning system. In *Winter Meeting - Atlanta, GA*. ASHRAE Transactions. Volume 96(1), pages 213–221.

- Hartley, H. O. (1959). Smallest Composite Designs for Quadratic Response Surfaces. *International Biometric Society*, 15(4):611–624.
- Heckert, N. A., Filliben, J. J., Croarkin, C. M., Hembree, B., Guthrie, W. F., Tobias, P., and Prinz, J. (2002). Handbook 151: NIST/SEMATECH e-Handbook of Statistical Methods.
- Hermes, C. J., Santos, G. Z., and Ronzoni, A. F. (2019). Performance characterization of small variable-capacity reciprocating compressors using a minimal dataset. *International Journal of Refrigeration*, 107:191–201.
- Hewitt, G. and Shires, G.L. Bott, T. (1994). *Process heat transfer*. CRC Press, Inc.
- HiRef (2020). Hiref - italian cooling solutions. Heat pumps manufacturer.
- Hole, G. (1994). Fluid Viscosity Effects on Centrifugal Pumps. *Pumps and Systems Magazine*, pages 14–19.
- Jähnig, D. I., Reindl, D. T., and Klein, S. A. (2000). A Semi-empirical Method for Representing Domestic Refrigerator/Freezer Compressor Calorimeter Test Data. In *Annual Meeting, Minneapolis, MN*. ASHRAE Transactions. Volume 106(2), pages 122–130.
- Jiang, H., Aute, V., and Radermacher, R. (2006). CoilDesigner: a general-purpose simulation and design tool for air-to-refrigerant heat exchangers. *International Journal of Refrigeration*, 29(4):601–610.
- Jin, H. (2002). *Parameter estimation based models of water source heat pumps*. PhD thesis, Oklahoma State University.
- Jin, H. and Spitler, J. (2002). A parameter estimation based model of water-to-water heat pumps for use in energy calculation programs. In *Winter Meeting, Atlantic City, NJ*. ASHRAE Transactions. Volume 108(1), pages 3–17.
- Jin, H. and Spitler, J. (2003). Parameter estimation based model of water-to-water heat pumps with scroll compressors and water/glycol solutions. *Building Services Engineering Research and Technology*, 24(3):203–219.
- Kabacoff, R. I. (2011). *R in action. Data analysis and graphics with R*. Manning Publications Co., 2nd edition.
- Kiefer, J. (1959). Optimum Experimental Designs. *Journal of the Royal Statistical Society*, 21(2):272–319.
- Kiefer, J. and Wolfowitz, J. (1959). Optimum Designs in Regression Problems. *The Annals of Mathematical Statistics*, 30(2):271–294.

- Kim, M., Payne, W. V., and Domanski, P. A. (2006). NISTIR 7350: Performance of a residential heat pump operating in the cooling mode with single faults imposed. Technical report, National Institute of Standards and Technology, Gaithersburg, MD.
- Kim, M., Payne, W. V., Domanski, P. A., Yoon, S. H., and Hermes, C. J. (2009). Performance of a residential heat pump operating in the cooling mode with single faults imposed. *Applied Thermal Engineering*, 29(4):770–778.
- Kim, M., Yoon, S. H., Payne, W. V., and Domanski, P. A. (2010). Development of the reference model for a residential heat pump system for cooling mode fault detection and diagnosis. *Journal of Mechanical Science and Technology*, 24(7):1481–1489.
- Klein, S.A. (2020). *EES: Engineering Equation Solver*. F-Chart Software, Madison, Wisconsin 53744, USA. Version 10.833.
- Knepell, P. L. and Arangno, D. C. (1993). *Simulation Validation: A Confidence Assessment Methodology*.
- Knuth, D. E. (1984). Literate Programming. *The Computer Journal*, 27(2):97–111.
- Koenig, H. E., Tokad, Y., and Kesavan, H. K. (1967). *Analysis of Discrete Physical Systems*. McGraw-Hill Electrical and Electronic Engineering Series, New York.
- Lemmon, E. W., Bell, I. H., Huber, M. L., and McLinden, M. O. (2018). NIST Standard Reference Database 23: Reference Fluid Thermodynamic and Transport Properties-REFPROP, Version 10.0, National Institute of Standards and Technology.
- Lemort, V. and Bertagnolio, S. (2010). A Generalized Simulation Model of Chillers and Heat Pumps to Be Calibrated on Published Manufacturer’s Data. In *International Symposium on Refrigeration Technology 2010, Zhuhai, China*.
- Lenz, J. R. and Shrestha (2016). TEST REPORT #59. Compressor Calorimeter Test of Refrigerants L41-1, DR-5A, ARM-71a, D2Y-60 and R-32 in a R-410A Reciprocating Piston Compressor. Technical report, Bristol compressor & Oak Ridge National Laboratory.
- TeXLive Team (2022). *TeXLive: A cross-platform, free software distribution for TeX/LaTeX typesetting system*. Version TeXLive 2022.
- Ma, J., Ding, X., Horton, W. T., and Ziviani, D. (2020). Development of an automated compressor performance mapping using artificial neural network and multiple compressor technologies. *International Journal of Refrigeration*, 120:66–80.

- Madani, H. (2012). *Capacity-controlled Ground Source Heat Pump Systems for Swedish single-family dwellings*. PhD thesis, KTH Royal Institute of Technology.
- Madani, H., Claesson, J., and Lundqvist, P. (2011a). Capacity control in ground source heat pump systems: Part I: Modeling and simulation. *International Journal of Refrigeration*, 34(6):1338–1347.
- Madani, H., Claesson, J., and Lundqvist, P. (2011b). Capacity control in ground source heat pump systems part II: Comparative analysis between on/off controlled and variable capacity systems. *International Journal of Refrigeration*, 34(8):1934–1942.
- Maertens, M. J. and Richardson, H. (1992). Scroll compressor operating envelope considerations. In *International Refrigeration and Air Conditioning Conference. Paper 850*, West Lafayette, Indiana. Purdue University.
- Myers, R. H., Montgomery, D. C., and Anderson-Cook, C. M. (2009). *Response Surface Methodology*. John Wiley & Sons, Inc., 3 edition.
- Navarro, E., Granryd, E., Urchueguía, J. F., and Corberán, J. M. (2007). A phenomenological model for analyzing reciprocating compressors. *International Journal of Refrigeration*, 30(7):1254–1265.
- Navarro-Peris, E., Corberán, J. M., Falco, L., and Martínez-Galván, I. O. (2013). New non-dimensional performance parameters for the characterization of refrigeration compressors. *International Journal of Refrigeration*, 36(7):1951–1964.
- Nebot-Andrés, L., Catalán-Gil, J., Sánchez, D., Calleja-Anta, D., Cabello, R., and Llopis, R. (2020). Experimental determination of the optimum working conditions of a transcritical CO₂ refrigeration plant with integrated mechanical subcooling. *International Journal of Refrigeration*, 113:266–275.
- Neelamkavil, F. (1987). *Computer Simulation and Modelling*. John Wiley & Sons, New York.
- Nishiguchi, J., Konda, T., and Dazai, R. (2010). Data-driven optimal control for building energy conservation. In *Proceedings of the SICE Annual Conference*, pages 116–120. IEEE.
- Pärisch, P., Mercker, O., Warmuth, J., Tepe, R., Bertram, E., and Rockendorf, G. (2014). Investigations and model validation of a ground-coupled heat pump for the combination with solar collectors. *Applied Thermal Engineering*, 62(2):375–381.

- Pérouffe, L. and Renevier, G. (2016a). TEST REPORT #64. Compressor Calorimeter Test of Refrigerant DR-7 (R-454A) in a R-404A Reciprocating Compressors. Technical report, Tecumseh Products Company.
- Pérouffe, L. and Renevier, G. (2016b). TEST REPORT #67. Compressor Calorimeter Test of Refrigerant ARM-25 in a R-404A Reciprocating Compressors. Technical report, Tecumseh Products Company.
- Pérouffe, L. and Renevier, G. (2016c). TEST REPORT #69. Compressor Calorimeter Test of Refrigerant ARM-20b in a R-404A Reciprocating Compressors. Technical report, Tecumseh Products Company.
- Pierre, B. (1982). Kylteknik, Allmän Kurs. Technical report, Inst. Mekanisk Värmeteori och Kylteknik. Kungl Tekniska Högskolan, Stockholm (Swedish).
- Rajendran, R. and Nicholson, A. (2013). TEST REPORT #24. Compressor Calorimeter Test of Refrigerant DR-5 in a R-410A Scroll Compressor. Technical report, Emerson Climate Technologies, Inc.
- Rajendran, R. and Nicholson, A. (2014a). TEST REPORT #34. Compressor Calorimeter Test of Refrigerant DR-7 in a R-404A Scroll Compressor. Technical report, Emerson Climate Technologies, Inc.
- Rajendran, R. and Nicholson, A. (2014b). TEST REPORT #35. Compressor Calorimeter Test of Refrigerant DR-7 in a R-404A Reciprocating Compressor. Technical report, Emerson Climate Technologies.
- Rajendran, R. and Nicholson, A. (2014c). TEST REPORT #36. Compressor Calorimeter Test of Refrigerant L-40 in a R-404A Scroll Compressor. Technical report, Emerson Climate Technologies, Inc.
- Rajendran, R. and Nicholson, A. (2014d). TEST REPORT #37. Compressor Calorimeter Test of Refrigerant L-40 in a R-404A Reciprocating Compressor. Technical report, Emerson Climate Technologies.
- Rajendran, R. and Nicholson, A. (2014e). TEST REPORT #38. Compressor Calorimeter Test of Refrigerant L-41b in a R-410A Scroll Compressor. Technical report, Emerson Climate Technologies, Inc.
- Rajendran, R. and Nicholson, A. (2014f). TEST REPORT #39. Compressor Calorimeter Test of Refrigerant R-32 in a R-410A Scroll Compressor. Technical report, Emerson Climate Technologies, Inc.
- Rajendran, R., Pham, H., Bella, B., and Skillen, T. (2016a). TEST REPORT #58. Compressor Calorimeter Test of Refrigerant DR-5 in a R-410A Scroll Compressor. Technical report, Emerson Climate Technologies, Inc.

- Rajendran, R., Pham, H., Bella, B., and Skillen, T. (2016b). TEST REPORT #65. Compressor Calorimeter Test of Refrigerant L-41-2 (R-447A) in a R-410A Scroll Compressor. Technical report, Emerson Climate Technologies, Inc.
- Rasmussen, B. D. and Jakobsen, A. (2000). Review of Compressor Models and Performance Characterizing Variables. In *International Refrigeration and Air Conditioning Conference. Paper 1429*, West Lafayette, Indiana. Purdue University.
- Rees, S. J. (2016). *Advances in Ground-Source Heat Pump Systems*. Elsevier Inc.
- Richardson, D. H. (2006). *An Object Oriented Simulation Framework For Steady-State Analysis Of Vapor Compression Refrigeration Systems And Components*. PhD thesis, University of Maryland.
- Richardson, D. H., Jiang, H., Lindsay, D., and Radermacher, R. (2002). Optimization of Vapor Compression Systems via Simulation. In *International Refrigeration and Air Conditioning Conference. Paper 529*, West Lafayette, Indiana. Purdue University.
- Ruschenburg, J., Ćutić, T., and Herkel, S. (2014). Validation of a black-box heat pump simulation model by means of field test results from five installations. *Energy and Buildings*, 84:506–515.
- Sedliak, J. (2013a). TEST REPORT #28. Compressor Calorimeter Test of R404A Alternative Refrigerant L-40 in Reciprocating Compressors. Technical report, Embraco.
- Sedliak, J. (2013b). TEST REPORT #29. Compressor Calorimeter Test of R404A Alternative Refrigerant DR-7 in Reciprocating Compressors. Technical report, Embraco.
- Sedliak, J. (2013c). TEST REPORT #30. Compressor Calorimeter Test of R134a Alternative Refrigerant R-1234yf in Reciprocating Compressors. Technical report, Embraco.
- Sedliak, J. (2015a). TEST REPORT #49. Compressor Calorimeter Test of Refrigerant Blend HDR110 in a R-404A Reciprocating Compressor. Technical report, Embraco.
- Sedliak, J. (2015b). TEST REPORT #50. Compressor Calorimeter Test of Refrigerant Blend DR-3 in a R-404A Reciprocating Compressor. Technical report, Embraco.
- Shao, S., Shi, W., Li, X., and Chen, H. (2004). Performance representation of variable-speed compressor for inverter air conditioners based on experimental data. *International Journal of Refrigeration*, 27(8):805 – 815.

- Shrestha, S., Mahderekal, I., Sharma, V., and Abdelaziz, O. (2013a). TEST REPORT #11. Compressor Calorimeter Test of R-410A Alternatives R-32, DR-5, and L-41a. Technical report, Oak Ridge National Laboratory.
- Shrestha, S., Sharma, V., and Abdelaziz, O. (2013b). TEST REPORT #21. Compressor Calorimeter Test of R-404A Alternatives ARM-31a, D2Y-65, L-40, and R-32/R-134a (50/50). Technical report, Oak Ridge National Laboratory.
- Shrestha, S., Sharma, V., and Abdelaziz, O. (2014). TEST REPORT #33. Compressor Calorimeter Test of R-410A Alternative: R-32/R-134a Mixture Using a Scroll Compressor. Technical report, Oak Ridge National Laboratory.
- Sinha, R., Paredis, C. J., Liang, V. C., and Khosla, P. K. (2001). Modeling and simulation methods for design of engineering systems. *Journal of Computing and Information Science in Engineering*, 1(1):84–91.
- Standard, B. (2018). Bs en 14511-3:2018. air conditioners, liquid chilling packages and heat pumps for space heating and cooling and process chillers, with electrically driven compressors. test methods.
- Stoecker, W. F. and Jones, J. W. (1982). *Refrigeration and air conditioning*. McGraw-Hill, Inc., New York, 2nd edition.
- Suindykov, S., Zhang, L., and Gernemann, A. (2016). TEST REPORT #66. Compressor Calorimeter Test of Refrigerant HPR2A in a R-410A Scroll Compressor. Technical report, Danfoss Commercial Compressors.
- Sürmeli, A. N., Ediger, V. S., Hoşgör, E., and Tatlıdil, H. (2007). Fossil fuel sustainability index: An application of resource management. *Energy Policy*, 35(5):2969–2977.
- SWEP (2018). *SWEP calculation software*. SWEP heat exchanger manufacturer. Version SSP G8.
- Tabatabaei, S. A., Treur, J., and Waumans, E. (2016). Comparative evaluation of different computational models for air source heat pump based on real word data. In *Energy Procedia*, volume 95, pages 459–466. Elsevier Ltd.
- Taguchi, G. (1987). *System of Experimental Design: Engineering Methods to Optimize Quality and Minimize*. Quality Resources (Kraus), New York.
- Taylor, B. N. and Kuyatt, C. E. (1994). Guidelines for evaluating and expressing the uncertainty of NIST measurement results. Technical report, National Bureau of Standards, Gaithersburg, MD.

- Tello-Oquendo, F. M., Navarro-Peris, E., Barceló-Ruescas, F., and González-Maciá, J. (2019). Semi-empirical model of scroll compressors and its extension to describe vapor-injection compressors. Model description and experimental validation. *International Journal of Refrigeration*, 106:308–326.
- Thermal Area IUIIE (2019). *IMST-ART: A simulation tool to assist the selection, design and optimization of refrigeration equipments and components*. IMST-GROUP, Instituto de Ingeniería Energética (Universitat Politècnica de València), Camino de Vera S/N, 46022, Valencia (Spain). Version 3.9.
- United Nations (2015). The Paris Agreement. United Nations Framework Convention on Climate Change (UNFCCC).
- Verhelst, C., Logist, F., Van Impe, J., and Helsen, L. (2012). Study of the optimal control problem formulation for modulating air-to-water heat pumps connected to a residential floor heating system. *Energy and Buildings*, 45:43–53.
- Winandy, E., Saavedra O, C., and Lebrun, J. (2002). Simplified modelling of an open-type reciprocating compressor. *International Journal of Thermal Sciences*, 41(2):183–192.
- Yuan, S. and Grabon, M. (2011). Optimizing energy consumption of a water-loop variable-speed heat pump system. In *Applied Thermal Engineering*, volume 31, pages 894–901. Pergamon.
- Zeigler, B. P., Luh, C. J., and Kim, T. G. (1991). Model Base Management for Multifaceted Systems. *ACM Transactions on Modeling and Computer Simulation*, 1(3):195–218.
- Zeigler, B. P., Praehofer, H., and Gon, K. T. (2000). *Theory of modeling and simulation: integrating discrete event and continuous complex dynamic systems*. Academic Press, 2nd edition.

R-Packages and software

- Arel-Bundock, V. (2022). *modelsummary: Summary Tables and Plots for Statistical Models and Data: Beautiful, Customizable, and Publication-Ready*. R package version 0.9.5.
- Arnold, J. B., Daroczi, G., Werth, B., and Weitzner, B. (2021). *ggthemes: Extra Themes, Scales and Geoms for 'ggplot2'*. R package version 4.2.4.
- Auguie, B. (2017). *gridExtra: Miscellaneous Functions for "Grid" Graphics*. R package version 2.3.
- Campitelli, E. (2022). *metR: Tools for Easier Analysis of Meteorological Fields*. R package version 0.12.0.
- Edwards, S. M. (2020). *lemon: Freshing Up your 'ggplot2' Plots*. R package version 0.4.5.
- Fox, J. (2021). *RcmdrMisc: R Commander Miscellaneous Functions*. R package version 2.7-2.
- Hamner, B. and Frasco, M. (2018). *Metrics: Evaluation Metrics for Machine Learning*. R package version 0.1.4.
- Henry, L. and Wickham, H. (2020). *purrr: Functional Programming Tools*. R package version 0.3.4.
- Hiebert, J. (2022). *udunits2: Uduunits-2 Bindings for R*. R package version 0.13.2.
- Horikoshi, M., Tang, Y., and Dickey, A. (2022). *gfortify: Data Visualization Tools for Statistical Analysis Results*. R package version 0.4.14.
- Iannone, R., Cheng, J., Schloerke, B., and RStudio (2021). *gt: Easily Create Presentation-Ready Display Tables*. R package version 0.3.1.
- Kassambara, A. (2020). *ggpubr: 'ggplot2' Based Publication Ready Plots*. R package version 0.4.0.
- Kim, S. (2015). *ppcor: Partial and Semi-Partial (Part) Correlation*. R package version 1.1.

- Müller, K. and Wickham, H. (2021). *tibble: Simple Data Frames*. R package version 3.1.6.
- Nychka, D., Furrer, R., and Paige, J. (2021). *fields: Tools for Spatial Data*. R package version 13.3.
- Padfield, D. and Matheson, G. (2020). *nls.multstart: Robust Non-Linear Regression using AIC Scores*. R package version 1.2.0.
- Pebesma, E., Mailund, T., and Hiebert, J. (2016). Measurement units in R. *R Journal*, 8(2):486–494.
- Pebesma, E., Mailund, T., Kalinowski, T., Hiebert, J., and Ucar, I. (2022). *units: Measurement Units for R Vectors*. R package version 0.8-0.
- R Core Team (2022). *R: A Language and Environment for Statistical Computing*. R Foundation for Statistical Computing, Vienna, Austria. Version 4.1.3.
- Rinker, T. and Kurkiewicz, D. (2019). *pacman: Package Management Tool*. R package version 0.5.1.
- RStudio Team (2022). *RStudio: Integrated Development Environment for R*. RStudio, PBC., Boston, MA.
- Schloerke, B., Cook, D., and Larmarange, J. (2021). *GGally: Extension to 'ggplot2'*. R package version 2.1.2.
- Sharpsteen, C., Bracken, C., and Xie, Y. (2020). *tikzDevice: R Graphics Output in LaTeX Format*. R package version 0.12.3.1.
- Ucar, I. (2021). *quantities: Quantity Calculus for R Vectors*. R package version 0.1.6.
- Ucar, I., Henry, L., and RStudio (2020). *errors: Uncertainty Propagation for R Vectors*. R package version 0.3.6.
- Ucar, I., Pebesma, E., and Azcorra, A. (2018). Measurement errors in R. *R Journal*, 10(2):549–557.
- Ushey, K., Allaire, J., RStudio, and Tang, Y. (2022). *reticulate: Interface to 'Python'*. R package version 1.24.
- Venables, W. N. and Ripley, B. D. (2022). *MASS: Support Functions and Datasets for Venables and Ripley's MASS*. R package version 7.3-55.
- Wheeler, B. (2019). *AlgDesign: Algorithmic Experimental Design*. R package version 1.2.0.

- Wickham, H. (2016). *ggplot2: Elegant Graphics for Data Analysis*. Springer-Verlag New York. ISBN 978-3-319-24277-4.
- Wickham, H. (2019). *stringr: Simple, Consistent Wrappers for Common String Operations*. R package version 1.4.0.
- Wickham, H. (2021). *forcats: Tools for Working with Categorical Variables (Factors)*. R package version 0.5.1.
- Wickham, H. (2022). *tidyr: Tidy Messy Data*. R package version 1.2.0.
- Wickham, H., Averick, M., and Bryan, J. (2019). Welcome to the tidyverse. *Journal of Open Source Software*, 4(43):1686.
- Wickham, H., Chang, W., Henry, L., Pedersen, T. L., Takahashi, K., Wilke, C. O., Woo, K., Yutani, H., Dunnington, D., and RStudio (2021a). *ggplot2: Create Elegant Data Visualisations Using the Grammar of Graphics*. R package version 3.3.5.
- Wickham, H., François, R., Henry, L., and Müller, K. (2022). *dplyr: A Grammar of Data Manipulation*. R package version 1.0.8.
- Wickham, H. and Hester, J. (2022). *readr: Read Rectangular Text Data*. R package version 2.1.2.
- Wickham, H., Hester, J., and Chang, W. (2021b). *devtools: Tools to Make Developing R Packages Easier*. R package version 2.4.3.
- Wickham, H. and RStudio (2021). *tidyverse: Easily Install and Load the 'Tidyverse'*. R package version 1.3.1.
- Wickham, H., Seidel, D., and RStudio (2020). *scales: Scale Functions for Visualization*. R package version 1.1.1.
- Wilke, C. O. (2020). *cowplot: Streamlined Plot Theme and Plot Annotations for 'ggplot2'*. R package version 1.1.1.
- Wilke, C. O. and Pedersen, T. L. (2021). *isoband: Generate Isolines and Isobands from Regularly Spaced Elevation Grids*. R package version 0.2.5.
- Xie, Y. (2014). knitr: A comprehensive tool for reproducible research in R. In Stodden, V., Leisch, F., and Peng, R. D., editors, *Implementing Reproducible Computational Research*. Chapman and Hall/CRC. ISBN 978-1466561595.
- Xie, Y. (2015). *Dynamic Documents with R and knitr*. Chapman and Hall/CRC, Boca Raton, Florida, 2nd edition. ISBN 978-1498716963.

Xie, Y. (2021). *knitr: A General-Purpose Package for Dynamic Report Generation in R*. R package version 1.37.

Zhu, H. (2021). *kableExtra: Construct Complex Table with 'kable' and Pipe Syntax*. R package version 1.3.4.

Python-Packages and software

- Anaconda Inc. (2022). *Anaconda Software Distribution*. Version 2022.05.
- Bell, I. (2020). *Coolprop: Open-source thermodynamic and transport properties database*. Python package version 6.4.1.
- Hunter, J. D. (2007). Matplotlib: A 2d graphics environment. *Computing in Science & Engineering*, 9(3):90–95.
- Hunter, J. D. and Droettboom, M. (2021). *Matplotlib: Python plotting package*. Python package version 3.5.1.
- Oliphant, T. E. (2021). *NumPy: the fundamental package for array computing with Python*. Python package version 1.21.5.
- Ostblom, J. (2021). *Session-info: Version information for modules loaded in the current session*. Python package version 1.0.0.
- Python Core Team (2022). *Python Language*. Python Software Foundation. Version 3.9.12.
- Team, P. D. (2022). *Pandas: Powerful data structures for data analysis, time series, and statistics*. Python package version 1.4.2.
- Virtanen, P., Gommers, R., Oliphant, T. E., and SciPy 1.0 Contributors (2020). SciPy 1.0: Fundamental Algorithms for Scientific Computing in Python. *Nature Methods*, 17:261–272.
- Wes McKinney (2010). Data Structures for Statistical Computing in Python. In Stéfan van der Walt and Jarrod Millman, editors, *Proceedings of the 9th Python in Science Conference*, pages 56 – 61.

Publications

- Cazorla-Marín, A., Corberán, J. M., Marchante-Avellaneda, J., and Montagud-Montalvá, C. (2018a). Dual source heat pump, a high efficiency and cost-effective alternative for heating, cooling and DHW production. *International Journal of Low-Carbon Technologies*, 13(2):161–176.
- Cazorla-Marín, A., Montagud-Montalvá, C., Corberán, J. M., and Marchante-Avellaneda, J. (2018b). Seasonal performance assessment of a dual source heat pump system for heating, cooling and domestic hot water production. In *International Ground Source Heat Pump Association Research Conference*, pages 180–189, Stockholm. IGSHA.
- Corberán, J. M., Cazorla-Marín, A., Marchante-Avellaneda, J., Montagud, C., and Masip, X. (2017a). Modelling and energy analysis of a dual source heat pump system in an office building. In *16th International Conference on Suitable Energy Technologies*, Bologna. SET.
- Corberán, J. M., Marchante-Avellaneda, J., Bortolin, S., Moro, L., Zanetti, E., Del Col, D., and Busato, G. (2017b). Deliverable D4.5. Experimental results of prototypes: 1-3. WP4 Plug&Play Geothermal System Development. GEOTeCH-656889.
- Corberán, J. M., Marchante-Avellaneda, J., and Juárez-López, E. (2016a). Deliverable D4.3. Final design of the refrigerant circuit and strategy of operation between the two different heat sources. WP4 Plug&Play Geothermal System Development. GEOTeCH-656889.
- Corberán, J. M., Marchante-Avellaneda, J., and Martínez-Ballester, S. (2016b). Deliverable D4.1. Dual source heat pump design. WP4 Plug&Play Geothermal System Development. GEOTeCH-656889.
- Corberán, J. M., Marchante-Avellaneda, J., Navarro-Peris, E., and Llopis, B. (2019). Design of experiments methodology for the characterization of the performance map of refrigeration and heat pump units. In *25th IIR International Congress of Refrigeration*, Montreal. International Institute of Refrigeration (IIR).
- Corberán, J. M., Marchante-Avellaneda, J., Navarro-Peris, E., and Shrestha, S. S.

- (2020). A critical analysis of the characterization of scroll compressors energy consumption. In *25th International Compressor Engineering Conference at Purdue. Paper 1558*, West Lafayette, Indiana. Purdue University.
- Corberán, J. M., Marchante-Avellaneda, J., Navarro-Peris, E., and Shrestha, S. S. (2021). A critical analysis of the characterization of scroll compressors mass flowrate. In *10th IIR Conference on Compressors and Refrigerants*, Bratislava, Slovak (Republic). International Institute of Refrigeration (IIR).
- Hervás, E., Marchante-Avellaneda, J., Navarro-Peris, E., and Corberán, J. M. (2018). Design of a system for the production of domestic hot water from wastewater heat recovery based on a heat pump optimized to work at high water temperature lift. In *International High Performance Building Conference at Purdue. Paper 259*, West Lafayette, Indiana. Purdue University.
- Marchante-Avellaneda, J. (2017). Diseño y ensayos de puesta a punto de una bomba de calor de 8 kW con foco de calor dual: aerotermia y geotermia. Master's thesis, Universitat Politècnica de València.
- Marchante-Avellaneda, J., Corberán, J. M., Cazorla-Marín, A., and Montagud-Montalvá, C. (2018a). Diseño de una bomba de calor de 8 kW con foco de calor dual: aerotermia y geotermia. In *IX Congreso Ibérico | VII Congreso Iberoamericano de las Ciencias y Técnicas del Frío*, Valencia. CYTEF.
- Marchante-Avellaneda, J., Corberán, J. M., Cazorla-Marín, A., and Montagud-Montalvá, C. (2018b). Initial Test Campaign of an Innovative Dual Source Heat Pump. In *IX Congreso Ibérico | VII Congreso Iberoamericano de las Ciencias y Técnicas del Frío*, Valencia. CYTEF.
- Marchante-Avellaneda, J., Corberán, J. M., and Navarro-Peris, E. (2020a). Comparación y selección de diseños experimentales óptimos para compresores scroll: Herramientas estadísticas para conformar las matrices de ensayo. In *X Congreso Ibérico | VIII Congreso Iberoamericano de las Ciencias y Técnicas del Frío*, Pamplona. CYTEF.
- Marchante-Avellaneda, J., Corberán, J. M., Navarro-Peris, E., and Llopis, B. (2019). Characterization of the performance for water-to-water and air-to-water heat pumps: Development of simple and compact polynomial correlations. In *XI National and II International Engineering Thermodynamics Congress*, Albacete. CNIT.
- Marchante-Avellaneda, J., Corberán, J. M., Navarro-Peris, E., and Shrestha, S. S. (2023a). A critical analysis of the AHRI polynomials for scroll compressor characterization. *Applied Thermal Engineering*, 219:119432.

- Marchante-Avellaneda, J., Corberán, J. M., Navarro-Peris, E., and Shrestha, S. S. (2023b). Analysis of map-based models for reciprocating compressors and optimum selection of rating points. *International Journal of Refrigeration*. Submitted article.
- Marchante-Avellaneda, J., López-Navarro, A., Navarro-Peris, E., and Corberán, J. M. (2020b). Performance analysis of a scroll compressor working with propane for heat recovery applications. In *IIR Gustav Lorentzen Conference on Natural Refrigerants*, Kyoto. International Institute of Refrigeration (IIR).
- Marchante-Avellaneda, J., Navarro-Peris, E., Corberán, J. M., and Shrestha, S. S. (2023c). Comparison and selection of experimental designs for the characterization of scroll compressors: Adjustment of polynomial models with compact experimental samples. *Case Studies in Thermal Engineering*. Submitted article.
- Marchante-Avellaneda, J., Navarro-Peris, E., Corberán, J. M., and Song, Y. (2023d). A new methodology for fitting polynomial models based on virtual-tests maps and experimental samples conducted by experimental designs for the performance characterization of heat pumps and refrigeration equipment. *Applied Thermal Engineering*. Preparing article for submission.
- Marchante-Avellaneda, J., Navarro-Peris, E., Corberán, J. M., and Song, Y. (2023e). Development of map-based models for the characterization of the performance in heat pumps and refrigeration equipment based on the external parameters. *Applied Thermal Engineering*. Preparing article for submission.
- Masip, X., Cazorla-Marín, A., Montagud-Montalvá, C., Marchante-Avellaneda, J., Barceló, F., and Corberán, J. M. (2019). Energy and techno-economic assessment of the effect of the coupling between an air source heat pump and the storage tank for sanitary hot water production. *Applied Thermal Engineering*, 159:113853.
- Song, Y., Rolando, D., Marchante-Avellaneda, J., Zucker, G., and Madani, H. (2023a). Data-driven soft sensors targeting heat pump systems. *Energy Conversion and Management*. Submitted article.
- Song, Y., Rolando, D., Marchante-Avellaneda, J., Zucker, G., and Madani, H. (2023b). Development and validation of data-driven soft sensors for heat pumps. In *14th IEA Heat Pump Conference*, Chicago, Illinois. IEA HPT. Accepted conference paper.
- Tarragona, J., Pisello, A. L., Fernández, C., Cabeza, L. F., Payá, J., Marchante-Avellaneda, J., and de Gracia, A. (2022). Analysis of thermal energy storage tanks and PV panels combinations in different buildings controlled through model predictive control. *Energy*, 239.

Part II

Appendixes


A

R workflow

CONTENTS

A.1	Introduction	a-1
A.2	How to calculate thermophysical properties and the error propagation in R	a-1
A.3	R extensions	a-3
A.4	Python extensions	a-12

A.1 Introduction

This appendix includes the workflow used in the  programming language to calculate thermophysical properties, including the error propagation analysis. The approach described below has been used for this purpose.

A.2 How to calculate thermophysical properties and the error propagation in R

Nowadays, there are several thermophysical property libraries that implement the highest-accuracy formulations for the thermophysical properties of fluids. The most widely used library is REFPROP, developed and maintained by the National Institute of Standards and Technology (NIST). Moreover, some other software and libraries also provide similar functionalities like CoolProp, EES, FLUIDCAL, among others. In this sense, Coolprop and Refprop 10 databases were selected in this work for the calculation of thermophysical properties in order to combine the advantages and strengths of both libraries.

Coolprop is an open-source library capable of obtaining refrigerants, mixtures, secondary fluids, and air psychrometry properties. This library is written in C++, with wrappers available for the majority of programming languages and platforms of technical interest. Coolprop is currently maintained by an active community, among them Ian Bell, also a member of the Refprop development team.

One of the most valuable and exciting features of Coolprop is the definition of several high-level functions that are easy to use and interact with the Refprop database. Specifically, this work uses these Coolprop high-level functions to obtain the thermophysical properties from the Refprop database. The wrapper selected in this PhD to use Coolprop was the Python wrapper¹, which can perform vector calculations for a specific fluid, significantly reducing the computation time.

Against this background, some extra tools and packages were necessary to use in a simple way Coolprop capabilities in an **R** working session. First of all, the **R** package “*reticulate*” (Ushey et al., 2022) was selected, providing **R** with a comprehensive set of tools for interoperability between Python and **R**. Thanks to the “*reticulate*” package we can use Python packages and modules in a simple way directly in **R**. Two functions were defined in a Python script (see Section A.4) calling the functions *PropsSI()*—properties of refrigerants— and *HAPropsSI()*—properties of moist air—from the Coolprop wrapper. Then, **R** loads these functions with the *py_run_file()* function of the *reticulate* package. This allows the *PropsSI()* and *HAPropsSI()* functions to be used as native **R** functions.

On the other hand, the **R** package “*quantities*” (Ucar, 2021) was selected to consider the uncertainties of the measurements and perform an appropriate analysis of the error propagation. The “*quantities*” package allows us to define our dataset, usually consisting of numeric vectors and matrices, as objects with two additional attributes, the units and uncertainty of the measurement. It also provides a comprehensive set of tools allowing the unit conversion and propagation of error automatically in arithmetical calculations. Last but not least, it was necessary to develop in **R** the function *therm_prop_error()* (see Section A.3) to consider also the error propagation in the thermophysical properties. This function performs the error propagation calculation by the classic Taylor Series Method (TSM) with high-order terms neglected, calculating the sensitivity coefficients of the input variables. Then, it returns a “*quantities*” object with the numerical values, units, and uncertainty of the property consulted in the Refprop database.

Figure A.1 shows a summary of the workflow discussed above.

¹The Python wrapper is one of the most developed wrappers currently offering additional functionalities such as plotting P-h diagrams. It allows vector calculations, i.e., call to Coolprop functions, including a vector of state points to return one (vector output) or several (matrix output) properties.

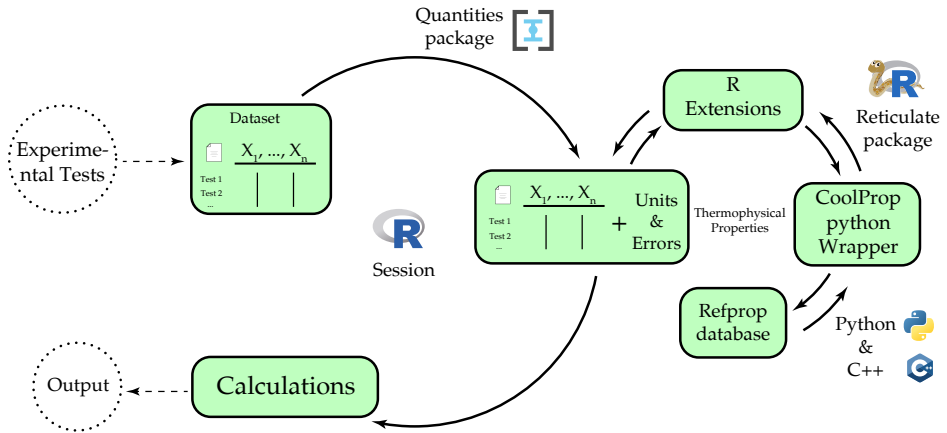


Figure A.1: R session workflow

A.3 R extensions

```
therm_prop_error <- function(outputname,
  input1name, input1values, input2name, input2values, fluid) {

  library(quantities)
  library(reticulate)
  py_run_file("00_sources/PropsSI_Python.py")
  source("00_sources/get_CoolProp_SI_units.R")
  source("00_sources/sensibility_coeff_high_resolution.R")

  options(errors.digits = 4)
  options(errors.notation = "plus-minus")

  if (!"quantities" %in% class(input1values))
    stop("input1values vector must be defined as quantities object")
  if (!"quantities" %in% class(input2values))
    stop("input2values vector must be defined as quantities object")

  fluid_ <- fluid
```

```

x_name <- input1name
x_q <- set_units(input1values, get_CoolProp_SI_units(x_name),
  mode = "standard")
x <- drop_quantities(x_q)
x_error <- errors(x_q)

y_name <- input2name
y_q <- set_units(input2values, get_CoolProp_SI_units(y_name),
  mode = "standard")
y <- drop_quantities(y_q)
y_error <- errors(y_q)

z_name <- outputname

z <- py$myPropsSI(outputs = z_name, input1name = x_name,
  input1values = x, input2name = y_name,
  input2values = y, fluid = fluid_)

if (all(x_error != 0)) {
  dx <- 2 * x_error
  z1_x <- py$myPropsSI(outputs = z_name,
    input1name = x_name, input1values = x +
      x_error, input2name = y_name,
    input2values = y, fluid = fluid_)
  z2_x <- py$myPropsSI(outputs = z_name,
    input1name = x_name, input1values = x -
      x_error, input2name = y_name,
    input2values = y, fluid = fluid_)

  dz_x <- z1_x - z2_x

  x_sensivity_coeff <- (dz_x)/dx
  whx_sen_coeff_is0 <- which(x_sensivity_coeff == 0)

  if (length(whx_sen_coeff_is0) != 0) {
    x_sensivity_coeff_recalc <- sensibility_coeff_high_resolution(
      output_name = z_name,
      varInput_name = x_name,
      varInput = x[whx_sen_coeff_is0],
      varInput_error = x_error,

```

```

        fixInput_name = y_name,
        fixInput = y[whx_sen_coeff_is0])
    x_sensivility_coeff[whx_sen_coeff_is0] <-
        x_sensivility_coeff_recalc
    }
} else {
    x_sensivility_coeff <- 0
}

if (all(y_error != 0)) {
    dy <- 2 * y_error
    z1_y <- py$myPropsSI(outputs = z_name,
        input1name = x_name, input1values = x,
        input2name = y_name, input2values = y +
            y_error, fluid = fluid_)
    z2_y <- py$myPropsSI(outputs = z_name,
        input1name = x_name, input1values = x,
        input2name = y_name, input2values = y -
            y_error, fluid = fluid_)

    dz_y <- z1_y - z2_y

    y_sensivility_coeff <- (z1_y - z2_y)/dy
    why_sen_coeff_is0 <- which(y_sensivility_coeff == 0)

    if (length(why_sen_coeff_is0) != 0) {
        y_sensivility_coeff_recalc <- sensibility_coeff_high_resolution(
            output_name = z_name,
            varInput_name = y_name,
            varInput = y[why_sen_coeff_is0],
            varInput_error = y_error,
            fixInput_name = x_name,
            fixInput = x[why_sen_coeff_is0])
        y_sensivility_coeff[why_sen_coeff_is0] <-
            y_sensivility_coeff_recalc
    }
} else {
    y_sensivility_coeff <- 0
}

z_error <- sqrt((x_sensivility_coeff *

```

```

x_error)^2 + (y_sensivity_coeff *
y_error)^2)

z_q <- set_quantities(as.numeric(z),
  get_CoolProp_SI_units(z_name), mode = "standard",
  errors = as.numeric(z_error))

return(z_q)
}

```

```

get_CoolProp_SI_units <- function(variable_name) {

  l <- list()

  # Molar density
  l[["DMOLAR"]] <- "mol/m^3"
  l[["Dmolar"]] <- "mol/m^3"
  # Mass density
  l[["D"]] <- "kg/m^3"
  l[["DMASS"]] <- "kg/m^3"
  l[["Dmass"]] <- "kg/m^3"
  # Molar specific enthalpy
  l[["HMOLAR"]] <- "J/mol"
  l[["Hmolar"]] <- "J/mol"
  # Mass specific enthalpy
  l[["H"]] <- "J/kg"
  l[["HMASS"]] <- "J/kg"
  l[["Hmass"]] <- "J/kg"
  # Pressure
  l[["P"]] <- "Pa"
  # Mass vapor quality
  l[["Q"]] <- "1"
  # Molar specific entropy
  l[["SMOLAR"]] <- "J/mol/K"
  l[["Smolar"]] <- "J/mol/K"
  # Mass specific entropy
  l[["S"]] <- "J/kg/K"
  l[["SMASS"]] <- "J/kg/K"
  l[["Smass"]] <- "J/kg/K"
  # Temperature

```



```
l[["T"]] <- "K"
# Molar specific internal energy
l[["UMOLAR"]] <- "J/mol"
l[["Umolar"]] <- "J/mol"
# Mass specific internal energy
l[["U"]] <- "J/kg"
l[["UMASS"]] <- "J/kg"
l[["Umass"]] <- "J/kg"
# Speed of sound
l[["A"]] <- "m/s"
l[["SPEED_OF_SOUND"]] <- "m/s"
l[["speed_of_sound"]] <- "m/s"
# Thermal conductivity
l[["CONDUCTIVITY"]] <- "W/m/K"
l[["L"]] <- "W/m/K"
l[["conductivity"]] <- "W/m/K"
# Ideal gas mass specific constant
# pressure specific heat
l[["CP0MASS"]] <- "J/kg/K"
l[["Cp0mass"]] <- "J/kg/K"
# Ideal gas molar specific constant
# pressure specific heat
l[["CP0MOLAR"]] <- "J/mol/K"
l[["Cp0molar"]] <- "J/mol/K"
# Molar specific constant pressure
# specific heat
l[["CPMOLAR"]] <- "J/mol/K"
l[["Cpmolar"]] <- "J/mol/K"
# Mass specific constant volume specific heat
l[["CVMASS"]] <- "J/kg/K"
l[["Cvmass"]] <- "J/kg/K"
# Molar specific constant volume specific heat
l[["CVMOLAR"]] <- "J/mol/K"
l[["Cvmolar"]] <- "J/mol/K"
# Mass specific constant pressure
# specific heat
l[["C"]] <- "J/kg/K"
l[["CPMASS"]] <- "J/kg/K"
l[["Cpmass"]] <- "J/kg/K"
# Dipole moment
l[["DIPOLE_MOMENT"]] <- "C*m"
```

```
l[["dipole_moment"]] <- "C*m"
# Molar gas constant
l[["GAS_CONSTANT"]] <- "J/mol/K"
l[["gas_constant"]] <- "J/mol/K"
# Residual molar Gibbs energy
l[["GMOLAR_RESIDUAL"]] <- "J/mol/K"
l[["Gmolar_residual"]] <- "J/mol/K"
# Molar specific Gibbs energy
l[["GMOLAR"]] <- "J/mol"
l[["Gmolar"]] <- "J/mol"
# Mass specific Gibbs energy
l[["G"]] <- "J/kg"
l[["GMASS"]] <- "J/kg"
l[["Gmass"]] <- "J/kg"
# Mass specific Helmholtz energy
l[["HELMHOLTZMASS"]] <- "J/kg"
l[["Helmholtzmass"]] <- "J/kg"
# Molar specific Helmholtz energy
l[["HELMHOLTZMOLAR"]] <- "J/mol"
l[["Helmholtzmolar"]] <- "J/mol"
# Residual molar enthalpy
l[["HMOLAR_RESIDUAL"]] <- "J/mol/K"
l[["Hmolar_residual"]] <- "J/mol/K"
# Isobaric expansion coefficient
l[["ISOBARIC_EXPANSION_COEFFICIENT"]] <- "1/K"
l[["isobaric_expansion_coefficient"]] <- "1/K"
# Isothermal compressibility
l[["ISOTHERMAL_COMPRESSIBILITY"]] <- "1/Pa"
l[["isothermal_compressibility"]] <- "1/Pa"
# Surface tension
l[["I"]] <- "N/m"
l[["SURFACE_TENSION"]] <- "N/m"
l[["surface_tension"]] <- "N/m"
# Molar mass
l[["M"]] <- "kg/mol"
l[["MOLARMASS"]] <- "kg/mol"
l[["MOLAR_MASS"]] <- "kg/mol"
l[["MOLEMASS"]] <- "kg/mol"
l[["molar_mass"]] <- "kg/mol"
l[["molarmass"]] <- "kg/mol"
l[["molemass"]] <- "kg/mol"
```

```
# Pressure at the critical point
l[["PCRIT"]] <- "Pa"
l[["P_CRITICAL"]] <- "Pa"
l[["Pcrit"]] <- "Pa"
l[["p_critical"]] <- "Pa"
l[["pcrit"]] <- "Pa"
# Maximum pressure limit
l[["PMAX"]] <- "Pa"
l[["P_MAX"]] <- "Pa"
l[["P_max"]] <- "Pa"
l[["pmax"]] <- "Pa"
# Minimum pressure limit
l[["PMIN"]] <- "Pa"
l[["P_MIN"]] <- "Pa"
l[["P_min"]] <- "Pa"
l[["pmin"]] <- "Pa"
# Pressure at the triple point (pure
# only)
l[["PTRIPLE"]] <- "Pa"
l[["P_TRIPLE"]] <- "Pa"
l[["p_triple"]] <- "Pa"
l[["ptriple"]] <- "Pa"
# Pressure at the reducing point
l[["P_REDUCING"]] <- "Pa"
l[["p_reducing"]] <- "Pa"
# Mass density at critical point
l[["RHOCRIT"]] <- "kg/m^3"
l[["RHOMASS_CRITICAL"]] <- "kg/m^3"
l[["rhocrit"]] <- "kg/m^3"
l[["rhomass_critical"]] <- "kg/m^3"
# Mass density at reducing point
l[["RHOMASS_REDUCING"]] <- "kg/m^3"
l[["rhomass_reducing"]] <- "kg/m^3"
# Molar density at critical point
l[["RHOMOLAR_CRITICAL"]] <- "mol/m^3"
l[["rhomolar_critical"]] <- "mol/m^3"
# Molar density at reducing point
l[["RHOMOLAR_REDUCING"]] <- "mol/m^3"
l[["rhomolar_reducing"]] <- "mol/m^3"
# Residual molar entropy (sr/R = s(T,rho)
# - s^0(T,rho))
```

```

l[["SMOLAR_RESIDUAL"]] <- "J/mol/K"
l[["Smolar_residual"]] <- "J/mol/K"
# Temperature at the critical point
l[["TCRIT"]] <- "K"
l[["T_CRITICAL"]] <- "K"
l[["T_critical"]] <- "K"
l[["Tcrit"]] <- "K"
# Maximum temperature limit
l[["TMAX"]] <- "K"
l[["T_MAX"]] <- "K"
l[["T_max"]] <- "K"
l[["Tmax"]] <- "K"
# Minimum temperature limit
l[["TMIN"]] <- "K"
l[["T_MIN"]] <- "K"
l[["T_min"]] <- "K"
l[["Tmin"]] <- "K"
# Temperature at the triple point
l[["TTRIPLE"]] <- "K"
l[["T_TRIPLE"]] <- "K"
l[["T_triple"]] <- "K"
l[["Ttriple"]] <- "K"
# Freezing temperature for incompressible
# solutions
l[["T_FREEZE"]] <- "K"
l[["T_freeze"]] <- "K"
# Temperature at the reducing point
l[["T_REDUCING"]] <- "K"
l[["T_reducing"]] <- "K"
# Viscosity
l[["V"]] <- "Pa*s"
l[["VISCOSITY"]] <- "Pa*s"
l[["viscosity"]] <- "Pa*s"

if (!variable_name %in% names(l))
  stop("The input variable name is not
      included in get_CoolProp_SI_units function")

return(l[[variable_name]])
}

```

```

sensibility_coeff_high_resolution <- function(output_name,
  varInput_name, varInput, varInput_error,
  fixInput_name, fixInput, fluid) {
  warning(paste0("called to sensibility_coeff_high_resolution
    function: ", output_name, " = f(", varInput_name,
    ",", fixInput_name, "). ", fixInput_name,
    " fixed for the propagation error"))
  mult <- 1
  mult_vec <- rep(1, length(varInput))
  # ptm <- proc.time()
  sensibility_coeff <- NA

  while (0 %in% sensibility_coeff || mult == 9999) {

    dvarInput <- 2 * mult_vec * varInput_error
    output_1 <- py$myPropsSI(outputs = output_name,
      input1name = varInput_name, input1values = varInput +
      mult_vec * varInput_error,
      input2name = fixInput_name, input2values = fixInput,
      fluid = fluid)
    output_2 <- py$myPropsSI(outputs = output_name,
      input1name = varInput_name, input1values = varInput -
      mult_vec * varInput_error,
      input2name = fixInput_name, input2values = fixInput,
      fluid = fluid)

    dvarOutput <- output_1 - output_2

    sensibility_coeff <- (dvarOutput)/dvarInput

    if (mult == 9999)
      stop("stop at 9999 iterations in
        sensibility_coeff_high_resolution function")

    wh_sen_coeff_is0 <- which(sensibility_coeff == 0)

    mult <- mult + 1

    mult_vec[wh_sen_coeff_is0] <- mult
  }
  # proc.time() - ptm

```

```

    return(sensivility_coeff)
}

```

A.4 Pyhton extensions

```

# from CMD: pip install CoolProp
import json, CoolProp.CoolProp as CP

#Refprop library path in the system
CP.set_config_string(CP.ALTERNATIVE_REFPROP_LIBRARY_PATH,
                    '/opt/Refprop_10/librefprop.so')
CP.set_config_string(CP.ALTERNATIVE_REFPROP_PATH, '/opt/Refprop_10/')

#json.loads(CP.get_config_as_json_string())
#CP.get_global_param_string("REFPROP_version")
#
def myPropsSI(outputs, input1name, input1values, input2name,
             input2values, fluid):
    res = CP.PropsSI(outputs, input1name, input1values, input2name,
                    input2values, fluid)
    return (res)

```

```

# from CMD: pip install CoolProp
import json, CoolProp.CoolProp as CP
from CoolProp.HumidAirProp import HAPropsSI

#Refprop library path in the system
CP.set_config_string(CP.ALTERNATIVE_REFPROP_LIBRARY_PATH,
                    '/opt/Refprop_10/librefprop.so')
CP.set_config_string(CP.ALTERNATIVE_REFPROP_PATH, '/opt/Refprop_10/')

#json.loads(CP.get_config_as_json_string())
#CP.get_global_param_string("REFPROP_version")
#

```

```
def myHAPropsSI(outputs, input1name, input1values, input2name,  
                input2values, input3name, input3values):  
    res = HAPropsSI(outputs, input1name, input1values, input2name,  
                    input2values, input3name, input3values)  
    return (res)
```


B

DSHP: Components description

CONTENTS

B.1	Refrigerant	b-1
B.2	Heat exchangers	b-2
B.3	Expansion valve	b-4
B.4	Compressor	b-5
B.5	Pipes and refrigerant charge	b-5

This appendix includes additional information related to the main components installed in the DSHP.

Section B.1 includes the refrigerant selected and its main advantages. Then, Section B.2 provides the geometry and circuits for the Air HX and the typology and dimensions of the selected plates in the User, DHW and Ground HXs.

Section B.3 and Section B.4 include information about the electronic expansion valve and the variable speed compressor installed.

Finally, Section B.5 shows the design criteria for selecting the diameter for the connection pipes and the total refrigerant charge.

B.1 Refrigerant

Due to the trends of the current regulation for refrigerant fluids (*F-gas regulation*), the use of HFCs¹ with high values of GWP² is being phased out. Nowadays, these refrigerants are replaced by HFOs³, HFCs with low values of GWP, or natural refrigerants like propane.

¹Hydrofluorocarbons: hydrogen, fluorine and carbon atoms connected by single bonds between the atoms.

²Global Warming Potential.

³Hydrofluoro-olefin: hydrogen, fluorine and carbon atoms. It contains at least one double bond between the carbon atoms.

The solution adopted in this unit was to use the refrigerant R32. In the past few years, many manufacturers selected the R32 as a short and medium-term substitute for the R410A. The main advantages of this refrigerant compared to R410A are:

1. Low GWP ($\approx 70\%$ less than R410A⁴. 675GWP-R32 vs 2088GWP-R410A)
2. Pure refrigerant (easy recycling).
3. Less refrigerant charge ($\approx 25\%$ less dense than R410A. Densities of R32 and R410A at temperature of 5°C on the saturated vapor are 25.769kg/m³ and 34.843kg/m³).
4. Low inflammability (safety group A2L).

B.2 Heat exchangers

In order to obtain an efficient heat transfer this unit includes internal Brazed Plate Heat Exchangers (BPHEs) for the User, DHW and Ground loops and a Round Tube Plate Fin Heat exchanger (RTPFHx) in the air side.

Figure B.1 shows the configuration for the circuits in the RTPFHx and Table B.1 includes its geometry.

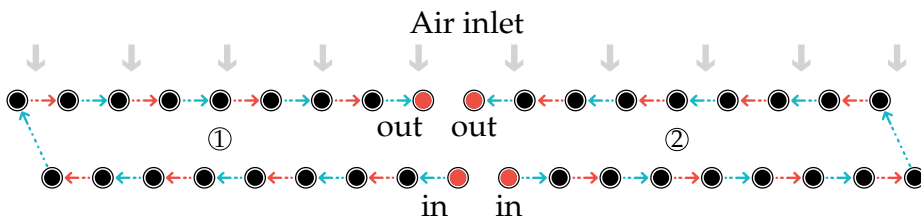


Figure B.1: RTPFHx: Circuits configuration⁵

⁴According to IPPCC-AR4/CIE.

⁵Configuration 1: First circuit. Configuration 2: Circuits 2, 3, 4 and 5.

Table B.1: Data of the designed RTPFHx

Element	Value
Height x Width	1125 x 750 mm
Longitudinal spacing	21.65 mm
Transversal spacing	25 mm
Tube	Thickness: 0.3 mm Outer Diameter: 7.94 mm (5/16") Material: Copper Surface: Smooth
Fin data	Thickness: 0.1 mm Fin Pitch 1.8 mm Material: Aluminium Type: Wavy
Circuitry	45 tubes/row 2 rows 5 circuits
Fans (2)	Diameter = 450 mm Type: EC Speed = Variable

The heat pump's frame dimensions were selected to ensure enough space for the RTPFHx and the rest of the components: (1500 × 1222 × 560)mm.

According to the operation mode, the RTPFHx operates in the following ways:

- Winter modes (RTPFHx as evaporator) ⇒ Counter-Current cross-flow.
- DHW (RTPFHx as evaporator) ⇒ Counter-Current cross-flow.
- Summer modes (RTPFHx as condenser) ⇒ Co-Current cross-flow.

Regarding the hydraulic loops, the secondary fluid selected for the Ground was propylene glycol with a 30% of mass concentration and water for the User and DHW. The DSHP also includes three internal circulation pumps and two 4-way valves at the connection with the outdoor hydraulic loops⁶. This configuration always allows keeping a counter-current arrangement in the BPHes.

⁶Ground and User loops.

Finally, Table B.2 shows the geometry and model for the BPHEs selected. DHW and Ground BPHEs were selected with asymmetric plate pitch in order to minimize the refrigerant charge and reduce the pressure drop on the water/brine loops.

Table B.2: BPHEs specifications

Geometry	User	DHW	Ground
n° Plates	20	18	20
Plate Pitch	1.84 mm	1.63* mm	2.25* mm
Height x Width	526x119 mm	376x119 mm	526x119 mm
Plate model	F85 (SWEP)	B26 (SWEP)	F80AS (SWEP)
Type	Symmetric	Asymmetric	Asymmetric
Port diameter	33 mm	18/24/27/27 mm	33 mm
Plate material	Stainless steel	Stainless steel	Stainless steel
Port material	Cooper	Cooper	Cooper

* Asymmetric plate. Medium value of plate pitch;

B.3 Expansion valve

An Electronic Expansion Valve (EEV) Model E2V14 by CAREL was employed to control the superheat level.

As the unit has a large number of different operation modes and the evaporator changes from one heat exchanger to another, the control of the superheat is measured at the compressor suction pipe, which corresponds to the same pipe for all operation modes. It also limits the maximum discharge temperature by injecting some liquid refrigerant at the compressor suction when the temperature rises to 120°C.

Finally, a liquid receiver is provided at the condenser outlet to store all liquid refrigerant that will be in excess for some of the modes and operating conditions, fixing the subcooling to 0K.

B.4 Compressor

This unit includes a variable speed compressor in order to adapt the performance to a wide range of operating conditions and minimize part load losses. The compressor selected was a scroll compressor due to the high efficiency of this technology.

Table B.3 shows the main characteristics of this compressor:

Table B.3: Compressor specifications

Compressor	
Manufacturer	Copeland
Model	XHV025
Type	Scroll
Displacement	25 cm ³ /rev
Refrigerant	R32*
Oil type	POE32
Speed	[15-120] rps

* Originally designed for R410A;

B.5 Pipes and refrigerant charge

The selection of the adequate diameters for the pipes of the different unit lines was performed by two main targets: first, avoiding excessive pressure losses, and second, ensuring a minimum velocity in order to get the return of the oil at low compressor velocities. This is especially critical for the suction line. Then, for those pipes that change their role from one operating mode to another, for instance, from part of the liquid line to part of an expansion line, the most critical criteria were selected to satisfy the design conditions.

Finally, the unit was provided with a refrigerant charge of 3 kg. This charge ensures the correct operation of the unit in all working modes.

C

Auxiliaries characterization

CONTENTS

C.1	DSHP parasitic consumption	c-1
C.2	Fan characterization	c-2
C.3	Fluid properties for the brine and water loops	c-3
C.4	BPHE pressure drop	c-4
C.5	Circulation pumps (secondary side)	c-7

This appendix includes how to characterize the auxiliary components in HP units. Typically these components are *fans*, *circulation pumps*, *connection pipes*, and the *control electronics*, among other secondary elements. The following sections include the characterization of the DSHP auxiliary components. These components are three circulation pumps and two fans with inverter technology. Additionally, correlations for the pressure drop in the secondary side of the BPHEs and the characterization of the parasitic losses are also included. The correlations of the pressure drop in the secondary side will be used to estimate the electrical consumption of the internal circulation pumps according to Section C.5.

We can consider the auxiliaries' effect on the HP performance by combining the correlations provided in this appendix with the empirical models performed in Chapter 3 (see equations on pages 61, 63 and 65).

C.1 DSHP parasitic consumption

The parasitic consumption in this unit is mainly composed of the control electronics consumption (42W). Furthermore, as described in Subsection 2.2.3, this unit includes 10 solenoid valves in order to select the desired operating mode. The normal operation is to energize only three solenoid valves¹ in any of the

¹Power consumption of 7.9W for each one.

possible working modes. Consequently, the parasitic consumption is calculated according to the following equations:

$$\dot{W}_{par}(W) = 42 + 3 \cdot 7.9 = 65.7W \quad (\text{HP compressor ON}) \quad (\text{C.1})$$

$$\dot{W}_{par}(W) = 42W \quad (\text{HP compressor OFF}) \quad (\text{C.2})$$

C.2 Fan characterization

This unit includes two variable speed fans (axial type). Both were characterized in the experimental campaign measuring the power consumptions and fan speed (Figure C.1). Then, a regression model² was adjusted to predict the power consumption for one fan (Equation C.3). Finally, as the unit mounts two fans, the total power consumption is calculated with the Equation C.4.

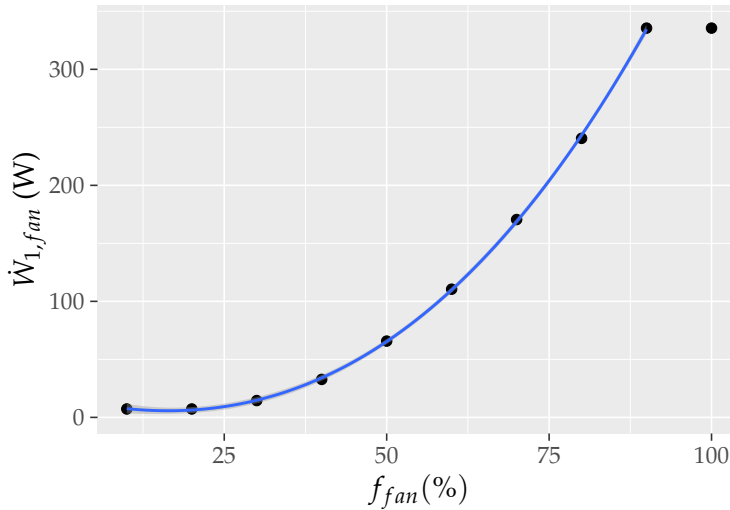


Figure C.1: Fan characterization

²The fan power consumption is limited to 90% of fan load by the fan electronics. This point is removed from the regression adjustment.

$$\dot{W}_{1,fan} = -2.402e-02f_{fan} + 8.652e-03f_{fan}^2 + 3.679e-04f_{fan}^3 \quad (C.3)$$

$$\dot{W}_{fan}(W) = 2\dot{W}_{1,fan} \quad (C.4)$$

The coefficients included in the equations above were adjusted for f_{fan} in (%) and $\dot{W}_{1,fan}$ in (W).

C.3 Fluid properties for the brine and water loops

The correlations provided in Section C.4 for the estimations of the pressure drop in the BPHEs depends on density and dynamic viscosity in order to correct them with the temperature change. These properties can be estimated in Refprop, EES, or Coolprop databases. However, it is possible to provide simple correlations for these properties as a function of the average temperature of the secondary fluid across the corresponding BPHE.

First of these properties, the density, can be estimated with a simple third-degree polynomial. Then, according to Hole (1994), the dynamic viscosity can be modelled as $\mu = Ae^{\frac{B}{T}}$. For simplicity, this expression has been linearized and added an extra term to improve the regression adjustment:

$$\ln\mu = \ln A + \frac{B}{T} + \frac{C}{T^2} \Rightarrow \mu = e^{\ln A + \frac{B}{T} + \frac{C}{T^2}} \quad (C.5)$$

The left expression allows a simple regression adjustment applying linear regression to obtain the coefficients $\ln A$, B and C and then, calculate the viscosity with equation on the right side.

Finally, Table C.1 and Table C.2 show the regression coefficients adjusted for the two secondary fluids, *water* and *propylenglycol*, used in this unit. The database used for the adjustment has been Coolprop and the average temperature in the secondary side has been calculated with Equation C.6 and Equation C.7.

$$T(K) = \frac{T_{co} - T_{ci}}{2} \quad (\text{Condenser side}) \quad (C.6)$$

$$T(K) = \frac{T_{ei} - T_{eo}}{2} \quad (\text{Evaporator side}) \quad (C.7)$$

Table C.1: Water Properties

Variable	Coeff.	Value	Range and equation	
$\rho(T)[kg/m^3]$	a_0	1.24e+01	Variable	$T[K]$
	a_1	8.94e+00	Range	$[273.25, 343.15]K$
	a_2	-2.59e-02	Equation	$\rho(T) = a_0 + a_1T + a_2T^2 + a_3T^3$
	a_3	2.35e-05		
$\mu(T)[Pa s]$	b_0	-7.11e+00	Variable	$T[K]$
	b_1	-2.00e+03	Range	$[273.25, 343.15]K$
	b_2	6.05e+05	Equation	$\mu(T) = e^{b_0+b_1\frac{1}{T}+b_2\frac{1}{T^2}}$

Table C.2: Propylenglycol Properties (30% mass fraction)

Variable	Coeff.	Value	Range and equation	
$\rho(T)[kg/m^3]$	a_0	5.40e+02	Variable	$T[K]$
	a_1	4.93e+00	Range	$[261.15, 313.15]K$
	a_2	-1.52e-02	Equation	$\rho(T) = a_0 + a_1T + a_2T^2 + a_3T^3$
	a_3	1.36e-05		
$\mu(T)[Pa s]$	b_0	-2.49e+00	Variable	$T[K]$
	b_1	-5.14e+03	Range	$[273.25, 343.15]K$
	b_2	1.22e+06	Equation	$\mu(T) = e^{b_0+b_1\frac{1}{T}+b_2\frac{1}{T^2}}$

C.4 BPHE pressure drop

Although BPHEs are manufactured with a wide range of plate measures and many different corrugation types, we can estimate the pressure drop in the secondary side with the Darcy-Weisbach equation for an incompressible fluid (Equation C.8):

$$\frac{\Delta P}{L} = 4f_f \frac{\rho v^2}{2D_h} \quad (C.8)$$

Where $\Delta P/L$ is the pressure loss per unit length (Pa/m), D_h is the hydraulic diameter (m), f_f is the fanning friction factor (-), ρ is the fluid density (kg/m^3) and v the mean flow velocity (m/s).

This equation requires an estimation for the fanning friction factor. Therefore, according to Hewitt and Shires (1994), this parameter can be obtained as a function of the Reynolds number with the Equation C.9³.

$$f_f = 2.78Re^{-0.18} \quad (C.9)$$

Where the Reynold number is calculated as $Re = \frac{vD_h\rho}{\mu}$.

Considering now the volume flow rate and mass flow rate as $\dot{V} = Av$ and $\dot{m} = \dot{V}\rho$ and the expression for the Reynolds number, the Equation C.8 can be rewritten as:

$$\Delta P = \frac{5.56L}{D_h^{1.18} A^{1.82}} \left(\frac{\mu^{0.18}}{\rho} \right) \dot{m}^{1.82} \quad (C.10)$$

The term $\frac{5.56L}{D_h^{1.18} A^{1.82}}$ is a constant value that we can adjust for the corresponding BPHE using catalog data from the manufacturer and a regression adjustment. For this purpose, the catalog data was extract from a simulation tool provided by the manufacturer (SWEP software). In order to increase the accuracy and prediction ranges for the pressure drop an extra term has been added to the equation above. Consequently, the pressure drop at the mean reference temperature is calculated according to the Equation C.11 for the three BPHEs:

$$\Delta P_{298.15K} = C_1 \dot{m} + C_2 \dot{m}^{1.9} \quad (C.11)$$

The regression coefficients adjusted at a mean reference temperature of 25°C (298.15K) for the three BPHEs are included in the Table C.3, Table C.4 and Table C.5.

Finally, the variation of the ΔP with the temperature is taken into account with the correlations adjusted in Section C.3 and the Equation C.12.

$$\Delta P(T) = \Delta P(298.15K) \left(\frac{\mu(T)}{\mu(298.15K)} \right)^{0.18} \left(\frac{\rho(298.15K)}{\rho(T)} \right) \quad (C.12)$$

³Approximate expresion for f_f in the turbulent flow region.

Table C.3: ΔP (User - Plate model: F85 SWEP)

Variable	Coeff.	Value	Range and equation	
$\Delta P_{298.15K}(\dot{m})[Pa]$	C_1	6.44e+03	Variable Range	$\dot{m}[kg/s]$ [0.005, 1]kg/s
	C_2	8.47e+04	Equation	$\Delta P(\dot{m}) = C_1\dot{m} + C_2\dot{m}^{1.9}$

Table C.4: ΔP (DHW - Plate model: B26 SWEP)

Variable	Coeff.	Value	Range and equation	
$\Delta P_{298.15K}(\dot{m})[Pa]$	C_1	1.85e+03	Variable Range	$\dot{m}[kg/s]$ [0.155, 0.6]kg/s
	C_2	8.63e+04	Equation	$\Delta P(\dot{m}) = C_1\dot{m} + C_2\dot{m}^2$

Table C.5: ΔP (Ground - Plate model: F80AS SWEP)

Variable	Coeff.	Value	Range and equation	
$\Delta P_{298.15K}(\dot{m})[Pa]$	C_1	2.44e+03	Variable Range	$\dot{m}[kg/s]$ [0.005, 1]kg/s
	C_2	4.59e+04	Equation	$\Delta P(\dot{m}) = C_1\dot{m} + C_2\dot{m}^{1.9}$

C.5 Circulation pumps (secondary side)

The DSHP tested includes three variable speed circulation pumps for the User, DHW and Ground BPHEs. Figure C.2 shows the typical representation for the performance maps in variable speed pumps.

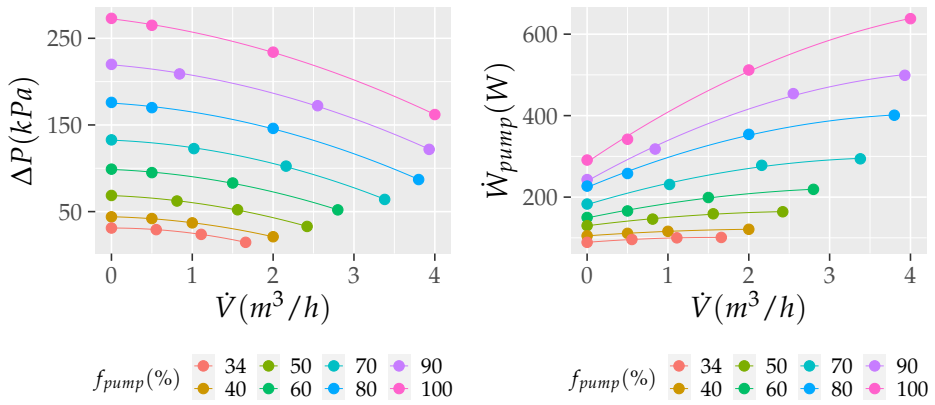


Figure C.2: Operating map of a variable speed circulation pump

The left graph represents the pressure of the pump as a set of curves depending on the volume flow rate and speed. Then, we can obtain the same representation in the right graph for the electrical consumption. This last variable, the electrical consumption, must be correlated to make the corrections proposed in the equations on pages 61, 63 and 65. Observing the previous figures, we can see that the consumption of the circulation pump is fixed by two independent variables, the volume flow rate, and the pump speed. The latter can be conveniently substituted by the ΔP , where a given volume flow rate and the ΔP provided by the pump will correspond to a specific pump speed. Therefore, we can propose a polynomial model for calculating the electrical consumption as a function of the pressure drop and the volume flow rate. Equation C.13 and Equation C.14 have been obtained by using the manufacturer’s catalog data. The ground circulation pump includes a small temperature correction with the $(\mu(T)^{0.07}/\rho(T))$ factor, where the coefficient 0.07 has been obtained by adjusting it to the catalog data⁴.

⁴The manufacturer Grunfos includes catalog data at different temperatures.

DHW and User pump:

$$\dot{W}_{pump} = a_0 + a_1\Delta P + a_2\Delta P^2 + a_3\dot{V} + a_4\Delta P\dot{V} \quad (\text{C.13})$$

Ground pump:

$$\dot{W}_{pump} = \left(b_0 + b_1\Delta P + b_2\Delta P^2 + b_3\dot{V} + b_4\dot{V}^2 + b_5\Delta P\dot{V} \right) \left(\frac{\mu(T)^{0.07}}{\rho(T)} \right) \quad (\text{C.14})$$

These correlations predict the electrical consumption (\dot{W}_{pump}) in W as a function of the pressure drop (ΔP) in kPa and the volume flow rate (\dot{V}) in m^3/h . Table C.6 and Table C.7 provide the values of the regression coefficients for a validated range of 0 to 4 m^3/h (volume flow rate).

Table C.6: Regression coefficients DHW and User pumps

Coeff.	Value
a_1	3.98e+00
a_2	7.88e-01
a_3	4.10e-03
a_4	2.30e+00
a_5	2.56e-01

Table C.7: Regression coefficients Ground pump

Coeff.	Value
b_1	9.72e+04
b_2	1.41e+03
b_3	-8.47e-01
b_4	-1.32e+04
b_5	1.14e+04
b_6	6.32e+02

Finally, to conclude this section, a brief description of the effect of circulation pumps on unit performance is included below. Figure C.3 shows a simple scheme of the hydraulic loop of a heat pump provided with internal circulation pumps. The example selected is the condenser side.

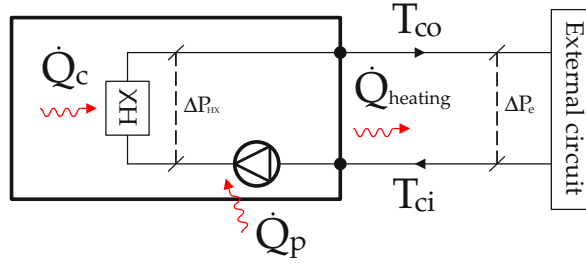


Figure C.3: Condenser capacity correction with the heat injected by the circulation pump

In this figure, we can see that the internal circulation pump is installed inside the unit. Thus, the temperature measurements made at the hydraulic connection ports include the heat injected by the pump (\dot{Q}_p) when calculating the capacity. As discussed in Chapter 3, the empirical models for the capacity prediction were adjusted by first eliminating the circulation pump's effect. They provide the values of the condenser capacity (\dot{Q}_c) and the evaporator capacity (\dot{Q}_e). For this purpose, the estimated values of the capacity were corrected with the same process that now is exposed to include the effect of the circulation pumps.

The process is simple. We consider the heating capacity of the unit as:

$$\dot{Q}_{heating} = \dot{Q}_c + \dot{Q}_p \quad (\text{C.15})$$

Then, we can estimate \dot{Q}_c with the DSHP models provided in Chapter 3. Therefore we only need to estimate the heat injected by the pump as:

$$\dot{Q}_p = \eta_p \cdot \dot{W}_{pump} - P_h = \eta_p \cdot \dot{W}_{pump} - \dot{V} \cdot \Delta P \quad (\text{C.16})$$

where η_p is the efficiency of the electric motor considered as a constant value⁵ of 0.9, \dot{W}_{pump} is the electric power in W and P_h is the hydraulic power in W. Both, the electric power and the hydraulic power depends on \dot{V} and ΔP . This ΔP compensated by the circulation pump is the sum of the pressure drop in the BPHEX (ΔP_{HX}) and the pressure drop in the external circuit (ΔP_e):

$$\Delta P = \Delta P_{HX} + \Delta P_e \quad (\text{C.17})$$

⁵BS EN Standard 14511-3:2018: η_p in dry-motor type pumps can be considered as a constant value of 0.9. In glandless pumps this efficiency value is 1.

Therefore, we are able to correct the circulation pump's effects by using the correlations provided for the estimation of the pressure drop in the BPHEs, the correlations provided for the estimation of the circulation pumps electric power and the measurement of the circulation pump volume flow rate. On the other hand, for the external circuit pressure drop, if we have additional information, we can estimate it, but it will depend on where the unit is installed and if the system has additional circulation pumps. In the absence of information and considering that the system should include additional circulation pumps if the pressure drop to be compensated is high, we can consider this pressure drop as negligible⁶.

Finally, to correct the energy consumption of the unit, the same correlations must be used, adding the electric power of the circulation pumps, the electric consumption of the fan and the parasitic consumption depending on the auxiliary components used in each operating mode.

⁶This pressure drop was considered during the experimental campaign when applying the correction in the capacities in order to obtain the DSHP polynomial models (\dot{Q}_c and \dot{Q}_e). The test rig included pressure drop sensors for the ΔP_e measurement in the hydraulic ports of the unit.

D

Uncertainty analysis

CONTENTS

D.1	Estimation of measurement uncertainty	d-1
D.2	Instrumentation uncertainty specifications	d-5
D.2.1	Pressure transducer Rosemount 2088A3S22A2B4Q4 ...	d-6
D.2.2	Pressure transducer Rosemount 3051CA3A02A1AH2Q4Q8TR	d-6
D.2.3	Power meter Gossen-Metrawatt A2000	d-7
D.2.4	Coriolis flowmeter Siemens Mass 2100 DL15	d-7
D.2.5	Coriolis flowmeter Siemens Mass 2100 DL15	d-7
D.2.6	Coriolis flowmeter Siemens Mass 2100 DL15	d-8
D.2.7	Vaisala HUMICAP 180	d-8
D.2.8	RTD Class 1/10DIN	d-9
D.2.9	Thermocouple Type T	d-9

This appendix includes information on the quality of the measurements obtained in the DSHP experimental campaign. It includes two sections, one with a brief explanation of the methodology used for calculating measurement uncertainties and the error propagation and another with a summary of the sensor's uncertainties installed in the experimental test bench. On the other hand, for calculating the uncertainties of the experimental measurements analyzed in the compressor chapter (Chapter 4), the uncertainties included in the AHRI reports have been considered by applying the same approach as in the experimental values of the DSHP.

D.1 Estimation of measurement uncertainty

When someone conducts experimental tests monitoring a process and recording data with sensors and data acquisition systems, there is no such thing as a per-

fect measurement value. All variable measurements contain inaccuracies and, if we use these experimental data in our analysis, we must consider how “good” the experimental information is. In this sense, we use the concept of uncertainty to describe the degree of goodness of measurement. There are different methodologies to quantify these uncertainties in our experimental data and new variables calculated from these data. In this PhD thesis, the corresponding error analysis and its propagation for the calculated variables were conducted according to Taylor and Kuyatt (1994), and also using some recommendations included in Coleman and Steele (2018).

First of all, it is important to note what types of error sources may be present when performing an experimental measurement. Using traditional nomenclature, we can assign the symbol β to designate an error that does not vary during the measurement period (systematic error) and the symbol ϵ to designate an error that does vary during the measurement period (random error). Considering both errors, we obtain the following equations for a measurement X :

$$X = X_{true} + \beta + \epsilon \quad (D.1)$$

$$\beta = \beta_1 + \beta_2 + \dots + \beta_n \quad \text{and} \quad \epsilon = \epsilon_1 + \epsilon_2 + \dots + \epsilon_n \quad (D.2)$$

To associate an uncertainty with a measured X value, we need to have elemental uncertainty estimates for all of the elemental error sources (systematic and random).

On the one hand, systematic standard uncertainties are designated with the symbol b . These types of uncertainties are due to the uncertainty of the sensor used and must be determined from the information available in the sensor’s datasheet. Furthermore, we must also determine the uncertainty of the data acquisition system when a sensor is connected to it. In this sense, Taylor and Kuyatt (1994) specifies that systematic standard uncertainties must be determined with the “type B¹” evaluation, where its estimation is based on scientific judgment using all the relevant information available. The approach selected in this work in order to obtain the sensor’s uncertainties was to make the following two assumptions:

¹Taylor and Kuyatt (1994) classifies uncertainties depending on the calculation process. Type A (those which are evaluated by statistical methods) and type B (those which are evaluated by other means).

- A normal distribution will be considered when the datasheet specifies a confidence interval for the uncertainty of the sensor. We must convert it to a standard uncertainty by dividing it by the appropriate factor for such distribution. 2 for a confidence interval of 95.45% (2σ) and 3 for 99.73% (3σ).
- A uniform rectangular distribution² will be considered when the datasheet does not specify a confidence interval for the uncertainty of the sensor. We must convert it to a standard uncertainty by dividing it by $\sqrt{3}$.

So, the first step will be to obtain all individual³ standard uncertainties for the sensor and the data acquisition system as:

$$\text{Gaussian distribution } \triangle \Rightarrow b = \frac{u_{95.45\%}}{2} \quad \text{or} \quad b = \frac{u_{99.73\%}}{3} \quad (\text{D.3})$$

$$\text{Rectangular distribution } \square \Rightarrow b = \frac{u}{\sqrt{3}} \quad (\text{D.4})$$

On the other hand, also according to Taylor and Kuyatt (1994), random standard uncertainties must be determined with the “type A” evaluation, i.e., using statistical methods. In this sense, in steady-state experiments, the random uncertainty for a measurement X is estimated as the standard deviation (s_x) for the N measurements⁴ of X (Equation D.5).

$$s_x = \sqrt{\frac{1}{N-1} \sum_{i=1}^N (X_i - \bar{X})^2} \quad (\text{D.5})$$

where N is the total number of readings taken by the datalogger during the test, and the mean value of the measurement X is calculated as:

$$\bar{X} = \frac{1}{N} \sum_{i=1}^N X_i \quad (\text{D.6})$$

Therefore, the abovementioned equations allow us to estimate all the individual standard uncertainties (systematic and random) for a specific X measurement.

²In practical cases, we can assume a uniform distribution for an invariant error source in the absence of other information.

³Commonly, the sensor’s datasheets include different sources of uncertainty (reference, temperature, stability, ...).

⁴The DSHP tests were conducted by recording at steady-state conditions over 45 minutes with an interval of 5 seconds between measurements.

Following the methodology included in Taylor and Kuyatt (1994), the second step implies combining all these individual standard uncertainties in order to obtain the “combined standard uncertainty” (u_c):

$$u_c(X) = \sqrt{\sum_{k=1}^M b_k^2 + s_x^2} \quad (\text{D.7})$$

where M is the number of systematic error sources.

Then, in order to associate a level of confidence with this combined uncertainty, Taylor and Kuyatt (1994) recommends a coverage factor such that:

$$U_{t\%}(X) = t_{t\%} u_c(X) \quad (\text{D.8})$$

where $U_{t\%}$ is the “expanded uncertainty” at a given percent level of confidence and $t_{t\%}$ the coverage factor from the t student⁵ distribution. Moreover, in most real engineering and scientific experiments, the degrees of freedom will be large enough to consider the $t_{t\%}$ value equal to a constant and, according to Taylor and Kuyatt (1994), we can approximate $t_{t\%}$ to the coverage factor of a Gaussian distribution. In this PhD, the coverage factor selected to obtain all expanded uncertainties for each X measurement was 2, considering a confidence interval of 95.45%. Therefore, by combining Equation D.7 and Equation D.8, we obtain a general expression —Equation D.9— in order to estimate the expanded uncertainty for an X measurement and report it in our experimental results.

$$U_{95.45\%}(X) = 2 \cdot \sqrt{s_x^2 + \sum_{k=1}^M b_k^2} \quad (\text{D.9})$$

Once the criteria for determining the uncertainties of the experimental measurements (X) have been established, it is also necessary to establish a criterion for obtaining the uncertainties of the calculated variables (Y). In this sense, this work performed the corresponding error propagation analysis using the classic Taylor Series Method (TSM) with higher-order terms neglected.

⁵The central limit theorem states that if X is not dominated by a single error source but instead is affected by multiple independent error sources, then the resulting distribution for X will be approximately normal.

Therefore, considering a calculated variable Y depending on the measured variables X_1, X_2, \dots, X_N (Equation D.10), the corresponding combined standard uncertainty and the expanded uncertainty will be obtained with Equation D.11 and Equation D.12.

$$Y = f(X_1, X_2, \dots, X_N) \tag{D.10}$$

$$u_c(Y) = \sqrt{\sum_{i=1}^N \left(\frac{\partial f}{\partial X_i}\right)^2 \cdot u_c^2(X_i)} \tag{D.11}$$

$$U_{95.45\%}(Y) = 2 \cdot u_c(Y) \tag{D.12}$$

Finally, to conclude this section, Figure D.1 shows a brief summary of the steps to determine the expanded uncertainties reported in the experimental data (Appendix F).

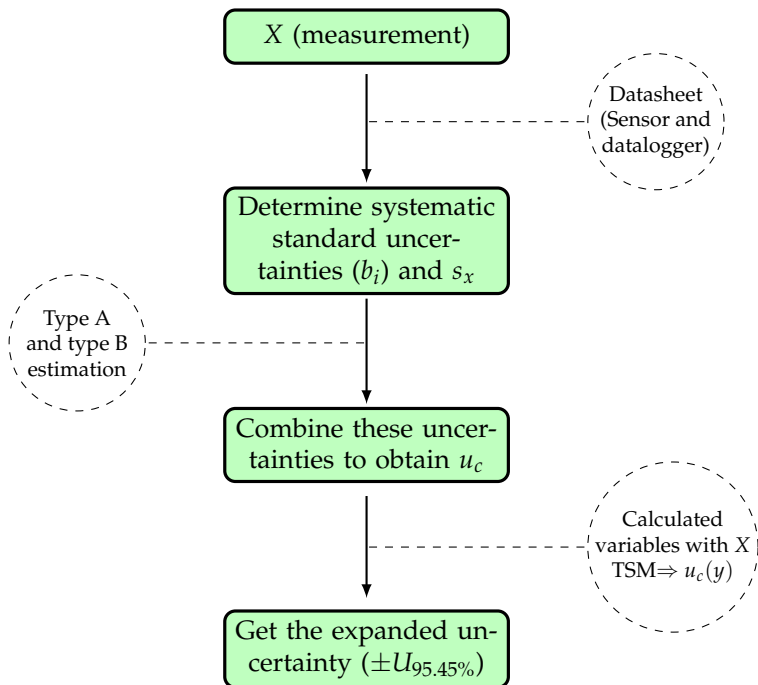


Figure D.1: Steps to obtain the expanded uncertainty to report

D.2 Instrumentation uncertainty specifications

This section includes a summary of the systematic uncertainties for the instrumentation installed in the test rig of the DSHP. They have been obtained by consulting the sensor's datasheets, including the type of distribution considered and the uncertainty added by the data acquisition system⁶ (Agilent 34972A).

D.2.1 Pressure transducer Rosemount 2088A3S22A2B4Q4

▲ Reference uncertainty (Gaussian 3σ): $\pm 0.10\% \cdot \text{calibrated span}$ (bar).

▲ Temperature effect (Gaussian 3σ):
 $\pm (0.15\% \cdot \text{URL} + 0.15\% \cdot \text{calibrated span})$ (bar).

▲ Stability (Gaussian 3σ): $\pm (0.10\% \cdot \text{URL})$ (bar) for 12 months.

Calibrated range: [0, 15] bar.

LRL catalog: 0 bar.

URL catalog: 55.2 bar.

Output signal: [4, 20] mA.

Calibration curve: $y[\text{bar}] = 937.5 \cdot x[\text{A}] - 3.75$.

▲ Datalogger (Gaussian 3σ): $0.05\% \cdot \text{reading}[\text{A}] + 0.005\% \cdot 0.1[\text{A}]$ (A).

Measurement variable: Suction pressure (P_e).

D.2.2 Pressure transducer Rosemount 3051CA3A02A1AH2Q4Q8TR

▲ Reference uncertainty (Gaussian 3σ):
 $\pm [0.0075 \cdot (\text{URL}/\text{calibrated span})] \cdot \% \text{calibrated span}$ (bar).

▲ Temperature effect (Gaussian 3σ):
 $\pm (0.025\% \cdot \text{URL} + 0.125\% \cdot \text{calibrated span})$ (bar).

▲ Stability (Gaussian 3σ): $\pm (0.125\% \cdot \text{URL})$ (bar) for 5 years.

Calibrated range: [10, 45] bar.

⁶This uncertainty is expressed in terms of the sensor output signal and must be converted to the units of measurement using the calibration curve.

LRL catalog: 0 bar.

URL catalog: 55.2 bar.

Output signal: [4, 20] mA.

Calibration curve: $y[\text{bar}] = 2187.5 \cdot x[\text{A}] + 1.25$.

▲ Datalogger (Gaussian 3σ): $0.05\% \cdot \text{reading}[\text{A}] + 0.005\% \cdot 0.1[\text{A}]$ (A).

Measurement variable: Discharge pressure (P_c).

D.2.3 Power meter Gossen-Metrawatt A2000

▲ Reference uncertainty (Gaussian 2σ): $\pm(0.5\% \cdot \text{reading}[\text{kW}] + 0.01)$ (kW).

Range: [0, 10] kW.

Output signal: [2, 10] V.

Calibration curve: $y[\text{bar}] = 1.25 \cdot x[\text{V}] - 2.5$.

▲ Datalogger (Gaussian 3σ): $0.0035\% \cdot \text{reading}[\text{V}] + 0.0005\% \cdot 10[\text{V}]$ (V).

Measurement variable: Unit and compressor energy consumption ($\dot{W}_{D\text{SHP}}$, \dot{W}_c).

D.2.4 Coriolis flowmeter Siemens Mass 2100 DL15

▲ Reference uncertainty (Gaussian 2σ): $\pm 0.15\% \cdot \text{URL}$ (kg/h) when flow rate $\geq 5\%$ URL.

▲ Output signal error (Gaussian 2σ): $\pm 0.1\% \cdot \text{URL} + 0.05\% \cdot \text{calibrated span}$ (kg/h).

Calibrated range: [0, 2000] kg/h.

LRL catalog: 0 kg/h.

URL catalog: 5600 kg/h.

Output signal: [4, 20] mA.

Calibration curve: $y[\text{bar}] = 124868.344 \cdot x[\text{A}] - 499.47$.

▲ Datalogger (Gaussian 3σ): $0.05\% \cdot \text{reading}[\text{A}] + 0.005\% \cdot 0.1[\text{A}]$ (A).

Measurement variable: Water mass flow rate in the User loop (\dot{m}_{user}).

D.2.5 Coriolis flowmeter Siemens Mass 2100 DL15

▲ Reference uncertainty (Gaussian 2σ): $\pm 0.15\% \cdot \text{URL}$ (kg/h) when flow rate $\geq 5\% \text{ URL}$.

▲ Output signal error (Gaussian 2σ): $\pm 0.1\% \cdot \text{URL} + 0.05\% \cdot \text{calibrated span}$ (kg/h).

Calibrated range: [0,5500] kg/h.

LRL catalog: 0 kg/h.

URL catalog: 5600 kg/h.

Output signal: [4, 20] mA.

Calibration curve: $y[\text{bar}] = 343750 \cdot x[\text{A}] - 1375$.

▲ Datalogger (Gaussian 3σ): $0.05\% \cdot \text{reading}[\text{A}] + 0.005\% \cdot 0.1[\text{A}]$ (A).

Measurement variable: Water mass flow rate in the DHW loop (\dot{m}_{dhw}).

D.2.6 Coriolis flowmeter Siemens Mass 2100 DL15

▲ Reference uncertainty (Gaussian 2σ): $\pm 0.15\% \cdot \text{URL}$ (kg/h) when flow rate $\geq 5\% \text{ URL}$.

▲ Output signal error (Gaussian 2σ): $\pm 0.1\% \cdot \text{URL} + 0.05\% \cdot \text{calibrated span}$ (kg/h).

Calibrated range: [0,5000] kg/h.

LRL catalog: 0 kg/h.

URL catalog: 5600 kg/h.

Output signal: [4, 20] mA.

Calibration curve: $y[\text{bar}] = 312324.93 \cdot x[\text{A}] - 1249.299$.

▲ Datalogger (Gaussian 3σ): $0.05\% \cdot \text{reading}[\text{A}] + 0.005\% \cdot 0.1[\text{A}]$ (A).

Measurement variable: Brine mass flow rate in the Ground loop (\dot{m}_{ground}).

D.2.7 Vaisala HUMICAP 180

▣ Reference uncertainty (rectangular distribution): $\pm 2\% \cdot RH$ (from 0 to 90) or $\pm 3\% \cdot RH$ (from 90 to 100).

▣ Temperature effect (rectangular distribution): $\pm 1.32\% \cdot RH$ (Maximum deviation at -10°C considered).

Range: [0, 100] %.

Output signal: [0, 10] V.

Calibration curve: $y[\%] = 10 \cdot x[\text{V}]$.

▲ Datalogger (Gaussian 3σ): $0.0035\% \cdot \text{reading}[\text{V}] + 0.0005\% \cdot 10[\text{V}]$ (V).

Measurement variable: Climatic chamber humidity (RH).

D.2.8 RTD Class 1/10DIN

▣ Reference uncertainty (rectangular distribution): $\pm(1/10 \cdot (0.3 + 0.005 \cdot |t|))$ ($^\circ\text{C}$).

Range: [-200, 850] $^\circ\text{C}$.

RTD: 100 Ω .

▲ Datalogger (Gaussian 3σ): 0.06 $^\circ\text{C}$.

Measurement variable: Air inlet temperature to the RTPFHx and inlet/outlet temperatures in the hydraulic loops ($T_d, T_{co}, T_{ci}, T_{eo}, T_{ei}$).

D.2.9 Thermocouple Type T

▲ Reference uncertainty (Gaussian 2σ): ± 0.3 $^\circ\text{C}$ (calibrated and compensated cold junction) for 6 months

Range: [-20, 150] $^\circ\text{C}$.

Measurement variable: Refrigerant inlet/outlet temperatures to the vapour compression cycle components ($T_s, T_d, T_{HX,in}, T_{HX,out}, T_{EEV,in}, T_{EEV,out}$).

E

Experimental test matrices

CONTENTS

E.1	Winter Ground	e-2
E.2	Summer Ground	e-3
E.3	DHW Ground	e-4
E.4	DHW User	e-5
E.5	Winter Air	e-6
E.6	Summer Air	e-7
E.7	DHW Air	e-8

E.1 Winter Ground

Table E.1: WG mode: CCD (30 test points)

f_c (Hz)	T_{co} (°C)	T_{ei} (°C)	dT_e (K)	dT_c (K)
Block I				
40	40	0	3	7
60	40	0	3	3
40	50	0	3	3
60	50	0	3	7
40	40	10	3	3
60	40	10	3	7
40	50	10	3	7
60	50	10	3	3
40	40	0	7	3
60	40	0	7	7
40	50	0	7	7
60	50	0	7	3
40	40	10	7	7
60	40	10	7	3
40	50	10	7	3
60	50	10	7	7
50	45	5	5	5
50	45	5	5	5
50	45	5	5	5
Block III				
30	45	5	5	5
70	45	5	5	5
50	35	5	5	5
50	55	5	5	5
50	45	-5	5	5
50	45	15	5	5
50	45	5	2	5
50	45	5	9	5
50	45	5	5	2
50	45	5	5	9
50	45	5	5	5

E.2 Summer Ground

Table E.2: SG mode: CCD (30 test points)

f_c (Hz)	T_{eo} (°C)	T_{ci} (°C)	dT_c (K)	dT_e (K)
Block I				
40	9	11	3	7
60	9	11	3	3
40	15	11	3	3
60	15	11	3	7
40	9	21	3	3
60	9	21	3	7
40	15	21	3	7
60	15	21	3	3
40	9	11	7	3
60	9	11	7	7
40	15	11	7	7
60	15	11	7	3
40	9	21	7	7
60	9	21	7	3
40	15	21	7	3
60	15	21	7	7
50	12	16	5	5
50	12	16	5	5
50	12	16	5	5
Block III				
30	12	16	5	5
70	12	16	5	5
50	6	16	5	5
50	18	16	5	5
50	12	6	5	5
50	12	26	5	5
50	12	16	2	5
50	12	16	9	5
50	12	16	5	2
50	12	16	5	9
50	12	16	5	5

E.3 DHW Ground

Table E.3: DHWG mode: CCD (20 test points)

f_c (Hz)	T_{co} (°C)	T_{ei} (°C)	dT_e (K)	dT_c (K)
Block I				
40	50	2.5	3	10
60	50	2.5	3	30
40	50	17.5	3	30
60	50	17.5	3	10
40	50	2.5	7	30
60	50	2.5	7	10
40	50	17.5	7	10
60	50	17.5	7	30
50	50	10.0	5	20
50	50	10.0	5	20
Block III				
30	50	10.0	5	20
70	50	10.0	5	20
50	50	-5.0	5	20
50	50	25.0	5	20
50	50	10.0	2	20
50	50	10.0	9	20
50	50	10.0	5	5
50	50	10.0	5	40
50	50	10.0	5	20
50	50	10.0	5	20

E.4 DHW User

Table E.4: DHWU mode: CCD (20 test points)

f_c (Hz)	T_{co} (°C)	T_{eo} (°C)	dT_e (K)	dT_c (K)
Block I				
40	50	9	3	10
60	50	9	3	30
40	50	15	3	30
60	50	15	3	10
40	50	9	7	30
60	50	9	7	10
40	50	15	7	10
60	50	15	7	30
50	50	12	5	20
50	50	12	5	20
Block III				
30	50	12	5	20
70	50	12	5	20
50	50	6	5	20
50	50	18	5	20
50	50	12	2	20
50	50	12	9	20
50	50	12	5	5
50	50	12	5	40
50	50	12	5	20
50	50	12	5	20

E.5 Winter Air

Table E.5: WA mode: CCD (30 test points)

f_c (Hz)	T_{co} (°C)	T_{ei} (°C)	f_{fan} (%)	dT_c (K)
Block I				
40	40	7	35	7
60	40	7	35	3
40	50	7	35	3
60	50	7	35	7
40	40	15	35	3
60	40	15	35	7
40	50	15	35	7
60	50	15	35	3
40	40	7	65	3
60	40	7	65	7
40	50	7	65	7
60	50	7	65	3
40	40	15	65	7
60	40	15	65	3
40	50	15	65	3
60	50	15	65	7
50	45	11	50	5
50	45	11	50	5
50	45	11	50	5
Block III				
30	45	11	50	5
70	45	11	50	5
50	35	11	50	5
50	55	11	50	5
50	45	4	50	5
50	45	19	50	5
50	45	11	20	5
50	45	11	80	5
50	45	11	50	2
50	45	11	50	9
50	45	11	50	5

E.6 Summer Air

Table E.6: SA mode: CCD (30 test points)

f_c (Hz)	T_{eo} (°C)	T_{ci} (°C)	f_{fan} (%)	dT_e (K)
Block I				
40	9	21	35	7
60	9	21	35	3
40	15	21	35	3
60	15	21	35	7
40	9	33	35	3
60	9	33	35	7
40	15	33	35	7
60	15	33	35	3
40	9	21	65	3
60	9	21	65	7
40	15	21	65	7
60	15	21	65	3
40	9	33	65	7
60	9	33	65	3
40	15	33	65	3
60	15	33	65	7
50	12	27	50	5
50	12	27	50	5
50	12	27	50	5
Block III				
30	12	27	50	5
70	12	27	50	5
50	6	27	50	5
50	18	27	50	5
50	12	15	50	5
50	12	39	50	5
50	12	27	20	5
50	12	27	80	5
50	12	27	50	2
50	12	27	50	9
50	12	27	50	5

E.7 DHW Air

Table E.7: DHWA mode: CCD (20 test points)

f_c (Hz)	T_{co} (°C)	T_{ei} (°C)	f_{fan} (%)	dT_c (K)
Block I				
40	50	11	35	10
60	50	11	35	30
40	50	23	35	30
60	50	23	35	10
40	50	11	65	30
60	50	11	65	10
40	50	23	65	10
60	50	23	65	30
50	50	17	50	20
50	50	17	50	20
Block III				
30	50	17	50	20
70	50	17	50	20
50	50	5	50	20
50	50	29	50	20
50	50	17	20	20
50	50	17	80	20
50	50	17	50	5
50	50	17	50	40
50	50	17	50	20
50	50	17	50	20

F

Experimental results DSHP

CONTENTS

F.1	Winter Ground	f-2
F.2	Summer Ground	f-4
F.3	DHW Ground	f-6
F.4	DHW User	f-8
F.5	Winter Air	f-10
F.6	Summer Air	f-13
F.7	DHW Air	f-16

F.1 Winter Ground

Table F.1: WG: Experimental results

	Test 1	Test 2	Test 3	Test 4	Test 5	Test 6	Test 7	Test 8	Test 9	Test 10
Compressor and fan speed										
f_c (Hz)	35	40	40	40	40	40	40	40	40	50
f_{fan} (%)	-	-	-	-	-	-	-	-	-	-
Secondary side										
T_{ci} (°C)	40.004 (±0.090)	46.995 (±0.093)	42.922 (±0.091)	33.096 (±0.088)	37.039 (±0.089)	33.012 (±0.088)	37.139 (±0.089)	42.961 (±0.091)	46.929 (±0.093)	40.114 (±0.090)
T_{co} (°C)	44.962 (±0.092)	49.930 (±0.094)	49.961 (±0.094)	40.088 (±0.090)	40.115 (±0.090)	39.910 (±0.090)	39.999 (±0.090)	49.385 (±0.094)	50.000 (±0.094)	45.173 (±0.092)
dT_c (K)	4.958 (±0.129)	2.936 (±0.132)	7.039 (±0.131)	6.992 (±0.126)	3.076 (±0.127)	6.898 (±0.126)	2.859 (±0.127)	6.424 (±0.131)	3.071 (±0.132)	5.059 (±0.129)
T_{ci} (°C)	4.950 (±0.079)	0.004 (±0.077)	10.002 (±0.080)	10.060 (±0.080)	10.057 (±0.080)	0.014 (±0.077)	0.011 (±0.077)	-0.007 (±0.077)	10.039 (±0.080)	5.060 (±0.079)
T_{co} (°C)	0.082 (±0.077)	-3.049 (±0.077)	7.066 (±0.079)	2.981 (±0.078)	6.953 (±0.079)	-2.958 (±0.077)	-6.889 (±0.076)	-7.074 (±0.076)	3.084 (±0.078)	0.064 (±0.077)
dT_c (K)	4.869 (±0.110)	3.053 (±0.109)	2.936 (±0.113)	7.079 (±0.112)	3.104 (±0.113)	2.972 (±0.109)	6.900 (±0.108)	7.067 (±0.108)	6.955 (±0.112)	4.996 (±0.111)
\dot{m}_{user} (kg/h)	831.385 (±2.274)	1441.231 (±3.338)	781.567 (±2.189)	752.720 (±2.140)	1915.149 (±4.185)	621.252 (±1.921)	1363.671 (±3.201)	576.762 (±1.848)	1659.926 (±3.727)	1134.966 (±2.798)
\dot{m}_{ground} (kg/h)	746.860 (±3.779)	1099.340 (±4.308)	1667.729 (±5.217)	704.158 (±3.717)	1733.343 (±5.325)	1276.397 (±4.585)	488.268 (±3.417)	431.814 (±3.341)	625.828 (±3.606)	990.963 (±4.142)
\dot{m}_{flow} (kg/h)	-	-	-	-	-	-	-	-	-	-
T_a^* (°C)	-	-	-	-	-	-	-	-	-	-
RH (%)	-	-	-	-	-	-	-	-	-	-
Refrigerant side										
P_c (bar)	7.713 (±0.080)	6.894 (±0.080)	9.246 (±0.080)	8.369 (±0.080)	9.222 (±0.080)	6.762 (±0.080)	6.045 (±0.080)	6.103 (±0.080)	8.390 (±0.080)	7.288 (±0.080)
P_e (bar)	27.478 (±0.060)	31.268 (±0.060)	30.725 (±0.060)	24.423 (±0.060)	25.304 (±0.060)	24.064 (±0.060)	24.699 (±0.060)	29.860 (±0.060)	31.558 (±0.060)	27.926 (±0.060)
P_r (-)	3.563 (±0.038)	4.536 (±0.053)	3.323 (±0.029)	2.918 (±0.029)	2.744 (±0.025)	3.558 (±0.043)	4.086 (±0.055)	4.893 (±0.065)	3.761 (±0.037)	3.832 (±0.043)
T_c (°C)	-1.638 (±0.320)	-5.054 (±0.348)	4.074 (±0.279)	0.904 (±0.301)	3.989 (±0.279)	-5.629 (±0.353)	-8.933 (±0.385)	-8.657 (±0.382)	0.981 (±0.300)	-3.373 (±0.334)
T_e (°C)	44.076 (±0.092)	49.608 (±0.083)	48.732 (±0.085)	39.058 (±0.101)	40.472 (±0.098)	38.527 (±0.102)	39.645 (±0.100)	47.637 (±0.086)	49.950 (±0.083)	44.608 (±0.091)
SC (K)	1.409 (±0.314)	1.542 (±0.311)	1.427 (±0.312)	1.110 (±0.317)	1.166 (±0.316)	1.084 (±0.317)	1.357 (±0.316)	1.556 (±0.312)	1.411 (±0.311)	0.973 (±0.314)
SH (K)	5.645 (±0.438)	3.832 (±0.460)	5.367 (±0.410)	5.445 (±0.425)	5.247 (±0.410)	5.666 (±0.463)	5.830 (±0.488)	3.592 (±0.486)	5.357 (±0.424)	5.377 (±0.449)
T_c (°C)	4.007 (±0.300)	-1.222 (±0.300)	9.441 (±0.300)	6.349 (±0.300)	9.236 (±0.300)	0.037 (±0.300)	-3.103 (±0.300)	-5.065 (±0.300)	6.338 (±0.300)	2.003 (±0.300)
T_d (°C)	95.169 (±0.300)	108.653 (±0.300)	93.580 (±0.300)	78.590 (±0.300)	77.985 (±0.300)	85.772 (±0.300)	93.092 (±0.300)	108.396 (±0.300)	100.808 (±0.300)	90.544 (±0.300)
$T_{w,in}$ (°C)	90.939 (±0.300)	103.767 (±0.300)	91.197 (±0.300)	76.709 (±0.300)	76.401 (±0.300)	82.917 (±0.300)	88.907 (±0.300)	102.845 (±0.300)	97.694 (±0.300)	88.953 (±0.300)
$T_{w,out}$ (°C)	43.049 (±0.300)	48.467 (±0.300)	47.813 (±0.300)	38.333 (±0.300)	39.700 (±0.300)	37.822 (±0.300)	38.734 (±0.300)	46.485 (±0.300)	49.047 (±0.300)	43.982 (±0.300)
$T_{a,in}$ (°C)	2.574 (±0.300)	0.872 (±0.300)	10.002 (±0.300)	6.115 (±0.300)	9.261 (±0.300)	-0.017 (±0.300)	-3.554 (±0.300)	-2.778 (±0.300)	6.741 (±0.300)	6.524 (±0.300)
$T_{a,out}$ (°C)	0.232 (±0.300)	-2.966 (±0.300)	8.852 (±0.300)	4.505 (±0.300)	9.143 (±0.300)	-1.749 (±0.300)	-7.408 (±0.300)	-7.010 (±0.300)	2.734 (±0.300)	0.747 (±0.300)
$T_{d,in}$ (°C)	-	-	-	-	-	-	-	-	-	-
$T_{d,out}$ (°C)	-	-	-	-	-	-	-	-	-	-
$T_{coil,in}$ (°C)	-	-	-	-	-	-	-	-	-	-
$T_{coil,out}$ (°C)	-	-	-	-	-	-	-	-	-	-
Performance variables										
\dot{W}_c (W)	1339.200 (±16.697)	1690.560 (±18.453)	1666.911 (±18.335)	1320.081 (±16.601)	1363.967 (±16.820)	1292.235 (±16.462)	1319.985 (±16.600)	1593.442 (±17.968)	1718.043 (±18.591)	1863.670 (±19.319)
\dot{Q}_c^* (W)	4771.491 (±125.126)	4871.009 (±221.390)	6374.909 (±120.270)	6098.924 (±111.369)	6753.178 (±282.511)	4966.347 (±92.038)	4489.743 (±201.166)	4292.952 (±88.743)	5861.316 (±254.994)	6641.246 (±170.793)
\dot{Q}_e^* (W)	3857.056 (±86.458)	3596.808 (±122.670)	5267.702 (±193.706)	5247.478 (±85.470)	5774.371 (±201.380)	4064.388 (±142.286)	3558.730 (±59.020)	3233.131 (±53.396)	4594.094 (±76.529)	5221.243 (±113.981)

(Continued on Next Page...)

Table F.1: WG: Experimental results (*continued*)

	Test 11	Test 12	Test 13	Test 14	Test 15	Test 16	Test 17	Test 18	Test 19	Test 20
Compressor and fan speed										
f_c (Hz)	50	50	50	50	50	50	50	50	50	50
f_{fan} (%)	-	-	-	-	-	-	-	-	-	-
Secondary side										
T_{ci} (°C)	40.063 (±0.090)	39.979 (±0.090)	40.019 (±0.090)	40.048 (±0.090)	36.024 (±0.089)	39.909 (±0.090)	30.061 (±0.087)	42.988 (±0.091)	50.014 (±0.094)	39.946 (±0.090)
T_{co} (°C)	45.156 (±0.092)	45.062 (±0.092)	45.099 (±0.092)	45.036 (±0.092)	45.104 (±0.092)	44.969 (±0.092)	35.157 (±0.088)	45.635 (±0.092)	55.090 (±0.096)	45.026 (±0.092)
dT_c (K)	5.093 (±0.129)	5.082 (±0.129)	5.080 (±0.129)	4.988 (±0.129)	9.081 (±0.128)	5.060 (±0.129)	5.096 (±0.124)	2.648 (±0.130)	5.076 (±0.134)	5.081 (±0.129)
T_{ci} (°C)	4.988 (±0.079)	4.973 (±0.079)	5.003 (±0.079)	-5.005 (±0.076)	4.986 (±0.079)	5.072 (±0.079)	5.018 (±0.079)	4.969 (±0.079)	5.014 (±0.079)	5.020 (±0.079)
T_{co} (°C)	0.019 (±0.077)	0.019 (±0.077)	0.036 (±0.077)	-9.934 (±0.075)	-0.060 (±0.077)	-3.922 (±0.076)	0.003 (±0.077)	0.086 (±0.077)	0.167 (±0.078)	2.968 (±0.078)
dT_c (K)	4.969 (±0.110)	4.955 (±0.110)	4.967 (±0.110)	4.929 (±0.107)	5.046 (±0.110)	8.994 (±0.110)	5.014 (±0.110)	4.883 (±0.111)	4.848 (±0.111)	2.051 (±0.111)
\dot{m}_{user} (kg/h)	1129.816 (±2.789)	1135.317 (±2.799)	1134.190 (±2.797)	831.472 (±2.274)	626.429 (±1.930)	1014.854 (±2.589)	1173.652 (±2.866)	2199.416 (±4.696)	1079.516 (±2.701)	1208.359 (±2.927)
\dot{m}_{ground} (kg/h)	1010.371 (±4.171)	1012.379 (±4.174)	1011.629 (±4.173)	679.717 (±3.682)	995.039 (±4.148)	490.128 (±3.419)	1096.346 (±4.303)	995.011 (±4.148)	907.168 (±4.015)	2549.224 (±6.703)
\dot{m}_{dhp} (kg/h)	-	-	-	-	-	-	-	-	-	-
T_{dhp} (°C)	-	-	-	-	-	-	-	-	-	-
RH (%)	-	-	-	-	-	-	-	-	-	-
Refrigerant side										
P_c (bar)	7.333 (±0.080)	7.344 (±0.080)	7.345 (±0.080)	5.303 (±0.080)	7.247 (±0.080)	6.456 (±0.080)	7.222 (±0.080)	7.234 (±0.080)	7.309 (±0.080)	7.841 (±0.080)
P_e (bar)	27.890 (±0.060)	27.834 (±0.060)	27.856 (±0.060)	27.331 (±0.060)	27.055 (±0.060)	27.579 (±0.060)	22.022 (±0.060)	28.836 (±0.060)	34.817 (±0.060)	27.989 (±0.060)
P_r (-)	3.804 (±0.042)	3.790 (±0.042)	3.792 (±0.042)	5.154 (±0.079)	3.733 (±0.042)	4.272 (±0.054)	3.049 (±0.035)	3.986 (±0.045)	4.764 (±0.053)	3.570 (±0.037)
T_c (°C)	-3.187 (±0.332)	-3.142 (±0.332)	-3.135 (±0.332)	-12.682 (±0.425)	-3.545 (±0.335)	-7.007 (±0.366)	-3.651 (±0.336)	-3.601 (±0.336)	-3.287 (±0.333)	-1.130 (±0.316)
T_e (°C)	44.554 (±0.091)	44.470 (±0.091)	44.508 (±0.091)	43.806 (±0.093)	43.239 (±0.094)	44.115 (±0.092)	34.763 (±0.110)	45.982 (±0.089)	54.227 (±0.077)	44.657 (±0.091)
SC (K)	1.256 (±0.314)	1.239 (±0.314)	1.296 (±0.314)	1.298 (±0.314)	0.956 (±0.314)	1.194 (±0.314)	0.697 (±0.319)	1.036 (±0.313)	1.386 (±0.310)	1.119 (±0.314)
SH (K)	5.505 (±0.448)	5.361 (±0.447)	5.338 (±0.447)	4.995 (±0.520)	5.448 (±0.450)	5.285 (±0.473)	5.408 (±0.450)	5.513 (±0.450)	5.421 (±0.448)	5.280 (±0.436)
T_s (°C)	2.318 (±0.300)	2.218 (±0.300)	2.203 (±0.300)	-7.687 (±0.300)	1.903 (±0.300)	-1.722 (±0.300)	1.757 (±0.300)	1.912 (±0.300)	2.133 (±0.300)	4.149 (±0.300)
T_d (°C)	96.062 (±0.300)	95.973 (±0.300)	96.843 (±0.300)	104.497 (±0.300)	88.032 (±0.300)	95.110 (±0.300)	73.235 (±0.300)	91.119 (±0.300)	108.320 (±0.300)	87.264 (±0.300)
$T_{d,in}$ (°C)	93.193 (±0.300)	93.235 (±0.300)	93.917 (±0.300)	100.599 (±0.300)	86.459 (±0.300)	92.950 (±0.300)	72.187 (±0.300)	89.534 (±0.300)	105.872 (±0.300)	85.904 (±0.300)
$T_{d,out}$ (°C)	43.669 (±0.300)	43.581 (±0.300)	43.596 (±0.300)	42.970 (±0.300)	42.647 (±0.300)	43.359 (±0.300)	34.201 (±0.300)	45.502 (±0.300)	53.526 (±0.300)	43.971 (±0.300)
$T_{s,in}$ (°C)	5.338 (±0.300)	5.134 (±0.300)	5.278 (±0.300)	-4.155 (±0.300)	6.379 (±0.300)	2.060 (±0.300)	4.322 (±0.300)	6.117 (±0.300)	7.160 (±0.300)	8.304 (±0.300)
$T_{s,out}$ (°C)	-0.999 (±0.300)	-1.186 (±0.300)	-1.406 (±0.300)	-10.740 (±0.300)	0.826 (±0.300)	-4.813 (±0.300)	0.526 (±0.300)	0.670 (±0.300)	0.468 (±0.300)	3.980 (±0.300)
$T_{d,in}^*$ (°C)	-	-	-	-	-	-	-	-	-	-
$T_{d,out}^*$ (°C)	-	-	-	-	-	-	-	-	-	-
$T_{coil,in}$ (°C)	-	-	-	-	-	-	-	-	-	-
$T_{coil,out}$ (°C)	-	-	-	-	-	-	-	-	-	-
Performance variables										
\dot{W}_c (W)	1856.218 (±19.282)	1851.680 (±19.259)	1854.879 (±19.275)	1724.122 (±18.621)	1812.194 (±19.062)	1819.712 (±19.099)	1492.779 (±17.464)	1912.774 (±19.564)	2287.123 (±21.436)	1864.435 (±19.323)
\dot{Q}_c^{\ddagger} (W)	6655.592 (±170.010)	6674.157 (±170.768)	6664.899 (±170.625)	4800.370 (±125.177)	6595.467 (±95.249)	5942.271 (±152.642)	6918.419 (±169.632)	6635.505 (±335.417)	6340.810 (±169.229)	7099.454 (±181.692)
\dot{Q}_e^{\ddagger} (W)	5294.698 (±116.117)	5289.785 (±116.327)	5299.146 (±116.265)	3542.625 (±75.993)	5293.243 (±114.438)	4629.873 (±63.457)	5790.572 (±125.831)	5127.251 (±114.322)	4648.128 (±104.435)	5777.009 (±289.478)

(Continued on Next Page...)

Table F.1: WG: Experimental results (*continued*)

	Test 21	Test 22	Test 23	Test 24	Test 25	Test 26	Test 27	Test 28	Test 29	Test 30
Compressor and fan speed										
f_c (Hz)	50	60	60	60	60	60	60	60	60	70
f_{fan} (%)	-	-	-	-	-	-	-	-	-	-
Secondary side										
T_{ci} (°C)	40.045 (±0.090)	46.968 (±0.093)	36.944 (±0.089)	33.007 (±0.088)	36.994 (±0.089)	42.989 (±0.091)	32.975 (±0.088)	42.961 (±0.091)	46.254 (±0.093)	40.001 (±0.090)
T_{co} (°C)	45.113 (±0.092)	49.760 (±0.094)	40.580 (±0.090)	39.891 (±0.090)	39.997 (±0.090)	50.039 (±0.094)	39.951 (±0.090)	49.937 (±0.094)	50.035 (±0.094)	45.118 (±0.092)
dT_c (K)	5.068 (±0.129)	2.792 (±0.132)	3.636 (±0.127)	6.884 (±0.126)	3.003 (±0.127)	7.050 (±0.131)	6.976 (±0.126)	6.976 (±0.131)	3.781 (±0.132)	5.118 (±0.129)
T_{ci} (°C)	14.963 (±0.082)	0.004 (±0.077)	9.952 (±0.080)	10.092 (±0.080)	-0.025 (±0.077)	10.032 (±0.080)	0.051 (±0.077)	-0.008 (±0.077)	10.008 (±0.080)	4.963 (±0.079)
T_{co} (°C)	9.951 (±0.080)	-6.914 (±0.076)	2.939 (±0.078)	6.967 (±0.079)	-3.009 (±0.077)	3.026 (±0.078)	-7.007 (±0.076)	-2.938 (±0.077)	7.085 (±0.079)	0.076 (±0.077)
dT_e (K)	5.012 (±0.114)	6.917 (±0.108)	7.013 (±0.112)	3.125 (±0.113)	2.983 (±0.109)	7.006 (±0.112)	7.058 (±0.108)	2.930 (±0.109)	2.923 (±0.113)	4.887 (±0.110)
\dot{m}_{inset} (kg/h)	1518.630 (±3.475)	2043.106 (±4.415)	2187.651 (±4.675)	1253.240 (±3.006)	2189.524 (±4.678)	1059.437 (±2.667)	830.821 (±2.273)	880.754 (±2.358)	2207.384 (±4.711)	1565.822 (±3.560)
\dot{m}_{ground} (kg/h)	1419.776 (±4.814)	636.571 (±3.621)	1013.567 (±4.176)	2528.562 (±6.668)	1847.823 (±5.515)	923.694 (±4.040)	718.739 (±3.738)	1692.513 (±5.257)	2400.143 (±6.448)	1387.098 (±4.761)
\dot{m}_{drip} (kg/h)	-	-	-	-	-	-	-	-	-	-
T_a^{\ddagger} (°C)	-	-	-	-	-	-	-	-	-	-
RH (%)	-	-	-	-	-	-	-	-	-	-
Refrigerant side										
P_e (bar)	10.004 (±0.080)	5.892 (±0.080)	8.094 (±0.080)	8.953 (±0.080)	6.547 (±0.080)	8.083 (±0.080)	5.860 (±0.080)	6.552 (±0.080)	8.994 (±0.080)	7.102 (±0.080)
P_c (bar)	28.623 (±0.060)	31.569 (±0.060)	25.877 (±0.060)	24.974 (±0.060)	25.245 (±0.060)	31.125 (±0.060)	24.192 (±0.060)	30.603 (±0.060)	32.365 (±0.060)	28.441 (±0.060)
P_r (-)	2.861 (±0.024)	5.358 (±0.074)	3.197 (±0.032)	2.789 (±0.026)	3.856 (±0.048)	3.851 (±0.039)	4.128 (±0.057)	4.671 (±0.058)	3.599 (±0.033)	4.005 (±0.046)
T_e (°C)	6.633 (±0.263)	-9.675 (±0.392)	-0.145 (±0.308)	3.041 (±0.286)	-6.591 (±0.362)	-0.186 (±0.309)	-9.834 (±0.394)	-6.570 (±0.362)	3.184 (±0.285)	-4.158 (±0.340)
T_c (°C)	45.376 (±0.090)	49.924 (±0.083)	41.165 (±0.097)	39.539 (±0.100)	40.338 (±0.099)	49.104 (±0.084)	38.624 (±0.102)	48.538 (±0.085)	50.717 (±0.082)	45.145 (±0.090)
SC (K)	1.065 (±0.313)	1.421 (±0.311)	1.044 (±0.315)	0.999 (±0.316)	1.120 (±0.316)	1.330 (±0.312)	1.057 (±0.317)	1.363 (±0.312)	1.358 (±0.311)	1.091 (±0.313)
SH (K)	5.129 (±0.399)	1.237 (±0.494)	5.120 (±0.430)	5.081 (±0.414)	5.441 (±0.470)	5.126 (±0.430)	5.459 (±0.495)	3.730 (±0.470)	5.167 (±0.414)	5.003 (±0.454)
T_a (°C)	11.763 (±0.300)	-8.438 (±0.300)	4.975 (±0.300)	8.122 (±0.300)	-1.150 (±0.300)	4.939 (±0.300)	-4.375 (±0.300)	-2.840 (±0.300)	8.351 (±0.300)	0.845 (±0.300)
T_d (°C)	77.972 (±0.300)	108.596 (±0.300)	83.059 (±0.300)	77.160 (±0.300)	92.203 (±0.300)	98.438 (±0.300)	94.408 (±0.300)	108.614 (±0.300)	95.938 (±0.300)	92.976 (±0.300)
$T_{a,in}$ (°C)	77.422 (±0.300)	104.569 (±0.300)	81.690 (±0.300)	76.025 (±0.300)	89.760 (±0.300)	96.531 (±0.300)	91.493 (±0.300)	105.384 (±0.300)	94.240 (±0.300)	91.514 (±0.300)
$T_{a,out}$ (°C)	44.792 (±0.300)	48.586 (±0.300)	40.418 (±0.300)	38.849 (±0.300)	39.541 (±0.300)	48.277 (±0.300)	37.842 (±0.300)	47.357 (±0.300)	49.848 (±0.300)	44.357 (±0.300)
$T_{e,in}$ (°C)	16.211 (±0.300)	2.980 (±0.300)	11.449 (±0.300)	14.081 (±0.300)	5.063 (±0.300)	12.440 (±0.300)	0.725 (±0.300)	5.366 (±0.300)	16.423 (±0.300)	12.206 (±0.300)
$T_{e,out}$ (°C)	12.203 (±0.300)	-9.098 (±0.300)	4.747 (±0.300)	8.656 (±0.300)	-1.968 (±0.300)	3.264 (±0.300)	-7.200 (±0.300)	-4.249 (±0.300)	8.673 (±0.300)	0.918 (±0.300)
$T_{d,in}$ (°C)	-	-	-	-	-	-	-	-	-	-
$T_{d,out}$ (°C)	-	-	-	-	-	-	-	-	-	-
$T_{coil,in}$ (°C)	-	-	-	-	-	-	-	-	-	-
$T_{coil,out}$ (°C)	-	-	-	-	-	-	-	-	-	-
Performance variables										
\dot{W}_c (W)	1910.473 (±19.553)	2442.529 (±22.213)	2099.276 (±20.497)	2029.381 (±20.147)	2026.783 (±20.134)	2481.863 (±22.410)	1935.385 (±19.677)	2401.594 (±22.009)	2588.417 (±22.943)	2662.644 (±23.314)
\dot{Q}_c^{\ddagger} (W)	8889.513 (±28.314)	6522.361 (±313.633)	9111.149 (±323.127)	9987.900 (±184.624)	7508.501 (±322.862)	8651.035 (±162.723)	6715.200 (±122.742)	7118.028 (±135.378)	9564.980 (±342.309)	9254.251 (±235.403)
\dot{Q}_e^{\ddagger} (W)	7528.125 (±69.379)	4619.246 (±74.767)	7449.625 (±120.500)	8517.341 (±293.540)	5904.377 (±205.656)	6789.170 (±110.266)	5305.828 (±83.788)	5313.441 (±188.399)	7578.290 (±278.565)	7134.430 (±158.518)

* The reported uncertainties are considered as the expanded uncertainties considering a confidence interval of 95.45%;

[†] $T_{a,i}$ is denoted as T_e or T_c in the DSHP models depending on the operating mode of the RTPFHx (evaporator or condenser);

[‡] Value corrected with the heat injected by the circulation pump;

F.2 Summer Ground

Table F.2: SG: Experimental results

	Test 1	Test 2	Test 3	Test 4	Test 5	Test 6	Test 7	Test 8	Test 9	Test 10	Test 11
Compressor and fan speed											
f_c (Hz)	30	40	40	40	40	50	50	50	50	50	50
f_{fan} (%)	-	-	-	-	-	-	-	-	-	-	-
Secondary side											
T_{ci} (°C)	15.949 (±0.082)	21.135 (±0.084)	20.940 (±0.084)	20.942 (±0.084)	20.998 (±0.084)	16.020 (±0.082)	16.028 (±0.082)	15.970 (±0.082)	15.933 (±0.082)	16.013 (±0.082)	16.013 (±0.082)
T_{co} (°C)	20.814 (±0.084)	24.089 (±0.085)	24.294 (±0.085)	27.974 (±0.086)	27.979 (±0.086)	19.566 (±0.083)	21.044 (±0.084)	20.905 (±0.084)	20.898 (±0.084)	20.985 (±0.084)	20.985 (±0.084)
ΔT_c (K)	4.865 (±0.117)	2.954 (±0.119)	3.354 (±0.119)	7.032 (±0.120)	6.981 (±0.120)	3.546 (±0.117)	5.016 (±0.117)	4.934 (±0.117)	4.965 (±0.117)	4.972 (±0.117)	4.972 (±0.117)
T_{ri} (°C)	16.975 (±0.082)	12.021 (±0.081)	22.073 (±0.084)	15.941 (±0.082)	18.048 (±0.083)	16.942 (±0.082)	11.021 (±0.081)	13.999 (±0.081)	16.760 (±0.082)	17.008 (±0.082)	17.008 (±0.082)
T_{ro} (°C)	12.035 (±0.081)	9.000 (±0.080)	15.027 (±0.082)	8.865 (±0.080)	14.928 (±0.082)	12.038 (±0.081)	6.120 (±0.079)	10.440 (±0.080)	11.791 (±0.081)	12.036 (±0.081)	12.036 (±0.081)
ΔT_r (K)	4.940 (±0.115)	3.021 (±0.114)	7.046 (±0.117)	7.076 (±0.114)	3.120 (±0.116)	4.904 (±0.115)	4.901 (±0.113)	3.559 (±0.114)	4.968 (±0.115)	4.972 (±0.115)	4.972 (±0.115)
\dot{m}_{user} (kg/h)	1044.464 (±2.640)	1874.149 (±4.111)	1048.602 (±2.648)	826.576 (±2.265)	2132.935 (±4.576)	1544.567 (±3.522)	1393.848 (±3.254)	2115.069 (±4.544)	1545.588 (±3.523)	1544.859 (±3.522)	1544.859 (±3.522)
\dot{m}_{ground} (kg/h)	1355.284 (±4.710)	2581.552 (±6.759)	2837.121 (±7.201)	1088.049 (±4.290)	1249.012 (±4.542)	2827.124 (±7.184)	1798.154 (±5.432)	2017.831 (±5.799)	2017.785 (±5.799)	2018.633 (±5.800)	2018.633 (±5.800)
\dot{m}_{flow} (kg/h)	-	-	-	-	-	-	-	-	-	-	-
$T_{s,i}$ (°C)	-	-	-	-	-	-	-	-	-	-	-
RH (%)	-	-	-	-	-	-	-	-	-	-	-
Refrigerant side											
P_c (bar)	11.306 (±0.080)	9.800 (±0.080)	12.336 (±0.080)	10.169 (±0.080)	11.657 (±0.080)	10.018 (±0.080)	9.098 (±0.080)	10.074 (±0.080)	10.186 (±0.080)	10.210 (±0.080)	10.210 (±0.080)
P_e (bar)	15.563 (±0.060)	17.300 (±0.060)	17.712 (±0.060)	18.745 (±0.060)	18.976 (±0.060)	15.646 (±0.060)	16.024 (±0.060)	16.155 (±0.060)	16.129 (±0.060)	16.162 (±0.060)	16.162 (±0.060)
P_r (-)	1.376 (±0.011)	1.765 (±0.016)	1.436 (±0.010)	1.843 (±0.016)	1.628 (±0.012)	1.562 (±0.014)	1.761 (±0.017)	1.604 (±0.014)	1.583 (±0.014)	1.583 (±0.014)	1.583 (±0.014)
T_c (°C)	10.712 (±0.240)	5.959 (±0.267)	13.692 (±0.224)	7.171 (±0.259)	11.751 (±0.234)	6.680 (±0.262)	3.555 (±0.282)	6.864 (±0.261)	7.228 (±0.259)	7.306 (±0.259)	7.306 (±0.259)
T_r (°C)	21.408 (±0.143)	25.060 (±0.132)	25.767 (±0.131)	28.109 (±0.125)	28.392 (±0.124)	21.013 (±0.144)	22.047 (±0.141)	22.143 (±0.141)	22.102 (±0.141)	22.181 (±0.140)	22.181 (±0.140)
SC (K)	0.606 (±0.332)	0.546 (±0.328)	0.726 (±0.327)	0.653 (±0.325)	0.704 (±0.325)	0.648 (±0.333)	0.658 (±0.331)	0.666 (±0.331)	0.662 (±0.331)	0.666 (±0.331)	0.666 (±0.331)
SH (K)	5.215 (±0.384)	5.207 (±0.401)	6.553 (±0.375)	5.408 (±0.397)	5.152 (±0.381)	9.127 (±0.399)	5.327 (±0.412)	5.866 (±0.398)	8.296 (±0.396)	8.462 (±0.396)	8.462 (±0.396)
T_s (°C)	15.927 (±0.300)	11.166 (±0.300)	20.245 (±0.300)	12.579 (±0.300)	16.903 (±0.300)	15.807 (±0.300)	8.883 (±0.300)	12.730 (±0.300)	15.523 (±0.300)	15.768 (±0.300)	15.768 (±0.300)
T_d (°C)	42.422 (±0.300)	50.635 (±0.300)	49.369 (±0.300)	55.012 (±0.300)	52.676 (±0.300)	51.062 (±0.300)	48.816 (±0.300)	47.888 (±0.300)	50.777 (±0.300)	51.219 (±0.300)	51.219 (±0.300)
$T_{u,in}$ (°C)	16.351 (±0.300)	11.645 (±0.300)	20.987 (±0.300)	11.908 (±0.300)	17.584 (±0.300)	16.494 (±0.300)	9.266 (±0.300)	13.497 (±0.300)	16.261 (±0.300)	16.512 (±0.300)	16.512 (±0.300)
$T_{u,out}$ (°C)	11.560 (±0.300)	8.419 (±0.300)	15.403 (±0.300)	9.727 (±0.300)	13.833 (±0.300)	9.811 (±0.300)	7.135 (±0.300)	10.187 (±0.300)	10.379 (±0.300)	10.527 (±0.300)	10.527 (±0.300)
$T_{g,in}$ (°C)	42.063 (±0.300)	50.216 (±0.300)	48.837 (±0.300)	54.460 (±0.300)	52.141 (±0.300)	50.373 (±0.300)	48.343 (±0.300)	47.314 (±0.300)	50.105 (±0.300)	50.575 (±0.300)	50.575 (±0.300)
$T_{g,out}$ (°C)	20.552 (±0.300)	24.452 (±0.300)	25.017 (±0.300)	27.508 (±0.300)	27.740 (±0.300)	20.244 (±0.300)	21.300 (±0.300)	21.382 (±0.300)	21.321 (±0.300)	21.398 (±0.300)	21.398 (±0.300)
$T_{d,in}$ (°C)	-	-	-	-	-	-	-	-	-	-	-
$T_{d,out}$ (°C)	-	-	-	-	-	-	-	-	-	-	-
$T_{coil,in}$ (°C)	-	-	-	-	-	-	-	-	-	-	-
$T_{coil,out}$ (°C)	-	-	-	-	-	-	-	-	-	-	-
Performance variables											
\dot{W}_c (W)	576.693 (±14.884)	910.365 (±14.552)	899.198 (±14.496)	987.866 (±14.940)	973.696 (±14.869)	1056.133 (±15.281)	1083.748 (±15.419)	1082.285 (±15.412)	1078.609 (±15.394)	1078.966 (±15.395)	1078.966 (±15.395)
\dot{Q}_c^+ (W)	6622.211 (±116.000)	7505.598 (±319.320)	9408.343 (±351.253)	7794.540 (±1139.498)	8887.640 (±159.498)	9885.953 (±342.479)	9067.813 (±219.993)	9998.515 (±246.483)	10063.360 (±246.482)	10081.264 (±246.684)	10081.264 (±246.684)
\dot{Q}_c^- (W)	6020.837 (±140.791)	6677.661 (±247.967)	8610.453 (±144.359)	6814.380 (±111.489)	7864.170 (±288.436)	8858.829 (±207.950)	7990.319 (±183.756)	8880.096 (±281.693)	8980.421 (±208.948)	8983.147 (±208.041)	8983.147 (±208.041)

(Continued on Next Page...)

Table F.2: SG: Experimental results (*continued*)

	Test 12	Test 13	Test 14	Test 15	Test 16	Test 17	Test 18	Test 19	Test 20	Test 21
Compressor and fan speed										
f_c (Hz)	50	50	50	50	50	60	60	60	60	70
f_{fan} (%)	-	-	-	-	-	-	-	-	-	-
Secondary side										
T_{ci} (°C)	15.947 (+0.082)	16.011 (+0.082)	16.019 (+0.082)	15.942 (+0.082)	26.115 (+0.085)	20.970 (+0.084)	21.079 (+0.084)	20.908 (+0.084)	21.016 (+0.084)	16.149 (+0.082)
T_{co} (°C)	20.923 (+0.084)	21.012 (+0.084)	21.045 (+0.084)	24.967 (+0.085)	31.060 (+0.087)	27.941 (+0.086)	28.092 (+0.086)	24.920 (+0.085)	25.098 (+0.085)	21.183 (+0.084)
dT_c (K)	4.976 (+0.117)	5.001 (+0.117)	5.026 (+0.117)	9.025 (+0.118)	4.945 (+0.122)	6.971 (+0.120)	7.013 (+0.120)	4.012 (+0.119)	4.082 (+0.119)	5.035 (+0.117)
T_{pi} (°C)	17.012 (+0.082)	21.089 (+0.084)	23.008 (+0.084)	17.065 (+0.082)	17.225 (+0.082)	12.028 (+0.081)	22.012 (+0.084)	15.811 (+0.082)	18.042 (+0.083)	16.997 (+0.082)
T_{po} (°C)	12.034 (+0.081)	12.087 (+0.081)	18.021 (+0.083)	12.009 (+0.081)	12.275 (+0.081)	8.226 (+0.080)	14.950 (+0.082)	8.837 (+0.080)	14.006 (+0.081)	11.946 (+0.081)
dT_c (°C)	4.978 (+0.115)	9.002 (+0.116)	4.987 (+0.118)	5.056 (+0.115)	4.950 (+0.115)	3.802 (+0.113)	7.062 (+0.117)	6.974 (+0.114)	4.036 (+0.116)	5.051 (+0.115)
\dot{m}_{user} (kg/h)	1544.819 (+3.522)	866.048 (+2.333)	1570.404 (+3.568)	1571.212 (+3.569)	1559.882 (+3.549)	2104.824 (+4.526)	1275.881 (+3.046)	1227.259 (+2.960)	2131.451 (+4.574)	1726.950 (+3.847)
\dot{m}_{ground} (kg/h)	2017.090 (+5.798)	2018.125 (+5.799)	2018.971 (+5.801)	1148.051 (+4.383)	2053.628 (+5.859)	1549.259 (+5.023)	1681.169 (+5.239)	2843.214 (+7.212)	2838.769 (+7.204)	2337.142 (+6.340)
\dot{m}_{dhw} (kg/h)	-	-	-	-	-	-	-	-	-	-
T_{pi}^\dagger (°C)	-	-	-	-	-	-	-	-	-	-
RH (%)	-	-	-	-	-	-	-	-	-	-
Refrigerant side										
P_c (bar)	10.210 (+0.080)	10.340 (+0.080)	10.433 (+0.080)	10.748 (+0.080)	11.014 (+0.080)	9.437 (+0.080)	10.464 (+0.080)	9.759 (+0.080)	9.972 (+0.080)	8.491 (+0.080)
P_e (bar)	16.136 (+0.060)	16.143 (+0.060)	16.139 (+0.060)	17.688 (+0.060)	21.046 (+0.060)	19.327 (+0.060)	19.464 (+0.060)	18.276 (+0.060)	18.332 (+0.060)	16.420 (+0.060)
P_r (-)	1.580 (+0.014)	1.561 (+0.013)	1.547 (+0.013)	1.646 (+0.013)	1.911 (+0.015)	2.048 (+0.018)	1.860 (+0.015)	1.873 (+0.017)	1.838 (+0.016)	1.934 (+0.020)
T_c (°C)	7.307 (+0.259)	7.723 (+0.256)	8.020 (+0.255)	9.010 (+0.249)	9.831 (+0.244)	4.732 (+0.275)	8.117 (+0.254)	5.822 (+0.268)	6.528 (+0.263)	1.356 (+0.297)
T_e (°C)	22.124 (+0.141)	22.158 (+0.141)	22.167 (+0.141)	25.452 (+0.131)	32.264 (+0.115)	28.694 (+0.123)	28.842 (+0.123)	26.409 (+0.129)	26.561 (+0.129)	22.529 (+0.139)
SC (K)	0.692 (+0.331)	0.647 (+0.331)	0.697 (+0.331)	0.685 (+0.328)	0.823 (+0.321)	0.674 (+0.324)	0.633 (+0.324)	0.562 (+0.327)	0.564 (+0.326)	0.676 (+0.331)
SH (K)	8.432 (+0.396)	12.035 (+0.395)	13.677 (+0.393)	6.577 (+0.390)	5.140 (+0.387)	5.173 (+0.407)	12.435 (+0.393)	7.507 (+0.402)	10.141 (+0.399)	14.331 (+0.422)
T_{si} (°C)	15.739 (+0.300)	19.759 (+0.300)	21.697 (+0.300)	15.587 (+0.300)	14.971 (+0.300)	9.906 (+0.300)	20.552 (+0.300)	13.329 (+0.300)	16.669 (+0.300)	15.686 (+0.300)
T_{so} (°C)	51.140 (+0.300)	54.963 (+0.300)	57.020 (+0.300)	52.076 (+0.300)	58.391 (+0.300)	58.319 (+0.300)	65.708 (+0.300)	57.163 (+0.300)	61.011 (+0.300)	65.012 (+0.300)
$T_{m,in}$ (°C)	16.513 (+0.300)	20.521 (+0.300)	22.485 (+0.300)	16.413 (+0.300)	15.689 (+0.300)	10.750 (+0.300)	21.444 (+0.300)	13.932 (+0.300)	17.545 (+0.300)	16.490 (+0.300)
$T_{m,out}$ (°C)	10.450 (+0.300)	10.772 (+0.300)	10.955 (+0.300)	12.609 (+0.300)	14.296 (+0.300)	10.757 (+0.300)	13.581 (+0.300)	11.439 (+0.300)	11.935 (+0.300)	7.820 (+0.300)
$T_{s,in}$ (°C)	50.491 (+0.300)	54.170 (+0.300)	56.138 (+0.300)	51.499 (+0.300)	57.821 (+0.300)	57.722 (+0.300)	64.793 (+0.300)	56.405 (+0.300)	60.210 (+0.300)	63.930 (+0.300)
$T_{s,out}$ (°C)	21.333 (+0.300)	21.381 (+0.300)	21.376 (+0.300)	24.750 (+0.300)	31.562 (+0.300)	28.086 (+0.300)	28.283 (+0.300)	25.895 (+0.300)	26.004 (+0.300)	21.786 (+0.300)
$T_{d,in}$ (°C)	-	-	-	-	-	-	-	-	-	-
$T_{d,out}$ (°C)	-	-	-	-	-	-	-	-	-	-
$T_{coil,in}$ (°C)	-	-	-	-	-	-	-	-	-	-
$T_{coil,out}$ (°C)	-	-	-	-	-	-	-	-	-	-
Performance variables										
\dot{W}_c (W)	1077.642 (+15.389)	1076.752 (+15.384)	1075.972 (+15.380)	1177.627 (+15.889)	1390.219 (+16.952)	1587.630 (+17.939)	1591.541 (+17.958)	1516.683 (+17.584)	1514.552 (+17.573)	1640.408 (+18.203)
\dot{Q}_c^\ddagger (W)	10081.269 (+246.429)	10140.243 (+246.664)	10197.240 (+246.813)	10575.853 (+146.872)	10296.554 (+262.877)	11013.074 (+196.941)	12024.671 (+213.588)	11373.827 (+353.076)	11563.102 (+352.821)	11812.044 (+285.675)
\dot{Q}_e^\ddagger (W)	8992.934 (+208.039)	9076.657 (+119.539)	9157.339 (+216.325)	9290.500 (+211.638)	9031.315 (+210.233)	9433.802 (+278.336)	10506.631 (+175.401)	9981.247 (+164.921)	10127.276 (+288.062)	10210.923 (+232.516)

* The reported uncertainties are considered as the expanded uncertainties considering a confidence interval of 95.45%;

† T_m is denoted as T_{si} or T_{so} in the DSHF models depending on the operating mode of the RTPPFs (evaporator or condenser);

‡ Value corrected with the heat injected by the circulation pump;

F.3 DHW Ground

Table F.3: DHWG: Experimental results

	Test 1	Test 2	Test 3	Test 4	Test 5	Test 6	Test 7	Test 8	Test 9	Test 10
Compressor and fan speed										
f_c (Hz)	35	40	40	40	40	50	50	50	50	50
f_{fan} (%)	-	-	-	-	-	-	-	-	-	-
Secondary side										
T_{ei} (°C)	30.097 (±0.087)	20.270 (±0.083)	19.985 (±0.083)	39.869 (±0.090)	39.907 (±0.090)	9.923 (±0.080)	29.860 (±0.087)	29.942 (±0.087)	30.030 (±0.087)	30.061 (±0.087)
T_{co} (°C)	49.975 (±0.094)	50.157 (±0.094)	49.969 (±0.094)	49.898 (±0.094)	49.959 (±0.094)	49.856 (±0.094)	49.891 (±0.094)	50.024 (±0.094)	50.135 (±0.094)	49.995 (±0.094)
dT_c (K)	19.879 (±0.128)	29.887 (±0.126)	29.985 (±0.126)	10.030 (±0.130)	10.052 (±0.130)	39.933 (±0.124)	20.031 (±0.128)	20.082 (±0.128)	20.105 (±0.128)	19.934 (±0.128)
T_{ei} (°C)	10.081 (±0.080)	2.417 (±0.078)	17.490 (±0.082)	2.505 (±0.078)	17.514 (±0.082)	10.073 (±0.080)	-4.924 (±0.076)	9.981 (±0.080)	9.990 (±0.080)	9.961 (±0.080)
T_{eo} (°C)	5.054 (±0.079)	-4.548 (±0.076)	14.388 (±0.082)	-0.555 (±0.077)	10.607 (±0.080)	5.046 (±0.079)	-10.076 (±0.075)	1.098 (±0.078)	5.052 (±0.079)	4.939 (±0.079)
dT_e (K)	5.028 (±0.112)	6.965 (±0.109)	3.102 (±0.116)	3.060 (±0.110)	6.907 (±0.115)	5.027 (±0.112)	5.152 (±0.107)	8.883 (±0.112)	4.938 (±0.112)	5.022 (±0.112)
\dot{m}_{user} (kg/h)	-	-	-	-	-	-	-	-	-	-
\dot{m}_{ground} (kg/h)	830.599 (±3.901)	503.624 (±3.437)	2035.853 (±5.829)	1205.932 (±4.474)	812.094 (±3.874)	1186.592 (±4.444)	630.620 (±3.613)	574.429 (±3.534)	1152.092 (±4.390)	1124.503 (±4.347)
\dot{m}_{dhw} (kg/h)	225.017 (±3.075)	127.961 (±2.968)	216.342 (±3.065)	435.168 (±3.345)	601.091 (±3.571)	156.402 (±2.999)	195.562 (±3.042)	282.350 (±3.149)	314.863 (±3.190)	313.364 (±3.188)
T_d^\dagger (°C)	-	-	-	-	-	-	-	-	-	-
RH (%)	-	-	-	-	-	-	-	-	-	-
Refrigerant side										
P_e (bar)	8.924 (±0.080)	6.521 (±0.080)	11.412 (±0.080)	7.371 (±0.080)	10.430 (±0.080)	8.492 (±0.080)	5.267 (±0.080)	7.595 (±0.080)	8.525 (±0.080)	8.442 (±0.080)
P_i (bar)	29.552 (±0.060)	27.359 (±0.060)	29.596 (±0.060)	30.815 (±0.060)	31.732 (±0.060)	27.877 (±0.060)	28.462 (±0.060)	29.898 (±0.060)	30.504 (±0.060)	30.397 (±0.060)
P_i (-)	3.312 (±0.030)	4.196 (±0.052)	2.593 (±0.019)	4.181 (±0.046)	3.042 (±0.024)	3.283 (±0.032)	5.404 (±0.083)	3.937 (±0.042)	3.578 (±0.042)	3.601 (±0.035)
T_e (°C)	2.935 (±0.286)	-6.710 (±0.363)	11.027 (±0.238)	-3.030 (±0.331)	8.010 (±0.255)	1.363 (±0.297)	-12.873 (±0.427)	-2.113 (±0.323)	1.484 (±0.296)	1.175 (±0.299)
T_c (°C)	47.098 (±0.087)	43.798 (±0.093)	46.842 (±0.088)	48.926 (±0.084)	50.004 (±0.083)	44.243 (±0.092)	45.535 (±0.090)	47.435 (±0.087)	48.183 (±0.086)	48.025 (±0.086)
SC (K)	1.370 (±0.312)	1.334 (±0.314)	1.323 (±0.313)	1.490 (±0.312)	1.437 (±0.311)	1.262 (±0.314)	1.388 (±0.313)	1.118 (±0.312)	1.015 (±0.312)	1.210 (±0.312)
SH (K)	5.439 (±0.415)	5.738 (±0.471)	5.122 (±0.383)	5.592 (±0.447)	5.186 (±0.393)	5.183 (±0.422)	5.360 (±0.522)	5.393 (±0.441)	5.189 (±0.422)	5.101 (±0.423)
T_s (°C)	8.373 (±0.300)	-0.972 (±0.300)	16.149 (±0.300)	2.562 (±0.300)	13.196 (±0.300)	6.546 (±0.300)	-7.513 (±0.300)	3.280 (±0.300)	6.672 (±0.300)	6.276 (±0.300)
T_d (°C)	94.577 (±0.300)	96.444 (±0.300)	82.655 (±0.300)	104.111 (±0.300)	90.720 (±0.300)	82.441 (±0.300)	107.559 (±0.300)	94.596 (±0.300)	89.042 (±0.300)	86.763 (±0.300)
$T_{i,in}$ (°C)	-	-	-	-	-	-	-	-	-	-
$T_{i,out}$ (°C)	-	-	-	-	-	-	-	-	-	-
$T_{g,in}$ (°C)	7.138 (±0.300)	-0.760 (±0.300)	16.482 (±0.300)	3.044 (±0.300)	13.992 (±0.300)	10.685 (±0.300)	-4.165 (±0.300)	7.586 (±0.300)	11.474 (±0.300)	11.314 (±0.300)
$T_{g,out}$ (°C)	6.570 (±0.300)	-4.584 (±0.300)	16.497 (±0.300)	0.252 (±0.300)	11.511 (±0.300)	6.099 (±0.300)	-10.628 (±0.300)	0.645 (±0.300)	6.233 (±0.300)	6.008 (±0.300)
$T_{d,in}$ (°C)	91.333 (±0.300)	92.775 (±0.300)	81.084 (±0.300)	100.118 (±0.300)	88.846 (±0.300)	81.373 (±0.300)	103.516 (±0.300)	92.658 (±0.300)	87.813 (±0.300)	85.730 (±0.300)
$T_{d,out}$ (°C)	45.893 (±0.300)	42.710 (±0.300)	45.867 (±0.300)	47.991 (±0.300)	49.187 (±0.300)	43.218 (±0.300)	44.557 (±0.300)	46.686 (±0.300)	47.522 (±0.300)	47.268 (±0.300)
$T_{coil,in}$ (°C)	-	-	-	-	-	-	-	-	-	-
$T_{coil,out}$ (°C)	-	-	-	-	-	-	-	-	-	-
Performance variables										
\dot{W}_c (W)	1451.279 (±17.257)	1466.395 (±17.332)	1594.442 (±17.973)	1677.604 (±18.389)	1731.844 (±18.660)	1867.943 (±19.340)	1790.562 (±18.953)	1995.180 (±19.976)	2045.743 (±20.229)	2028.482 (±20.143)
\dot{Q}_c^\dagger (W)	5188.684 (±78.534)	4435.797 (±104.717)	7527.529 (±111.358)	5060.851 (±76.539)	7006.078 (±100.020)	7247.443 (±140.903)	4543.535 (±76.557)	6578.582 (±84.642)	7344.934 (±88.017)	7247.908 (±87.321)
\dot{Q}_c^\ddagger (W)	4427.696 (±98.010)	3705.201 (±61.239)	6810.250 (±244.388)	3953.784 (±135.875)	5923.084 (±100.554)	6296.945 (±138.930)	3436.725 (±70.965)	5360.054 (±73.418)	6010.398 (±134.856)	5963.824 (±131.712)

(Continued on Next Page...)

Table E.3: DHWG: Experimental results (*continued*)

	Test 11	Test 12	Test 13	Test 14	Test 15	Test 16	Test 17	Test 18	Test 19	Test 20
Compressor and fan speed										
f_c (Hz)	50	50	50	50	50	60	60	60	60	70
f_{fan} (%)	-	-	-	-	-	-	-	-	-	-
Secondary side										
T_{ci} (°C)	30.031 (±0.087)	30.119 (±0.087)	30.110 (±0.087)	30.042 (±0.087)	44.942 (±0.092)	19.850 (±0.083)	19.963 (±0.083)	40.118 (±0.090)	40.090 (±0.090)	30.085 (±0.087)
T_{co} (°C)	50.171 (±0.094)	50.136 (±0.094)	50.099 (±0.094)	50.125 (±0.094)	49.985 (±0.094)	49.902 (±0.094)	49.918 (±0.094)	50.081 (±0.094)	49.882 (±0.094)	50.919 (±0.094)
dT_c (K)	20.140 (±0.128)	20.017 (±0.128)	19.988 (±0.128)	20.083 (±0.128)	5.043 (±0.132)	30.051 (±0.126)	29.955 (±0.126)	9.963 (±0.130)	9.791 (±0.130)	19.934 (±0.128)
T_{ci} (°C)	9.997 (±0.080)	9.997 (±0.080)	10.000 (±0.080)	25.165 (±0.085)	10.028 (±0.080)	2.595 (±0.078)	17.536 (±0.082)	2.554 (±0.078)	17.478 (±0.082)	9.892 (±0.080)
T_{co} (°C)	5.072 (±0.079)	4.989 (±0.079)	7.966 (±0.080)	20.066 (±0.083)	5.118 (±0.079)	-0.466 (±0.077)	10.572 (±0.080)	-4.411 (±0.076)	14.536 (±0.082)	5.016 (±0.079)
dT_c (K)	4.925 (±0.112)	5.009 (±0.112)	2.034 (±0.113)	5.099 (±0.119)	4.910 (±0.112)	3.060 (±0.110)	6.964 (±0.115)	6.966 (±0.109)	2.941 (±0.116)	4.877 (±0.112)
\dot{m}_{user} (kg/h)	-	-	-	-	-	-	-	-	-	-
\dot{m}_{ground} (kg/h)	1161.955 (±4.405)	1140.261 (±4.371)	2885.621 (±7.285)	1843.522 (±5.507)	1125.963 (±4.349)	1793.016 (±5.424)	1231.755 (±4.514)	679.343 (±3.682)	2987.607 (±7.463)	1576.074 (±5.067)
\dot{m}_{dhw} (kg/h)	314.258 (±3.189)	315.460 (±3.190)	336.610 (±3.217)	482.940 (±3.409)	1275.868 (±4.584)	208.892 (±3.057)	303.004 (±3.175)	579.401 (±3.541)	1006.637 (±4.165)	437.550 (±3.348)
T_{RH} (°C)	-	-	-	-	-	-	-	-	-	-
RH (%)	-	-	-	-	-	-	-	-	-	-
Refrigerant side										
P_c (bar)	8.534 (±0.080)	8.496 (±0.080)	9.118 (±0.080)	13.538 (±0.080)	8.568 (±0.080)	6.898 (±0.080)	10.237 (±0.080)	6.226 (±0.080)	11.148 (±0.080)	8.400 (±0.080)
P_e (bar)	30.519 (±0.060)	30.477 (±0.060)	30.776 (±0.060)	31.923 (±0.060)	32.662 (±0.060)	28.609 (±0.060)	30.298 (±0.060)	31.166 (±0.060)	32.910 (±0.060)	30.826 (±0.060)
P_s (°C)	3.576 (±0.034)	3.587 (±0.034)	3.375 (±0.030)	2.358 (±0.015)	3.812 (±0.036)	4.147 (±0.049)	2.960 (±0.024)	5.006 (±0.065)	2.952 (±0.022)	3.670 (±0.036)
T_c (°C)	1.516 (±0.296)	1.376 (±0.297)	3.624 (±0.282)	16.944 (±0.209)	1.642 (±0.295)	-5.033 (±0.348)	7.393 (±0.258)	-8.074 (±0.376)	10.237 (±0.242)	1.017 (±0.300)
T_e (°C)	48.192 (±0.086)	48.144 (±0.086)	48.494 (±0.085)	49.570 (±0.083)	51.243 (±0.081)	45.400 (±0.090)	47.364 (±0.087)	49.310 (±0.084)	50.975 (±0.081)	48.169 (±0.086)
SC (K)	1.201 (±0.312)	1.241 (±0.312)	1.123 (±0.312)	1.186 (±0.311)	1.263 (±0.311)	1.199 (±0.313)	1.209 (±0.312)	1.423 (±0.312)	1.319 (±0.311)	1.081 (±0.312)
SH (K)	5.109 (±0.422)	5.100 (±0.422)	5.124 (±0.412)	5.183 (±0.366)	5.018 (±0.421)	5.149 (±0.459)	4.987 (±0.396)	5.586 (±0.481)	4.982 (±0.386)	5.204 (±0.424)
T_s (°C)	6.625 (±0.300)	6.476 (±0.300)	8.747 (±0.300)	22.128 (±0.300)	6.660 (±0.300)	0.115 (±0.300)	12.381 (±0.300)	-2.487 (±0.300)	15.219 (±0.300)	6.221 (±0.300)
T_d (°C)	87.625 (±0.300)	88.979 (±0.300)	86.556 (±0.300)	81.643 (±0.300)	95.796 (±0.300)	91.638 (±0.300)	84.873 (±0.300)	113.562 (±0.300)	88.388 (±0.300)	93.210 (±0.300)
$T_{s,in}$ (°C)	-	-	-	-	-	-	-	-	-	-
$T_{s,out}$ (°C)	-	-	-	-	-	-	-	-	-	-
$T_{e,in}$ (°C)	11.515 (±0.300)	11.248 (±0.300)	13.771 (±0.300)	25.812 (±0.300)	11.773 (±0.300)	7.951 (±0.300)	20.072 (±0.300)	4.504 (±0.300)	23.627 (±0.300)	18.539 (±0.300)
$T_{e,out}$ (°C)	6.356 (±0.300)	6.065 (±0.300)	9.033 (±0.300)	22.976 (±0.300)	5.969 (±0.300)	-0.158 (±0.300)	12.916 (±0.300)	-6.588 (±0.300)	16.143 (±0.300)	6.687 (±0.300)
$T_{d,in}$ (°C)	86.462 (±0.300)	87.687 (±0.300)	85.370 (±0.300)	80.449 (±0.300)	94.216 (±0.300)	90.150 (±0.300)	83.711 (±0.300)	110.001 (±0.300)	87.099 (±0.300)	91.822 (±0.300)
$T_{d,out}$ (°C)	47.434 (±0.300)	47.369 (±0.300)	47.790 (±0.300)	48.817 (±0.300)	50.582 (±0.300)	44.568 (±0.300)	46.540 (±0.300)	48.473 (±0.300)	50.212 (±0.300)	47.637 (±0.300)
$T_{coil,in}$ (°C)	-	-	-	-	-	-	-	-	-	-
$T_{coil,out}$ (°C)	-	-	-	-	-	-	-	-	-	-
Performance variables										
\dot{W}_c (W)	2044.500 (±20.223)	2036.700 (±20.184)	2069.653 (±20.349)	2111.747 (±20.599)	2188.790 (±20.944)	2278.703 (±21.394)	2455.372 (±22.277)	2432.805 (±22.165)	2659.243 (±23.297)	2909.725 (±24.549)
\dot{Q}_c^{\dagger} (W)	7343.564 (±88.066)	7326.646 (±87.808)	7806.926 (±89.947)	11254.975 (±107.104)	7439.252 (±196.779)	7284.320 (±111.000)	10534.103 (±119.013)	6693.579 (±96.797)	11425.162 (±139.488)	10121.430 (±101.187)
\dot{Q}_c^{\ddagger} (W)	6045.684 (±135.988)	6031.315 (±133.538)	6525.599 (±334.916)	10004.986 (±229.805)	5842.716 (±181.853)	5874.380 (±201.749)	9025.049 (±150.205)	4963.861 (±80.179)	9570.986 (±358.663)	8112.500 (±183.673)

* The reported uncertainties are considered as the expanded uncertainties considering a confidence interval of 95.45%;

† T_{in} is denoted as T_{co} or T_{ci} in the DSHF models depending on the operating mode of the RTPFHs (evaporator or condenser);

‡ Value corrected with the heat injected by the circulation pump;

F.4 DHW User

Table F.4: DHWU: Experimental results

	Test 1	Test 2	Test 3	Test 4	Test 5	Test 6	Test 7	Test 8	Test 9	Test 10
Compressor and fan speed										
f_c (Hz)	30	40	40	40	40	50	50	50	50	50
f_{fan} (%)	-	-	-	-	-	-	-	-	-	-
Secondary side										
T_{ci} (°C)	29.746 (±0.087)	20.075 (±0.083)	20.129 (±0.083)	39.997 (±0.090)	40.029 (±0.090)	10.109 (±0.080)	30.001 (±0.087)	30.065 (±0.087)	30.106 (±0.087)	30.011 (±0.087)
T_{co} (°C)	49.695 (±0.094)	50.082 (±0.094)	50.163 (±0.094)	50.002 (±0.094)	50.050 (±0.094)	50.189 (±0.094)	50.114 (±0.094)	50.153 (±0.094)	50.137 (±0.094)	50.029 (±0.094)
dT_c (K)	19.949 (±0.128)	30.007 (±0.126)	30.034 (±0.126)	10.005 (±0.130)	10.021 (±0.130)	40.080 (±0.124)	20.112 (±0.128)	20.088 (±0.128)	20.032 (±0.128)	20.018 (±0.128)
T_{ci} (°C)	17.023 (±0.082)	16.202 (±0.082)	18.003 (±0.083)	12.056 (±0.081)	21.986 (±0.084)	17.046 (±0.082)	10.967 (±0.080)	14.005 (±0.081)	17.047 (±0.082)	16.981 (±0.082)
T_{co} (°C)	12.084 (±0.081)	9.160 (±0.080)	15.061 (±0.082)	9.076 (±0.080)	15.048 (±0.082)	12.016 (±0.081)	5.967 (±0.079)	11.186 (±0.081)	11.992 (±0.081)	11.956 (±0.081)
dT_e (K)	4.939 (±0.115)	7.042 (±0.115)	2.942 (±0.116)	2.979 (±0.114)	6.938 (±0.117)	5.030 (±0.115)	5.000 (±0.113)	2.819 (±0.115)	5.054 (±0.115)	5.025 (±0.115)
\dot{m}_{user} (kg/h)	797.919 (±2.217)	706.407 (±2.063)	1896.230 (±4.151)	1498.428 (±3.440)	834.743 (±2.279)	1337.536 (±3.154)	1052.048 (±2.654)	2111.303 (±4.537)	1282.859 (±3.058)	1292.117 (±3.074)
\dot{m}_{ground} (kg/h)	-	-	-	-	-	-	-	-	-	-
\dot{m}_{dhw} (kg/h)	238.312 (±3.090)	198.742 (±3.046)	221.670 (±3.071)	575.128 (±3.535)	705.319 (±3.719)	197.930 (±3.045)	334.515 (±3.215)	379.094 (±3.272)	400.758 (±3.300)	399.516 (±3.298)
T_{ci}^\dagger (°C)	-	-	-	-	-	-	-	-	-	-
RH (%)	-	-	-	-	-	-	-	-	-	-
Refrigerant side										
P_c (bar)	11.251 (±0.080)	10.346 (±0.080)	11.690 (±0.080)	9.845 (±0.080)	12.321 (±0.080)	10.945 (±0.080)	9.076 (±0.080)	10.344 (±0.080)	10.984 (±0.080)	10.940 (±0.080)
P_e (bar)	29.785 (±0.060)	29.196 (±0.060)	29.818 (±0.060)	31.530 (±0.060)	32.081 (±0.060)	29.139 (±0.060)	30.642 (±0.060)	31.045 (±0.060)	31.223 (±0.060)	31.200 (±0.060)
P_s (-)	2.647 (±0.020)	2.822 (±0.023)	2.551 (±0.018)	3.203 (±0.027)	2.604 (±0.018)	2.662 (±0.020)	3.376 (±0.030)	3.001 (±0.024)	2.843 (±0.021)	2.852 (±0.022)
T_c (°C)	10.548 (±0.240)	7.744 (±0.256)	11.847 (±0.234)	6.111 (±0.266)	13.652 (±0.225)	9.619 (±0.246)	3.478 (±0.283)	7.738 (±0.256)	9.739 (±0.245)	9.602 (±0.246)
T_e (°C)	47.398 (±0.087)	46.336 (±0.088)	47.135 (±0.087)	49.764 (±0.083)	50.343 (±0.082)	45.816 (±0.089)	48.295 (±0.085)	48.743 (±0.085)	48.916 (±0.084)	48.881 (±0.085)
SC (K)	1.429 (±0.312)	1.255 (±0.313)	1.444 (±0.312)	1.560 (±0.311)	1.503 (±0.311)	1.435 (±0.313)	1.244 (±0.312)	1.222 (±0.312)	1.159 (±0.312)	1.385 (±0.312)
SH (K)	5.520 (±0.384)	5.157 (±0.394)	5.154 (±0.380)	5.342 (±0.401)	5.246 (±0.375)	5.114 (±0.388)	5.044 (±0.412)	5.081 (±0.394)	5.044 (±0.387)	5.257 (±0.388)
T_s (°C)	16.068 (±0.300)	12.901 (±0.300)	17.001 (±0.300)	11.452 (±0.300)	18.898 (±0.300)	14.734 (±0.300)	8.522 (±0.300)	12.818 (±0.300)	14.783 (±0.300)	14.859 (±0.300)
T_{ci} (°C)	86.308 (±0.300)	83.110 (±0.300)	81.892 (±0.300)	91.224 (±0.300)	86.161 (±0.300)	78.741 (±0.300)	85.335 (±0.300)	85.418 (±0.300)	84.396 (±0.300)	83.741 (±0.300)
$T_{ci,in}$ (°C)	12.342 (±0.300)	11.555 (±0.300)	15.447 (±0.300)	10.090 (±0.300)	17.335 (±0.300)	15.535 (±0.300)	10.281 (±0.300)	14.105 (±0.300)	16.129 (±0.300)	15.972 (±0.300)
$T_{ci,out}$ (°C)	15.648 (±0.300)	12.791 (±0.300)	17.554 (±0.300)	11.687 (±0.300)	19.183 (±0.300)	15.456 (±0.300)	8.942 (±0.300)	13.442 (±0.300)	15.372 (±0.300)	15.501 (±0.300)
$T_{e,in}$ (°C)	-	-	-	-	-	-	-	-	-	-
$T_{e,out}$ (°C)	-	-	-	-	-	-	-	-	-	-
$T_{ci,in}$ (°C)	83.991 (±0.300)	81.894 (±0.300)	80.579 (±0.300)	89.463 (±0.300)	84.754 (±0.300)	77.783 (±0.300)	84.467 (±0.300)	84.473 (±0.300)	83.475 (±0.300)	82.734 (±0.300)
$T_{ci,out}$ (°C)	46.362 (±0.300)	45.391 (±0.300)	46.181 (±0.300)	48.967 (±0.300)	49.491 (±0.300)	44.838 (±0.300)	47.521 (±0.300)	47.947 (±0.300)	48.106 (±0.300)	48.121 (±0.300)
$T_{coil,in}$ (°C)	-	-	-	-	-	-	-	-	-	-
$T_{coil,out}$ (°C)	-	-	-	-	-	-	-	-	-	-
Performance variables										
\dot{W}_c (W)	1261.374 (±16.307)	1570.237 (±17.852)	1594.319 (±17.972)	1712.414 (±18.563)	1726.600 (±18.634)	1933.364 (±19.667)	2053.498 (±20.268)	2078.732 (±20.394)	2082.466 (±20.413)	2081.750 (±20.409)
\dot{Q}_c^\dagger (W)	5514.962 (±79.910)	6919.804 (±110.074)	7725.742 (±111.956)	6672.131 (±96.224)	8195.476 (±115.170)	9206.928 (±144.583)	7806.496 (±90.104)	8836.566 (±94.913)	9315.453 (±97.201)	9280.492 (±97.003)
\dot{Q}_c^\ddagger (W)	4596.048 (±107.711)	5794.549 (±95.541)	6577.404 (±256.436)	5245.074 (±198.321)	6746.379 (±115.075)	7859.570 (±180.216)	6144.631 (±138.795)	7046.982 (±281.354)	7572.353 (±172.866)	7582.858 (±174.065)

(Continued on Next Page...)

Table F.4: DHWU: Experimental results (*continued*)

	Test 11	Test 12	Test 13	Test 14	Test 15	Test 16	Test 17	Test 18	Test 19	Test 20
Compressor and fan speed										
f_c (Hz)	50	50	50	50	50	60	60	60	60	70
f_{fan} (%)	-	-	-	-	-	-	-	-	-	-
Secondary side										
T_{ei} (°C)	30.035 (+0.087)	29.974 (+0.087)	29.994 (+0.087)	30.060 (+0.087)	45.044 (+0.092)	20.012 (+0.083)	20.047 (+0.083)	40.061 (+0.090)	40.040 (+0.090)	29.979 (+0.087)
T_{eo} (°C)	50.007 (+0.094)	50.035 (+0.094)	50.035 (+0.094)	50.121 (+0.094)	50.057 (+0.094)	50.010 (+0.094)	50.051 (+0.094)	50.098 (+0.094)	50.021 (+0.094)	50.074 (+0.094)
dT_e (K)	19.972 (+0.128)	20.061 (+0.128)	20.041 (+0.128)	20.061 (+0.128)	5.013 (+0.132)	29.998 (+0.126)	30.005 (+0.126)	10.037 (+0.130)	9.981 (+0.130)	20.094 (+0.128)
T_{ei} (°C)	16.956 (+0.082)	16.984 (+0.082)	20.923 (+0.084)	22.967 (+0.084)	16.966 (+0.082)	12.068 (+0.081)	21.877 (+0.084)	15.974 (+0.082)	17.939 (+0.083)	16.889 (+0.082)
T_{eo} (°C)	11.949 (+0.081)	11.944 (+0.081)	11.959 (+0.081)	17.903 (+0.083)	11.934 (+0.081)	8.847 (+0.080)	14.925 (+0.082)	8.921 (+0.080)	14.246 (+0.081)	11.975 (+0.081)
dT_e (K)	5.006 (+0.115)	5.040 (+0.115)	8.964 (+0.116)	5.064 (+0.118)	5.032 (+0.115)	3.221 (+0.114)	6.952 (+0.117)	7.052 (+0.114)	3.694 (+0.116)	4.914 (+0.115)
\dot{m}_{user} (kg/h)	1292.663 (+3.075)	1289.448 (+3.070)	745.182 (+2.128)	1561.806 (+3.552)	1245.892 (+2.993)	2107.079 (+4.530)	1266.716 (+3.029)	988.212 (+2.543)	2133.182 (+4.577)	1806.836 (+3.990)
\dot{m}_{ground} (kg/h)	-	-	-	-	-	-	-	-	-	-
\dot{m}_{dhw} (kg/h)	401.116 (+3.300)	399.243 (+3.298)	408.755 (+3.310)	470.779 (+3.393)	1624.041 (+5.145)	287.586 (+3.155)	352.575 (+3.238)	895.792 (+3.998)	1011.412 (+4.172)	557.405 (+3.510)
T_a^\dagger (°C)	-	-	-	-	-	-	-	-	-	-
RH (%)	-	-	-	-	-	-	-	-	-	-
Refrigerant side										
P_e (bar)	10.955 (+0.080)	10.961 (+0.080)	11.221 (+0.080)	13.085 (+0.080)	10.962 (+0.080)	9.628 (+0.080)	12.024 (+0.080)	10.032 (+0.080)	11.375 (+0.080)	10.689 (+0.080)
P_c (bar)	31.233 (+0.060)	31.186 (+0.060)	31.253 (+0.060)	31.630 (+0.060)	33.214 (+0.060)	29.996 (+0.060)	31.074 (+0.060)	32.508 (+0.060)	32.888 (+0.060)	31.671 (+0.060)
P_r (-)	2.851 (+0.022)	2.845 (+0.021)	2.785 (+0.021)	2.417 (+0.015)	3.030 (+0.023)	3.116 (+0.027)	2.584 (+0.018)	3.240 (+0.027)	2.891 (+0.021)	2.963 (+0.023)
T_e (°C)	9.648 (+0.245)	9.668 (+0.245)	10.457 (+0.241)	15.745 (+0.215)	9.671 (+0.245)	5.383 (+0.270)	12.810 (+0.229)	6.728 (+0.262)	10.916 (+0.239)	8.826 (+0.250)
T_c (°C)	48.928 (+0.084)	48.861 (+0.085)	48.915 (+0.084)	49.225 (+0.084)	51.735 (+0.080)	47.032 (+0.087)	48.101 (+0.086)	50.608 (+0.082)	50.884 (+0.082)	48.938 (+0.084)
SC (K)	1.328 (+0.312)	1.408 (+0.312)	1.347 (+0.312)	1.378 (+0.312)	1.508 (+0.311)	1.193 (+0.312)	1.323 (+0.312)	1.431 (+0.311)	1.378 (+0.311)	1.364 (+0.312)
SH (K)	5.173 (+0.388)	5.251 (+0.387)	5.152 (+0.385)	5.237 (+0.369)	5.130 (+0.387)	5.009 (+0.404)	5.181 (+0.377)	5.068 (+0.398)	5.090 (+0.383)	5.205 (+0.390)
T_g (°C)	14.821 (+0.300)	14.918 (+0.300)	15.609 (+0.300)	20.982 (+0.300)	14.802 (+0.300)	10.392 (+0.300)	17.991 (+0.300)	11.796 (+0.300)	16.006 (+0.300)	14.031 (+0.300)
$T_{g,i}$ (°C)	84.215 (+0.300)	84.089 (+0.300)	83.277 (+0.300)	81.939 (+0.300)	89.335 (+0.300)	86.138 (+0.300)	81.729 (+0.300)	90.839 (+0.300)	87.462 (+0.300)	88.075 (+0.300)
$T_{w,in}$ (°C)	15.916 (+0.300)	15.905 (+0.300)	16.695 (+0.300)	21.573 (+0.300)	16.205 (+0.300)	14.125 (+0.300)	21.253 (+0.300)	15.729 (+0.300)	19.887 (+0.300)	19.878 (+0.300)
$T_{w,out}$ (°C)	15.487 (+0.300)	15.548 (+0.300)	15.424 (+0.300)	21.811 (+0.300)	15.518 (+0.300)	11.138 (+0.300)	18.806 (+0.300)	12.289 (+0.300)	17.008 (+0.300)	14.942 (+0.300)
$T_{g,out}$ (°C)	-	-	-	-	-	-	-	-	-	-
$T_{s,out}$ (°C)	-	-	-	-	-	-	-	-	-	-
$T_{d,in}$ (°C)	83.273 (+0.300)	83.054 (+0.300)	82.340 (+0.300)	80.795 (+0.300)	88.264 (+0.300)	85.091 (+0.300)	80.664 (+0.300)	89.682 (+0.300)	86.387 (+0.300)	86.686 (+0.300)
$T_{d,out}$ (°C)	48.150 (+0.300)	48.067 (+0.300)	48.135 (+0.300)	48.367 (+0.300)	51.015 (+0.300)	46.183 (+0.300)	47.299 (+0.300)	49.857 (+0.300)	50.168 (+0.300)	48.123 (+0.300)
$T_{coil,in}$ (°C)	-	-	-	-	-	-	-	-	-	-
$T_{coil,out}$ (°C)	-	-	-	-	-	-	-	-	-	-
Performance variables										
\dot{W}_c (W)	2086.745 (+20.434)	2084.279 (+20.422)	2083.708 (+20.419)	2090.291 (+20.452)	2230.891 (+21.155)	2423.105 (+22.116)	2494.310 (+22.472)	2614.473 (+23.073)	2654.011 (+23.271)	3010.937 (+25.055)
\dot{Q}_c^\ddagger (W)	9296.137 (+97.046)	9293.937 (+97.099)	9505.698 (+98.132)	10959.617 (+105.559)	9398.182 (+250.029)	10012.506 (+117.725)	12278.759 (+124.046)	10424.386 (+143.366)	11701.673 (+160.506)	12998.171 (+116.454)
\dot{Q}_e^\ddagger (W)	7558.768 (+174.121)	7589.744 (+173.709)	7775.760 (+103.044)	9247.362 (+215.106)	7320.641 (+167.860)	8021.137 (+278.772)	10268.140 (+174.041)	8121.977 (+133.086)	9286.479 (+288.236)	10400.570 (+243.147)

* The reported uncertainties are considered as the expanded uncertainties considering a confidence interval of 95.45%;

† T_a is denoted as T_{ei} or T_{eo} in the DSHP models depending on the operating mode of the RTPFHx (evaporator or condenser);

‡ Value corrected with the heat injected by the circulation pump;

F.5 Winter Air

Table F.5: WA: Experimental results

	Test 1	Test 2	Test 3	Test 4	Test 5	Test 6	Test 7	Test 8	Test 9	Test 10
Compressor and fan speed										
f_c (Hz)	30	40	40	40	40	40	40	40	40	50
f_{fan} (%)	50	35	35	35	35	65	65	65	65	20
Secondary side										
T_{ci} (°C)	40.048 (±0.090)	46.913 (±0.093)	33.044 (±0.088)	42.931 (±0.091)	37.016 (±0.089)	37.020 (±0.089)	42.943 (±0.091)	32.958 (±0.088)	46.955 (±0.093)	40.043 (±0.090)
T_{co} (°C)	44.931 (±0.094)	49.955 (±0.094)	39.992 (±0.090)	49.957 (±0.094)	40.069 (±0.090)	40.094 (±0.090)	49.907 (±0.094)	39.984 (±0.090)	49.930 (±0.094)	44.995 (±0.092)
dT_c (K)	4.884 (±0.129)	3.042 (±0.132)	6.949 (±0.126)	7.025 (±0.131)	3.053 (±0.127)	3.074 (±0.127)	6.964 (±0.131)	7.026 (±0.126)	2.975 (±0.132)	4.952 (±0.129)
T_{ci} (°C)	-	-	-	-	-	-	-	-	-	-
T_{co} (°C)	-	-	-	-	-	-	-	-	-	-
dT_e (K)	-	-	-	-	-	-	-	-	-	-
\dot{m}_{user} (kg/h)	842.591 (±2.293)	1551.809 (±3.535)	693.082 (±2.040)	789.087 (±2.202)	1939.852 (±4.229)	1635.371 (±3.684)	676.624 (±2.013)	877.694 (±2.353)	2009.014 (±4.353)	1214.441 (±2.938)
\dot{m}_{ground} (kg/h)	-	-	-	-	-	-	-	-	-	-
\dot{m}_{dhw} (kg/h)	-	-	-	-	-	-	-	-	-	-
T_{di}^{\ddagger} (°C)	10.994 (±0.080)	6.987 (±0.079)	6.973 (±0.079)	15.048 (±0.082)	14.983 (±0.082)	6.975 (±0.079)	6.996 (±0.079)	14.994 (±0.082)	14.846 (±0.082)	10.989 (±0.080)
RH (%)	88.376 (±2.309)	86.844 (±2.321)	87.796 (±2.321)	70.116 (±2.309)	68.882 (±2.309)	86.957 (±2.321)	86.948 (±2.321)	70.206 (±2.309)	70.420 (±2.309)	89.769 (±2.309)
Refrigerant side										
P_c (bar)	9.412 (±0.080)	7.994 (±0.080)	7.812 (±0.080)	9.552 (±0.080)	9.445 (±0.080)	8.088 (±0.080)	8.184 (±0.080)	10.106 (±0.080)	10.224 (±0.080)	7.762 (±0.080)
P_e (bar)	27.575 (±0.060)	31.464 (±0.060)	24.291 (±0.060)	30.800 (±0.060)	25.303 (±0.060)	25.062 (±0.060)	30.521 (±0.060)	24.667 (±0.060)	31.952 (±0.060)	27.973 (±0.060)
P_s (-)	2.930 (±0.026)	3.936 (±0.040)	3.109 (±0.033)	3.224 (±0.028)	2.679 (±0.024)	3.099 (±0.032)	3.729 (±0.037)	2.441 (±0.020)	3.125 (±0.025)	3.604 (±0.038)
T_c (°C)	4.648 (±0.275)	-0.531 (±0.311)	-1.244 (±0.317)	5.127 (±0.272)	4.761 (±0.274)	-0.169 (±0.308)	0.200 (±0.306)	6.968 (±0.261)	7.350 (±0.258)	-1.443 (±0.318)
T_e (°C)	44.208 (±0.092)	49.819 (±0.083)	38.844 (±0.101)	48.811 (±0.085)	40.452 (±0.098)	40.123 (±0.099)	48.479 (±0.085)	39.333 (±0.101)	50.383 (±0.082)	44.626 (±0.091)
SC (K)	2.239 (±0.314)	2.518 (±0.311)	1.964 (±0.317)	1.997 (±0.312)	1.646 (±0.316)	2.210 (±0.316)	2.739 (±0.312)	1.683 (±0.316)	2.240 (±0.311)	2.001 (±0.314)
SH (K)	5.600 (±0.407)	5.262 (±0.432)	5.364 (±0.436)	5.208 (±0.405)	5.350 (±0.407)	5.343 (±0.430)	5.240 (±0.428)	5.347 (±0.397)	5.236 (±0.396)	5.107 (±0.437)
T_s (°C)	10.249 (±0.300)	4.730 (±0.300)	4.120 (±0.300)	10.335 (±0.300)	10.110 (±0.300)	5.175 (±0.300)	5.440 (±0.300)	12.315 (±0.300)	12.586 (±0.300)	3.664 (±0.300)
T_{di} (°C)	84.645 (±0.300)	97.877 (±0.300)	75.667 (±0.300)	90.285 (±0.300)	75.487 (±0.300)	76.720 (±0.300)	92.195 (±0.300)	70.722 (±0.300)	89.656 (±0.300)	86.120 (±0.300)
$T_{di,in}$ (°C)	80.128 (±0.300)	93.128 (±0.300)	72.656 (±0.300)	86.932 (±0.300)	72.912 (±0.300)	73.227 (±0.300)	87.611 (±0.300)	68.230 (±0.300)	86.065 (±0.300)	83.977 (±0.300)
$T_{di,out}$ (°C)	43.199 (±0.300)	48.593 (±0.300)	37.861 (±0.300)	47.660 (±0.300)	39.474 (±0.300)	39.006 (±0.300)	47.142 (±0.300)	38.376 (±0.300)	49.171 (±0.300)	43.674 (±0.300)
$T_{si,in}$ (°C)	-	-	-	-	-	-	-	-	-	-
$T_{si,out}$ (°C)	-	-	-	-	-	-	-	-	-	-
$T_{di,in}$ (°C)	-	-	-	-	-	-	-	-	-	-
$T_{di,out}$ (°C)	-	-	-	-	-	-	-	-	-	-
$T_{coi,in}$ (°C)	5.263 (±0.300)	0.760 (±0.300)	0.068 (±0.300)	6.442 (±0.300)	5.972 (±0.300)	1.086 (±0.300)	1.495 (±0.300)	8.121 (±0.300)	8.698 (±0.300)	0.895 (±0.300)
$T_{coi,out}$ (°C)	9.524 (±0.300)	4.305 (±0.300)	4.032 (±0.300)	10.294 (±0.300)	10.140 (±0.300)	5.212 (±0.300)	5.331 (±0.300)	12.606 (±0.300)	12.756 (±0.300)	3.604 (±0.300)
Performance variables										
\dot{W}_c (W)	1176.470 (±185.883)	1705.045 (±18.526)	1314.583 (±16.573)	1666.146 (±18.331)	1363.746 (±16.819)	1352.165 (±16.761)	1652.494 (±18.263)	1320.906 (±16.605)	1734.401 (±18.673)	1870.568 (±19.353)
\dot{Q}_c^{\ddagger} (W)	4762.510 (±126.788)	5432.162 (±238.360)	5581.025 (±102.590)	6423.139 (±121.412)	6787.878 (±286.118)	5779.937 (±241.241)	5460.119 (±104.232)	7144.689 (±129.639)	6844.309 (±308.539)	6953.828 (±182.589)
\dot{Q}_e^{\ddagger} (W)	3945.000 (±105.400)	4266.000 (±187.500)	4715.000 (±87.330)	5234.000 (±99.810)	5792.000 (±244.500)	4884.000 (±204.100)	4393.000 (±84.550)	6222.000 (±113.800)	5631.000 (±254.300)	5685.000 (±149.900)

(Continued on Next Page...)

Table F.5: WA: Experimental results (continued)

	Test 11	Test 12	Test 13	Test 14	Test 15	Test 16	Test 17	Test 18	Test 19	Test 20
Compressor and fan speed										
f_c (Hz)	50	50	50	50	50	50	50	50	50	50
f_{fan} (%)	80	50	50	50	50	50	50	50	50	50
Secondary side										
T_{ci} (°C)	40.050 (±0.090)	39.986 (±0.090)	30.017 (±0.087)	35.952 (±0.089)	41.865 (±0.091)	40.043 (±0.090)	39.984 (±0.090)	40.000 (±0.090)	40.048 (±0.090)	50.064 (±0.094)
T_{co} (°C)	45.021 (±0.092)	44.933 (±0.092)	35.062 (±0.088)	44.915 (±0.092)	45.018 (±0.092)	45.058 (±0.092)	44.947 (±0.092)	44.982 (±0.092)	45.067 (±0.092)	55.013 (±0.096)
dT_c (K)	4.971 (±0.129)	4.947 (±0.129)	5.045 (±0.124)	8.963 (±0.128)	3.153 (±0.129)	5.015 (±0.129)	4.963 (±0.129)	4.982 (±0.129)	5.018 (±0.129)	4.949 (±0.134)
T_{ci} (°C)	-	-	-	-	-	-	-	-	-	-
T_{co} (°C)	-	-	-	-	-	-	-	-	-	-
dT_e (K)	-	-	-	-	-	-	-	-	-	-
\dot{m}_{inset} (kg/h)	1379.069 (±3.228)	1151.225 (±2.827)	1399.913 (±3.265)	755.987 (±2.146)	2196.107 (±4.690)	1351.012 (±3.178)	1370.545 (±3.213)	1360.925 (±3.196)	1354.666 (±3.185)	1327.068 (±3.136)
\dot{m}_{ground} (kg/h)	-	-	-	-	-	-	-	-	-	-
\dot{m}_{dirt} (kg/h)	-	-	-	-	-	-	-	-	-	-
T_a^* (°C)	10.943 (±0.080)	4.061 (±0.079)	10.973 (±0.080)	11.043 (±0.081)	11.033 (±0.081)	10.992 (±0.080)	10.980 (±0.080)	10.996 (±0.080)	11.055 (±0.081)	11.020 (±0.081)
RH (%)	88.455 (±2.309)	87.789 (±2.354)	87.045 (±2.309)	88.953 (±2.309)	88.762 (±2.309)	87.499 (±2.309)	88.960 (±2.309)	88.776 (±2.309)	88.240 (±2.309)	88.057 (±2.309)
Refrigerant side										
P_c (bar)	9.028 (±0.080)	7.241 (±0.080)	8.745 (±0.080)	8.904 (±0.080)	8.918 (±0.080)	8.862 (±0.080)	8.893 (±0.080)	8.878 (±0.080)	8.899 (±0.080)	9.089 (±0.080)
P_e (bar)	28.364 (±0.060)	27.811 (±0.060)	22.297 (±0.060)	27.451 (±0.060)	28.760 (±0.060)	28.318 (±0.060)	28.282 (±0.060)	28.306 (±0.060)	28.345 (±0.060)	35.348 (±0.060)
P_s (-)	3.142 (±0.029)	3.841 (±0.043)	2.550 (±0.024)	3.083 (±0.029)	3.225 (±0.030)	3.195 (±0.030)	3.180 (±0.029)	3.188 (±0.030)	3.185 (±0.029)	3.889 (±0.035)
T_c (°C)	3.307 (±0.284)	-3.570 (±0.335)	2.292 (±0.291)	2.865 (±0.287)	2.914 (±0.286)	2.715 (±0.288)	2.826 (±0.287)	2.773 (±0.287)	2.848 (±0.287)	3.520 (±0.282)
T_e (°C)	45.079 (±0.090)	44.434 (±0.092)	35.043 (±0.109)	43.686 (±0.093)	45.692 (±0.089)	45.030 (±0.091)	44.966 (±0.091)	44.999 (±0.091)	45.060 (±0.091)	54.762 (±0.076)
SC (K)	2.010 (±0.313)	2.395 (±0.314)	1.473 (±0.319)	1.893 (±0.314)	1.939 (±0.313)	1.887 (±0.313)	1.996 (±0.313)	1.986 (±0.313)	1.999 (±0.313)	2.341 (±0.310)
SH (K)	5.272 (±0.413)	5.021 (±0.450)	5.154 (±0.418)	4.985 (±0.415)	5.077 (±0.415)	5.199 (±0.416)	4.998 (±0.415)	5.009 (±0.415)	4.987 (±0.415)	4.990 (±0.412)
T_g (°C)	8.579 (±0.300)	1.451 (±0.300)	7.446 (±0.300)	7.851 (±0.300)	7.991 (±0.300)	7.914 (±0.300)	7.824 (±0.300)	7.781 (±0.300)	7.834 (±0.300)	8.511 (±0.300)
T_d (°C)	78.770 (±0.300)	90.752 (±0.300)	63.991 (±0.300)	77.046 (±0.300)	80.677 (±0.300)	79.957 (±0.300)	79.333 (±0.300)	79.176 (±0.300)	79.412 (±0.300)	97.309 (±0.300)
$T_{H,in}$ (°C)	76.966 (±0.300)	86.703 (±0.300)	62.906 (±0.300)	75.721 (±0.300)	79.152 (±0.300)	78.395 (±0.300)	77.851 (±0.300)	77.595 (±0.300)	77.812 (±0.300)	95.061 (±0.300)
$T_{H,out}$ (°C)	44.026 (±0.300)	43.129 (±0.300)	34.255 (±0.300)	42.712 (±0.300)	44.706 (±0.300)	44.088 (±0.300)	44.013 (±0.300)	44.017 (±0.300)	44.084 (±0.300)	53.590 (±0.300)
$T_{g,in}$ (°C)	-	-	-	-	-	-	-	-	-	-
$T_{g,out}$ (°C)	-	-	-	-	-	-	-	-	-	-
$T_{d,in}$ (°C)	-	-	-	-	-	-	-	-	-	-
$T_{d,out}$ (°C)	-	-	-	-	-	-	-	-	-	-
$T_{coil,in}$ (°C)	5.850 (±0.300)	-1.631 (±0.300)	4.511 (±0.300)	5.342 (±0.300)	5.440 (±0.300)	5.250 (±0.300)	5.298 (±0.300)	5.275 (±0.300)	5.340 (±0.300)	6.225 (±0.300)
$T_{coil,out}$ (°C)	9.061 (±0.300)	1.540 (±0.300)	8.044 (±0.300)	8.468 (±0.300)	8.573 (±0.300)	8.428 (±0.300)	8.350 (±0.300)	8.303 (±0.300)	8.364 (±0.300)	8.850 (±0.300)
Performance variables										
\dot{W}_c (W)	1903.285 (±19.517)	1889.668 (±19.449)	1506.138 (±17.531)	1837.659 (±19.189)	1925.449 (±19.628)	1898.874 (±19.495)	1894.100 (±19.471)	1898.670 (±19.494)	1900.072 (±19.501)	2366.007 (±21.831)
\dot{Q}_c^{\ddagger} (W)	7921.715 (±207.307)	6586.451 (±173.063)	8162.228 (±202.172)	7855.784 (±114.437)	7914.613 (±333.840)	7830.092 (±203.130)	7860.169 (±205.971)	7835.450 (±204.561)	7857.142 (±203.686)	7592.328 (±207.885)
\dot{Q}_c^{\S} (W)	6746.000 (±177.300)	5263.000 (±138.900)	7200.000 (±179.100)	6707.000 (±99.070)	6681.000 (±282.300)	6621.000 (±172.500)	6662.000 (±175.300)	6646.000 (±174.300)	6657.000 (±173.400)	6061.000 (±166.800)

(Continued on Next Page...)

Table F.5: WA: Experimental results (continued)

	Test 21	Test 22	Test 23	Test 24	Test 25	Test 26	Test 27	Test 28	Test 29	Test 30
Compressor and fan speed										
f_c (Hz)	50	60	60	60	60	60	60	60	60	70
f_{fan} (%)	50	35	35	35	35	65	65	65	65	50
Secondary side										
T_{ci} (°C)	40.000 (±0.090)	46.204 (±0.093)	36.768 (±0.089)	42.957 (±0.091)	32.965 (±0.088)	33.003 (±0.088)	46.708 (±0.093)	35.919 (±0.089)	42.932 (±0.091)	39.977 (±0.090)
T_{co} (°C)	44.973 (±0.092)	49.915 (±0.094)	40.064 (±0.090)	49.990 (±0.094)	40.074 (±0.090)	40.085 (±0.090)	50.010 (±0.094)	39.974 (±0.090)	50.035 (±0.094)	45.008 (±0.092)
dT_c (K)	4.973 (±0.129)	3.711 (±0.132)	3.297 (±0.127)	7.032 (±0.131)	7.110 (±0.126)	7.081 (±0.126)	3.302 (±0.132)	4.055 (±0.126)	7.103 (±0.131)	5.031 (±0.129)
T_{ci} (°C)	-	-	-	-	-	-	-	-	-	-
T_{co} (°C)	-	-	-	-	-	-	-	-	-	-
dT_c (K)	-	-	-	-	-	-	-	-	-	-
\dot{m}_{user} (kg/h)	1597.365 (±3.616)	2205.928 (±4.708)	2185.209 (±4.671)	976.910 (±2.523)	1146.627 (±2.819)	1043.333 (±2.639)	2195.712 (±4.689)	2183.941 (±4.668)	1208.375 (±2.927)	1844.683 (±4.058)
\dot{m}_{ground} (kg/h)	-	-	-	-	-	-	-	-	-	-
\dot{m}_{dhu} (kg/h)	-	-	-	-	-	-	-	-	-	-
T_a^3 (°C)	19.138 (±0.083)	14.970 (±0.082)	6.961 (±0.079)	6.973 (±0.079)	14.853 (±0.082)	7.014 (±0.079)	6.979 (±0.079)	14.670 (±0.082)	15.235 (±0.082)	11.031 (±0.081)
RH (%)	52.250 (±2.309)	69.371 (±2.309)	87.806 (±2.321)	86.947 (±2.321)	68.781 (±2.309)	86.388 (±2.321)	86.917 (±2.321)	69.543 (±2.309)	70.126 (±2.309)	86.935 (±2.309)
Refrigerant side										
P_c (bar)	10.492 (±0.080)	8.931 (±0.080)	7.351 (±0.080)	7.533 (±0.080)	8.555 (±0.080)	7.740 (±0.080)	7.884 (±0.080)	9.267 (±0.080)	9.623 (±0.080)	8.454 (±0.080)
P_e (bar)	28.674 (±0.060)	32.319 (±0.060)	25.458 (±0.060)	30.936 (±0.060)	25.046 (±0.060)	24.799 (±0.060)	32.181 (±0.060)	25.780 (±0.060)	31.678 (±0.060)	28.849 (±0.060)
P_r (-)	2.733 (±0.022)	3.619 (±0.033)	3.463 (±0.039)	4.107 (±0.044)	2.928 (±0.028)	3.204 (±0.034)	4.082 (±0.042)	2.782 (±0.025)	3.292 (±0.028)	3.412 (±0.033)
T_e (°C)	8.208 (±0.253)	2.960 (±0.286)	-3.112 (±0.332)	-2.364 (±0.325)	1.593 (±0.296)	-1.531 (±0.319)	-0.961 (±0.314)	4.146 (±0.278)	5.366 (±0.270)	1.219 (±0.298)
T_c (°C)	45.389 (±0.090)	50.640 (±0.082)	40.561 (±0.098)	48.889 (±0.085)	39.664 (±0.100)	39.379 (±0.100)	50.570 (±0.082)	40.771 (±0.098)	49.642 (±0.083)	45.501 (±0.090)
SC (K)	1.585 (±0.313)	1.878 (±0.311)	1.929 (±0.316)	2.361 (±0.312)	1.483 (±0.316)	1.958 (±0.316)	2.409 (±0.311)	1.600 (±0.316)	1.948 (±0.311)	1.878 (±0.313)
SH (K)	5.070 (±0.393)	5.005 (±0.415)	5.337 (±0.447)	5.215 (±0.443)	5.146 (±0.421)	5.129 (±0.438)	5.200 (±0.435)	5.219 (±0.409)	5.073 (±0.404)	5.033 (±0.423)
T_g (°C)	13.278 (±0.300)	7.965 (±0.300)	2.225 (±0.300)	2.852 (±0.300)	6.739 (±0.300)	3.598 (±0.300)	4.239 (±0.300)	9.366 (±0.300)	10.439 (±0.300)	6.252 (±0.300)
T_d (°C)	75.679 (±0.300)	93.993 (±0.300)	83.365 (±0.300)	99.806 (±0.300)	74.593 (±0.300)	77.684 (±0.300)	98.041 (±0.300)	73.184 (±0.300)	87.822 (±0.300)	85.390 (±0.300)
$T_{u,in}$ (°C)	74.377 (±0.300)	91.755 (±0.300)	80.926 (±0.300)	96.493 (±0.300)	73.087 (±0.300)	75.543 (±0.300)	94.699 (±0.300)	71.533 (±0.300)	85.732 (±0.300)	83.782 (±0.300)
$T_{u,out}$ (°C)	44.468 (±0.300)	49.524 (±0.300)	39.566 (±0.300)	47.712 (±0.300)	38.828 (±0.300)	38.371 (±0.300)	49.272 (±0.300)	39.860 (±0.300)	48.534 (±0.300)	44.558 (±0.300)
$T_{g,in}$ (°C)	-	-	-	-	-	-	-	-	-	-
$T_{g,out}$ (°C)	-	-	-	-	-	-	-	-	-	-
$T_{d,in}$ (°C)	-	-	-	-	-	-	-	-	-	-
$T_{d,out}$ (°C)	-	-	-	-	-	-	-	-	-	-
$T_{coil,in}$ (°C)	10.598 (±0.300)	6.330 (±0.300)	-0.161 (±0.300)	0.649 (±0.300)	4.863 (±0.300)	1.480 (±0.300)	2.324 (±0.300)	7.312 (±0.300)	8.697 (±0.300)	5.623 (±0.300)
$T_{coil,out}$ (°C)	13.898 (±0.300)	8.474 (±0.300)	2.547 (±0.300)	3.085 (±0.300)	7.298 (±0.300)	4.236 (±0.300)	4.630 (±0.300)	10.200 (±0.300)	11.255 (±0.300)	7.159 (±0.300)
Performance variables										
\dot{W}_c (W)	1908.285 (±19.542)	2598.327 (±22.992)	2075.961 (±20.380)	2463.148 (±22.316)	2049.425 (±20.248)	2029.921 (±20.150)	2568.552 (±22.843)	2103.487 (±20.518)	2553.408 (±22.768)	2739.555 (±23.698)
\dot{Q}_c^{\ddagger} (W)	9170.089 (±240.021)	9379.700 (±341.933)	8240.038 (±322.204)	7958.029 (±150.089)	9441.007 (±169.136)	8558.063 (±153.983)	8294.892 (±340.529)	10158.787 (±321.664)	9938.268 (±185.479)	10699.270 (±277.154)
\dot{Q}_e^{\S} (W)	7962.000 (±209.400)	7530.000 (±275.200)	6754.000 (±264.600)	6179.000 (±117.500)	8052.000 (±145.500)	7176.000 (±130.200)	6518.000 (±268.100)	8776.000 (±278.700)	8223.000 (±154.900)	8828.000 (±229.700)

* The reported uncertainties are considered as the expanded uncertainties considering a confidence interval of 95.45%;

† $T_{u,i}$ is denoted as $T_{u,e}$ or $T_{u,c}$ in the DSHP models depending on the operating mode of the RTPFHx (evaporator or condenser);

‡ Value corrected with the heat injected by the circulation pump;

§ The evaporator capacity is estimated from the refrigerant side;

F.6 Summer Air

Table F.6: SA: Experimental results

	Test 1	Test 2	Test 3	Test 4	Test 5	Test 6	Test 7	Test 8	Test 9	Test 10
Compressor and fan speed										
f_c (Hz)	30	40	40	40	40	40	40	40	40	50
f_{fan} (%)	50	35	35	35	35	65	65	65	65	20
Secondary side										
T_{ci} (°C)	-	-	-	-	-	-	-	-	-	-
T_{co} (°C)	-	-	-	-	-	-	-	-	-	-
dT_c (K)	-	-	-	-	-	-	-	-	-	-
T_{ci} (°C)	17.031 (± 0.082)	16.001 (± 0.082)	17.971 (± 0.083)	11.943 (± 0.081)	21.887 (± 0.084)	12.010 (± 0.081)	21.924 (± 0.084)	15.955 (± 0.082)	17.854 (± 0.083)	17.007 (± 0.082)
T_{co} (°C)	12.032 (± 0.082)	8.984 (± 0.080)	14.992 (± 0.082)	8.963 (± 0.080)	14.981 (± 0.082)	9.073 (± 0.080)	14.894 (± 0.082)	9.074 (± 0.080)	14.932 (± 0.082)	12.021 (± 0.081)
dT_c (K)	4.999 (± 0.115)	7.017 (± 0.115)	2.979 (± 0.116)	2.980 (± 0.114)	6.905 (± 0.117)	2.937 (± 0.114)	7.030 (± 0.117)	6.881 (± 0.115)	2.922 (± 0.116)	4.985 (± 0.115)
\dot{m}_{user} (kg/h)	905.782 (± 2.401)	805.759 (± 2.230)	2131.955 (± 4.575)	1602.991 (± 3.626)	876.979 (± 2.352)	1866.089 (± 4.096)	1016.921 (± 2.593)	754.987 (± 2.144)	2025.606 (± 4.383)	1321.010 (± 3.125)
\dot{m}_{ground} (kg/h)	-	-	-	-	-	-	-	-	-	-
\dot{m}_{dhw} (kg/h)	-	-	-	-	-	-	-	-	-	-
T_w^\dagger (°C)	26.906 (± 0.086)	21.006 (± 0.084)	20.912 (± 0.084)	32.858 (± 0.088)	33.128 (± 0.088)	20.935 (± 0.084)	21.070 (± 0.084)	32.930 (± 0.088)	32.629 (± 0.088)	27.054 (± 0.086)
RH (%)	31.087 (± 2.309)	35.625 (± 2.309)	41.741 (± 2.309)	18.297 (± 2.312)	23.004 (± 2.313)	37.126 (± 2.309)	36.183 (± 2.309)	19.036 (± 2.312)	19.040 (± 2.312)	29.996 (± 2.309)
Refrigerant side										
P_c (bar)	11.270 (± 0.080)	10.196 (± 0.080)	11.587 (± 0.080)	9.938 (± 0.080)	12.283 (± 0.080)	9.763 (± 0.080)	12.329 (± 0.080)	10.300 (± 0.080)	11.760 (± 0.080)	10.909 (± 0.080)
P_e (bar)	21.950 (± 0.060)	20.722 (± 0.060)	21.147 (± 0.060)	27.309 (± 0.060)	28.457 (± 0.060)	18.771 (± 0.060)	19.631 (± 0.060)	25.392 (± 0.060)	25.731 (± 0.060)	29.607 (± 0.060)
P_e (-)	1.948 (± 0.015)	2.032 (± 0.017)	1.825 (± 0.014)	2.748 (± 0.023)	2.317 (± 0.016)	1.923 (± 0.017)	1.592 (± 0.011)	2.465 (± 0.020)	2.188 (± 0.016)	2.714 (± 0.021)
T_c (°C)	10.605 (± 0.240)	7.260 (± 0.259)	11.544 (± 0.235)	6.416 (± 0.264)	13.545 (± 0.225)	5.837 (± 0.268)	13.674 (± 0.225)	7.595 (± 0.257)	12.051 (± 0.233)	9.507 (± 0.246)
T_e (°C)	34.837 (± 0.109)	32.467 (± 0.114)	33.207 (± 0.113)	43.799 (± 0.093)	45.483 (± 0.090)	28.582 (± 0.123)	30.199 (± 0.120)	40.729 (± 0.098)	41.230 (± 0.097)	47.108 (± 0.087)
SC (K)	0.773 (± 0.319)	0.957 (± 0.321)	0.954 (± 0.321)	0.810 (± 0.314)	0.869 (± 0.313)	0.776 (± 0.324)	0.801 (± 0.323)	0.740 (± 0.316)	0.681 (± 0.315)	1.098 (± 0.312)
SH (K)	5.495 (± 0.384)	5.345 (± 0.396)	5.174 (± 0.381)	5.424 (± 0.400)	5.257 (± 0.375)	5.489 (± 0.402)	5.380 (± 0.375)	5.379 (± 0.395)	5.293 (± 0.380)	5.320 (± 0.388)
T_s (°C)	16.099 (± 0.300)	12.605 (± 0.300)	16.718 (± 0.300)	11.840 (± 0.300)	18.801 (± 0.300)	11.326 (± 0.300)	19.053 (± 0.300)	12.974 (± 0.300)	17.343 (± 0.300)	14.827 (± 0.300)
T_d (°C)	62.968 (± 0.300)	60.123 (± 0.300)	57.890 (± 0.300)	80.046 (± 0.300)	77.859 (± 0.300)	54.541 (± 0.300)	52.124 (± 0.300)	73.819 (± 0.300)	70.272 (± 0.300)	78.305 (± 0.300)
$T_{i,in}$ (°C)	12.071 (± 0.300)	10.012 (± 0.300)	14.326 (± 0.300)	10.368 (± 0.300)	17.116 (± 0.300)	8.435 (± 0.300)	15.863 (± 0.300)	11.353 (± 0.300)	15.623 (± 0.300)	16.080 (± 0.300)
$T_{i,out}$ (°C)	15.753 (± 0.300)	12.074 (± 0.300)	17.447 (± 0.300)	11.668 (± 0.300)	18.262 (± 0.300)	11.612 (± 0.300)	19.354 (± 0.300)	11.911 (± 0.300)	17.546 (± 0.300)	15.337 (± 0.300)
$T_{e,in}$ (°C)	-	-	-	-	-	-	-	-	-	-
$T_{e,out}$ (°C)	-	-	-	-	-	-	-	-	-	-
$T_{d,in}$ (°C)	-	-	-	-	-	-	-	-	-	-
$T_{d,out}$ (°C)	-	-	-	-	-	-	-	-	-	-
$T_{evil,in}$ (°C)	61.879 (± 0.300)	59.460 (± 0.300)	57.233 (± 0.300)	79.084 (± 0.300)	76.981 (± 0.300)	53.823 (± 0.300)	51.390 (± 0.300)	72.858 (± 0.300)	69.479 (± 0.300)	77.767 (± 0.300)
$T_{evil,out}$ (°C)	33.799 (± 0.300)	31.225 (± 0.300)	31.829 (± 0.300)	42.699 (± 0.300)	44.313 (± 0.300)	27.454 (± 0.300)	29.021 (± 0.300)	39.773 (± 0.300)	40.221 (± 0.300)	45.704 (± 0.300)
Performance variables										
\dot{W}_c (W)	883.107 (± 14.416)	1098.516 (± 15.493)	1098.402 (± 15.493)	1469.119 (± 17.346)	1518.479 (± 17.593)	993.827 (± 14.970)	999.372 (± 14.997)	1363.734 (± 16.819)	1363.314 (± 16.817)	1969.937 (± 19.850)
\dot{Q}_c^\ddagger (W)	5933.000 (± 138.000)	7376.000 (± 122.900)	8295.000 (± 138.900)	6661.000 (± 252.000)	8204.000 (± 142.000)	7154.000 (± 273.600)	9033.000 (± 153.100)	7028.000 (± 119.500)	7956.000 (± 312.200)	8926.000 (± 207.800)
\dot{Q}_c^\ddagger (W)	5282.029 (± 122.206)	6587.153 (± 108.724)	7511.988 (± 288.253)	5618.504 (± 212.074)	7054.932 (± 120.795)	6466.434 (± 246.911)	8330.575 (± 139.954)	6052.644 (± 101.897)	6991.577 (± 273.774)	7693.134 (± 177.963)

(Continued on Next Page...)

Table F.6: SA: Experimental results (continued)

	Test 11	Test 12	Test 13	Test 14	Test 15	Test 16	Test 17	Test 18	Test 19	Test 20
Compressor and fan speed										
f_c (Hz)	50	50	50	50	50	50	50	50	50	50
f_{fan} (%)	50	50	50	50	50	50	50	50	50	50
Secondary side										
T_{ci} (°C)	-	-	-	-	-	-	-	-	-	-
T_{co} (°C)	-	-	-	-	-	-	-	-	-	-
dT_c (K)	-	-	-	-	-	-	-	-	-	-
T_{ci} (°C)	17.035 (±0.082)	10.975 (±0.080)	13.998 (±0.081)	17.023 (±0.082)	17.044 (±0.082)	16.894 (±0.082)	16.941 (±0.082)	21.020 (±0.084)	22.997 (±0.084)	16.920 (±0.082)
T_{co} (°C)	11.916 (±0.081)	6.019 (±0.079)	10.862 (±0.080)	12.056 (±0.081)	12.077 (±0.081)	11.929 (±0.081)	11.990 (±0.081)	12.020 (±0.081)	18.029 (±0.083)	12.044 (±0.081)
dT_c (K)	5.118 (±0.115)	4.956 (±0.113)	3.136 (±0.114)	4.967 (±0.115)	4.967 (±0.115)	4.964 (±0.115)	4.951 (±0.115)	9.000 (±0.116)	4.968 (±0.118)	4.876 (±0.115)
\dot{m}_{user} (kg/h)	1533.302 (±3.502)	1192.348 (±2.899)	2118.826 (±4.551)	1447.814 (±3.350)	1447.645 (±3.349)	1436.725 (±3.330)	1445.543 (±3.346)	823.631 (±2.280)	1748.836 (±3.886)	1311.346 (±3.108)
\dot{m}_{ground} (kg/h)	-	-	-	-	-	-	-	-	-	-
\dot{m}_{dhu} (kg/h)	-	-	-	-	-	-	-	-	-	-
T_{s1} (°C)	18.241 (±0.083)	27.225 (±0.086)	27.053 (±0.086)	26.947 (±0.086)	26.982 (±0.086)	27.008 (±0.086)	27.075 (±0.086)	26.829 (±0.086)	26.971 (±0.086)	39.028 (±0.090)
RH (%)	60.821 (±2.309)	29.238 (±2.309)	29.353 (±2.309)	25.825 (±2.309)	31.919 (±2.309)	29.502 (±2.309)	32.804 (±2.309)	26.529 (±2.309)	26.070 (±2.309)	10.766 (±2.335)
Refrigerant side										
P_c (bar)	10.865 (±0.080)	9.058 (±0.080)	10.242 (±0.080)	10.897 (±0.080)	10.887 (±0.080)	10.816 (±0.080)	10.873 (±0.080)	11.143 (±0.080)	13.089 (±0.080)	11.055 (±0.080)
P_e (bar)	19.174 (±0.060)	23.247 (±0.060)	23.688 (±0.060)	23.983 (±0.060)	23.965 (±0.060)	23.970 (±0.060)	24.020 (±0.060)	24.051 (±0.060)	25.234 (±0.060)	31.521 (±0.060)
P_r (-)	1.765 (±0.014)	2.567 (±0.024)	2.313 (±0.019)	2.201 (±0.017)	2.201 (±0.017)	2.216 (±0.017)	2.209 (±0.017)	2.158 (±0.016)	1.928 (±0.013)	2.851 (±0.021)
T_e (°C)	9.371 (±0.247)	3.411 (±0.283)	7.408 (±0.258)	9.472 (±0.246)	9.440 (±0.247)	9.221 (±0.248)	9.398 (±0.247)	10.222 (±0.242)	15.755 (±0.215)	9.955 (±0.244)
T_c (°C)	29.161 (±0.122)	37.009 (±0.105)	37.714 (±0.104)	38.187 (±0.103)	38.148 (±0.103)	38.149 (±0.103)	38.243 (±0.103)	38.288 (±0.103)	40.187 (±0.099)	49.840 (±0.083)
SC (K)	0.972 (±0.324)	0.650 (±0.318)	0.623 (±0.317)	0.728 (±0.317)	0.715 (±0.317)	0.692 (±0.317)	0.727 (±0.317)	0.736 (±0.317)	0.916 (±0.316)	0.690 (±0.311)
SH (K)	5.296 (±0.389)	5.285 (±0.413)	5.450 (±0.396)	5.189 (±0.388)	5.235 (±0.388)	5.202 (±0.389)	5.186 (±0.388)	5.165 (±0.386)	5.069 (±0.369)	5.143 (±0.386)
T_s (°C)	14.667 (±0.300)	8.697 (±0.300)	12.858 (±0.300)	14.661 (±0.300)	14.675 (±0.300)	14.423 (±0.300)	14.584 (±0.300)	15.388 (±0.300)	20.825 (±0.300)	15.098 (±0.300)
T_d (°C)	53.401 (±0.300)	67.346 (±0.300)	64.939 (±0.300)	64.847 (±0.300)	64.613 (±0.300)	63.957 (±0.300)	64.684 (±0.300)	64.656 (±0.300)	65.952 (±0.300)	85.184 (±0.300)
$T_{u,in}$ (°C)	13.048 (±0.300)	9.065 (±0.300)	13.031 (±0.300)	14.859 (±0.300)	14.949 (±0.300)	14.724 (±0.300)	14.901 (±0.300)	15.485 (±0.300)	20.583 (±0.300)	16.750 (±0.300)
$T_{u,out}$ (°C)	15.499 (±0.300)	8.881 (±0.300)	13.233 (±0.300)	15.213 (±0.300)	15.160 (±0.300)	14.972 (±0.300)	15.101 (±0.300)	14.845 (±0.300)	21.661 (±0.300)	15.269 (±0.300)
$T_{g,in}$ (°C)	-	-	-	-	-	-	-	-	-	-
$T_{g,out}$ (°C)	-	-	-	-	-	-	-	-	-	-
$T_{d,in}$ (°C)	-	-	-	-	-	-	-	-	-	-
$T_{d,out}$ (°C)	-	-	-	-	-	-	-	-	-	-
$T_{coil,in}$ (°C)	52.880 (±0.300)	67.023 (±0.300)	64.455 (±0.300)	64.486 (±0.300)	64.220 (±0.300)	63.610 (±0.300)	64.330 (±0.300)	64.286 (±0.300)	65.507 (±0.300)	84.611 (±0.300)
$T_{coil,out}$ (°C)	27.890 (±0.300)	36.077 (±0.300)	36.701 (±0.300)	37.234 (±0.300)	37.188 (±0.300)	37.182 (±0.300)	37.273 (±0.300)	37.224 (±0.300)	39.056 (±0.300)	48.951 (±0.300)
Performance variables										
\dot{W}_c (W)	1268.572 (±16.343)	1563.654 (±17.819)	1576.889 (±17.885)	1592.445 (±17.963)	1591.070 (±17.956)	1584.236 (±17.922)	1594.795 (±17.974)	1595.292 (±17.977)	1652.887 (±18.265)	2107.397 (±20.538)
\dot{Q}_c^S (W)	10060.000 (±227.500)	7899.000 (±180.800)	8827.000 (±317.900)	9426.000 (±219.800)	9415.000 (±219.600)	9316.000 (±217.300)	9375.000 (±219.300)	9665.000 (±129.500)	11356.000 (±270.400)	8908.000 (±211.900)
\dot{Q}_c^t (W)	9175.486 (±206.512)	6905.935 (±157.236)	7853.968 (±282.273)	8405.865 (±195.017)	8404.889 (±195.009)	8336.264 (±193.430)	8365.711 (±194.651)	8630.107 (±113.744)	10169.782 (±240.840)	7470.043 (±176.601)

(Continued on Next Page...)

Table F.6: SA: Experimental results (*continued*)

	Test 21	Test 22	Test 23	Test 24	Test 25	Test 26	Test 27	Test 28	Test 29	Test 30
Compressor and fan speed										
f_c (Hz)	50	60	60	60	60	60	60	60	60	70
f_{fan} (%)	80	35	35	35	35	65	65	65	65	50
Secondary side										
T_{ei} (°C)	-	-	-	-	-	-	-	-	-	-
T_{eo} (°C)	-	-	-	-	-	-	-	-	-	-
ΔT_e (K)	-	-	-	-	-	-	-	-	-	-
T_{ei} (°C)	17.088 (±0.082)	12.140 (±0.081)	21.931 (±0.084)	16.056 (±0.082)	18.073 (±0.083)	16.099 (±0.082)	18.078 (±0.083)	12.056 (±0.081)	21.969 (±0.084)	17.017 (±0.082)
T_{eo} (°C)	12.050 (±0.081)	8.549 (±0.080)	14.934 (±0.082)	9.073 (±0.080)	14.312 (±0.081)	9.145 (±0.080)	13.826 (±0.081)	8.733 (±0.080)	14.986 (±0.082)	11.986 (±0.081)
ΔT_e (K)	5.037 (±0.115)	3.591 (±0.114)	6.997 (±0.117)	6.982 (±0.115)	3.762 (±0.116)	6.953 (±0.115)	4.252 (±0.116)	3.323 (±0.114)	6.982 (±0.117)	5.032 (±0.115)
\dot{m}_{user} (kg/h)	1455.389 (±3.363)	2104.108 (±4.524)	1363.552 (±3.200)	1023.047 (±2.603)	2132.201 (±4.575)	1206.318 (±2.923)	2128.288 (±4.568)	2110.183 (±4.535)	1293.775 (±3.077)	1891.424 (±4.142)
\dot{m}_{ground} (kg/h)	-	-	-	-	-	-	-	-	-	-
\dot{m}_{dilu} (kg/h)	-	-	-	-	-	-	-	-	-	-
T_a^\ddagger (°C)	27.188 (±0.086)	21.125 (±0.084)	21.063 (±0.084)	32.944 (±0.088)	32.819 (±0.088)	21.154 (±0.084)	21.503 (±0.084)	32.943 (±0.088)	32.989 (±0.088)	26.997 (±0.086)
RH (%)	32.011 (±2.309)	47.286 (±2.309)	50.259 (±2.309)	15.243 (±2.312)	14.553 (±2.312)	49.685 (±2.309)	49.807 (±2.309)	13.587 (±2.312)	15.573 (±2.312)	32.770 (±2.309)
Refrigerant side										
P_r (bar)	10.888 (±0.080)	9.495 (±0.080)	11.767 (±0.080)	10.021 (±0.080)	11.418 (±0.080)	9.961 (±0.080)	10.868 (±0.080)	9.595 (±0.080)	12.034 (±0.080)	10.618 (±0.080)
P_c (bar)	22.765 (±0.060)	22.726 (±0.060)	24.108 (±0.060)	30.146 (±0.060)	31.408 (±0.060)	20.642 (±0.060)	21.191 (±0.060)	27.054 (±0.060)	28.598 (±0.060)	26.134 (±0.060)
P_r (-)	2.091 (±0.016)	2.394 (±0.021)	2.049 (±0.015)	3.008 (±0.025)	2.751 (±0.020)	2.072 (±0.018)	1.950 (±0.015)	2.820 (±0.024)	2.376 (±0.017)	2.461 (±0.019)
T_r (°C)	9.444 (±0.246)	4.929 (±0.273)	12.071 (±0.233)	6.691 (±0.262)	11.047 (±0.238)	6.492 (±0.264)	9.381 (±0.247)	5.270 (±0.271)	12.839 (±0.229)	8.604 (±0.251)
T_c (°C)	36.030 (±0.107)	35.957 (±0.107)	38.182 (±0.103)	47.847 (±0.086)	49.560 (±0.083)	31.994 (±0.116)	32.964 (±0.113)	43.209 (±0.094)	45.418 (±0.090)	41.515 (±0.097)
SC (K)	0.669 (±0.319)	0.941 (±0.319)	1.171 (±0.317)	0.859 (±0.312)	0.919 (±0.311)	0.906 (±0.321)	0.982 (±0.321)	0.684 (±0.314)	0.868 (±0.313)	1.061 (±0.315)
SH (K)	5.312 (±0.388)	5.365 (±0.406)	6.894 (±0.380)	5.191 (±0.399)	5.221 (±0.383)	5.298 (±0.399)	6.922 (±0.388)	5.285 (±0.404)	5.114 (±0.377)	5.077 (±0.391)
T_g (°C)	14.756 (±0.300)	10.295 (±0.300)	18.965 (±0.300)	11.882 (±0.300)	16.268 (±0.300)	11.790 (±0.300)	16.303 (±0.300)	10.555 (±0.300)	17.952 (±0.300)	13.681 (±0.300)
$T_{g,in}$ (°C)	61.856 (±0.300)	66.971 (±0.300)	67.040 (±0.300)	85.117 (±0.300)	84.074 (±0.300)	59.783 (±0.300)	61.539 (±0.300)	77.986 (±0.300)	76.082 (±0.300)	73.777 (±0.300)
$T_{g,out}$ (°C)	14.643 (±0.300)	12.099 (±0.300)	18.665 (±0.300)	15.623 (±0.300)	20.000 (±0.300)	12.851 (±0.300)	15.422 (±0.300)	13.875 (±0.300)	21.047 (±0.300)	18.513 (±0.300)
$T_{d,in}$ (°C)	15.153 (±0.300)	10.976 (±0.300)	20.029 (±0.300)	11.622 (±0.300)	16.871 (±0.300)	11.935 (±0.300)	17.341 (±0.300)	10.796 (±0.300)	18.279 (±0.300)	14.582 (±0.300)
$T_{g,in}$ (°C)	-	-	-	-	-	-	-	-	-	-
$T_{g,out}$ (°C)	-	-	-	-	-	-	-	-	-	-
$T_{d,in}$ (°C)	-	-	-	-	-	-	-	-	-	-
$T_{d,out}$ (°C)	-	-	-	-	-	-	-	-	-	-
$T_{cool,in}$ (°C)	61.375 (±0.300)	66.249 (±0.300)	66.450 (±0.300)	84.443 (±0.300)	83.379 (±0.300)	59.068 (±0.300)	60.790 (±0.300)	77.339 (±0.300)	75.507 (±0.300)	73.146 (±0.300)
$T_{cool,out}$ (°C)	35.139 (±0.300)	34.625 (±0.300)	36.790 (±0.300)	46.729 (±0.300)	48.333 (±0.300)	30.820 (±0.300)	31.730 (±0.300)	42.287 (±0.300)	44.430 (±0.300)	40.317 (±0.300)
Performance variables										
\dot{W}_c (W)	1516.022 (±17.581)	1850.995 (±19.256)	1933.395 (±19.668)	2440.629 (±22.204)	2531.032 (±22.656)	1686.799 (±18.435)	1723.788 (±18.619)	2201.445 (±21.008)	2294.191 (±21.472)	2494.291 (±22.472)
\dot{Q}_c^\S (W)	9543.000 (±219.500)	10189.000 (±319.000)	12465.000 (±211.900)	9997.000 (±167.400)	11190.000 (±342.600)	10947.000 (±183.300)	11853.000 (±321.300)	9750.000 (±329.400)	12137.000 (±207.200)	12904.000 (±296.300)
\dot{Q}_c^\ddagger (W)	8568.566 (±196.088)	8915.075 (±278.383)	11127.372 (±187.335)	8325.698 (±137.765)	9450.337 (±288.237)	9780.977 (±162.280)	10645.821 (±287.647)	8283.136 (±279.149)	10534.033 (±177.801)	11153.573 (±254.624)

* The reported uncertainties are considered as the expanded uncertainties considering a confidence interval of 95.45%;

† T_{ei} is denoted as T_{ei} or T_{eo} in the DSHP models depending on the operating mode of the RTPFHs (evaporator or condenser);

‡ Value corrected with the heat injected by the circulation pump;

§ The condenser capacity is estimated from the refrigerant side;

E.7 DHW Air

Table E.7: DHWA: Experimental results

	Test 1	Test 2	Test 3	Test 4	Test 5	Test 6	Test 7	Test 8	Test 9	Test 10
Compressor and fan speed										
f_c (Hz)	30	40	40	40	40	50	50	50	50	50
f_{fan} (%)	50	35	35	65	65	50	20	50	50	50
Secondary side										
T_{ci} (°C)	29.813 (±0.087)	20.113 (±0.083)	39.887 (±0.090)	19.961 (±0.083)	39.934 (±0.090)	10.107 (±0.080)	29.898 (±0.087)	30.007 (±0.087)	29.965 (±0.087)	29.935 (±0.087)
T_{co} (°C)	49.781 (±0.094)	50.034 (±0.094)	49.971 (±0.094)	49.906 (±0.094)	49.896 (±0.094)	50.006 (±0.094)	49.983 (±0.094)	49.901 (±0.094)	49.982 (±0.094)	50.096 (±0.094)
dT_c (K)	19.968 (±0.128)	29.921 (±0.126)	10.084 (±0.130)	29.945 (±0.126)	9.962 (±0.130)	39.898 (±0.124)	20.084 (±0.128)	19.894 (±0.128)	20.017 (±0.128)	20.161 (±0.128)
T_{ti} (°C)	-	-	-	-	-	-	-	-	-	-
T_{to} (°C)	-	-	-	-	-	-	-	-	-	-
dT_e (K)	-	-	-	-	-	-	-	-	-	-
\dot{m}_{user} (kg/h)	-	-	-	-	-	-	-	-	-	-
\dot{m}_{ground} (kg/h)	-	-	-	-	-	-	-	-	-	-
\dot{m}_{dhw} (kg/h)	225.034 (±3.075)	216.435 (±3.065)	513.931 (±3.451)	172.644 (±3.017)	712.244 (±3.728)	177.516 (±3.022)	359.995 (±3.247)	362.826 (±3.251)	362.867 (±3.251)	359.604 (±3.247)
T_{dt} (°C)	17.133 (±0.082)	23.108 (±0.084)	10.999 (±0.081)	10.922 (±0.080)	23.064 (±0.084)	17.134 (±0.082)	17.098 (±0.082)	16.826 (±0.082)	17.010 (±0.082)	17.001 (±0.082)
RH (%)	59.930 (±2.309)	41.292 (±2.309)	89.408 (±2.309)	89.373 (±2.309)	39.186 (±2.309)	64.088 (±2.309)	59.658 (±2.309)	60.280 (±2.309)	60.549 (±2.309)	59.966 (±2.309)
Refrigerant side										
P_c (bar)	10.942 (±0.080)	11.470 (±0.080)	9.034 (±0.080)	9.152 (±0.080)	12.629 (±0.080)	9.848 (±0.080)	10.019 (±0.080)	10.024 (±0.080)	10.075 (±0.080)	10.063 (±0.080)
P_e (bar)	29.923 (±0.060)	29.692 (±0.060)	31.289 (±0.060)	28.817 (±0.060)	32.139 (±0.060)	28.673 (±0.060)	31.032 (±0.060)	31.017 (±0.060)	31.057 (±0.060)	31.115 (±0.060)
P_r (-)	2.735 (±0.021)	2.589 (±0.019)	3.463 (±0.031)	3.149 (±0.028)	2.545 (±0.017)	2.911 (±0.024)	3.097 (±0.025)	3.094 (±0.025)	3.083 (±0.025)	3.092 (±0.025)
T_c (°C)	9.609 (±0.246)	11.199 (±0.237)	3.329 (±0.284)	3.744 (±0.281)	14.507 (±0.221)	6.121 (±0.266)	6.683 (±0.262)	6.700 (±0.262)	6.866 (±0.261)	6.828 (±0.262)
T_e (°C)	47.607 (±0.086)	46.972 (±0.087)	49.489 (±0.084)	45.869 (±0.089)	50.387 (±0.082)	45.285 (±0.090)	48.735 (±0.085)	48.716 (±0.085)	48.765 (±0.085)	48.844 (±0.085)
SC (K)	2.100 (±0.312)	1.676 (±0.312)	2.210 (±0.311)	2.243 (±0.313)	1.738 (±0.311)	1.880 (±0.313)	1.851 (±0.312)	1.832 (±0.312)	1.810 (±0.312)	1.825 (±0.312)
SH (K)	5.567 (±0.388)	5.307 (±0.382)	5.443 (±0.413)	5.442 (±0.411)	5.405 (±0.372)	5.417 (±0.401)	5.199 (±0.399)	5.370 (±0.399)	5.295 (±0.398)	5.277 (±0.398)
T_s (°C)	15.176 (±0.300)	16.507 (±0.300)	8.772 (±0.300)	9.186 (±0.300)	19.912 (±0.300)	11.537 (±0.300)	11.882 (±0.300)	12.070 (±0.300)	12.161 (±0.300)	12.106 (±0.300)
T_{dt} (°C)	84.990 (±0.300)	81.728 (±0.300)	93.879 (±0.300)	84.737 (±0.300)	83.705 (±0.300)	79.845 (±0.300)	82.572 (±0.300)	82.716 (±0.300)	82.562 (±0.300)	82.390 (±0.300)
$T_{ti,in}$ (°C)	-	-	-	-	-	-	-	-	-	-
$T_{ti,out}$ (°C)	-	-	-	-	-	-	-	-	-	-
$T_{to,in}$ (°C)	-	-	-	-	-	-	-	-	-	-
$T_{to,out}$ (°C)	-	-	-	-	-	-	-	-	-	-
$T_{ci,in}$ (°C)	80.713 (±0.300)	79.573 (±0.300)	90.180 (±0.300)	81.328 (±0.300)	81.301 (±0.300)	77.773 (±0.300)	80.629 (±0.300)	80.582 (±0.300)	80.475 (±0.300)	80.362 (±0.300)
$T_{ci,out}$ (°C)	46.496 (±0.300)	45.996 (±0.300)	48.499 (±0.300)	44.813 (±0.300)	49.553 (±0.300)	44.195 (±0.300)	47.894 (±0.300)	47.880 (±0.300)	47.924 (±0.300)	48.009 (±0.300)
$T_{coil,in}$ (°C)	10.169 (±0.300)	12.510 (±0.300)	4.692 (±0.300)	5.138 (±0.300)	15.897 (±0.300)	8.466 (±0.300)	9.265 (±0.300)	9.309 (±0.300)	9.488 (±0.300)	9.447 (±0.300)
$T_{coil,out}$ (°C)	15.039 (±0.300)	16.797 (±0.300)	8.689 (±0.300)	9.344 (±0.300)	20.336 (±0.300)	11.917 (±0.300)	12.515 (±0.300)	12.550 (±0.300)	12.664 (±0.300)	12.654 (±0.300)
Performance variables										
\dot{W}_c (W)	1258.721 (±16.294)	1591.803 (±17.960)	1703.368 (±18.517)	1555.577 (±17.778)	1730.749 (±18.654)	1911.622 (±19.559)	2076.740 (±20.384)	2076.789 (±20.384)	2077.332 (±20.387)	2079.268 (±20.397)
\dot{Q}_c (W)	5212.507 (±78.811)	7514.748 (±111.152)	6009.583 (±87.633)	5998.193 (±107.934)	8227.465 (±116.039)	8219.441 (±142.367)	8389.586 (±92.759)	8375.415 (±92.486)	8428.118 (±92.871)	8412.653 (±92.963)
\dot{Q}_s (W)	4365.000 (±66.910)	6383.000 (±95.810)	4825.000 (±71.390)	4985.000 (±90.520)	7017.000 (±100.700)	6996.000 (±122.400)	7118.000 (±80.840)	7110.000 (±80.640)	7158.000 (±81.030)	7152.000 (±81.190)

(Continued on Next Page...)

Table F.7: DHWA: Experimental results (continued)

	Test 11	Test 12	Test 13	Test 14	Test 15	Test 16	Test 17	Test 18	Test 19	Test 20
Compressor and fan speed										
f_c (Hz)	50	50	50	50	50	60	60	60	60	70
f_{fan} (%)	50	50	50	80	50	35	35	65	65	50
Secondary side										
T_{ci} (°C)	29.903 (+0.087)	30.034 (+0.087)	30.010 (+0.087)	29.942 (+0.087)	45.081 (+0.092)	19.910 (+0.083)	39.939 (+0.090)	19.957 (+0.083)	39.899 (+0.090)	29.991 (+0.087)
T_{co} (°C)	49.909 (+0.094)	50.032 (+0.094)	50.046 (+0.094)	49.994 (+0.094)	49.997 (+0.094)	49.927 (+0.094)	50.059 (+0.094)	49.920 (+0.094)	49.855 (+0.094)	49.961 (+0.094)
dT_c (K)	20.006 (+0.128)	19.999 (+0.128)	20.036 (+0.128)	20.052 (+0.128)	4.916 (+0.132)	30.017 (+0.126)	10.120 (+0.130)	29.963 (+0.126)	9.956 (+0.130)	19.969 (+0.128)
T_{ci} (°C)	-	-	-	-	-	-	-	-	-	-
T_{co} (°C)	-	-	-	-	-	-	-	-	-	-
dT_e (K)	-	-	-	-	-	-	-	-	-	-
\dot{m}_{user} (kg/h)	-	-	-	-	-	-	-	-	-	-
\dot{m}_{ground} (kg/h)	-	-	-	-	-	-	-	-	-	-
\dot{m}_{flow} (kg/h)	362.488 (+3.250)	263.952 (+3.119)	478.073 (+3.402)	374.483 (+3.266)	1503.091 (+4.948)	247.741 (+3.100)	918.423 (+4.032)	331.504 (+3.211)	786.480 (+3.836)	486.274 (+3.413)
T_{e}^{\dagger} (°C)	16.842 (+0.082)	5.018 (+0.079)	29.056 (+0.086)	17.004 (+0.082)	16.967 (+0.082)	10.893 (+0.080)	23.216 (+0.084)	22.879 (+0.084)	10.841 (+0.080)	16.901 (+0.082)
RH (%)	60.576 (+2.309)	73.108 (+2.341)	31.294 (+2.309)	59.904 (+2.309)	59.855 (+2.309)	88.107 (+2.309)	40.694 (+2.309)	41.517 (+2.309)	88.185 (+2.309)	59.106 (+2.309)
Refrigerant side										
P_e (bar)	10.041 (+0.080)	7.256 (+0.080)	13.379 (+0.080)	10.507 (+0.080)	10.189 (+0.080)	8.328 (+0.080)	10.538 (+0.080)	11.383 (+0.080)	8.833 (+0.080)	9.317 (+0.080)
P_c (bar)	31.012 (+0.060)	29.825 (+0.060)	31.859 (+0.060)	31.280 (+0.060)	33.190 (+0.060)	29.393 (+0.060)	32.722 (+0.060)	30.835 (+0.060)	32.077 (+0.060)	31.375 (+0.060)
P_r (-)	3.088 (+0.025)	4.111 (+0.046)	2.381 (+0.015)	2.977 (+0.023)	3.258 (+0.026)	3.529 (+0.035)	3.105 (+0.024)	2.709 (+0.020)	3.632 (+0.034)	3.368 (+0.030)
T_e (°C)	6.757 (+0.262)	-3.509 (+0.335)	16.527 (+0.211)	8.255 (+0.253)	7.237 (+0.259)	0.749 (+0.302)	8.354 (+0.253)	10.941 (+0.238)	2.607 (+0.289)	4.319 (+0.277)
T_c (°C)	48.701 (+0.085)	47.362 (+0.087)	49.495 (+0.084)	49.022 (+0.084)	51.755 (+0.080)	46.372 (+0.088)	50.801 (+0.082)	47.887 (+0.086)	50.182 (+0.083)	48.815 (+0.085)
SC (K)	1.811 (+0.312)	2.515 (+0.312)	1.352 (+0.311)	1.965 (+0.312)	1.943 (+0.311)	1.961 (+0.313)	1.567 (+0.311)	1.571 (+0.312)	2.143 (+0.311)	1.791 (+0.312)
SH (K)	5.217 (+0.398)	5.646 (+0.450)	5.252 (+0.367)	5.204 (+0.393)	5.287 (+0.396)	5.262 (+0.425)	5.203 (+0.392)	5.175 (+0.383)	5.315 (+0.416)	5.341 (+0.408)
T_e (°C)	11.973 (+0.300)	2.137 (+0.300)	21.779 (+0.300)	13.459 (+0.300)	12.524 (+0.300)	6.011 (+0.300)	13.557 (+0.300)	16.116 (+0.300)	7.922 (+0.300)	9.660 (+0.300)
T_c (°C)	82.155 (+0.300)	94.445 (+0.300)	81.197 (+0.300)	81.417 (+0.300)	87.422 (+0.300)	88.646 (+0.300)	88.668 (+0.300)	81.170 (+0.300)	91.598 (+0.300)	89.483 (+0.300)
$T_{e,in}$ (°C)	-	-	-	-	-	-	-	-	-	-
$T_{e,out}$ (°C)	-	-	-	-	-	-	-	-	-	-
$T_{g,in}$ (°C)	-	-	-	-	-	-	-	-	-	-
$T_{g,out}$ (°C)	-	-	-	-	-	-	-	-	-	-
$T_{d,in}$ (°C)	80.470 (+0.300)	90.266 (+0.300)	79.652 (+0.300)	79.278 (+0.300)	85.252 (+0.300)	86.381 (+0.300)	87.018 (+0.300)	79.354 (+0.300)	89.143 (+0.300)	87.184 (+0.300)
$T_{d,out}$ (°C)	47.901 (+0.300)	46.359 (+0.300)	48.700 (+0.300)	48.207 (+0.300)	50.992 (+0.300)	45.412 (+0.300)	50.085 (+0.300)	47.046 (+0.300)	49.333 (+0.300)	47.954 (+0.300)
$T_{oil,in}$ (°C)	9.359 (+0.300)	-1.217 (+0.300)	18.767 (+0.300)	10.845 (+0.300)	9.922 (+0.300)	4.056 (+0.300)	11.921 (+0.300)	14.288 (+0.300)	6.138 (+0.300)	8.749 (+0.300)
$T_{oil,out}$ (°C)	12.642 (+0.300)	2.208 (+0.300)	22.522 (+0.300)	14.212 (+0.300)	13.155 (+0.300)	6.516 (+0.300)	14.296 (+0.300)	16.942 (+0.300)	8.638 (+0.300)	10.415 (+0.300)
Performance variables										
\dot{W}_c (W)	2073.853 (+20.370)	1986.506 (+19.933)	2111.413 (+20.558)	2093.133 (+20.466)	2229.417 (+21.148)	2370.298 (+21.852)	2632.507 (+23.163)	2481.178 (+22.406)	2577.277 (+22.887)	2968.861 (+24.845)
\dot{Q}_c^{\ddagger} (W)	8414.914 (+92.789)	6124.123 (+82.438)	11115.330 (+106.359)	8713.345 (+94.267)	8533.015 (+231.457)	8630.140 (+114.017)	10775.813 (+146.814)	11528.633 (+121.795)	9078.914 (+126.936)	11268.705 (+107.158)
$\dot{Q}_{e,\S}$ (W)	7155.000 (+81.060)	4858.000 (+66.450)	9595.000 (+95.450)	7460.000 (+83.040)	7139.000 (+194.600)	7033.000 (+94.490)	8942.000 (+124.100)	9872.000 (+107.400)	7380.000 (+104.900)	9248.000 (+91.020)

* The reported uncertainties are considered as the expanded uncertainties considering a confidence interval of 95.45%;

† T_{e} is denoted as T_{ci} or T_{co} in the DSHP models depending on the operating mode of the R1PFHx (evaporator or condenser);

‡ Value corrected with the heat injected by the circulation pump;

§ The evaporator capacity is estimated from the refrigerant side;

G

Empirical models DSHP

CONTENTS

G.1	Introduction	g-1
G.2	Winter Ground	g-2
G.3	Summer Ground	g-5
G.4	DHW Ground	g-8
G.5	DHW User	g-11
G.6	Winter Air	g-14
G.7	Summer Air	g-17
G.8	DHW Air	g-20

G.1 Introduction

This appendix includes the \dot{W}_c , \dot{Q}_c and \dot{Q}_e models for all operating modes summarized in:

- A first table for each operating mode contains the \dot{W}_c/f_c , \dot{Q}_c/f_c and \dot{Q}_e/f_c polynomial models adjusted with the virtual database. In said table, the polynomial model prediction errors (MRE, RMSE and CV_{RMSE}) are calculated with respect to the simulation results, thus reconverting the values for the estimation of \dot{W}_c , \dot{Q}_c and \dot{Q}_e .
- A second table is also attached with values for the k_i adjustment coefficients obtained from the readjustments with the experimental data. In this case, the prediction errors are expressed with respect to the experimental results. Thus we can obtain the final regression models based on these two tables and Equation 3.24 on page 100.
- Lastly, a series of figures is included as a visual comparison of the adjustment of these models, the model adjusted with the virtual database and the final regression model readjusted with the experimental data.

G.2 Winter Ground

Table G.1: Winter Ground: Polynomial models adjusted with the virtual database

	\dot{W}_c / f_c (W/Hz)	\dot{Q}_c / f_c (W/Hz)	\dot{Q}_e / f_c (W/Hz)
(Int.)	1.162e+03 ($\pm 1.35e+01$)***	4.617e+03 ($\pm 7.31e+01$)***	3.710e+03 ($\pm 7.33e+01$)***
(T_{co}^2)	7.612e-03 ($\pm 1.00e-04$)***	9.011e-03 ($\pm 5.43e-04$)***	3.644e-03 ($\pm 5.45e-04$)***
T_{co}	-6.997e+00 ($\pm 6.74e-02$)***	-1.003e+01 ($\pm 3.65e-01$)***	-4.674e+00 ($\pm 3.66e-01$)***
(T_{eo}^2)	-3.968e-03 ($\pm 7.56e-05$)***	4.359e-02 ($\pm 4.09e-04$)***	4.690e-02 ($\pm 4.10e-04$)***
T_{eo}	-1.214e+00 ($\pm 4.83e-02$)***	-2.405e+01 ($\pm 2.62e-01$)***	-2.307e+01 ($\pm 2.62e-01$)***
dT_c	3.013e+00 ($\pm 7.38e-02$)***	2.669e-01 ($\pm 8.87e-03$)***	4.470e-01 ($\pm 8.90e-03$)***
dT_e	3.174e-02 ($\pm 1.74e-03$)***	8.238e-01 ($\pm 9.44e-03$)***	7.968e-01 ($\pm 9.47e-03$)***
f_c	-1.602e-01 ($\pm 1.08e-02$)***	2.826e-01 ($\pm 5.87e-02$)***	3.247e-01 ($\pm 5.89e-02$)***
($1/f_c$)	2.991e+02 ($\pm 2.53e+00$)***	-1.275e+02 ($\pm 1.37e+01$)***	-2.816e+02 ($\pm 1.38e+01$)***
$T_{co} \times T_{eo}$	1.089e-02 ($\pm 7.90e-05$)***	1.278e-02 ($\pm 4.27e-04$)***	3.737e-03 ($\pm 4.29e-04$)***
$T_{co} \times dT_c$	-1.029e-02 ($\pm 2.32e-04$)***		
$T_{eo} \times f_c$	1.125e-03 ($\pm 3.95e-05$)***	-1.270e-03 ($\pm 2.14e-04$)***	-1.814e-03 ($\pm 2.14e-04$)***
Num.Obs.	3125	3125	3125
R2 Adj.	1.000	0.999	0.999
AIC	-4384.6	6170.0	6187.4
MRE (%)	1.385	1.867	3.204
RMSE (W)	5.524	32.030	31.981
CV _{RMSE} (%)	0.293	0.477	0.596
Range (W)	[890, 3558]	[2415, 13500]	[1531, 11939]

^a + p < 0.1, * p < 0.05, ** p < 0.01, *** p < 0.001; Confidence interval of 95% for regression coefficients;

^b Temperatures (K);

^c Compressor frequency (Hz);

Table G.2: Winter Ground: Experimental readjustment

	\dot{W}_c^* (W)	\dot{Q}_c^* (W)	\dot{Q}_e^* (W)
$k_0(\dot{W}_{c0}, \dot{Q}_{c0}, \dot{Q}_{e0})$	1.000e+00 ($\pm 3.06e-03$)***	1.012e+00 ($\pm 5.66e-03$)***	1.007e+00 ($\pm 6.16e-03$)***
$k_1(x_1 = f_c)$	9.815e-01 ($\pm 1.27e-02$)***	9.997e-01 ($\pm 3.33e-02$)***	9.548e-01 ($\pm 3.68e-02$)***
$k_2(x_2 = T_{e0})$	1.070e+00 ($\pm 1.81e-01$)***	1.070e+00 ($\pm 4.47e-02$)***	1.084e+00 ($\pm 3.98e-02$)***
$k_3(x_3 = dT_e)$	1.274e+00 ($\pm 2.22e+00$)	7.679e-01 ($\pm 5.68e-01$)*	8.376e-01 ($\pm 5.06e-01$)**
$k_4(x_4 = T_{c0})$	1.046e+00 ($\pm 3.34e-02$)***	7.735e-01 ($\pm 2.14e-01$)***	9.212e-01 ($\pm 1.10e-01$)***
$k_5(x_5 = dT_c)$	1.163e+00 ($\pm 2.68e-01$)***		7.768e-01 ($\pm 8.94e-01$)+
Num.Obs.	30	30	30
R2 Adj.	1.000	1.000	1.000
AIC	255.2	368.1	359.8
MRE (%)	2.131	3.543	3.351
RMSE (W)	13.488	91.488	77.069
CV_{RMSE} (%)	0.720	1.354	1.434
Range (W)	[1292, 2663]	[4293, 9988]	[3233, 8517]

^a + p < 0.1, * p < 0.05, ** p < 0.01, *** p < 0.001; Confidence interval of 95% for regression coefficients;

^b Temperatures (K);

^c Compressor frequency (Hz);

CCD central point:

$$\dot{W}_{c0} = 1856.612 \text{ (W)} \quad \dot{Q}_{c0} = 5276.218 \text{ (W)} \quad T_{e0} = 273.184 \text{ (K)} \quad T_{c0} = 318.272 \text{ (K)}$$

$$\dot{Q}_{e0} = 6658.974 \text{ (W)} \quad f_{c0} = 50 \text{ (Hz)} \quad dT_{e0} = 4.972 \text{ (K)} \quad dT_{c0} = 5.078 \text{ (K)}$$

Partial derivatives at CCD center point:

$$\left. \frac{\partial \dot{W}_c}{\partial f_c} \right|_0 = 5.186e+01 \quad \left. \frac{\partial \dot{W}_c}{\partial dT_c} \right|_0 = -1.304e+01 \quad \left. \frac{\partial \dot{Q}_c}{\partial T_{c0}} \right|_0 = -3.992e+01 \quad \left. \frac{\partial \dot{Q}_e}{\partial T_{c0}} \right|_0 = -6.668e+01$$

$$\left. \frac{\partial \dot{W}_c}{\partial T_{e0}} \right|_0 = 7.033e+00 \quad \left. \frac{\partial \dot{Q}_c}{\partial f_c} \right|_0 = 1.315e+02 \quad \left. \frac{\partial \dot{Q}_e}{\partial f_c} \right|_0 = 1.027e+02 \quad \left. \frac{\partial \dot{Q}_e}{\partial dT_c} \right|_0 = 2.235e+01$$

$$\left. \frac{\partial \dot{W}_c}{\partial dT_e} \right|_0 = 1.587e+00 \quad \left. \frac{\partial \dot{Q}_c}{\partial T_{e0}} \right|_0 = 1.884e+02 \quad \left. \frac{\partial \dot{Q}_e}{\partial T_{e0}} \right|_0 = 1.824e+02$$

$$\left. \frac{\partial \dot{W}_c}{\partial T_{c0}} \right|_0 = 3.859e+01 \quad \left. \frac{\partial \dot{Q}_c}{\partial dT_e} \right|_0 = 4.119e+01 \quad \left. \frac{\partial \dot{Q}_e}{\partial dT_e} \right|_0 = 3.984e+01$$

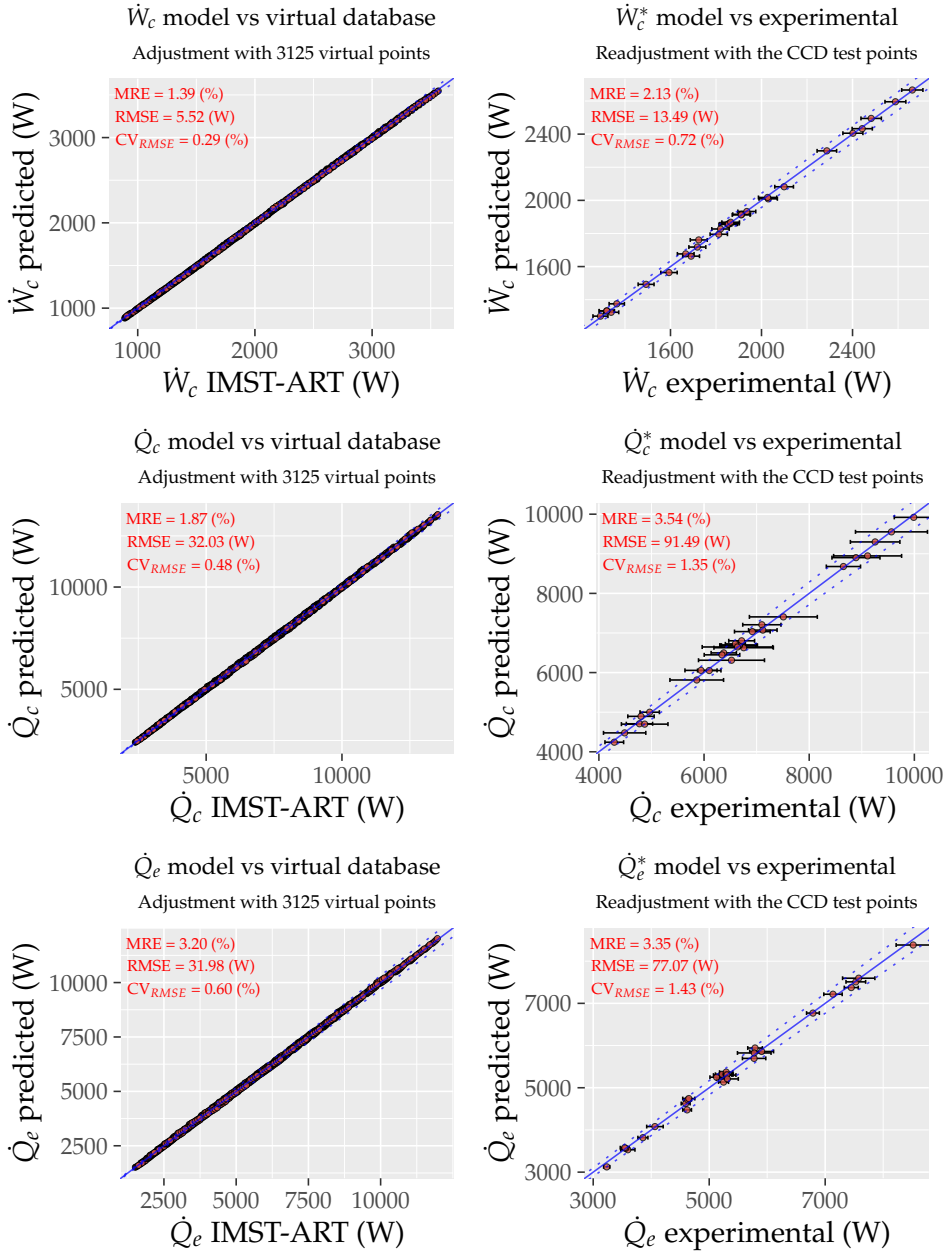


Figure G.1: Winter Ground mode: Empirical model

G.3 Summer Ground

Table G.3: Summer Ground: Polynomial models adjusted with the virtual database

	\dot{W}_c/f_c (W/Hz)	\dot{Q}_c/f_c (W/Hz)	\dot{Q}_e/f_c (W/Hz)
(Int.)	1.267e+03 ($\pm 1.82e+01$)***	6.361e+03 ($\pm 1.92e+02$)***	5.469e+03 ($\pm 1.94e+02$)***
$(T_{co})^2$	8.446e-03 ($\pm 1.03e-04$)***	7.825e-03 ($\pm 9.53e-04$)***	2.714e-03 ($\pm 9.64e-04$)***
T_{co}	-7.624e+00 ($\pm 5.66e-02$)***	-1.115e+01 ($\pm 5.41e-01$)***	-6.019e+00 ($\pm 5.46e-01$)***
$(T_{eo})^2$	-4.286e-03 ($\pm 2.23e-04$)***	6.029e-02 ($\pm 2.37e-03$)***	6.323e-02 ($\pm 2.39e-03$)***
T_{eo}	-1.186e+00 ($\pm 1.19e-01$)***	-3.540e+01 ($\pm 1.27e+00$)***	-3.430e+01 ($\pm 1.28e+00$)***
dT_c	1.429e+00 ($\pm 7.03e-02$)***	1.377e-01 ($\pm 1.34e-02$)***	2.019e-01 ($\pm 1.35e-02$)***
dT_e	-5.151e-02 ($\pm 1.19e-03$)***	1.321e+00 ($\pm 1.27e-02$)***	1.360e+00 ($\pm 1.29e-02$)***
f_c	-3.521e-01 ($\pm 1.52e-02$)***		
$(1/f_c)$	1.857e+02 ($\pm 1.86e+00$)***	-4.043e+02 ($\pm 1.97e+01$)***	-5.444e+02 ($\pm 2.00e+01$)***
$T_{co} \times T_{eo}$	1.125e-02 ($\pm 1.79e-04$)***	1.968e-02 ($\pm 1.89e-03$)***	1.091e-02 ($\pm 1.91e-03$)***
$T_{co} \times dT_c$	-5.116e-03 ($\pm 2.36e-04$)***		
$T_{eo} \times f_c$	1.653e-03 ($\pm 5.35e-05$)***	-6.639e-04 ($\pm 3.27e-05$)***	-9.717e-04 ($\pm 3.31e-05$)***
Num.Obs.	2096	2096	2096
R2 Adj.	0.999	0.998	0.998
AIC	-5147.7	4777.8	4823.0
MRE (%)	1.269	1.141	1.286
RMSE (W)	3.578	38.031	38.663
CV _{RMSE} (%)	0.287	0.373	0.417
Range (W)	[584, 2188]	[4869, 16826]	[4191, 15668]

^a + p < 0.1, * p < 0.05, ** p < 0.01, *** p < 0.001; Confidence interval of 95% for regression coefficients;

^b Temperatures (K);

^c Compressor frequency (Hz);

Table G.4: Summer Ground: Experimental readjustment

	\dot{W}_c^* (W)	\dot{Q}_c^* (W)	\dot{Q}_e^* (W)
$k_0(\dot{W}_{c0}, \dot{Q}_{c0}, \dot{Q}_{e0})$	9.870e-01 ($\pm 1.83\text{e-}02$)***	1.016e+00 ($\pm 2.51\text{e-}02$)***	9.851e-01 ($\pm 2.73\text{e-}02$)***
$k_1(x_1 = f_c)$	1.107e+00 ($\pm 5.63\text{e-}02$)***	9.696e-01 ($\pm 8.64\text{e-}02$)***	9.110e-01 ($\pm 9.17\text{e-}02$)***
$k_2(x_2 = T_{eo})$	5.389e-01 ($\pm 4.05\text{e-}01$)*	1.149e+00 ($\pm 2.53\text{e-}01$)***	1.087e+00 ($\pm 2.35\text{e-}01$)***
$k_3(x_3 = T_{co})$	1.088e+00 ($\pm 1.16\text{e-}01$)***	8.479e-01 ($\pm 7.73\text{e-}01$)*	8.874e-01 ($\pm 5.41\text{e-}01$)*
Num.Obs.	8	8	8
R2 Adj.	1.000	1.000	1.000
AIC	62.9	103.5	103.0
MRE (%)	1.087	2.235	2.122
RMSE (W)	6.612	83.672	80.695
CV _{RMSE} (%)	0.616	0.940	1.029
Range (W)	[577, 1588]	[6622, 11013]	[6021, 9434]

^a + p < 0.1, * p < 0.05, ** p < 0.01, *** p < 0.001; Confidence interval of 95% for regression coefficients;

^b Temperatures (K);

^c Compressor frequency (Hz);

CCD central point:

$$\dot{W}_{c0} = 1082.285 \text{ (W)} \quad \dot{Q}_{e0} = 8880.096 \text{ (W)} \quad T_{eo0} = 283.59 \text{ (K)}$$

$$\dot{Q}_{c0} = 9998.515 \text{ (W)} \quad f_{c0} = 50 \text{ (Hz)} \quad T_{co0} = 294.055 \text{ (K)}$$

Partial derivatives at CCD center point:

$$\left. \frac{\partial \dot{W}_c}{\partial f_c} \right|_0 = 2.381\text{e}+01 \quad \left. \frac{\partial \dot{Q}_c}{\partial f_c} \right|_0 = 1.963\text{e}+02 \quad \left. \frac{\partial \dot{Q}_e}{\partial f_c} \right|_0 = 1.783\text{e}+02$$

$$\left. \frac{\partial \dot{W}_c}{\partial T_{eo}} \right|_0 = -1.123\text{e}+01 \quad \left. \frac{\partial \dot{Q}_c}{\partial T_{eo}} \right|_0 = 2.273\text{e}+02 \quad \left. \frac{\partial \dot{Q}_e}{\partial T_{eo}} \right|_0 = 2.359\text{e}+02$$

$$\left. \frac{\partial \dot{W}_c}{\partial T_{co}} \right|_0 = 2.547\text{e}+01 \quad \left. \frac{\partial \dot{Q}_c}{\partial T_{co}} \right|_0 = -4.824\text{e}+01 \quad \left. \frac{\partial \dot{Q}_e}{\partial T_{co}} \right|_0 = -6.648\text{e}+01$$

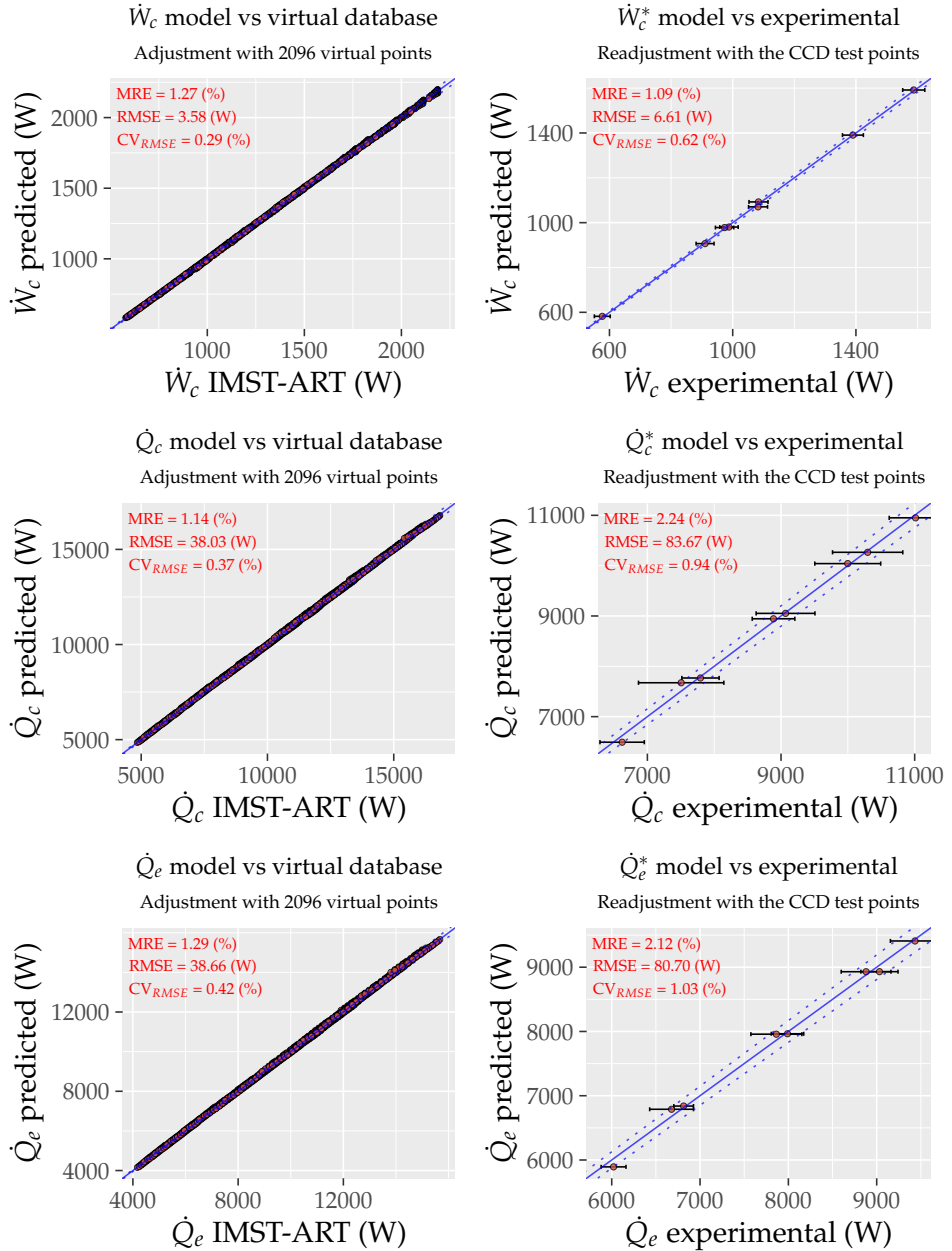


Figure G.2: Summer Ground mode: Empirical model

G.4 DHW Ground

Table G.5: DHW Ground: Polynomial models adjusted with the virtual database

	\dot{W}_c / f_c (W/Hz)	\dot{Q}_c / f_c (W/Hz)	\dot{Q}_e / f_c (W/Hz)
<i>(Int.)</i>	9.213e+02 ($\pm 6.27e+01$)***	2.666e+03 ($\pm 8.42e+01$)***	2.276e+03 ($\pm 9.37e+01$)***
(T_{co}^2)	4.745e-03 ($\pm 5.66e-04$)***		
T_{co}	-5.277e+00 ($\pm 3.74e-01$)***	-9.170e-01 ($\pm 2.46e-01$)***	1.116e+00 ($\pm 2.73e-01$)***
(T_{eo}^2)	-3.769e-03 ($\pm 5.44e-05$)***	4.408e-02 ($\pm 3.13e-04$)***	4.739e-02 ($\pm 3.49e-04$)***
T_{eo}	-1.485e+00 ($\pm 5.88e-02$)***	-2.056e+01 ($\pm 3.38e-01$)***	-1.948e+01 ($\pm 3.76e-01$)***
(dT_c^2)	2.853e-03 ($\pm 4.77e-05$)***		
dT_c	2.271e+00 ($\pm 4.30e-02$)***	1.839e-01 ($\pm 2.66e-03$)***	3.434e-01 ($\pm 2.96e-03$)***
dT_e	5.316e-02 ($\pm 2.38e-03$)***	9.658e-01 ($\pm 1.37e-02$)***	9.227e-01 ($\pm 1.52e-02$)***
f_c	-2.510e-01 ($\pm 1.08e-02$)***		
$(1/f_c)$	3.284e+02 ($\pm 3.57e+00$)***	-1.533e+02 ($\pm 2.03e+01$)***	-3.142e+02 ($\pm 2.26e+01$)***
$T_{co} \times T_{eo}$	1.137e-02 ($\pm 1.53e-04$)***	9.794e-04 ($\pm 8.84e-04$)*	-8.406e-03 ($\pm 9.83e-04$)***
$T_{co} \times dT_c$	-8.011e-03 ($\pm 1.31e-04$)***		
$T_{eo} \times f_c$	1.522e-03 ($\pm 3.84e-05$)***	-2.976e-04 ($\pm 3.50e-05$)***	-7.576e-04 ($\pm 3.89e-05$)***
Num.Obs.	3125	3125	3125
R2 Adj.	0.999	1.000	0.999
AIC	-2235.7	8700.7	9367.3
MRE (%)	1.506	4.259	7.834
RMSE (W)	8.963	50.027	56.302
CV _{RMSE} (%)	0.411	0.658	0.929
Range (W)	[999, 4107]	[2313, 16783]	[1391, 14773]

^a + p < 0.1, * p < 0.05, ** p < 0.01, *** p < 0.001; Confidence interval of 95% for regression coefficients;

^b Temperatures (K);

^c Compressor frequency (Hz);

Table G.6: DHW Ground: Experimental readjustment

	\dot{W}_c^* (W)	\dot{Q}_c^* (W)	\dot{Q}_e^* (W)
$k_0(\dot{W}_{c0}, \dot{Q}_{c0}, \dot{Q}_{e0})$	1.033e+00 ($\pm 5.11e-03$)***	9.714e-01 ($\pm 9.38e-03$)***	9.886e-01 ($\pm 5.94e-03$)***
$k_1(x_1 = f_c)$	1.007e+00 ($\pm 3.00e-02$)***	9.586e-01 ($\pm 5.42e-02$)***	9.122e-01 ($\pm 3.57e-02$)***
$k_2(x_2 = T_{e0})$	1.197e+00 ($\pm 1.83e-01$)***	1.031e+00 ($\pm 4.79e-02$)***	1.047e+00 ($\pm 2.57e-02$)***
$k_3(x_3 = dT_e)$	3.517e-01 ($\pm 2.45e+00$)	9.280e-01 ($\pm 8.88e-01$)*	1.041e+00 ($\pm 4.83e-01$)***
$k_4(x_4 = dT_c)$	9.181e-01 ($\pm 1.21e-01$)***		7.931e-01 ($\pm 2.46e-01$)***
Num.Obs.	20	20	20
R2 Adj.	1.000	1.000	1.000
AIC	186.4	261.3	235.6
MRE (%)	1.756	4.721	2.100
RMSE (W)	18.918	129.369	64.792
CV _{RMSE} (%)	0.927	1.732	1.046
Range (W)	[1451, 2910]	[4436, 11425]	[3437, 10005]

^a + p < 0.1, * p < 0.05, ** p < 0.01, *** p < 0.001; Confidence interval of 95% for regression coefficients;

^b Temperatures (K);

^c Compressor frequency (Hz);

CCD central point:

$$\dot{W}_{c0} = 2038.856 \text{ (W)} \quad \dot{Q}_{c0} = 6012.805 \text{ (W)} \quad T_{e0} = 278.163 \text{ (K)} \quad dT_{c0} = 20.049 \text{ (K)}$$

$$\dot{Q}_{c0} = 7315.763 \text{ (W)} \quad f_{c0} = 50 \text{ (Hz)} \quad dT_{e0} = 4.974 \text{ (K)}$$

Partial derivatives at CCD center point:

$$\left. \frac{\partial \dot{W}_c}{\partial f_c} \right|_0 = 4.119e+01 \quad \left. \frac{\partial \dot{W}_c}{\partial dT_c} \right|_0 = -1.020e+01 \quad \left. \frac{\partial \dot{Q}_c}{\partial dT_e} \right|_0 = 4.829e+01 \quad \left. \frac{\partial \dot{Q}_e}{\partial dT_e} \right|_0 = 4.614e+01$$

$$\left. \frac{\partial \dot{W}_c}{\partial T_{e0}} \right|_0 = 8.459e+00 \quad \left. \frac{\partial \dot{Q}_c}{\partial f_c} \right|_0 = 1.498e+02 \quad \left. \frac{\partial \dot{Q}_e}{\partial f_c} \right|_0 = 1.184e+02 \quad \left. \frac{\partial \dot{Q}_e}{\partial dT_c} \right|_0 = 1.717e+01$$

$$\left. \frac{\partial \dot{W}_c}{\partial dT_e} \right|_0 = 2.658e+00 \quad \left. \frac{\partial \dot{Q}_c}{\partial T_{e0}} \right|_0 = 2.132e+02 \quad \left. \frac{\partial \dot{Q}_e}{\partial T_{e0}} \right|_0 = 2.063e+02$$

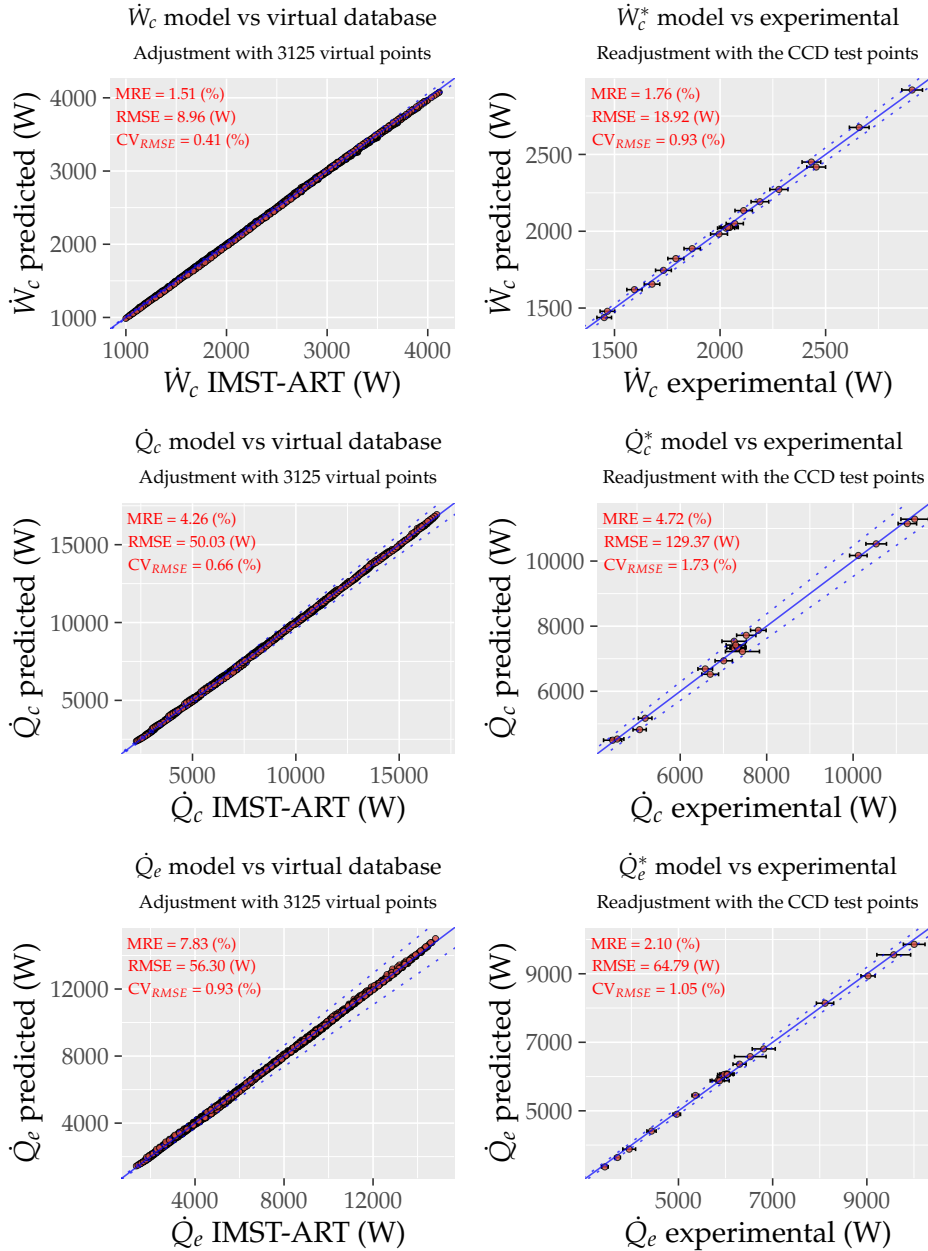


Figure G.3: DHW Ground mode: Empirical model

G.5 DHW User

Table G.7: DHW User: Polynomial models adjusted with the virtual database

	\dot{W}_c/f_c (W/Hz)	\dot{Q}_c/f_c (W/Hz)	\dot{Q}_e/f_c (W/Hz)
(Int.)	8.516e+02 ($\pm 6.26e+01$)***	2.085e+03 ($\pm 2.36e+02$)***	1.767e+03 ($\pm 2.85e+02$)***
(T_{co}^2)	4.540e-03 ($\pm 4.54e-04$)***		
T_{co}	-5.095e+00 ($\pm 3.11e-01$)***	1.393e+00 ($\pm 5.44e-01$)***	3.245e+00 ($\pm 6.56e-01$)***
(T_{eo}^2)	-4.236e-03 ($\pm 3.15e-04$)***	4.654e-02 ($\pm 1.90e-03$)***	5.003e-02 ($\pm 2.29e-03$)***
T_{eo}	-1.188e+00 ($\pm 2.08e-01$)***	-1.923e+01 ($\pm 1.25e+00$)***	-1.845e+01 ($\pm 1.51e+00$)***
(dT_c^2)	2.879e-03 ($\pm 3.83e-05$)***		
dT_c	2.183e+00 ($\pm 3.44e-02$)***	1.604e-01 ($\pm 2.23e-03$)***	3.302e-01 ($\pm 2.69e-03$)***
dT_e	4.699e-02 ($\pm 1.85e-03$)***	1.425e+00 ($\pm 1.12e-02$)***	1.387e+00 ($\pm 1.35e-02$)***
f_c	-3.203e-01 ($\pm 2.26e-02$)***		
$(1/f_c)$	3.372e+02 ($\pm 2.86e+00$)***	-1.982e+02 ($\pm 1.72e+01$)***	-4.137e+02 ($\pm 2.08e+01$)***
$T_{co} \times T_{eo}$	1.121e-02 ($\pm 3.16e-04$)***	-7.054e-03 ($\pm 1.91e-03$)***	-1.585e-02 ($\pm 2.30e-03$)***
$T_{co} \times dT_c$	-7.767e-03 ($\pm 1.05e-04$)***		
$T_{eo} \times f_c$	1.786e-03 ($\pm 7.91e-05$)***	-3.569e-04 ($\pm 2.89e-05$)***	-8.473e-04 ($\pm 3.49e-05$)***
Num.Obs.	3125	3125	3125
R2 Adj.	0.999	0.999	0.998
AIC	-3617.9	7606.1	8775.3
MRE (%)	1.150	1.458	2.587
RMSE (W)	7.123	39.704	49.260
CV _{RMSE} (%)	0.313	0.432	0.655
Range (W)	[1104, 4072]	[4297, 15772]	[3145, 13731]

^a + p < 0.1, * p < 0.05, ** p < 0.01, *** p < 0.001; Confidence interval of 95% for regression coefficients;

^b Temperatures (K);

^c Compressor frequency (Hz);

Table G.8: DHW User: Experimental readjustment

	\dot{W}_c^* (W)	\dot{Q}_c^* (W)	\dot{Q}_e^* (W)
$k_0(\dot{W}_{c0}, \dot{Q}_{c0}, \dot{Q}_{e0})$	1.032e+00 ($\pm 4.05e-03$)***	9.968e-01 ($\pm 6.40e-03$)***	9.660e-01 ($\pm 4.09e-03$)***
$k_1(x_1 = f_c)$	1.029e+00 ($\pm 2.20e-02$)***	1.021e+00 ($\pm 3.59e-02$)***	9.548e-01 ($\pm 2.27e-02$)***
$k_2(x_2 = T_{eo})$	8.159e-01 ($\pm 5.83e-01$)**	1.031e+00 ($\pm 8.98e-02$)***	1.031e+00 ($\pm 4.76e-02$)***
$k_3(x_3 = dT_e)$	4.703e-01 ($\pm 2.29e+00$)	1.226e+00 ($\pm 5.32e-01$)***	1.324e+00 ($\pm 2.84e-01$)***
$k_4(x_4 = dT_c)$	8.079e-01 ($\pm 9.38e-02$)***		8.725e-01 ($\pm 2.22e-01$)***
Num.Obs.	20	20	20
R2 Adj.	1.000	1.000	1.000
AIC	177.8	255.5	229.9
MRE (%)	1.505	2.776	1.672
RMSE (W)	15.290	111.968	56.137
CV _{RMSE} (%)	0.730	1.208	0.745
Range (W)	[1261, 3011]	[5515, 12998]	[4596, 10401]

^a + p < 0.1, * p < 0.05, ** p < 0.01, *** p < 0.001; Confidence interval of 95% for regression coefficients;

^b Temperatures (K);

^c Compressor frequency (Hz);

CCD central point:

$$\dot{W}_{c0} = 2083.81 \text{ (W)} \quad \dot{Q}_{e0} = 7575.931 \text{ (W)} \quad T_{eo0} = 285.111 \text{ (K)} \quad dT_{c0} = 20.021 \text{ (K)}$$

$$\dot{Q}_{c0} = 9296.505 \text{ (W)} \quad f_{c0} = 50 \text{ (Hz)} \quad dT_{e0} = 5.031 \text{ (K)}$$

Partial derivatives at CCD center point:

$$\left. \frac{\partial \dot{W}_c}{\partial f_c} \right|_0 = 4.281e+01 \quad \left. \frac{\partial \dot{W}_c}{\partial dT_c} \right|_0 = -1.063e+01 \quad \left. \frac{\partial \dot{Q}_c}{\partial dT_e} \right|_0 = 7.123e+01 \quad \left. \frac{\partial \dot{Q}_e}{\partial dT_e} \right|_0 = 6.935e+01$$

$$\left. \frac{\partial \dot{W}_c}{\partial T_{eo}} \right|_0 = 5.470e+00 \quad \left. \frac{\partial \dot{Q}_c}{\partial f_c} \right|_0 = 1.848e+02 \quad \left. \frac{\partial \dot{Q}_e}{\partial f_c} \right|_0 = 1.522e+02 \quad \left. \frac{\partial \dot{Q}_e}{\partial dT_c} \right|_0 = 1.651e+01$$

$$\left. \frac{\partial \dot{W}_c}{\partial dT_e} \right|_0 = 2.350e+00 \quad \left. \frac{\partial \dot{Q}_c}{\partial T_{eo}} \right|_0 = 2.503e+02 \quad \left. \frac{\partial \dot{Q}_e}{\partial T_{eo}} \right|_0 = 2.459e+02$$

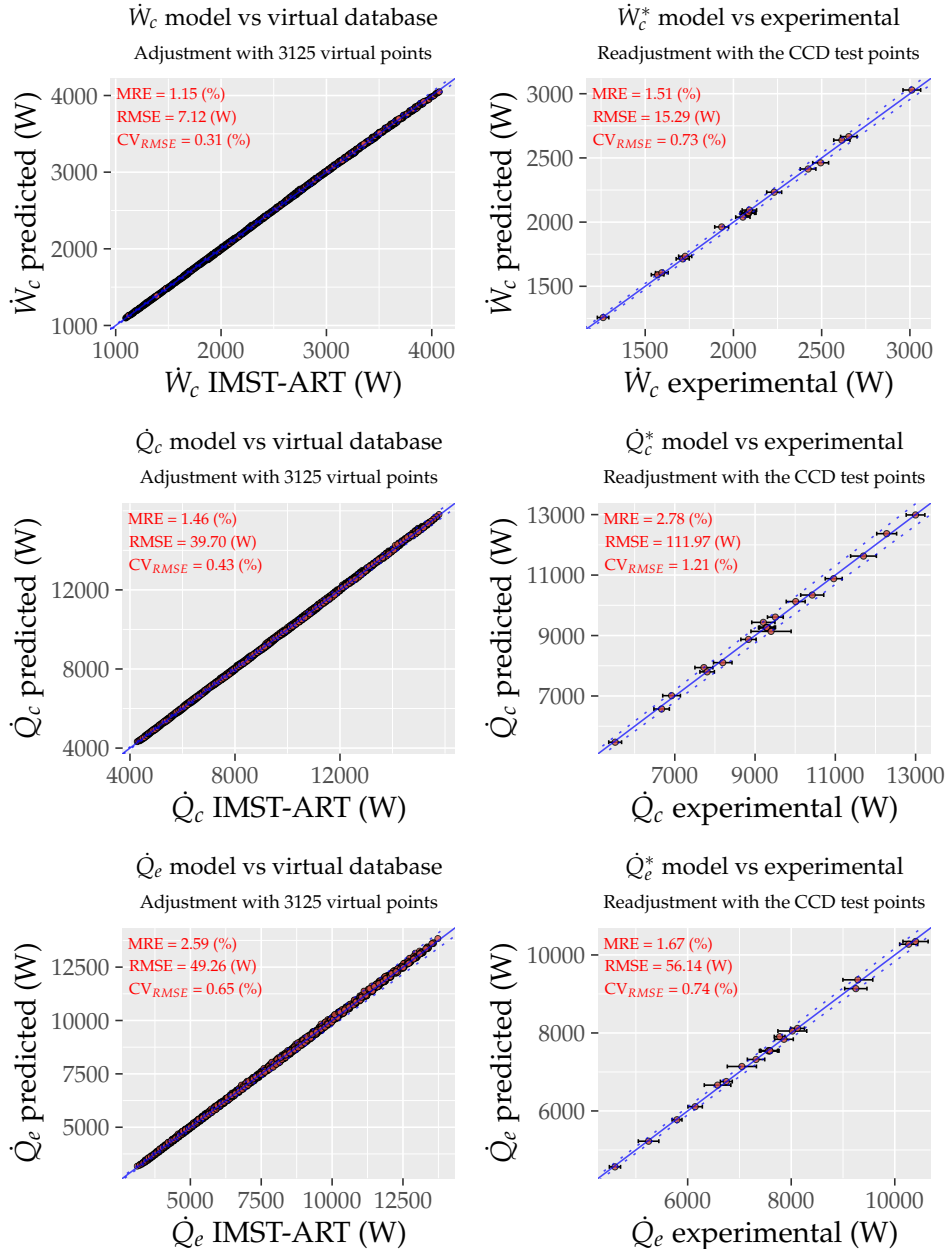


Figure G.4: DHW User mode: Empirical model

G.6 Winter Air

Table G.9: Winter Air: Polynomial models adjusted with the virtual database

	\dot{W}_c/f_c (W/Hz)	\dot{Q}_c/f_c (W/Hz)	\dot{Q}_e/f_c (W/Hz)
(Int.)	1.022e+03 ($\pm 2.73e+01$)***	-1.255e+03 ($\pm 1.62e+01$)***	-1.073e+03 ($\pm 1.45e+01$)***
(T_{co}^2)	7.564e-03 ($\pm 1.33e-04$)***		
T_{co}	-6.643e+00 ($\pm 9.46e-02$)***	-6.682e-01 ($\pm 6.64e-03$)***	-1.275e+00 ($\pm 5.94e-03$)***
(T_{ei}^2)	-4.325e-03 ($\pm 2.42e-04$)***		
T_{ei}	-6.008e-01 ($\pm 1.45e-01$)***	5.833e+00 ($\pm 5.57e-02$)***	5.806e+00 ($\pm 4.98e-02$)***
dT_c	2.873e+00 ($\pm 9.81e-02$)***	2.098e-01 ($\pm 1.83e-02$)***	4.023e-01 ($\pm 1.64e-02$)***
($1/f_{fan}$)	-3.337e+00 ($\pm 9.72e-01$)***	1.347e+04 ($\pm 4.31e+02$)***	1.348e+04 ($\pm 3.85e+02$)***
f_c	-1.608e-01 ($\pm 2.16e-02$)***	4.969e+00 ($\pm 2.60e-01$)***	5.044e+00 ($\pm 2.32e-01$)***
($1/f_c$)	2.969e+02 ($\pm 3.41e+00$)***	-4.158e+02 ($\pm 2.93e+01$)***	-5.731e+02 ($\pm 2.62e+01$)***
$T_{co} \times T_{ei}$	9.634e-03 ($\pm 1.47e-04$)***		
$T_{co} \times dT_c$	-9.887e-03 ($\pm 3.08e-04$)***		
$T_{ei} \times f_c$	1.113e-03 ($\pm 7.56e-05$)***	-1.825e-02 ($\pm 8.97e-04$)***	-1.893e-02 ($\pm 8.03e-04$)***
$\Delta w'$		-2.626e+03 ($\pm 3.43e+02$)***	-2.723e+03 ($\pm 3.07e+02$)***
$\Delta w' \times f_c$		9.920e+01 ($\pm 6.75e+00$)***	9.865e+01 ($\pm 6.04e+00$)***
$T_{ei} \times (1/f_{fan})$		-4.701e+01 ($\pm 1.51e+00$)***	-4.707e+01 ($\pm 1.35e+00$)***
($1/f_{fan}$) $\times f_c$		-1.027e+01 ($\pm 6.64e-01$)***	-1.003e+01 ($\pm 5.94e-01$)***
Num.Obs.	2375	2375	2375
R2 Adj.	0.999	0.997	0.998
AIC	-2627.1	7485.9	6955.2
MRE (%)	1.806	2.465	2.891
RMSE (W)	6.319	58.656	51.994
CV _{RMSE} (%)	0.333	0.720	0.766
Range (W)	[872, 3586]	[3826, 14063]	[2829, 12507]

^a + p < 0.1, * p < 0.05, ** p < 0.01, *** p < 0.001; Confidence interval of 95% for regression coefficients;

^b Temperatures (K);

^c Compressor frequency (Hz);

^d Fan frequency (%);

^e $\Delta w'$ (kg_{water}/kg_{dry air});

^f $\delta T_e = 6$ K;

Table G.10: Winter Air: Experimental readjustment

	\dot{W}_c^* (W)	\dot{Q}_c^* (W)	\dot{Q}_e^* (W)
$k_0(\dot{W}_{c0}, \dot{Q}_{c0}, \dot{Q}_{e0})$	9.985e-01 ($\pm 2.68\text{e-}03$)***	9.244e-01 ($\pm 7.08\text{e-}03$)***	9.336e-01 ($\pm 8.27\text{e-}03$)***
$k_1(x_1 = f_c)$	9.924e-01 ($\pm 1.42\text{e-}02$)***	9.118e-01 ($\pm 2.41\text{e-}02$)***	9.120e-01 ($\pm 2.92\text{e-}02$)***
$k_2(x_2 = T_{ei})$	1.024e+00 ($\pm 4.67\text{e-}01$)***	9.588e-01 ($\pm 6.59\text{e-}02$)***	1.020e+00 ($\pm 6.63\text{e-}02$)***
$k_3(x_3 = f_{fan})$	5.713e+00 ($\pm 5.65\text{e+}00$)*	1.395e+00 ($\pm 3.27\text{e-}01$)***	1.603e+00 ($\pm 3.27\text{e-}01$)***
$k_4(x_4 = T_{co})$	9.852e-01 ($\pm 2.65\text{e-}02$)***	8.280e-01 ($\pm 2.39\text{e-}01$)***	9.077e-01 ($\pm 1.24\text{e-}01$)***
$k_5(x_5 = dT_c)$	1.107e+00 ($\pm 2.35\text{e-}01$)***		
$k_6(x_6 = \Delta w')$		1.066e+00 ($\pm 5.93\text{e-}01$)**	1.826e+00 ($\pm 6.21\text{e-}01$)***
Num.Obs.	30	30	30
R2 Adj.	1.000	1.000	1.000
AIC	248.2	365.1	364.5
MRE (%)	1.966	2.783	3.325
RMSE (W)	12.000	84.117	83.303
CV_{RMSE} (%)	0.629	1.095	1.302
Range (W)	[1176, 2740]	[4763, 10699]	[3945, 8828]

^a + p < 0.1, * p < 0.05, ** p < 0.01, *** p < 0.001; Confidence interval of 95% for regression coefficients;

^b Temperatures (K);

^c Compressor frequency (Hz);

^d Fan frequency (%);

^e $\Delta w'$ (kg_{water}/kg_{dry air});

^f $\delta T_c = 6$ K;

CCD central point:

$$\dot{W}_{c0} = 1897.929 \text{ (W)} \quad f_{c0} = 50 \text{ (Hz)} \quad T_{co0} = 318.163 \text{ (K)}$$

$$\dot{Q}_{c0} = 7845.713 \text{ (W)} \quad T_{ei0} = 284.156 \text{ (K)} \quad dT_{c0} = 4.994 \text{ (K)}$$

$$\dot{Q}_{e0} = 6646.5 \text{ (W)} \quad f_{fan0} = 50 \text{ (%)} \quad \Delta w'_0 = 0.00181 \text{ (kg}_{water}\text{/kg}_{dry air})}$$

Partial derivatives at CCD center point:

$$\left. \frac{\partial \dot{W}_c}{\partial f_c} \right|_0 = 3.979\text{e+}01 \quad \left. \frac{\partial \dot{W}_c}{\partial dT_c} \right|_0 = -1.362\text{e+}01 \quad \left. \frac{\partial \dot{Q}_c}{\partial T_{co}} \right|_0 = -3.341\text{e+}01 \quad \left. \frac{\partial \dot{Q}_e}{\partial f_{fan}} \right|_0 = 8.002\text{e+}00$$

$$\left. \frac{\partial \dot{W}_c}{\partial T_{ei}} \right|_0 = 3.092\text{e+}00 \quad \left. \frac{\partial \dot{Q}_c}{\partial f_c} \right|_0 = 1.643\text{e+}02 \quad \left. \frac{\partial \dot{Q}_c}{\partial \Delta w'} \right|_0 = 1.167\text{e+}05 \quad \left. \frac{\partial \dot{Q}_e}{\partial T_{co}} \right|_0 = -6.374\text{e+}01$$

$$\left. \frac{\partial \dot{W}_c}{\partial f_{fan}} \right|_0 = 6.673\text{e-}02 \quad \left. \frac{\partial \dot{Q}_c}{\partial T_{ei}} \right|_0 = 1.990\text{e+}02 \quad \left. \frac{\partial \dot{Q}_e}{\partial f_c} \right|_0 = 1.343\text{e+}02 \quad \left. \frac{\partial \dot{Q}_e}{\partial \Delta w'} \right|_0 = 1.105\text{e+}05$$

$$\left. \frac{\partial \dot{W}_c}{\partial T_{co}} \right|_0 = 4.294\text{e+}01 \quad \left. \frac{\partial \dot{Q}_c}{\partial f_{fan}} \right|_0 = 8.081\text{e+}00 \quad \left. \frac{\partial \dot{Q}_e}{\partial T_{ei}} \right|_0 = 1.959\text{e+}02$$

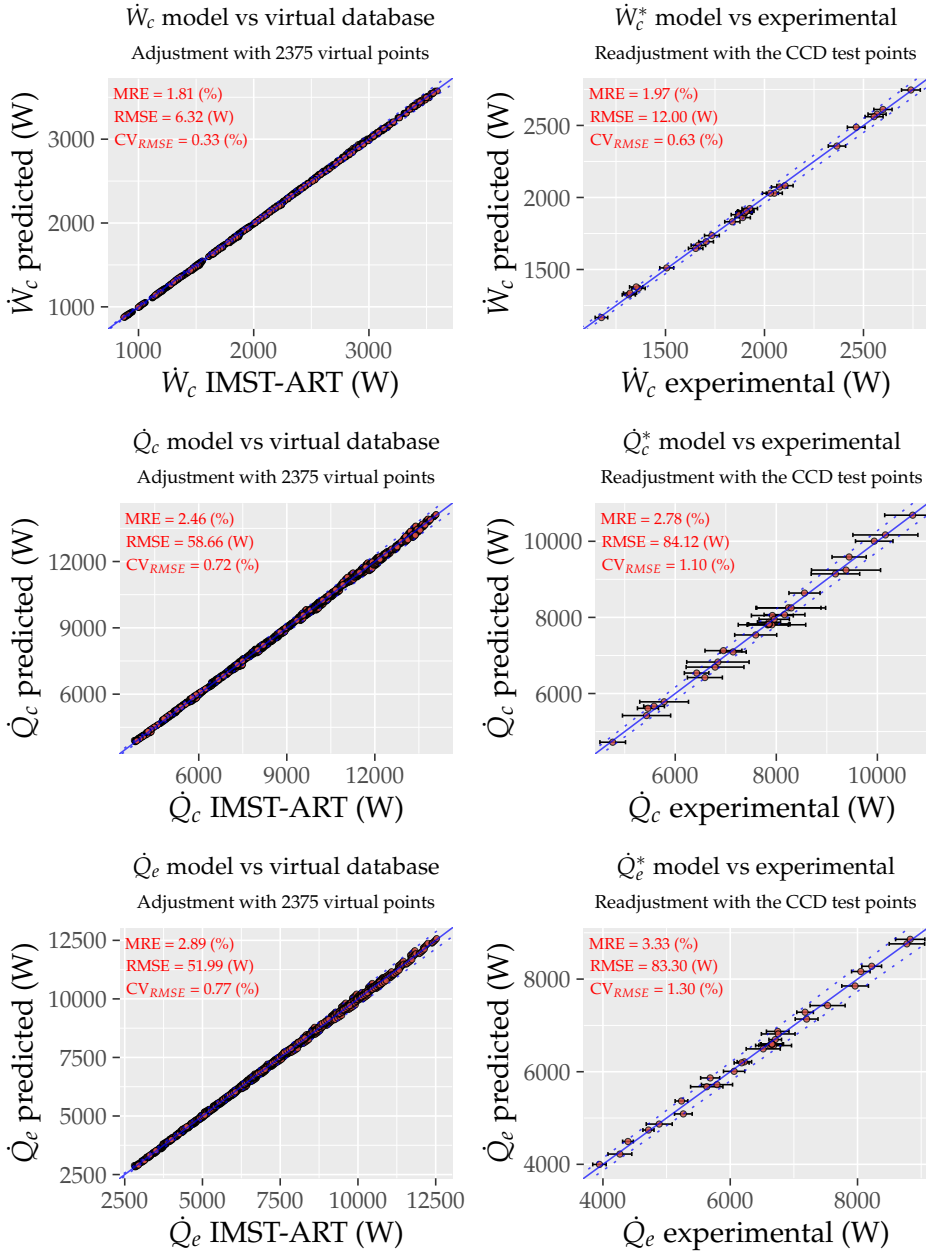


Figure G.5: Winter Air mode: Empirical model

G.7 Summer Air

Table G.11: Summer Air: Polynomial models adjusted with the virtual database

	\dot{W}_c/f_c (W/Hz)	\dot{Q}_c/f_c (W/Hz)	\dot{Q}_e/f_c (W/Hz)
(Int.)	1.946e+03 ($\pm 1.93\text{e}+01$)***	3.700e+03 ($\pm 1.62\text{e}+02$)***	3.787e+03 ($\pm 1.57\text{e}+02$)***
T_{ci}	-8.491e+00 ($\pm 8.54\text{e}-02$)***	-7.865e-01 ($\pm 3.62\text{e}-03$)***	-1.334e+00 ($\pm 3.49\text{e}-03$)***
T_{eo}	-4.827e+00 ($\pm 6.11\text{e}-02$)***	-2.765e+01 ($\pm 1.14\text{e}+00$)***	-2.750e+01 ($\pm 1.10\text{e}+00$)***
dT_e	1.591e-02 ($\pm 2.65\text{e}-03$)***	-7.937e+00 ($\pm 7.96\text{e}-01$)***	-7.889e+00 ($\pm 7.68\text{e}-01$)***
$(1/f_{fan})$	-3.872e+03 ($\pm 8.83\text{e}+01$)***	6.246e+02 ($\pm 3.51\text{e}+02$)***	2.578e+03 ($\pm 3.39\text{e}+02$)***
f_c	-2.067e+00 ($\pm 3.76\text{e}-02$)***	4.075e-01 ($\pm 1.51\text{e}-01$)***	1.572e+00 ($\pm 1.46\text{e}-01$)***
(T_{ci}^2)	8.178e-03 ($\pm 1.15\text{e}-04$)**		
$(1/f_c)$	2.261e+02 ($\pm 4.28\text{e}+00$)***	-2.868e+02 ($\pm 1.85\text{e}+01$)***	-4.170e+02 ($\pm 1.78\text{e}+01$)***
$T_{ci} \times T_{eo}$	1.467e-02 ($\pm 1.98\text{e}-04$)**		
$T_{ci} \times (1/f_{fan})$	4.046e+00 ($\pm 1.42\text{e}-01$)***		
$T_{ci} \times f_c$	1.673e-03 ($\pm 6.18\text{e}-05$)***		
$T_{eo} \times (1/f_{fan})$	9.272e+00 ($\pm 2.80\text{e}-01$)***	-2.933e+00 ($\pm 1.23\text{e}+00$)***	-1.031e+01 ($\pm 1.19\text{e}+00$)***
$T_{eo} \times f_c$	6.031e-03 ($\pm 1.21\text{e}-04$)***	-2.277e-03 ($\pm 5.29\text{e}-04$)***	-6.927e-03 ($\pm 5.10\text{e}-04$)***
$(1/f_{fan}) \times f_c$	4.707e+00 ($\pm 9.67\text{e}-02$)***		
(T_{eo}^2)		5.691e-02 ($\pm 2.00\text{e}-03$)***	5.724e-02 ($\pm 1.93\text{e}-03$)***
(dT_e^2)		-9.823e-02 ($\pm 6.05\text{e}-03$)***	-9.787e-02 ($\pm 5.84\text{e}-03$)***
$T_{eo} \times dT_e$		3.640e-02 ($\pm 2.78\text{e}-03$)***	3.618e-02 ($\pm 2.68\text{e}-03$)***
Num.Obs.	2297	2297	2297
R2 Adj.	0.999	0.999	0.999
AIC	-1717.4	5106.6	4938.1
MRE (%)	3.355	1.477	1.894
RMSE (W)	8.381	36.179	35.344
CV_{RMSE} (%)	0.534	0.375	0.417
Range (W)	[611, 3356]	[4613, 16780]	[3757, 15563]

^a + p < 0.1, * p < 0.05, ** p < 0.01, *** p < 0.001; Confidence interval of 95% for regression coefficients;

^b Temperatures (K);

^c Compressor frequency (Hz);

^d Fan frequency (%);

Table G.12: Summer Air: Experimental readjustment

	\dot{W}_c^* (W)	\dot{Q}_c^* (W)	\dot{Q}_e^* (W)
$k_0(\dot{W}_{c0}, \dot{Q}_{c0}, \dot{Q}_{e0})$	1.043e+00 ($\pm 2.95e-03$)***	9.646e-01 ($\pm 4.28e-03$)***	9.684e-01 ($\pm 3.58e-03$)***
$k_1(x_1 = f_c)$	1.054e+00 ($\pm 1.38e-02$)***	9.142e-01 ($\pm 2.38e-02$)***	9.104e-01 ($\pm 2.09e-02$)***
$k_2(x_2 = T_{ci})$	1.036e+00 ($\pm 2.42e-02$)***	1.323e+00 ($\pm 2.01e-01$)***	1.205e+00 ($\pm 8.84e-02$)***
$k_3(x_3 = f_{fan})$	1.135e+00 ($\pm 7.80e-02$)***	1.660e+00 ($\pm 6.97e-01$)***	1.478e+00 ($\pm 3.04e-01$)***
$k_4(x_4 = T_{eo})$	1.977e+00 ($\pm 5.48e-01$)***	1.138e+00 ($\pm 6.25e-02$)***	1.108e+00 ($\pm 4.71e-02$)***
$k_5(x_5 = dT_e)$		1.439e+00 ($\pm 3.41e-01$)***	1.357e+00 ($\pm 2.56e-01$)***
Num.Obs.	28	28	28
R2 Adj.	1.000	1.000	1.000
AIC	224.1	344.5	328.2
MRE (%)	1.225	2.791	2.399
RMSE (W)	10.685	88.533	66.111
CV _{RMSE} (%)	0.652	0.963	0.818
Range (W)	[883, 2531]	[5933, 12904]	[5282, 11154]

^a + p < 0.1, * p < 0.05, ** p < 0.01, *** p < 0.001; Confidence interval of 95% for regression coefficients;

^b Temperatures (K);

^c Compressor frequency (Hz);

^d Fan frequency (%);

CCD central point:

$$\dot{W}_{c0} = 1590.636 \text{ (W)} \quad \dot{Q}_{e0} = 8378.182 \text{ (W)} \quad T_{ci0} = 300.153 \text{ (K)} \quad T_{eo0} = 285.163 \text{ (K)}$$

$$\dot{Q}_{c0} = 9383 \text{ (W)} \quad f_{c0} = 50 \text{ (Hz)} \quad f_{fan0} = 50 \text{ (%)} \quad dT_{e0} = 4.962 \text{ (K)}$$

Partial derivatives at CCD center point:

$$\left. \frac{\partial \dot{W}_c}{\partial f_c} \right|_0 = 3.849e+01 \quad \left. \frac{\partial \dot{Q}_c}{\partial f_c} \right|_0 = 1.895e+02 \quad \left. \frac{\partial \dot{Q}_c}{\partial dT_e} \right|_0 = 7.344e+01 \quad \left. \frac{\partial \dot{Q}_e}{\partial T_{eo}} \right|_0 = 2.386e+02$$

$$\left. \frac{\partial \dot{W}_c}{\partial T_{ci}} \right|_0 = 3.834e+01 \quad \left. \frac{\partial \dot{Q}_c}{\partial T_{ci}} \right|_0 = -3.932e+01 \quad \left. \frac{\partial \dot{Q}_e}{\partial f_c} \right|_0 = 1.608e+02 \quad \left. \frac{\partial \dot{Q}_e}{\partial dT_e} \right|_0 = 7.290e+01$$

$$\left. \frac{\partial \dot{W}_c}{\partial f_{fan}} \right|_0 = -4.446e+00 \quad \left. \frac{\partial \dot{Q}_c}{\partial f_{fan}} \right|_0 = 4.234e+00 \quad \left. \frac{\partial \dot{Q}_e}{\partial T_{ci}} \right|_0 = -6.670e+01$$

$$\left. \frac{\partial \dot{W}_c}{\partial T_{eo}} \right|_0 = 3.230e+00 \quad \left. \frac{\partial \dot{Q}_c}{\partial T_{eo}} \right|_0 = 2.409e+02 \quad \left. \frac{\partial \dot{Q}_e}{\partial f_{fan}} \right|_0 = 7.245e+00$$

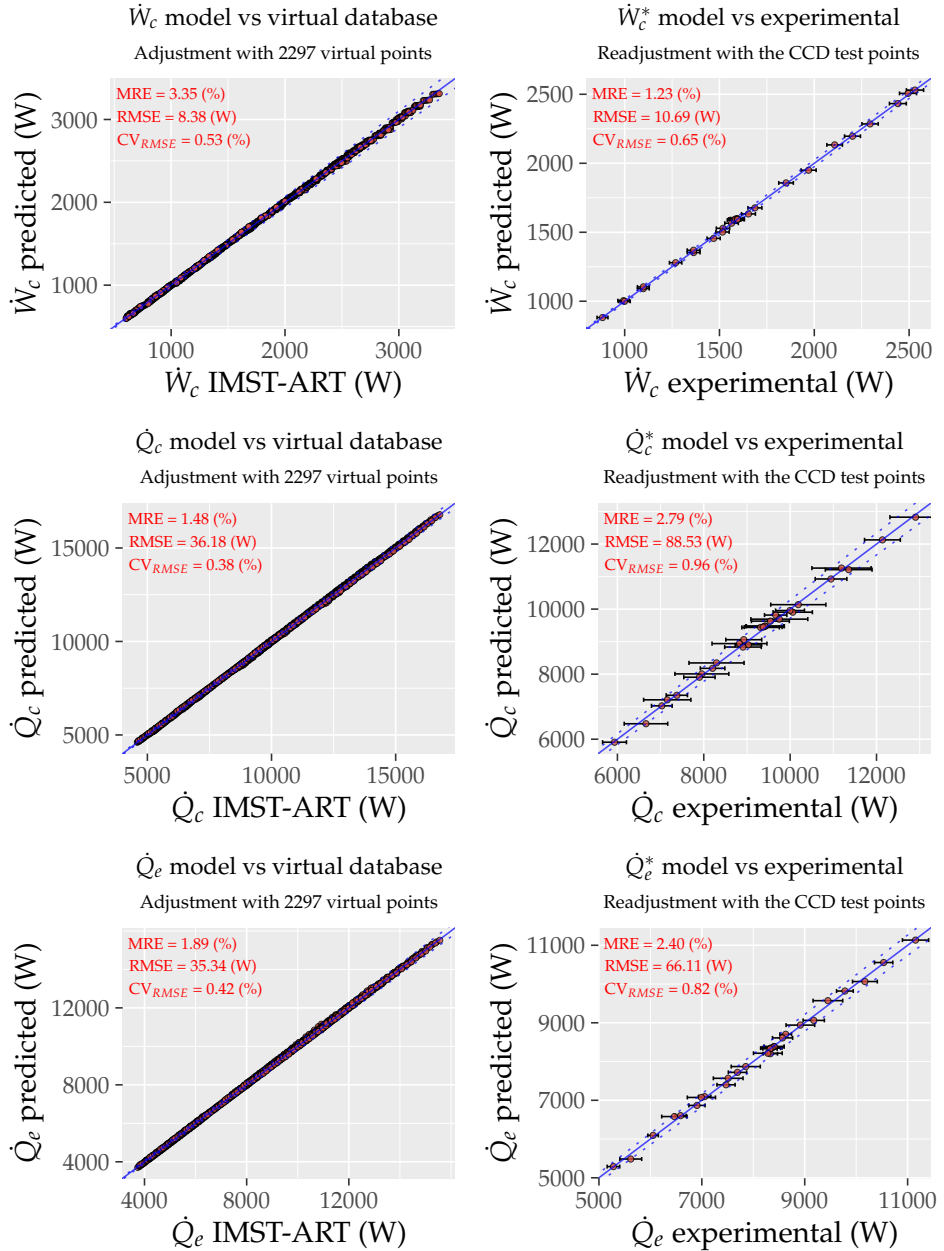


Figure G.6: Summer Air mode: Empirical model

G.8 DHW Air

Table G.13: DHW Air: Polynomial models adjusted with the virtual database

	\dot{W}_c / f_c (W/Hz)	\dot{Q}_c / f_c (W/Hz)	\dot{Q}_e / f_c (W/Hz)
(Int.)	2.732e+02 ($\pm 2.61e+01$)***	1.109e+02 ($\pm 6.77e+01$)**	5.899e+02 ($\pm 7.20e+01$)***
f_c	-1.592e-01 ($\pm 1.89e-02$)***	7.975e+00 ($\pm 1.20e-01$)***	8.021e+00 ($\pm 1.28e-01$)***
T_{co}	-1.708e+00 ($\pm 7.29e-02$)***	-5.437e-01 ($\pm 1.34e-02$)***	-1.198e+00 ($\pm 1.42e-02$)***
T_{ei}	-1.011e+00 ($\pm 1.10e-01$)***	-4.837e+00 ($\pm 4.62e-01$)***	-6.745e+00 ($\pm 4.92e-01$)***
dT_c	2.191e+00 ($\pm 5.46e-02$)***	1.400e-01 ($\pm 3.69e-03$)***	3.065e-01 ($\pm 3.93e-03$)***
$(1/f_{fan})$	-1.499e+01 ($\pm 1.31e+00$)***	1.492e+04 ($\pm 2.82e+02$)***	1.479e+04 ($\pm 3.00e+02$)***
(T_{ei}^2)	-3.580e-03 ($\pm 1.25e-04$)***	1.997e-02 ($\pm 7.92e-04$)***	2.310e-02 ($\pm 8.44e-04$)***
(dT_c^2)	2.874e-03 ($\pm 6.07e-05$)**		
$(1/f_c)$	3.264e+02 ($\pm 4.60e+00$)***	-3.529e+02 ($\pm 2.95e+01$)***	-5.114e+02 ($\pm 3.14e+01$)***
$T_{co} \times T_{ei}$	9.639e-03 ($\pm 2.51e-04$)***		
$T_{co} \times dT_c$	-7.786e-03 ($\pm 1.66e-04$)***		
$f_c \times T_{ei}$	1.167e-03 ($\pm 6.46e-05$)**		
$\Delta w'$		2.382e+03 ($\pm 8.25e+01$)***	2.288e+03 ($\pm 8.78e+01$)***
$T_{ei} \times (1/f_{fan})$		-5.134e+01 ($\pm 9.64e-01$)***	-5.093e+01 ($\pm 1.03e+00$)***
$T_{ei} \times f_c$		-2.808e-02 ($\pm 4.09e-04$)***	-2.872e-02 ($\pm 4.36e-04$)***
$(1/f_{fan}) \times f_c$		-1.437e+01 ($\pm 6.69e-01$)***	-1.380e+01 ($\pm 7.12e-01$)***
Num.Obs.	2375	2375	2375
R2 Adj.	0.998	0.999	0.999
AIC	-1209.9	7517.6	7814.8
MRE (%)	1.383	2.648	3.878
RMSE (W)	9.953	57.066	60.869
CV _{RMSE} (%)	0.448	0.626	0.808
Range (W)	[1095, 4120]	[3888, 16922]	[2805, 14910]

^a + p < 0.1, * p < 0.05, ** p < 0.01, *** p < 0.001; Confidence interval of 95% for regression coefficients;

^b Temperatures (K);

^c Compressor frequency (Hz);

^d Fan frequency (%);

^e $\Delta w'$ (kg_{water}/kg_{dry air});

^f $\delta T_e = 7$ K;

Table G.14: DHW Air: Experimental readjustment

	\dot{W}_c^* (W)	\dot{Q}_c^* (W)	\dot{Q}_e^* (W)
$k_0(\dot{W}_{c0}, \dot{Q}_{c0}, \dot{Q}_{e0})$	1.028e+00 ($\pm 4.92e-03$)***	8.940e-01 ($\pm 1.21e-02$)***	8.921e-01 ($\pm 1.72e-02$)***
$k_1(x_1 = f_c)$	1.012e+00 ($\pm 2.59e-02$)***	9.019e-01 ($\pm 5.11e-02$)***	9.032e-01 ($\pm 7.57e-02$)***
$k_2(x_2 = T_{ei})$	1.120e+00 ($\pm 4.29e-01$)***	9.695e-01 ($\pm 8.92e-02$)***	9.215e-01 ($\pm 1.10e-01$)***
$k_3(x_3 = f_{fan})$	2.431e+00 ($\pm 2.86e+00$) ^a	1.083e+00 ($\pm 4.89e-01$)***	1.230e+00 ($\pm 6.00e-01$)***
$k_4(x_4 = dT_c)$	8.466e-01 ($\pm 1.12e-01$)***		
$k_5(x_5 = \Delta w')$		1.264e+00 ($\pm 1.01e+00$) ^a	7.464e-01 ($\pm 1.26e+00$)
Num.Obs.	19	19	19
R2 Adj.	1.000	1.000	0.999
AIC	175.0	253.3	260.3
MRE (%)	1.681	4.378	5.854
RMSE (W)	17.653	138.660	166.491
CV _{RMSE} (%)	0.849	1.641	2.349
Range (W)	[1259, 2969]	[5213, 11529]	[4365, 9872]

^a + p < 0.1, * p < 0.05, ** p < 0.01, *** p < 0.001; Confidence interval of 95% for regression coefficients;

^b Temperatures (K);

^c Compressor frequency (Hz);

^d Fan frequency (%);

^e $\Delta w'$ (kg_{water}/kg_{dry air});

^f $\delta T_c = 7$ K;

CCD central point:

$$\dot{W}_{c0} = 2076.81 \text{ (W)} \quad f_{c0} = 50 \text{ (Hz)} \quad dT_{c0} = 20.02 \text{ (K)}$$

$$\dot{Q}_{c0} = 8407.775 \text{ (W)} \quad T_{ei0} = 290.07 \text{ (K)} \quad \Delta w'_0 = 0^1 \text{ (kg}_{\text{water}}/\text{kg}_{\text{dry air}})$$

$$\dot{Q}_{e0} = 7143.75 \text{ (W)} \quad f_{fan0} = 50 \text{ (\%)}$$

Partial derivatives at CCD center point:

$$\left. \frac{\partial \dot{W}_c}{\partial f_c} \right|_0 = 4.252e+01 \quad \left. \frac{\partial \dot{W}_c}{\partial dT_c} \right|_0 = -1.047e+01 \quad \left. \frac{\partial \dot{Q}_c}{\partial f_{fan}} \right|_0 = 1.383e+01 \quad \left. \frac{\partial \dot{Q}_e}{\partial T_{ei}} \right|_0 = 2.100e+02$$

$$\left. \frac{\partial \dot{W}_c}{\partial T_{ei}} \right|_0 = 4.250e+00 \quad \left. \frac{\partial \dot{Q}_c}{\partial f_c} \right|_0 = 1.696e+02 \quad \left. \frac{\partial \dot{Q}_c}{\partial \Delta w'} \right|_0 = 1.191e+05 \quad \left. \frac{\partial \dot{Q}_e}{\partial f_{fan}} \right|_0 = 1.355e+01$$

$$\left. \frac{\partial \dot{W}_c}{\partial f_{fan}} \right|_0 = 2.998e-01 \quad \left. \frac{\partial \dot{Q}_c}{\partial T_{ei}} \right|_0 = 2.158e+02 \quad \left. \frac{\partial \dot{Q}_e}{\partial f_c} \right|_0 = 1.374e+02 \quad \left. \frac{\partial \dot{Q}_e}{\partial \Delta w'} \right|_0 = 1.144e+05$$

¹There are no dehumidification conditions at the center point.

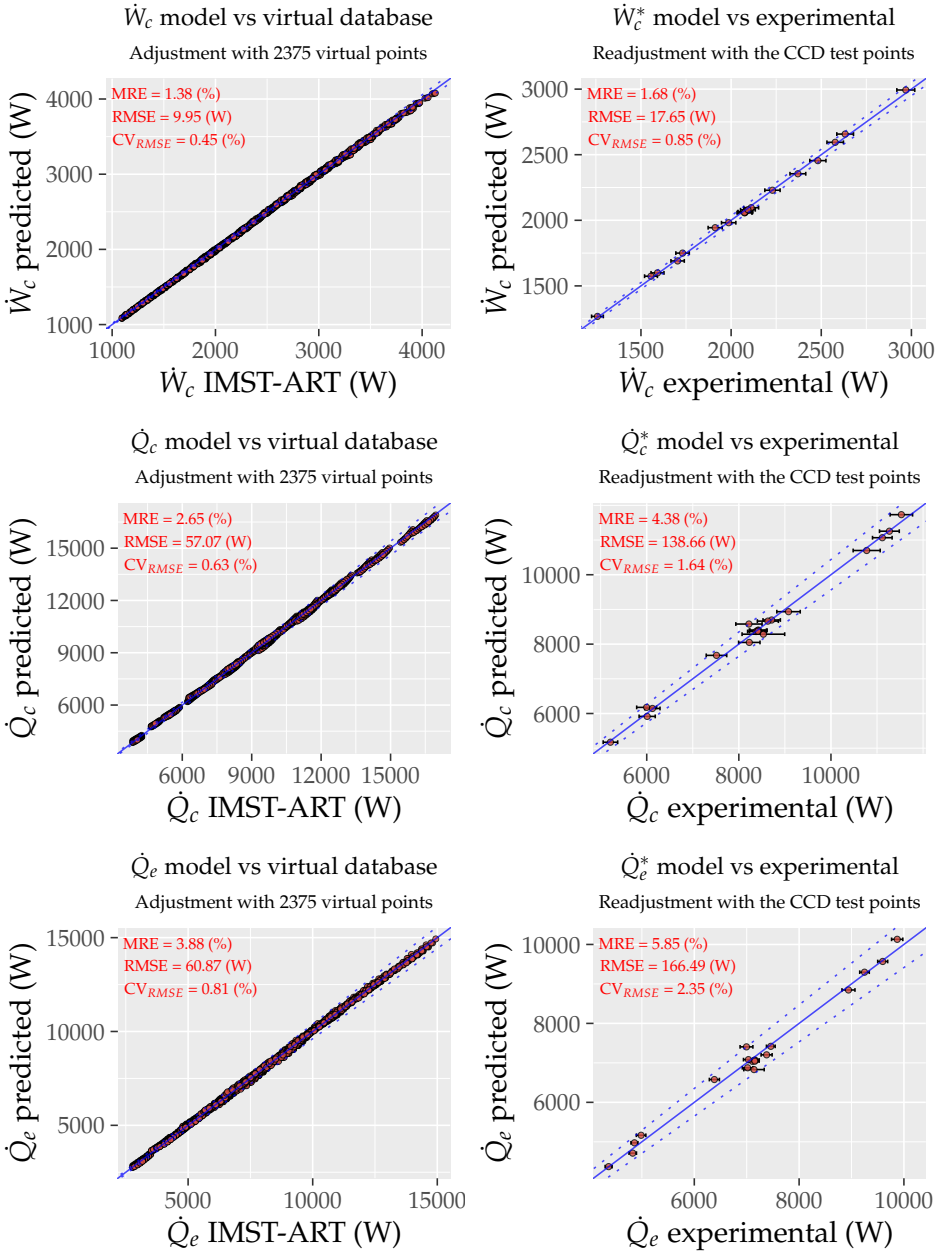


Figure G.7: DHW Air mode: Empirical model

H

Contour plots scroll compressors

CONTENTS

H.1	Contour plots of scroll performance variables	h-1
H.1.1	Compressor ZP21K5E-PFV (AHRI 11, 33)	h-2
H.1.2	Compressor ZS21KAE-PFV (AHRI 21)	h-4
H.1.3	Compressor ZP31K5E-PFV (AHRI 24, 38, 39, 58)	h-5
H.1.4	Compressor ZF18K4E-TFD (AHRI 34, 36)	h-9
H.1.5	Compressor ZP122KCE-TFD (AHRI 65)	h-11
H.1.6	Compressor SH161A4 (AHRI 66)	h-12
H.1.7	Compressor Cuevas(2009)	h-13

H.1 Contour plots of scroll performance variables

This appendix includes additional information on the contour plots generated for each relevant variable analyzed in this work related to the characterization of scroll compressors. These diagrams have been generated covering the entire experimental domain of each compressor analyzed, considering its reference refrigerant and a single suction condition (generally at constant SH).

The variables represented include compressor consumption (\dot{W}_c), mass flow rate (\dot{m}_{ref}), specific consumption ($\dot{W}_{esp} = \dot{W}_c / \dot{m}_{ref}$), and non-dimensional consumption ($\dot{W}_{ad} = \dot{W}_c / (P_e V_s n)$), plotting them as a function of evaporation and condensation pressure. These plots also include the pressure ratio isolines, increasing the information. Furthermore, the same plots for the energy consumption and the mass flow rate are replicated but plotting them in temperatures due to their wide use in the refrigeration field.

H.1.1 Compressor ZP21K5E-PFV (AHRI 11, 33)

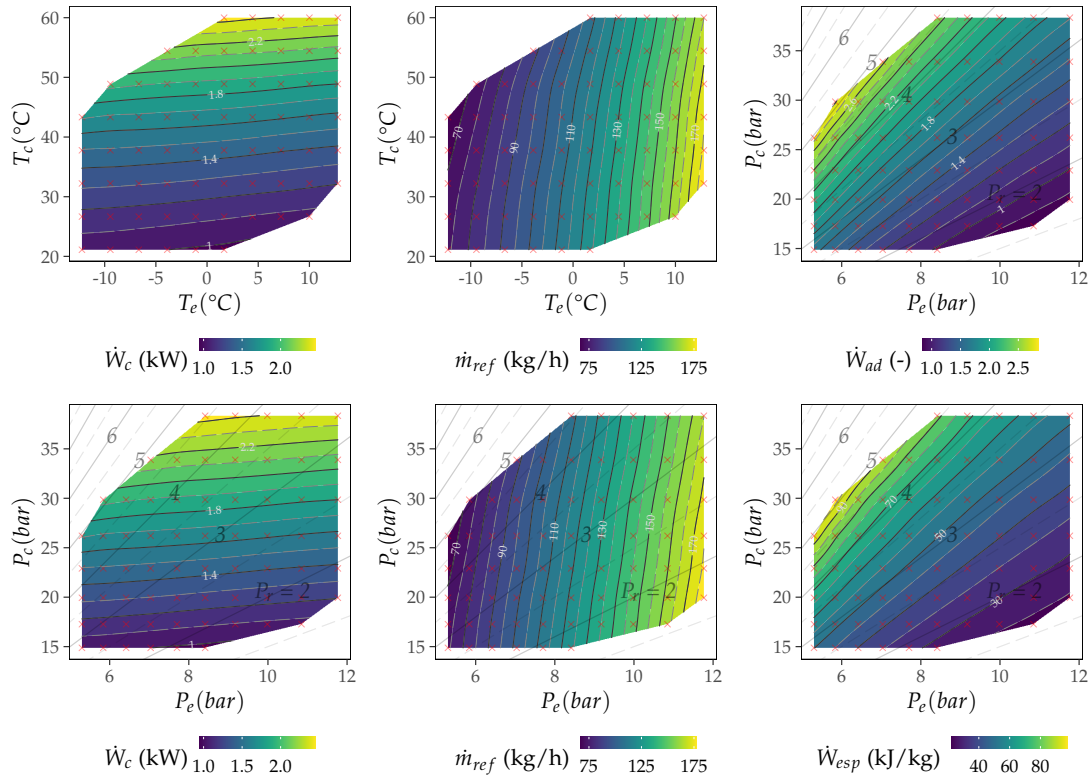


Figure H.1: Contour plots AHRI 11 ; R410A ; SH=11K

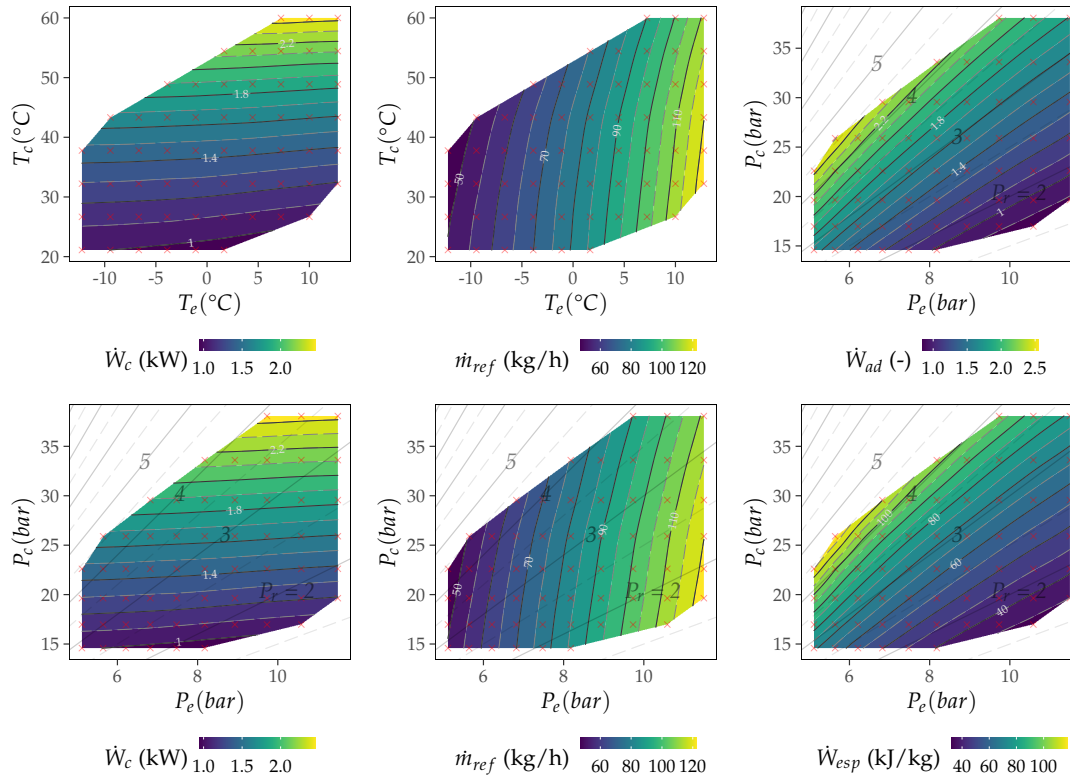


Figure H.2: Contour plots AHRI 33 ; R32+R134a ; SH=11K

H.1.2 Compressor ZS21KAE-PFV (AHRI 21)

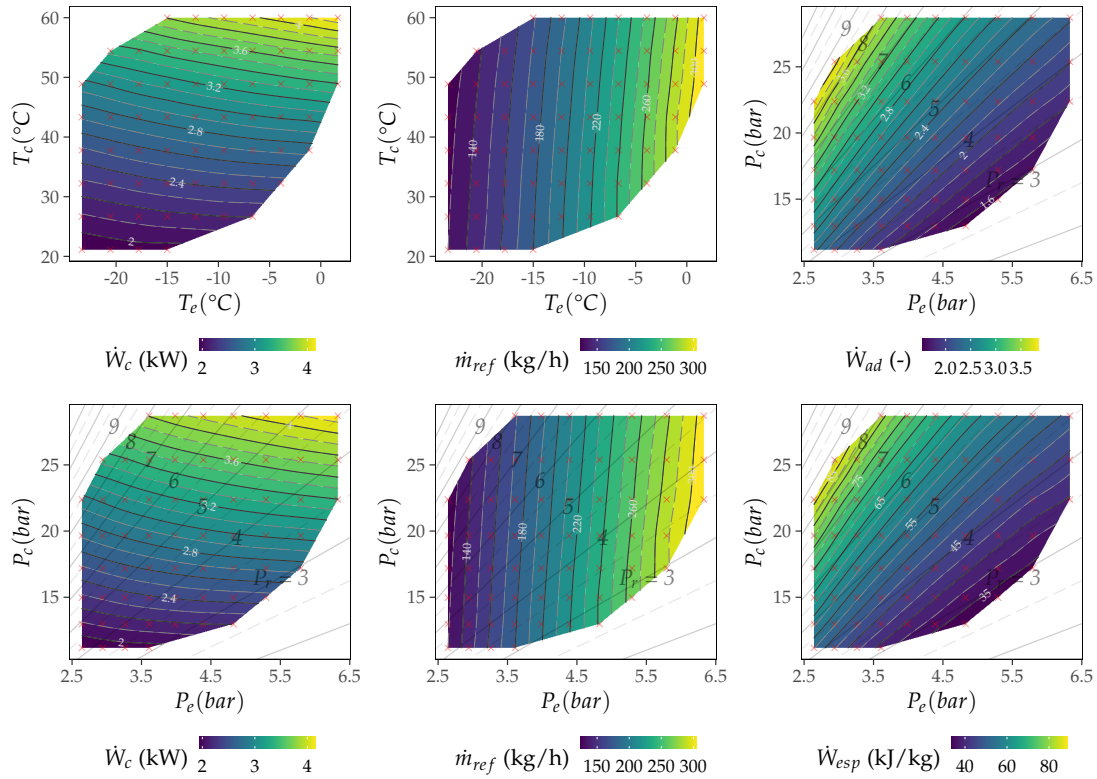


Figure H.3: Contour plots AHRI 21 ; R404A ; SH=11K

H.1.3 Compressor ZP31K5E-PFV (AHRI 24, 38, 39, 58)

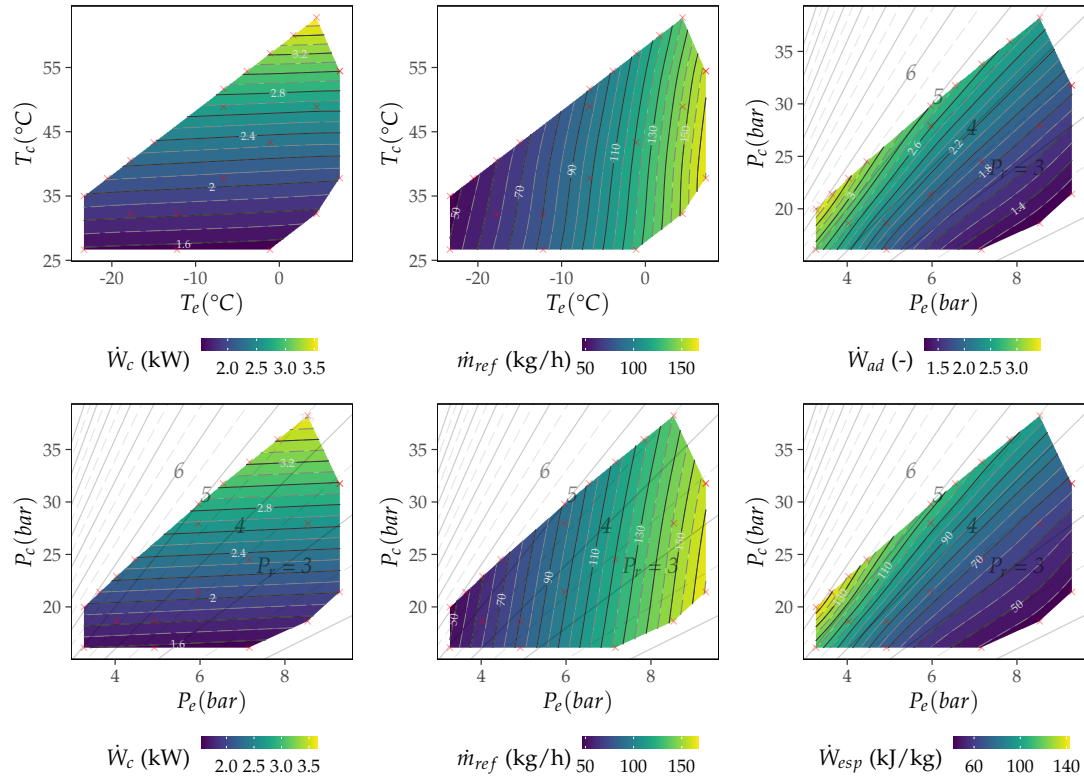


Figure H.4: Contour plots AHRI 24 ; DR5 ; SH=11K

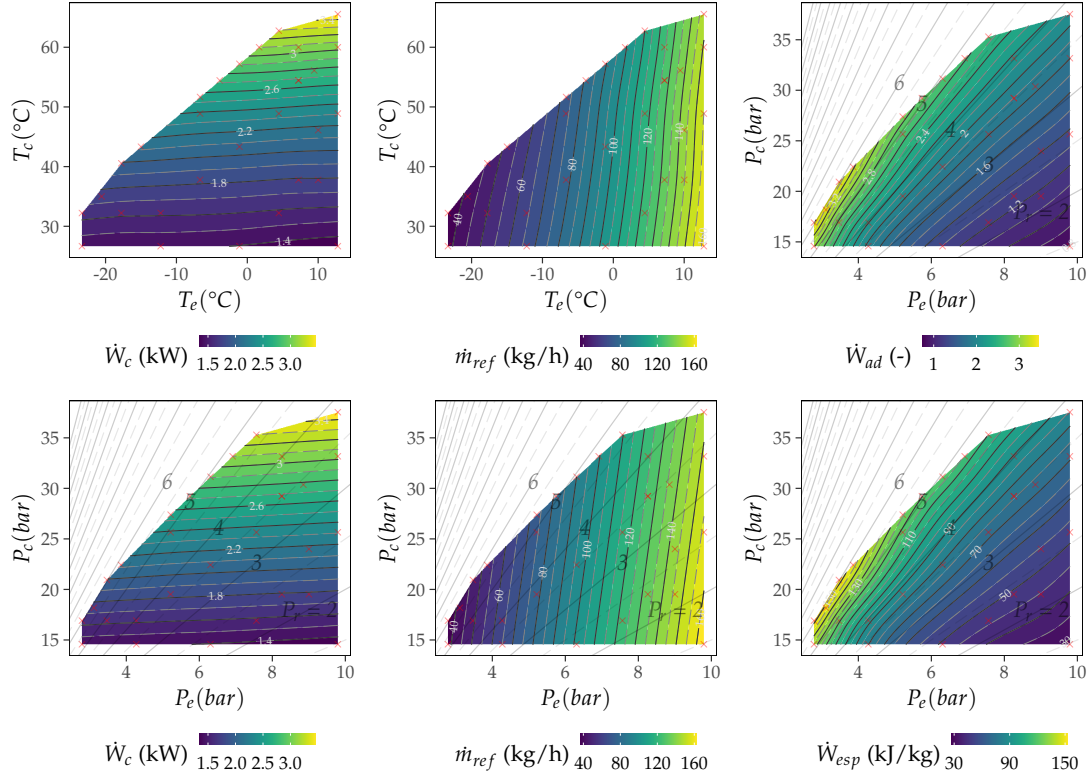


Figure H.5: Contour plots AHRI 38 ; L41b ; SH=11K

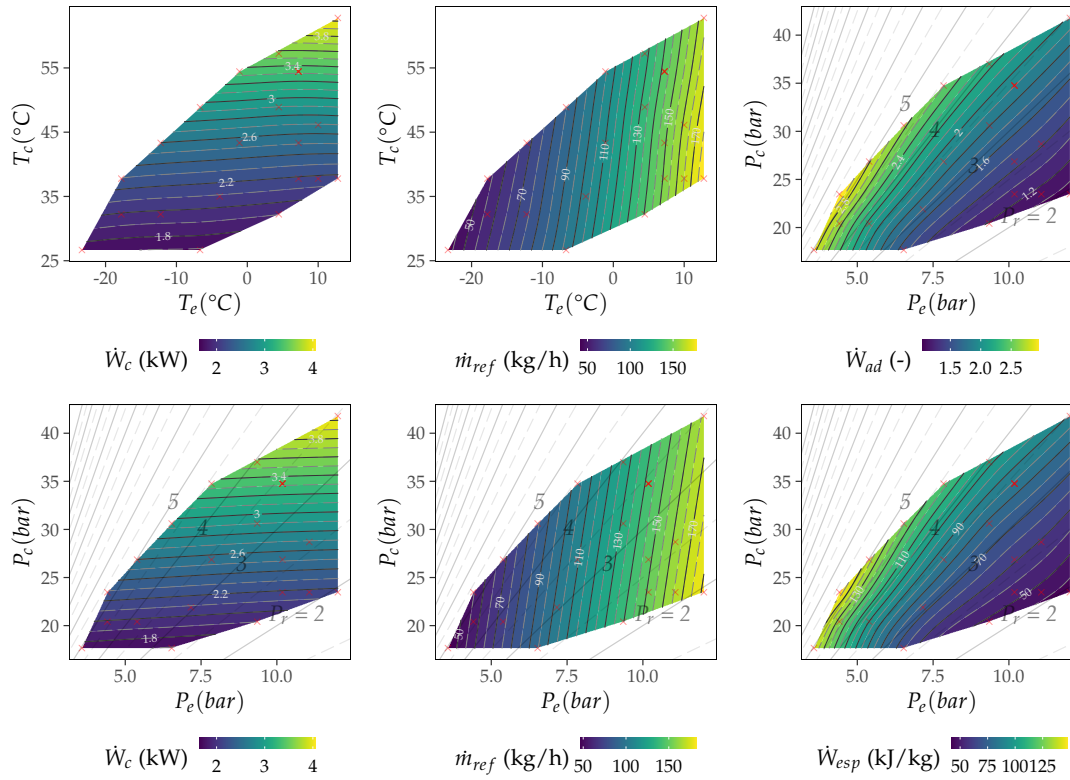


Figure H.6: Contour plots AHRI 39 ; R32 ; SH=11K

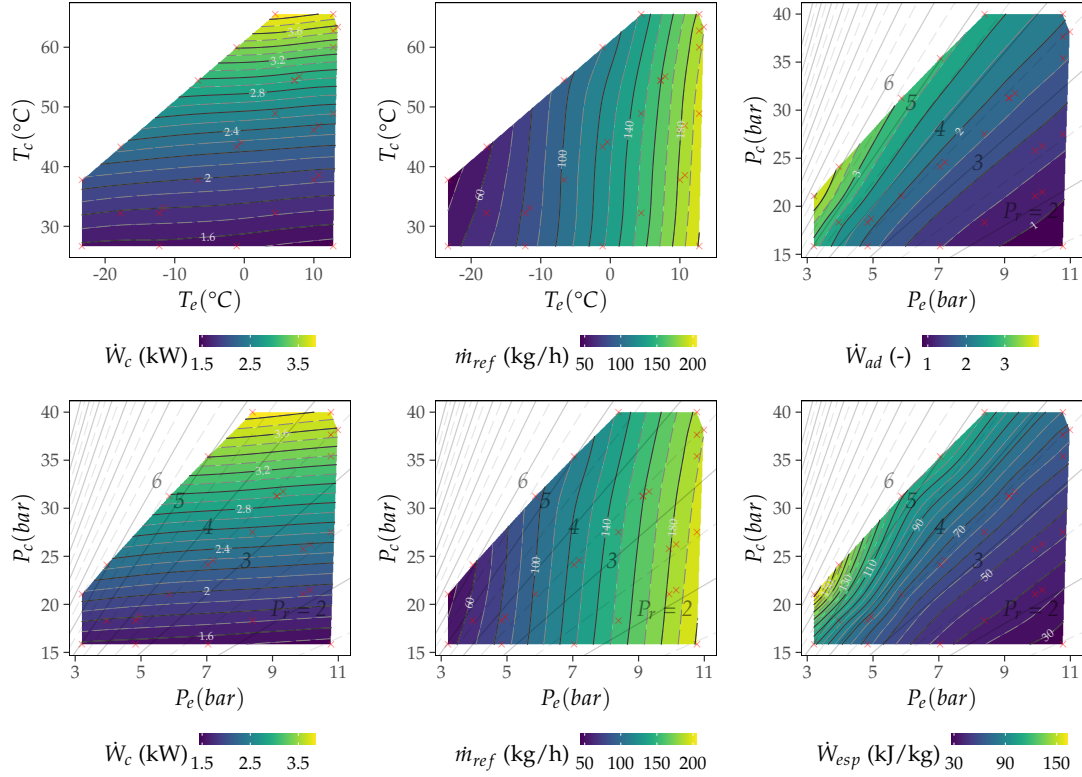


Figure H.7: Contour plots AHRI 58 ; R454B ; SH=11K

H.1.4 Compressor ZF18K4E-TFD (AHRI 34, 36)

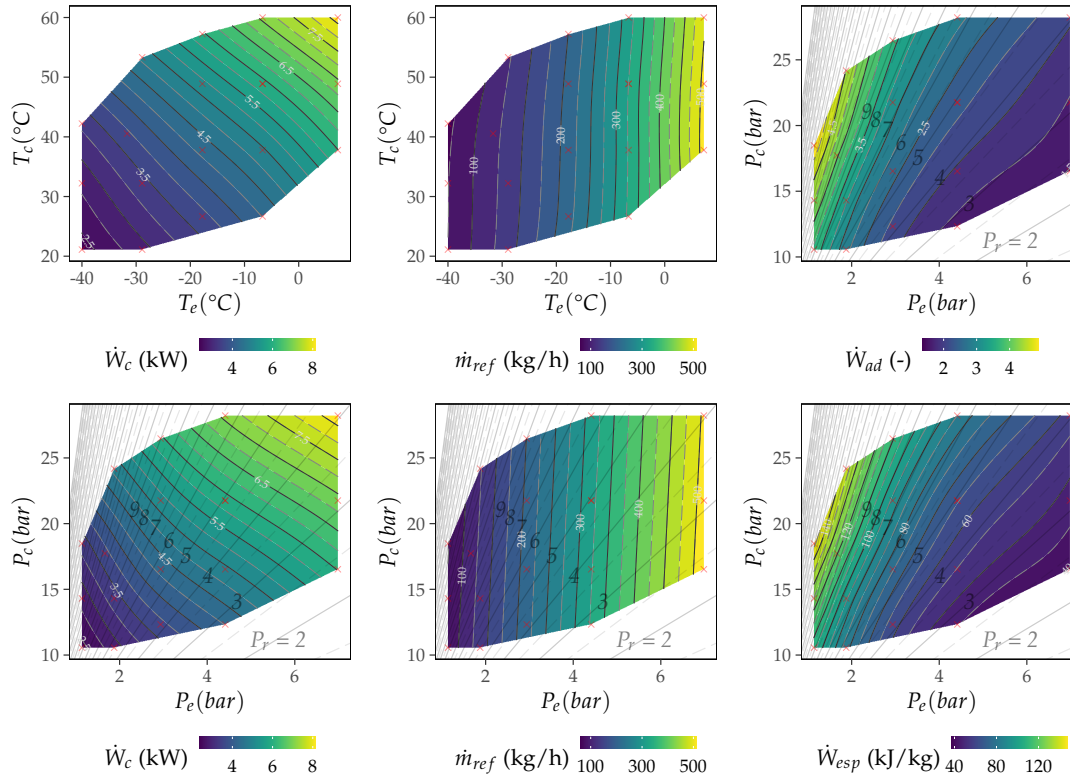


Figure H.8: Contour plots AHRI 34 ; DR7 ; SH=11K

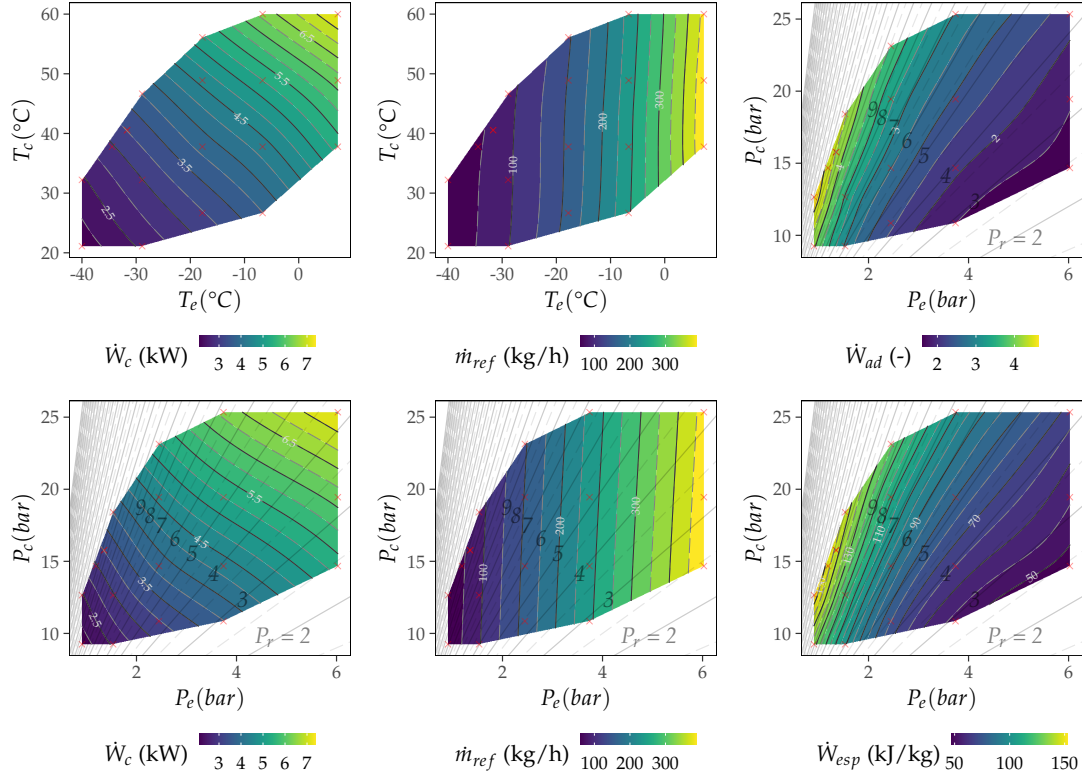


Figure H.9: Contour plots AHRI 36 ; L40 ; SH=11K

H.1.5 Compressor ZP122KCE-TFD (AHRI 65)

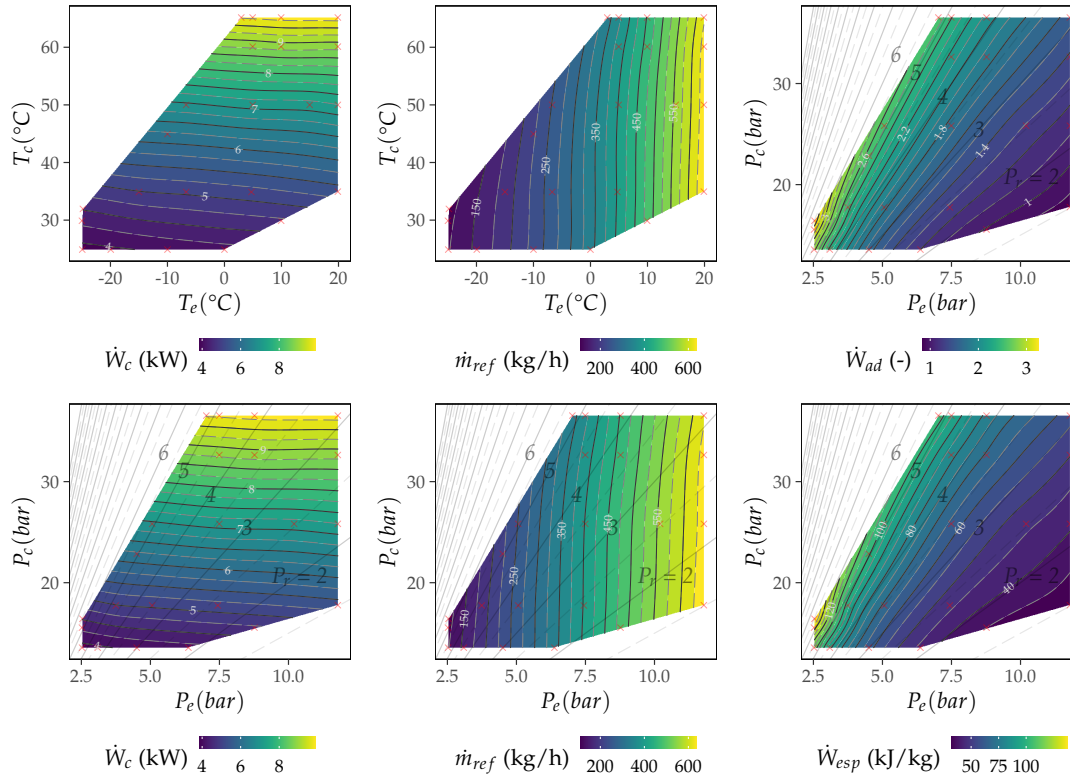


Figure H.10: Contour plots AHRI 65 ; R447A ; SH=11K

H.1.6 Compressor SH161A4 (AHRI 66)

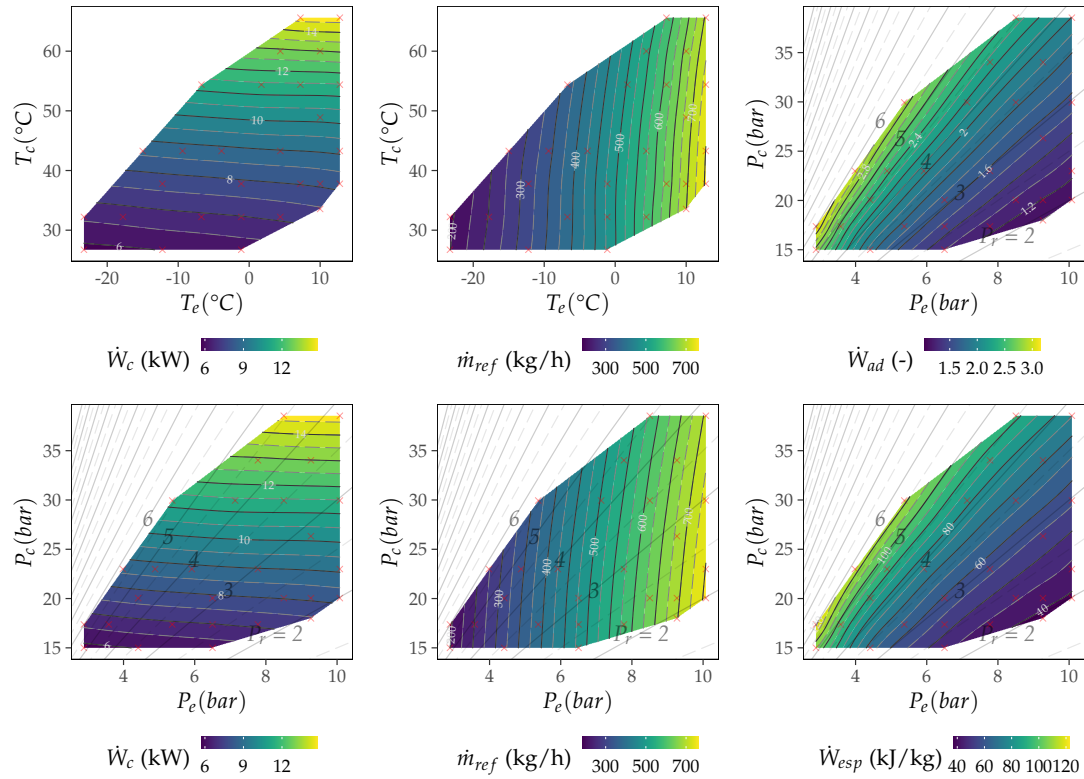


Figure H.11: Contour plots AHRI 66 ; HPR2A ; SH=11K

H.1.7 Compressor Cuevas(2009)

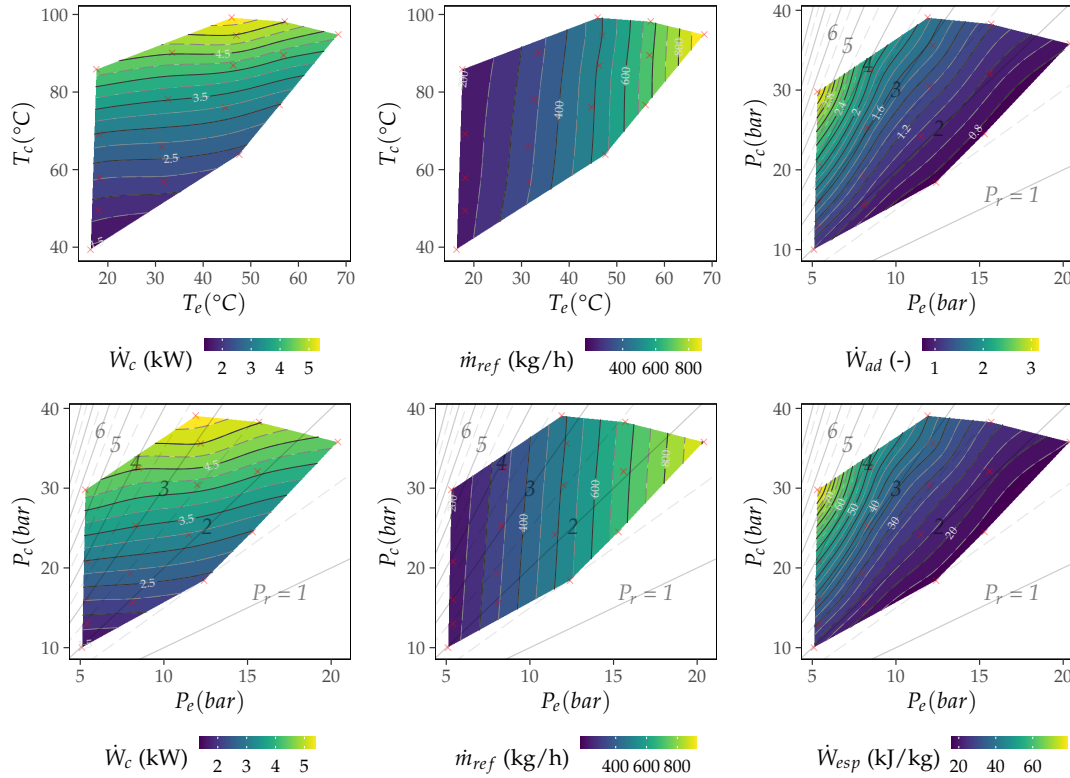


Figure H.12: Contour plots Cuevas(2009) 50Hz ; R134a ; SH=6.8K

I

Contour plots reciprocating compressors

CONTENTS

I.1	Contour plots of reciprocating performance variables	i-1
I.1.1	Compressor NJ7240F (AHRI 17)	i-2
I.1.2	Compressor EG80HLR (AHRI 18)	i-3
I.1.3	Compressor NEK2134GK (AHRI 28, 29, 49, 50)	i-4
I.1.4	Compressor NEK6214Z (AHRI 30)	i-8
I.1.5	Compressor CS14K6E-TF5 (AHRI 35, 37)	i-9
I.1.6	Compressor 4GE-23-40P (AHRI 51)	i-11
I.1.7	Compressor H84B223ABC (AHRI 59)	i-12
I.1.8	Compressor FH2511Z (AHRI 64a, 67a, 69a)	i-13
I.1.9	Compressor FH4540Z (AHRI 64b, 67b, 69b)	i-16

I.1 Contour plots of reciprocating performance variables

This appendix includes additional information on the contour plots generated for each relevant variable analyzed in this work related to the characterization of reciprocating compressors. These diagrams have been generated covering the entire experimental domain of each compressor analyzed, considering its reference refrigerant and a single suction condition (generally at constant SH).

The variables represented include compressor consumption (\dot{W}_c), mass flow rate (\dot{m}_{ref}), specific consumption ($\dot{W}_{esp} = \dot{W}_c / \dot{m}_{ref}$), and non-dimensional consumption ($\dot{W}_{ad} = \dot{W}_c / (P_e V_s n)$), plotting them as a function of evaporation and condensation pressure. These plots also include the pressure ratio isolines, increasing the information. Furthermore, the same plots for the energy consumption and the mass flow rate are replicated but plotting them in temperatures due to their wide use in the refrigeration field.

I.1.1 Compressor NJ7240F (AHRI 17)

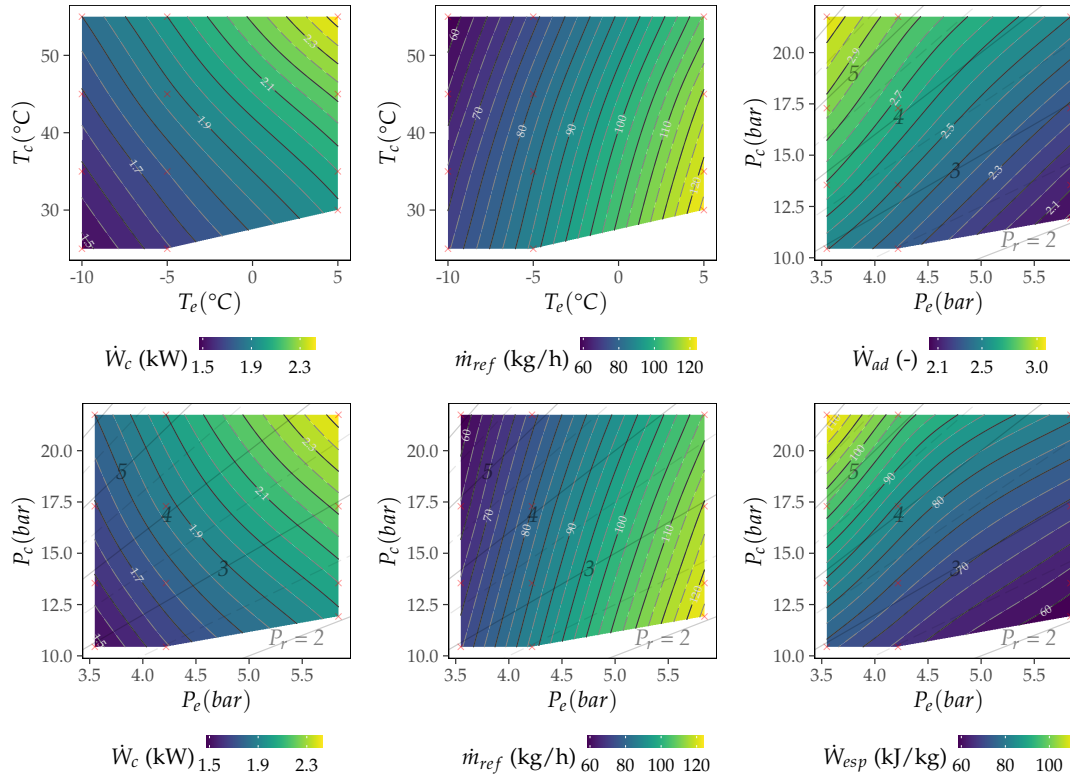


Figure I.1: Contour plots AHRI 17 ; R22 ; SH=11K

I.1.2 Compressor EG80HLR (AHRI 18)

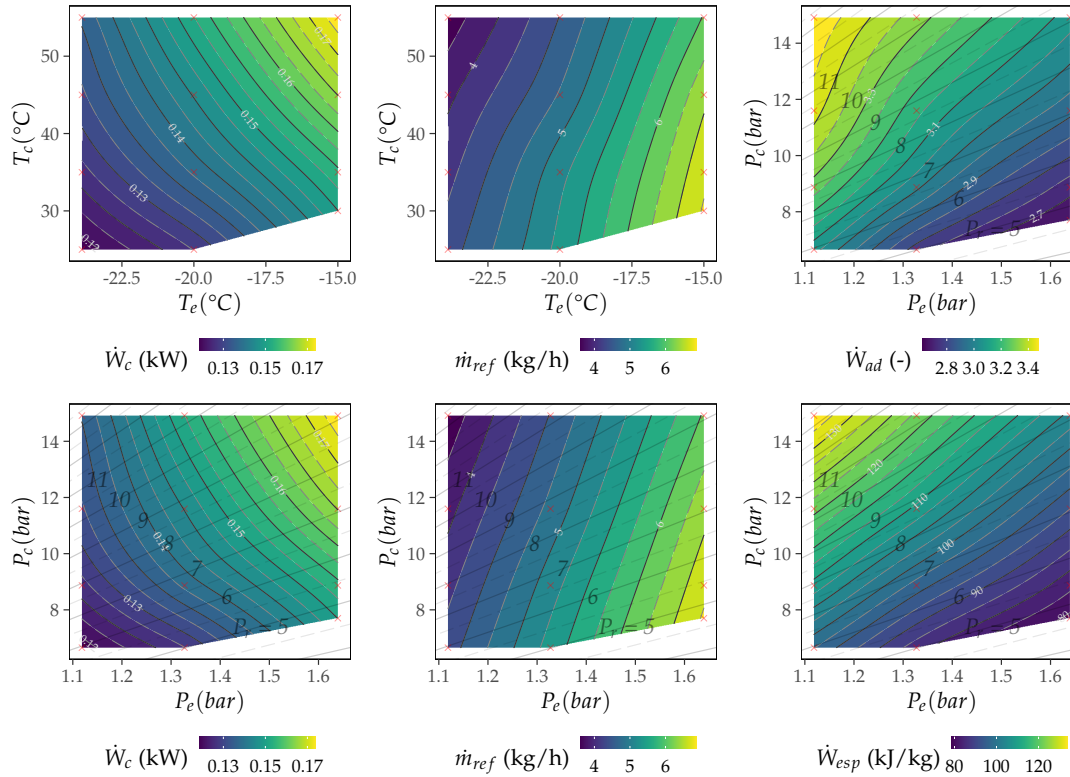


Figure I.2: Contour plots AHRI 18 ; R134a ; SH=22K

I.1.3 Compressor NEK2134GK (AHRI 28, 29, 49, 50)

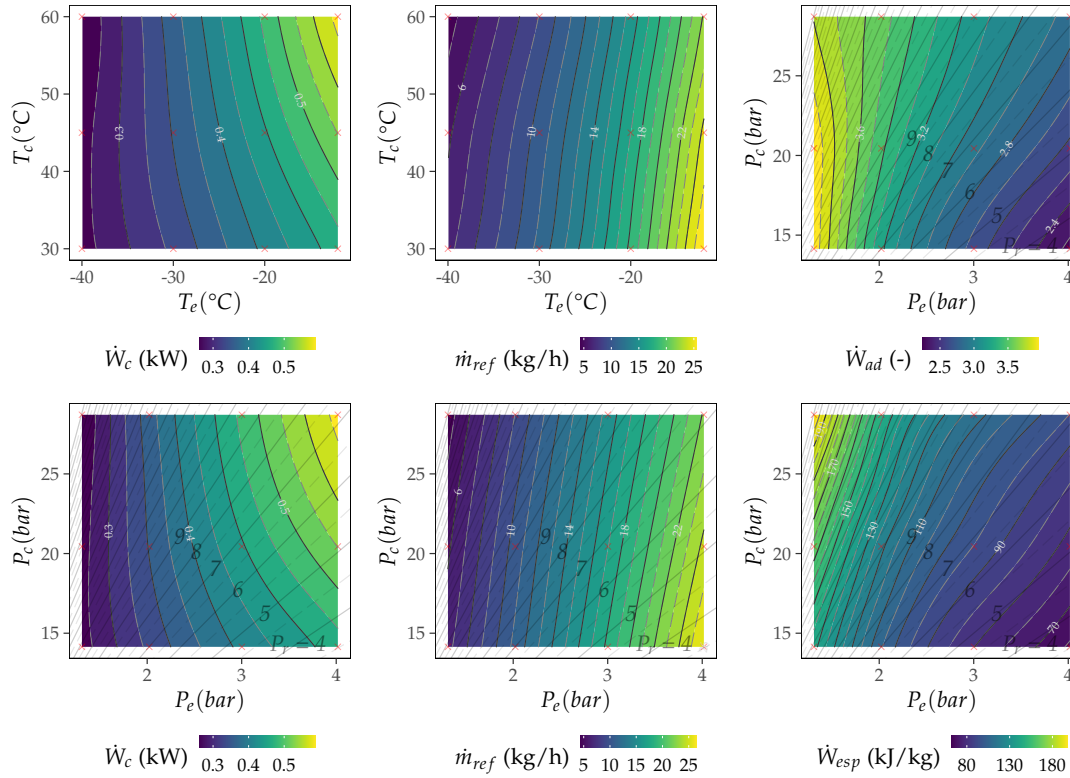


Figure I.3: Contour plots AHRI 28 ; R404A ; SH=11K

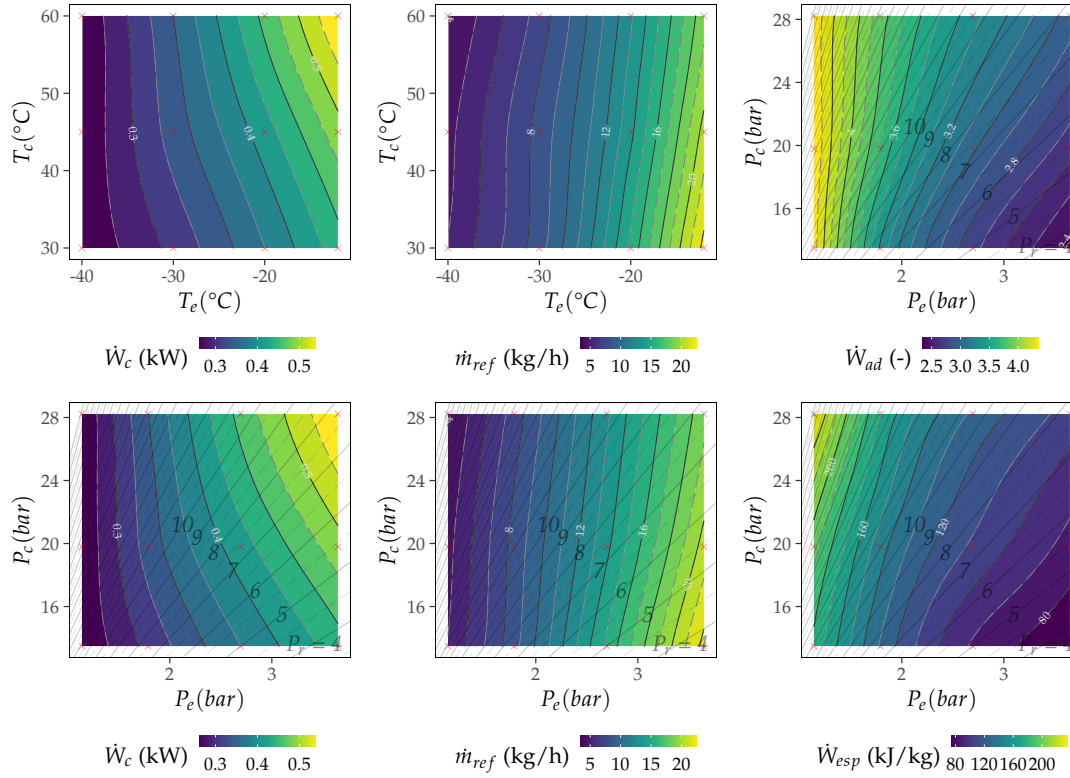


Figure I.4: Contour plots AHRI 29 ; DR7 ; SH=11K

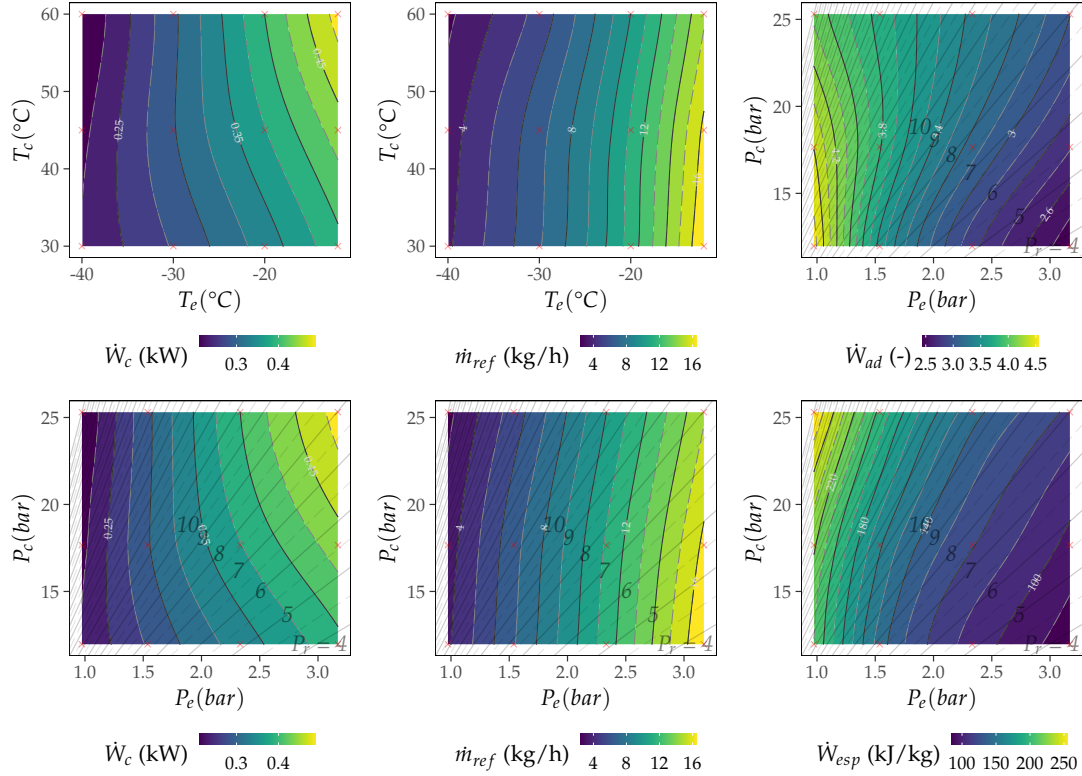


Figure I.5: Contour plots AHRI 49 ; R455A ; SH=11K

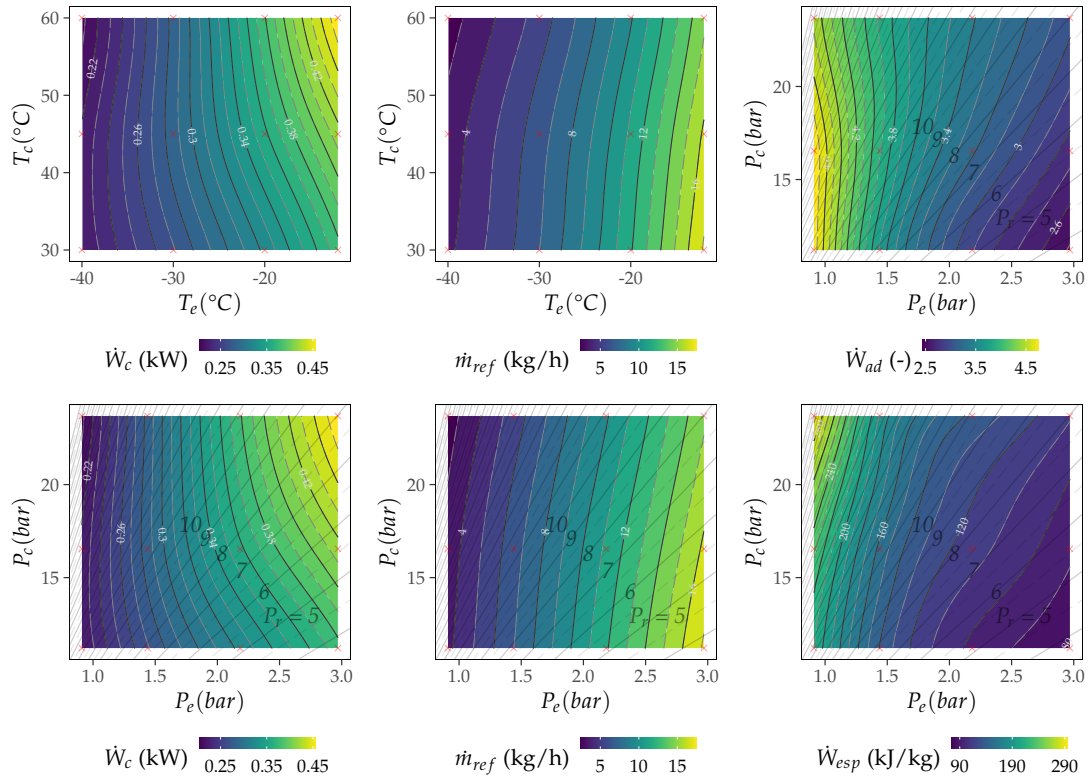


Figure I.6: Contour plots AHRI 50 ; DR3 ; SH=11K

I.1.4 Compressor NEK6214Z (AHRI 30)

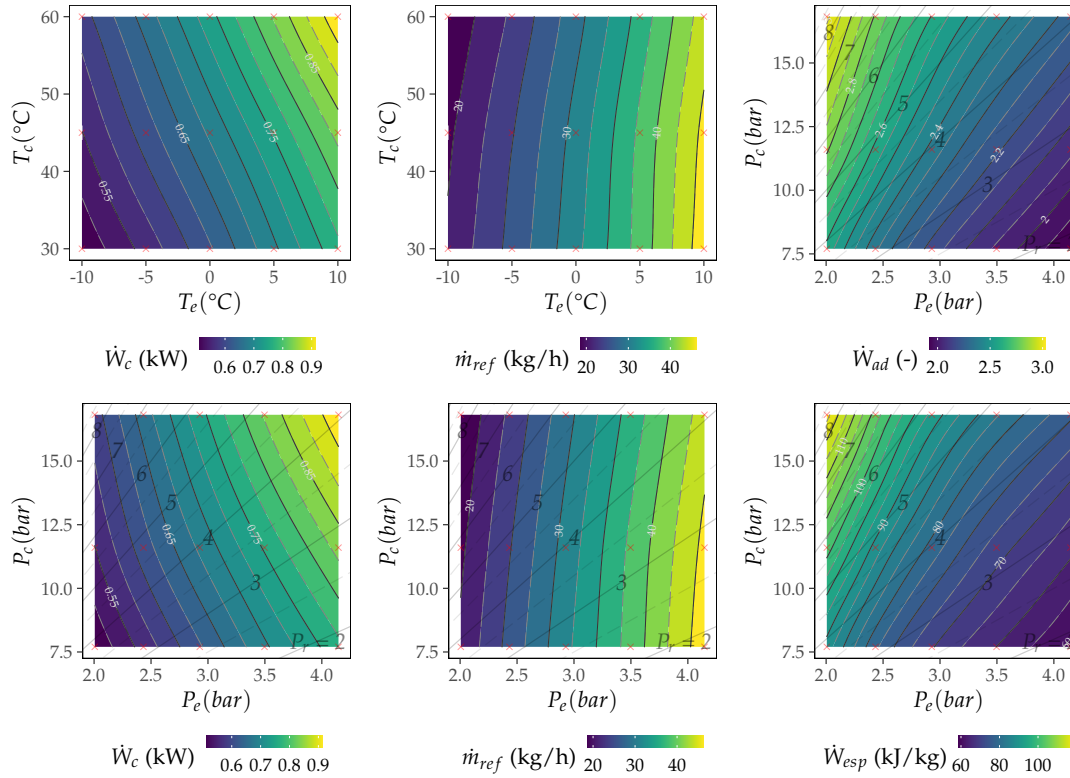


Figure I.7: Contour plots AHRI 30 ; R134a ; SH=11K

I.1.5 Compressor CS14K6E-TF5 (AHRI 35, 37)

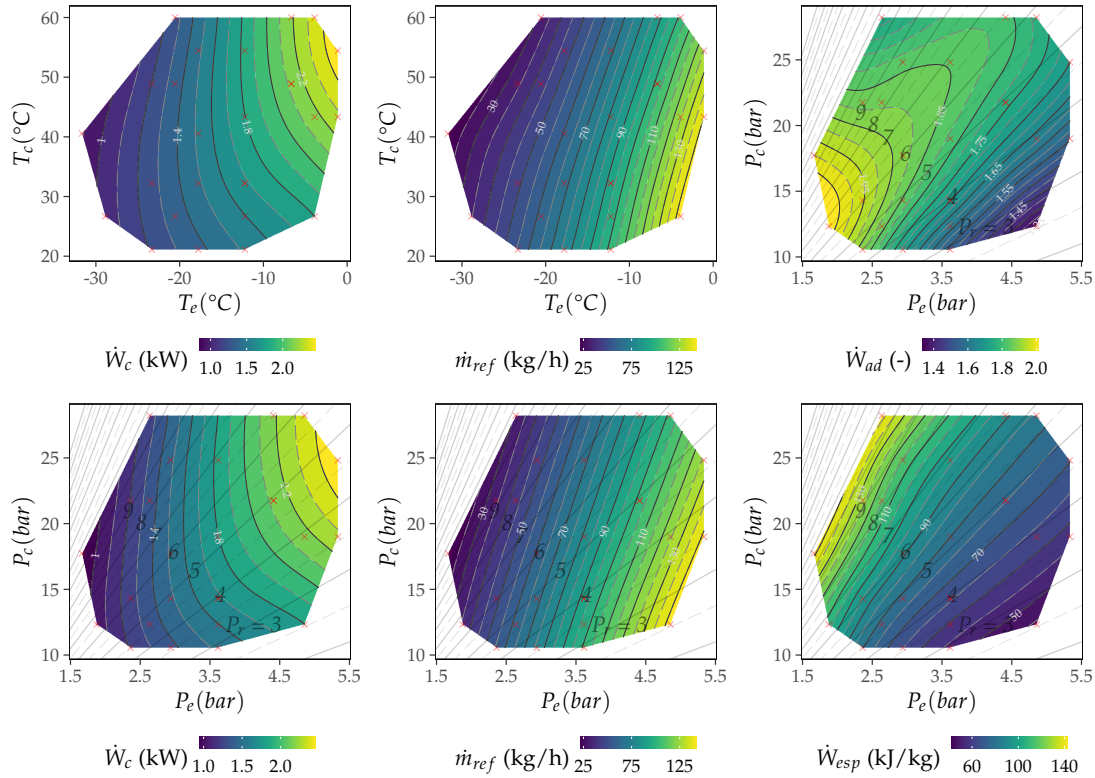


Figure I.8: Contour plots AHRI 35 ; DR7 ; SH=11K

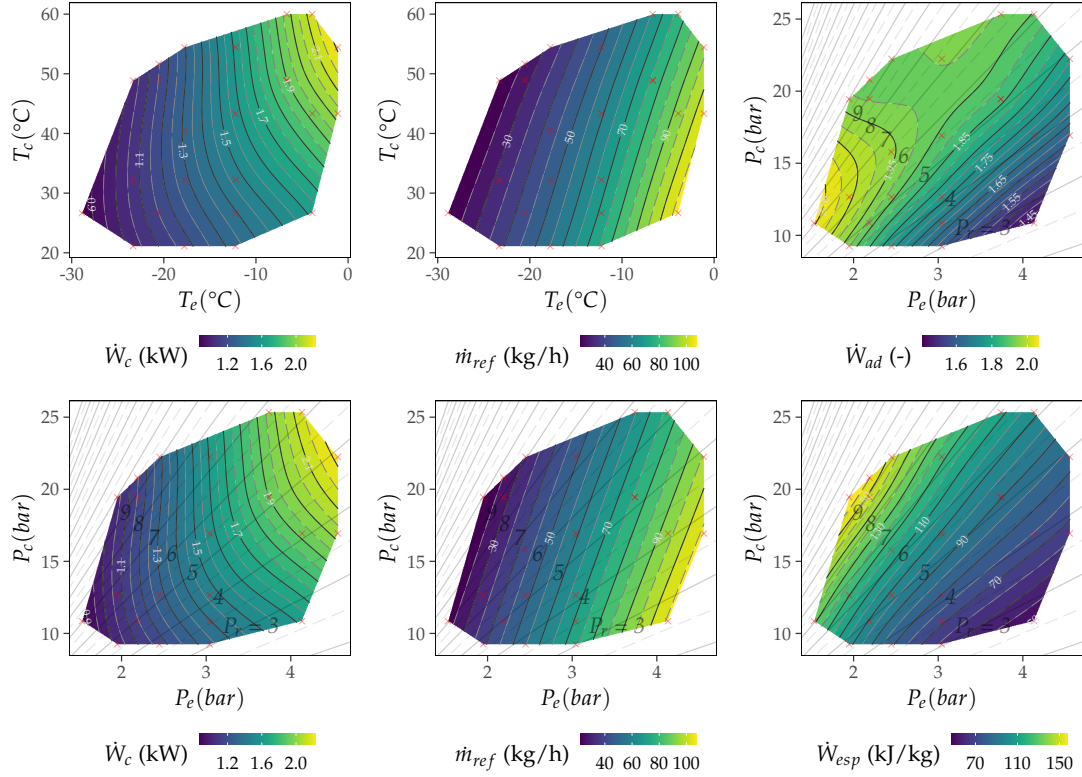


Figure I.9: Contour plots AHRI 37 ; L40 ; SH=11K

I.1.6 Compressor 4GE-23-40P (AHRI 51)

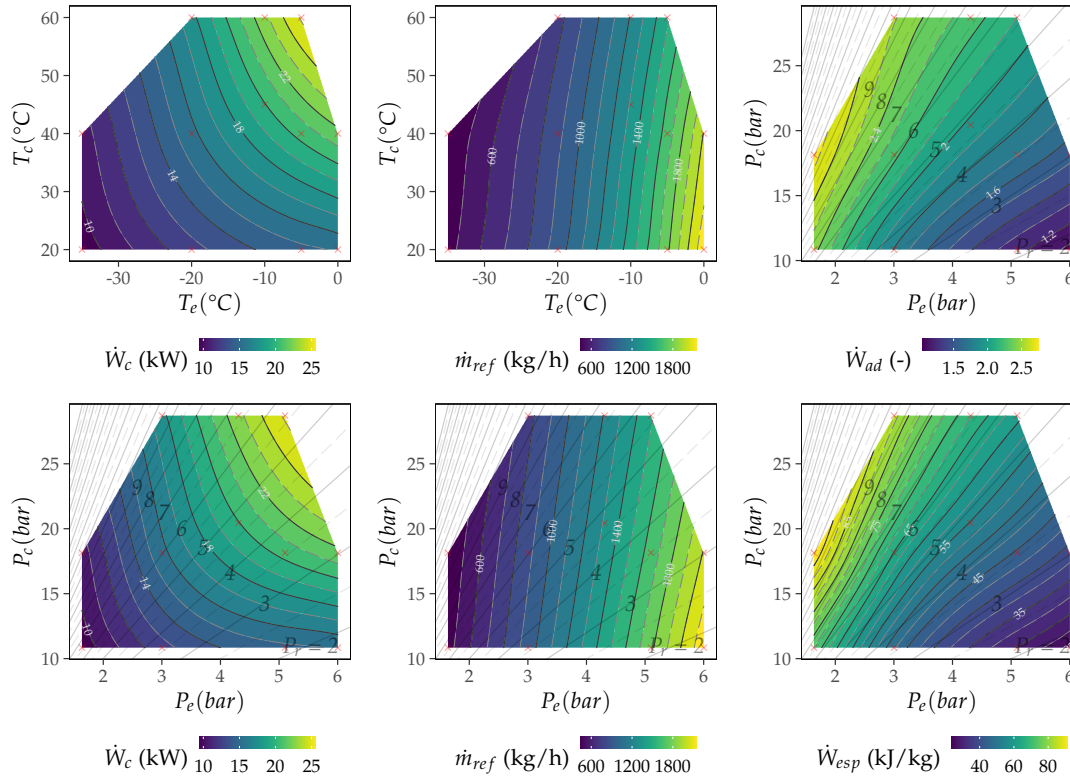


Figure I.10: Contour plots AHRI 51 ; R404A ; $T_s=20^\circ\text{C}$

I.1.7 Compressor H84B223ABC (AHRI 59)

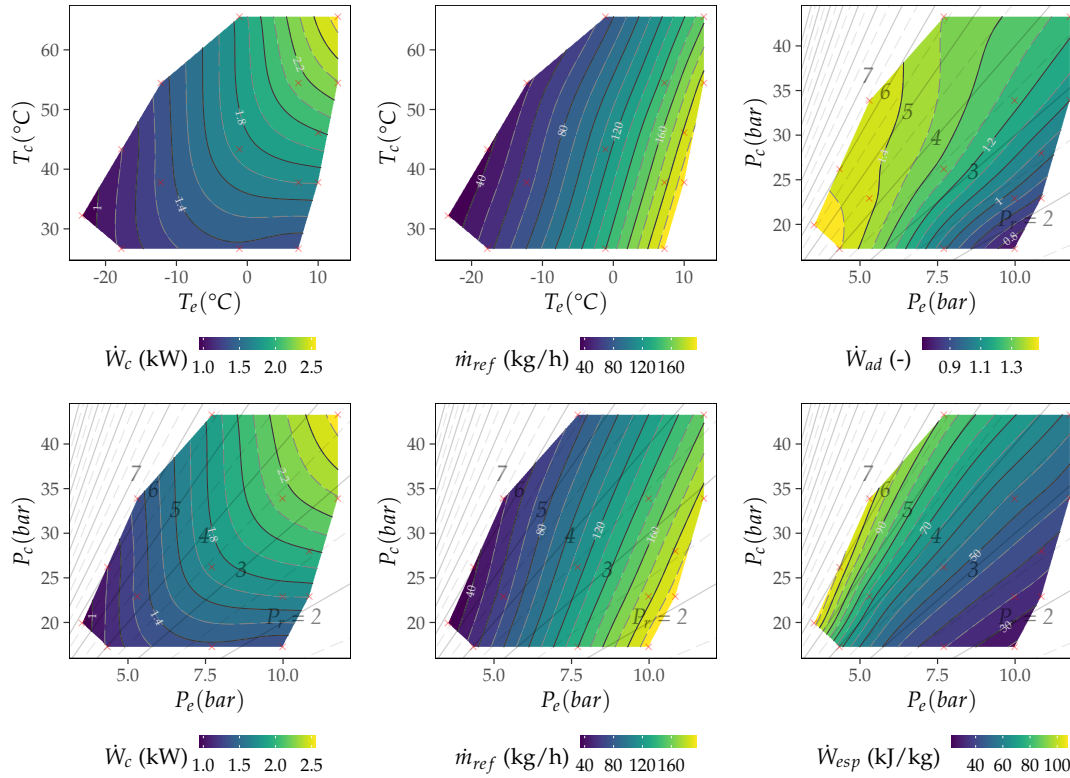


Figure I.11: Contour plots AHRI 59 ; R410A ; SH=11K

I.1.8 Compressor FH2511Z (AHRI 64a, 67a, 69a)

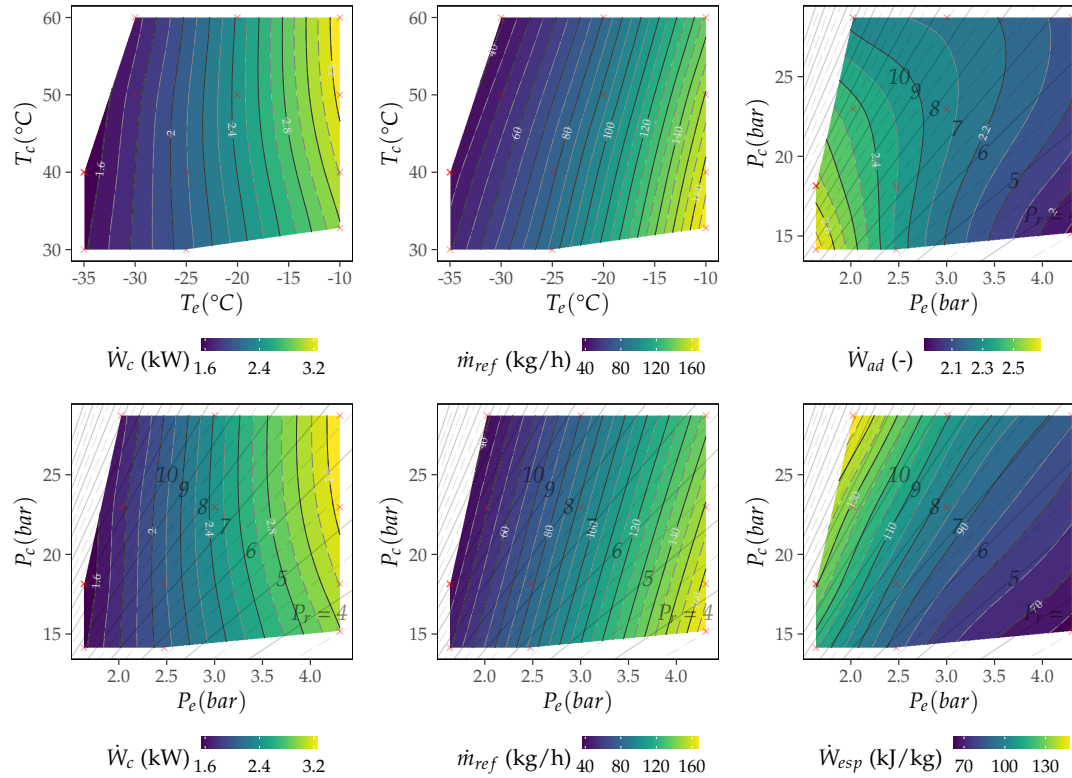


Figure I.12: Contour plots AHRI 64a ; R404A ; SH=10K

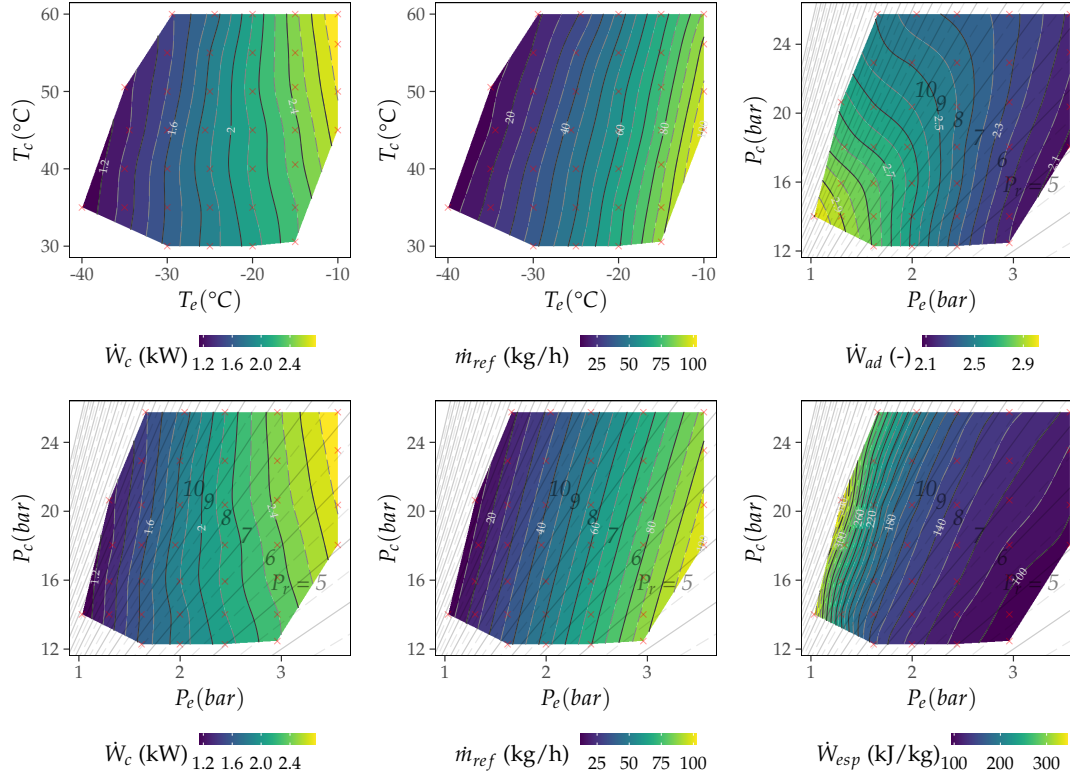


Figure I.13: Contour plots AHRI 67a ; ARM25 ; SH=10K

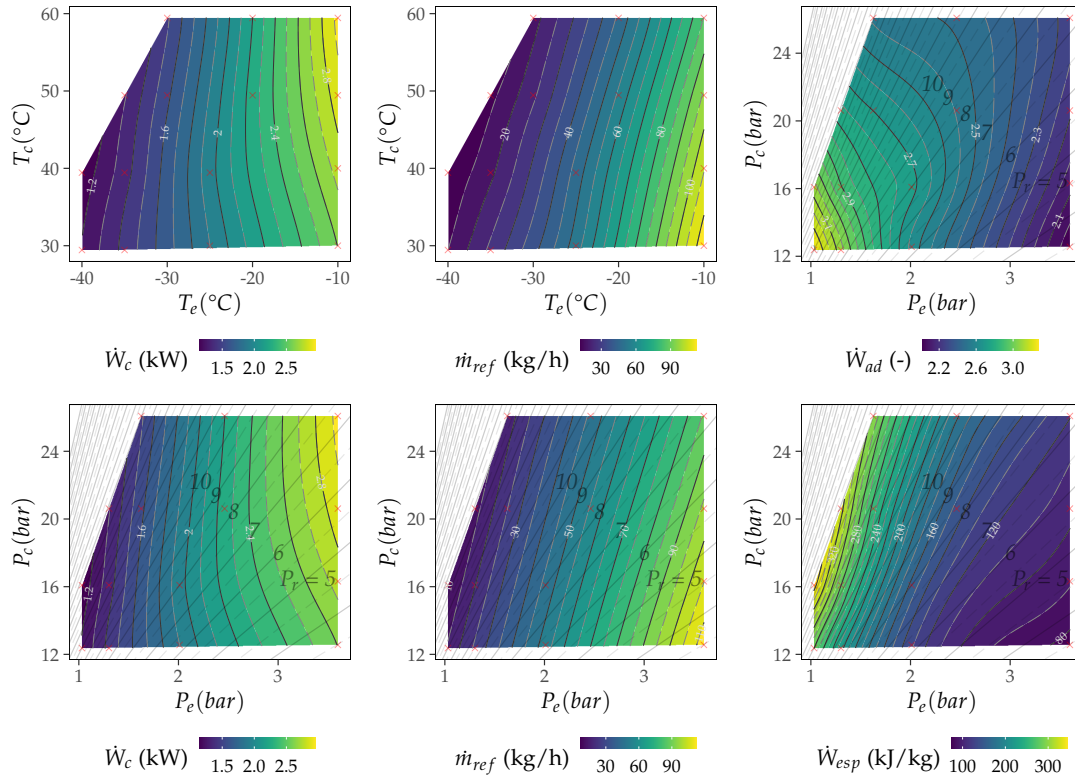


Figure I.14: Contour plots AHRI 69a ; ARM20b ; SH=10K

I.1.9 Compressor FH4540Z (AHRI 64b, 67b, 69b)

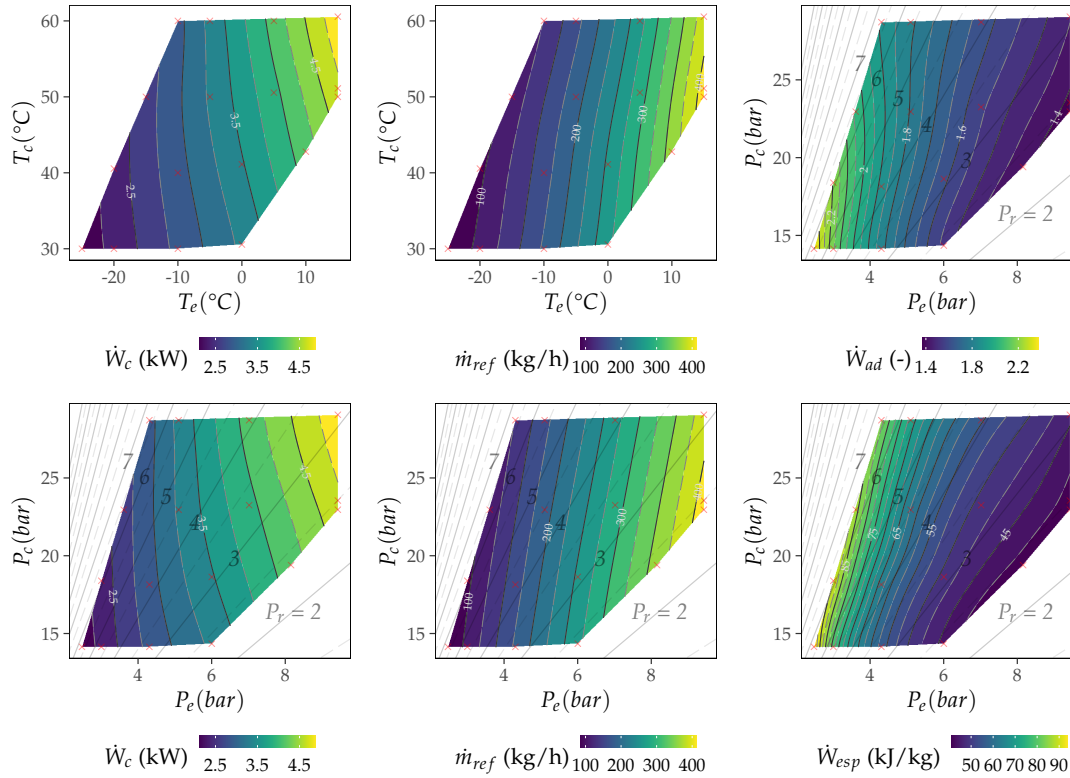


Figure I.15: Contour plots AHRI 64b ; R404A ; SH=10K

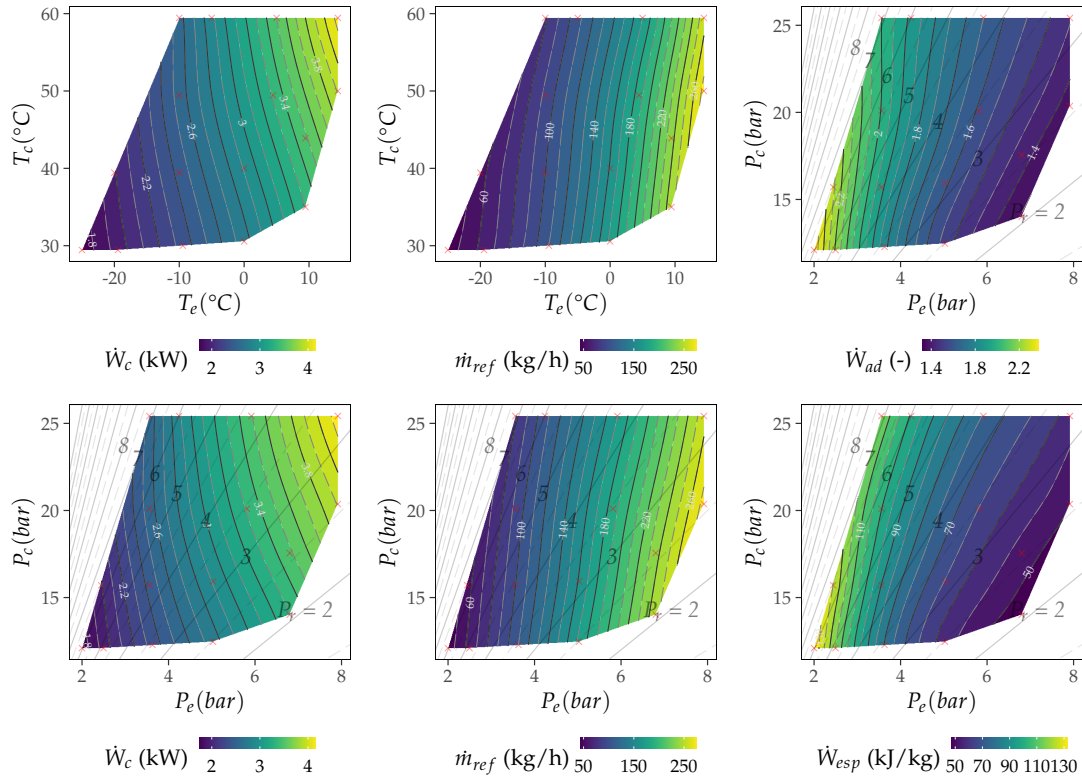


Figure I.16: Contour plots AHRI 67b ; ARM25 ; SH=10K

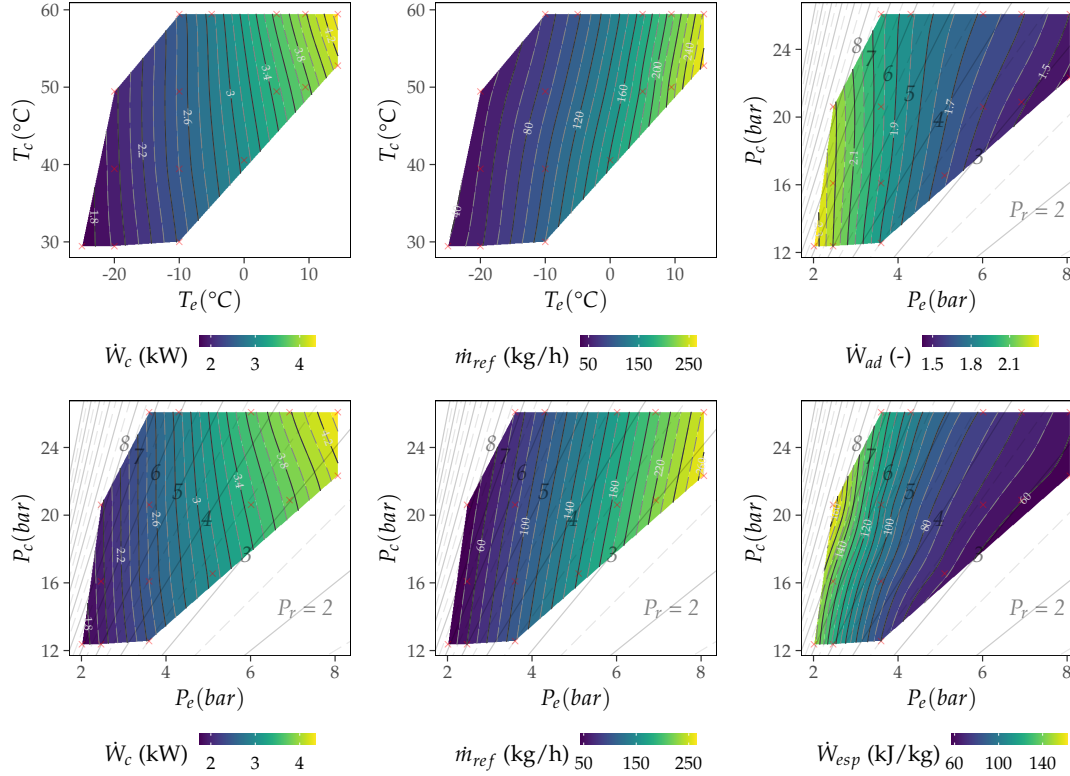


Figure I.17: Contour plots AHRI 69b ; ARM20b ; SH=10K

J

Model summary tables for scroll compressors

CONTENTS

J.1	Model summary tables for the characterization of \dot{W}_c , \dot{W}_{esp} and \dot{m}_{ref}	j-1
J.1.1	Compressor ZP21K5E-PFV (AHRI 11, 33)	j-2
J.1.2	Compressor ZS21KAE-PFV (AHRI 21)	j-4
J.1.3	Compressor ZP31K5E-PFV (AHRI 24, 38, 39, 58)	j-6
J.1.4	Compressor ZF18K4E-TFD (AHRI 34, 36)	j-8
J.1.5	Compressor ZP122KCE-TFD (AHRI 65)	j-9
J.1.6	Compressor SH161A4 (AHRI 66)	j-10
J.1.7	Compressor Cuevas(2009)	j-11

J.1 Model summary tables for the characterization of \dot{W}_c , \dot{W}_{esp} and \dot{m}_{ref}

This appendix includes summary tables of the models considered in Chapter 4 in scroll compressor characterization. They include the value of the coefficients and its uncertainty. It also includes the values of MRE, RMSE and CV_{RMSE} , the range of variation of \dot{W}_c and \dot{m}_{ref} , and the number of points considered in the adjustment. The units to be considered in each correlation is included at the bottom of each table. The polynomial expressions were reported in Chapter 4. Finally, the error values for \dot{W}_{esp} are included in terms of energy consumption. As already mentioned in Chapter 4, we must multiply by the predicted mass flow rate at the same suction conditions used in the adjustment of \dot{W}_{esp} to reconvert to \dot{W}_c values. These conditions are the same used in the summary table of the mass flow rate models.

J.1.1 Compressor ZP21K5E-PFV (AHRI 11, 33)

Table J.1: Energy consumption models (AHRI 11, 33)

\dot{W}_c (kW)		MRE (%) RMSE [†] (W)	\dot{W}_c (kW)		MRE (%) RMSE [†] (W)	\dot{W}_c (kW)		MRE (%) RMSE [†] (W)	\dot{W}_{esp} (kJ/kg)	MRE (%) RMSE [†] (W)	Fluid W_c Range [W] (N° tests)	
Correlation 1a			Correlation 2a			Correlation 3a						
AHRI 11												
c_0, z_c	2.758e-01 (±3.21e-02)***	2.57 12.86 (0.93)	c_0, z_c	3.242e-01 (±1.71e-02)**	0.72 4.95 (0.32)	c_0, z_c	7.719e-01 (±1.52e-02)***	1.21 7.26 (0.46)	c_0, z_c	-6.835e+00 (±5.43e-01)***	1.63 8.46 (0.54)	R410A [973, 2454] (66/64/66)
c_1, z_c	-2.954e-02 (±3.78e-03)***		c_1, z_c	-1.080e-02 (±3.35e-03)***		c_1, z_c	-3.930e-03 (±7.03e-04)***		c_1, z_c	-8.978e-01 (±4.41e-01)***		
c_2, k_0	5.846e-02 (±1.32e-03)***		c_2, k_0	4.813e-02 (±8.03e-04)**		c_2, k_0	1.002e-03 (±8.13e-04)*		c_2, k_0	-5.731e-01 (±7.18e-01)***		
c_3, k_1	4.317e-04 (±1.49e-04)***		c_3, k_1	-1.346e-04 (±7.70e-05)***		c_3, k_1	-2.073e-05 (±1.79e-05)*		c_3, k_1	8.220e+00 (±6.26e-01)***		
c_4, k_2			c_4, k_2	-2.900e-04 (±2.19e-04)**		c_4, k_2	-7.612e-05 (±2.16e-05)***		c_4, k_2	1.750e+00 (±1.25e-01)***		
c_5, k_3		c_5, k_3	2.913e-04 (±1.87e-05)***	c_5, k_3	4.470e-04 (±1.02e-05)***							
c_0, z_c	4.033e-01 (±4.90e-02)***	2.71 16.88 (1.09)	c_0, z_c	3.962e-01 (±4.44e-02)***	3.19 12.53 (0.91)	c_0, z_c	7.952e-01 (±3.69e-02)***	3.12 14.43 (0.93)	c_0, z_c	-2.095e+00 (±1.15e+00)***	5.67 32.97 (2.12)	R32 [1005, 2607] (59/52/55)
c_1, z_c	-4.484e-02 (±5.35e-03)***		c_1, z_c	-1.635e-02 (±9.11e-03)***		c_1, z_c	-6.163e-03 (±1.90e-03)***		c_1, z_c	4.272e-02 (±3.35e-01)		
c_2, k_0	5.235e-02 (±2.17e-03)***		c_2, k_0	4.307e-02 (±2.28e-03)***		c_2, k_0	6.100e-04 (±2.09e-03)		c_2, k_0	-1.822e+01 (±3.95e+00)***		
c_3, k_1	1.305e-03 (±2.24e-04)***		c_3, k_1	5.302e-04 (±2.86e-04)**		c_3, k_1	6.753e-05 (±5.38e-05)*		c_3, k_1	2.873e+01 (±1.22e+00)***		
c_4, k_2			c_4, k_2	-6.050e-04 (±6.31e-04)+		c_4, k_2	-7.108e-05 (±5.18e-05)**		c_4, k_2			
c_5, k_3		c_5, k_3	3.195e-04 (±6.40e-05)***	c_5, k_3	3.195e-04 (±6.40e-05)***	c_5, k_3	4.836e-04 (±2.82e-05)***					
c_0, z_c	2.880e-01 (±4.59e-02)***	4.95 17.94 (1.31)	c_0, z_c	3.566e-01 (±3.65e-02)***	4.19 10.61 (0.71)	c_0, z_c	7.815e-01 (±2.79e-02)***	4.62 13.00 (0.87)	c_0, z_c	-6.887e+00 (±9.46e-01)***	5.33 15.00 (1.01)	DR5 [929, 2401] (66/61/62)
c_1, z_c	-3.288e-02 (±5.73e-03)***		c_1, z_c	-1.259e-02 (±7.84e-03)***		c_1, z_c	-2.703e-03 (±1.34e-03)***		c_1, z_c	-1.112e+00 (±2.50e-01)***		
c_2, k_0	5.778e-02 (±2.07e-03)***		c_2, k_0	4.479e-02 (±1.86e-03)***		c_2, k_0	-1.732e-03 (±1.51e-03)*		c_2, k_0	1.700e+00 (±1.84e+00)+		
c_3, k_1	6.835e-04 (±2.46e-04)***		c_3, k_1	-2.444e-04 (±2.03e-04)*		c_3, k_1	-3.607e-05 (±3.49e-05)*		c_3, k_1	8.288e+00 (±1.64e+00)***		
c_4, k_2			c_4, k_2	3.952e-05 (±5.62e-04)		c_4, k_2	-4.084e-05 (±4.05e-05)*		c_4, k_2	2.716e+00 (±3.28e-01)***		
c_5, k_3		c_5, k_3	4.213e-04 (±4.72e-05)***	c_5, k_3	4.213e-04 (±4.72e-05)***	c_5, k_3	4.626e-04 (±1.91e-05)***					
c_0, z_c	2.959e-01 (±2.68e-02)***	2.29 10.48 (0.75)	c_0, z_c	3.021e-01 (±1.56e-02)**	1.02 4.64 (0.33)	c_0, z_c	6.949e-01 (±1.39e-02)***	1.25 6.33 (0.45)	c_0, z_c	-6.200e+00 (±4.92e-01)***	2.31 7.30 (0.52)	L41a [888, 2211] (65/60/61)
c_1, z_c	-3.105e-02 (±3.48e-03)***		c_1, z_c	-7.373e-03 (±3.52e-03)***		c_1, z_c	-4.315e-03 (±6.73e-04)***		c_1, z_c	-7.167e-01 (±1.25e-01)***		
c_2, k_0	5.503e-02 (±1.26e-03)***		c_2, k_0	4.661e-02 (±8.34e-04)**		c_2, k_0	1.556e-03 (±2.57e-04)***		c_2, k_0	7.395e-01 (±9.86e-01)		
c_3, k_1	7.344e-04 (±1.56e-04)***		c_3, k_1	2.042e-04 (±9.94e-05)***		c_3, k_1	2.430e-05 (±1.78e-05)**		c_3, k_1	1.011e+01 (±8.47e-01)***		
c_4, k_2			c_4, k_2	-8.129e-04 (±2.66e-04)***		c_4, k_2	-8.312e-05 (±1.99e-05)***		c_4, k_2	2.224e+00 (±1.65e-01)***		
c_5, k_3		c_5, k_3	2.678e-04 (±2.27e-05)**	c_5, k_3	3.922e-04 (±9.70e-06)**	c_5, k_3						
AHRI 33												
c_0, z_c	3.108e-01 (±3.10e-02)***	2.49 12.40 (0.80)	c_0, z_c	3.418e-01 (±1.68e-02)**	0.94 4.87 (0.31)	c_0, z_c	7.328e-01 (±1.62e-02)***	1.70 7.72 (0.50)	c_0, z_c	-6.539e+00 (±7.31e-01)***	2.46 12.31 (0.79)	R410A [945, 2432] (66/64/66)
c_1, z_c	-3.749e-02 (±3.64e-03)***		c_1, z_c	-1.578e-02 (±3.29e-03)***		c_1, z_c	-6.348e-03 (±7.48e-04)***		c_1, z_c	-9.907e-01 (±1.95e-01)***		
c_2, k_0	5.597e-02 (±1.28e-03)***		c_2, k_0	4.611e-02 (±7.90e-04)**		c_2, k_0	1.747e-03 (±8.64e-04)**		c_2, k_0	-4.754e+00 (±8.91e-01)***		
c_3, k_1	7.780e-04 (±1.44e-04)***		c_3, k_1	2.871e-04 (±7.57e-05)**		c_3, k_1	4.515e-05 (±1.91e-05)**		c_3, k_1	1.072e+01 (±7.33e-01)***		
c_4, k_2			c_4, k_2	-5.720e-04 (±2.15e-04)***		c_4, k_2	-9.265e-05 (±2.30e-05)**		c_4, k_2	1.358e+00 (±1.53e-01)***		
c_5, k_3		c_5, k_3	2.696e-04 (±1.84e-05)**	c_5, k_3	2.696e-04 (±1.84e-05)**	c_5, k_3	4.403e-04 (±1.08e-05)***					
c_0, z_c	3.480e-01 (±3.01e-02)***	1.80 10.67 (0.72)	c_0, z_c	3.405e-01 (±1.73e-02)***	0.89 5.01 (0.34)	c_0, z_c	7.230e-01 (±2.09e-02)***	1.42 8.31 (0.56)	c_0, z_c	-1.625e+00 (±7.99e-01)***	4.43 23.55 (1.59)	R32+R134a [943, 2452] (59/53/56)
c_1, z_c	-4.097e-02 (±3.44e-03)***		c_1, z_c	-1.627e-02 (±3.73e-03)***		c_1, z_c	-6.223e-03 (±1.09e-03)***		c_1, z_c	2.123e-01 (±2.27e-01)+		
c_2, k_0	5.388e-02 (±1.38e-03)***		c_2, k_0	4.610e-02 (±9.15e-04)**		c_2, k_0	2.024e-03 (±1.18e-03)**		c_2, k_0	-1.503e+01 (±2.66e+00)***		
c_3, k_1	1.107e-03 (±1.49e-04)***		c_3, k_1	4.505e-04 (±1.20e-04)**		c_3, k_1	6.219e-05 (±3.06e-05)**		c_3, k_1	2.598e+01 (±8.05e-01)***		
c_4, k_2			c_4, k_2	-5.988e-04 (±2.71e-04)**		c_4, k_2	-7.656e-05 (±2.98e-05)**		c_4, k_2			
c_5, k_3		c_5, k_3	2.716e-04 (±2.63e-05)**	c_5, k_3	2.716e-04 (±2.63e-05)**	c_5, k_3	4.461e-04 (±1.58e-05)***					

^a + p < 0.1, * p < 0.05, ** p < 0.01, *** p < 0.001; Confidence interval of 95% for regression coefficients;

^b Temperatures (°C);

^c Pressures (bar);

^d The values in brackets are the CV_{RMSE} (%);

Table J.2: Mass flow rate models (AHRI 11, 33)

	\dot{m}_{ref} (kg/h) Correlation 1b	MRE (%) RMSE ^d (kg/h)	\dot{m}_{ref} (kg/h) Correlation 2b	MRE (%) RMSE ^d (kg/h)	\dot{m}_{ref} (kg/h) Correlation 3b	MRE (%) RMSE ^d (kg/h)	Fluid \dot{m} Range [kg/h] (N° tests)
AHRI 11 (SH = 11K)							
c ₀	-4.472e+00 (±7.47e-01)***	1.61 0.61 (0.52)	-1.032e+00 (±2.55e+00)	1.37 0.57 (0.49)	1.170e+02 (±1.45e+00)***	1.42 0.40 (0.34)	R410A [66, 178] (66)
c ₁	1.658e+01 (±8.24e-02)***		1.617e+01 (±2.98e-01)***		4.082e+00 (±6.73e-02)***		
c ₂	-6.726e-01 (±2.38e-02)***		-8.171e-01 (±1.05e-01)***		1.242e-01 (±7.82e-02)**		
c ₃			1.661e-02 (±1.18e-02)**		4.019e-03 (±1.73e-03)***		
c ₄					5.603e-02 (±2.12e-03)***		
c ₅					-6.558e-03 (±9.85e-04)***		
c ₀	-3.185e-01 (±1.10e+00)	2.24 0.86 (1.05)	-9.252e+00 (±3.49e+00)***	1.67 0.70 (0.86)	7.745e+01 (±2.33e+00)***	2.16 0.54 (0.66)	R32 [46, 123] (59)
c ₁	1.129e+01 (±1.28e-01)***		1.227e+01 (±3.84e-01)***		2.960e+00 (±1.17e-01)***		
c ₂	-6.301e-01 (±3.93e-02)***		-2.390e-01 (±1.51e-01)**		3.423e-01 (±1.31e-01)***		
c ₃			-4.173e-02 (±1.58e-02)***		9.063e-05 (±3.25e-03)		
c ₄					3.534e-02 (±3.34e-03)***		
c ₅					-9.097e-03 (±1.74e-03)***		
c ₀	-2.305e+00 (±3.87e-01)***	1.33 0.32 (0.36)	-2.829e-01 (±1.29e+00)	1.02 0.29 (0.33)	8.896e+01 (±6.93e-01)***	0.65 0.19 (0.21)	DR5 [49, 134] (66)
c ₁	1.346e+01 (±4.59e-02)***		1.320e+01 (±1.62e-01)***		3.075e+00 (±3.21e-02)***		
c ₂	-6.068e-01 (±1.31e-02)***		-6.976e-01 (±5.68e-02)***		9.685e-02 (±3.73e-02)***		
c ₃			1.121e-02 (±6.85e-03)**		3.664e-03 (±8.23e-04)***		
c ₄					3.874e-02 (±1.01e-03)***		
c ₅					-5.486e-03 (±4.70e-04)***		
c ₀	-3.876e+00 (±5.04e-01)***	1.87 0.41 (0.52)	1.350e+00 (±1.17e+00)*	1.22 0.27 (0.33)	8.315e+01 (±9.38e-01)***	0.99 0.25 (0.32)	L41a [43, 122] (65)
c ₁	1.291e+01 (±6.38e-02)***		1.222e+01 (±1.53e-01)***		2.803e+00 (±4.49e-02)***		
c ₂	-5.266e-01 (±1.79e-02)***		-7.731e-01 (±5.42e-02)***		-7.364e-02 (±5.07e-02)**		
c ₃			3.171e-02 (±6.81e-03)***		4.679e-03 (±1.17e-03)***		
c ₄					3.476e-02 (±1.40e-03)***		
c ₅					-2.793e-03 (±6.41e-04)***		
AHRI 33 (SH = 11K)							
c ₀	-3.538e+00 (±6.18e-01)***	1.08 0.50 (0.42)	-5.008e+00 (±2.20e+00)***	1.14 0.49 (0.41)	1.181e+02 (±9.69e-01)***	0.75 0.26 (0.22)	R410A [68, 181] (66)
c ₁	1.675e+01 (±6.82e-02)***		1.692e+01 (±2.58e-01)***		4.203e+00 (±4.49e-02)***		
c ₂	-6.515e-01 (±1.97e-02)***		-5.898e-01 (±9.10e-02)***		2.138e-01 (±5.21e-02)***		
c ₃			-7.096e-03 (±1.02e-02)		2.178e-03 (±1.15e-03)***		
c ₄					5.285e-02 (±1.41e-03)***		
c ₅					-7.474e-03 (±6.57e-04)***		
c ₀	-9.958e-01 (±6.30e-01)**	1.46 0.50 (0.61)	-4.578e+00 (±2.23e+00)***	1.33 0.46 (0.55)	7.815e+01 (±9.68e-01)***	1.10 0.23 (0.27)	R32+R134a [46, 123] (59)
c ₁	1.175e+01 (±7.69e-02)***		1.216e+01 (±2.57e-01)***		2.838e+00 (±4.87e-02)***		
c ₂	-5.731e-01 (±2.34e-02)***		-4.102e-01 (±1.00e-01)***		2.916e-01 (±5.44e-02)***		
c ₃			-1.819e-02 (±1.09e-02)**		3.701e-03 (±1.35e-03)***		
c ₄					3.430e-02 (±1.39e-03)***		
c ₅					-8.067e-03 (±7.23e-04)***		

^a + p < 0.1, * p < 0.05, ** p < 0.01, *** p < 0.001; Confidence interval of 95% for regression coefficients;

^b Temperatures (°C);

^c Pressures (bar);

^d The values in brackets are the CV_{RMSE} (%);

J.1.2 Compressor ZS21KAE-PFV (AHRI 21)

Table J.3: Energy consumption models (AHRI 21)

\dot{W}_c (kW)		MRE (%)	RMSE ^d (W)	\dot{W}_c (kW)		MRE (%)	RMSE ^d (W)	\dot{W}_c (kW)		MRE (%)	RMSE ^d (W)	\dot{W}_{esp} (kJ/kg)	MRE (%)	RMSE ^d (W)	Fluid W_r Range [W] (N° tests)
Correlation 1a				Correlation 2a				Correlation 3a							
AHRI 21															
c_0, z_c	7.650e-01 (±5.09e-02)**	2.34	21.50 (0.74)	5.876e-01 (±4.24e-02)**	1.54	13.44 (0.46)	1.364e+00 (±4.87e-02)**	2.19	14.04 (0.48)	-6.117e+00 (±6.01e-01)**	2.84	24.07 (0.83)	2.84	16.73 (0.68)	R404A [1856, 4172] (64/63/64)
c_1, z_c	-2.086e-03 (±1.26e-02)			1.100e-01 (±1.53e-02)**			-1.109e-02 (±2.35e-03)**			-6.089e-01 (±1.05e-01)**					
c_2, k_0	8.803e-02 (±2.51e-03)**			8.301e-02 (±2.97e-03)**			2.082e-02 (±1.91e-03)**			-2.652e+00 (±1.38e+00)**					
c_3, k_1	4.986e-03 (±5.92e-04)**			7.071e-03 (±5.14e-04)**			4.832e-04 (±3.59e-05)**			1.013e+01 (±2.59e-01)**					
c_4, k_2				-1.782e-02 (±2.11e-03)**			-2.083e-04 (±4.68e-05)**								
c_5, k_3		-8.686e-05 (±8.80e-05)+	4.177e-04 (±1.93e-05)**												
c_0, z_c	6.718e-01 (±3.77e-02)**	1.89	17.42 (0.70)	5.179e-01 (±2.66e-02)**	1.29	9.40 (0.30)	1.165e+00 (±3.50e-02)**	1.65	9.73 (0.30)	-4.855e+00 (±3.57e-01)**	2.18	16.73 (0.68)	2.18	16.73 (0.68)	ARM31a [1582, 3615] (58/64/64)
c_1, z_c	1.598e-02 (±1.16e-02)**			1.197e-01 (±1.21e-02)**			-8.665e-03 (±1.68e-03)**			-2.704e-01 (±5.44e-02)**					
c_2, k_0	8.459e-02 (±2.19e-03)**			8.342e-02 (±2.20e-03)**			1.830e-02 (±1.38e-03)**			4.238e-01 (±1.28e+00)					
c_3, k_1	5.617e-03 (±6.37e-04)**			8.578e-03 (±4.93e-04)**			4.503e-04 (±2.64e-05)**			1.155e+01 (±2.09e-01)**					
c_4, k_2				-2.242e-02 (±2.11e-03)**			-1.556e-04 (±3.31e-05)**								
c_5, k_3		-2.473e-04 (±7.69e-05)**	3.626e-04 (±1.40e-05)**												
c_0, z_c	7.080e-01 (±4.13e-02)**	2.61	18.41 (0.68)	5.574e-01 (±3.23e-02)**	1.61	11.01 (0.41)	1.260e+00 (±4.30e-02)**	1.85	11.98 (0.44)	-5.108e+00 (±4.78e-01)**	2.48	20.85 (0.77)	2.48	20.85 (0.77)	D2Y65 [1724, 3988] (56/64/63)
c_1, z_c	1.104e-03 (±1.11e-02)			1.028e-01 (±1.33e-02)**			-1.027e-02 (±2.11e-03)**			-4.011e-01 (±7.94e-02)**					
c_2, k_0	8.712e-02 (±2.20e-03)**			8.351e-02 (±2.41e-03)**			1.873e-02 (±1.71e-03)**			-1.482e+00 (±1.57e+00)+					
c_3, k_1	5.247e-03 (±5.58e-04)**			7.683e-03 (±4.92e-04)**			4.824e-04 (±3.30e-05)**			1.269e+01 (±2.77e-01)**					
c_4, k_2				-1.886e-02 (±2.10e-03)**			-1.699e-04 (±4.21e-05)**								
c_5, k_3		-1.473e-04 (±7.70e-05)**	4.285e-04 (±1.75e-05)**												
c_0, z_c	6.125e-01 (±3.49e-02)**	2.27	15.79 (0.64)	5.073e-01 (±2.52e-02)**	1.50	9.04 (0.37)	1.164e+00 (±3.69e-02)**	1.29	9.12 (0.37)	-4.686e+00 (±3.98e-01)**	2.02	16.78 (0.68)	2.02	16.78 (0.68)	L40 [1570, 3655] (53/61/59)
c_1, z_c	1.549e-02 (±1.07e-02)**			1.149e-01 (±1.24e-02)**			-8.714e-03 (±1.87e-03)**			-3.070e-01 (±6.20e-02)**					
c_2, k_0	9.143e-02 (±2.16e-03)**			8.526e-02 (±2.20e-03)**			1.627e-02 (±1.47e-03)**			-1.793e+00 (±1.61e+00)+					
c_3, k_1	5.172e-03 (±6.15e-04)**			8.141e-03 (±5.88e-04)**			4.321e-04 (±3.04e-05)**			1.365e+01 (±2.70e-01)**					
c_4, k_2				-2.182e-02 (±2.41e-03)**			-1.650e-04 (±3.60e-05)**								
c_5, k_3		-1.149e-04 (±8.41e-05)**	4.079e-04 (±1.50e-05)**												
c_0, z_c	6.068e-01 (±3.96e-02)**	1.46	15.50 (0.58)	5.295e-01 (±2.68e-02)**	0.91	8.89 (0.33)	1.306e+00 (±8.29e-02)**	1.28	13.62 (0.51)	-4.049e+00 (±7.28e-01)**	2.03	22.48 (0.84)	2.03	22.48 (0.84)	R32+R134a [1740, 4268] (40/48/45)
c_1, z_c	-5.817e-03 (±1.03e-02)			1.081e-01 (±1.53e-02)**			-1.140e-02 (±4.77e-03)**			-4.138e-01 (±1.33e-01)**					
c_2, k_0	1.029e-01 (±2.53e-03)**			8.812e-02 (±2.52e-03)**			1.395e-02 (±3.43e-03)**			-8.245e+00 (±3.16e+00)**					
c_3, k_1	5.034e-03 (±5.82e-04)**			7.895e-03 (±9.05e-04)**			4.759e-04 (±8.47e-05)**			1.752e+01 (±5.95e-01)**					
c_4, k_2				-2.128e-02 (±3.22e-03)**			-2.337e-04 (±9.03e-05)**								
c_5, k_3		9.119e-05 (±1.11e-04)	5.739e-04 (±3.56e-05)**												

^a + p < 0.1, * p < 0.05, ** p < 0.01, *** p < 0.001; Confidence interval of 95% for regression coefficients;

^b Temperatures (°C);

^c Pressures (bar);

^d The values in brackets are the CV_{RMSE} (%);

Table J.4: Mass flow rate models (AHRI 21)

	\dot{m}_{ref} (kg/h) Correlation 1b	MIRE (%) RMSE ^d (kg/h)	\dot{m}_{ref} (kg/h) Correlation 2b	MIRE (%) RMSE ^d (kg/h)	\dot{m}_{ref} (kg/h) Correlation 3b	MIRE (%) RMSE ^d (kg/h)	Fluid \dot{m} Range [kg/h] (N ^o tests)
AHRI 21 (SH = 11K)							
c ₀	4.801e+00 (±9.67e-01)***	1.09 0.80 (0.40)	-4.720e+00 (±2.29e+00)***	0.85 0.53 (0.26)	3.056e+02 (±3.24e+00)***	0.75 0.49 (0.24)	R404A [124, 308] (63)
c ₁	5.093e+01 (±2.12e-01)***		5.332e+01 (±5.70e-01)***		9.744e+00 (±1.57e-01)***		
c ₂	-7.107e-01 (±4.24e-02)**		-2.385e-01 (±1.13e-01)***		-1.708e-02 (±1.25e-01)		
c ₃			-1.156e-01 (±2.67e-02)**		-5.005e-03 (±2.38e-03)***		
c ₄					9.452e-02 (±3.07e-03)***		
c ₅					-4.410e-03 (±1.25e-03)***		
c ₀	1.362e+00 (±3.74e-01)***	0.73 0.33 (0.26)	-7.923e-01 (±1.09e+00)	0.92 0.29 (0.23)	1.966e+02 (±1.67e+00)***	0.92 0.28 (0.22)	ARM31a [73, 200] (64)
c ₁	4.077e+01 (±1.01e-01)***		4.145e+01 (±3.35e-01)***		6.563e+00 (±8.21e-02)***		
c ₂	-5.273e-01 (±1.85e-02)**		-4.026e-01 (±6.20e-02)**		-7.248e-02 (±6.65e-02)*		
c ₃			-3.794e-02 (±1.82e-02)**		-1.204e-03 (±1.24e-03)+		
c ₄					6.842e-02 (±1.71e-03)***		
c ₅					-1.931e-03 (±6.86e-04)**		
c ₀	2.573e+00 (±6.38e-01)***	1.24 0.55 (0.40)	-6.429e-01 (±1.95e+00)	1.62 0.50 (0.37)	2.089e+02 (±2.58e+00)***	1.33 0.44 (0.32)	D2Y65 [81, 214] (64)
c ₁	3.888e+01 (±1.52e-01)***		3.977e+01 (±5.30e-01)***		6.772e+00 (±1.27e-01)***		
c ₂	-5.252e-01 (±2.84e-02)**		-3.566e-01 (±1.01e-01)***		5.783e-02 (±1.03e-01)		
c ₃			-4.516e-02 (±2.61e-02)**		2.105e-04 (±1.92e-03)		
c ₄					6.698e-02 (±2.66e-03)***		
c ₅					-3.509e-03 (±1.06e-03)**		
c ₀	1.311e+00 (±4.82e-01)***	1.04 0.42 (0.38)	-4.331e-01 (±1.55e+00)	1.29 0.41 (0.36)	1.661e+02 (±2.13e+00)***	1.04 0.32 (0.29)	L40 [64, 175] (61)
c ₁	3.668e+01 (±1.41e-01)***		3.723e+01 (±4.83e-01)***		5.692e+00 (±1.09e-01)***		
c ₂	-5.020e-01 (±2.56e-02)**		-3.967e-01 (±9.25e-02)**		2.149e-01 (±8.51e-02)***		
c ₃			-3.196e-02 (±2.71e-02)*		2.328e-03 (±1.70e-03)**		
c ₄					6.098e-02 (±2.20e-03)**		
c ₅					-4.778e-03 (±8.68e-04)**		
c ₀	2.304e+00 (±7.79e-01)***	1.76 0.61 (0.51)	1.800e+00 (±2.71e+00)	1.75 0.61 (0.51)	1.697e+02 (±5.23e+00)***	1.33 0.53 (0.44)	R32+R134a [68, 179] (48)
c ₁	3.519e+01 (±2.50e-01)***		3.532e+01 (±7.17e-01)***		5.883e+00 (±3.05e-01)***		
c ₂	-8.091e-01 (±4.61e-02)**		-7.783e-01 (±1.65e-01)***		4.069e-01 (±2.15e-01)***		
c ₃			-7.643e-03 (±3.93e-02)		7.470e-03 (±5.21e-03)**		
c ₄					6.584e-02 (±6.07e-03)***		
c ₅					-8.758e-03 (±2.22e-03)**		

^a + p < 0.1, * p < 0.05, ** p < 0.01, *** p < 0.001; Confidence interval of 95% for regression coefficients;

^b Temperatures (°C);

^c Pressures (bar);

^d The values in brackets are the CV_{RMSE} (%);

J.1.3 Compressor ZP31K5E-PFV (AHRI 24, 38, 39, 58)

Table J.5: Energy consumption models (AHRI 24, 38, 39, 58)

\dot{W}_c (kW)		MRE (%)	RMSE ^d (W)	\dot{W}_c (kW)		MRE (%)	RMSE ^d (W)	\dot{W}_c (kW)		MRE (%)	RMSE ^d (W)	\dot{W}_{esp} (kJ/kg)		MRE (%)	RMSE ^d (W)	Fluid
Correlation 1a				Correlation 2a				Correlation 3a								\dot{W}_{Range} [W] (N ^c tests)
AHRI 24																
c_0, z_c	1.850e-01 (±2.67e-01)			4.408e-01 (±1.94e-01)***				1.526e+00 (±2.38e-01)***				-3.750e+00 (±1.95e+00)***				
c_1, z_c	-2.583e-02 (±3.81e-02)			3.311e-03 (±3.88e-02)				9.172e-03 (±9.35e-03)+				-5.827e-01 (±3.98e-01)**				
c_2, k_0	9.239e-02 (±1.22e-02)***	3.54	32.58 (1.36)	6.363e-02 (±1.33e-02)***				-2.063e-02 (±1.13e-02)**				1.118e+01 (±7.07e+00)**				DR5
c_3, k_1	3.966e-04 (±1.64e-03)			-1.946e-03 (±1.70e-03)*		1.91	18.67 (0.78)	-3.113e-04 (±2.02e-04)**		1.71	18.40 (0.77)	6.059e+00 (±5.11e+00)*			3.00	[1591, 3681]
c_4, k_2				1.748e-03 (±1.17e-03)*				7.699e-05 (±1.57e-04)				2.697e+00 (±7.93e-01)***				(22)
c_5, k_3				8.805e-04 (±3.43e-04)***				8.824e-04 (±1.28e-04)***								
AHRI 38																
c_0, z_c	1.657e-01 (±9.69e-02)**			3.316e-01 (±4.94e-02)***				1.091e+00 (±8.42e-02)***				-2.644e+00 (±8.22e-01)***				
c_1, z_c	-2.257e-02 (±1.33e-02)**			-3.014e-03 (±1.05e-02)				-1.454e-03 (±2.69e-03)				-3.411e-01 (±1.61e-01)***				
c_2, k_0	9.010e-02 (±4.76e-03)***	2.29	19.98 (0.90)	7.038e-02 (±1.18e-03)***		1.25	7.75 (0.35)	-6.246e-03 (±4.01e-03)**		1.77	11.21 (0.50)	3.762e+00 (±2.53e+00)**			2.68	L41b
c_3, k_1	3.322e-04 (±6.10e-04)			-5.091e-04 (±3.60e-04)**				-5.537e-05 (±6.34e-05)+				1.227e+01 (±1.83e+00)**				[1335, 3481]
c_4, k_2				-2.129e-04 (±9.86e-04)				-3.220e-05 (±5.50e-05)				1.976e+00 (±2.96e-01)***				(30)
c_5, k_3				5.271e-04 (±9.40e-05)***				6.634e-04 (±4.60e-05)***								
AHRI 39																
c_0, z_c	2.397e-01 (±1.22e-01)***			3.880e-01 (±6.98e-02)***				1.392e+00 (±1.70e-01)***				2.934e+00 (±1.50e+00)***				
c_1, z_c	-4.278e-02 (±1.34e-02)***			-1.042e-02 (±1.34e-02)				1.808e-03 (±5.45e-03)				9.263e-01 (±2.90e-01)***				
c_2, k_0	9.041e-02 (±5.23e-03)***	1.93	16.25 (0.62)	6.984e-02 (±6.01e-03)***		0.60	7.26 (0.28)	-1.199e-02 (±8.23e-03)**		0.86	10.00 (0.38)	-7.124e+00 (±5.16e+00)**			3.65	R32
c_3, k_1	1.073e-03 (±5.39e-04)***			-5.215e-04 (±5.41e-04)+				-1.382e-04 (±1.32e-04)*				2.670e+01 (±1.23e+00)***				[1714, 4064]
c_4, k_2				4.606e-04 (±9.04e-04)				2.466e-05 (±7.91e-05)								(23)
c_5, k_3				6.159e-04 (±1.58e-04)***				8.850e-04 (±9.62e-05)***								
AHRI 58																
c_0, z_c	1.431e-01 (±1.55e-01)+			3.864e-01 (±5.95e-02)***				1.265e+00 (±9.05e-02)***				-1.800e+00 (±1.17e+00)**				
c_1, z_c	-2.852e-02 (±1.83e-02)**			-1.277e-02 (±1.15e-02)*				-3.079e-04 (±2.81e-03)				-3.068e-01 (±2.55e-01)*				
c_2, k_0	9.504e-02 (±7.07e-03)***	4.29	29.78 (1.22)	7.075e-02 (±4.36e-03)***		0.87	8.95 (0.37)	-1.117e-02 (±4.20e-03)**		1.56	13.07 (0.53)	1.776e+00 (±2.98e+00)			2.51	R454B
c_3, k_1	2.736e-04 (±7.73e-04)			-8.491e-04 (±3.30e-04)***				-1.207e-04 (±6.62e-05)***				1.238e+01 (±2.33e+00)***				[1451, 3878]
c_4, k_2				7.100e-04 (±9.15e-04)				-1.631e-05 (±5.76e-05)				1.741e+00 (±4.10e-01)***				(29)
c_5, k_3				6.219e-04 (±8.48e-05)***				7.798e-04 (±4.72e-05)***								

a + p < 0.1, * p < 0.05, ** p < 0.01, *** p < 0.001; Confidence interval of 95% for regression coefficients;

b Temperatures (°C);

c Pressures (bar);

d The values in brackets are the CV_{RMSE} (%);

Table J.6: Mass flow rate models (AHRI 24, 38, 39, 58)

	\dot{m}_{ref} (kg/h) Correlation 1b	MRE (%) RMSE ^d (kg/h)	\dot{m}_{ref} (kg/h) Correlation 2b	MRE (%) RMSE ^d (kg/h)	\dot{m}_{ref} (kg/h) Correlation 3b	MRE (%) RMSE ^d (kg/h)	Fluid <i>m</i> Range [kg/h] (N° tests)
AHRI 24 (<i>SH</i> = 11K)							
<i>c</i> ₀	-1.220e+00 (±1.85e+00)		5.781e+00 (±6.81e+00)+		1.250e+02 (±6.94e+00)***		
<i>c</i> ₁	1.993e+01 (±2.66e-01)***		1.893e+01 (±9.73e-01)***		4.439e+00 (±2.72e-01)***		
<i>c</i> ₂	-8.663e-01 (±8.06e-02)**	2.69	-1.187e+00 (±3.12e-01)***	1.58	5.482e-01 (±3.30e-01)**	1.41	DR5
<i>c</i> ₃		0.94 (0.91)	4.437e-02 (±4.18e-02)*	0.83 (0.80)	8.922e-03 (±5.90e-03)**	0.54 (0.52)	[47, 166]
<i>c</i> ₄					5.370e-02 (±4.57e-03)***		(22)
<i>c</i> ₅					-1.199e-02 (±3.72e-03)***		
AHRI 38 (<i>SH</i> = 11K)							
<i>c</i> ₀	-1.335e+00 (±1.70e+00)		4.829e+00 (±4.75e+00)*		1.060e+02 (±7.54e+00)***		
<i>c</i> ₁	1.786e+01 (±2.24e-01)***		1.701e+01 (±6.54e-01)***		3.709e+00 (±2.41e-01)***		
<i>c</i> ₂	-6.834e-01 (±7.44e-02)**	2.80	-9.896e-01 (±2.33e-01)***	2.60	1.310e-01 (±3.59e-01)	2.64	L41b
<i>c</i> ₃		1.12 (1.12)	4.096e-02 (±2.99e-02)**	0.98 (0.98)	5.641e-03 (±5.68e-03)+	1.00 (1.01)	[38, 162]
<i>c</i> ₄					4.553e-02 (±4.93e-03)***		(30)
<i>c</i> ₅					-6.023e-03 (±4.12e-03)**		
AHRI 39 (<i>SH</i> = 11K)							
<i>c</i> ₀	1.233e-02 (±2.47e+00)		-7.728e+00 (±8.05e+00)+		1.206e+02 (±1.71e+01)***		
<i>c</i> ₁	1.671e+01 (±2.63e-01)***		1.756e+01 (±8.83e-01)***		4.304e+00 (±5.49e-01)***		
<i>c</i> ₂	-8.146e-01 (±9.90e-02)***	1.88	-4.823e-01 (±3.44e-01)**	1.70	2.677e-01 (±8.28e-01)	1.62	R32
<i>c</i> ₃		1.19 (1.00)	-3.556e-02 (±3.55e-02)*	1.07 (0.90)	1.467e-03 (±1.33e-02)	1.01 (0.85)	[44, 182]
<i>c</i> ₄					4.500e-02 (±7.96e-03)***		(23)
<i>c</i> ₅					-9.181e-03 (±9.69e-03)+		
AHRI 58 (<i>SH</i> = 11K)							
<i>c</i> ₀	9.802e-01 (±2.82e+00)		3.689e+00 (±9.49e+00)		1.276e+02 (±1.04e+01)***		
<i>c</i> ₁	2.005e+01 (±3.43e-01)***		1.973e+01 (±1.12e+00)***		4.312e+00 (±3.23e-01)***		
<i>c</i> ₂	-8.330e-01 (±1.14e-01)***	6.30	-9.575e-01 (±4.32e-01)***	5.53	5.306e-01 (±4.83e-01)*	5.64	R454B
<i>c</i> ₃		1.83 (1.35)	1.412e-02 (±4.71e-02)	1.82 (1.34)	1.034e-02 (±7.61e-03)**	1.50 (1.10)	[46, 201]
<i>c</i> ₄					4.828e-02 (±6.62e-03)***		(29)
<i>c</i> ₅					-1.187e-02 (±5.42e-03)**		

^a + *p* < 0.1, * *p* < 0.05, ** *p* < 0.01, *** *p* < 0.001; Confidence interval of 95% for regression coefficients;

^b Temperatures (°C);

^c Pressures (bar);

^d The values in brackets are the *CV*_{RMSE} (%);

J.1.4 Compressor ZF18K4E-TFD (AHRI 34, 36)

Table J.7: Energy consumption models (AHRI 34, 36)

\dot{W}_L (kW)		MRE (%) RMSE ^d (W)	\dot{W}_L (kW)		\dot{W}_L (kW)		\dot{W}_{esp} (kJ/kg)		Fluid \dot{W} Range [W] (N° tests)
Correlation 1a			Correlation 2a		Correlation 3a				
AHRI 34									
c_0, z_c	2.821e-01 (±5.97e-01)	11.03 147.02 (0.05)	6.269e-01 (±5.18e-01)*	4.10 67.32 (0.40)	3.813e+00 (±5.00e-01)***	1.69 39.80 (0.83)	-2.859e+00 (±9.55e-01)***	2.01 56.23 (1.17)	DR7 [2422, 8147] (19)
c_1, z_e	4.213e-01 (±1.67e-01)***		6.640e-01 (±1.14e-01)***		4.493e-02 (±1.22e-02)***		-3.591e-01 (±1.02e-01)***		
c_2, k_0	1.530e-01 (±3.32e-02)***		7.645e-02 (±5.93e-02)*		8.917e-03 (±2.18e-02)		1.380e+01 (±2.95e+00)***		
c_3, k_1	3.447e-03 (±8.28e-03)		6.555e-03 (±5.98e-03)*		5.684e-04 (±2.21e-04)***		1.034e+01 (±5.24e-01)***		
c_4, k_2			-3.686e-02 (±1.37e-02)***		1.930e-04 (±1.32e-04)***				
c_5, k_3		1.602e-03 (±1.81e-03)+	8.963e-04 (±2.33e-04)***						
AHRI 36									
c_0, z_c	1.562e-01 (±4.75e-01)	7.74 116.54 (0.82)	5.390e-01 (±4.13e-01)*	3.28 54.13 (1.31)	3.454e+00 (±5.83e-01)***	1.83 38.86 (0.94)	-3.232e+00 (±1.20e+00)***	2.45 61.10 (1.48)	L40 [2108, 7268] (19)
c_1, z_e	4.589e-01 (±1.51e-01)***		6.809e-01 (±1.04e-01)***		4.523e-02 (±1.59e-02)***		-2.960e+01 (±1.13e-01)***		
c_2, k_0	1.620e-01 (±3.09e-02)***		8.193e-02 (±5.29e-02)**		3.978e-03 (±2.56e-02)		1.660e+01 (±4.08e+00)***		
c_3, k_1	1.794e-03 (±8.57e-03)		4.265e-03 (±7.43e-03)		4.288e-04 (±2.96e-04)**		1.119e+01 (±6.35e-01)***		
c_4, k_2			-3.736e-02 (±1.74e-02)***		2.268e-04 (±1.68e-04)*				
c_5, k_3		1.996e-03 (±1.96e-03)*	8.511e-04 (±2.71e-04)***						

^a + p < 0.1, * p < 0.05, ** p < 0.01, *** p < 0.001; Confidence interval of 95% for regression coefficients;

^b Temperatures (°C);

^c Pressures (bar);

^d The values in brackets are the CV_{RMSE} (%);

Table J.8: Mass flow rate models (AHRI 34, 36)

\dot{m}_{ref} (kg/h)		MRE (%) RMSE ^d (kg/h)	\dot{m}_{ref} (kg/h)		\dot{m}_{ref} (kg/h)		Fluid \dot{m} Range [kg/h] (N° tests)
Correlation 1b			Correlation 2b		Correlation 3b		
AHRI 34 (SH = 11K)							
c_0	7.474e+00 (±7.44e+00)*	3.75 3.95 (1.60)	1.663e+00 (±1.56e+01)	3.56 3.85 (1.55)	3.931e+02 (±4.60e+01)***	4.80 3.66 (1.48)	DR7 [76, 520] (19)
c_1	7.569e+01 (±1.21e+00)***		7.746e+01 (±4.37e+00)***		1.352e+01 (±1.13e+00)***		
c_2	-1.103e+00 (±4.20e-01)***		-7.815e-01 (±8.69e-01)+		1.319e+00 (±2.01e+00)		
c_3			-9.196e-02 (±2.17e-01)		2.305e-03 (±2.03e-02)		
c_4					1.328e-01 (±1.22e-02)***		
c_5			-2.141e-02 (±2.15e-02)+				
AHRI 36 (SH = 11K)							
c_0	4.905e+00 (±2.37e+00)***	3.04 1.28 (0.72)	4.505e-01 (±4.41e+00)	2.40 1.08 (0.61)	3.155e+02 (±3.17e+01)***	8.09 2.11 (1.19)	L40 [54, 396] (19)
c_1	6.922e+01 (±4.56e-01)***		6.846e+01 (±1.40e+00)***		1.107e+01 (±8.64e-01)***		
c_2	-9.148e-01 (±1.60e-01)***		-6.288e-01 (±2.86e-01)***		1.960e-01 (±1.39e+00)		
c_3			-9.107e-02 (±7.95e-02)*		-6.993e-03 (±1.61e-02)		
c_4					1.115e-01 (±9.12e-03)***		
c_5			-7.849e-03 (±1.48e-02)				

^a + p < 0.1, * p < 0.05, ** p < 0.01, *** p < 0.001; Confidence interval of 95% for regression coefficients;

^b Temperatures (°C);

^c Pressures (bar);

^d The values in brackets are the CV_{RMSE} (%);

J.1.5 Compressor ZP122KCE-TFD (AHRI 65)

Table J.9: Energy consumption models (AHRI 65)

	\dot{W}_c (kW) Correlation 1a	MRE (%) RMSE ^d (W)	\dot{W}_c (kW) Correlation 2a	MRE (%) RMSE ^d (W)	\dot{W}_c (kW) Correlation 3a	MRE (%) RMSE ^d (W)	\dot{W}_{esp} (kJ/kg)	MRE (%) RMSE ^d (W)	Fluid \dot{W}_c Range [W] (N° tests)
AHRI 65									
c_0, z_c	3.263e-01 (±2.07e-01)**		7.012e-01 (±1.45e-01)**		3.386e+00 (±2.20e-01)**		-3.530e+00 (±7.69e-01)**		
c_1, z_e	6.592e-02 (±2.91e-02)**		1.128e-01 (±2.18e-02)**		1.915e-02 (±7.03e-03)**		-2.673e-01 (±1.49e-01)**		
c_2, k_0	2.525e-01 (±1.05e-02)**	2.02	2.061e-01 (±1.27e-02)**	0.79	-7.749e-03 (±1.09e-02)	1.07	2.599e+00 (±1.82e+00)**	0.89	R447A
c_3, k_1	-1.110e-03 (±1.29e-03)*	52.65 (0.80)	-1.149e-03 (±9.38e-04)*	22.96 (0.35)	-2.303e-04 (±1.75e-04)*		1.396e+01 (±1.34e+00)**	33.77 (0.52)	[3902, 9868]
c_4, k_2			-2.790e-03 (±2.03e-03)*		5.362e-05 (±1.18e-04)		7.045e-01 (±2.13e-01)**		(23)
c_5, k_3			8.946e-04 (±2.79e-04)**		1.621e-03 (±1.24e-04)**				

^a + p < 0.1, * p < 0.05, ** p < 0.01, *** p < 0.001; Confidence interval of 95% for regression coefficients;

^b Temperatures (°C);

^c Pressures (bar);

^d The values in brackets are the CV_{RMSE} (%);

Table J.10: Mass flow rate models (AHRI 65)

	\dot{m}_{ref} (kg/h) Correlation 1b	MRE (%) RMSE ^d (kg/h)	\dot{m}_{ref} (kg/h) Correlation 2b	MRE (%) RMSE ^d (kg/h)	\dot{m}_{ref} (kg/h) Correlation 3b	MRE (%) RMSE ^d (kg/h)	Fluid \dot{m} Range [kg/h] (N° tests)
AHRI 65 (SH = 11K)							
c_0	-4.831e+00 (±6.44e+00)		-1.962e+00 (±1.76e+01)		3.087e+02 (±1.83e+01)**		
c_1	5.799e+01 (±8.25e-01)**		5.758e+01 (±2.48e+00)**		1.118e+01 (±5.85e-01)**		
c_2	-1.475e+00 (±3.00e-01)**	2.51	-1.622e+00 (±8.91e-01)**	2.58	2.306e+00 (±9.05e-01)**	1.49	R447A
c_3		4.49 (1.23)	1.931e-02 (±1.10e-01)	4.47 (1.23)	3.730e-02 (±1.46e-02)**	2.35 (0.64)	[116, 644]
c_4					1.293e-01 (±9.85e-03)**		(23)
c_5					-3.707e-02 (±1.03e-02)**		

^a + p < 0.1, * p < 0.05, ** p < 0.01, *** p < 0.001; Confidence interval of 95% for regression coefficients;

^b Temperatures (°C);

^c Pressures (bar);

^d The values in brackets are the CV_{RMSE} (%);

J.1.6 Compressor SH161A4 (AHRI 66)

Table J.11: Energy consumption models (AHRI 66)

\dot{W}_c (kW) Correlation 1a		MRE (%) RMSE ^d (W)	\dot{W}_c (kW) Correlation 2a		MRE (%) RMSE ^d (W)	\dot{W}_c (kW) Correlation 3a		MRE (%) RMSE ^d (W)	\dot{W}_{esp} (kJ/kg)	MRE (%) RMSE ^d (W)	Fluid \dot{W}_c Range [W] (N° tests)
AHRI 66											
c_0, z_c	4.960e-01 ($\pm 4.00e-01$)*	1.77 69.52 (0.76)	9.021e-01 ($\pm 1.36e-01$)**	0.35 19.53 (0.21)	5.253e+00 ($\pm 3.80e-01$)**	11.6 38.52 (0.42)	2.543e-01 ($\pm 1.07e+00$)	2.51 114.44 (1.26)	1.978e-01 ($\pm 2.00e-01$)+	2.51 114.44 (1.26)	HPR2A [5851, 14745] (28)
c_1, z_p	5.760e-02 ($\pm 5.13e-02$)*		1.804e-01 ($\pm 2.69e-02$)**		3.714e-02 ($\pm 1.36e-02$)**		1.978e-01 ($\pm 2.00e-01$)+				
c_2, k_0	3.435e-01 ($\pm 1.97e-02$)**		2.769e-01 ($\pm 1.04e-02$)**		-3.023e-02 ($\pm 1.81e-02$)*		-1.441e-02 ($\pm 2.96e+00$)				
c_3, k_1	9.248e-04 ($\pm 2.37e-03$)		-3.072e-03 ($\pm 1.21e-03$)**		-4.760e-04 ($\pm 3.25e-04$)**		1.917e+01 ($\pm 6.88e-01$)**				
c_4, k_2			-2.506e-03 ($\pm 2.49e-03$)*		1.942e-04 ($\pm 2.16e-04$)+						
c_5, k_3			1.871e-03 ($\pm 2.75e-04$)**		2.628e-03 ($\pm 2.05e-04$)**						

^a + p < 0.1, * p < 0.05, ** p < 0.01, *** p < 0.001; Confidence interval of 95% for regression coefficients;
^b Temperatures (°C);
^c Pressures (bar);
^d The values in brackets are the CV_{RMSE} (%).

Table J.12: Mass flow rate models (AHRI 66)

\dot{m}_{ref} (kg/h) Correlation 1b		MRE (%) RMSE ^d (kg/h)	\dot{m}_{ref} (kg/h) Correlation 2b		MRE (%) RMSE ^d (kg/h)	\dot{m}_{ref} (kg/h) Correlation 3b		MRE (%) RMSE ^d (kg/h)	Fluid \dot{m} Range [kg/h] (N° tests)
AHRI 66 (SH = 11K)									
c_0	1.244e+01 ($\pm 6.04e+00$)**	2.35 3.78 (0.74)	-1.168e+01 ($\pm 1.90e+01$)	1.88 3.30 (0.65)	4.610e+02 ($\pm 2.29e+01$)**	2.18 2.33 (0.46)	1.736e+01 ($\pm 8.23e-01$)**	2.18 2.33 (0.46)	HPR2A [195, 754] (28)
c_1	7.891e+01 ($\pm 7.82e-01$)**		8.200e+01 ($\pm 2.44e+00$)**		1.736e+01 ($\pm 8.23e-01$)**				
c_2	-2.513e+00 ($\pm 2.58e-01$)**		-1.312e+00 ($\pm 9.36e-01$)**		2.682e+00 ($\pm 1.09e+00$)**				
c_3			-1.493e-01 ($\pm 1.13e-01$)*		8.622e-03 ($\pm 1.96e-02$)				
c_4					2.016e-01 ($\pm 1.31e-02$)*				
c_5					-4.545e-02 ($\pm 1.24e-02$)**				

^a + p < 0.1, * p < 0.05, ** p < 0.01, *** p < 0.001; Confidence interval of 95% for regression coefficients;
^b Temperatures (°C);
^c Pressures (bar);
^d The values in brackets are the CV_{RMSE} (%).

J.1.7 Compressor Cuevas(2009)

Table J.13: Energy consumption models (Cuevas(2009))

\dot{W}_c (kW) Correlation 1a		MRE (%) RMSE ^d (W)	\dot{W}_c (kW) Correlation 2a		MRE (%) RMSE ^d (W)	\dot{W}_c (kW) Correlation 3a		MRE (%) RMSE ^d (W)	\dot{W}_{esp} (kJ/kg)	MRE (%) RMSE ^d (W)	Fluid \dot{W}_c Range [W] (N° tests)
Cuevas(2009)											
c_0, z_c	9.187e-02 (±2.82e-01)		1.779e-01 (±3.01e-01)		1.384e+00 (±6.61e-01)***		1.384e+00 (±6.61e-01)***		-3.241e+00 (±3.12e+00)*		R134a [1449, 5424] (18)
c_1, z_c	-3.761e-02 (±3.32e-02)*		-2.548e-03 (±4.63e-02)		1.959e-02 (±2.08e-02)+		1.959e-02 (±2.08e-02)+		-5.485e-01 (±1.07e-00)		
c_2, k_0	1.549e-01 (±1.11e-02)***	3.16	1.321e-01 (±2.82e-02)***		-3.100e-02 (±2.45e-02)*		-3.100e-02 (±2.45e-02)*		-2.828e-01 (±3.38e+00)	3.68	
c_3, k_1	-6.756e-04 (±1.08e-03)	60.75 (0.75)	-1.101e-03 (±2.41e-03)		-1.686e-04 (±3.38e-04)		-1.686e-04 (±3.38e-04)	3.05	7.239e+00 (±3.60e+00)***		
c_4, k_2			-9.498e-04 (±2.62e-03)		-2.660e-04 (±2.11e-04)*		-2.660e-04 (±2.11e-04)*		1.352e+00 (±8.94e-01)**	71.45 (2.86)	
c_5, k_3			5.152e-04 (±8.52e-04)	2.58	7.654e-04 (±2.24e-04)***	51.17 (1.47)	7.654e-04 (±2.24e-04)***	54.48 (0.57)			

^a + p < 0.1, * p < 0.05, ** p < 0.01, *** p < 0.001; Confidence interval of 95% for regression coefficients;
^b Temperatures (°C);
^c Pressures (bar);
^d The values in brackets are the CV_{RMSE} (%);

Table J.14: Mass flow rate models (Cuevas(2009))

\dot{m}_{ref} (kg/h) Correlation 1b		MRE (%) RMSE ^d (kg/h)	\dot{m}_{ref} (kg/h) Correlation 2b		MRE (%) RMSE ^d (kg/h)	\dot{m}_{ref} (kg/h) Correlation 3b		MRE (%) RMSE ^d (kg/h)	Fluid \dot{m} Range [kg/h] (N° tests)
Cuevas(2009) (SH = 6.8K)									
c_0	-1.155e+01 (±1.04e+01)*		4.247e+00 (±2.63e+01)		1.332e+02 (±5.43e+01)***		1.332e+02 (±5.43e+01)***		R134a [198, 904] (18)
c_1	4.766e+01 (±1.01e+00)***		4.575e+01 (±3.08e+00)***		6.381e-01 (±1.71e+00)		6.381e-01 (±1.71e+00)		
c_2	-1.706e+00 (±4.99e-01)***		-2.297e+00 (±1.03e+00)***		1.318e+00 (±2.01e+00)		1.318e+00 (±2.01e+00)		
c_3		3.93	6.580e-02 (±1.01e-01)	4.70	7.263e-03 (±2.78e-02)		7.263e-03 (±2.78e-02)	2.76	
c_4					1.500e-01 (±1.73e-02)***		1.500e-01 (±1.73e-02)***	4.48 (1.02)	
c_5					-1.610e-02 (±1.84e-02)+		-1.610e-02 (±1.84e-02)+		

^a + p < 0.1, * p < 0.05, ** p < 0.01, *** p < 0.001; Confidence interval of 95% for regression coefficients;
^b Temperatures (°C);
^c Pressures (bar);
^d The values in brackets are the CV_{RMSE} (%);

K

Model summary tables for reciprocating compressors

CONTENTS

K.1	Model summary tables for the characterization of \dot{W}_c , \dot{W}_{esp} and \dot{m}_{ref}	k-1
K.1.1	Compressor NJ7240F (AHRI 17)	k-2
K.1.2	Compressor EG80HLR (AHRI 18)	k-3
K.1.3	Compressor NEK2134GK (AHRI 28, 29, 49, 50)	k-5
K.1.4	Compressor NEK6214Z (AHRI 30)	k-7
K.1.5	Compressor CS14K6E-TF5 (AHRI 35, 37)	k-8
K.1.6	Compressor 4GE-23-40P (AHRI 51)	k-9
K.1.7	Compressor H84B223ABC (AHRI 59)	k-10
K.1.8	Compressor FH2511Z (AHRI 64a, 67a, 69a)	k-12
K.1.9	Compressor FH4540Z (AHRI 64b, 67b, 69b)	k-14

K.1 Model summary tables for the characterization of \dot{W}_c , \dot{W}_{esp} and \dot{m}_{ref}

This appendix includes summary tables of the models considered in Chapter 4 in reciprocating compressor characterization. They include the value of the coefficients and its uncertainty. It also includes the values of MRE, RMSE and CV_{RMSE} , the range of variation of \dot{W}_c and \dot{m}_{ref} , and the number of points considered in the adjustment. The units to be considered in each correlation is included at the bottom of each table. The polynomial expressions were reported in Chapter 4. Finally, the error values for \dot{W}_{esp} are included in terms of energy consumption. As already mentioned in Chapter 4, we must multiply by the predicted mass flow rate at the same suction conditions used in the adjustment of \dot{W}_{esp} to reconvert to \dot{W}_c values. These conditions are the same used in the summary table of the mass flow rate models.

K.1.1 Compressor NJ7240F (AHRI 17)

Table K.1: Energy consumption models (AHRI 17)

	\dot{W}_c (kW) AHRI (T-SW)	MRE (%) RMSE ^d (W)	\dot{W}_c (kW) AHRI (P-SW)	MRE (%) RMSE ^d (W)	\dot{W}_c (kW) AHRI (T)	MRE (%) RMSE ^d (W)	\dot{W}_c (kW) AHRI (P)	MRE (%) RMSE ^d (W)	W_{exp} (kJ/kg)	MRE (%) RMSE ^d (W)	Fluid \dot{W}_c Range [W] (N° tests)
AHRI 17											
c_0, z_c	1.614e+00 (±5.48e-02)**		-7.986e-01 (±3.46e-01)**		1.665e+00 (±2.83e-01)**		-7.812e-01 (±5.24e-01)*		-4.513e+00 (±5.64e+00)		
c_1, z_c	3.532e-02 (±7.93e-03)**		6.829e-01 (±1.38e-01)**		3.624e-02 (±1.11e-02)**		6.826e-01 (±1.82e-01)**		-3.994e-01 (±1.42e+00)		
c_2, k_0	3.918e-03 (±2.75e-03)*		1.113e-01 (±2.94e-02)**		-6.644e-05 (±2.18e-02)		1.079e-01 (±6.37e-02)*		2.266e+01 (±1.63e+01)**		
c_3, k_1	-6.657e-04 (±3.80e-04)**	0.21	-2.171e-02 (±9.53e-03)**	0.12	-7.049e-04 (±5.22e-04)*	0.17	-2.180e-02 (±1.26e-02)*	0.13	1.340e+01 (±4.73e-07)**	2.19	R22 [147e, 2427] (12)
c_4, k_2	-7.993e-04 (±3.50e-04)**	1.50 (0.08)	-4.910e-02 (±1.44e-02)**	1.32 (0.07)	-7.788e-04 (±5.52e-04)*	1.42 (0.08)	-4.888e-02 (±1.93e-02)**	1.31 (0.07)		20.59 (1.10)	
c_5, k_3	1.260e-04 (±3.30e-05)**		-2.415e-03 (±7.35e-04)**		2.259e-04 (±5.42e-04)		-2.184e-03 (±3.95e-03)				
c_6	1.448e-05 (±3.42e-06)**		4.648e-04 (±1.69e-04)**		1.489e-05 (±5.96e-06)**		4.703e-04 (±2.36e-04)**				
c_7	1.674e-05 (±8.35e-06)**		1.491e-03 (±8.82e-04)**		1.631e-05 (±1.07e-05)*		1.480e-03 (±1.17e-03)*				
c_8					(NA)		(NA)				
c_9					-8.052e-07 (±4.35e-06)		-5.238e-06 (±7.84e-05)				
c_0, z_c	1.422e+00 (±8.35e-02)**		-7.142e-01 (±7.81e-01)+		1.478e+00 (±4.43e-01)**		-8.052e-01 (±1.14e+00)		-2.032e+01 (±3.03e+01)		
c_1, z_c	4.058e-02 (±1.21e-02)**		3.584e-01 (±2.64e-01)*		4.158e-02 (±1.74e-02)**		3.603e-01 (±3.35e-01)*		-6.840e+00 (±1.02e+01)		
c_2, k_0	1.277e-02 (±4.19e-03)**	0.19	9.584e-02 (±6.19e-02)*	0.21	8.417e-03 (±3.41e-02)	0.16	1.122e-01 (±1.29e-01)*	0.20	-6.627e+01 (±1.58e+02)	1.99	R1270 [1510, 2485] (12)
c_3, k_1	-1.222e-03 (±5.79e-04)**	2.29 (0.12)	9.534e-03 (±1.70e-02)	2.36 (0.12)	-1.264e-03 (±8.16e-04)*	2.23 (0.11)	9.887e-03 (±2.17e-02)	2.27 (0.12)	6.227e+01 (±5.38e+01)**	29.04 (1.49)	
c_4, k_2	-1.703e-04 (±5.32e-04)**		-9.547e-03 (±2.35e-02)**		-1.478e-04 (±7.07e-04)		-1.041e-02 (±3.03e-02)				
c_5, k_3	7.901e-05 (±5.03e-05)*		-4.451e-03 (±1.46e-02)**		1.881e-04 (±8.48e-04)		-5.487e-03 (±6.65e-03)*				
c_6	1.881e-05 (±6.72e-06)**		6.627e-04 (±1.35e-04)**		1.926e-05 (±9.33e-06)**		6.409e-04 (±3.83e-04)*				
c_7	-1.931e-05 (±1.27e-05)*		-2.360e-03 (±1.35e-03)**		-1.978e-05 (±1.68e-05)*		-2.317e-03 (±1.73e-03)*				
c_8					(NA)		(NA)				
c_9					-8.793e-07 (±6.81e-06)		2.210e-05 (±1.36e-04)				

^a + p < 0.1, * p < 0.05, ** p < 0.01, *** p < 0.001; Confidence interval of 95% for regression coefficients;
^b Temperatures (°C);
^c Pressures (bar);
^d The values in brackets are the CV_{RMSE} (%).

Table K.2: Mass flow rate models (AHRI 17)

	\dot{m}_{ref} (kg/h) 2 nd order polynomial (T-SW)	MRE (%) RMSE (kg/h)	\dot{m}_{ref} (kg/h) 2 nd order polynomial (P-SW)	MRE (%) RMSE (kg/h)	\dot{m}_{ref} (kg/h) 2 nd order polynomial (T)	MRE (%) RMSE (kg/h)	\dot{m}_{ref} (kg/h) 2 nd order polynomial (P)	MRE (%) RMSE (kg/h)	Fluid \dot{m} Range [kg/h] (N° tests)
AHRI 17 (SH = 11K)									
c_0	1.134e+02 (±4.83e+00)**		-2.914e+01 (±9.65e+00)**		1.134e+02 (±4.83e+00)**		-3.001e+01 (±1.12e+01)**		
c_1	3.873e+00 (±1.89e-01)**		3.650e+01 (±3.97e+00)**		3.873e+00 (±1.89e-01)**		3.649e+01 (±4.32e+00)**		
c_2	-1.326e-01 (±2.42e-01)	0.71	-7.843e-01 (±2.43e-01)**	0.58	-1.326e-01 (±2.42e-01)	0.71	-6.663e-01 (±5.74e-01)**	0.68	R22 [58, 123] (12)
c_3	-7.447e-03 (±4.26e-03)**	0.26 (0.30)	-1.336e-01 (±5.36e-02)**	0.23 (0.26)	-7.447e-03 (±4.26e-03)**	0.26 (0.30)	-1.309e-01 (±5.95e-02)**	0.22 (0.25)	
c_4	1.629e-02 (±1.13e-02)*		-1.229e+00 (±4.08e-01)**		1.629e-02 (±1.13e-02)*		-1.233e+00 (±4.45e-01)**		
c_5	-5.189e-03 (±2.90e-03)**				-5.189e-03 (±2.90e-03)**		-3.968e-03 (±1.71e-02)		
c_0	7.505e+01 (±2.76e+00)**		1.244e+01 (±6.93e+00)**		7.505e+01 (±2.76e+00)**		1.226e+01 (±8.19e+00)*		
c_1	2.581e+00 (±1.08e-01)**	0.36	8.486e+00 (±2.41e+00)**	0.39	2.581e+00 (±1.08e-01)**	0.36	8.485e+00 (±2.69e+00)**	0.39	R1270 [40, 81] (12)
c_2	-1.512e-01 (±1.38e-01)*	0.15 (0.26)	-2.883e-01 (±1.63e-01)**	0.14 (0.24)	-1.512e-01 (±1.38e-01)*	0.15 (0.26)	-2.656e-01 (±3.86e-01)	0.14 (0.24)	
c_3	-8.067e-03 (±2.43e-03)**		-1.269e-01 (±3.05e-02)**		-8.067e-03 (±2.43e-03)**		-1.264e-01 (±3.47e-02)**		
c_4	3.749e-02 (±6.48e-03)**		5.591e-01 (±2.11e-01)**		3.749e-02 (±6.48e-03)**		5.584e-01 (±2.36e-01)**		
c_5	-2.995e-03 (±1.66e-03)**				-2.995e-03 (±1.66e-03)**		-7.190e-04 (±1.08e-02)		

^a + p < 0.1, * p < 0.05, ** p < 0.01, *** p < 0.001; Confidence interval of 95% for regression coefficients;
^b Temperatures (°C);
^c Pressures (bar);
^d The values in brackets are the CV_{RMSE} (%).

K.1.2 Compressor EG80HLR (AHRI 18)

Table K.3: Energy consumption models (AHRI 18)

	\dot{W}_c (kW) AHRI (T-SW)	MRE (%) RMSE ² (W)	\dot{W}_c (kW) AHRI (P-SW)	MRE (%) RMSE ² (W)	\dot{W}_c (kW) AHRI (T)	MRE (%) RMSE ² (W)	\dot{W}_c (kW) AHRI (P)	MRE (%) RMSE ² (W)	\dot{W}_{esp} (kJ/kg)	MRE (%) RMSE ² (W)	Fluid \dot{W}_c range [W] (N° tests)
AHRI 18											
c_0, z_c	2.444e-01 (+1.26e-01)**		1.133e-01 (+1.50e-01)		2.263e-01 (+2.16e-01)*		1.076e-01 (+1.91e-01)		-1.108e+01 (+7.36e+00)**		
c_1, z_p	1.180e-02 (+1.07e-02)		-1.028e-01 (+1.97e-01)		1.109e-02 (+1.48e-02)+		-1.002e-01 (+2.48e-01)		-3.426e+01 (+5.83e+01)		
c_2, k_0	-9.560e-04 (+4.44e-03)		3.077e-03 (+2.12e-02)		6.556e-05 (+9.85e-03)		4.483e-03 (+2.77e-02)		1.372e+01 (+1.08e+01)		
c_3, k_1	-2.017e-04 (+3.05e-04)		1.594e-02 (+1.79e-02)+		-1.812e-04 (+4.25e-04)		1.430e-02 (+2.42e-02)		6.914e+00 (+2.52e+00)**		
c_4, k_2	2.180e-04 (+2.42e-04)+	0.53	4.639e-02 (+7.15e-02)	0.64	2.058e-04 (+3.26e-04)	0.52	5.017e-02 (+9.20e-02)	0.57		1.35	R134a [119, 174] (12)
c_5, k_3	1.580e-05 (+4.09e-05)	0.40 (0.29)	-1.045e-03 (+1.54e-03)	0.43 (0.30)	-4.843e-06 (+1.70e-04)	0.39 (0.27)	-1.068e-03 (+1.94e-03)	0.41 (0.28)		1.01 (0.70)	
c_6	1.198e-06 (+1.95e-06)		-4.581e-03 (+6.48e-03)		1.081e-06 (+2.67e-06)		1.092e-04 (+5.96e-04)				
c_7	-4.000e-06 (+5.74e-06)				-3.745e-06 (+7.67e-06)		-4.878e-03 (+8.29e-03)				
c_8					(NA)		(NA)				
c_9			2.566e-05 (+4.73e-05)		1.501e-07 (+1.18e-06)		2.196e-05 (+6.27e-05)				
c_0, z_c	2.804e-01 (+3.25e-01)+	0.11	-5.072e-03 (+2.88e-01)	0.16	2.804e-01 (+3.25e-01)+	0.11	-5.072e-03 (+2.88e-01)	0.16	-9.722e+00 (+3.50e+01)	1.87	N13a [125, 169] (8)
c_1, z_p	6.961e-03 (+1.24e-02)+	0.09 (0.06)	8.846e-02 (+2.45e-01)	0.13 (0.09)	6.961e-03 (+1.24e-02)+	0.09 (0.06)	8.846e-02 (+2.45e-01)	0.13 (0.09)	-3.910e-01 (+3.21e+00)	1.52 (1.03)	
c_2, k_0	-7.019e-03 (+1.90e-02)		1.071e-02 (+6.39e-02)		-7.019e-03 (+1.90e-02)		1.071e-02 (+6.39e-02)		1.865e+01 (+1.28e+02)		
c_3, k_1	-2.156e-04 (+6.05e-04)		-8.582e-03 (+4.84e-02)		-2.156e-04 (+6.05e-04)		-8.582e-03 (+4.84e-02)		6.470e+00 (+1.19e+01)		
c_4, k_2					(NA)		(NA)				
c_5, k_3	1.744e-04 (+3.50e-04)+	0.11	-5.297e-07 (+5.19e-03)	0.16	1.744e-04 (+3.50e-04)+	0.11	-5.297e-07 (+5.19e-03)	0.16			
c_6	3.229e-06 (+7.06e-06)		5.888e-04 (+2.27e-03)		3.229e-06 (+7.06e-06)		5.888e-04 (+2.27e-03)				
c_7					(NA)		(NA)				
c_8					(NA)		(NA)				
c_9	-1.080e-06 (+2.19e-06)		-3.850e-05 (+1.86e-04)		-1.080e-06 (+2.19e-06)		-3.850e-05 (+1.86e-04)				
c_0, z_c	1.524e-01 (+2.36e-02)**	0.48	1.882e-02 (+3.38e-02)	0.58	1.648e-01 (+2.31e-01)	0.46	-4.123e-03 (+2.37e-01)	0.49	-1.218e+01 (+4.70e+00)**	0.89	ARM42a [131, 185] (12)
c_1, z_p	1.341e-03 (+2.78e-03)	0.42 (0.27)	6.838e-02 (+4.16e-02)**	0.46 (0.30)	2.128e-03 (+1.58e-02)	0.42 (0.27)	7.567e-02 (+2.70e-01)	0.43 (0.28)	-2.438e-01 (+3.70e-01)	0.66 (0.43)	
c_2, k_0	1.050e-03 (+1.20e-03)+		7.964e-03 (+1.57e-03)**		5.026e-04 (+1.05e-02)		1.365e-02 (+3.33e-02)		1.266e+01 (+1.52e+01)+		
c_3, k_1					-2.328e-05 (+4.54e-04)		-9.211e-04 (+2.59e-02)		5.632e+00 (+1.24e+00)**		
c_4, k_2	-4.195e-05 (+1.12e-04)		-1.094e-02 (+1.31e-02)+		-2.682e-05 (+3.48e-04)		-1.239e-02 (+8.85e-02)				
c_5, k_3	1.558e-05 (+2.51e-05)		-4.627e-04 (+9.19e-05)**		2.350e-05 (+1.82e-04)		-9.350e-04 (+2.25e-03)				
c_6	1.283e-06 (+1.21e-06)*		1.480e-04 (+3.18e-05)**		1.394e-06 (+2.86e-06)		1.768e-04 (+6.23e-04)				
c_7	1.231e-06 (+2.59e-06)				8.800e-07 (+8.20e-06)		1.025e-04 (+7.84e-03)				
c_8					(NA)		(NA)				
c_9					-4.593e-08 (+1.26e-06)		1.298e-05 (+7.16e-05)				

^a + p < 0.1, * p < 0.05, ** p < 0.01, *** p < 0.001; Confidence interval of 95% for regression coefficients;
^b Temperatures (°C);
^c Pressures (bar);
^d The values in brackets are the CV_{RMSE} (%).

Table K.4: Mass flow rate models (AHRI 18)

	\dot{m}_{ref} (kg/h) 2 nd order polynomial (T-SW)	MRE (%) RMSE (kg/h)	\dot{m}_{ref} (kg/h) 2 nd order polynomial (P-SW)	MRE (%) RMSE (kg/h)	\dot{m}_{ref} (kg/h) 2 nd order polynomial (T)	MRE (%) RMSE (kg/h)	\dot{m}_{ref} (kg/h) 2 nd order polynomial (P)	MRE (%) RMSE (kg/h)	Fluid <i>m</i> Range [kg/h] (N° tests)
AHRI 18 (<i>SH</i> = 22K)									
<i>C</i> ₀	1.428e+01 (±1.07e+00)***	1.51 0.03 (0.64)	1.824e+00 (±1.72e+00)*	1.38 0.03 (0.66)	1.461e+01 (±1.62e+00)***	1.48 0.03 (0.59)	1.445e+00 (±2.05e+00)	1.51 0.03 (0.59)	R134a [4, 7] (12)
<i>C</i> ₁	6.051e-01 (±1.14e-01)***		1.646e+00 (±2.53e+00)		6.218e-01 (±1.35e-01)***		1.873e+00 (±2.81e+00)		
<i>C</i> ₂			-1.002e-01 (±9.29e-03)***		-8.128e-03 (±3.52e-02)		-5.658e-02 (±1.08e-01)		
<i>C</i> ₃					-3.528e-04 (±8.32e-04)		-2.232e-02 (±4.97e-02)		
<i>C</i> ₄	8.397e-03 (±2.94e-03)***		1.129e+00 (±9.10e-01)*		8.456e-03 (±3.33e-03)***		1.132e+00 (±9.98e-01)*		
<i>C</i> ₅	-3.426e-04 (±3.07e-05)**		-3.295e-04 (±3.34e-04)+	-6.190e-04 (±4.40e-03)					
<i>C</i> ₀	1.162e+01 (±1.13e+00)***	0.49 0.01 (0.25)	-2.825e-01 (±2.36e-01)*	0.79 0.02 (0.34)	1.162e+01 (±1.13e+00)***	0.49 0.01 (0.25)	-2.166e-02 (±1.09e+00)	0.57 0.02 (0.27)	N13a [5, 7] (8)
<i>C</i> ₁	2.900e-01 (±4.73e-02)***		5.272e+00 (±1.58e-01)***		2.900e-01 (±4.73e-02)***		4.981e+00 (±7.83e-01)***		
<i>C</i> ₂	1.205e-02 (±3.79e-02)		-1.166e-01 (±8.52e-03)***		1.205e-02 (±3.79e-02)		-1.261e-01 (±1.33e-01)+		
<i>C</i> ₃	4.618e-04 (±1.11e-03)				4.618e-04 (±1.11e-03)		2.835e-02 (±7.54e-02)		
<i>C</i> ₄					(NA)		(NA)		
<i>C</i> ₅	-4.152e-04 (±3.24e-04)*		-4.152e-04 (±3.24e-04)*	-1.447e-03 (±5.19e-03)					
<i>C</i> ₀	1.551e+01 (±1.16e+00)***	0.96 0.03 (0.43)	-9.694e-01 (±1.57e-01)***	1.15 0.03 (0.44)	1.541e+01 (±1.53e+00)***	0.97 0.03 (0.43)	-7.397e-01 (±2.22e+00)	1.05 0.03 (0.44)	ARM42a [5, 9] (12)
<i>C</i> ₁	5.465e-01 (±1.10e-01)***		5.358e+00 (±9.71e-02)***		5.419e-01 (±1.28e-01)***		5.135e+00 (±2.67e+00)**		
<i>C</i> ₂	2.231e-02 (±2.27e-02)+				2.488e-02 (±3.33e-02)		-1.101e-02 (±1.12e-01)		
<i>C</i> ₃					9.300e-05 (±7.88e-04)		2.182e-03 (±4.60e-02)		
<i>C</i> ₄	5.420e-03 (±2.83e-03)**				5.400e-03 (±3.15e-03)**		6.362e-02 (±8.36e-01)		
<i>C</i> ₅	-6.783e-04 (±2.77e-04)***		-5.492e-03 (±3.42e-04)***	-6.870e-04 (±3.17e-04)**	-5.153e-03 (±4.48e-03)*				

^a + p < 0.1, * p < 0.05, ** p < 0.01, *** p < 0.001; Confidence interval of 95% for regression coefficients;

^b Temperatures (°C);

^c Pressures (bar);

^d The values in brackets are the CV_{RMSE} (%);

K.1.3 Compressor NEK2134GK (AHRI 28, 29, 49, 50)

Table K.5: Energy consumption models (AHRI 28, 29, 49, 50)

	\dot{W}_c (kW) AHRI (T-SW)	MRE (%) RMSE ² (W)	\dot{W}_c (kW) AHRI (P-SW)	MRE (%) RMSE ² (W)	\dot{W}_c (kW) AHRI (T)	MRE (%) RMSE ² (W)	\dot{W}_c (kW) AHRI (P)	MRE (%) RMSE ² (W)	\dot{W}_{esp} (kJ/kg)	MRE (%) RMSE ² (W)	Fluid \dot{W}_c Range [W] (N° tests)
AHRI 28											
c_0, z_c	4.002e-01 (±4.06e-02)***	2.23 (0.87)	1.349e-01 (±3.93e-02)***	1.51	3.768e-01 (±4.90e-02)***	1.42	1.519e-01 (±5.54e-02)***	1.56	-6.262e+00 (±3.93e-00)***	3.81	R404A [247, 587] (12/12/12)
c_1, z_c	5.919e-03 (±1.55e-03)***		7.987e-02 (±4.03e-02)***		3.256e-03 (±3.67e-03)+		7.330e-02 (±4.32e-02)***		1.192e-01 (±2.10e-01)		
c_2, k_0	5.204e-03 (±1.88e-03)***		-8.72e-04 (±1.94e-03)		5.501e-03 (±1.92e-03)***		-2.586e-03 (±1.36e-03)		2.564e+01 (±7.37e+01)***		
c_3, k_1	6.483e-05 (±6.87e-05)+		5.526e-03 (±9.93e-04)***		9.209e-05 (±7.96e-05)*		6.186e-03 (±1.81e-03)***		8.177e+00 (±7.14e-01)***		
c_4, k_2	3.294e-05 (±9.49e-06)***		-1.824e-02 (±1.44e-02)***		-5.118e-05 (±1.22e-04)		-1.824e-02 (±1.45e-02)*		-8.601e-02 (±1.64e-02)***		
c_5, k_3	8.717e-06 (±2.99e-05)		-1.536e-04 (±3.54e-05)***		8.717e-06 (±2.07e-05)		-1.141e-04 (±9.70e-05)				
c_6	1.084e-06 (±7.59e-07)*				1.084e-06 (±7.30e-07)*		-1.529e-05 (±3.49e-05)				
c_7			-3.921e-04 (±1.84e-04)***		5.226e-07 (±8.01e-07)		-3.921e-04 (±1.85e-04)***				
c_8			1.846e-03 (±1.73e-03)*		-7.778e-07 (±1.49e-06)		1.846e-03 (±1.74e-03)*				
c_9			(NA)	(NA)							
c_0, z_c	2.741e-01 (±2.12e-02)***	0.99	1.459e-01 (±2.27e-02)***	1.10	2.644e-01 (±3.14e-02)***	0.98	1.499e-01 (±2.81e-02)***	1.00	-2.672e+00 (±2.44e-00)*	4.55	L470 [216, 476] (12/12/12)
c_1, z_c	-1.233e-04 (±2.15e-03)		6.398e-02 (±1.16e-02)***		-4.245e-04 (±2.35e-03)		6.286e-02 (±2.95e-02)***		4.330e-01 (±1.07e-01)***		
c_2, k_0	6.217e-03 (±5.47e-04)***		-2.815e-03 (±2.56e-03)*		6.585e-03 (±1.23e-03)***		-3.327e-03 (±2.59e-03)*		5.030e+01 (±9.21e+01)***		
c_3, k_1	1.822e-04 (±2.68e-05)***		6.010e-03 (±1.23e-03)***		1.967e-04 (±5.11e-05)***		6.625e-03 (±1.43e-03)***		1.143e+01 (±9.80e-01)***		
c_4, k_2	-9.892e-05 (±2.74e-05)*		-1.242e-02 (±1.10e-03)***		-9.892e-05 (±7.82e-05)*		-1.521e-02 (±1.34e-02)***		-1.626e+01 (±4.46e-02)***		
c_5, k_3	-1.161e-05 (±5.00e-06)***		1.069e-05 (±6.78e-05)		-1.571e-05 (±1.33e-05)		1.069e-05 (±6.64e-05)		1.043e-03 (±4.50e-04)***		
c_6			-7.726e-05 (±3.26e-05)***		-1.606e-07 (±4.81e-07)		-7.726e-05 (±3.19e-05)***				
c_7	1.424e-06 (±5.08e-07)***				1.424e-06 (±5.14e-07)***		-1.539e-04 (±1.95e-04)				
c_8	-1.105e-06 (±9.45e-07)*				-1.105e-06 (±9.56e-07)*		9.407e-04 (±2.16e-03)				
c_9			(NA)	(NA)							
AHRI 29											
c_0, z_c	4.269e-01 (±2.04e-02)***	2.03	1.191e-01 (±4.23e-02)***	2.19	3.888e-01 (±6.02e-02)***	1.88	1.382e-01 (±5.91e-02)***	2.00	-8.587e+00 (±3.40e+00)***	4.19	DR7 [244, 548] (12/12/12)
c_1, z_c	7.295e-03 (±6.59e-04)***		9.969e-02 (±4.86e-02)***		5.649e-03 (±4.50e-03)*		9.144e-02 (±5.19e-02)***		2.533e-01 (±1.42e-01)***		
c_2, k_0	2.489e-03 (±8.68e-04)***		-5.721e-04 (±2.17e-03)		4.220e-03 (±2.36e-03)***		-2.556e-03 (±4.79e-03)		2.199e+01 (±9.32e+01)***		
c_3, k_1			5.086e-03 (±1.22e-03)***		7.796e-05 (±9.78e-05)		5.942e-03 (±2.21e-03)***		8.282e+00 (±8.11e-02)***		
c_4, k_2	3.812e-05 (±1.19e-05)***		-2.686e-02 (±1.95e-02)***		4.053e-05 (±1.30e-04)		-2.686e-02 (±1.95e-02)***		-8.437e-02 (±1.41e-02)***		
c_5, k_3	3.239e-05 (±9.86e-06)***		-1.038e-04 (±4.13e-05)***		1.545e-05 (±2.54e-05)		-5.651e-05 (±1.10e-04)				
c_6	1.468e-06 (±8.74e-08)***				8.033e-07 (±9.20e-07)+		-2.036e-05 (±4.38e-05)				
c_7			-4.372e-04 (±2.52e-04)***		3.375e-07 (±9.84e-07)		-4.372e-04 (±2.53e-04)***				
c_8			3.335e-03 (±2.61e-03)*		2.259e-07 (±1.83e-06)		3.335e-03 (±2.62e-03)*				
c_9			(NA)	(NA)							
AHRI 49											
c_0, z_c	3.635e-01 (±1.86e-02)***	1.94	1.345e-01 (±3.40e-02)***	1.93	3.631e-01 (±5.68e-02)***	2.13	1.266e-01 (±5.08e-02)***	1.88	-2.029e+00 (±1.25e+00)*	3.95	R455A [200, 485] (12/12/12)
c_1, z_c	6.036e-03 (±6.01e-04)***		8.434e-02 (±4.79e-02)***		6.652e-03 (±4.25e-03)*		8.831e-02 (±5.17e-02)***		6.957e-01 (±3.66e-02)***		
c_2, k_0	3.114e-03 (±2.92e-04)***		-2.230e-03 (±2.08e-03)*		3.434e-03 (±2.23e-03)*		-1.303e-03 (±4.62e-03)		4.388e+01 (±5.92e+01)***		
c_3, k_1			7.930e-03 (±1.35e-03)***		3.262e-06 (±9.24e-05)		7.468e-03 (±2.47e-03)***		7.847e+00 (±7.43e-01)***		
c_4, k_2	2.833e-05 (±1.09e-05)***		-3.140e-02 (±2.22e-02)***		5.483e-05 (±1.41e-04)		-3.140e-02 (±2.25e-02)***		-1.263e-01 (±2.24e-02)***		
c_5, k_3	1.951e-05 (±9.00e-06)***		-1.697e-04 (±4.45e-05)***		1.405e-05 (±2.40e-05)		-1.944e-04 (±1.18e-04)		7.067e-04 (±1.98e-04)***		
c_6	1.564e-06 (±7.97e-08)***				1.350e-06 (±8.70e-07)*		1.231e-05 (±5.46e-05)				
c_7			-9.474e-04 (±3.20e-04)***		-3.102e-07 (±9.29e-07)		-9.474e-04 (±3.25e-04)***				
c_8			5.258e-03 (±4.43e-03)*		1.609e-07 (±1.73e-06)		5.258e-03 (±4.49e-03)*				
c_9			(NA)	(NA)							
AHRI 50											
c_0, z_c	3.461e-01 (±1.90e-02)***	2.59	1.265e-01 (±3.90e-02)***	2.71	3.543e-01 (±6.06e-02)***	2.50	1.085e-01 (±5.44e-02)***	2.53	-1.243e+01 (±2.95e+00)***	4.92	DR3 [197, 458] (12/12/12)
c_1, z_c	5.477e-03 (±3.85e-04)***		7.200e-02 (±5.54e-02)***		6.138e-03 (±4.53e-03)*		8.161e-02 (±5.91e-02)***		9.506e-02 (±1.07e-01)+		
c_2, k_0	3.234e-03 (±3.84e-04)***		9.357e-05 (±2.42e-03)		2.999e-03 (±2.38e-03)*		2.331e-03 (±5.29e-03)		3.472e+01 (±1.01e+01)***		
c_3, k_1			7.153e-03 (±1.67e-03)***		-1.034e-05 (±9.84e-05)		5.960e-03 (±3.02e-03)***		5.734e+00 (±7.34e-01)***		
c_4, k_2	1.022e-05 (±9.47e-06)*		-2.210e-02 (±2.74e-02)		1.825e-05 (±1.31e-04)		-2.210e-02 (±2.75e-02)				
c_5, k_3	1.291e-06 (±8.40e-08)***		-2.021e-04 (±5.52e-05)***		1.259e-05 (±2.56e-05)		-2.657e-04 (±1.45e-04)***				
c_6					1.383e-06 (±9.27e-07)*		3.391e-05 (±7.13e-05)				
c_7			-8.706e-04 (±4.23e-04)***		-3.677e-08 (±9.90e-07)		-8.706e-04 (±4.24e-04)***				
c_8	-4.752e-07 (±1.47e-07)***		3.835e-03 (±4.53e-03)+		-2.638e-07 (±1.84e-06)		3.835e-03 (±4.54e-03)+				
c_9			(NA)	(NA)							

^a + p < 0.1, * p < 0.05, ** p < 0.01, *** p < 0.001; Confidence interval of 95% for regression coefficients;

^b Temperature (°C);

^c Pressures (bar);

^d The values in brackets are the CV_{RMSE} (%);

Table K.6: Mass flow rate models (AHRI 28, 29, 49, 50)

\dot{m}_{ref} (kg/h) 2 nd order polynomial (T-SW)		MRE (%) RMSE (kg/h)	\dot{m}_{ref} (kg/h) 2 nd order polynomial (P-SW)		MRE (%) RMSE (kg/h)	\dot{m}_{ref} (kg/h) 2 nd order polynomial (T)		MRE (%) RMSE (kg/h)	\dot{m}_{ref} (kg/h) 2 nd order polynomial (P)		MRE (%) RMSE (kg/h)	Fluid <i>m</i> Range [kg/h] (N° tests)
AHRI 28 (SH = 11K)												
c_0	4.240e+01 (±2.76e+00)***	3.16 0.13 (0.91)	-5.405e-01 (±8.96e-01)	2.49 0.08 (0.36)	4.240e+01 (±2.76e+00)***	3.16 0.13 (0.91)	-6.922e-01 (±1.71e+00)	2.37 0.08 (0.35)	-6.922e-01 (±1.71e+00)	2.37 0.08 (0.35)	R404A [5, 26] (12)	
c_1	1.357e+00 (±9.17e-02)***		6.679e+00 (±5.43e-01)***		1.357e+00 (±9.17e-02)***		6.679e+00 (±5.43e-01)***					
c_2	-6.179e-02 (±1.13e-01)		-7.789e-02 (±3.24e-02)***		-6.179e-02 (±1.13e-01)		-7.789e-02 (±3.24e-02)***					
c_3	-2.018e-03 (±1.00e-03)**		-4.422e-02 (±1.16e-02)***		-2.018e-03 (±1.00e-03)**		-4.422e-02 (±1.16e-02)***					
c_4	1.172e-02 (±1.51e-03)***		2.010e-01 (±8.96e-02)**		1.172e-02 (±1.51e-03)***		2.010e-01 (±8.96e-02)**					
c_5	-9.222e-04 (±1.22e-03)				-9.222e-04 (±1.22e-03)							
AHRI 28 (SH = 11K)												
c_0	2.356e+01 (±8.66e-01)***	4.43 0.08 (1.18)	7.770e-02 (±1.68e+00)	6.71 0.09 (1.30)	2.378e+01 (±1.70e+00)***	4.86 0.08 (1.17)	7.770e-02 (±1.68e+00)	6.71 0.09 (1.30)	7.770e-02 (±1.68e+00)	6.71 0.09 (1.30)	L40 [2, 13] (12)	
c_1	7.834e-01 (±5.12e-02)***		4.474e+00 (±7.98e-01)***		7.834e-01 (±5.12e-02)***		4.474e+00 (±7.98e-01)***					
c_2	-9.265e-02 (±1.54e-02)**		-1.116e-01 (±1.65e-01)		-1.036e-01 (±6.96e-02)*		-1.116e-01 (±1.65e-01)					
c_3	-1.810e-03 (±5.60e-04)***		-5.206e-02 (±1.97e-02)***		-1.810e-03 (±5.60e-04)***		-5.206e-02 (±1.97e-02)***					
c_4	6.999e-03 (±8.46e-04)***		2.233e-01 (±1.76e-01)*		6.999e-03 (±8.46e-04)***		2.233e-01 (±1.76e-01)*					
c_5			2.889e-03 (±4.25e-03)				2.889e-03 (±4.25e-03)					
AHRI 29 (SH = 11K)												
c_0	3.969e+01 (±2.22e+00)***	6.99 0.21 (1.76)	-1.551e+00 (±2.15e+00)	4.34 0.20 (1.72)	3.937e+01 (±4.40e+00)***	6.66 0.21 (1.75)	-6.987e-01 (±3.94e+00)	4.83 0.20 (1.67)	-6.987e-01 (±3.94e+00)	4.83 0.20 (1.67)	DR7 [4, 22] (12)	
c_1	1.331e+00 (±1.31e-01)***		5.982e+00 (±1.46e+00)***		1.331e+00 (±1.31e-01)***		5.982e+00 (±1.46e+00)***					
c_2	-1.477e-01 (±3.96e-02)**		2.101e-02 (±7.97e-02)		-1.322e-01 (±1.80e-01)		-1.322e-01 (±1.80e-01)					
c_3	-3.049e-03 (±1.44e-03)**		-7.019e-02 (±3.18e-02)**		-3.049e-03 (±1.44e-03)**		-3.049e-03 (±1.44e-03)**					
c_4	1.206e-02 (±2.17e-03)**		3.798e-01 (±2.68e-01)*		1.206e-02 (±2.17e-03)**		3.798e-01 (±2.68e-01)*					
c_5					-1.722e-04 (±1.94e-03)		-1.722e-04 (±1.94e-03)					
AHRI 49 (SH = 11K)												
c_0	2.614e+01 (±2.20e+00)***	3.78 0.10 (1.13)	-2.115e+00 (±1.65e+00)*	3.07 0.08 (0.92)	2.614e+01 (±2.20e+00)***	3.78 0.10 (1.13)	-2.115e+00 (±1.65e+00)*	3.07 0.08 (0.92)	-2.115e+00 (±1.65e+00)*	3.07 0.08 (0.92)	R455A [3, 17] (12)	
c_1	9.703e-01 (±7.31e-02)***		4.988e+00 (±7.63e-01)***		9.703e-01 (±7.31e-02)***		4.988e+00 (±7.63e-01)***					
c_2	7.009e-02 (±9.01e-02)		1.655e-01 (±1.60e-01)*		7.009e-02 (±9.01e-02)		1.655e-01 (±1.60e-01)*					
c_3	-1.029e-03 (±7.99e-04)**		-2.988e-02 (±1.86e-02)**		-1.029e-03 (±7.99e-04)**		-2.988e-02 (±1.86e-02)**					
c_4	9.147e-03 (±1.21e-03)**		3.149e-01 (±1.62e-01)**		9.147e-03 (±1.21e-03)**		3.149e-01 (±1.62e-01)**					
c_5	-1.633e-03 (±9.70e-04)**		-5.893e-03 (±4.13e-03)*		-1.633e-03 (±9.70e-04)**		-5.893e-03 (±4.13e-03)*					
AHRI 50 (SH = 11K)												
c_0	2.732e+01 (±8.96e-01)***	1.19 0.04 (0.46)	-2.026e+00 (±8.63e-01)**	0.98 0.04 (0.48)	2.732e+01 (±8.96e-01)***	1.19 0.04 (0.46)	-2.026e+00 (±8.63e-01)**	0.98 0.04 (0.48)	-2.026e+00 (±8.63e-01)**	0.98 0.04 (0.48)	DR3 [3, 17] (12)	
c_1	9.525e-01 (±2.98e-02)***		6.234e+00 (±4.25e-01)***		9.525e-01 (±2.98e-02)***		6.234e+00 (±4.25e-01)***					
c_2	2.173e-02 (±3.67e-02)		8.236e-02 (±8.96e-02)+		2.173e-02 (±3.67e-02)		8.236e-02 (±8.96e-02)+					
c_3	-1.321e-03 (±3.25e-04)***		-4.251e-02 (±1.11e-02)***		-1.321e-03 (±3.25e-04)***		-4.251e-02 (±1.11e-02)***					
c_4	8.402e-03 (±4.92e-04)***		1.867e-01 (±9.64e-02)**		8.402e-03 (±4.92e-04)***		1.867e-01 (±9.64e-02)**					
c_5	-1.272e-03 (±3.95e-04)***		-4.148e-03 (±2.46e-03)**		-1.272e-03 (±3.95e-04)***		-4.148e-03 (±2.46e-03)**					

a + p < 0.1, * p < 0.05, ** p < 0.01, *** p < 0.001; Confidence interval of 95% for regression coefficients;

b Temperatures (°C);

c Pressures (bar);

d The values in brackets are the CV_{RMSE} (%);

K.1.4 Compressor NEK6214Z (AHRI 30)

Table K.7: Energy consumption models (AHRI 30)

	\dot{W}_c (kW) AHRI (T-SW)	MRE (%) RMSE ^d (W)	\dot{W}_c (kW) AHRI (P-SW)	MRE (%) RMSE ^d (W)	\dot{W}_c (kW) AHRI (T)	MRE (%) RMSE ^d (W)	\dot{W}_c (kW) AHRI (P)	MRE (%) RMSE ^d (W)	\dot{W}_{esp} (kJ/kg)	MRE (%) RMSE ^d (W)	Fluid \dot{m} Range [W] (N° tests)
AHRI 30											
c_0, z_c	5.292e-01 (±1.03e-02)**		9.481e-02 (±1.42e-02)**		5.292e-01 (±1.05e-02)**		1.481e-01 (±2.60e-02)**		-7.732e+00 (±8.98e-01)**		R134a [503, 922] (15/15/15)
c_1, z_c	1.517e-02 (±1.45e-03)**		1.407e-01 (±1.14e-02)**		1.535e-02 (±1.46e-03)**		9.525e-02 (±6.64e-02)**		8.332e-02 (±1.15e-01)		
c_2, k_0	2.639e-03 (±4.84e-04)**		2.254e-02 (±2.59e-03)**		2.640e-03 (±4.85e-04)**		2.002e-02 (±6.61e-03)**		3.434e+01 (±2.18e+00)**		
c_3, k_1	-1.543e-04 (±6.84e-05)**		-2.438e-03 (±2.93e-03)	0.78	-1.543e-04 (±6.82e-05)**		1.138e-03 (±2.74e-03)		6.649e+00 (±3.39e-01)**	1.65	
c_4, k_2	1.327e-04 (±1.96e-05)**	0.78	-9.158e-04 (±1.77e-04)**		1.338e-04 (±5.15e-05)**		1.059e-02 (±2.08e-02)	0.75		4.75 (0.69)	
c_5, k_3	1.489e-05 (±5.35e-06)**		2.182e-04 (±5.54e-05)**		1.489e-05 (±5.33e-06)**		-8.479e-04 (±2.41e-04)**				
c_6	2.948e-05 (±7.56e-07)**		-3.189e-04 (±2.23e-04)**		2.948e-06 (±7.54e-07)**		1.956e-04 (±7.78e-05)**				
c_7					-2.540e-08 (±1.10e-06)		-4.119e-04 (±3.16e-04)*				
c_8					-2.022e-06 (±2.67e-06)		-1.290e-03 (±2.21e-03)				
c_9					(NA)		(NA)				
c_0, z_c	5.727e-01 (±1.43e-02)**		2.098e-01 (±5.93e-02)**		5.727e-01 (±1.46e-02)**		1.301e-01 (±1.26e-01)*		-9.501e+00 (±1.08e+00)**		R1234YF [531, 919] (15/15/15)
c_1, z_c	1.004e-02 (±4.12e-04)**		1.245e-01 (±2.02e-02)**		9.293e-03 (±2.02e-03)**		1.886e-01 (±1.04e-01)**		4.370e-02 (±1.42e-01)		
c_2, k_0	2.420e-03 (±6.57e-04)**		-2.399e-03 (±9.96e-03)		2.420e-03 (±6.70e-04)**		9.614e-04 (±1.10e-02)		3.132e+01 (±1.83e+00)**		
c_3, k_1	8.642e-05 (±8.84e-06)**		6.421e-03 (±3.00e-03)**		1.226e-04 (±9.42e-05)*		4.268e-03 (±4.26e-03)*		5.147e+00 (±2.88e-01)**	1.58	
c_4, k_2	-1.710e-05 (±6.97e-05)	0.81	-7.460e-03 (±1.63e-03)**	0.85	-1.710e-05 (±7.11e-05)		-2.338e-02 (±3.03e-02)	0.78		3.94 (0.56)	
c_5, k_3	9.289e-06 (±7.22e-06)*		2.101e-04 (±4.05e-04)		9.289e-06 (±7.37e-06)*		2.101e-04 (±4.02e-04)				
c_6			-1.484e-04 (±1.22e-04)*		-4.015e-07 (±1.04e-06)		-1.484e-04 (±1.21e-04)*				
c_7	2.422e-06 (±1.49e-06)**				2.422e-06 (±1.52e-06)**		3.262e-04 (±4.61e-04)				
c_8					-1.185e-07 (±3.68e-06)		1.216e-03 (±3.01e-03)				
c_9					(NA)		(NA)				

^a * p < 0.1, * p < 0.05, ** p < 0.01, *** p < 0.001; Confidence interval of 95% for regression coefficients;

^b Temperatures (°C);

^c Pressures (bar);

^d The values in brackets are the CV_{RMSE} (%);

Table K.8: Mass flow rate models (AHRI 30)

	\dot{m}_{ref} (kg/h) 2 nd order polynomial (T-SW)	MRE (%) RMSE (kg/h)	\dot{m}_{ref} (kg/h) 2 nd order polynomial (P-SW)	MRE (%) RMSE (kg/h)	\dot{m}_{ref} (kg/h) 2 nd order polynomial (T)	MRE (%) RMSE (kg/h)	\dot{m}_{ref} (kg/h) 2 nd order polynomial (P)	MRE (%) RMSE (kg/h)	Fluid \dot{m} Range [kg/h] (N° tests)
AHRI 30 ($S_H = 11$K)									
c_0	3.048e+01 (±1.13e+00)**		-4.131e+00 (±1.17e+00)**		3.048e+01 (±1.21e+00)**		-4.598e+00 (±1.80e+00)**		R134a [18, 46] (15)
c_1	1.301e+00 (±8.84e-03)**		1.284e+01 (±7.91e-01)**		1.302e+00 (±3.60e-02)**		1.286e+01 (±9.00e-01)**		
c_2	1.104e-01 (±5.33e-02)**	0.66		0.66	1.104e-01 (±5.70e-02)**	0.65	7.743e-02 (±1.85e-01)	0.69	
c_3					-2.000e-05 (±7.72e-04)		-1.455e-03 (±2.33e-02)		
c_4	1.678e-02 (±1.94e-03)**	0.09 (0.28)	-1.097e-01 (±1.28e-01)+	0.09 (0.28)	1.678e-02 (±1.60e-03)**	0.09 (0.28)	-1.097e-01 (±1.38e-01)	0.09 (0.28)	
c_5	-2.222e-03 (±5.89e-04)**		-1.208e-02 (±6.57e-04)**		-2.222e-03 (±6.31e-04)**		-1.501e-02 (±6.90e-03)**		
c_0	3.757e+01 (±4.76e+00)**		1.871e+00 (±1.14e+00)		3.757e+01 (±4.76e+00)**		-3.628e+00 (±8.08e+00)		R1234YF [24, 55] (15)
c_1	1.334e+00 (±1.42e-01)**	2.18	1.245e+01 (±1.25e+00)**	2.19	1.334e+00 (±1.42e-01)**	2.18	1.445e+01 (±3.77e+00)**	2.20	
c_2	1.118e-01 (±2.24e-01)	0.35 (0.90)	-5.278e-01 (±3.33e-01)**	0.41 (1.05)	1.118e-01 (±2.24e-01)	0.35 (0.90)	-1.034e-01 (±8.23e-01)	0.35 (0.90)	
c_3	2.440e-03 (±3.04e-03)		7.869e-02 (±1.00e-01)		2.440e-03 (±3.04e-03)		7.869e-02 (±9.78e-02)		
c_4	1.479e-02 (±6.28e-03)**				1.479e-02 (±6.28e-03)**		-3.030e-01 (±5.41e-01)		
c_5	-2.102e-03 (±2.48e-03)+				-2.102e-03 (±2.48e-03)+		-1.736e-02 (±3.09e-02)		

^a * p < 0.1, * p < 0.05, ** p < 0.01, *** p < 0.001; Confidence interval of 95% for regression coefficients;

^b Temperatures (°C);

^c Pressures (bar);

^d The values in brackets are the CV_{RMSE} (%);

K.1.5 Compressor CS14K6E-TF5 (AHRI 35, 37)

Table K.9: Energy consumption models (AHRI 35, 37)

	\dot{W}_c (kW) AHRI (T-SW)	MRE (%) RMSE ^d (W)	\dot{W}_c (kW) AHRI (P-SW)	MRE (%) RMSE ^d (W)	\dot{W}_c (kW) AHRI (T)	MRE (%) RMSE ^d (W)	\dot{W}_c (kW) AHRI (P)	MRE (%) RMSE ^d (W)	\dot{W}_{esp} (kJ/kg)	MRE (%) RMSE ^d (W)	Fluid \dot{W}_c Range [W] (N° tests)
AHRI 35											
c_0, z_c	7.771e-01 (±7.51e-02)**		3.686e-01 (±2.41e-01)**		6.827e-01 (±2.80e-01)**		2.755e-01 (±3.46e-01)		-1.153e+00 (±6.67e-01)**		DR7 [887, 2487] (26/20)
c_1, z_r	-4.070e-02 (±9.51e-03)**		2.353e-01 (±5.74e-02)**		-4.867e-02 (±1.77e-02)**		2.985e-01 (±1.73e-01)**		3.892e-01 (±7.64e-02)**		
c_2, k_0	4.038e-02 (±2.02e-03)**		3.958e-03 (±3.52e-02)		4.524e-02 (±1.81e-03)**		8.482e-03 (±3.78e-02)		-8.873e+00 (±6.23e+00)**		
c_3, k_1	1.630e-03 (±1.86e-04)**		3.898e-02 (±5.63e-03)**		1.922e-03 (±5.78e-04)**		3.791e-02 (±7.84e-03)**		2.173e+01 (±2.31e+00)**		
c_4, k_2	-1.808e-03 (±4.28e-04)**	1.79	-5.927e-02 (±1.13e-03)**	2.29	-1.991e-03 (±5.51e-04)**	1.91	-7.540e-02 (±4.28e-02)**	2.05	-1.544e+00 (±2.93e-01)**	2.87	
c_5, k_3		13.10 (0.80)	-2.986e-03 (±1.81e-03)**	13.13 (0.80)	-7.251e-05 (±4.01e-04)	12.91 (0.79)	-3.127e-03 (±1.88e-03)**	13.04 (0.80)	5.699e-02 (±1.27e-02)**	16.96 (0.60)	
c_6	1.644e-05 (±6.25e-06)**		-4.922e-04 (±1.43e-04)**		1.862e-05 (±7.68e-06)**		6.694e-05 (±1.12e-03)				
c_7	-1.919e-05 (±6.56e-06)**				2.967e-04 (±7.85e-04)		-1.468e-04 (±5.78e-04)				
c_9	-2.863e-06 (±2.58e-07)**		4.706e-05 (±3.20e-05)**		-2.589e-06 (±2.99e-06)		4.844e-05 (±3.29e-05)**				
AHRI 37											
c_0, z_c	6.470e-01 (±1.05e-01)**		2.511e-01 (±7.41e-02)**		8.976e-01 (±5.22e-01)**		2.772e-01 (±3.75e-01)		5.690e-01 (±5.58e-01)**		L40 [766, 2212] (24/27)
c_1, z_r	-5.090e-02 (±1.26e-02)**		2.169e-01 (±2.38e-02)**		-3.407e-02 (±2.85e-02)**		1.513e-01 (±2.24e-01)		7.223e-01 (±4.61e-02)**		
c_2, k_0	3.627e-02 (±2.91e-03)**		1.446e-02 (±7.06e-03)**		2.089e-02 (±3.54e-02)		2.141e-02 (±4.94e-02)		6.915e-01 (±7.97e-01)		
c_3, k_1	1.678e-03 (±2.38e-04)**		2.488e-02 (±1.52e-03)**	4.32	9.945e-04 (±1.08e-03)	4.24	2.904e-02 (±1.24e-02)**	4.38	2.068e+01 (±2.53e+00)**	3.62	
c_4, k_2	-2.611e-03 (±5.77e-04)**	3.60	-2.172e-03 (±2.61e-04)**	15.53 (0.8)	-2.268e-03 (±7.68e-04)**	15.55 (0.8)	1.204e-02 (±6.70e-02)	15.38 (0.7)	-1.309e+00 (±2.78e-01)**	20.96 (0.46)	
c_5, k_3		15.94 (0.11)		15.53 (0.8)	2.967e-04 (±7.85e-04)	4.24	-3.007e-03 (±3.03e-03)	4.38	4.561e-02 (±1.05e-02)**		
c_6	2.103e-05 (±7.85e-06)**				7.032e-06 (±1.08e-05)		-1.468e-04 (±5.78e-04)				
c_7	-3.447e-05 (±8.73e-06)**		-8.304e-03 (±7.50e-04)**		1.588e-05 (±1.13e-05)**		6.534e-05 (±2.64e-03)				
c_9	-2.221e-06 (±3.80e-07)**				-3.096e-05 (±1.00e-05)**		-9.688e-03 (±9.34e-03)**				

^a $p < 0.1$, * $p < 0.05$, ** $p < 0.01$, *** $p < 0.001$; Confidence interval of 95% for regression coefficients;
^b Temperatures (°C);
^c Pressures (bar);
^d The values in brackets are the CV_{RMSE} (%).

Table K.10: Mass flow rate models (AHRI 35, 37)

	\dot{m}_{ref} (kg/h) 2 nd order polynomial (T-SW)	MRE (%) RMSE (kg/h)	\dot{m}_{ref} (kg/h) 2 nd order polynomial (P-SW)	MRE (%) RMSE (kg/h)	\dot{m}_{ref} (kg/h) 2 nd order polynomial (T)	MRE (%) RMSE (kg/h)	\dot{m}_{ref} (kg/h) 2 nd order polynomial (P)	MRE (%) RMSE (kg/h)	Fluid \dot{m} Range [kg/h] (N° tests)
AHRI 35 (SH = 11K)									
c_0	1.955e+02 (±5.41e+00)**		-6.040e+00 (±7.63e+00)		1.955e+02 (±5.41e+00)**		-6.040e+00 (±7.63e+00)		DR7 [23, 144] (26)
c_1	7.425e+00 (±2.50e-01)**		3.370e+01 (±2.90e+00)**		7.425e+00 (±2.50e-01)**		3.370e+01 (±2.90e+00)**		
c_2	-8.194e-01 (±2.21e-01)**		-1.507e+00 (±5.69e-01)**	11.46	-8.194e-01 (±2.21e-01)**	3.26	-1.507e+00 (±5.69e-01)**	11.46	
c_3	-2.274e-02 (±3.76e-03)**	3.26	-3.781e-01 (±8.71e-02)**	0.88 (0.12)	-2.274e-02 (±3.76e-03)**	0.65 (0.83)	-3.781e-01 (±8.71e-02)**	0.88 (0.12)	
c_5	-6.245e-03 (±2.41e-03)**		1.052e+00 (±4.29e-01)**		7.595e-02 (±4.62e-03)**		1.052e+00 (±4.29e-01)**		
AHRI 37 (SH = 11K)									
c_0	1.583e+02 (±5.65e+00)**		-1.343e+01 (±8.95e+00)**		1.554e+02 (±1.15e+01)**		-9.067e+00 (±1.15e+01)		L40 [22, 111] (24)
c_1	6.168e+00 (±5.12e-01)**		3.740e+01 (±3.10e+00)**		6.098e+00 (±5.77e-01)**		3.444e+01 (±5.83e+00)**		
c_2	-1.066e+00 (±1.08e-01)**		-1.933e+00 (±9.68e-01)**	8.05	-9.329e-01 (±4.78e-01)**	4.60	-1.968e+00 (±9.59e-01)**	4.90	
c_3	-2.159e-02 (±7.02e-03)**	5.02	-3.600e-01 (±1.80e-01)**	1.34 (2.80)	-2.044e-02 (±8.21e-03)**	1.16 (0.98)	-4.167e-01 (±2.02e-01)**	1.29 (2.21)	
c_5	6.473e-02 (±1.11e-02)**	1.17 (2.00)			6.382e-02 (±1.18e-02)**		6.262e-01 (±1.05e+00)		

^a $p < 0.1$, * $p < 0.05$, ** $p < 0.01$, *** $p < 0.001$; Confidence interval of 95% for regression coefficients;
^b Temperatures (°C);
^c Pressures (bar);
^d The values in brackets are the CV_{RMSE} (%).

K.1.6 Compressor 4GE-23-40P (AHRI 51)

Table K.11: Energy consumption models (AHRI 51)

\dot{W}_c (kW) AHRI (T-SW)		MRE (%) RMSE ^d (W)	\dot{W}_c (kW) AHRI (P-SW)		MRE (%) RMSE ^d (W)	\dot{W}_c (kW) AHRI (I)		MRE (%) RMSE ^d (W)	\dot{W}_c (kW) AHRI (P)		MRE (%) RMSE ^d (W)	W_{esp} (kJ/kg)	MRE (%) RMSE ^d (W)	Fluid \dot{W}_c Range [W] (N° tests)							
AHRI 51																					
$c_{0,z}$	3.665e+00 (±1.24e+01)	0.49 32.81 (0.22)	-1.864e+00 (±1.79e+01)	0.68 48.02 (0.32)	3.665e+00 (±1.24e+01)	0.49 32.81 (0.22)	-1.864e+00 (±1.79e+01)	0.68 48.02 (0.32)	3.665e+00 (±1.24e+01)	0.49 32.81 (0.22)	-1.864e+00 (±1.79e+01)	0.68 48.02 (0.32)	-1.114e+00 (±1.48e+00)	1.94 117.56 (0.79)	R449A [2872, 2295] (12)						
$c_{1,z}$	-1.587e-01 (±1.88e-01)		2.439e+00 (±4.12e+00)		-1.587e-01 (±1.88e-01)		2.439e+00 (±4.12e+00)		-1.587e-01 (±1.88e-01)		2.439e+00 (±4.12e+00)		-1.587e-01 (±1.88e-01)			2.439e+00 (±4.12e+00)	-1.587e-01 (±1.88e-01)	2.439e+00 (±4.12e+00)	-1.587e-01 (±1.88e-01)	2.439e+00 (±4.12e+00)	1.565e-01 (±1.75e-01)
$c_{2,k0}$	5.795e-01 (±1.12e+00)		9.732e-01 (±3.62e+00)		5.795e-01 (±1.12e+00)		9.732e-01 (±3.62e+00)		5.795e-01 (±1.12e+00)		9.732e-01 (±3.62e+00)		5.795e-01 (±1.12e+00)			9.732e-01 (±3.62e+00)	5.795e-01 (±1.12e+00)	9.732e-01 (±3.62e+00)	5.795e-01 (±1.12e+00)	9.732e-01 (±3.62e+00)	1.687e+00 (±5.99e+00)
$c_{3,k1}$	7.606e-03 (±6.78e-03)*		3.725e-01 (±2.14e-01)*		7.606e-03 (±6.78e-03)*		3.725e-01 (±2.14e-01)*		7.606e-03 (±6.78e-03)*		3.725e-01 (±2.14e-01)*		7.606e-03 (±6.78e-03)*			3.725e-01 (±2.14e-01)*	7.606e-03 (±6.78e-03)*	3.725e-01 (±2.14e-01)*	7.606e-03 (±6.78e-03)*	3.725e-01 (±2.14e-01)*	1.613e+01 (±1.71e+00)***
$c_{4,k2}$	-7.165e-03 (±8.08e-03)*		-8.844e-01 (±1.10e+00)*		-7.165e-03 (±8.08e-03)*		-8.844e-01 (±1.10e+00)*		-7.165e-03 (±8.08e-03)*		-8.844e-01 (±1.10e+00)*		-7.165e-03 (±8.08e-03)*			-8.844e-01 (±1.10e+00)*	-7.165e-03 (±8.08e-03)*	-8.844e-01 (±1.10e+00)*	-7.165e-03 (±8.08e-03)*	-8.844e-01 (±1.10e+00)*	-8.600e-01 (±2.02e-01)***
$c_{5,k3}$	-6.646e-03 (±3.02e-02)		-7.119e-02 (±2.24e-01)		-6.646e-03 (±3.02e-02)		-7.119e-02 (±2.24e-01)		-6.646e-03 (±3.02e-02)		-7.119e-02 (±2.24e-01)		-6.646e-03 (±3.02e-02)			-7.119e-02 (±2.24e-01)	-6.646e-03 (±3.02e-02)	-7.119e-02 (±2.24e-01)	-6.646e-03 (±3.02e-02)	-7.119e-02 (±2.24e-01)	1.987e-02 (±2.77e-03)***
c_6	3.423e-05 (±6.93e-05)		-2.997e-03 (±3.75e-03)+		3.423e-05 (±6.93e-05)		-2.997e-03 (±3.75e-03)+		3.423e-05 (±6.93e-05)		-2.997e-03 (±3.75e-03)+		3.423e-05 (±6.93e-05)			-2.997e-03 (±3.75e-03)+	3.423e-05 (±6.93e-05)	-2.997e-03 (±3.75e-03)+	3.423e-05 (±6.93e-05)	-2.997e-03 (±3.75e-03)+	
c_7	4.655e-05 (±9.35e-05)		-1.349e-02 (±3.02e-02)		4.655e-05 (±9.35e-05)		-1.349e-02 (±3.02e-02)		4.655e-05 (±9.35e-05)		-1.349e-02 (±3.02e-02)		4.655e-05 (±9.35e-05)			-1.349e-02 (±3.02e-02)	4.655e-05 (±9.35e-05)	-1.349e-02 (±3.02e-02)	4.655e-05 (±9.35e-05)	-1.349e-02 (±3.02e-02)	
c_8	-6.460e-05 (±1.36e-04)		6.053e-02 (±1.09e-01)		-6.460e-05 (±1.36e-04)		6.053e-02 (±1.09e-01)		-6.460e-05 (±1.36e-04)		6.053e-02 (±1.09e-01)		-6.460e-05 (±1.36e-04)			6.053e-02 (±1.09e-01)	-6.460e-05 (±1.36e-04)	6.053e-02 (±1.09e-01)	-6.460e-05 (±1.36e-04)	6.053e-02 (±1.09e-01)	
c_9	4.759e-05 (±2.48e-04)	1.215e-03 (±4.14e-03)	4.759e-05 (±2.48e-04)	1.215e-03 (±4.14e-03)	4.759e-05 (±2.48e-04)	1.215e-03 (±4.14e-03)	4.759e-05 (±2.48e-04)	1.215e-03 (±4.14e-03)	4.759e-05 (±2.48e-04)	1.215e-03 (±4.14e-03)	4.759e-05 (±2.48e-04)	1.215e-03 (±4.14e-03)									
$c_{0,z}$	7.260e+00 (±7.83e-01)***	0.03 2.08 (0.00)	-1.182e+00 (±5.04e-00)	0.11 11.38 (0.07)	7.260e+00 (±7.83e-01)***	0.03 2.08 (0.00)	-1.182e+00 (±5.04e-00)	0.11 11.38 (0.07)	7.260e+00 (±7.83e-01)***	0.03 2.08 (0.00)	-1.182e+00 (±5.04e-00)	0.11 11.38 (0.07)	-1.761e+00 (±9.11e-01)**	0.52 56.52 (0.33)	R404A [9353, 25132] (12)						
$c_{1,z}$	-1.328e-01 (±1.18e-02)**		2.637e+00 (±9.60e-01)**		-1.328e-01 (±1.18e-02)**		2.637e+00 (±9.60e-01)**		-1.328e-01 (±1.18e-02)**		2.637e+00 (±9.60e-01)**		-1.328e-01 (±1.18e-02)**			2.637e+00 (±9.60e-01)**	-1.328e-01 (±1.18e-02)**	2.637e+00 (±9.60e-01)**	-1.328e-01 (±1.18e-02)**	2.637e+00 (±9.60e-01)**	8.370e-02 (±1.24e-01)
$c_{2,k0}$	4.335e-01 (±7.99e-02)**		7.823e-01 (±9.29e-01)+		4.335e-01 (±7.99e-02)**		7.823e-01 (±9.29e-01)+		4.335e-01 (±7.99e-02)**		7.823e-01 (±9.29e-01)+		4.335e-01 (±7.99e-02)**			7.823e-01 (±9.29e-01)+	4.335e-01 (±7.99e-02)**	7.823e-01 (±9.29e-01)+	4.335e-01 (±7.99e-02)**	7.823e-01 (±9.29e-01)+	4.420e+00 (±2.91e-00)**
$c_{3,k1}$	8.421e-03 (±4.29e-04)**		2.884e-01 (±4.49e-02)**		8.421e-03 (±4.29e-04)**		2.884e-01 (±4.49e-02)**		8.421e-03 (±4.29e-04)**		2.884e-01 (±4.49e-02)**		8.421e-03 (±4.29e-04)**			2.884e-01 (±4.49e-02)**	8.421e-03 (±4.29e-04)**	2.884e-01 (±4.49e-02)**	8.421e-03 (±4.29e-04)**	2.884e-01 (±4.49e-02)**	1.606e+01 (±1.05e-00)***
$c_{4,k2}$	-5.988e-03 (±5.12e-04)**		-7.479e-01 (±2.16e-01)**		-5.988e-03 (±5.12e-04)**		-7.479e-01 (±2.16e-01)**		-5.988e-03 (±5.12e-04)**		-7.479e-01 (±2.16e-01)**		-5.988e-03 (±5.12e-04)**			-7.479e-01 (±2.16e-01)**	-5.988e-03 (±5.12e-04)**	-7.479e-01 (±2.16e-01)**	-5.988e-03 (±5.12e-04)**	-7.479e-01 (±2.16e-01)**	-1.069e+00 (±1.44e-01)**
$c_{5,k3}$	-2.278e-03 (±1.91e-03)**		-5.024e-02 (±5.26e-02)+		-2.278e-03 (±1.91e-03)**		-5.024e-02 (±5.26e-02)+		-2.278e-03 (±1.91e-03)**		-5.024e-02 (±5.26e-02)+		-2.278e-03 (±1.91e-03)**			-5.024e-02 (±5.26e-02)+	-2.278e-03 (±1.91e-03)**	-5.024e-02 (±5.26e-02)+	-2.278e-03 (±1.91e-03)**	-5.024e-02 (±5.26e-02)+	3.171e-02 (±6.68e-03)***
c_6	2.466e-05 (±4.39e-00)**		-2.276e-03 (±7.49e-04)**		2.466e-05 (±4.39e-00)**		-2.276e-03 (±7.49e-04)**		2.466e-05 (±4.39e-00)**		-2.276e-03 (±7.49e-04)**		2.466e-05 (±4.39e-00)**			-2.276e-03 (±7.49e-04)**	2.466e-05 (±4.39e-00)**	-2.276e-03 (±7.49e-04)**	2.466e-05 (±4.39e-00)**	-2.276e-03 (±7.49e-04)**	
c_7	6.214e-05 (±5.92e-00)***		-6.988e-03 (±5.38e-03)*		6.214e-05 (±5.92e-00)***		-6.988e-03 (±5.38e-03)*		6.214e-05 (±5.92e-00)***		-6.988e-03 (±5.38e-03)*		6.214e-05 (±5.92e-00)***			-6.988e-03 (±5.38e-03)*	6.214e-05 (±5.92e-00)***	-6.988e-03 (±5.38e-03)*	6.214e-05 (±5.92e-00)***	-6.988e-03 (±5.38e-03)*	
c_8	-3.851e-05 (±8.59e-06)**		4.359e-02 (±1.81e-02)**		-3.851e-05 (±8.59e-06)**		4.359e-02 (±1.81e-02)**		-3.851e-05 (±8.59e-06)**		4.359e-02 (±1.81e-02)**		-3.851e-05 (±8.59e-06)**			4.359e-02 (±1.81e-02)**	-3.851e-05 (±8.59e-06)**	4.359e-02 (±1.81e-02)**	-3.851e-05 (±8.59e-06)**	4.359e-02 (±1.81e-02)**	
c_9	1.130e-05 (±1.57e-05)+	7.624e-04 (±8.99e-04)+	1.130e-05 (±1.57e-05)+	7.624e-04 (±8.99e-04)+	1.130e-05 (±1.57e-05)+	7.624e-04 (±8.99e-04)+	1.130e-05 (±1.57e-05)+	7.624e-04 (±8.99e-04)+	1.130e-05 (±1.57e-05)+	7.624e-04 (±8.99e-04)+	1.130e-05 (±1.57e-05)+	7.624e-04 (±8.99e-04)+									

a + p < 0.1, * p < 0.05, ** p < 0.01, *** p < 0.001; Confidence interval of 95% for regression coefficients;
b Temperatures (°C);
c Pressures (bar);
d The values in brackets are the CV_{RMSE} (%).

Table K.12: Mass flow rate models (AHRI 51)

\dot{m}_{ref} (kg/h) 2 nd order polynomial (T-SW)		MRE (%) RMSE (kg/h)	\dot{m}_{ref} (kg/h) 2 nd order polynomial (P-SW)		MRE (%) RMSE (kg/h)	\dot{m}_{ref} (kg/h) 2 nd order polynomial (I)		MRE (%) RMSE (kg/h)	\dot{m}_{ref} (kg/h) 2 nd order polynomial (P)		MRE (%) RMSE (kg/h)	Fluid \dot{m} Range [kg/h] (N° tests)				
AHRI 51 (T_i = 20°C)																
c_0	1.706e+03 (±8.01e+01)***	4.79 9.41 (1.03)	-2.901e+01 (±3.75e+01)	1.48 2.95 (0.32)	1.706e+03 (±8.01e+01)***	4.79 9.41 (1.03)	-2.901e+01 (±3.75e+01)	1.48 2.95 (0.32)	1.706e+03 (±8.01e+01)***	4.79 9.41 (1.03)	-2.901e+01 (±3.75e+01)	1.48 2.95 (0.32)	R449A [259, 1623] (12)			
c_1	6.133e+01 (±3.95e+00)***		3.108e+02 (±1.59e+01)**		6.133e+01 (±3.95e+00)***		3.108e+02 (±1.59e+01)**		6.133e+01 (±3.95e+00)***		3.108e+02 (±1.59e+01)**		6.133e+01 (±3.95e+00)***	3.108e+02 (±1.59e+01)**	6.133e+01 (±3.95e+00)***	3.108e+02 (±1.59e+01)**
c_2	-3.891e+00 (±4.12e+00)+		-5.143e+00 (±3.33e+00)**		-3.891e+00 (±4.12e+00)+		-5.143e+00 (±3.33e+00)**		-3.891e+00 (±4.12e+00)+		-5.143e+00 (±3.33e+00)**		-3.891e+00 (±4.12e+00)+	-5.143e+00 (±3.33e+00)**	-3.891e+00 (±4.12e+00)+	-5.143e+00 (±3.33e+00)**
c_3	-1.187e-01 (±6.58e-02)**		-2.338e+00 (±4.40e-01)**		-1.187e-01 (±6.58e-02)**		-2.338e+00 (±4.40e-01)**		-1.187e-01 (±6.58e-02)**		-2.338e+00 (±4.40e-01)**		-1.187e-01 (±6.58e-02)**	-2.338e+00 (±4.40e-01)**	-1.187e-01 (±6.58e-02)**	-2.338e+00 (±4.40e-01)**
c_4	6.158e-01 (±8.58e-02)**		7.987e+00 (±2.29e+00)**		6.158e-01 (±8.58e-02)**		7.987e+00 (±2.29e+00)**		6.158e-01 (±8.58e-02)**		7.987e+00 (±2.29e+00)**		6.158e-01 (±8.58e-02)**	7.987e+00 (±2.29e+00)**	6.158e-01 (±8.58e-02)**	7.987e+00 (±2.29e+00)**
c_5	-3.276e-02 (±4.99e-02)	5.286e-02 (±8.24e-02)	-3.276e-02 (±4.99e-02)	5.286e-02 (±8.24e-02)	-3.276e-02 (±4.99e-02)	5.286e-02 (±8.24e-02)	-3.276e-02 (±4.99e-02)	5.286e-02 (±8.24e-02)	-3.276e-02 (±4.99e-02)	5.286e-02 (±8.24e-02)						
c_0	2.334e+03 (±4.24e+01)***	2.49 11.03 (0.88)	-1.517e+01 (±6.00e+01)	0.80 4.24 (0.34)	2.334e+03 (±4.24e+01)***	2.49 11.03 (0.88)	-1.517e+01 (±6.00e+01)	0.80 4.24 (0.34)	2.334e+03 (±4.24e+01)***	2.49 11.03 (0.88)	-1.517e+01 (±6.00e+01)	0.80 4.24 (0.34)	R404A [409, 2172] (12)			
c_1	8.018e+01 (±4.05e+00)***		3.420e+02 (±2.12e+01)**		8.018e+01 (±4.05e+00)***		3.420e+02 (±2.12e+01)**		8.018e+01 (±4.05e+00)***		3.420e+02 (±2.12e+01)**		8.018e+01 (±4.05e+00)***	3.420e+02 (±2.12e+01)**	8.018e+01 (±4.05e+00)***	3.420e+02 (±2.12e+01)**
c_2	-8.504e+00 (±1.10e+00)**		-6.547e+00 (±4.86e+00)*		-8.504e+00 (±1.10e+00)**		-6.547e+00 (±4.86e+00)*		-8.504e+00 (±1.10e+00)**		-6.547e+00 (±4.86e+00)*		-8.504e+00 (±1.10e+00)**	-6.547e+00 (±4.86e+00)*	-8.504e+00 (±1.10e+00)**	-6.547e+00 (±4.86e+00)*
c_3	-1.840e-01 (±6.82e-02)**		-3.018e+00 (±5.44e-01)**		-1.840e-01 (±6.82e-02)**		-3.018e+00 (±5.44e-01)**		-1.840e-01 (±6.82e-02)**		-3.018e+00 (±5.44e-01)**		-1.840e-01 (±6.82e-02)**	-3.018e+00 (±5.44e-01)**	-1.840e-01 (±6.82e-02)**	-3.018e+00 (±5.44e-01)**
c_4	7.951e-01 (±8.84e-02)**		1.053e+01 (±2.56e+00)**		7.951e-01 (±8.84e-02)**		1.053e+01 (±2.56e+00)**		7.951e-01 (±8.84e-02)**		1.053e+01 (±2.56e+00)**		7.951e-01 (±8.84e-02)**	1.053e+01 (±2.56e+00)**	7.951e-01 (±8.84e-02)**	1.053e+01 (±2.56e+00)**
c_5		1.343e-01 (±1.12e-01)*		1.343e-01 (±1.12e-01)*		1.343e-01 (±1.12e-01)*		1.343e-01 (±1.12e-01)*		1.343e-01 (±1.12e-01)*						

a + p < 0.1, * p < 0.05, ** p < 0.01, *** p < 0.001; Confidence interval of 95% for regression coefficients;
b Temperatures (°C);
c Pressures (bar);
d The values in brackets are the CV_{RMSE} (%).

K.1.7 Compressor H84B223ABC (AHRI 59)

Table K.13: Energy consumption models (AHRI 59)

	\dot{W}_c (kW) AHRI (T-SW)	MRE (%) RMSE ^b (W)	\dot{W}_c (kW) AHRI (P-SW)	MRE (%) RMSE ^b (W)	\dot{W}_c (kW) AHRI (T)	MRE (%) RMSE ^b (W)	\dot{W}_c (kW) AHRI (P)	MRE (%) RMSE ^b (W)	\dot{W}_{exp} (kJ/kg)	MRE (%) RMSE ^b (W)	Fluid \dot{W}_c Range [W] (N° tests)	
AHRI 59												
c_0, z_c	8.272e-01 (±5.28e-01)**	1.87 10.80 (0.60)	2.277e-01 (±5.74e-01)	1.97 12.91 (0.70)	8.259e-01 (±7.13e-01)*	1.92 9.86 (0.60)	7.319e-02 (±1.01e+00)	2.01 12.35 (0.70)	2.092e+00 (±4.05e+00)	4.06 34.69 (3.13)	R410A [918, 2552] (15)	
c_1, z_c	-4.112e-02 (±5.52e-03)**		3.157e-01 (±1.81e-01)**		-4.476e-02 (±3.13e-02)*		4.708e-04 (±1.28e-03)		3.260e-01 (±2.26e-01)**		-1.096e-04 (±2.28e-04)	1.259e+00 (±6.84e-01)**
c_2, k_0	1.176e-02 (±3.83e-02)		-3.486e-02 (±3.77e-03)**		1.594e-02 (±2.23e-03)**		1.664e-03 (±1.50e-03)*		-1.998e-02 (±9.05e-02)		-1.685e-02 (±7.54e-03)**	-2.115e+00 (±7.02e+00)
c_3, k_1	1.475e-03 (±1.12e-04)**		-5.184e-02 (±2.50e-02)**		-1.477e-03 (±1.15e-03)*		-1.914e-06 (±1.67e-05)		-5.502e-02 (±3.48e-02)**		-8.609e-04 (±2.97e-03)	1.625e+01 (±2.78e+00)**
c_4, k_2	-1.168e-03 (±3.61e-04)**		-1.221e-04 (±7.30e-05)**		1.399e-03 (±1.09e-03)*		1.574e-05 (±2.46e-05)		-1.096e-04 (±2.28e-04)		-9.845e-05 (±1.02e-05)	-3.059e-01 (±3.52e-01)+
c_5, k_3	5.033e-04 (±8.80e-04)											
c_6	1.033e-05 (±8.36e-06)*											
c_7												
c_9	-6.563e-06 (±6.42e-06)*											
c_0, z_c	3.903e-01 (±1.21e-01)**	1.64 7.04 (0.53)	-1.029e-01 (±6.01e-01)	1.78 8.23 (0.60)	4.161e-01 (±5.03e-01)+	1.65 6.94 (0.50)	-1.029e-01 (±6.01e-01)	1.78 8.23 (0.60)	1.134e+00 (±3.55e+00)	4.72 26.43 (1.91)	L41-1 [779, 2173] (15)	
c_1, z_c	-4.238e-02 (±1.51e-02)**		1.208e-01 (±1.71e-01)		-4.044e-02 (±2.20e-02)*		4.708e-04 (±1.28e-03)		1.208e-01 (±1.71e-01)		-1.096e-04 (±2.28e-04)	1.193e+00 (±3.43e-01)**
c_2, k_0	3.906e-02 (±5.42e-03)**		5.558e-02 (±6.59e-02)+		3.353e-02 (±3.80e-02)+		-1.876e-04 (±9.02e-04)		5.558e-02 (±6.59e-02)+		-1.935e+00 (±3.32e-01)**	3.298e+01 (±1.79e-01)**
c_3, k_1	1.940e-03 (±7.44e-04)**		1.082e-02 (±6.88e-03)**		1.846e-03 (±1.06e-03)*		-1.866e-04 (±9.02e-04)		1.082e-02 (±6.88e-03)**		-3.082e-03 (±2.61e-03)**	-1.827e-01 (±2.07e-01)+
c_4, k_2	-2.378e-03 (±3.26e-04)**		-1.248e-02 (±3.34e-02)		-2.320e-03 (±8.08e-04)**		-3.569e-04 (±2.54e-04)*		-1.248e-02 (±3.34e-02)		-3.569e-04 (±2.54e-04)*	1.827e-01 (±2.07e-01)+
c_5, k_3	-3.194e-04 (±6.62e-05)**		-3.082e-03 (±2.61e-03)**		-1.866e-04 (±9.02e-04)		3.537e-05 (±1.73e-05)**		-3.082e-03 (±2.61e-03)**		1.275e-03 (±1.20e-03)*	
c_6	-7.662e-03 (±8.26e-06)**		1.275e-03 (±1.20e-03)*		-2.038e-03 (±2.72e-03)		-3.106e-05 (±1.23e-05)**		-7.662e-03 (±8.26e-06)**		-2.038e-03 (±2.72e-03)	
c_7	3.675e-05 (±1.28e-05)**		1.275e-03 (±1.20e-03)*		5.484e-05 (±4.61e-05)*		-9.946e-07 (±6.74e-06)		3.675e-05 (±1.28e-05)**		5.484e-05 (±4.61e-05)*	
c_9	-3.144e-05 (±1.06e-05)**		-2.038e-03 (±2.72e-03)						-3.144e-05 (±1.06e-05)**			
c_0, z_c	6.378e-01 (±2.12e-01)**	0.73 3.83 (0.28)	-2.728e-01 (±4.45e-01)	0.96 5.56 (0.36)	6.057e-01 (±2.66e-01)**	0.63 3.68 (0.26)	-2.728e-01 (±4.45e-01)	0.96 5.56 (0.36)	5.346e-01 (±2.77e-00)	2.72 23.63 (1.53)	DR5A [884, 2416] (15)	
c_1, z_c	-3.622e-02 (±2.19e-03)**		2.738e-01 (±1.10e-01)**		-3.914e-02 (±1.17e-02)**		1.508e-03 (±5.59e-03)**		2.738e-01 (±1.10e-01)**		1.138e-01 (±3.40e-02)**	-2.314e+01 (±1.21e-01)**
c_2, k_0	2.351e-02 (±1.54e-02)**		3.476e-02 (±4.34e-02)+		2.627e-02 (±2.01e-02)*		-1.857e-03 (±4.28e-04)**		3.476e-02 (±4.34e-02)**		1.288e-02 (±3.99e-03)**	-3.487e+00 (±2.52e-00)**
c_3, k_1	1.566e-03 (±4.77e-05)**		1.288e-02 (±3.99e-03)**		1.508e-03 (±5.59e-03)**		1.031e-04 (±4.78e-04)		1.566e-03 (±4.77e-05)**		-4.188e-02 (±1.86e-02)**	2.054e-01 (±1.71e-01)**
c_4, k_2	-1.770e-03 (±2.35e-04)**		-4.188e-02 (±1.86e-02)**		-2.077e-03 (±1.54e-03)*		-1.594e-06 (±6.24e-06)		-1.770e-03 (±2.35e-04)**		-1.607e-04 (±1.31e-04)*	
c_5, k_3	1.739e-04 (±3.52e-04)**		-2.077e-03 (±1.54e-03)*		1.031e-04 (±4.78e-04)		2.491e-05 (±9.18e-06)**		1.739e-04 (±3.52e-04)**		3.376e-04 (±5.96e-04)	
c_6	2.290e-05 (±4.30e-06)**		-1.607e-04 (±1.31e-04)*		-1.594e-06 (±6.24e-06)		-1.566e-05 (±6.52e-06)**		2.290e-05 (±4.30e-06)**		6.263e-04 (±1.30e-03)	
c_7	-1.481e-05 (±5.09e-06)**		3.376e-04 (±5.96e-04)		2.491e-05 (±9.18e-06)**		-3.416e-06 (±3.57e-06)+		-1.481e-05 (±5.09e-06)**		2.512e-05 (±2.35e-05)*	
c_9	-3.968e-06 (±2.57e-06)**		2.512e-05 (±2.45e-05)*		-3.416e-06 (±3.57e-06)+				-3.968e-06 (±2.57e-06)**			
c_0, z_c	6.062e-01 (±2.21e-01)**	0.53 3.05 (0.20)	-1.965e-01 (±2.87e-01)	0.76 4.25 (0.28)	6.062e-01 (±2.21e-01)**	0.53 3.05 (0.20)	-1.946e-01 (±3.34e-01)	0.73 4.25 (0.28)	1.126e+00 (±2.48e+00)	3.23 25.45 (1.68)	ARM71a [866, 2371] (15)	
c_1, z_c	-3.960e-02 (±9.70e-03)**		2.343e-01 (±5.51e-02)**		-3.960e-02 (±9.70e-03)**		1.508e-03 (±5.59e-03)**		-3.960e-02 (±9.70e-03)**		1.180e-01 (±3.56e-01)**	-2.173e+00 (±2.70e-00)
c_2, k_0	2.614e-02 (±1.67e-02)*		3.609e-02 (±2.83e-02)*		2.614e-02 (±1.67e-02)*		-1.857e-03 (±4.28e-04)**		2.614e-02 (±1.67e-02)*		3.636e-02 (±3.34e-02)**	-2.699e+01 (±1.95e-01)**
c_3, k_1	1.617e-03 (±4.64e-04)**		1.166e-02 (±2.06e-03)**		1.617e-03 (±4.64e-04)**		1.031e-04 (±4.78e-04)		1.617e-03 (±4.64e-04)**		1.159e-02 (±3.15e-03)**	3.380e-01 (±1.15e-01)**
c_4, k_2	-2.016e-03 (±3.55e-04)**		-3.376e-02 (±5.96e-03)**		-2.016e-03 (±3.55e-04)**		-3.325e-06 (±5.18e-06)		-2.016e-03 (±3.55e-04)**		-3.329e-02 (±1.48e-02)**	-3.635e+00 (±1.37e-00)**
c_5, k_3	6.141e-05 (±3.97e-04)		-2.154e-03 (±1.05e-03)*		6.141e-05 (±3.97e-04)		2.839e-05 (±7.32e-06)**		6.141e-05 (±3.97e-04)		-2.157e-03 (±1.21e-03)*	2.160e-01 (±1.58e-01)**
c_6	-3.325e-06 (±5.18e-06)		-2.006e-04 (±7.07e-05)**		-3.325e-06 (±5.18e-06)		-2.067e-05 (±5.41e-06)**		-3.325e-06 (±5.18e-06)		-2.031e-04 (±1.06e-04)*	
c_7	2.839e-05 (±7.32e-06)**		5.608e-04 (±2.60e-04)**		2.839e-05 (±7.32e-06)**		-2.067e-05 (±5.41e-06)**		2.839e-05 (±7.32e-06)**		5.747e-04 (±4.86e-04)*	
c_9	-2.881e-06 (±2.96e-06)**		2.887e-05 (±1.59e-05)**		-2.881e-06 (±2.96e-06)**		-2.881e-06 (±2.96e-06)**		-2.881e-06 (±2.96e-06)**		2.914e-05 (±1.98e-05)*	
c_0, z_c	5.652e-01 (±1.11e-01)**	1.93 7.79 (0.68)	1.719e-01 (±7.66e-01)	2.41 11.03 (0.92)	6.993e-01 (±4.56e-01)**	2.00 7.51 (0.63)	1.885e-01 (±9.19e-01)	2.35 11.03 (0.91)	-2.173e+00 (±2.70e-00)	2.08 14.61 (1.21)	D2Y60 [787, 1838] (17)	
c_1, z_c	-6.267e-02 (±1.43e-02)**		3.368e-01 (±1.84e-01)**		-5.921e-02 (±1.98e-02)**		1.666e-02 (±3.46e-02)		-6.267e-02 (±1.43e-02)**		3.264e-01 (±3.10e-01)*	3.097e-01 (±3.56e-01)**
c_2, k_0	2.706e-02 (±5.13e-03)**		-3.258e-02 (±7.74e-02)		1.666e-02 (±3.46e-02)		1.666e-02 (±3.46e-02)		2.706e-02 (±5.13e-03)**		-3.222e-02 (±8.52e-02)	-3.296e+01 (±1.93e-01)**
c_3, k_1	2.985e-03 (±4.94e-04)**		1.644e-02 (±2.58e-03)**		2.813e-03 (±9.26e-04)**		2.813e-03 (±9.26e-04)**		2.985e-03 (±4.94e-04)**		1.624e-02 (±9.42e-03)**	3.338e-01 (±9.42e-00)**
c_4, k_2	-2.241e-03 (±5.70e-04)**		-5.908e-02 (±2.10e-02)**		-2.113e-03 (±7.39e-04)**		-2.049e-05 (±1.03e-05)**		-2.241e-03 (±5.70e-04)**		-5.677e-02 (±5.70e-02)+	-4.097e+00 (±1.66e-00)**
c_5, k_3	-2.238e-04 (±5.50e-05)**		-2.635e-04 (±3.26e-03)		2.561e-05 (±8.21e-04)		2.561e-05 (±8.21e-04)		-2.238e-04 (±5.50e-05)**		-2.671e-04 (±3.54e-03)	2.327e-01 (±9.82e-02)**
c_6	-2.244e-04 (±5.50e-06)**		-6.326e-04 (±2.48e-04)**		-2.049e-05 (±1.03e-05)**		-1.879e-05 (±1.48e-05)**		-2.244e-04 (±5.50e-06)**		-6.445e-04 (±3.81e-04)*	
c_7	3.761e-05 (±1.16e-05)**		1.728e-03 (±1.05e-03)**		3.467e-05 (±1.56e-05)**		-1.879e-05 (±1.48e-05)**		3.761e-05 (±1.16e-05)**		1.788e-03 (±1.78e-03)*	
c_9	-2.007e-05 (±1.35e-05)**		4.260e-05 (±5.77e-05)		-1.864e-06 (±6.12e-06)		-1.864e-06 (±6.12e-06)		-2.007e-05 (±1.35e-05)**		-2.030e-04 (±4.58e-03)	
c_0, z_c	1.682e+00 (±1.81e+00)+	1.11 9.94 (0.83)	3.755e-01 (±1.28e-01)**	2.13 15.22 (0.84)	1.682e+00 (±1.81e+00)+	1.11 9.94 (0.83)	3.750e-01 (±1.48e-00)	2.11 15.22 (0.84)	6.101e+00 (±2.70e+00)**	5.57 54.65 (3.02)	R32 [946, 3083] (15)	
c_1, z_c	6.653e-02 (±1.03e-01)		2.646e-01 (±2.35e-01)**		6.653e-02 (±1.03e-01)		1.682e+00 (±1.81e+00)+		6.653e-02 (±1.03e-01)		2.663e-01 (±3.17e-01)**	2.041e+00 (±3.08e-01)**
c_2, k_0	-5.384e-02 (±1.34e-01)		-2.654e-02 (±1.07e-01)		-5.384e-02 (±1.34e-01)		-5.384e-02 (±1.34e-01)		-5.384e-02 (±1.34e-01)		-2.699e-02 (±1.31e-01)	-1.118e+01 (±3.08e-01)**
c_3, k_1	-4.311e-03 (±4.89e-03)+		3.930e-02 (±1.14e-02)**		-4.311e-03 (±4.90e-03)		2.181e-03 (±2.43e-03)*		-4.311e-03 (±4.89e-03)+		3.930e-02 (±1.14e-02)**	3.532e+01 (±2.05e-01)**
c_4, k_2	2.181e-03 (±2.43e-03)*		-8.266e-02 (±2.94e-02)**		2.181e-03 (±2.43e-03)*		2.350e-03 (±1.19e-03)*		2.181e-03 (±2.43e-03)*		-8.255e-02 (±3.56e-02)**	-2.539e+00 (±1.39e-00)**
c_5, k_3	2.350e-03 (±1.19e-03)*		-3.992e-03 (±2.71e-03)*		2.350e-03 (±1.19e-03)*		7.572e-05 (±5.66e-05)*		2.350e-03 (±1.19e-03)*		-3.940e-03 (±6.00e-03)**	1.207e-01 (±2.96e-01)**
c_6	7.572e-05 (±5.66e-05)*		2.858e-04 (±2.51e-04)*		7.572e-05 (±5.66e-05)*		-8.098e-05 (±5.18e-05)**		7.572e-05 (±5.66e-05)*		2.957e-04 (±1.02e-03)	
c_7	-8.098e-05 (±5.18e-05)**		-2.451e-03 (±9.79e-04)**		-8.098e-05 (±5.18e-05)**		2.706e-05 (±2.59e-05)**		-8.098e-05 (±5.18e-05)**		-2.469e-03 (±2.19e-03)*	
c_9	2.706e-05 (±2.59e-05)**		4.892e-03 (±1.84e-03)**		2.706e-05 (±2.59e-05)**		-2.169e-05 (±2.47e-05)+		2.706e-05 (±2.59e-05)**		4.908e-03 (±2.66e-03)**	
c_9	-2.169e-05 (±2.47e-05)+		-2.169e-05 (±2.47e-05)+		-2.169e-05 (±2.47e-05)+	-1.643e-06 (±1.63e-04)						

^a $p < 0.1$, ^b $p < 0.05$, ^c $p < 0.01$, ^d $p < 0.001$; Confidence interval of 95% for regression coefficients;
^b Temperatures (°C);
^c Pressures (bar);
^d The values in brackets are the CV_{BASE} (%).

Table K.14: Mass flow rate models (AHRI 59)

\dot{m}_{ref} (kg/h)		MRE (%) RMSE (kg/h)	\dot{m}_{ref} (kg/h)		MRE (%) RMSE (kg/h)	\dot{m}_{ref} (kg/h)		MRE (%) RMSE (kg/h)	\dot{m}_{ref} (kg/h)		MRE (%) RMSE (kg/h)	Fluid \dot{m} Range [kg/h] (N° tests)
2 nd order polynomial (T-SW)			2 nd order polynomial (P-SW)			2 nd order polynomial (T)			2 nd order polynomial (P)			
AHRI 59 (SH = 11K)												
C0	1.777e+02 (±1.15e+01)**	5.41 1.10 (0.91)	-2.200e+01 (±1.20e+01)**	6.04 1.18 (0.98)	1.777e+02 (±1.15e+01)**	5.41 1.10 (0.91)	-2.041e+01 (±1.39e+01)**	5.66 1.15 (0.96)	R410A			
C1	7.194e+00 (±4.54e-01)**		2.770e+01 (±1.15e+00)**		7.194e+00 (±4.54e-01)**		2.710e+01 (±2.51e+00)**		[31, 196]			
C2	-9.504e-01 (±5.47e-01)**		-1.885e+00 (±7.50e-01)**		-9.504e-01 (±5.47e-01)**		-1.867e+00 (±7.90e-01)**		(15)			
C3	-3.083e-02 (±9.40e-03)**		-1.798e-01 (±4.20e-02)**		-3.083e-02 (±9.40e-03)**		-1.924e-01 (±6.39e-02)**					
C4	6.819e-02 (±1.09e-02)**		1.380e-02 (±1.29e-02)*		6.819e-02 (±1.09e-02)**		6.013e-02 (±2.21e-01)					
C5	-8.085e-03 (±6.04e-03)*		1.897e-02 (±2.22e-02)+		-8.085e-03 (±6.04e-03)*		1.528e-02 (±1.46e-02)*					
C0	1.112e+02 (±9.50e+00)**	4.32 0.91 (1.22)	-1.340e+01 (±1.45e+01)+	9.08 1.29 (1.74)	1.112e+02 (±9.50e+00)**	4.32 0.91 (1.22)	-1.340e+01 (±1.45e+01)+	9.08 1.29 (1.74)	L41-1			
C1	5.180e+00 (±3.77e-01)**		1.992e+01 (±3.30e+00)**		5.180e+00 (±3.77e-01)**		1.992e+01 (±3.30e+00)**		[17, 126]			
C2	-7.081e-01 (±4.54e-01)**		-1.265e+00 (±1.00e+00)*		-7.081e-01 (±4.54e-01)**		-1.265e+00 (±1.00e+00)*		(15)			
C3	-2.792e-02 (±7.80e-03)**		-2.369e-01 (±1.02e-01)**		-2.792e-02 (±7.80e-03)**		-2.369e-01 (±1.02e-01)**					
C4	5.887e-02 (±9.04e-03)**		3.145e-01 (±3.70e-01)+		5.887e-02 (±9.04e-03)**		3.145e-01 (±3.70e-01)+					
C5	-3.810e-03 (±5.01e-03)		1.897e-02 (±2.22e-02)+		-3.810e-03 (±5.01e-03)		1.897e-02 (±2.22e-02)+					
C0	1.329e+02 (±4.99e+00)**	2.04 0.48 (0.52)	-1.817e+01 (±1.01e+01)**	4.72 0.85 (0.92)	1.329e+02 (±4.99e+00)**	2.04 0.48 (0.52)	-1.817e+01 (±1.01e+01)**	4.72 0.85 (0.92)	DR5A			
C1	5.708e+00 (±1.98e-01)**		2.189e+01 (±2.01e+00)**		5.708e+00 (±1.98e-01)**		2.189e+01 (±2.01e+00)**		[23, 151]			
C2	-6.890e-01 (±2.38e-01)**		-1.926e+00 (±6.22e-01)**		-6.890e-01 (±2.38e-01)**		-1.926e+00 (±6.22e-01)**		(15)			
C3	-2.747e-02 (±4.10e-03)**		-1.962e-01 (±5.51e-02)**		-2.747e-02 (±4.10e-03)**		-1.962e-01 (±5.51e-02)**					
C4	5.757e-02 (±4.75e-03)**		1.443e-01 (±1.93e-01)		5.757e-02 (±4.75e-03)**		1.443e-01 (±1.93e-01)					
C5	-5.910e-03 (±2.63e-03)**		1.406e-02 (±1.24e-02)*		-5.910e-03 (±2.63e-03)**		1.406e-02 (±1.24e-02)*					
C0	1.316e+02 (±5.93e+00)**	2.52 0.57 (0.64)	-1.580e+01 (±1.16e+01)**	4.93 0.98 (1.10)	1.316e+02 (±5.93e+00)**	2.52 0.57 (0.64)	-1.580e+01 (±1.16e+01)**	4.93 0.98 (1.10)	ARM71a			
C1	5.652e+00 (±2.35e-01)**		2.190e+01 (±2.36e+00)**		5.652e+00 (±2.35e-01)**		2.190e+01 (±2.36e+00)**		[23, 147]			
C2	-7.848e-01 (±2.83e-01)**		-1.428e+00 (±7.30e-01)**		-7.848e-01 (±2.83e-01)**		-1.428e+00 (±7.30e-01)**		(15)			
C3	-2.836e-02 (±4.87e-03)**		-2.097e-01 (±6.65e-02)**		-2.836e-02 (±4.87e-03)**		-2.097e-01 (±6.65e-02)**					
C4	5.795e-02 (±5.64e-03)**		1.636e-01 (±2.35e-01)		5.795e-02 (±5.64e-03)**		1.636e-01 (±2.35e-01)					
C5	-4.531e-03 (±3.13e-03)**		1.825e-02 (±1.49e-02)*		-4.531e-03 (±3.13e-03)**		1.825e-02 (±1.49e-02)*					
C0	1.415e+02 (±3.85e+00)**	6.55 1.51 (1.80)	-2.416e+01 (±1.41e+01)**	8.78 1.52 (1.81)	1.375e+02 (±1.47e+01)**	7.19 1.48 (1.77)	-1.933e+01 (±1.81e+01)*	7.37 1.46 (1.74)	D2Y60			
C1	5.983e+00 (±4.51e-01)**		2.993e+01 (±1.88e+00)**		5.917e+00 (±5.21e-01)**		2.817e+01 (±4.44e+00)**		[25, 147]			
C2	-1.258e+00 (±8.43e-02)**		-1.920e+00 (±1.14e+00)**		-1.056e+00 (±7.11e-01)**		-1.974e+00 (±1.16e+00)**		(17)			
C3	-3.242e-02 (±9.56e-03)**		-3.040e-01 (±9.00e-02)**		-3.103e-02 (±1.10e-02)**		-3.391e-01 (±1.21e-01)**					
C4	5.958e-02 (±1.32e-02)**		2.951e-02 (±2.53e-02)*		5.771e-02 (±1.52e-02)**		2.148e-01 (±4.91e-01)					
C5					-2.234e-03 (±7.79e-03)		3.524e-02 (±2.88e-02)*					
C0	1.179e+02 (±2.13e+00)**	15.45 1.16 (1.41)	-1.346e+01 (±9.14e+00)**	13.19 1.19 (1.45)	1.123e+02 (±2.02e+01)**	10.26 1.08 (1.32)	-1.582e+01 (±1.32e+01)*	13.09 1.16 (1.42)	R32			
C1	4.419e+00 (±1.11e-01)**		2.177e+01 (±2.26e+00)**		4.090e+00 (±7.20e-01)**		2.144e+01 (±2.72e+00)**		[18, 144]			
C2			-2.101e+00 (±1.51e-01)**		2.779e-01 (±9.74e-01)		-1.825e+00 (±9.03e-01)**		(15)			
C3					7.716e-03 (±1.67e-02)		2.191e-02 (±1.25e-01)					
C4	3.515e-02 (±7.61e-03)**		-2.891e-01 (±1.45e-01)**		3.165e-02 (±1.08e-02)**		-3.034e-01 (±2.25e-01)*					
C5	-1.574e-02 (±1.07e-03)**				-1.904e-02 (±1.13e-02)**		-8.210e-03 (±2.92e-02)*					

^a $p < 0.1$, * $p < 0.05$, ** $p < 0.01$, *** $p < 0.001$; Confidence interval of 95% for regression coefficients;

^b Temperatures (°C);

^c Pressures (bar);

^d The values in brackets are the CV_{RMSE} (%);

K.1.8 Compressor FH2511Z (AHRI 64a, 67a, 69a)

Table K.15: Energy consumption models (AHRI 64a, 67a, 69a)

	\dot{W}_c (kW) AHRI (T-SW)	MRE (%) RMSE ^b (W)	\dot{W}_c (kW) AHRI (P-SW)	MRE (%) RMSE ^b (W)	\dot{W}_c (kW) AHRI (T)	MRE (%) RMSE ^b (W)	\dot{W}_c (kW) AHRI (P)	MRE (%) RMSE ^b (W)	\dot{W}_{exp} (kJ/kg)	MRE (%) RMSE ^b (W)	Fluid \dot{W} Range [W] (N° tests)
AHRI 64a											
c_0, z_c	2.788e+00 (+1.56e-01)**		1.106e+00 (+3.87e-01)**		2.856e+00 (+1.26e+00)**		1.259e+00 (+9.70e-01)*		-1.577e+00 (+2.06e+00)		
c_1, z_e	5.041e-02 (+6.57e-03)**		3.856e-01 (+1.43e-01)**		1.887e-02 (+5.28e-02)		4.789e-01 (+4.07e-01)*		3.503e-01 (+1.30e-01)**		
c_2, k_0	3.058e-02 (+4.36e-03)**		-5.485e-02 (+3.76e-02)**		1.227e-02 (+7.95e-02)		-8.841e-02 (+1.37e-01)		3.811e+01 (+4.80e+00)**		
c_3, k_1	7.906e-04 (+8.06e-05)**		3.566e-02 (+1.28e-02)**		1.638e-03 (+1.17e-03)**		3.992e-02 (+2.25e-02)**		6.267e+00 (+4.82e-01)**		
c_4, k_2	4.260e-04 (+9.80e-05)**		-4.640e-02 (+9.47e-03)**		-2.647e-04 (+1.61e-03)		-1.021e-01 (+1.83e-01)				
c_5, k_3		2.03	3.741e-04 (+8.84e-04)		6.043e-04 (+1.17e-03)		1.737e-03 (+9.86e-03)				
c_6		16.54 (0.75)	-5.003e-04 (+2.98e-04)*		-5.167e-06 (+8.95e-06)		-4.396e-04 (+3.89e-04)				
c_7				1.59	9.509e-06 (+1.41e-05)	171	-1.006e-03 (+3.28e-03)	198			
c_8				15.86 (0.70)	-4.520e-06 (+1.67e-05)	15.01 (0.68)	8.886e-03 (+2.66e-02)	15.24 (0.69)			
c_9	-1.896e-06 (+5.71e-07)**				-7.142e-06 (+1.22e-05)		-2.466e-05 (+1.11e-04)				2.90
c_0, z_c	2.156e+00 (+3.51e-01)**		9.377e-01 (+7.06e-01)*		1.388e+00 (+2.85e+00)		4.116e-01 (+1.68e+00)		-1.078e+01 (+8.83e+00)*		
c_1, z_e	2.158e-02 (+6.90e-03)**		5.723e-01 (+2.67e-01)**		-3.598e-02 (+1.32e-01)		4.469e-01 (+9.30e-01)		-3.141e-01 (+5.60e-01)		
c_2, k_0	4.436e-02 (+1.40e-02)**		-5.264e-02 (+7.63e-02)		7.430e-02 (+1.76e-01)		4.393e-02 (+2.86e-01)		-8.877e+01 (+1.28e+02)		
c_3, k_1	9.269e-04 (+1.40e-04)**		3.773e-02 (+2.75e-02)**		2.154e-03 (+2.66e-03)+		3.642e-02 (+5.92e-02)		4.544e+01 (+3.39e+01)**		
c_4, k_2		3.76	-9.159e-02 (+2.42e-02)**		-1.613e-03 (+4.53e-03)		-2.923e-02 (+4.94e-01)		-3.745e+00 (+3.15e+00)*		
c_5, k_3	-2.409e-04 (+1.41e-04)**		2.947e-04 (+1.81e-03)		-6.804e-04 (+3.79e-03)		-4.516e-03 (+1.44e-02)		1.313e-01 (+9.66e-02)*		
c_6		26.59 (0.39)	-5.019e-04 (+6.64e-04)		-7.130e-06 (+2.00e-05)		-6.189e-04 (+8.01e-04)				
c_7				3.42	1.521e-05 (+3.65e-05)	347	1.107e-03 (+8.40e-03)	3.36			
c_8				25.64 (0.15)	-1.501e-05 (+8.81e-05)	25.33 (0.14)	-1.095e-02 (+7.80e-02)	25.04 (0.13)			
c_9					2.161e-06 (+2.69e-05)		8.238e-05 (+2.40e-04)				3.89
c_0, z_c	1.713e+00 (+3.49e-01)**		1.732e-01 (+2.68e-01)		1.275e+00 (+1.57e+00)		2.209e-01 (+9.66e-01)		-1.031e+01 (+4.28e+00)**		
c_1, z_e	-1.721e-02 (+2.73e-02)		1.275e+00 (+3.17e-01)**		-5.753e-02 (+8.34e-02)		1.173e+00 (+4.15e-01)**		-5.533e-02 (+2.06e-01)		
c_2, k_0	3.539e-02 (+7.94e-03)**		-1.178e-02 (+1.57e-02)		4.584e-02 (+8.10e-02)		-6.500e-03 (+1.37e-01)		-1.366e+02 (+1.06e+02)*		
c_3, k_1	1.489e-03 (+3.85e-04)**		2.191e-02 (+2.83e-03)**		1.996e-03 (+1.97e-03)*		3.198e-02 (+2.63e-02)*		5.033e+01 (+2.27e+01)**		
c_4, k_2	-7.020e-04 (+5.66e-04)**		-3.363e-01 (+1.48e-01)**		-1.999e-03 (+2.03e-03)		-3.300e-01 (+1.47e-01)**		-3.478e+00 (+1.68e+00)**		
c_5, k_3		2.47	-1.033e-03 (+1.93e-04)**		-1.072e-04 (+1.93e-03)		-1.983e-03 (+6.91e-03)		9.774e-02 (+4.08e-02)**		
c_6		18.37 (0.64)	-9.640e-07 (+1.43e-05)		-9.640e-07 (+1.43e-05)		-4.201e-04 (+8.03e-04)				
c_7	1.307e-05 (+1.26e-05)*			2.94	2.235e-02 (+2.07e-05)*	2.21	1.296e-03 (+5.73e-03)	2.41			
c_8			2.965e-02 (+1.96e-02)**		-1.241e-05 (+1.78e-05)		2.521e-02 (+2.71e-02)+				
c_9	-1.506e-06 (+6.30e-07)**			18.19 (0.65)	-9.178e-07 (+1.10e-05)	17.65 (0.60)	3.339e-05 (+1.22e-04)	17.74 (0.63)			4.83
AHRI 67a											
c_0, z_c	1.741e+00 (+2.60e-01)**		7.605e-01 (+2.92e-01)**		1.605e+00 (+1.12e+00)**		5.052e-01 (+7.56e-01)		-5.111e+00 (+2.33e+00)**		
c_1, z_e	-3.149e-02 (+3.48e-02)+		7.008e-01 (+1.28e-01)**		-3.596e-02 (+4.92e-02)		6.204e-01 (+3.66e-01)**		1.907e-01 (+1.09e-01)*		
c_2, k_0	4.266e-02 (+7.12e-03)**		-4.377e-02 (+3.30e-02)*		5.025e-02 (+7.07e-02)		7.951e-03 (+1.21e-01)		-1.827e+01 (+2.95e+01)		
c_3, k_1	1.387e-03 (+3.57e-04)**		3.501e-02 (+1.33e-03)*		1.532e-03 (+1.13e-03)*		3.456e-02 (+2.24e-02)**		2.534e+01 (+6.73e+00)**		
c_4, k_2	-1.969e-03 (+1.28e-03)**		-1.144e-01 (+1.09e-02)**		-2.038e-03 (+1.46e-03)**		-7.317e-02 (+1.96e-01)		-1.465e+00 (+5.62e-01)**		
c_5, k_3	-2.030e-04 (+7.51e-05)**		-2.353e-05 (+8.72e-04)		-3.426e-04 (+1.52e-03)		-2.808e-03 (+6.66e-03)		4.528e-02 (+1.48e-02)**		
c_6		2.02	-4.018e-04 (+3.47e-04)*		-1.250e-06 (+8.56e-06)	1.93	-4.589e-04 (+4.03e-04)*	2.00			
c_7	1.248e-05 (+1.07e-05)*			14.70 (0.73)	1.332e-05 (+1.31e-05)*	14.37 (0.71)	5.012e-04 (+4.20e-03)	14.32 (0.71)			
c_8	-2.057e-05 (+1.37e-05)**				-2.106e-05 (+1.50e-05)**		-7.162e-03 (+3.44e-02)				
c_9					8.365e-07 (+1.08e-05)		5.086e-05 (+1.17e-04)				3.11
AHRI 69a											
c_0, z_c	1.741e+00 (+2.60e-01)**		7.605e-01 (+2.92e-01)**		1.605e+00 (+1.12e+00)**		5.052e-01 (+7.56e-01)		-5.111e+00 (+2.33e+00)**		
c_1, z_e	-3.149e-02 (+3.48e-02)+		7.008e-01 (+1.28e-01)**		-3.596e-02 (+4.92e-02)		6.204e-01 (+3.66e-01)**		1.907e-01 (+1.09e-01)*		
c_2, k_0	4.266e-02 (+7.12e-03)**		-4.377e-02 (+3.30e-02)*		5.025e-02 (+7.07e-02)		7.951e-03 (+1.21e-01)		-1.827e+01 (+2.95e+01)		
c_3, k_1	1.387e-03 (+3.57e-04)**		3.501e-02 (+1.33e-03)*		1.532e-03 (+1.13e-03)*		3.456e-02 (+2.24e-02)**		2.534e+01 (+6.73e+00)**		
c_4, k_2	-1.969e-03 (+1.28e-03)**		-1.144e-01 (+1.09e-02)**		-2.038e-03 (+1.46e-03)**		-7.317e-02 (+1.96e-01)		-1.465e+00 (+5.62e-01)**		
c_5, k_3	-2.030e-04 (+7.51e-05)**		-2.353e-05 (+8.72e-04)		-3.426e-04 (+1.52e-03)		-2.808e-03 (+6.66e-03)		4.528e-02 (+1.48e-02)**		
c_6		2.02	-4.018e-04 (+3.47e-04)*		-1.250e-06 (+8.56e-06)	1.93	-4.589e-04 (+4.03e-04)*	2.00			
c_7	1.248e-05 (+1.07e-05)*			14.70 (0.73)	1.332e-05 (+1.31e-05)*	14.37 (0.71)	5.012e-04 (+4.20e-03)	14.32 (0.71)			
c_8	-2.057e-05 (+1.37e-05)**				-2.106e-05 (+1.50e-05)**		-7.162e-03 (+3.44e-02)				
c_9					8.365e-07 (+1.08e-05)		5.086e-05 (+1.17e-04)				3.11

^a * p < 0.1, ** p < 0.05, *** p < 0.01, **** p < 0.001; Confidence interval of 95% for regression coefficients;

^b Temperatures (°C);

^c Pressures (bar);

^d The values in brackets are the CV_{RMSE} (%).

Table K.16: Mass flow rate models (AHRI 64a, 67a, 69a)

\dot{m}_{ref} (kg/h)		MRE (%) RMSE (kg/h)	\dot{m}_{ref} (kg/h)		MRE (%) RMSE (kg/h)	\dot{m}_{ref} (kg/h)		MRE (%) RMSE (kg/h)	\dot{m}_{ref} (kg/h)		MRE (%) RMSE (kg/h)	Fluid <i>m</i> Range [kg/h] (<i>N</i> ^c tests)
2 nd order polynomial (T-SW)			2 nd order polynomial (P-SW)			2 nd order polynomial (T)			2 nd order polynomial (P)			
AHRI 64a (<i>SH</i> = 10K)												
<i>C</i> ₀	2.775e+02 (+1.23e+01)**	1.67 0.51 (0.39)	1.642e+00 (+6.92e+00)	1.18 0.34 (0.39)	2.775e+02 (+1.23e+01)**	1.67 0.51 (0.39)	1.642e+00 (+6.92e+00)	1.18 0.34 (0.39)	2.775e+02 (+1.23e+01)**	1.67 0.51 (0.39)	1.642e+00 (+6.92e+00)	R404A [39, 169] (14)
<i>C</i> ₁	8.912e+00 (+4.21e-01)**		4.446e+01 (+2.48e+00)**		8.912e+00 (+4.21e-01)**		4.446e+01 (+2.48e+00)**					
<i>C</i> ₂	-7.434e-01 (+4.62e-01)**		-1.666e+00 (+5.66e-01)**		-7.434e-01 (+4.62e-01)**		-1.666e+00 (+5.66e-01)**					
<i>C</i> ₃	-1.420e-02 (+4.93e-03)**		-2.455e-01 (+5.75e-02)**		-1.420e-02 (+4.93e-03)**		-2.455e-01 (+5.75e-02)**					
<i>C</i> ₄	7.859e-02 (+6.85e-03)**		8.603e-01 (+4.09e-01)**		7.859e-02 (+6.85e-03)**		8.603e-01 (+4.09e-01)**					
<i>C</i> ₅	-6.390e-03 (+4.67e-03)*		7.271e-03 (+1.30e-02)		-6.390e-03 (+4.67e-03)*		7.271e-03 (+1.30e-02)					
AHRI 67a (<i>SH</i> = 10K)												
<i>C</i> ₀	2.050e+02 (+2.01e+01)**	1.63 0.40 (0.63)	-6.944e+00 (+5.23e+00)*	2.02 0.44 (0.69)	2.050e+02 (+2.01e+01)**	1.63 0.40 (0.63)	-9.423e+00 (+9.32e+00)*	1.83 0.40 (0.63)	2.050e+02 (+2.01e+01)**	1.63 0.40 (0.63)	-8.879e-03 (+2.28e-02)	DR7 [31, 122] (11)
<i>C</i> ₁	6.928e+00 (+7.63e-01)**		4.261e+01 (+2.07e+00)**		6.928e+00 (+7.63e-01)**		4.219e+01 (+5.49e+00)**					
<i>C</i> ₂	-1.444e-01 (+6.51e-01)		-1.427e+00 (+2.64e-01)**		-1.444e-01 (+6.51e-01)		-1.123e+00 (+8.88e-01)*					
<i>C</i> ₃	-9.502e-03 (+9.13e-03)*		-1.934e-01 (+9.73e-02)**		-9.502e-03 (+9.13e-03)*		-1.660e-01 (+1.49e-01)*					
<i>C</i> ₄	5.950e-02 (+1.07e-02)**				5.950e-02 (+1.07e-02)**		-3.180e-02 (+1.06e+00)					
<i>C</i> ₅	-1.119e-02 (+5.74e-03)**				-1.119e-02 (+5.74e-03)**							
AHRI 69a (<i>SH</i> = 10K)												
<i>C</i> ₀	1.718e+02 (+8.08e+00)**	5.96 0.58 (1.12)	-1.123e+01 (+3.34e+00)**	6.38 0.58 (1.11)	1.718e+02 (+8.08e+00)**	5.96 0.58 (1.12)	-1.216e+01 (+5.31e+00)**	6.24 0.57 (1.10)	1.718e+02 (+8.08e+00)**	5.96 0.58 (1.12)	-2.942e-03 (+1.30e-02)	ARM25 [12, 101] (37)
<i>C</i> ₁	5.528e+00 (+2.99e-01)**		4.407e+01 (+2.02e+00)**		5.528e+00 (+2.99e-01)**		4.409e+01 (+2.06e+00)**					
<i>C</i> ₂	-1.479e-01 (+2.72e-01)		-1.412e+00 (+1.97e-01)**		-1.479e-01 (+2.72e-01)		-1.312e+00 (+4.85e-01)**					
<i>C</i> ₃	-4.649e-03 (+3.61e-03)*		-1.126e-01 (+8.32e-02)**		-4.649e-03 (+3.61e-03)*		-1.075e-01 (+8.73e-02)*					
<i>C</i> ₄	4.339e-02 (+3.79e-03)**		-9.648e-01 (+4.72e-01)**		4.339e-02 (+3.79e-03)**		-9.900e-01 (+4.92e-01)**					
<i>C</i> ₅	-7.799e-03 (+2.66e-03)**				-7.799e-03 (+2.66e-03)**							
AHRI 69a (<i>SH</i> = 10K)												
<i>C</i> ₀	1.928e+02 (+1.08e+01)**	5.34 0.54 (1.12)	-5.984e+00 (+7.65e+00)	7.57 0.60 (1.23)	1.928e+02 (+1.08e+01)**	5.34 0.54 (1.12)	-6.616e+00 (+8.41e+00)	9.03 0.59 (1.21)	1.928e+02 (+1.08e+01)**	5.34 0.54 (1.12)	1.664e-02 (+2.23e-02)	ARM20b [11, 113] (15)
<i>C</i> ₁	6.157e+00 (+3.44e-01)**		4.200e+01 (+1.78e+00)**		6.157e+00 (+3.44e-01)**		4.281e+01 (+3.67e+00)**					
<i>C</i> ₂	-7.837e-01 (+4.25e-01)**		-1.680e+00 (+7.96e-01)**		-7.837e-01 (+4.25e-01)**		-1.690e+00 (+8.37e-01)**					
<i>C</i> ₃	-1.281e-02 (+4.22e-03)**		-2.957e-01 (+9.74e-02)**		-1.281e-02 (+4.22e-03)**		-2.878e-01 (+1.07e-01)**					
<i>C</i> ₄	4.972e-02 (+5.04e-03)**				4.972e-02 (+5.04e-03)**		-1.944e-01 (+7.63e-01)					
<i>C</i> ₅	-3.343e-03 (+4.37e-03)		1.706e-02 (+2.11e-02)		-3.343e-03 (+4.37e-03)							

^a + *p* < 0.1, * *p* < 0.05, ** *p* < 0.01, *** *p* < 0.001; Confidence interval of 95% for regression coefficients;

^b Temperatures (°C);

^c Pressures (bar);

^d The values in brackets are the CV_{RMSE} (%);

K.1.9 Compressor FH4540Z (AHRI 64b, 67b, 69b)

Table K.17: Energy consumption models (AHRI 64b, 67b, 69b)

	\dot{W}_c (kW) AHRI (T-SW)	MRE (%) RMSE ^d (W)	\dot{W}_c (kW) AHRI (P-SW)	MRE (%) RMSE ^d (W)	\dot{W}_c (kW) AHRI (T)	MRE (%) RMSE ^d (W)	\dot{W}_c (kW) AHRI (P)	MRE (%) RMSE ^d (W)	\dot{W}_{exp} (kJ/kg)	MRE (%) RMSE ^d (W)	Fluid \dot{W}_c Range [W] (N° tests)
AHRI 64b											
c_0, z_c	2.541e+00 (±3.70e-01)**	34.88 (0.0)	8.491e-01 (±2.81e-01)**	35.71 (0.0)	3.043e+00 (±2.64e+00)*	2.16	3.771e-01 (±1.94e+00)	34.47 (0.0)	-4.087e+00 (±1.63e+00)**	2.24	R404A [2097, 4918] (17/17)
c_1, z_c	4.426e-02 (±5.09e-03)**		3.687e-01 (±4.68e-02)**		5.628e-02 (±2.72e-02)		4.673e-01 (±2.63e-01)**		8.777e-01 (±1.54e-01)**		
c_2, k_0	3.028e-02 (±1.61e-02)**		2.633e-02 (±2.87e-02)+		-1.539e-03 (±1.78e-01)		7.325e-02 (±2.93e-01)		1.934e+01 (±1.72e+00)**		
c_3, k_1			8.045e-03 (±1.92e-03)**		-4.851e-04 (±3.11e-03)		1.148e-02 (±1.98e-02)		6.658e+00 (±2.82e-01)**		
c_4, k_2	1.561e-04 (±1.45e-04)*		-1.643e-02 (±4.32e-03)**		9.085e-05 (±1.47e-05)		-4.071e-02 (±4.47e-02)				
c_5, k_3	-1.905e-04 (±1.70e-04)*		-1.150e-03 (±7.17e-04)*		4.696e-04 (±3.88e-05)		-3.851e-03 (±1.48e-02)				
c_6	8.839e-06 (±2.05e-06)**				1.376e-05 (±3.24e-05)		8.491e-05 (±5.95e-04)				
c_7					1.627e-06 (±3.06e-05)		-5.262e-04 (±1.45e-03)				
c_8					-2.403e-06 (±1.75e-05)		1.868e-03 (±2.77e-03)				
c_9			-4.495e-06 (±2.75e-05)	3.252e-02 (±2.88e-04)							
c_0, z_c	9.850e-01 (±1.05e+00)	1.19	2.960e-02 (±9.37e-01)	1.30	1.445e+00 (±1.53e+00)*	1.53	5.673e-03 (±0.27e-01)	1.28	-8.296e+00 (±1.13e+00)**	1.51	DR7 [1886, 4570] (14/13)
c_1, z_c	6.336e-03 (±5.29e-02)		5.618e-01 (±1.16e-01)**		1.995e-02 (±3.26e-02)		5.494e-01 (±1.43e-01)**		5.975e-01 (±0.01e-02)**		
c_2, k_0	1.198e-01 (±2.37e-02)**		1.004e-01 (±1.45e-01)		8.851e-02 (±1.04e-01)+		1.076e-01 (±1.56e-01)		1.409e+01 (±1.88e+00)**		
c_3, k_1	1.172e-03 (±1.09e-04)**		2.714e-02 (±1.00e-02)**		5.518e-04 (±1.42e-05)		2.826e-02 (±1.25e-02)**		9.852e+00 (±2.90e-01)**		
c_4, k_2	-2.147e-04 (±8.75e-05)**		-8.568e-02 (±2.52e-02)**		-3.701e-05 (±8.75e-04)		-8.533e-02 (±2.60e-02)**				
c_5, k_3	-2.222e-03 (±1.68e-03)*		-7.924e-03 (±7.80e-03)*		-1.535e-03 (±2.33e-03)		-8.445e-03 (±8.67e-03)+				
c_6					6.500e-06 (±1.48e-05)		-5.272e-05 (±3.31e-04)				
c_7					-1.298e-03 (±8.44e-04)**		-1.192e-03 (±1.09e-03)*				
c_8					4.826e-03 (±2.16e-03)**		4.670e-03 (±2.43e-03)**				
c_9	1.518e-05 (±1.24e-05)*		1.107e-04 (±1.25e-04)+	1.234e-04 (±1.51e-04)							
AHRI 67b											
c_0, z_c	3.222e+00 (±1.50e+00)**	0.50	7.145e-01 (±1.07e+00)	0.58	3.222e+00 (±1.50e+00)**	0.69	7.145e-01 (±1.07e+00)	0.83	-7.576e+00 (±1.39e+00)**	0.83	ARM25 [1736, 4150] (16)
c_1, z_c	6.752e-02 (±3.18e-02)**		5.090e-01 (±1.53e-01)**		6.752e-02 (±3.18e-02)**		5.090e-01 (±1.53e-01)**		6.141e-01 (±9.44e-02)**		
c_2, k_0	-5.600e-02 (±1.05e-01)		-1.523e-02 (±1.88e-01)		-5.600e-02 (±1.05e-01)		-1.523e-02 (±1.88e-01)		1.849e+01 (±2.20e+00)**		
c_3, k_1	-1.355e-03 (±1.40e-03)+		6.872e-03 (±1.53e-02)		-1.355e-03 (±1.40e-03)+		6.872e-03 (±1.53e-02)		8.681e+00 (±3.21e-01)**		
c_4, k_2	8.369e-04 (±8.30e-04)+		4.965e-02 (±3.35e-02)*		8.369e-04 (±8.30e-04)+		4.966e-02 (±3.35e-02)*				
c_5, k_3	1.754e-03 (±2.38e-03)		2.104e-03 (±1.13e-02)		1.754e-03 (±2.38e-03)		2.104e-03 (±1.13e-02)				
c_6	2.168e-05 (±1.48e-05)*		4.392e-04 (±4.50e-04)+		2.168e-05 (±1.48e-05)*		4.392e-04 (±4.50e-04)+				
c_7	-1.349e-05 (±1.76e-05)		-1.473e-03 (±1.57e-03)+		-1.349e-05 (±1.76e-05)		-1.473e-03 (±1.57e-03)+				
c_8	7.981e-06 (±1.15e-05)		3.837e-03 (±3.47e-03)*		7.981e-06 (±1.15e-05)		3.837e-03 (±3.47e-03)*				
c_9	-1.382e-05 (±1.74e-05)	-1.004e-04 (±2.16e-04)	-1.382e-05 (±1.74e-05)	-1.004e-04 (±2.16e-04)							
AHRI 69b											
c_0, z_c	2.483e+00 (±3.58e-01)**	0.82	2.200e-01 (±2.70e-01)+	0.73	2.293e+00 (±3.12e+00)	0.69	2.077e-01 (±1.30e+00)	0.83	-6.436e+00 (±6.28e+00)*	0.83	ARM20b [1714, 4355] (16)
c_1, z_c	3.738e-02 (±6.40e-03)**		6.451e-01 (±1.18e-01)**		2.153e-02 (±1.47e-01)		6.700e-01 (±2.44e-01)**		4.041e-01 (±6.12e-01)		
c_2, k_0	1.572e-02 (±1.44e-02)*		4.983e-02 (±2.41e-02)**		2.503e-02 (±1.91e-01)		4.730e-02 (±2.28e-01)		3.807e+01 (±1.58e+01)**		
c_3, k_1			5.895e-04 (±5.55e-03)		5.895e-04 (±5.55e-03)		-6.368e-03 (±3.18e-02)		3.447e+00 (±6.65e+00)		
c_4, k_2	-8.102e-04 (±5.22e-04)**		-5.037e-02 (±2.56e-02)**		-1.088e-03 (±2.57e-03)		-4.182e-02 (±5.53e-02)		5.390e-01 (±5.14e-01)*		
c_5, k_3	-4.603e-05 (±1.42e-04)		-2.078e-03 (±7.88e-04)**		-1.862e-04 (±3.89e-03)		-1.327e-03 (±1.27e-02)				
c_6	1.090e-05 (±2.11e-06)**		2.775e-04 (±5.41e-05)**		5.500e-06 (±5.18e-05)		5.554e-04 (±5.36e-03)				
c_7	1.714e-05 (±9.51e-06)**				2.220e-05 (±4.74e-05)		-6.058e-04 (±3.38e-03)				
c_8	-1.027e-05 (±9.17e-06)*		1.550e-03 (±1.60e-03)+		-1.168e-05 (±1.70e-05)		1.895e-03 (±3.71e-03)				
c_9			6.174e-07 (±2.63e-05)	-2.990e-05 (±2.51e-04)							

* $p < 0.1$, * $p < 0.05$, ** $p < 0.01$, *** $p < 0.001$; Confidence interval of 95% for regression coefficients;

^b Temperatures (°C);

^c Pressures (bar);

^d The values in brackets are the CV_{RMSE} (%).

Table K.18: Mass flow rate models (AHRI 64b, 67b, 69b)

\dot{m}_{ref} (kg/h)		MRE (%) RMSE (kg/h)	\dot{m}_{ref} (kg/h)		MRE (%) RMSE (kg/h)	\dot{m}_{ref} (kg/h)		MRE (%) RMSE (kg/h)	\dot{m}_{ref} (kg/h)		MRE (%) RMSE (kg/h)	Fluid <i>m</i> Range [kg/h] (<i>N</i> ^c tests)
2 nd order polynomial (T-SW)			2 nd order polynomial (P-SW)			2 nd order polynomial (T)			2 nd order polynomial (P)			
AHRI 64b (<i>SH</i> = 10K)												
<i>C</i> ₀	2.869e+02 (±1.23e+01)***	0.89 0.68 (0.30)	-1.971e+01 (±7.23e+00)***	0.95 0.55 (0.24)	2.869e+02 (±1.23e+01)***	0.89 0.68 (0.30)	-1.971e+01 (±7.23e+00)***	0.95 0.55 (0.24)			R404A [79, 413] (17)	
<i>C</i> ₁	1.048e+01 (±3.62e-01)***		5.751e+01 (±1.09e+00)***		1.048e+01 (±3.62e-01)***		5.751e+01 (±1.09e+00)***					
<i>C</i> ₂	6.433e-02 (±5.41e-01)		-2.490e+00 (±7.08e-01)***		6.433e-02 (±5.41e-01)		-2.490e+00 (±7.08e-01)***					
<i>C</i> ₃	-8.083e-03 (±7.25e-03)*		-5.944e-02 (±5.91e-02)*		-8.083e-03 (±7.25e-03)*		-5.944e-02 (±5.91e-02)*					
<i>C</i> ₄	1.053e-01 (±5.26e-03)***		-3.217e-01 (±1.17e-01)***		1.053e-01 (±5.26e-03)***		-3.217e-01 (±1.17e-01)***					
<i>C</i> ₅	-2.106e-02 (±5.68e-03)***		-2.132e-02 (±1.91e-02)*		-2.106e-02 (±5.68e-03)***		-2.132e-02 (±1.91e-02)*					
AHRI 67b (<i>SH</i> = 10K)												
<i>C</i> ₀	2.351e+02 (±5.58e+00)***	3.23 1.36 (0.88)	-1.129e+01 (±1.23e+01)+	1.48 0.75 (0.48)	2.256e+02 (±2.93e+01)***	2.88 1.32 (0.85)	-1.129e+01 (±1.23e+01)+	1.48 0.75 (0.48)			DR7 [46, 303] (14)	
<i>C</i> ₁	9.301e+00 (±6.88e-01)***		4.316e+01 (±1.80e+00)***		9.142e+00 (±8.64e-01)***		4.316e+01 (±1.80e+00)***					
<i>C</i> ₂	-1.524e+00 (±1.17e-01)***		-2.991e+00 (±1.29e+00)***		-1.097e+00 (±1.30e+00)+		-2.991e+00 (±1.29e+00)***					
<i>C</i> ₃	-2.778e-02 (±1.41e-02)**		-2.580e-01 (±1.01e-01)***		-2.480e-02 (±1.73e-02)*		-2.580e-01 (±1.01e-01)***					
<i>C</i> ₄	1.094e-01 (±1.17e-02)***		4.392e-01 (±2.29e-01)***		1.076e-01 (±1.34e-02)**		4.392e-01 (±2.29e-01)***					
<i>C</i> ₅			3.351e-02 (±3.37e-02)+		-4.493e-03 (±1.36e-02)		3.351e-02 (±3.37e-02)+					
AHRI 69b (<i>SH</i> = 10K)												
<i>C</i> ₀	1.848e+02 (±2.05e+01)***	1.74 1.18 (0.81)	-2.499e+01 (±7.36e+00)***	1.51 1.07 (0.73)	1.848e+02 (±2.05e+01)***	1.74 1.18 (0.81)	-2.913e+01 (±1.41e+01)***	1.82 1.04 (0.71)			ARM25 [45, 274] (16)	
<i>C</i> ₁	8.504e+00 (±5.51e-01)***		4.226e+01 (±2.39e+00)***		8.504e+00 (±5.51e-01)***		4.212e+01 (±2.49e+00)***					
<i>C</i> ₂	-1.032e-02 (±9.30e-01)		-7.253e-01 (±5.81e-01)*		-1.032e-02 (±9.30e-01)		-2.096e-01 (±1.60e+00)					
<i>C</i> ₃	-2.949e-02 (±1.14e-02)**		-3.982e-01 (±1.16e-01)***		-2.949e-02 (±1.14e-02)**		-3.817e-01 (±1.29e-01)***					
<i>C</i> ₄	1.013e-01 (±9.55e-03)**		7.081e-01 (±3.21e-01)***		1.013e-01 (±9.55e-03)**		6.871e-01 (±3.36e-01)**					
<i>C</i> ₅	-1.349e-02 (±1.01e-02)*				-1.349e-02 (±1.01e-02)*		-1.548e-02 (±4.45e-02)					
AHRI 69b (<i>SH</i> = 10K)												
<i>C</i> ₀	2.293e+02 (±7.02e+00)***	2.13 1.21 (0.92)	-2.230e+01 (±1.04e+01)***	6.05 1.43 (1.08)	2.176e+02 (±3.63e+01)***	1.88 1.18 (0.89)	-2.314e+01 (±1.87e+01)*	4.22 1.36 (1.03)			ARM20b [41, 264] (16)	
<i>C</i> ₁	9.167e+00 (±6.09e-01)***		4.609e+01 (±2.76e+00)***		8.892e+00 (±1.04e+00)***		4.528e+01 (±4.07e+00)***					
<i>C</i> ₂	-1.653e+00 (±1.38e-01)***		-1.938e+00 (±5.23e-01)***		-1.166e+00 (±1.48e+00)		-1.670e+00 (±2.26e+00)					
<i>C</i> ₃	-3.883e-02 (±1.12e-02)**		-2.290e-01 (±1.24e-01)**		-3.373e-02 (±1.93e-02)*		-2.745e-01 (±2.72e-01)*					
<i>C</i> ₄	9.788e-02 (±9.00e-03)***				9.547e-02 (±1.18e-02)**		1.730e-01 (±4.78e-01)					
<i>C</i> ₅					-4.851e-03 (±1.47e-02)		-1.521e-03 (±7.48e-02)					

^a + *p* < 0.1, * *p* < 0.05, ** *p* < 0.01, *** *p* < 0.001; Confidence interval of 95% for regression coefficients;
^b Temperatures (°C);
^c Pressures (bar);
^d The values in brackets are the CV_{RMSE} (%).

L

Design of experiments in compressor characterization

CONTENTS

L.1	Introduction	1-1
L.2	Classical experimental designs	1-3
L.3	Computer-aided experimental designs	1-5
L.4	Generating the experimental samples	1-6
L.5	Analysis of results	1-8
	L.5.1 Obtained samples with the experimental designs	1-8
	L.5.2 Results from the adjusted models with the experimental designs	1-11
L.6	Summary of results	1-14
L.7	Summary tables DoE samples	1-16
L.8	Source code to obtain computer-aided designs	1-19

L.1 Introduction

The Design of Experiments (DoE) methodologies is a branch of statistics aimed to prepare and plan the experimental matrices and, along with the Response Surface Methodologies (RSM), they provide researchers with powerful tools when selecting experimental samples for empirical model adjustments. Therefore, the main objective of the DoE is to specify where to take the tests within the experimental domain to define an optimal ratio between the number of points to test and experimental information with statistical inference to make the model adjustment.

These experimental design methodologies can be divided into classical experimental designs and computer-aided designs. The first group defines experimental designs for mainly orthogonal domains, while the second one presents the

advantage of defining designs for irregular domains. In Figure L.1-left, it can be seen an example of a non-orthogonal domain illustrated in Atkinson and Donev's book (see Atkinson et al., 2007, chap. 12, pg. 180). It describes the experimental design proposed to characterize the torque of an internal combustion engine based on the ignition advance of the spark plug. It can be seen that the shown experimental domain is similar to the working area of a scroll compressor (Figure L.1-right). They both are characterized by having areas where it is not possible to work, creating a convex polygon in contrast with other types of processes without limitations and with orthogonal domains. In the case of compressors, they have two areas of no operation, one limited by the high discharge temperatures, where the integrity of the compressor would be compromised, and another area limited by a low-pressure ratio with a considerable loss of efficiency (Maertens and Richardson, 1992).

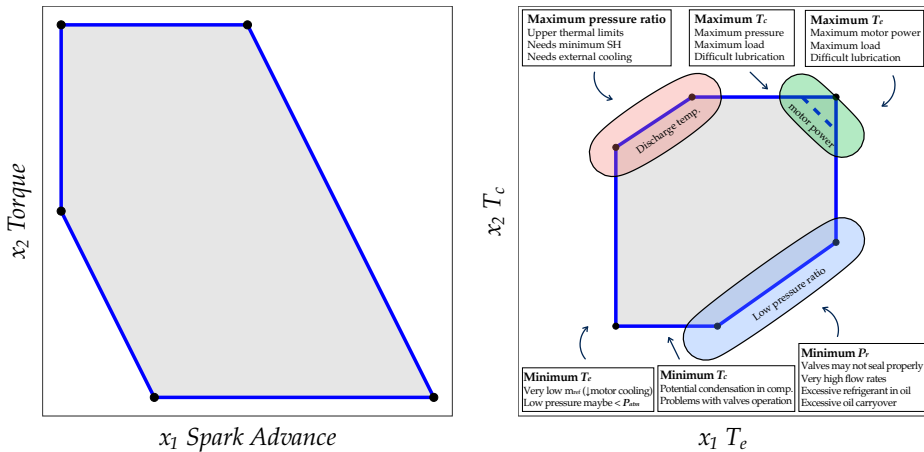


Figure L.1: Non-orthogonal experimental domains. Internal combustion engine (left-hand) and scroll compressor (right-hand)

The following sections show an example of a comparison of different experimental designs. Some of them use designs available in the literature (classical designs), and others are more advanced, using algorithms and computation (computer aided-designs). This information can be considered complementary to the main chapters of the thesis, where only the designs with the best results are shown. This appendix compares the designs in the AHRI reports with the greater number of data (AHRI 11, 21, and 33 \Rightarrow scroll compressors), selecting as the base model for the adjustment with the samples the proposed model for scroll compressors and using temperatures as independent variables (Equation L.1 and

Equation L.2). This is only to simplify the reading of this appendix. The other models were also checked with similar results.

$$\dot{W}_c = a_0 + a_1 T_e + a_2 T_c + a_3 T_e T_c + a_4 T_e^2 + a_5 T_c^2 \quad (\text{L.1})$$

$$\dot{m}_{ref} = b_0 + b_1 T_e + b_2 T_c + b_3 T_e T_c + b_4 T_e^2 + b_5 T_c^2 \quad (\text{L.2})$$

L.2 Classical experimental designs

Nowadays, in the literature exists a huge diversity of methodologies and experimental designs which can be used to obtain a good experimental plan as well as relevant statistical results. The use of one methodology or another will be established according to the experimentation capacity (number of tests), the quantity of independent variables that we shall control during the experiment, and the complexity of the response surface to be characterized.

In the compressors field, we only have two factors of control (T_e and T_c) and two response variables to characterize (\dot{W}_c y \dot{m}_{ref}). Based on this scenario, one of the most extended methodologies is the use of X^k designs. A full factorial design X^k with k factors of control is obtained by selecting a determined number of levels X for each factor. These levels are considered discrete values selected at the continuous range of the control factors. The selection of 2 or more levels will depend on whether the effects of the factors over the response variable are or not linear.

Normally this modest methodology is very useful when completing experimental orthogonal matrices in a great number of scenarios. Said propriety of orthogonality is especially interesting because it grants, in regression models, to estimate the effects of every factor and interaction among factors free from influences with other factors or interactions.

On the other hand, in the 1950s George E.P. Box and K.B. Wilson proposed an alternative to the X^k factorial designs. Starting first from a 2^k design and with the addition of central and axial points, it can be built the Central Composite Design (CCD) (Box and Wilson, 1951). Currently, this design is the most used one when adjusting second-order polynomial models. The addition of central and axial points allows the estimation of quadratic terms and interactions. Furthermore, it allows the use of a great number of levels for the factors, reducing the number of total points if it is compared to a complete factorial design with the same number of levels.

Additionally, with the objective of obtaining even more compact designs, exists a variant of the CCD known as Small Composite Design (SCD) (Hartley, 1959). These designs come originally from a CCD eliminating some points and trying to lose a lesser amount of information, which can be justified in the analysis of processes with elevated experimentation costs, where an agreement between the accuracy of the model and the experimentation costs is sought.

Finally, in the event of having just two factors, other alternatives such as hexagonal designs (HD) exist (see Myers et al., 2009, chap. 7, pg. 331). Having CCD as an octagonal equiradial design, this alternative shows an alternative design, which is also equiradial and could be of greater interest depending on the experimental domain that one tries to cover.

Taking into account the irregular experimental domain of the scroll compressor, we can select the following classical experimental design alternatives for two factors (T_e y T_c): 3^2 , CCD, SCD, and HD. The total number of points goes from 7 to 9 tests for the four methodologies. Said designs were built trying to cover the greatest possible experimental design among the analyzed compressors and selecting available points on the experimental matrices included in the AHRI reports.

Figure L.2 shows an example of how the points were distributed in the envelope for the AHRI 21 compressor considering its reference refrigerant (R404A) and SH=11K as suction conditions. In this figure, the black points include the set of given points in the AHRI report, and the red points are the selected ones to build the different samples. With the SCD methodology, the selected points are the same ones as in the CCD design, eliminating the two highlighted points on the diagonal.

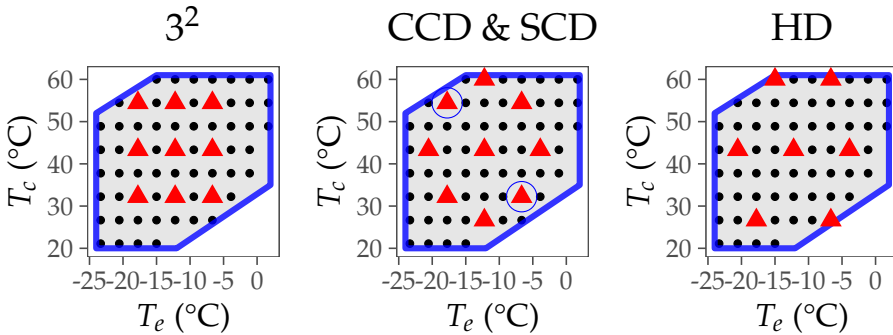


Figure L.2: Classical designs: 3^2 , CCD, SCD and HD (AHRI 21 R404A and SH=11K)

L.3 Computer-aided experimental designs

Nowadays, the development of informatics has allowed us to have a great processing power on problem-solving at our disposal. In the field of experimental designs, the increase in this potential for calculation has allowed researchers to use sophisticated algorithms to plan and generate experimental matrices. These kinds of methodologies are known as computer-aided experimental designs because they generate the samples from algorithms and calculations by computer (see Heckert et al., 2002, chap 5, sec. 5). In contrast with classical factorial designs, these methodologies are used in particular situations. For example, two of the most common situations are:

- The physical or chemical phenomena analyzed include a great number of factors. In this situation, classical designs with completed or fractionated factorials result in a high number of tests.
- Not all combinations of factors are possible. Therefore, we have an irregular experimental domain instead of an orthogonal one.

Focusing on our case of study, experimental planning of compressors, it might be possible that the first situation does not justify using these methodologies. We only have two control factors (T_e and T_c), so the samples for classical methodologies will be compact. As it is mentioned above, the selected designs only include 7 to 9 experimental points.

However, we must keep in mind that the working domain in compressors is irregular and, as can be seen in Figure L.2, classical methodologies do not cover it completely. Inscribing the designs in the central area, there are two remaining excluded areas of the design (high T_e , T_c and low T_e , T_c). This can lead to extrapolation errors if these excluded areas are significant.

For this last reason, this work also includes the use of experimental designs assisted by computer in the comparative analysis. The selected methodologies are 2 of the most used ones in experimental planning, the Optimal Designs (OD) and Cluster Design (CD). Additionally, one more typology has been added; it derives from Cluster Designs, the Polygonal Designs (PD), Aute et al. (2015, section 8.1.2).

The first methodology, optimal experimental designs, was firstly proposed by Kieffer and Wolfowitz in the 1950s (Kieffer and Wolfowitz, 1959; Kiefer, 1959) and later was published as a more relevant work in the Atkinson & Donev's book (Atkinson and Donev, 1992). This type of methodology assumes knowing the mathematical function of the model to apply, able to reproduce the response variable accurately. Having this function and knowing the experimental domain (set

of candidate points), these designs lay out the selection of points depending on an optimality criterion. Hence, the obtained design normally will be optimal for a specific model. Using matrix notation, the adjustment of a linear regression model is given by:

$$Y = \hat{\beta}X \quad \text{and} \quad X = \begin{bmatrix} f_1(x_1) & \cdots & f_m(x_1) \\ \vdots & \ddots & \vdots \\ f_1(x_n) & \cdots & f_m(x_n) \end{bmatrix} \quad (\text{L.3})$$

Being able to calculate the regression coefficients $\hat{\beta}$ as:

$$\hat{\beta} = (X^T X)^{-1} X^T Y \quad (\text{L.4})$$

Within this context, it is common to use the determinant of the matrix of covariance as a measure (scalar) of the adjustment precision. This generalized variance for the estimation of $\hat{\beta}$ is calculated as:

$$VG(\hat{\beta}) = |Var(\hat{\beta})| = \left| (X^T X)^{-1} \right| \sigma^2 \quad (\text{L.5})$$

Based on the previous equations, the optimality criteria will select the experimental points to maximize or reduce a statistical estimator of the matrix of information. In this case, it is selected one of the most used ones, the Optimal-D criterion, which intends to maximize the determinant of the matrix of information $|X^T X|$. Therefore, it minimizes the generalized variance (Equation L.5) for the regression coefficients ($\hat{\beta}$). In other words, it selects the points intending to obtain the minimum error for the prediction of the regression coefficients ($\hat{\beta}$).

On the other hand, the cluster design is based on the automatic grouping of points considering their location in the experimental domain. Therefore, when talking about compressors, it just needs as main input a series of candidate points on evaporation and condensation temperature coordinates. With this information, this methodology is able to analyze the experimental domain and classify in a number of k clusters the complete set of candidate points. Once the clustering is made, the experimental design will be considered as the set of k points located in the center of each cluster. This study has used the algorithm *k-means* to obtain the clustering. In this case, the algorithm calculates the average of T_e and T_c in the k clusters assigning the candidate points to the cluster whose average value of T_e and T_c is closer.


Finally, the polygonal design methodology (Aute et al., 2015, sec 8.1.2) combines the manual selection of points with cluster design. In a first stage, the vertices of the polygon defining the compressor envelope are selected. The rest of the points to be included in the experimental design will be selected using the clustering methodology.

L.4 Generating the experimental samples

As the experimental data disclosed in the AHRI 11, 21, and 33 reports include many tests resulting in a very thin mesh of points over the entire working map, it has been possible to compare all the methodologies mentioned above.

With the classical experimental designs, it has been sought to draw the designs centering them on the compressor working map and trying to cover the largest possible experimental area. No additional tools have been needed as designs were of common use and perfectly documented in the technical literature.

On the other hand, for the use of designs assisted by computer, it was selected a specific open-source software with pre-programmed functions of experimental design. The objective is to facilitate the use of the methodologies described here.

Particularly, it has been used the statistical software  (R Core Team, 2022) together with the package **AlgDesign** (Wheeler, 2019). For the optimal designs methodology, it has been used the function *optFederov()*, which is an implementation of the Fedorov's algorithm (Fedorov, 1972). This algorithm automatically obtains the optimal experimental designs needing:

1. A set of candidate points on coordinates of T_e and T_c .
2. A rescaling of said coordinates from -1 to 1.
3. To know the mathematical functional of the model to apply.
4. To specify the desired number of points for the sample.
5. To select the optimality criterion to apply and run the algorithm.
6. To rescale the coordinates of the design to the original range.

The size samples selected to illustrate the use of these methodologies are 6, 9, and 12 points. The candidate points given to the algorithm are available on the AHRI reports, and the optimality criterion selected is the Optimal-D criterion.

Furthermore, the cluster design has been obtained with the *k-mean* function of the base package **stats**. This methodology needs the following steps to get the designs:

1. To select a set of candidate points on coordinates of T_e and T_c .
2. A rescaling of said coordinates from -1 to 1.
3. To specify the number of clusters. This number will be the same as the number of tests desired for the design.

4. To execute the clustering algorithm.
5. To rescale the coordinates of the design to the original range.

The obtained designs include the centroid of every cluster. As these points are not included in the revised reports, it has been necessary to estimate their value by a smooth interpolation. A non-parametric model, the Thin-Plate-Spline (Nychka et al., 2021), was used for this purpose.

Finally, the polygonal designs have been obtained by manually selecting the vertexes of the compressor envelope (6 points) and applying the steps above described on the cluster designs to define the remainder points. The designs included for the polygonal and cluster designs also include 6, 9, and 12 points.

The final part of this appendix includes the source code of how to obtain experimental designs assisted by computer applying the optimal designs and the cluster designs methodologies described here (Section L.8).

L.5 Analysis of results

To simplify the analysis, only the results using the candidate points as tests in SH=11K to generate the different experimental designs will be shown below. These designs were proposed for every refrigerant included in the AHRI 11, 21, and 33 reports. Similar results were obtained, taking the SH=22K and $T_s=18^\circ\text{C}$ tests as candidate points. As mentioned before, classical designs will include a total of 7 to 9 points. On the other hand, for the designs assisted by computer, three designs per methodology were considered, including a total of 6, 9, and 12 points. The objective is to evaluate the prediction power of the adjusted model with the different samples. Now, a visual analysis is presented of how the different samples are distributed within the experimental domain and a comparison of the prediction errors.

L.5.1 Obtained samples with the experimental designs

Figure L.2 already presented an example of how the experimental samples in classical designs were distributed. The main limitation detected is that they are not able to adapt to irregular experimental domains. Hence, centering the designs on the experimental domain, we will be able to cover a larger or smaller working area depending on the limits of the compressor envelope. Figure L.3 shows an example of how the working range of the compressor AHRI 11 is modified using R410A and R32 as refrigerants. We can observe that having higher discharge tem-

peratures, the refrigerant R32 shows a lower range of work when having high T_c and low T_e values.

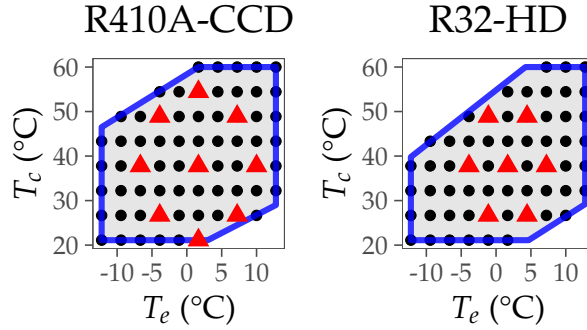


Figure L.3: AHRI 11 R410A-CCD vs R32-HD (SH=11K)

As can be seen in the figure above, depending on the compressor, the refrigerant, and the fixed suction conditions, these methodologies cannot be appropriate in the case of not covering a significant area of the working domain.

Analyzing the cluster designs in the second place, Figure L.4 shows an example of the selected points for a design of 6, 9, and 12 points using the data from the AHRI 11 report and the reference refrigerant (R410A).

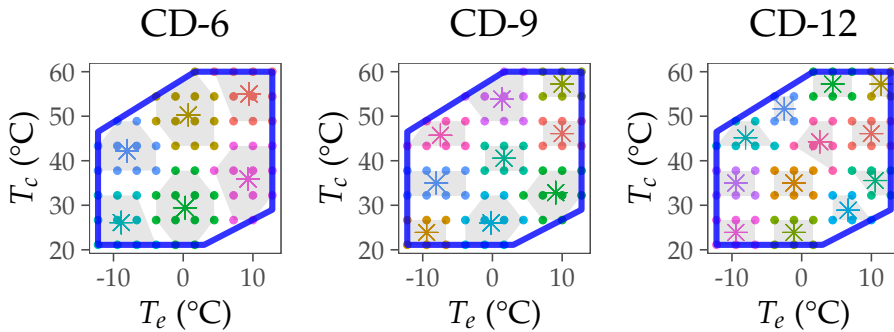


Figure L.4: Clustering 6, 9, and 12 points (AHRI 11 R410A and SH=11K)

In the figure above, it can be seen how the clustering algorithm operates. Having a number n of points to include in the design, the algorithm classifies the candidate points in n clusters. The centroid obtained from every cluster will be the point to include in the experimental design. Therefore, this methodology obtains an equidistant distribution of points to test within the experimental design and presents the advantage of being able to adapt to an irregular experimental domain. It is possible to notice that, considering a low number of clusters when building the design, the points obtained show a high distance from the compressor's operation limits. However, this distance is minimized as we include a larger number of points and, in contrast with the classical designs, they always cover a larger area in the experimental domain.

Additionally, Figure L.5 presents the experimental designs obtained with the optimal design methodology and Fedorov's algorithm for an Optimal-D criterion.

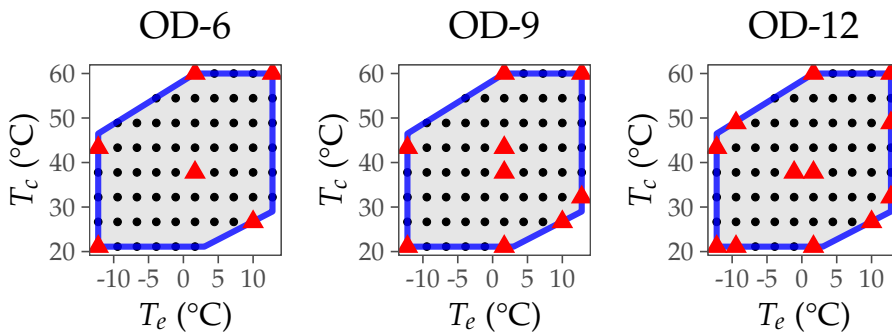


Figure L.5: Optimal design using Fedorov's algorithm for 6, 9, and 12 points (AHRI 11 R410A and SH=11K)

In this case, it can be noticed that the algorithm makes the selection of points mainly on the compressor's operation limits and 1 or 2 central points. These results are coherent with the model that we wish to adjust, which contains only linear terms (T_e and T_c) and quadratic terms (T_e^2 and T_c^2) along with a two-factor interaction term ($T_e T_c$). When placing the points on the limits of operation, we obtain a greater accuracy in the adjustment of linear terms. Concerning the addition of central points, these are needed to adjust the quadratic terms, where a higher number of levels are required to characterize the curvature of the response variable (\dot{W}_c or \dot{m}_{ref}). In contrast with the cluster design, it has the advantage of including in the design the 100% of the experimental design.

Finally, Figure L.6 shows the selection of points for the polygonal design. Selecting the envelope's vertexes of the compressor and adding the remaining points with the clustering methodology could be considered a hybrid methodology between the both abovementioned. However, with the borderline case of considering the most compact design (6 tests), this methodology does not include central points, which complicates the estimation of quadratic terms in the model.

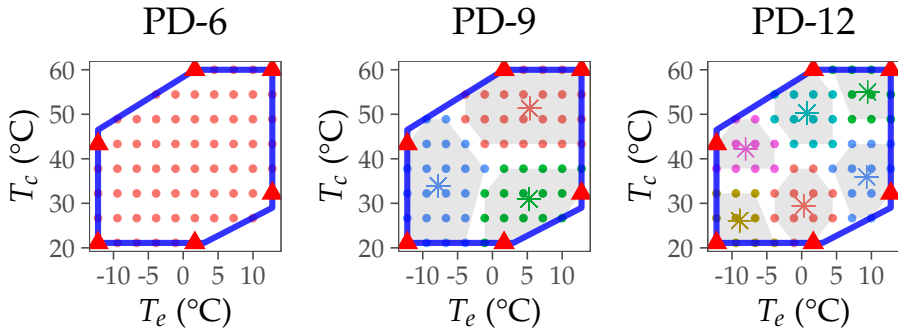


Figure L.6: Polygon Design 6, 9, and 12 points (AHRI 11 R410A and SH=11K)

L.5.2 Results from the adjusted models with the experimental designs

In order to evaluate and compare the experimental designs obtained, the adjustment of the models presented in Equation L.1 and Equation L.2 has been carried out. Once the models were adjusted, it has been confirmed their prediction power with the remaining available points for the evaluated refrigerant and compressor. These points include the three suction conditions tests for the prediction of \dot{W}_c , and the SH=11K tests for the prediction of \dot{m}_{ref} . It was already confirmed in Chapter 4 that compressors' suction conditions mainly affect the mass flow rate and have no apparent effect on the energy consumption. The errors used on the comparative have been the Maximum Relative Error (MRE) and the Root Mean Square Error (RMSE).

It shall be pointed out that, due to the experimental error, the tested points on the operation limits of the compressor usually have a higher measurement error than central points. Because of this, it is important to bear in mind the precision of measurement when making a regression adjustment. Therefore, we use a weighted regression method selecting the Inverse-Variance Weighting (IVW) for the adjustment instead of the classical adjustment by Ordinary Least Squares (OLS). It includes a weight vector with the same length as the experimental sample. This vector must be constructed as the inverse of the experimental variance,

i.e., the inverse-square of the combined standard uncertainty (Taylor and Kuyatt, 1994).

Table L.1 and Table L.2 show an example of the results obtained for the AHRI 11 compressor and the base refrigerant (R410A). The first columns includes the results obtained by performing the adjustment on every available point (reference model).

Table L.1: AHRI 11 (R410A). Energy consumption

	All tests	3k	CCD	SCD	HD	OD6	OD9	OD12	CD6	CD9	CD12	PD6	PD9	PD12
(Int.)	7.7e-01 ***	7.1e-01 ***	7.0e-01 ***	7.1e-01 *	8.0e-01 *	7.6e-01	7.4e-01 ***	7.5e-01 ***	-1.4e+00	7.6e-01 ***	7.6e-01 ***	9.9e-01	7.3e-01 ***	7.4e-01 ***
T_c	-3.9e-03 ***	-5.3e-03 **	-5.2e-03 *	-5.7e-03	-3.0e-03	-3.7e-03	-3.8e-03 **	-3.6e-03 **	-7.8e-02	-4.5e-03	-4.9e-03 *	4.9e-03	-4.0e-03 *	-4.3e-03 *
T_c	1.0e-03 *	4.9e-03 *	5.3e-03 *	5.0e-03	-3.2e-04	1.8e-03	2.4e-03 *	2.0e-03	1.2e-01	2.0e-03	2.2e-03	-1.4e-02	3.4e-03	2.6e-03
$(T_c)^2$	-7.6e-05 ***	-1.0e-04	-1.2e-04	-1.2e-04	-1.4e-04	-7.0e-05	-3.2e-05	-4.9e-05	-1.2e-03	-5.8e-05	-7.3e-05	3.2e-04	-4.3e-05	-4.0e-05
$(T_c)^2$	4.5e-04 ***	3.9e-04 **	3.8e-04 **	3.9e-04 *	4.6e-04	4.4e-04	4.3e-04 **	4.4e-04 **	-1.0e-03	4.3e-04 *	4.3e-04 **	6.5e-04	4.2e-04 **	4.3e-04 **
$T_c \times T_c$	-2.1e-05 *	5.2e-06	7.9e-06	1.2e-05	-4.0e-05	-2.9e-05	-2.6e-05	-3.8e-05	1.9e-03	-1.1e-05	1.5e-06	-2.7e-04	-2.1e-05	-1.1e-05
Num.Obs.	196	9	9	7	7	6	9	12	6	9	12	6	9	12
RMSE (W)	7.26	17.76	14.84	13.43	8.96	8.78	8.79	8.14	161.72	10.22	9.28	44.29	9.15	8.04
MRE (%)	1.21	2.77	2.46	2.27	1.90	1.24	1.33	1.13	39.56	2.06	1.98	6.32	1.31	1.30

^a * p < 0.1, ** p < 0.05, *** p < 0.01, **** p < 0.001;
^b Temperatures (°C);
^c Energy consumption (kW); Range: [973, 2454] (W);

Table L.2: AHRI 11 (R410A). Mass flow rate

	All tests	3k	CCD	SCD	HD	OD6	OD9	OD12	CD6	CD9	CD12	PD6	PD9	PD12
(Int.)	1.2e+02 ***	1.2e+02 ***	1.2e+02 ***	1.2e+02 *	1.2e+02 **	1.2e+02	1.2e+02 ***	1.2e+02 ***	2.7e+02	1.2e+02 ***	1.2e+02 ***	1.5e+02	1.2e+02 ***	1.2e+02 ***
T_c	4.1e+00 ***	4.1e+00 ***	4.1e+00 ***	3.9e+00 *	4.0e+00 **	4.1e+00	4.1e+00 ***	4.2e+00 ***	9.3e+00	4.1e+00 ***	4.1e+00 ***	5.2e+00	4.0e+00 ***	4.0e+00 ***
T_c	1.2e-01 **	-1.8e-01	5.8e-03	5.8e-03	1.8e-01 *	8.1e-03	1.1e-01	2.7e-02	-8.3e+00	1.1e-01	8.1e-02	-2.0e+00	2.1e-01	2.3e-01
$(T_c)^2$	5.6e-02 ***	6.1e-02 **	6.1e-02 **	6.2e-02 *	6.7e-02 **	5.5e-02	5.6e-02 **	5.7e-02 **	1.4e-01	5.8e-02 **	5.7e-02 **	1.0e-01	5.4e-02 **	5.2e-02 **
$(T_c)^2$	-6.6e-03 ***	-2.1e-03	-4.7e-03	-4.9e-03	-7.3e-03 **	-5.4e-03	-6.6e-03 **	-5.6e-03 **	1.0e-01	-6.2e-03 **	-5.8e-03 **	2.0e-02	-7.9e-03 *	-8.2e-03 *
$T_c \times T_c$	4.0e-03 ***	2.9e-03	2.0e-03	6.0e-03	3.5e-03 *	3.6e-03	4.6e-03 *	2.8e-03	-1.3e-01	2.7e-03	3.1e-03 *	-2.6e-02	6.5e-03 *	6.4e-03 *
Num.Obs.	66	9	9	7	7	6	9	12	6	9	12	6	9	12
RMSE (kg/h)	0.40	1.03	0.76	0.76	1.02	0.62	0.56	0.55	11.78	0.49	0.46	5.94	0.52	0.50
MRE (%)	1.42	3.84	4.11	3.20	5.44	1.80	1.74	1.66	28.94	2.65	2.17	9.75	1.49	1.17

^a * p < 0.1, ** p < 0.05, *** p < 0.01, **** p < 0.001;
^b Temperatures (°C);
^c Mass flow rate (kg/h); Range: [66, 178] (kg/h);

The tables above show that the adjustment with different samples obtains a similar error to the one obtained considering the adjustment with all the available points.

In the case of the energy consumption, we have an RMSE=7.3W and an MRE=1.2%, adjusting with 196 points. The variation range of the energy consumption is between 973W and 2454W. Taking these values of error as a reference, we can see how the prediction of these 196 points gets an error similar to the optimal designs.

We can point out the optimal design of 6 points (OD6) where we obtain an RMSE=8.8W and an MRE=1.2% with only using 6 points for the adjustment. This sample of 6 points is the most possible compact design considering the number of terms to adjust in the model.

On the other hand, cluster designs and polygonal designs obtain similar results except for the designs of 6 points (CD6 and PD6). In this case, these methodologies obtain a considerable error compared to the other designs.

Finally, classical designs show an error slightly higher than the rest of the designs, without considering the cluster and polygonal designs with 6 points. Regarding the mass flow rate prediction, we obtained similar results to the ones described in the consumption.

As we can see from the results, the errors obtained on the different designs are low except for those obtained in CD6 and PD6. However, if we take a closer look at the results, we will notice in some designs that the regression coefficients reverse the sign when comparing them with the reference model. These coefficients have been highlighted in red in the tables above. Considering that in the reference model, all of the regression coefficients are significant ($p\text{-value} < 0.05$) and that this model has been adjusted with a large number of experimental points, this change in trend is an effect that we must try to avoid. This effect is motivated by the reduction of experimental information in the selected samples, which can lead to:

- A change in trend in second-order effects.
- A change in trend in first-order effects.

In the first case, we only lose some accuracy being terms of low weight in the model. For example, despite reversing the sign of the term $T_e T_c$ for classical designs in Table L.1, this just means a slight rise in the prediction error. Another example would be the term T_c of the design 3² in Table L.2. In this case, the model for the mass flow rate depends mainly on T_e instead of T_c .

In the second case, the prediction error may increase considerably. Considering that the energy consumption in scroll compressors depends mainly on T_c , it can be observed in the CD6 and PD6 designs that the terms T_c and T_c^2 invert their sign concerning the ones obtained in the reference model with a considerable increase in the prediction error. In the case of the HD design, we only obtain a change of tendency in T_c without a significant increase in the error because it is compensated with the quadratic term T_c^2 .

Considering what has been described above, Section L.7 includes a summary table per analyzed AHRI report (Table L.3, Table L.4 and Table L.5). These tables show the error in the \dot{W}_c and \dot{m}_{ref} models for the whole set of refrigerants. They have been adjusted with the different experimental designs next to an additional column ("*sign*") indicating whether there is a change in trend, or not, in some of the regression coefficients. Additionally, to facilitate the analysis, a column with the design's label has been colored according to the obtained value of RMSE.

According to the results on the summary tables, it can be seen that similar results to the ones described above for the AHRI 11 compressor and the reference refrigerant are obtained. CD6 and PD6 methodologies always get high values of RMSE and MRE. Concerning the rest of the designs, classical methodologies

generally have acceptable prediction errors but are higher than computer-aided methodologies. On the other hand, having analyzed the tendencies in the coefficients, methodologies with optimal designs get a better prediction of the regression coefficients showing the same trend if they are compared with the results obtained when adjusting them to all available points per compressor and refrigerant. Regarding cluster and polygonal designs with more than 6 points in the design, despite not getting the same trend in all coefficients for some of the analyzed refrigerants, this does not become a significant increase in the prediction error. Therefore, it can be concluded that all methodologies assisted by computer generally obtain the lower prediction errors if more than 6 points on the experimental design are included.

L.6 Summary of results

Finally, a brief summary of the most relevant results is shown below to conclude this appendix:

- The response surfaces for the energy consumption and mass flow rate are smooth, and generally, all of the analyzed designs obtain acceptable prediction errors, except for the CD6 and PD6 designs.
- Classical designs are not able to adapt to irregular experimental domains. They do not obtain errors as low as the computer-aided designs. However, they do not show high errors of prediction, which makes it appropriate if they can cover a significant area within the limits of the compressor envelope. These designs should be used only in the case of not having the necessary tools to use computer-aided designs. Based on the obtained results, the most appropriate classical methodology has been the CCD.
- In most cases, computer-aided designs have obtained the lowest errors of prediction. The cluster and polygonal designs considering 6 test points shall be excluded. These methodologies allow to adapt the designs to irregular experimental domains minimizing the extrapolation errors. Therefore, computer-aided designs are more appropriate than classical methodologies in irregular experimental domains.

- Optimal designs show the advantage of selecting an optimal sample for adjusting the target model, being more recommendable in case of knowing the functional to adjust. They show the limitation of considering the same functional for the prediction of \dot{W}_c and \dot{m}_{ref} . Considering different functional would lead to consider two designs, one for the adjustment of \dot{W}_c and the other for the adjustment of \dot{m}_{ref} . In this case, we must consider the model with higher number of terms in the polynomial.
- The use of 9 experimental points in the design has shown to be an appropriate number of tests balancing accuracy and experimentation costs. The use of 9 points allows to obtain similar results among the three methodologies of computer-aided designs.
- The use of 6 points using the optimal designs methodology is the most reliable compact design when minimizing the experimentation costs to the maximum is critical. This sample size has the drawback of assuming 0 degrees of freedom in the adjustment of the model. Therefore it is able to obtain the value of the regression coefficients but without the different statistical indicators of the regression model (*p-value*, *std.Error*, ...). However, in the analyzed cases, using the optimal designs methodology has obtained a great prediction of the regression coefficients with a low prediction error considering the 6 points samples. When considering the different statistical indicators of the regression adjustment, the most compact size will be 7 points.
- The use of the three methodologies of computer-aided designs allows to define the total number of points to include in the sample. This allows the adjustment of models considering a greater number of terms in the functional; Maybe necessary for a more complex response surface like in reciprocating compressors. Therefore, they are appropriate for adjusting the AHRI polynomial (AHRI 540, 2020), which includes 10 coefficients in the functional. In these cases, building the design with 12 points, as proposed in (Aute et al., 2015), would be the most suitable option. More compact designs of 10-11 points may be considered to reduce the costs and time of experimentation, recommending, in this case, the use of optimal design methodologies.

L.7 Summary tables DoE samples

Table L.3: AHRI 11. Summary table DoE samples results

DoE	Energy consumption					Fluid	mass flowrate					DoE
	MRE (%)	RMSE (W)	Sample	Range (W)	sign		sign	Range (kg/h)	Sample	RMSE (kg/h)	MRE (%)	
All tests	1.21	7.26	196		✓		✓		66	0.396	1.415	All tests
3k	2.77	17.76	9		✗		✗		9	1.028	3.837	3k
CCD	2.46	14.84	9		✗		✓		9	0.755	4.109	CCD
SCD	2.27	13.43	7		✗		✓		7	0.759	3.197	SCD
HD	1.90	8.96	7		✗		✓		7	1.024	5.443	HD
OD6	1.24	8.78	6		✓		✓		6	0.619	1.799	OD6
OD9	1.33	8.79	9		✓		✓		9	0.561	1.740	OD9
OD12	1.13	8.14	12	[973, 2454]	✓	R410A	✓	[66, 178]	12	0.546	1.661	OD12
CD6	39.56	161.72	6		✗		✗		6	11.781	28.937	CD6
CD9	2.06	10.22	9		✓		✓		9	0.487	2.650	CD9
CD12	1.98	9.28	12		✗		✓		12	0.461	2.166	CD12
PD6	6.32	44.29	6		✗		✗		6	5.941	9.754	PD6
PD9	1.31	9.15	9		✓		✓		9	0.525	1.488	PD9
PD12	1.30	8.04	12		✓		✓		12	0.497	1.173	PD12
All tests	3.12	14.43	166		✓		✓		59	0.545	2.164	All tests
3k	5.66	26.86	9		✓		✓		9	1.211	3.878	3k
CCD	4.68	20.61	9		✓		✓		9	1.453	7.485	CCD
SCD	4.53	20.26	7		✓		✓		7	1.348	7.366	SCD
HD	5.52	25.89	7		✓		✓		7	1.476	6.351	HD
OD6	4.00	26.97	6		✓		✓		6	0.671	2.727	OD6
OD9	2.67	20.53	9		✓		✓		9	0.587	2.254	OD9
OD12	2.80	20.05	12	[1005, 2607]	✓	R32	✓	[46, 123]	12	0.578	2.332	OD12
CD6	12.84	57.22	6		✗		✓		6	1.435	3.817	CD6
CD9	3.46	21.39	9		✓		✓		9	0.664	1.944	CD9
CD12	2.85	17.04	12		✗		✓		12	0.559	2.043	CD12
PD6	31.30	288.88	6		✗		✗		6	5.384	12.235	PD6
PD9	3.12	19.95	9		✓		✓		9	0.656	2.425	PD9
PD12	3.64	23.79	12		✓		✓		12	0.610	2.127	PD12
All tests	4.62	13.00	189		✓		✓		66	0.189	0.647	All tests
3k	6.15	20.37	9		✗		✓		9	0.331	1.296	3k
CCD	5.72	17.19	9		✗		✓		9	0.400	2.214	CCD
SCD	5.51	16.85	7		✗		✓		7	0.377	2.005	SCD
HD	4.17	15.15	7		✓		✓		7	0.386	2.407	HD
OD6	4.15	18.52	6		✓		✓		6	0.234	1.026	OD6
OD9	4.06	15.62	9		✓		✓		9	0.222	1.062	OD9
OD12	4.17	16.94	12	[929, 2401]	✓	DR5	✓	[49, 134]	12	0.209	0.615	OD12
CD6	60.36	225.08	6		✗		✗		6	5.105	16.214	CD6
CD9	5.27	14.84	9		✗		✓		9	0.197	0.799	CD9
CD12	5.00	14.08	12		✗		✓		12	0.205	0.592	CD12
PD6	24.74	191.08	6		✗		✗		6	2.111	4.893	PD6
PD9	4.39	15.15	9		✗		✓		9	0.223	1.048	PD9
PD12	4.60	13.96	12		✗		✓		12	0.210	0.957	PD12
All tests	1.25	6.33	186		✓		✓		65	0.254	0.993	All tests
3k	3.39	10.90	9		✓		✗		9	0.650	1.901	3k
CCD	2.46	8.47	9		✓		✓		9	0.449	2.076	CCD
SCD	2.81	8.80	7		✓		✓		7	0.610	3.280	SCD
HD	3.90	11.41	7		✓		✗		7	0.480	1.415	HD
OD6	1.47	9.90	6		✓		✓		6	0.305	1.063	OD6
OD9	1.33	9.13	9		✓		✓		9	0.314	0.950	OD9
OD12	1.41	9.43	12	[888, 2211]	✓	L41a	✓	[43, 122]	12	0.267	0.995	OD12
CD6	6.99	28.14	6		✓		✗		6	1.721	6.001	CD6
CD9	1.89	7.74	9		✓		✓		9	0.268	0.962	CD9
CD12	1.84	7.20	12		✓		✓		12	0.260	0.968	CD12
PD6	1.90	9.57	6		✗		✗		6	1.287	3.941	PD6
PD9	1.29	8.37	9		✓		✓		9	0.277	1.012	PD9
PD12	1.08	7.11	12		✓		✓		12	0.269	1.004	PD12

Table L.4: AHRI 21. Summary table DoE samples results

DoE	Energy consumption					Fluid	mass flowrate					DoE
	MRE (%)	RMSE (W)	Sample	Range (W)	sign		sign	Range (kg/h)	Sample	RMSE (kg/h)	MRE (%)	
All tests	2.19	14.04	191		✓		✓		63	0.491	0.751	All tests
3k	4.88	26.57	9		✓		✓		9	0.521	0.746	3k
CCD	4.81	22.45	9		✓		✓		9	0.576	0.912	CCD
SCD	4.83	22.38	7		✓		✓		7	0.596	0.973	SCD
HD	3.95	18.95	7		✓		✓		7	0.541	0.779	HD
OD6	2.64	16.49	6		✓		✓		6	0.633	0.995	OD6
OD9	2.50	15.69	9		✓		✓		9	0.584	0.872	OD9
OD12	2.62	15.83	12	[1856, 4172]	✓	R404A	✓	[124, 308]	12	0.558	0.895	OD12
CD6	5.07	44.57	6		✓		✗		6	2.691	4.845	CD6
CD9	3.58	21.72	9		✓		✓		9	0.591	0.867	CD9
CD12	3.51	19.68	12		✓		✓		12	0.524	0.789	CD12
PD6	2.64	16.73	6		✓		✗		6	5.686	5.540	PD6
PD9	2.78	17.81	9		✓		✗		9	0.761	1.181	PD9
PD12	2.79	18.36	12		✓		✓		12	0.603	0.980	PD12
All tests	1.65	9.73	186		✓		✓		64	0.283	0.922	All tests
3k	4.05	19.35	9		✓		✓		9	0.430	0.917	3k
CCD	3.13	15.54	9		✓		✓		9	0.320	1.169	CCD
SCD	3.65	16.19	7		✓		✓		7	0.335	0.969	SCD
HD	2.83	15.08	7		✓		✓		7	0.322	0.986	HD
OD6	1.71	14.54	6		✓		✓		6	0.476	0.957	OD6
OD9	1.75	16.11	9		✓		✓		9	0.400	0.872	OD9
OD12	1.83	12.87	12	[1582, 3615]	✓	ARM31a	✓	[73, 200]	12	0.346	0.600	OD12
CD6	3.06	15.56	6		✓		✓		6	0.436	1.931	CD6
CD9	2.77	15.13	9		✓		✓		9	0.315	0.748	CD9
CD12	2.63	14.08	12		✓		✓		12	0.297	1.185	CD12
PD6	4.76	50.34	6		✗		✗		6	1.764	2.629	PD6
PD9	1.86	13.62	9		✓		✗		9	0.384	1.025	PD9
PD12	1.98	12.88	12		✓		✗		12	0.481	1.216	PD12
All tests	1.85	11.98	183		✓		✓		64	0.439	1.326	All tests
3k	5.06	24.99	9		✓		✓		9	0.539	1.385	3k
CCD	3.66	17.73	9		✓		✓		9	0.501	1.548	CCD
SCD	4.76	20.00	7		✓		✓		7	0.515	1.776	SCD
HD	3.42	18.18	7		✓		✓		7	0.539	1.765	HD
OD6	1.91	16.27	6		✓		✓		6	0.484	1.434	OD6
OD9	1.88	17.74	9		✓		✓		9	0.486	1.302	OD9
OD12	1.99	14.68	12	[1724, 3988]	✓	D2Y65	✓	[81, 214]	12	0.471	1.397	OD12
CD6	3.55	18.68	6		✓		✓		6	0.709	2.983	CD6
CD9	3.25	17.84	9		✓		✓		9	0.530	1.497	CD9
CD12	3.01	16.30	12		✓		✓		12	0.464	1.412	CD12
PD6	3.26	30.33	6		✗		✗		6	2.658	4.189	PD6
PD9	2.08	15.53	9		✓		✓		9	0.591	1.054	PD9
PD12	2.19	14.47	12		✓		✓		12	0.564	1.485	PD12
All tests	1.29	9.12	173		✓		✓		61	0.324	1.040	All tests
3k	4.64	22.01	9		✓		✓		9	0.710	2.878	3k
CCD	2.33	11.73	9		✓		✓		9	0.417	1.742	CCD
SCD	3.87	16.50	7		✓		✗		7	0.488	1.929	SCD
HD	2.79	16.27	7		✓		✗		7	0.866	3.737	HD
OD6	1.49	17.04	6		✓		✓		6	0.363	0.808	OD6
OD9	1.34	15.35	9		✓		✓		9	0.409	0.775	OD9
OD12	1.37	13.63	12	[1570, 3655]	✓	L40	✓	[64, 175]	12	0.341	0.855	OD12
CD6	2.74	13.84	6		✓		✓		6	0.985	2.704	CD6
CD9	2.02	12.68	9		✓		✓		9	0.394	1.492	CD9
CD12	2.10	11.99	12		✓		✓		12	0.351	1.128	CD12
PD6	1.41	13.59	6		✓		✗		6	0.803	1.648	PD6
PD9	1.53	12.54	9		✓		✗		9	0.560	1.128	PD9
PD12	1.76	11.22	12		✓		✓		12	0.354	0.716	PD12

(Continued on Next Page...)

Table L.4: AHRI 21. Summary table DoE samples results (*continued*)

DoE	Energy consumption					Fluid	mass flowrate					DoE
	MRE (%)	RMSE (W)	Sample	Range (W)	sign		sign	Range (kg/h)	Sample	RMSE (kg/h)	MRE (%)	
All tests	1.28	13.6	133		✓		✓		48	0.533	1.33	All tests
3k	2.58	27.3	9		✓		✓		9	0.563	1.44	3k
CCD	6.03	35.1	9		✗		✓		9	1.045	3.56	CCD
SCD	4.47	40.9	7		✗		✓		7	1.861	7.92	SCD
HD	4.31	28.1	7		✓		✓		7	1.725	7.88	HD
OD6	2.39	21.2	6		✓		✓		6	0.810	1.61	OD6
OD9	1.21	15.4	9		✓		✓		9	0.658	1.44	OD9
OD12	1.24	15.7	12	[1740, 4268]	✓	R32/R134a	✓	[68, 179]	12	0.645	1.50	OD12
CD6	3.78	37.3	6		✓		✗		6	2.353	7.03	CD6
CD9	2.40	16.0	9		✓		✓		9	0.599	1.74	CD9
CD12	2.17	16.4	12		✓		✓		12	0.574	1.67	CD12
PD6	43.17	346.2	6		✗		✗		6	18.468	33.55	PD6
PD9	2.17	21.0	9		✓		✓		9	1.069	3.31	PD9
PD12	1.39	15.0	12		✓		✓		12	0.973	2.32	PD12

Table L.5: AHRI 33. Summary table DoE samples results

DoE	Energy consumption					Fluid	mass flowrate					DoE
	MRE (%)	RMSE (W)	Sample	Range (W)	sign		sign	Range (kg/h)	Sample	RMSE (kg/h)	MRE (%)	
All tests	1.70	7.72	196		✓		✓		66	0.264	0.751	All tests
3k	3.52	14.32	9		✓		✓		9	0.345	1.233	3k
CCD	2.33	13.74	9		✓		✓		9	0.368	1.468	CCD
SCD	3.38	12.56	7		✓		✓		7	0.383	1.827	SCD
HD	3.19	10.24	7		✗		✓		7	0.457	2.510	HD
OD6	2.37	12.64	6		✓		✓		6	0.390	0.642	OD6
OD9	2.38	11.94	9		✓		✓		9	0.361	0.768	OD9
OD12	1.97	10.16	12	[945, 2432]	✓	R410A	✓	[68, 181]	12	0.328	0.664	OD12
CD6	60.02	233.14	6		✗		✗		6	14.395	33.587	CD6
CD9	2.97	9.86	9		✓		✓		9	0.335	0.928	CD9
CD12	2.76	9.60	12		✓		✓		12	0.300	0.788	CD12
PD6	3.61	19.60	6		✗		✗		6	7.040	11.387	PD6
PD9	2.42	12.55	9		✓		✓		9	0.332	0.739	PD9
PD12	2.09	10.42	12		✓		✓		12	0.332	0.560	PD12
All tests	1.42	8.31	168		✓		✓		59	0.226	1.102	All tests
3k	2.23	12.34	9		✓		✓		9	0.261	1.147	3k
CCD	2.12	11.29	9		✓		✓		9	0.262	1.617	CCD
SCD	2.19	10.46	7		✓		✓		7	0.257	1.539	SCD
HD	2.42	12.64	7		✓		✓		7	0.388	1.895	HD
OD6	2.20	13.22	6		✓		✓		6	0.289	1.511	OD6
OD9	1.74	11.92	9		✓		✓		9	0.276	0.964	OD9
OD12	1.85	12.04	12	[943, 2452]	✓	R32/R134a	✓	[46, 123]	12	0.286	0.995	OD12
CD6	3.19	10.96	6		✗		✓		6	0.601	1.991	CD6
CD9	1.72	10.27	9		✓		✓		9	0.285	1.097	CD9
CD12	1.97	9.20	12		✓		✓		12	0.245	1.284	CD12
PD6	8.97	63.77	6		✗		✗		6	3.019	6.886	PD6
PD9	1.96	12.19	9		✓		✓		9	0.313	1.258	PD9
PD12	1.78	10.99	12		✓		✓		12	0.276	0.911	PD12

L.8 Source code to obtain computer-aided designs

```

library(AlgDesign)
library(geoR)
library(scales)

# Define data.frame with compressor
# envelope
df_env <- data.frame(Te = c(-24, -24, -15, 2, 2, -12),
  Tc = c(20, 52, 61, 61, 35, 20))
# Define number of points to include in
# the experimental design
test_points <- 9

# Extra variables to build the mesh
# grid inside the compressor envelope
dTe <- 1
dTc <- 1

# Generate the mesh grid
grid <- polygrid(xgrid = seq(from = min(df_env$Te),
  to = max(df_env$Te), by = dTe), ygrid = seq(from = min(df_env$Tc),
  to = max(df_env$Tc), by = dTc), borders = df_env)
names(grid) <- c("Te", "Tc")

# Rescale Tc, Te coordinates to -1, 1
# range
grid$Te_N <- rescale(grid$Te, to = c(-1, 1))
grid$Tc_N <- rescale(grid$Tc, to = c(-1, 1))

# Optimal design Fedorov D-optimal
# criteria
Fedorov <- optFedorov(~Te_N + Tc_N + I(Te_N^2) +
  I(Tc_N^2) + Te_N:Tc_N, data = grid, nTrials = test_points,
  criterion = "D")

df_Fedorov <- Fedorov$design[, c("Te", "Tc")]

# Cluster design

```

```

cluster <- kmeans(x = grid[, c("Te_N", c("Tc_N"))],
  centers = test_points, iter.max = 10000,
  nstart = nrow(grid))

df_cluster <- data.frame(Te = rescale(c(-1,
  1, cluster$centers[, "Te_N"]), to = c(min(df_env$Te),
  max(df_env$Te))[-c(1:2)]), Tc = rescale(c(-1,
  1, cluster$centers[, "Tc_N"]), to = c(min(df_env$Tc),
  max(df_env$Tc))[-c(1:2)])

# Experimental matrices
print(df_Fedorov, row.names = F)

##   Te Tc
## -24 20
## -12 20
##   2 35
## -24 36
## -11 42
## -11 43
## -24 52
## -15 61
##   2 61

print(df_cluster, row.names = F)

##      Te   Tc
## -11.11 55.3
##  -1.59 41.8
## -19.40 50.2
## -13.36 27.2
## -20.31 37.8
## -11.42 42.2
## -20.73 25.3
##  -2.00 55.0
##  -6.23 32.6

# Model adjustment. The df data.frame
# includes the experimental results
# (including the experimental error)

```

```
Wc <- lm(data = df, formula = Wc ~ Te + Tc +  
         I(Te^2) + I(Tc^2) + Te:Tc, weights = 1/(df$Wc_error^2))  
  
m <- lm(data = df, formula = m ~ Te + Tc +  
         I(Te^2) + I(Tc^2) + Te:Tc, weights = 1/(df$m^2))
```